The Thesis Committee for Umesh Gupta
Certifies that this is the approved version of the following thesis:

Cyclic Loading Analysis of Doubler Plate Attachment Details for Steel Moment Resisting Frames

APPROVED BY
SUPERVISING COMMITTEE:

Supervisor:

Michael D. Engelhardt

Todd Helwig

Cyclic Loading Analysis of Doubler Plate Attachment Details for Steel Moment Resisting Frames

by

Umesh Gupta, B.Tech., M.Tech.

Thesis

Presented to the Faculty of the Graduate School of

The University of Texas at Austin

in Partial Fulfillment

of the Requirements

for the Degree of

Master of Science in Engineering

The University of Texas at Austin

May 2013

Dedication

Dedicated to my wife and parents.

Acknowledgements

I would like to express my gratitude towards my advisor Dr. Michael Engelhardt for giving me an opportunity to work on this simulating work involving finite element study on structural steel. My learning in the initial stage was enhanced greatly by his continuous critical appraisal and positive feedback. His advice to break the bigger problem into a number of smaller questions helped me throughout the course of work. While working with him, I developed good engineering skills and professional approach.

I would also like to thank Dr. Todd Helwig who agreed to become reader for my thesis and provide constructive feedback. I also want to thank Donkada Shravya and Priyanka Shirsat who helped me initially to learn the basic skills in finite element modeling.

Finally I want to thank my wife and parents for their continuous support during my study period. I am grateful to all my friends in Austin.

Abstract

Cyclic Loading Analysis of Doubler Plate Attachment Details for Steel Moment Resisting Frames

Umesh Gupta, MSE

The University of Texas at Austin, 2013

Supervisor: Michael D. Engelhardt

The panel zone region in columns of seismic resistant steel moment frames are subject to very high shear forces during earthquake loading. Doubler plates are often used to increase the stiffness and strength of the panel zone. The methods and details used to attach doubler plates to columns can affect seismic performance of the panel zone and can also affect cost. The research reported in this thesis was aimed at developing an improved understanding of the advantages and disadvantages of various approaches for detailing and welding doubler plates to columns and how various details perform under cyclic inelastic loading. An extensive series of finite element analyses were conducted to study doubler plate attachment details. Both a shallow W14x398 column and a deep W40x264 column were studied in this research. This thesis provides a detailed description of the finite element modeling techniques used for the research and presents the results of an extensive series of analyses examining a wide variety of issues related to doubler plate design and detailing.

Table of Contents

CHAPTER 1

Introduction

1.1 STATEMENT OF THE PROBLEM

The columns in a seismic-resistant moment frames are subjected to large forces and deformations during seismic lateral loading. The high moment gradient at the connection produces a high shear in the column near the connection (see Figure 1.1). This region of the high shear in the column within the beam flanges is known as 'panel zone' (see Figure 1.1). The glossary of *Specification for Steel Structural Buildings* (AISC 2010a) defines the panel zone as '*Web area of beam-to-column connection delineated by the extension of beam and column flanges through the connection, transmitting moment through a shear panel*.' The available shear strength of the panel zone can be calculated according to section J10 of *Specification for Steel Structural Buildings* (AISC 2010a) and the required shear strength of the panel zone can be determined as given in section E3 of *Seismic Provisions for Steel Structural Buildings* (AISC 2010b). Whenever the required shear strength exceeds the available shear strength, doubler plates (DP) are often used to increase the available strength and stiffness of the panel zone. The DP is a plate that acts as an additional web in the column and is generally attached or separated from the web (see Figure 1.2) as per details given in *Seismic Provisions for Steel Structural Buildings* (AISC 2010b). As per section E3 of AISC (2010b), sometimes continuity plates (CP) are required to provide a different 'load-path' to the concentrated force delivered to the column by the beam flanges and to control the local limit states like flange bending and web / DP crippling in the column. The DP and CP can be welded to the column using groove welds or fillet welds and the amount of welding can increase the construction cost of moment frames.

In the past, many researchers have conducted investigations on the strength and stiffness of the panel zone and its effect on beam – column joint connection behavior as well as overall frame behavior. However, very little research has been conducted on the

different ways of attaching the DP to the column. Some of the current guidelines in the *Seismic Provisions for Steel Structural Buildings* (AISC 2010b) are not very clear about sizing of the DP and the methods to be used for welding the doubler plate to the column, both in cases with and without the presence of CPs. These issues are researched in this thesis using finite element studies of beam – column assembly subjected to cyclic loading.

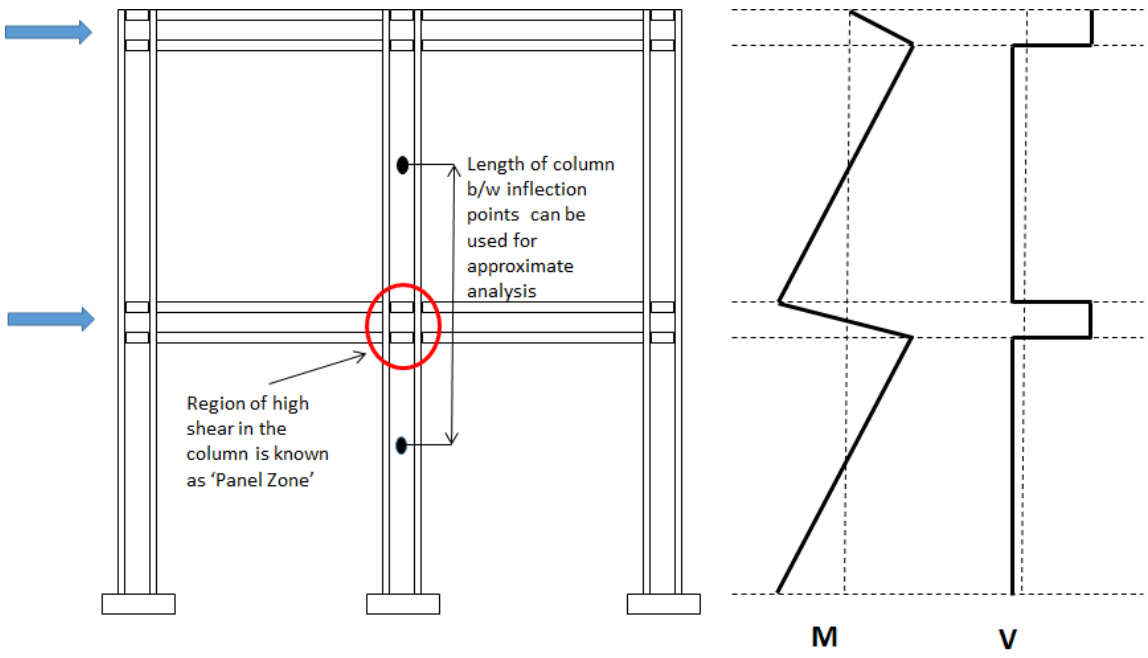

Figure 1.1: Panel zone in the steel moment frame

1.2 RESEARCH OBJECTIVES

The research done here is an extension of the previous work done by Shirsat (2011) and Donkada (2012). The research is aimed to provide the answers to the following questions using cyclic loading analysis:

- Are there any benefits of extension of the DP above the beam joints if only vertical groove welds are used to attach the DP to the column?

- Is there any advantage of providing horizontal fillet welds at the top and bottom of the DP when vertical groove welds are already in place and the DP is terminated at the level of the beam flanges?
- When are the CP's critical elements in the panel zone assembly? How does the load path of the beam flange force applied to the column change with introduction of CP's?
- Does the DP get overstressed when the DP is extended and CP's are welded directly to the DP?
- What are the different limiting strength states in shallow and deep columns when the panel zone is cyclically loaded to a rotation of 0.05 radian?
- What are the major stresses along the depth of vertical groove weld? Should the weld be designed to develop shear strength or tensile strength of the DP?
- What are the consequences if DP is undersized or oversized as compared to the requirement by *Seismic Provisions for Steel Structural Buildings* (AISC 2010b)?

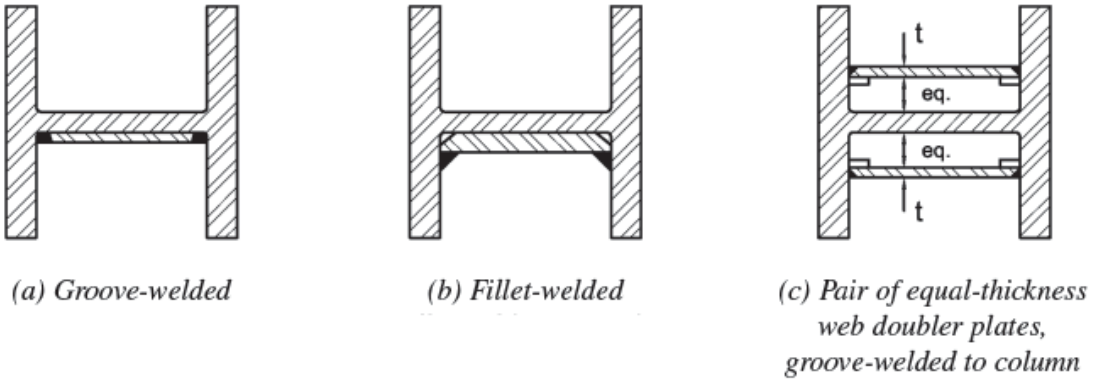

Figure 1.2: Doubler plate attachment details as per *AISC Seismic Provisions for Steel Structural Buildings* (2010b)

1.3 ORGANIZATION OF THE THESIS

The thesis is divided into nine chapters. Chapter 2 provides a brief summary of the previous work done by other researchers regarding doubler plate attachment details and cyclic stress–strain response of structural steel. Chapter 3 discusses the modeling techniques used in ABAQUS 6.12 to develop a finite element model of the beam – column assembly. It also outlines the development of a cyclic material model for this research. Chapters 4 and 5 list all the results pertaining to analysis of a shallow column (W14X398) and of a deep column (W40X264) respectively. The limit states predominant in different simulation cases are also discussed in Chapters 4 and 5. Chapters 6, 7 and 8 address the specific questions asked in the objectives of this thesis regarding the benefits of horizontal welds, used of undersized or oversized DP and advantage of extending the DP respectively. Finally, Chapter 9 summarizes the work done, the major conclusions and the future research that can be done to investigate some other areas in DP attachment detailing.

1.4 NOMENCLATURE

The abbreviations used in this thesis are given below:

FE	Finite Element
FEM	Finite Element Method
CP	Continuity Plate
DP	Doubler Plate
LP	Loading Plate
VMS	Von Mises Stress
PEEQ	Cumulative Equivalent Plastic Strain
PEMAG	Plastic Strain Magnitude
CJP	Complete Joint Penetration weld

CJP1	Complete Joint Penetration weld between column flange and DP
CJP2	Complete Joint Penetration weld between column flange and CP
CJP3	Complete Joint Penetration weld between column web and CP
EBF	Eccentrically Braced Frames
FBD	Free Body Diagram

CHAPTER 2

Literature Review

2.1 OVERVIEW

This chapter provides a brief literature review of previous work done relevant to attachment details of doubler plates in panel zones of steel moment resisting frames designed for seismic loads. In addition, since the research reported in this thesis involves modeling of panel zone regions under cyclic load, a brief review is also provided on data and material models for the cyclic stress-strain response of structural steel. A substantial amount of work has been done examining the strength and deformation characteristics of panel zones but very few studies has been done specifically on doubler plate attachment details. Section 2.2 reviews past finite element studies on the doubler plate attachment details while section 2.3 talks about the previous work done by researchers on cyclic stress-strain response of structural steel. An overall summary is given in section 2.4.

2.2 FINITE ELEMENT STUDIES ON DOUBLER PLATE ATTACHMENT DETAILS

A review of some previous studies including Becker (1975), Slutter (1982), research at the University of Minnesota (2005) and Ciutina and Dubina (2008) can be found in the literature review section of Shirsat (2011) and Donkada (2012). Interesting FE studies on doubler plate attachment details was done by Mays (2000), Shirsat (2011) and Donkada (2012). These studies are summarized below:

2.2.1 Research by Mays (2000)

Mays studied the seismic design and analysis of moment end plate connections using the finite element method. A part of the study also focused on doubler plate (DP) welding requirements on the column web. Mays developed some key recommendations regarding the welding details of doubler plate by investigating how the horizontal welds can alter the load path of the concentrated force across the column web of the panel zone.

He studied the combined effect of extension of doubler plates beyond the continuity plate (CP) and the provision of horizontal welds at the DP-column web interface. The study was done on a W14x311 column with a weak panel zone so that the DP was required to provide the required shear strength of the panel zone. The total FE assembly consisted of the W14x311 column, nominal W36 section girders, 0.705 inch thick DP, 0.5 inch thick CP's and 0.5 inch horizontal/vertical welds. Vertical welds were included in all cases.

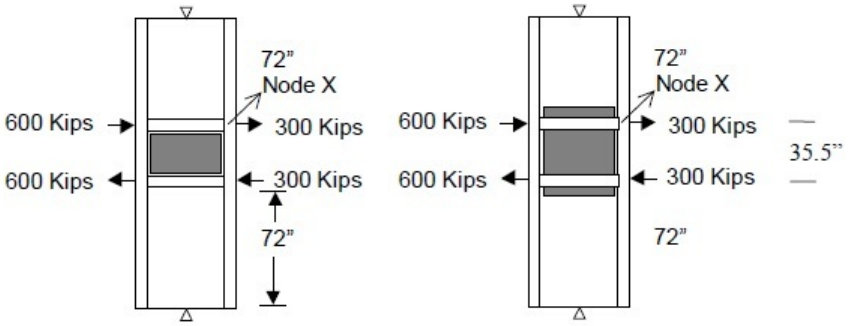

Figure 2.1: Loading assembly (*Mays (2000)*)

The loading and overall assembly was as shown in Figure 2.1. A total of four cases were considered:

1. DP between CP's with horizontal welds at DP and column web interface.
2. DP extended 2.5 times "k" beyond CP's with horizontal welds at DP and column web interface.
3. DP between CP's with no horizontal welds at DP and column web interface.
4. DP extended 2.5 times "k" beyond CP with no horizontal welds between DP and column web.

The Von Mises Stress (VMS) in the column web, VMS in the DP, and the horizontal and vertical shear stresses in the DP were studied for the above four cases by examining the stress contours. Stress contours for VMS and vertical shear stress in the DP were as shown in Figure 2.2 and Figure 2.3 respectively. In case 1, it was found that uniform low horizontal shear stresses occurred in the DP but concentrated vertical shear

stress occurred along the vertical welds. Case 2 had similar stress patterns. In case 3, there was noticeable change in the load path of the concentrated force and high VMS gradient near corners of the DP was noticed. This high stress gradient was due to localized yielding at corners. The vertical shear stress at corners increased slightly as compared to case 2. Case 4 eliminated some of the disadvantages in case 3 and considerable decrease in VMS stress gradient and vertical shear stress was found. The region above the CP had much smaller stresses. In this study, the DP was modeled elastically. Similar results were obtained when the DP material was considered plastic with a much lesser yield stress than the column web. Another interesting observation suggested that yielding started at the center of DP and extended towards the corners which were in line with the physical observations in the experiments. These results clearly manifested that exclusions of horizontal weld and extending the DP beyond the CPs presented an ideal load path.

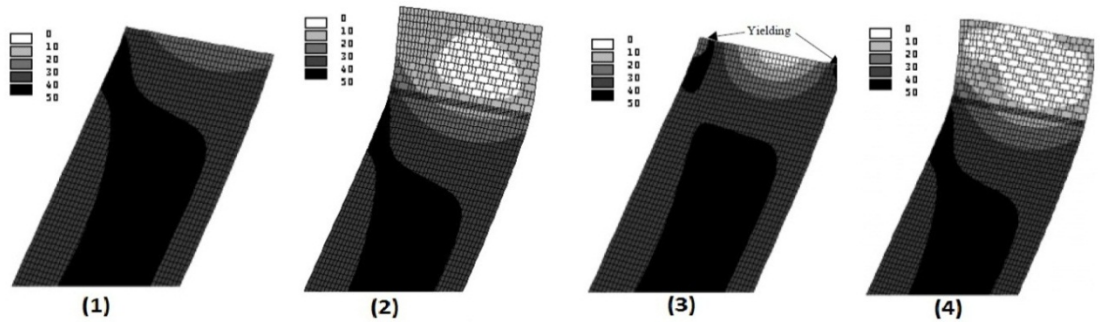

Figure 2.2: VMS in the Doubler Plate (*Mays (2000)*)

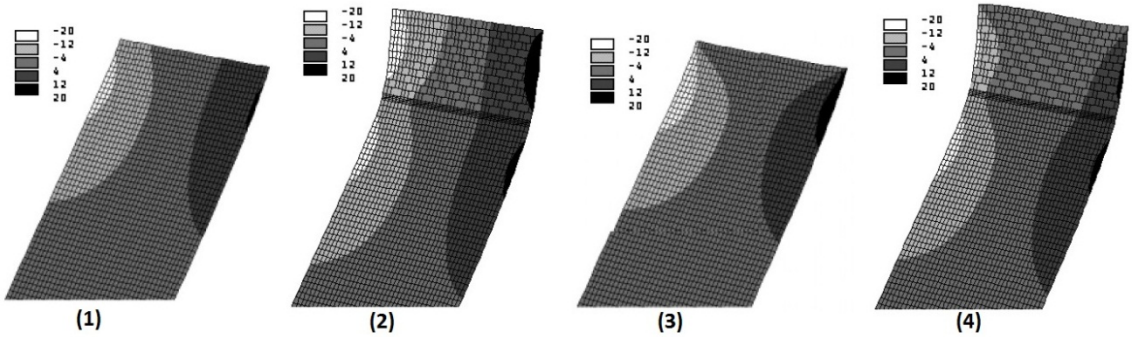

Figure 2.3: Vertical shear stress in the Doubler Plate (*Mays (2000)*)

2.2.2 Research by Shirsat (2011)

Shirsat (2011) conducted preliminary FE studies that provided several insights on issues related to doubler plate attachment details to columns. The parametric studies were made using ABAQUS 6.9. The earthquake loading is cyclic in nature but for preliminary studies the material model considered was representative of only monotonic loading. The trilinear material model used for steel was as shown in Figure 2.4. A different trilinear model was used for modeling welds (*Shirsat (2011)*). The beam flanges on either side of the column was represented by loading plates. The key variables used in these simulations were: (a) column size (W14X398 and W33X264); (b) doubler plate thickness (1/2-inch and 9/8-inch); (c) location of welds (horizontal, vertical, both horizontal and vertical); (d) distance between loading plates (24-inch and 36-inch); (e) extension of DP beyond loading plates; and (f) replacement of thick DP with two thin DP's on both sides of the column web. The FE model was as shown in Figure 2.5.The key variables investigated in this study are shown pictorially in Figure 2.6. Note that none of the cases investigated by Shirsat included CP's.

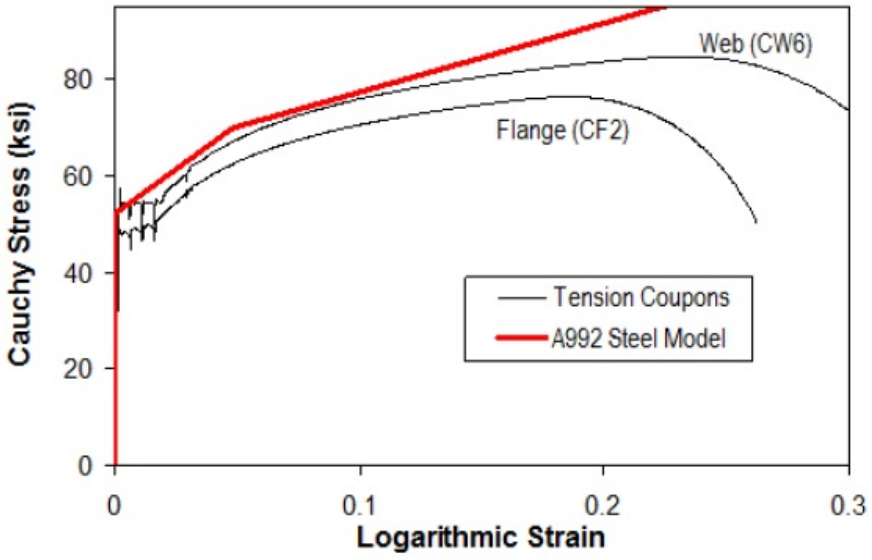

Figure 2.4: Material Model (taken from *Okazaki (2004)*)

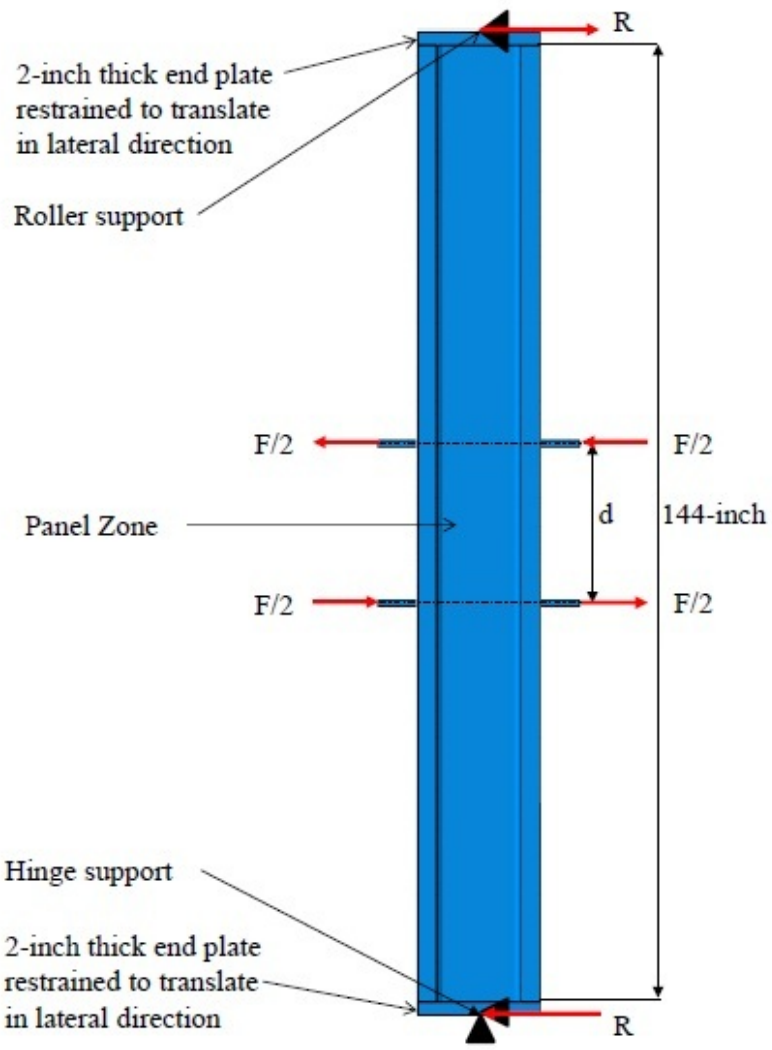

Figure 2.5: FE Model by *Shirsat (2011)*

An analysis case consisted of combination of the above described variables. A total of 21 cases were analyzed on ABAQUS 6.9. The key outputs considered in the study included panel zone shear versus panel zone rotation, shear forces in the column web and DP, VMS contour plots in the column and the DP, and VMS variation along the depth of column and DP and forces in the welds. The major conclusions of the research were as follows:

- Welding the DP only at the top and bottom was not an effective way of attaching the doubler plates. Instead providing only vertical groove welds helped increase panel zone strength and stiffness. There was little benefit in providing horizontal welds when the DP was welded vertically except in cases where there were buckling concerns of thin doubler plates.
- Extending the DP beyond the loading plates increased panel zone strength and stiffness in the deeper column (W33X264) while there was little effect in the shallow column (W14X398).
- Providing two thin plates on either side of the web instead of one thick DP on one side resulted in the same stiffness and strength of the panel zone.
- Recommendations in the 2005 AISC Seismic Provisions for designing the horizontal welds for a doubler plate appear inaccurate compared to the analysis results, but were conservative.

The research by Shirsat (2011) was followed by Donkada (2012). The FE simulations carried out by Shirsat (2011) did not included continuity plates in the model. The role of the CP in altering the load path of the concentrated force across the column web was studied extensively by Donkada (2012). A brief review of the work is provided in the next section.

2.2.3 Research by Donkada (2012)

Donkada (2012) extended the work done by Shirsat (2011) and carried out more extensive FE studies on the attachment details of doubler plates. A main objective of Donkada's research was to study load paths when continuity plates are welded directly to the doubler plate and the effects of the continuity plate in terms of increased forces or stresses in the doubler plate. As the controlling limit state for the welds is fracture, the fracture initiation propensity in the welds was also studied. The modeling techniques and material model used by Donkada were similar to those of Shirsat (2011). The loading in the Donkada (2012) models were displacement-controlled instead of load-controlled as used in Shirsat (2011). All the models in this study were loaded up to a target level

rotation of 0.05 radians. The rotation angle of the panel zone was defined as shown in Figure 2.7. Similar to Shirsat (2011), Donkada considered only monotonic loading.

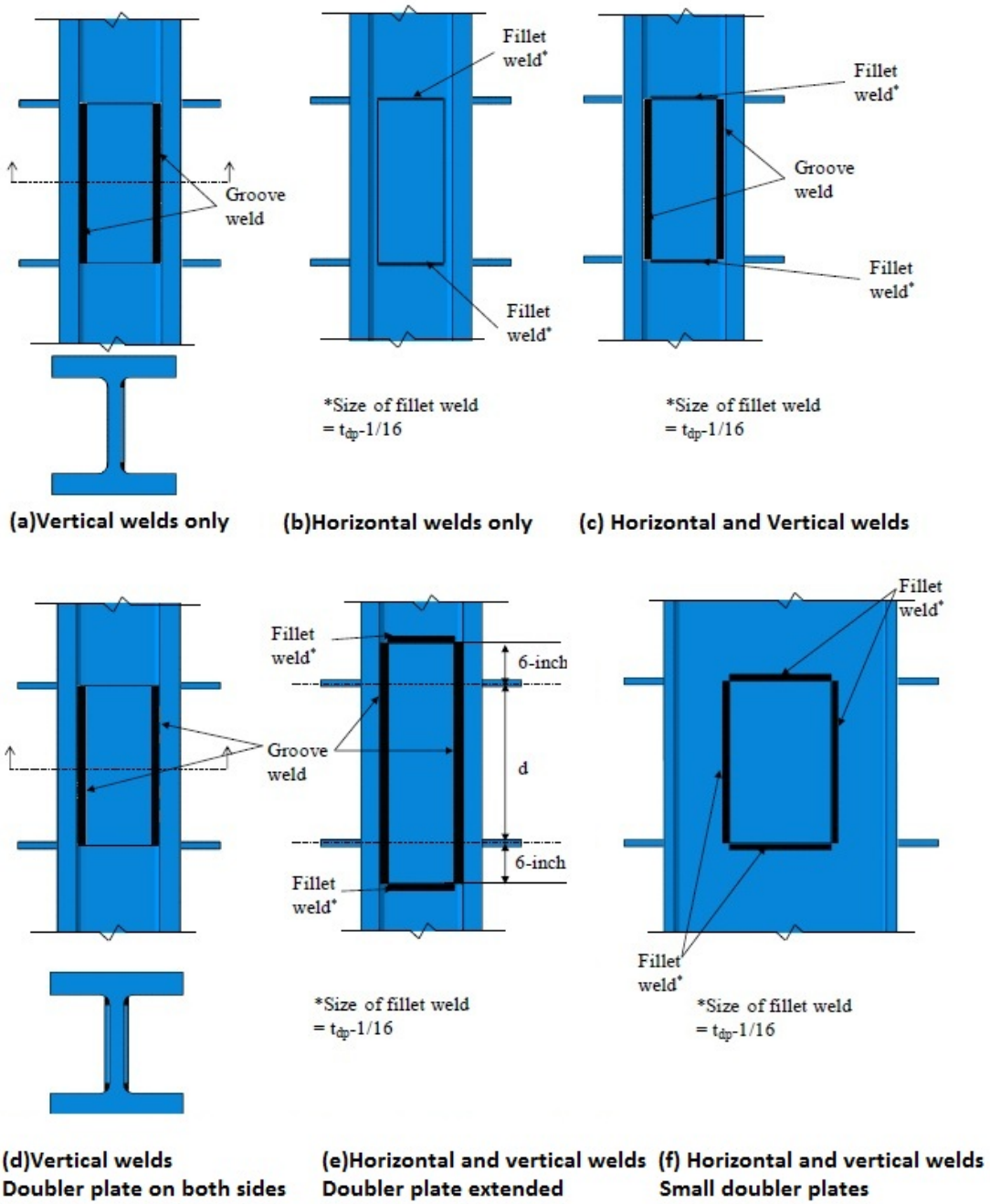

Figure 2.6: Various doubler plate configurations investigated by *Shirsat (2011)*

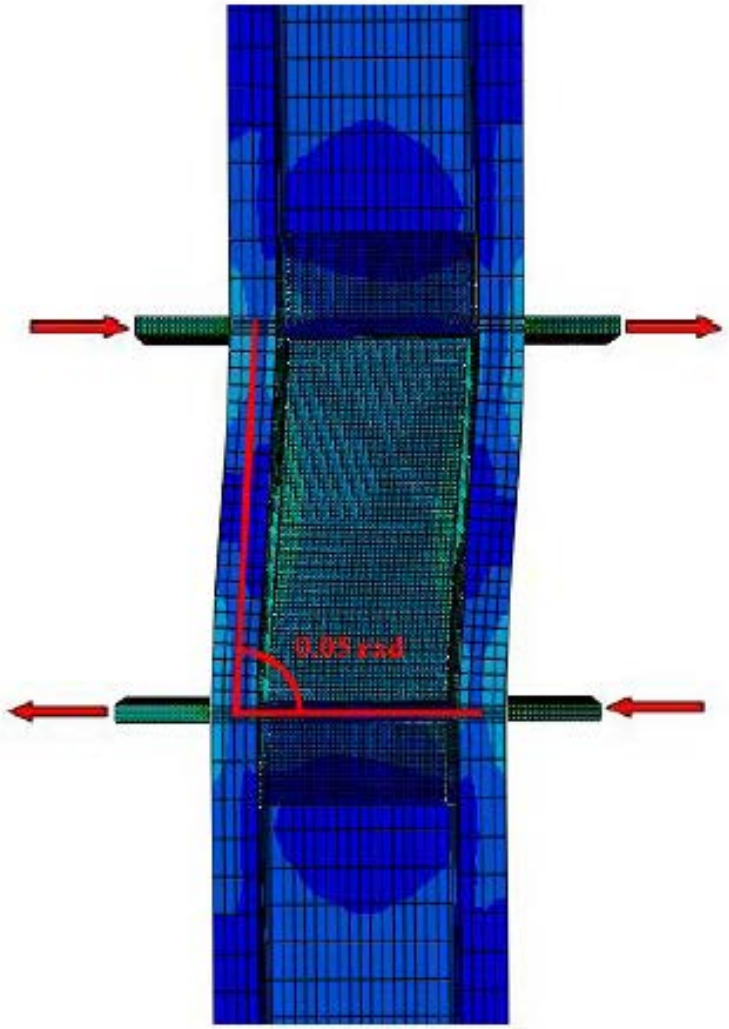

Figure 2.7: Panel zone rotation in FE model by *Donkada (2012)*

The items studied in the simulations included: (a) force on the loading plates; (b) shear forces in the CP and DP; (c) VMS contours in the column, DP, CP's and welds; (d) peak equivalent plastic strain (PEEQ); and (e) hydrostatic stress (p).The last three quantities were used to calculate the triaxiality ratio and rupture index at the weld nodes. Higher values of rupture index indicate higher fracture initiation tendency in the welds.

The first three quantities were analyzed to study the effect of changed load path on the DP and the overall panel zone strength. Free body diagrams of the DP and CP were compared to investigate load paths. These FBD were cut from the parts in ABAQUS as shown in Figure 2.8.

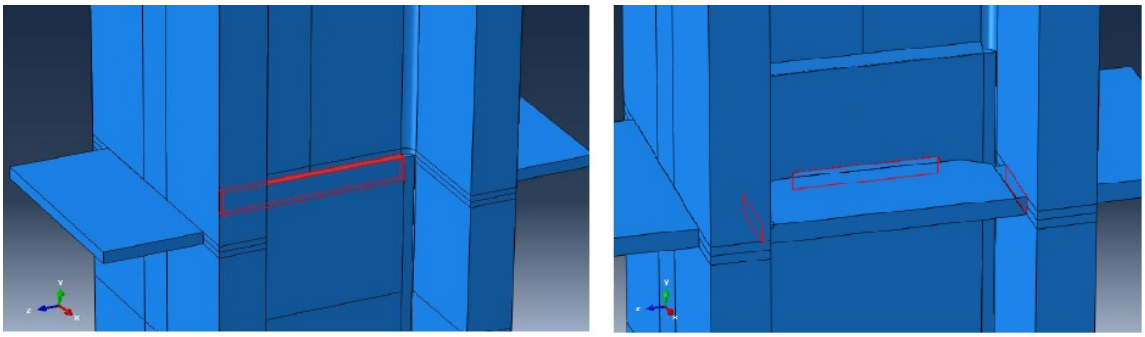

Figure 2.8: FBD of doubler plate and continuity plate in ABAQUS assembly by *Donkada (2012)*

The simulations were carried out on two columns: a W14X398 (shallow column) and a W40X264 (deep column). All the models, except those used for the fracture initiation study, had only vertical CJP groove welds connecting the DP to the column. The different cases in the simulations were as follows:

1. No DP.
2. DP without any extension.
3. DP with extension of 6-inches on both sides beyond loading plates.
4. No DP but with CP's between column flange.
5. DP with extension of 6-inches on both sides beyond loading plates and CP between column flanges, with CP's welded to DP.

It was found that in all the above five cases, the amount of load passing through the CP's decreased as column flange thickness increased. In order to study the effect of the CP's on the load path, a new set of cases were made by progressively decreasing the column flange thickness in steps. The flange thickness (inches) of the W14X398 column

was decreased in 3 steps (2.85->2.00->1.00->0.5) while the flange thickness (inches) of the W40X264 was decreased in 1 step (1.75->0.75).The major conclusions of the research were as outlined below:

- Welding the DP only along the vertical edges with CJP groove welds was adequate to develop the full required strength and stiffness of the panel zone. The provision of horizontal welds were helpful in reducing the localized stress in the top region of the vertical CJP welds and in restraining the buckling of the doubler plate but the fracture initiation study suggested that vertical welds were not likely to fracture under the applied monotonic load.
- Extending the DP in the deep column (W40X264) led to a 10% gain in the panel zone shear strength while it had little effect on the strength of the shallow column (W14X398).
- The continuity plates did not add to the strength of the panel zone in both the columns when the web shear was the governing limit state but had a major role in increasing the strength when the limit states were localized flange bending, web crippling, web compression buckling and localized web yielding.
- Welding the CP's to the doubler plate in both the shallow and deeper column did not increase the stresses significantly in the doubler plate. On the other hand, the CP provided an alternate load path from the column flanges to the CP's and then to the column web. This in effect reduced the stresses on the vertical CJP welds.
- The deep column with thin flanges had a much higher percentage of force flow through the CP's as compared to the shallow column with thin flanges. Thus continuity plates were found to be critical elements in the deeper column system.

The studies carried out by Shirsat (2011) and Donkada (2012) provided significant insights on the behavior of the panel zone and the load path though different

parts of the assembly. However, both Shirsat (2011) and Donkada (2012) considered only monotonic loading of the panel zone. For earthquake response, cyclic loading behavior is of interest, and will be considered in this current study. Developing an FE model of the panel zone region under cyclic loading requires a cyclic stress-strain model. The next section briefly reviews a few studies done in the past on the cyclic stress-strain behavior of structural steel.

2.3 CYCLIC STRESS-STRAIN RESPONSE OF STRUCTURAL STEEL

2.3.1 Research by Cofie and Krawinkler (1985)

This research proposed a model for uniaxial cyclic stress-strain behavior of structural steel subjected to arbitrary loading cycles in the inelastic range. Various other models like elastic-perfectly plastic, bilinear models and three parameter model of *Ramberg and Osgood (1943)* performed well for the gross analysis of structural components but a thorough assessment of local buckling and crack propagation could be achieved by using the model developed in this study.

The behavior of steel under cyclic loading depends on the monotonic stress-strain curve and cyclic stress-strain curve (backbone curve).The two curves were as shown in Figure 2.9.The cyclic stress-strain (backbone curve) is the locus of saturated peak stresses obtained by cycling the material at various strain amplitudes. At any given cycle at a given strain amplitude, the material tries to work its way to achieve the saturated peak stress corresponding to the strain amplitude in the backbone curve. These movements of cyclic curves were achieved through three properties of steel: cyclic hardening, cyclic softening and the mean stress relaxation. Cyclic hardening is the increase in stress amplitude while cyclic softening is the decrease in stress amplitude with the increasing number of cycles at constant strain amplitude. The mean stress, if present in the cycles dies out to zero with increasing number of reversals. This process is called mean stress relaxation. The cyclic hardening and cyclic softening are as shown in Figure 2.10(a) and Figure 2.10(b) respectively. The hardening or softening takes place in Figure 2.10 until the stress amplitude coincides with stress on the dashed backbone curve.

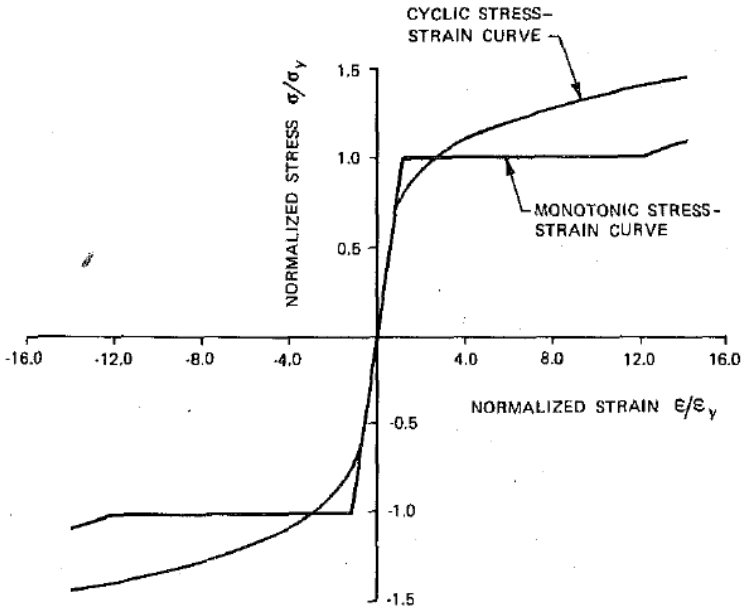

Figure 2.9: Monotonic and Cyclic stress-strain curve (*Cofie and Krawinkler (1985)*)

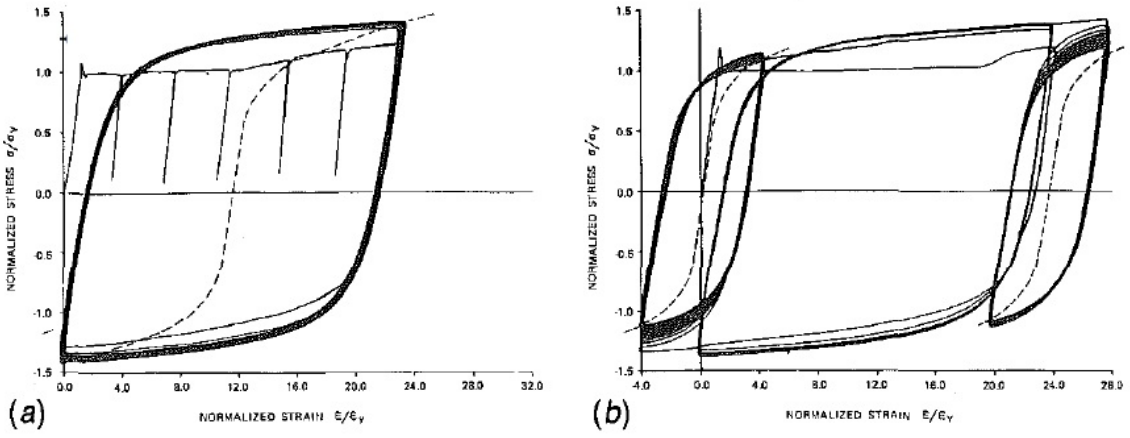

Figure 2.10: (a) Cyclic hardening (b) Cyclic softening and mean stress relaxation (*Cofie and Krawinkler (1985)*)

The model developed by Cofie and Krawinkler (1985) was compared with experimental results. It was found that the predictions were not very accurate at small strain amplitude cycles but were quite accurate at large strain amplitude cycles.

2.3.2 Research by Yongjiu et al. (2011)

Yongjiu et al. (2011) developed cyclic constitutive material models for two types of steel: Q235B and Q345B. A total of fifty experiments were carried out and a mathematical material model for the two types of steel was developed using the test data. A finite element model of a structural system using beam elements was developed and the material stress-strain model developed was input as a user defined material model (UMAT) in ABAQUS. The experimental results matched satisfactorily with the ABAQUS results.

The specimen tested under monotonic and cyclic loading was a plate tension coupon with an extensometer on the sides to measure the vertical and lateral displacements. By comparing the monotonic test results with that of cyclic test results, it was found that fracture occurs at a much lesser strain percentage in cyclic loading but the fracture stress remained same as in monotonic loading. There was a marked decrease in ductility when the specimen was subjected to cyclic loading. The outputs of these experiments were the monotonic stress-strain curve and the cyclic stress-strain curve (back bone curve) for Q235b and Q345B steel. A mathematical model was developed for these two types of stress-strain curve along with hysteresis criteria which included: the first time loading curve of steel, the unloading curve of steel, the reloading direction of steel and the reloading curve of the steel. These three parts of a cyclic constitutive model were as shown in Figure 2.11.

The mathematical model developed above was used as an input to UMAT (User defined material) in the finite element software ABAQUS. A validation of the FEM studies with the experimental studies were made by running simulations on a ‘line’ FEM model of a typical beam-column frame structure. The experimental results matched satisfactorily with the ABAQUS outputs. The section 2.3.1 and 2.3.2 discussed the cyclic studies mainly at the material level only; the following section 2.3.3 enumerates a study on the structural system (shear links) response to cyclic loading.

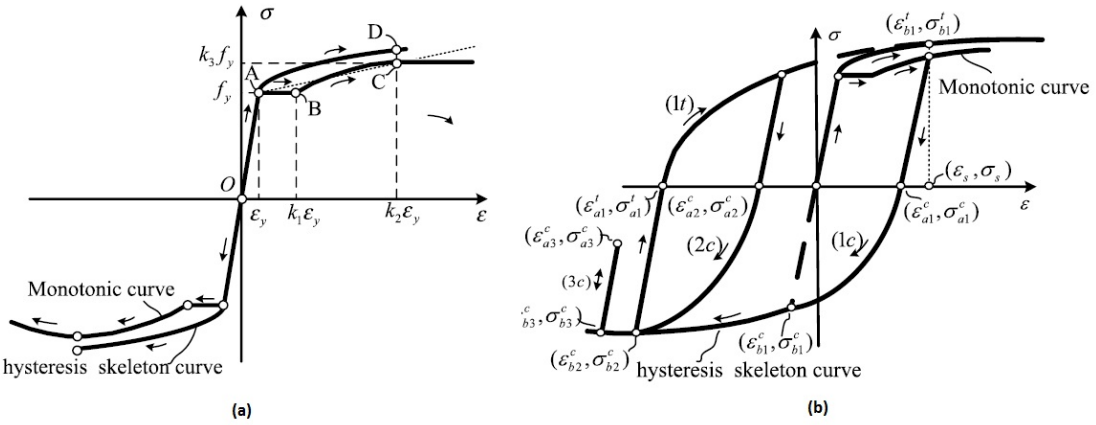

Figure 2.11: (a) Monotonic and Cyclic Stress-Strain Curve (b) Hysteresis Criteria developed by *Yongjiu et al. (2011)*

2.3.3 Research by Richards (2004).

Richard (2004) studied the cyclic loading behavior of links in steel eccentrically braced frames. In this research, FE models were developed for short, intermediate and long links and compared with cyclic loading experiments on links. ABAQUS (2001) was used to develop the FE models, and incorporated a cyclic stress-strain model for steel that incorporated a nonlinear kinematic hardening rule. The links were modeled using S4R shell elements. The models predicted the experimentally observed global load-deflection behavior of the links quite accurately. The link model and the boundary conditions were as shown in Figure 2.12.The correlation of FEM results with the experimental results was as shown in Figure 2.13.The buckling initiation (rotation and amplitude) captured in the model correlated well with that of experimental observations. This study showed that a reasonable material model representative of cyclic loading permitted good correlation with the experimental findings.

2.4 SUMMARY

From the above reviews, it can be concluded that interesting conclusions and recommendations were made by Shirsat (2011) and Donkada (2012) regarding the most effective way of attaching a doubler plate to the column web in the panel zone of the steel

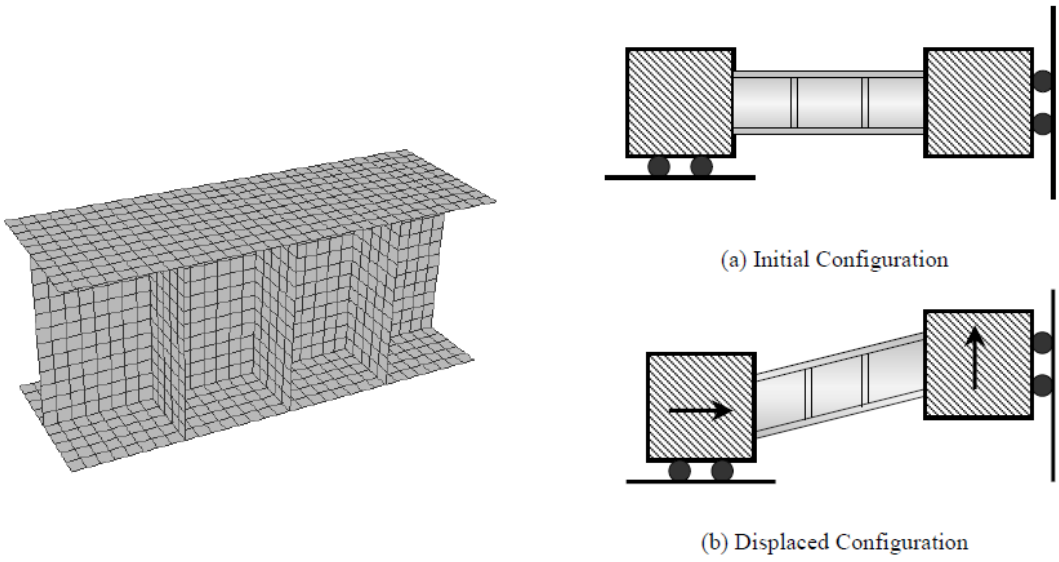

Figure 2.12: Shear Link FE model and the boundary conditions by *Richards (2004)*

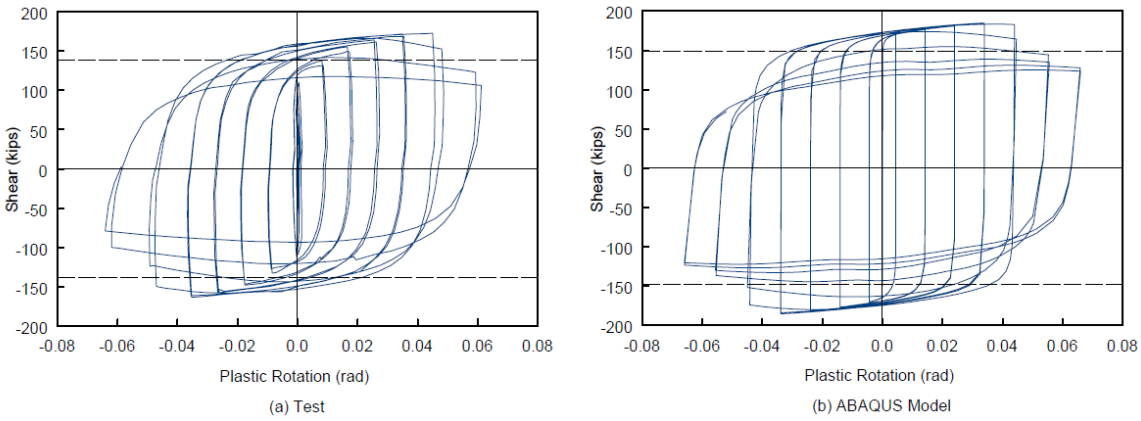

Figure 2.13: Correlation of FEM results with experimental results for a link test specimen *(Richards (2004)*)

moment frame connections. These recommendations were made with caution in both the works as the material models in these FE studies were representative of monotonic loading only.

The literature review sections also highlighted some of the key parameters of the hysteresis curve which were cyclic hardening, cyclic softening and mean stress relaxation. The monotonic stress-strain curve, the cyclic stress-strain curve (backbone curve) and the hysteresis criteria will be sufficient to predict the behavior of the structures subjected to cyclic loading. It can be concluded from the results of studies enumerated in section 2.3 that a reasonable cyclic material model can be developed in ABAQUS where the model FE results can correlate well with the experimental results.

The following questions, previously considered by Shirsat (2011) and Donkada (2012) using monotonic material models are evaluated in this study by developing FE models capable of predicting the global and local behavior under cyclic loading in the panel zone:

- Should the doubler plates be welded from all four sides or at vertical locations only?
- Is there any benefit of extending the doubler plate 6 inch on both sides of the loading plate?
- Does the welding of continuity plates directly to the doubler plate increases the overall forces or stress in the doubler plate?
- What are the stresses developed in the vertical and horizontal welds?

Some additional issues that are addressed in this research are listed below:

- Does the welding of continuity plates to a very thin doubler plate increase the overall forces or stresses in the doubler plate? Can similar conclusions be made for thick doubler plates?
- Do columns with thin flanges combined with thin doubler plates change the load path of the concentrated forces through the column web?
- Are there any localized stresses at the loading plate level when the continuity plates are welded directly to thin doubler plates?
- How does the stress pattern changes when continuity plates are introduced in the panel zone assembly?

These issues are addressed by generating a FE model assembly in ABAQUS 6.12 and analyzing the models under a specific cyclic loading protocol. The analysis results are discussed in chapter 4 onwards. The modeling techniques to generate this FE models are discussed in next chapter.

CHAPTER 3

Modeling Techniques

The major objectives of this research are to simulate panel zone behavior under cyclic loading and to evaluate various methods of attaching the doubler plate to the column web. All simulations were conducted on the general purpose finite element program ABAQUS. This chapter focuses on the techniques used in ABAQUS 6.12 to create a finite element model assembly of typical panel zone in steel moment frames. An overview of the modeling steps is provided in section 3.1 while detailed explanation of each step in modeling is described from section 3.2 to section 3.9. Section 3.10 summarizes the overall modeling process.

3.1 OVERVIEW

ABAQUS/CAE was used to create models, submit and monitor ABAQUS jobs and evaluating results while ABAQUS, VIEWER (a subset of ABAQUS/CAE) was used for post-processing the results. ABAQUS/Standard was used for analysis of the models created in ABAQUS/CAE. ABAQUS/CAE is divided into functional units called modules in ABAQUS. Specific task of the modeling are performed in each module of ABAQUS. The subsequent sections in this chapter correspond to each of these modules and explain the modeling process in each module. These modules are Part, Property, Assembly, Step, Interaction, Load, Mesh, Optimization, Job, Visualization and Sketch. A material model representative of cyclic loading was developed as described in section 3.3 and simulations results of some abaqus models were compared with experimental studies to validate the material model. The material model is capable of capturing the behavior of steel loaded well into the inelastic range. To keep the simulation model size and analysis time manageable, an approximate model of the actual steel beam-column frame was created. The columns were modeled only between the inflection points and the beams were replaced by loading plates which represented the flanges of the beams. The two types of columns modeled in this study were W14X398 (shallow column) and W40X264

(deep column). The modeling techniques used in this research are very similar to those of Shirsat (2011). As noted in Chapter 1, this study is an extension of the work done by Shirsat (2011) and Donkada (2012). A more detailed explanation of these modeling techniques and their validation with experimental results can be found in Shirsat (2011).

3.2 ABAQUS MODEL PARTS

The sketcher in the Part module is used to create the two dimensional profile sketch of the part which can be extruded to a certain thickness to form a deformable 3D solid part. The entire model assembly consists of one or more of following parts:

1. Column
2. Loading Plate
3. Doubler Plate (DP)
4. Vertical groove welds between DP and column flanges (CJP1)
5. Horizontal Fillet welds between DP and column web
6. Continuity Plate (CP)
7. Groove weld between CP and column flanges(CJP2)
8. Groove weld between CP and column web(CJP3)

The column height is 144 inches and distance between the loading plates is 24 inches for both the columns. The dimensions of the columns are labeled as shown in Figure 3.1 and values of these dimensions for the two columns (W14X398, W40X264) are as given in *AISC Steel Construction Manual* (AISC, 2010c). Figure 3.2 shows the dimensions of the loading plate, doubler plate and continuity plates while Figure 3.3 shows the dimensions of the different welds. The loading plate and continuity plate thickness is 1 inch in all the models. The structural steel and the welds were provided with a material model which is discussed in the next section.

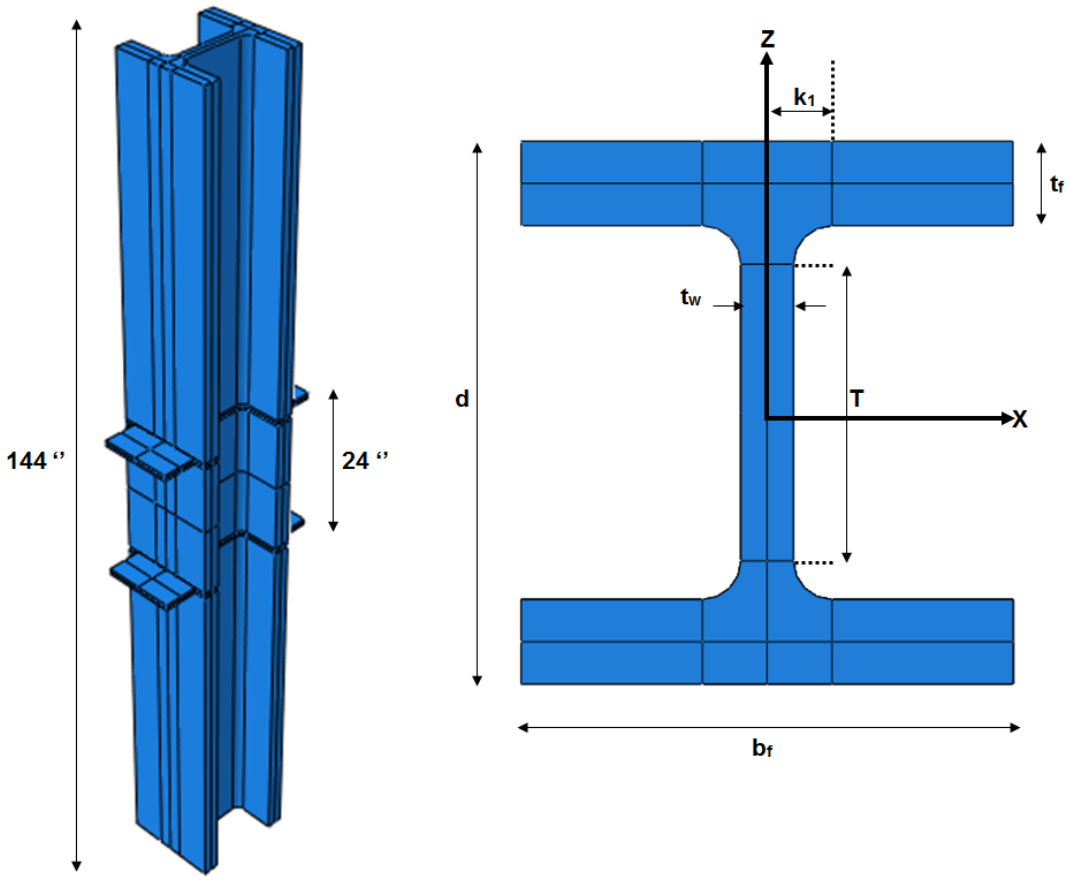

Figure 3.1: Column dimensions

3.3 Cyclic Material Model

The work on doubler plate attachment details conducted by Shirsat (2011) and Donkada (2012) considered monotonic loading. A primary goal of this current research is to determine if the conclusions of these previous studies are still valid when cyclic loading is considered. Consequently, the development of a material model representative of cyclic loading is needed. This section describes the steps taken in order to develop the cyclic material model.

3.3.1 Overview

Shirsat (2011) and Donkada (2012) used an inelastic monotonic material model for steel from *Okazaki (2004)* as shown already in Figure 2.4. A more detailed

explanation of this material model for steel and welds can be found in Shirsat (2011). The monotonic material model represented A992 steel for both wide flange members and for continuity and doubler plates. Continuity and doubler plates are typically made of A572 Gr. 50 steel. However, the properties of A992 steel and A572 Gr. 50 steel are very similar, and so the same material model was used for both.

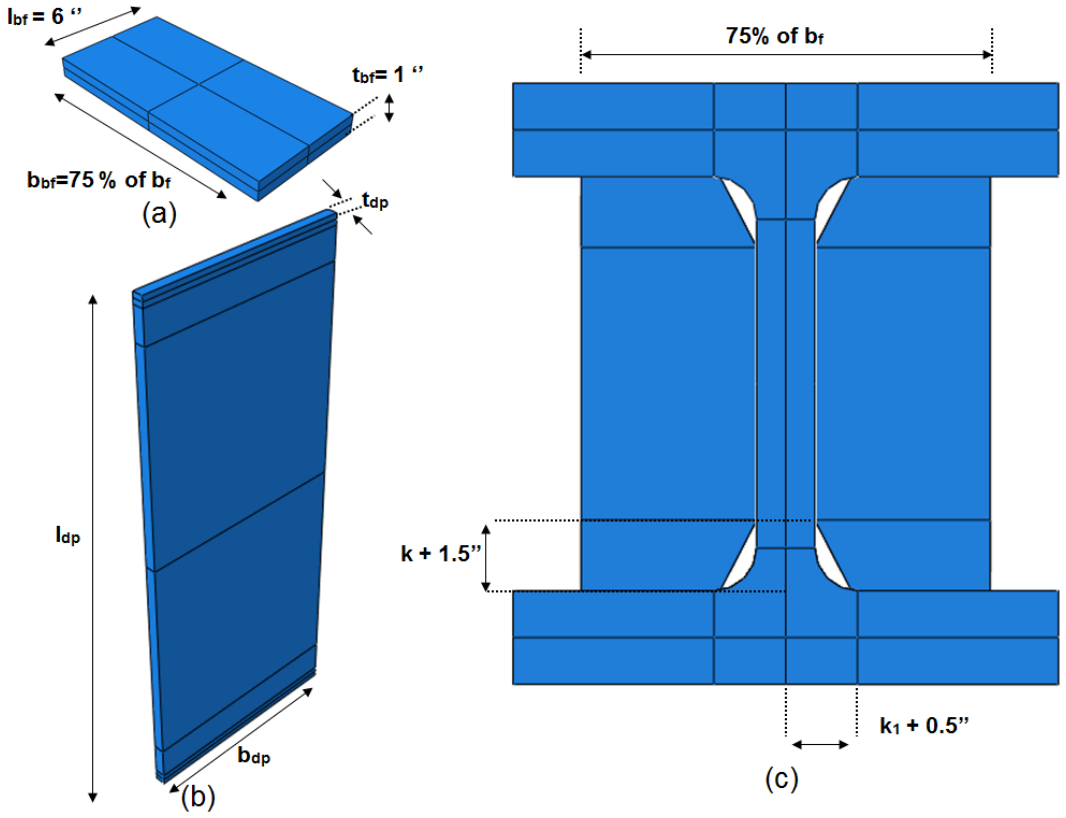

Figure 3.2: (a) Loading Plate dimensions (b) Doubler plate dimensions (c) Continuity plate dimensions

In this study also a single material model was used for all structural steel and a different material model was developed for the welds. The loading plates were modeled elastically with a young modulus of 60 ksi and a Poisson’s ratio of 0.3. This was done because the intent of this study was not to investigate inelastic behavior in the beam, but rather in the column panel zone.

In order to develop cyclic material models for this research, different cyclic material models available in ABAQUS were examined. Once a suitable material model was chosen, it was validated using cyclic loading experiments on shear links and on beam-column assemblies reported in the literature by *Ryu (2005)* and by *Engelhardt et al. (2000)*. The most suitable definition of this cyclic material model was input in ABAQUS. This material model was used in the model of shear links and dog bone specimens which were used in the validation studies. A validation of material model was done by comparing the finite element simulation results of shear link and dog bone specimen with that of experiments done by *Ryu (2005)* and *Engelhardt et al. (2000)* respectively. This validation is described in section 3.3.3 and 3.3.4 of this chapter. The cyclic material model developed did not show a distinct yield stress point in contrast to the trilinear material monotonic models used in previous studies. This finding is also evident from the Figure 2.9 of the research by *Cofie and Krawinkler (1985)*. The determination of yield stress and a backbone curve for these types of cyclic material models was done by simulating a tension coupon test in ABAQUS which is described in section 3.3.5. At last some limitations of this cyclic material model are discussed in section 3.3.6.

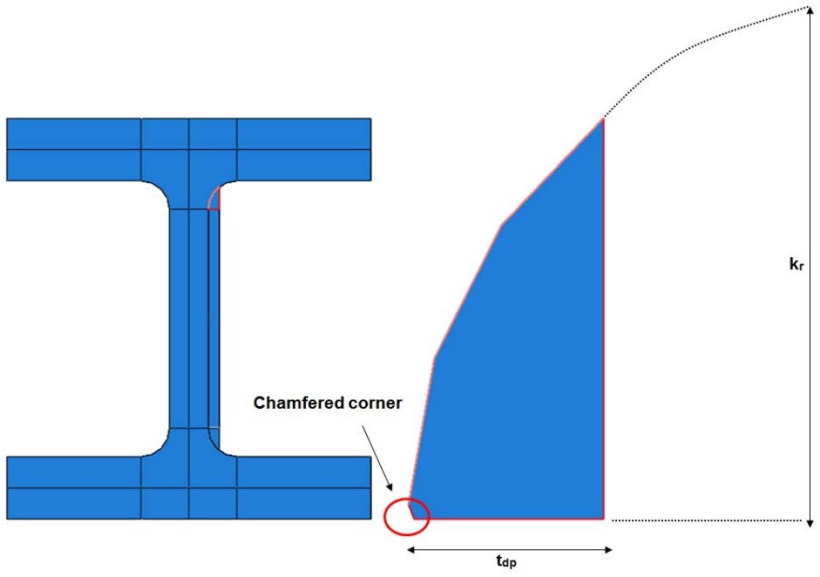

Figure 3.3a: CJP1 in the model assembly

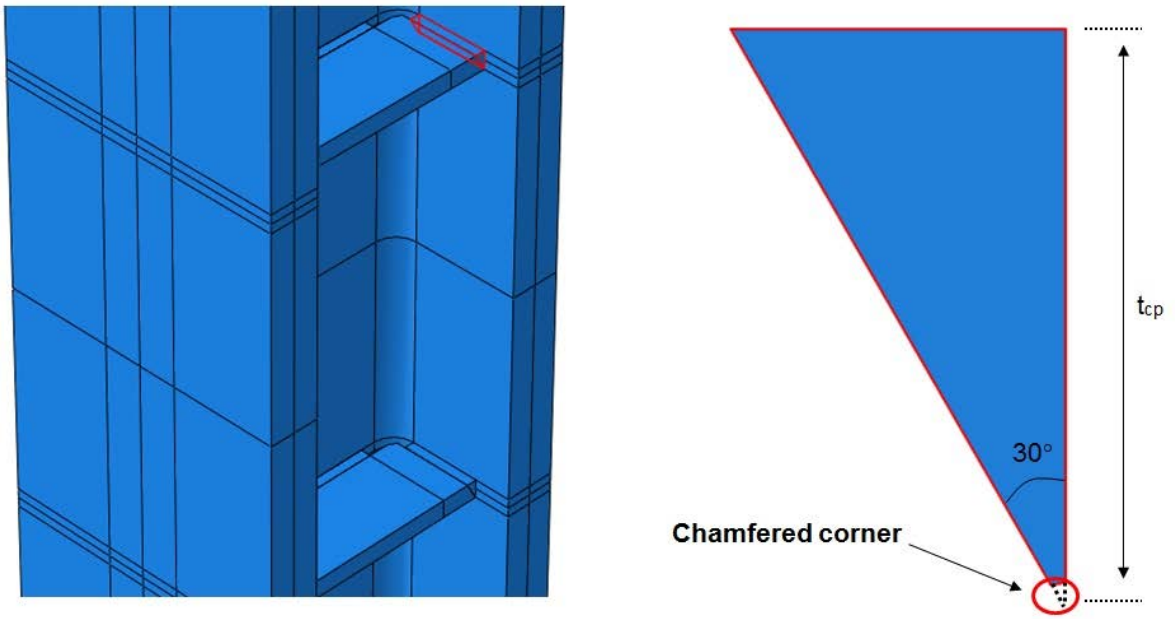

Figure 3.3b: CJP2 in the model assembly

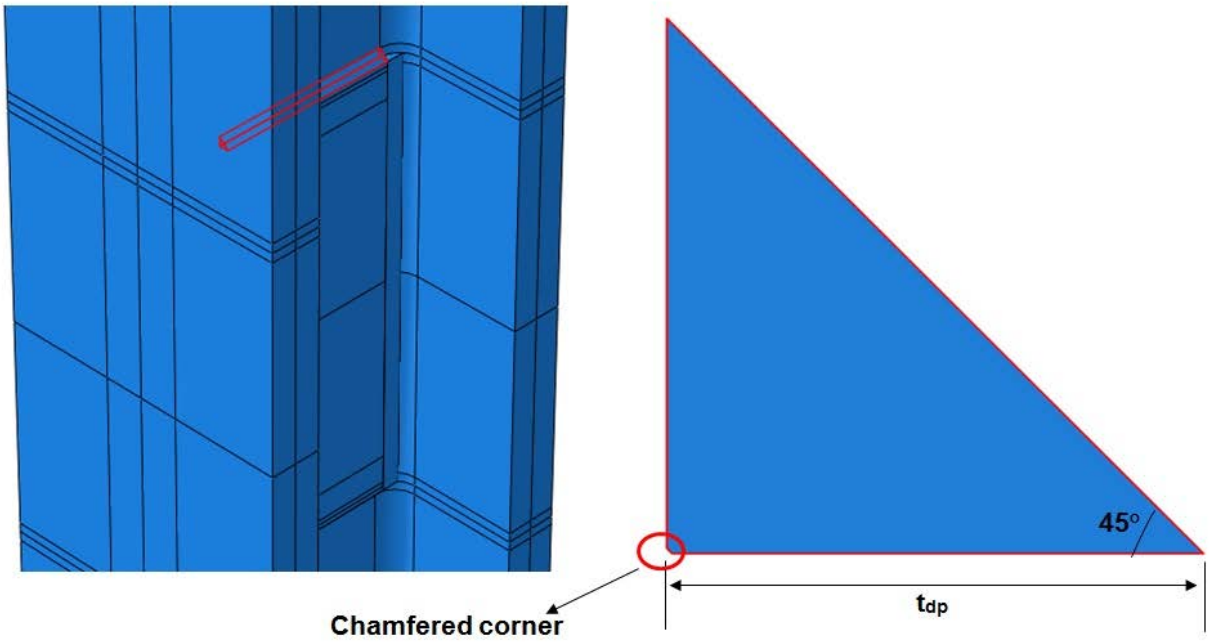

Figure 3.3c: Fillet weld in the model assembly

3.3.2 Development of the model

Steel subjected to constant strain amplitude cycles may exhibit isotropic or kinematic hardening with increasing number of cycles until a steady state condition is reached. Thus the cyclic hardening of structural steel can be modeled accurately by providing the appropriate kinematic and isotropic hardening parameters in ABAQUS. A list of different ways of providing these parameters for modeling of metals subjected to cyclic loading are discussed in *ABAQUS 6.12 Analysis User's Manual, Section 23.2.2*. A combination of one or more of these methods were tried in ABAQUS to match the finite element results of experiments on a shear link and on a beam-column assembly as described in section 3.3.3 and 3.3.4 respectively. A non-linear kinematic plastic hardening law defined by data over a stabilized cycle was found to be best method and provided a reasonable match of experimental and finite element simulation results. This data over a single stabilized cycle was based on a single half-loop (maximum compression to maximum tension).Such a cycle with data in pairs (σ_i , ε_i^{pl}) is shown in Figure 3.4. Each data pair (σ_i , ε_i^{pl}) must be specified with the strain axis shifted to $\varepsilon_p^{\ 0}$, so that

$\varepsilon_i^{pl} = \varepsilon_i - \frac{\sigma_i}{E} - \varepsilon_P^0$ and $\varepsilon_1^{pl} = 0$.

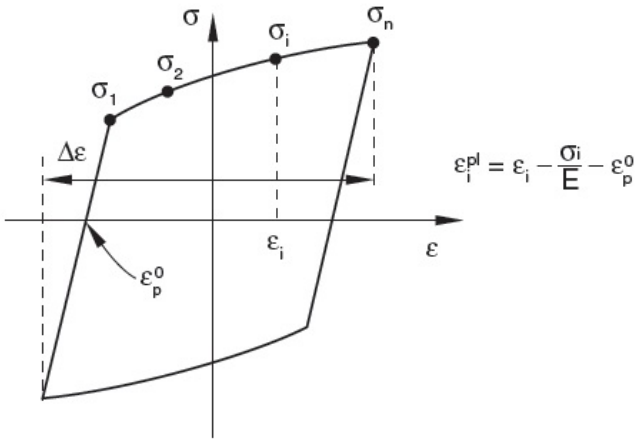

Figure 3.4: Nonlinear kinematic hardening law by defining data over a stabilized half-cycle (*ABAQUS 6.12 Analysis User's Manual, Section 23.2.2*)

The calibrated kinematic stabilized cycle and its conversion to a shifted strain axis for steel and welds are shown in Figure 3.5a. The input lines in ABAQUS keywords for this non-linear kinematic hardening model are as shown in Figure 3.5b. The material named 'Elastic_steel', 'Plastic_weld' and 'Plastic_steel' in Figure 3.5b are material model for loading plates, welds and structural steel respectively. Here the line below the keyword 'Elastic' specifies a young modulus of 29000 ksi and Poisson ratio of 0.3 for welds and structural steel. Notice that the young modulus of the loading plate is 60000 ksi. The lines below the keyword 'Plastic' specify the true stress and true shifted plastic strain of the largest stabilized cycle (Figure 3.5a) for the kinematic hardening model. The definition of engineering stress and engineering strain and their conversion to true stress and true plastic strain can be found in Shirsat (2011). The engineering stress-strain data points were taken from *Kauffmann et al. (2001)*. The largest stabilized cycle of Steel C in the *Kauffmann et al. (2001)* was calibrated such that the shear link experimental results described in section 3.3.3 correlate well with that of finite element results. Note that several iteration cycles of material modeling and simulations was done in ABAQUS to arrive at a reasonable cyclic material model for structural steel. However, no cyclic material test data was available for weld metal, so the cyclic material model for weld metal was developed using considerable judgment. The hardening ratio of the cyclic material model to the monotonic material model for steel was kept same as the hardening ratio of the cyclic material model to the monotonic material model for welds while developing the weld cyclic material model. The next sections 3.3.3 and 3.3.4 shows the validation of this cyclic material model with the finite element studies performed on the shear links and on a beam-column assembly experiments respectively.

3.3.3 Comparison of ABAQUS model with Shear Link experiments

The techniques used to model the panel zone in ABAQUS were intended to study the behavior of panel zones subject to large shear forces. It was therefore of interest to validate the cyclic material model by comparing the finite element results to some experimental studies on steel members subjected to large shear forces. So, an ABAQUS

model of shear links which are used in eccentrically braced frames was developed. This model was similar to the shear links used in the experiments done by *Ryu (2005)*. The cyclic material model was validated and developed simultaneously by iterating the initially approximate material model (Steel C – largest stabilized cycle) from *Kauffmann et al. (2001)* such that the finite element results for shear links matched well with the experimental results on shear links performed by *Ryu (2005).*

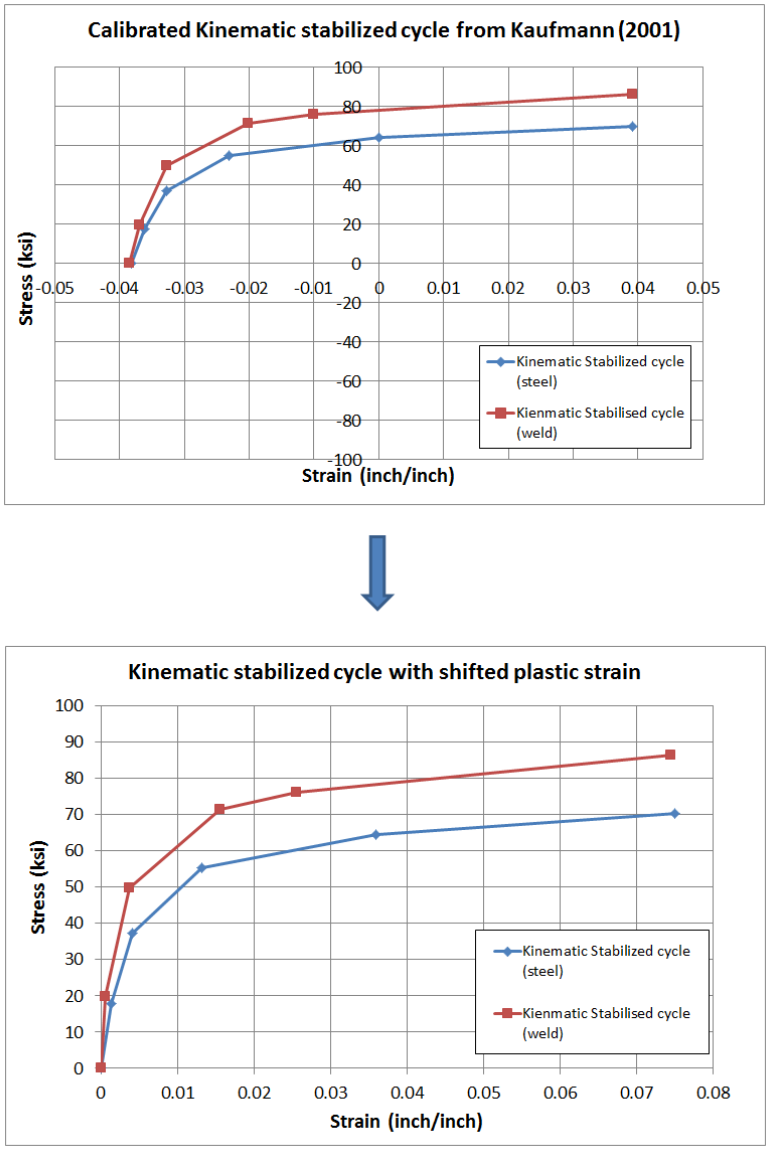

Figure 3.5a: Material model input in ABAQUS

```
**
** MATERIALS
**
*Material, name=Elastic_steel
*Elastic
60000., 0.3

*Material, name=Plastic_WELD
*Elastic
29000., 0.3
*Plastic, hardening=COMBINED, datatype=STABILIZED, number
backstresses=6
   0.001,          0.
 19.7558, 0.000463528
 49.8417,   0.0036715
   71.54,   0.0154504
   76.23,    0.025441
   86.32,   0.0743642

*Material, name=Plastic_steel
*Elastic
29000., 0.3
*Plastic, hardening=COMBINED, datatype=STABILIZED, number
backstresses=6
   0.001,          0.
 17.8433, 0.00135927
 37.2603, 0.00410534
 55.2118,  0.0131522
    64.5,  0.0358959
    70.2,    0.07492
```

Figure 3.5b: Keyword edit for defining the material model in ABAQUS.

The overall test setup and rigid body kinematics in Ryu's experiments is shown in Figure 3.6 and Figure 3.7 respectively. The set up consisted of a W18X76 beam, a shear link and a W12X120 column. The column was moved vertically in a manner which produced high shear forces and high inelastic deformations in the link similar to an actual shear link in EBF's. High shear forces in the links are also evident from the qualitative shear diagram in Figure 3.7.

The specimen validated in this study was a W18X40 shear link. The shear link in the experimental study was subjected to different loading protocols and shear in the link versus rotation of the link was plotted. The same specimen under a loading protocol was named differently. The specimens which were validated in this study were '12MON',

'12RAN', '12AISC', '12RLP' and '12SEV'. The protocol '12MON' was a monotonic loading while others loading were cyclic in nature with different cyclic loading histories. A more detailed explanation of the different shear links and the loading protocols can be found in *Ryu (2005)*. The finite element model of the shear link setup is described in section 3.3.3.1 and comparison of experimental results with ABAQUS predictions is provided in section 3.3.3.2.

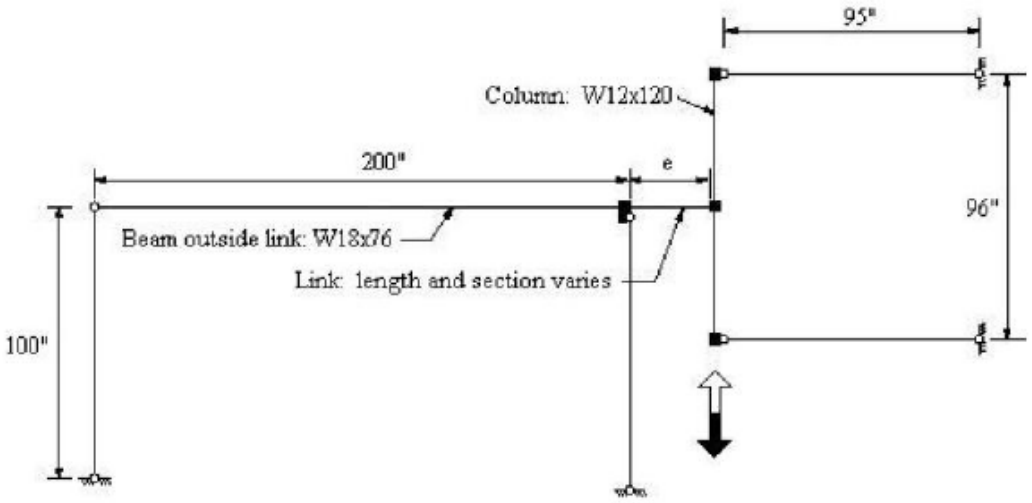

Figure 3.6a: Test set for experiments done by *Ryu (2005)*

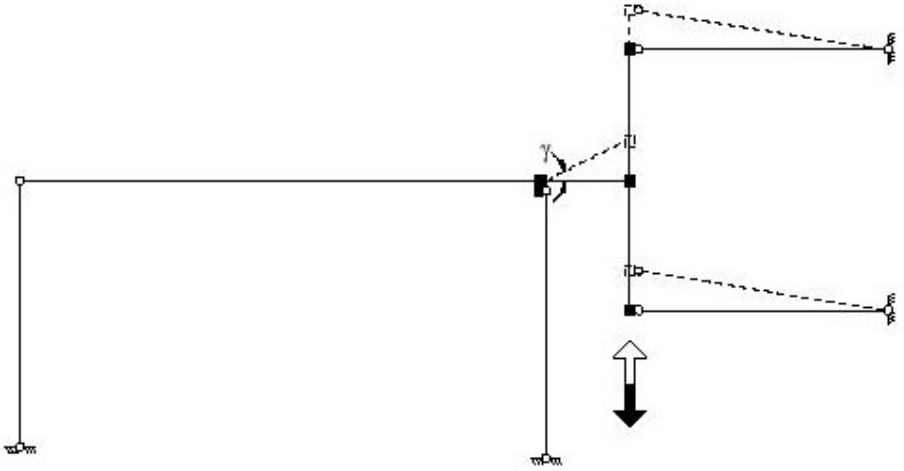

Figure 3.6b: Rigid-plastic kinematics of test setup (*Ryu (2005)*)

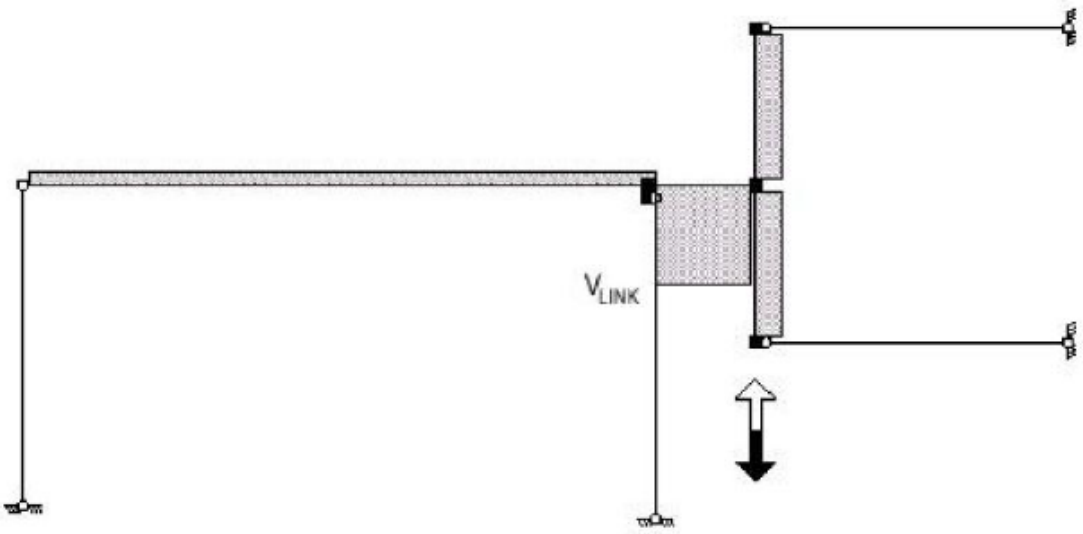

Figure 3.7: Qualitative shear diagram for experiment set up (*Ryu (2005)*)

3.3.3.1 Finite element model of the shear link experimental setup

The shear link finite element model assembly consisted of following parts: shear link (W18X40 section), beam outside shear link (W18X76 section), column outside shear link (W12X120 section), three stiffeners on one side of shear link (3/8 inch thick) and end plates at both end of shear link (2 inches thick). The shear link was 23 inches long with end plates on both sides to connect to the beam on the left end and to the column on the right end. The beam was 200 inches long while the column was 96 inches in height. The web of link was stiffened with three stiffeners which were placed at 5-3/4 inches apart (center to center). The welds were not modeled explicitly in the model and tie constraints were used between stiffeners and the link web, stiffeners and the link flanges, link and end plates and between end plates and the beam/column. The link and stiffeners had the same cyclic material model (‘Plastic_Steel’) as given in Figure 3.5b while the beam, column and the end plates were modeled elastically with an elastic modulus of 29000 ksi. Geometric nonlinearity was considered by activating the ‘nlgeom’ option in the analysis step of ABAQUS. The ‘Structured’ mesh in ABAQUS with ‘C3D8R’ elements was used for link, stiffener, end plates, column and beam. An approximate

global seed size of 0.4 inch was used for the link and the stiffeners and 1 inch for the end plates. The beam and columns were meshed with a much coarser global seed size of 5 inches and 2.4 inches respectively as the focus here is on the behavior of shear links rather than beams and columns. The finite element mesh of the shear link portion of the model is shown in Figure 3.9.

The beam and columns were modeled explicitly to simulate the actual boundary condition of the shear link in the experiment. The boundary conditions for the full model are shown in Figure 3.8. The shear link is subjected to different loading protocols as discussed in section 3.3.3.1. These protocols were applied as displacement U2 (Amp1) at the column ends. The variation of Amp1 is equal to 23 times (length) the rotation angle (γ). The cyclic loading protocols were defined as shown in Figure 3.10. The monotonic loading protocol '12MON' was a static displacement of approximately 8.5 inches in the 'Y' direction. A more detailed description of loading protocols can be found in *Ryu (2005)*. In the test done by Ryu, the test specimens '12SEV' and '12 RAN' showed a severe strength degradation due to buckling and crack propagation at γ=0.08 radian (second cycle) and γ = -0.1304 radian respectively. Therefore the loading Amp1 in these two ABAQUS models has also been limited to the severe strength degradation cycles corresponding to Ryu's experiment.

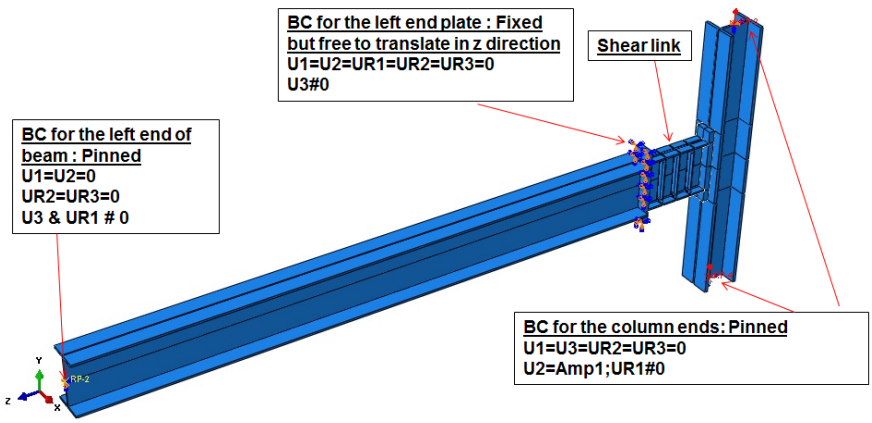

Figure 3.8: Boundary conditions for the shear link models

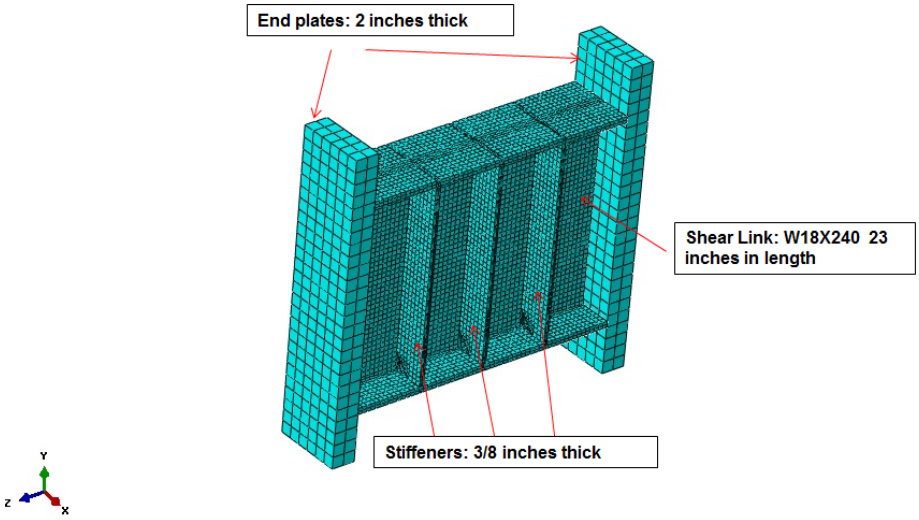

Figure 3.9: Finite element assembly for shear link only

3.3.3.2 Comparison of ABAQUS results with experimental results

The finite element models described above were analyzed in ABAQUS. Results are shown as plots of shear in the link versus the total link rotation (γ) and were compared with actual results from Ryu's experiments. The link shear is the total force applied at the column ends as the shear is uniform along the length of the link and the rotations (γ) is equal to the relative vertical displacement of the link ends divided by the link length.

Figure 3.11 to Figure 3.14 shows the comparison of ABAQUS results with that of experimental data from *Ryu (2005)* for the cyclic loading protocols while Figure 3.15 shows the comparison for the monotonic loading protocol. The ABAQUS results correlate well with the experimental data for '12 RLP', '12AISC' and '12 SEV' loading protocols but ABAQUS underpredicts the strength of the shear link by approximately 18% for '12 RAN' loading protocol. This suggests that the cyclic material model developed is good for progressively increasing amplitude loading protocols but is less accurate for loading which is random in nature. It can also be inferred that for the '12 RLP' loading protocol that severe degradation in strength in the experiment after $\gamma = 0.15$

radian due to cracking and the buckling enhanced by cracking is not captured accurately in the ABAQUS model.

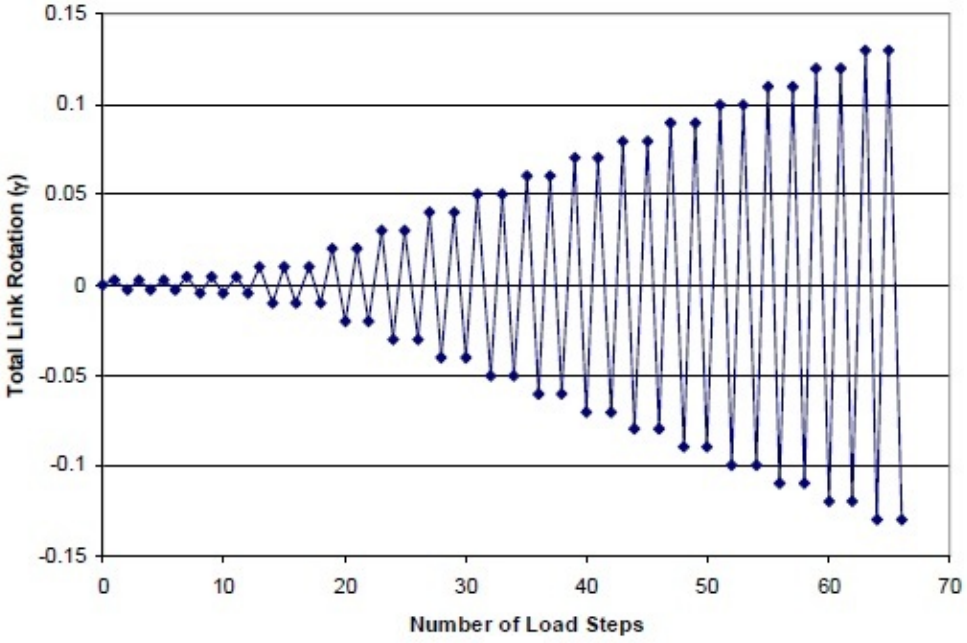

(a)

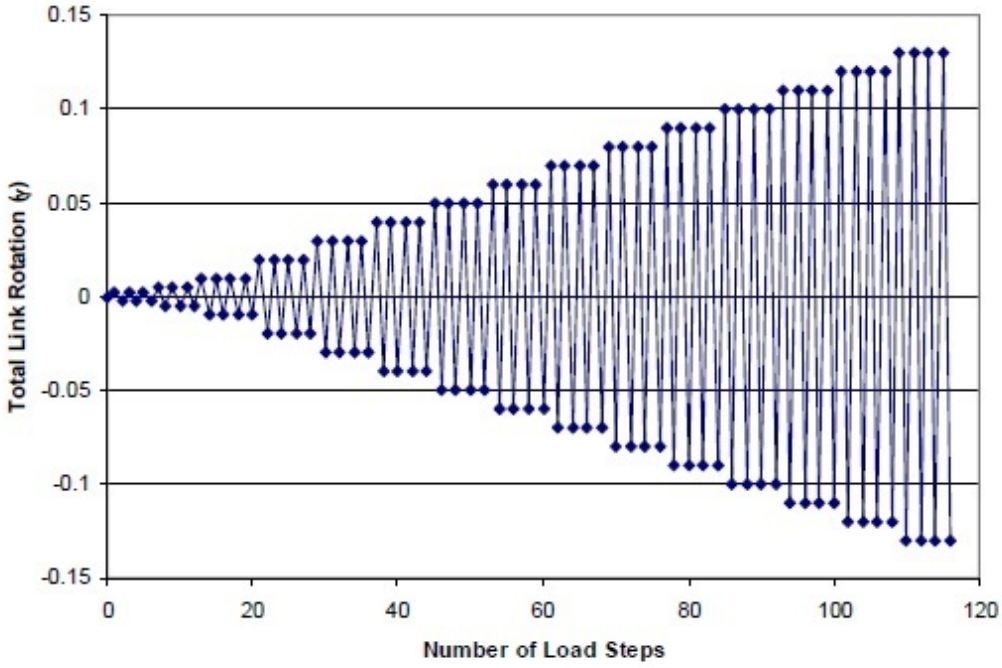

(b)

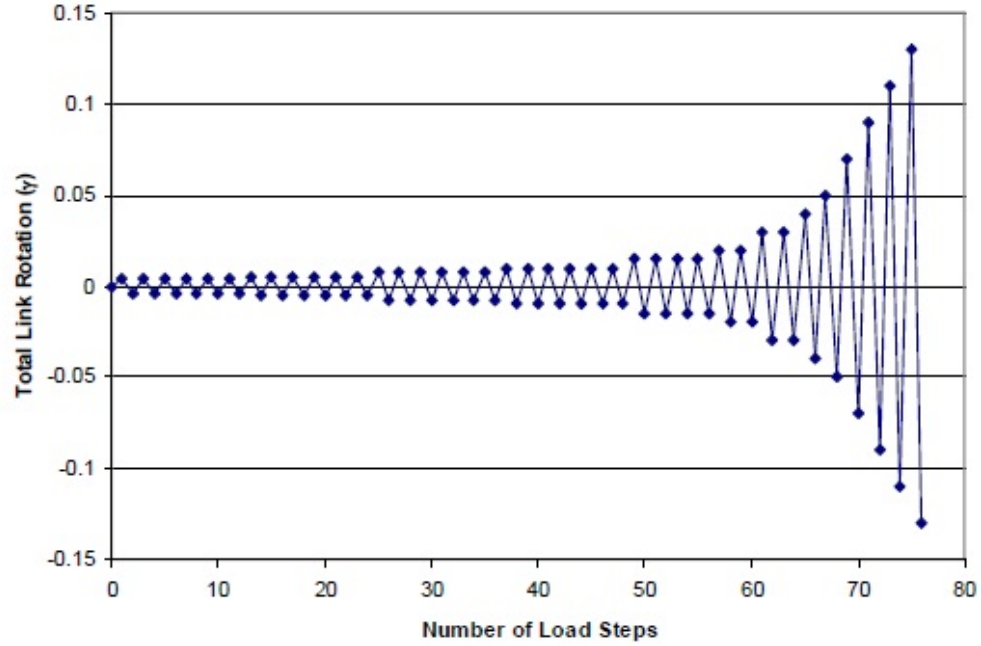

(c)

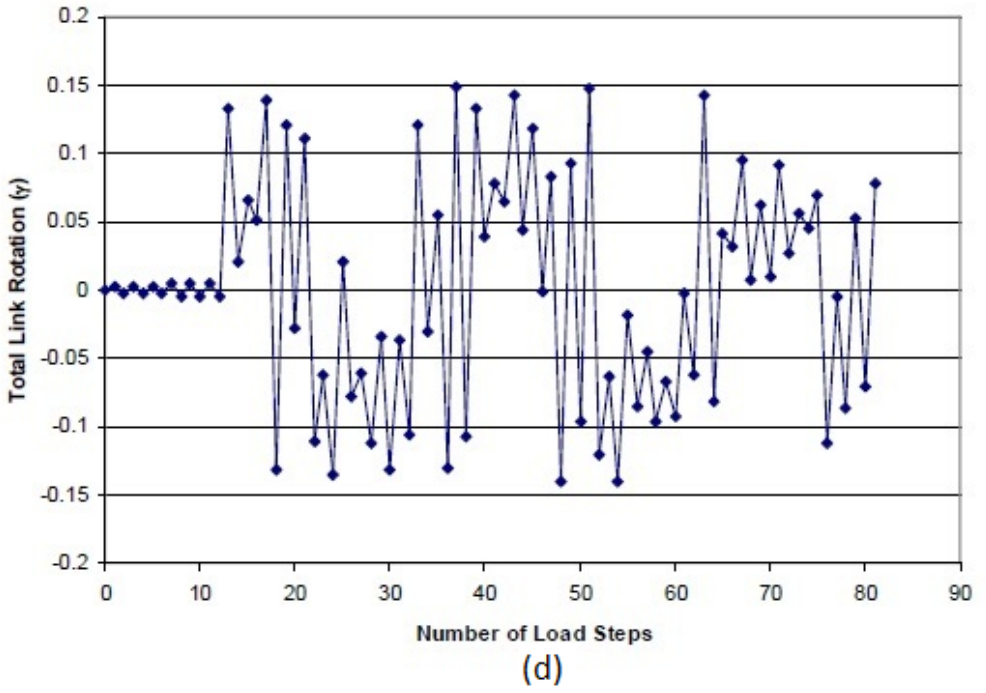

(d)

Figure 3.10: Loading protocol (a) AISC (b) RLP (c) SEV (d) RAN as used in Ryu's experiments (*Ryu (2005)*)

The same conclusion can be drawn for ’12 AISC’ and ’12 SEV’ loading protocols. This is due to the fact that the cyclic material model used in ABAQUS did not consider fracture modeling in the material. The behavior of the shear links up to the severe strength degradation point is simulated quite accurately by ABAQUS cyclic material model.

The comparison of ABAQUS results with experimental results for ’12 MON’ (Figure 3.15) specimen predicts the overall behavior and strength degradation due to severe buckling quite closely. The first yield point in the shear versus gamma plot from the experimental results is not seen in the ABAQUS results. The ABAQUS overpredicts the shear force at first yield, but captures the subsequent strain hardening behavior quite well. Figure 3.16 and Figure 3.17 shows the deformed configurations of shear links after the test and from the ABAQUS analysis. By comparing these figures, it can be seen that buckling of the left and right stiffener, buckling of web and flanges and the straight middle stiffener is very well captured by the ABAQUS model.

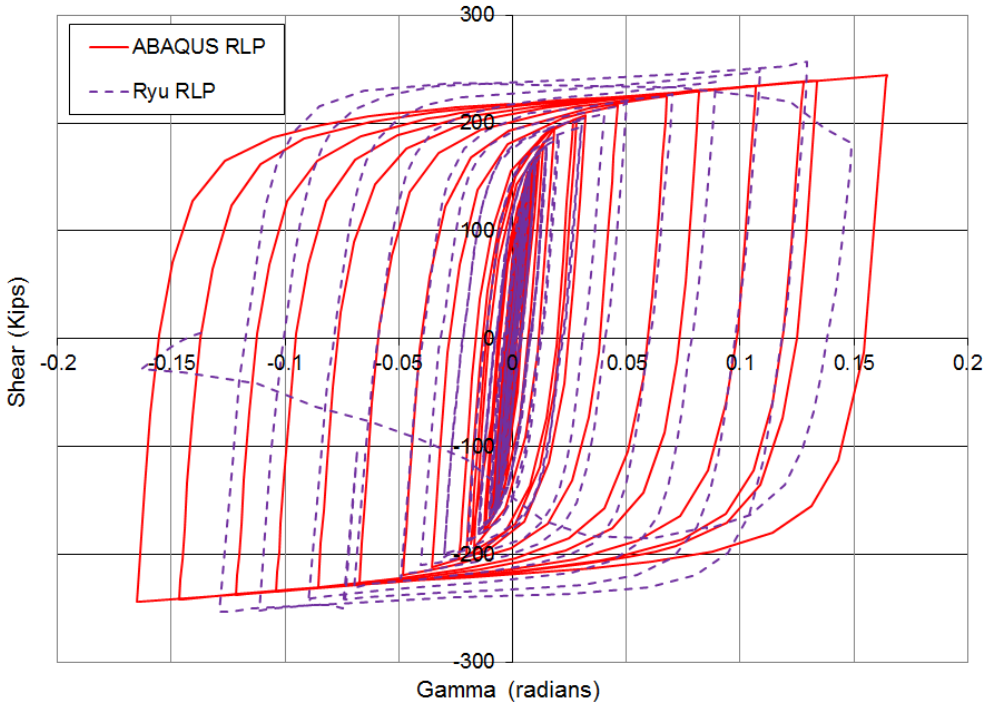

Figure 3.11: Shear versus gamma for revised loading protocol (RLP)

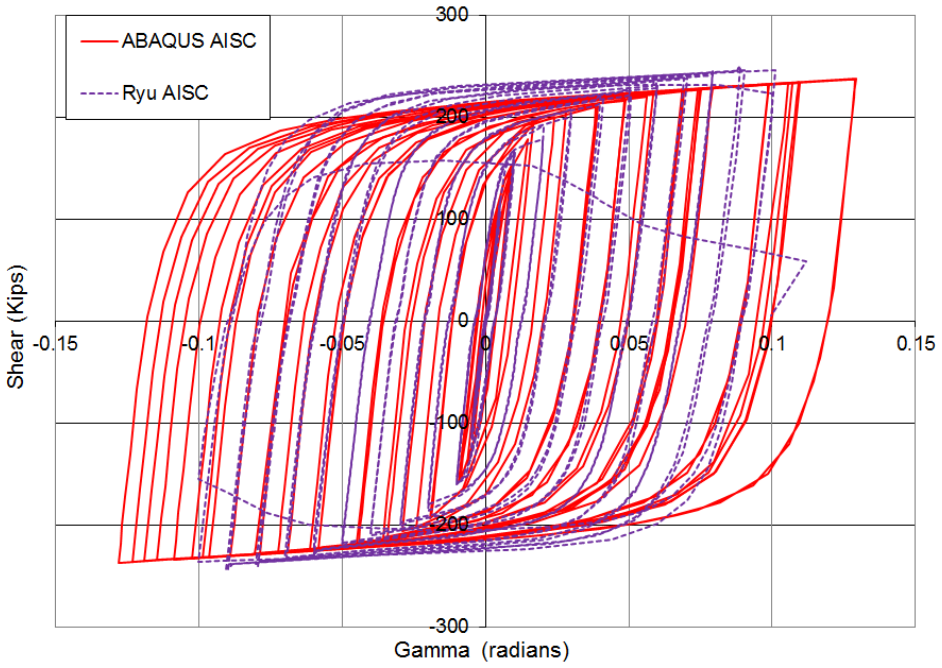

Figure 3.12: Shear versus gamma for AISC loading protocol

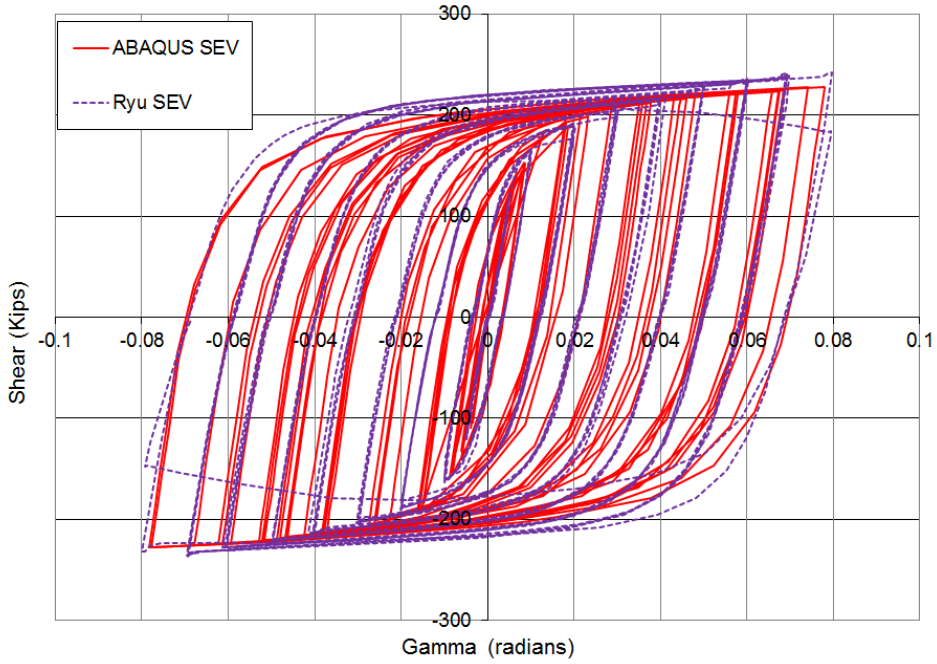

Figure 3.13: Shear versus gamma for severe loading protocol (SEV)

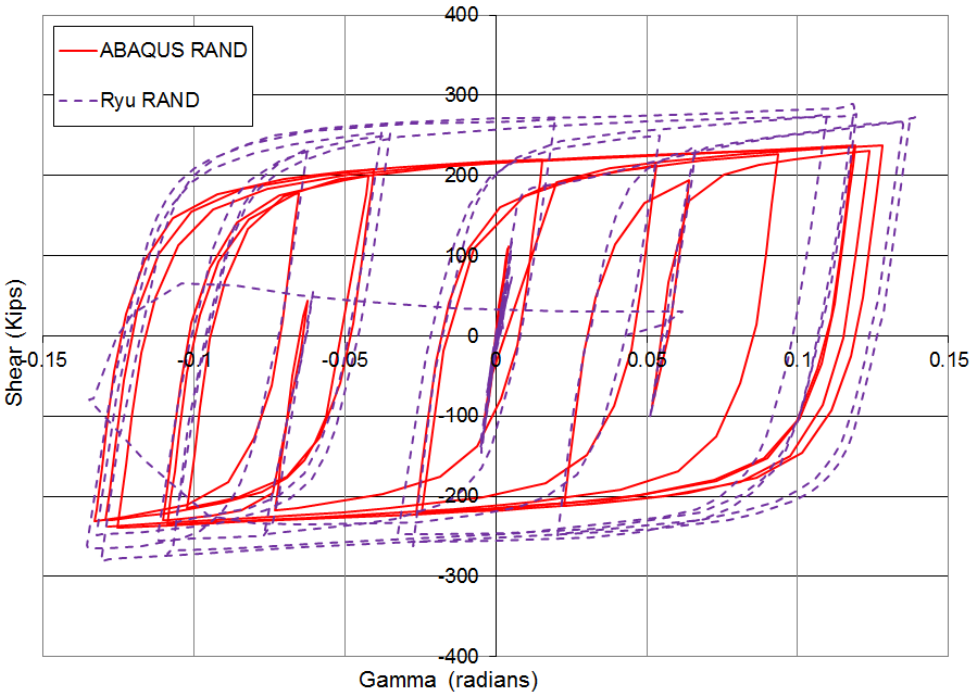

Figure 3.14: Shear versus gamma for random loading protocol (RAN)

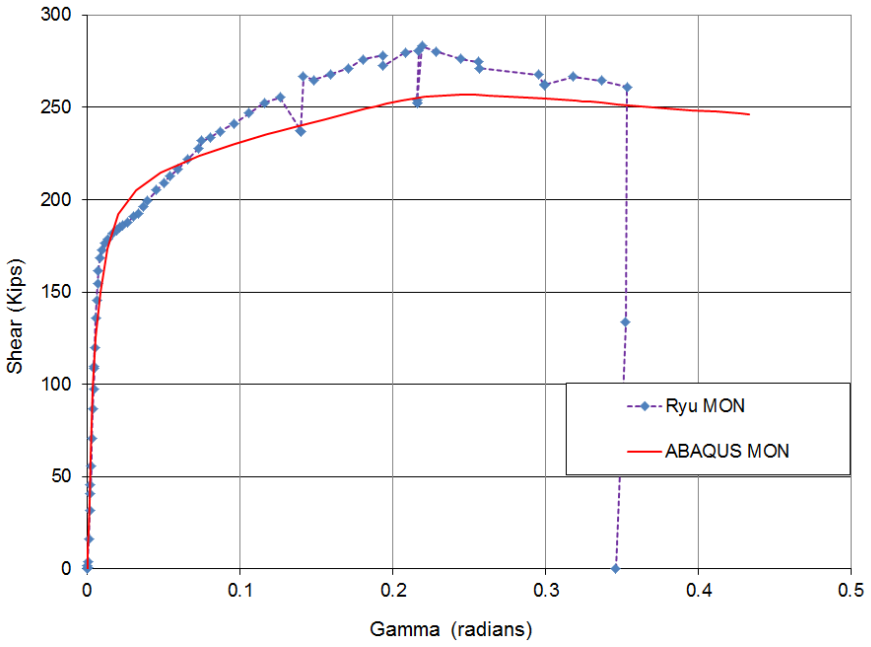

Figure 3.15: Shear versus gamma for monotonic loading protocol (MON)

Figure 3.16: Specimen ‘12 MON’ after testing (*Ryu (2005)*)

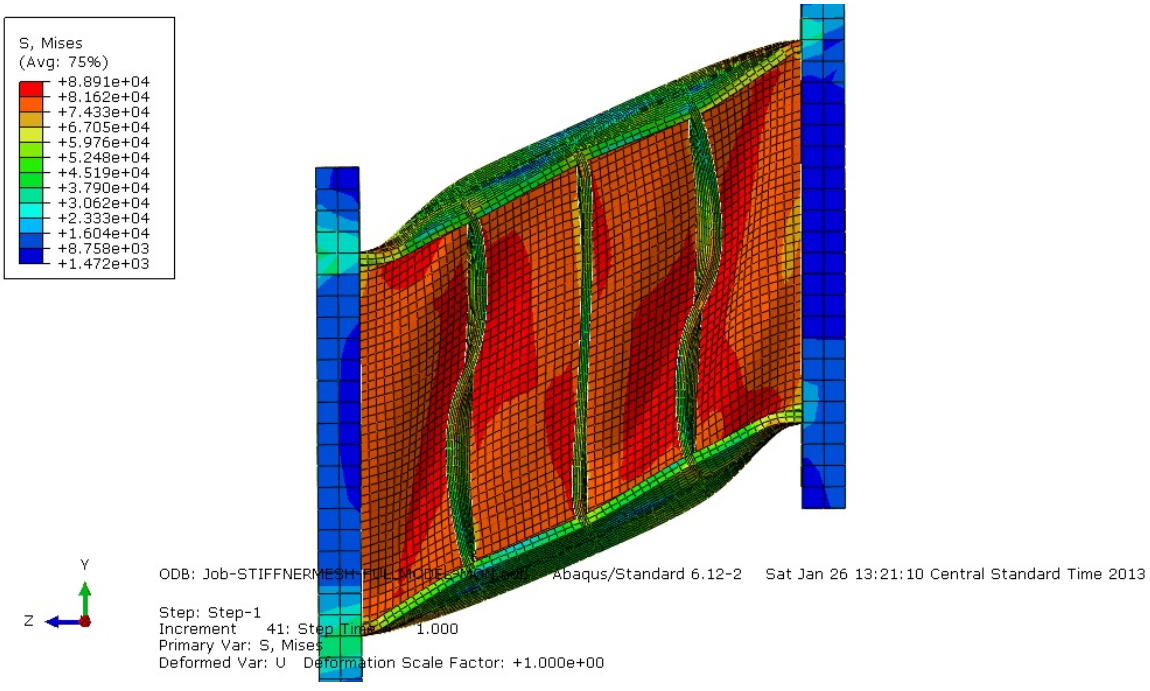

Figure 3.17: Specimen ‘12 MON’ after testing from ABAQUS

3.3.4 Comparison of ABAQUS model with DBBWWPZ experiment

In order to further validate the cyclic material model, one more validation study was done on beam-column assembly with a weak panel zone. The specimen was designated as DBBWWPZ (Dog bone bolted web weak panel zone) and is reported by Engelhardt et al. (2000). This specimen included reduced beam sections but had a weak panel zone such that most of the inelastic action was concentrated in the panel zone. The details of the model are given in Figure 3.18. Section 3.3.4.1 outlines the finite element model of the DBBWWPZ specimen while section 3.3.4.2 compares the ABAQUS results with the experimental data.

3.3.4.1 Finite element model of the DBBWWPZ experimental set up

The DBBWWPZ specimen consisted of a column (W14X283 section), two beams (W36X150 sections), continuity plates and end plates. The model assembly is shown in Figure 3.18. The cyclic material model for steel as given in Figure 3.5b was used for all the steel members in the specimen. The 'nlgeom' option to consider the geometric non-linearity was activated in the analysis step of the simulation. The reduced section of the beam was not modeled as the main goal was to study the deformation in the panel zone. In the experiments, welding was done to develop the moment connection between beam and column. In the ABAQUS model, the welds were not modeled explicitly but rather a tie constraint was used between the joining pairs to realize the connection. The tie constraint was used between continuity plate and column, beam and column and between end plates and beam/column. The meshing technique discussed in section 3.3.3.1 was also used here. The beam and column were meshed with a global seed size of 1.5 inches but the region of the column in the panel zone was given a local seed size of 0.80 inches. The continuity plate and the end plates had a mesh size of 0.3 inches and 1 inch respectively. The beam ends were modeled to behave as rollers while the column bottom end was modeled as pinned. All the ends were constrained to prevent out-of-plane displacement. The displacement loading condition (Amp1) was given at the column top as shown in Figure 3.19. This loading condition is same as described in section K2 of the *Seismic Provisions for Steel Structural Buildings* (AISC 2010b). The loading cycles are

given in terms of drift angle in Figure 3.19. Drift angle was converted to horizontal displacement at the column tip by multiplying the drift angle with the column height.

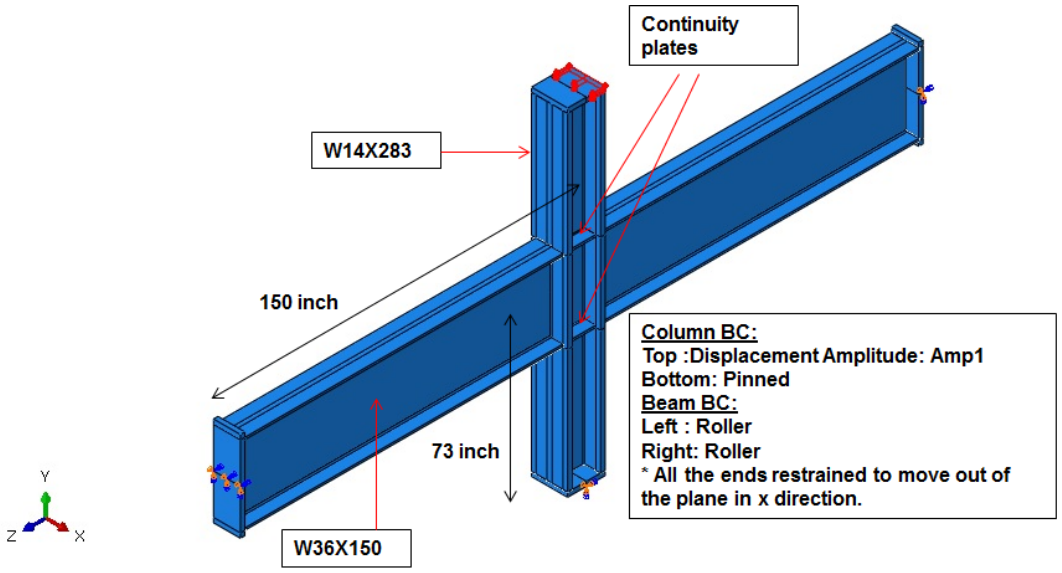

Figure 3.18: DBBWWPZ specimen

1) 6 cycles at Θ = 0.00375 rad
2) 6 cycles at Θ = 0.005 rad
3) 6 cycles at Θ = 0.0075 rad
4) 4 cycles at Θ = 0.01 rad
5) 2 cycles at Θ = 0.015 rad
6) 2 cycles at Θ = 0.02 rad
7) 2 cycles at Θ = 0.03 rad
8) 2 cycles at Θ = 0.04 rad

Figure 3.19: Amp1 loading at column tip in DBBWWPZ specimen (*Continue loading in 0.01 rad increment for 2 cycles, Θ=interstory drift angle)

3.3.4.2 Comparison of ABAQUS results with experimental results

The global response of the DBBWWPZ specimen was compared by comparing the plot of column tip load versus the column tip displacement in the ABAQUS simulation and the experimental results. The comparison is shown in Figure 3.20. The ABAQUS results match well with the experimental results up to a certain column displacement where fracture of the beam-column connection occurred in the experiment. As the cyclic material model developed in this study did not consider fracture, the connection failure in the specimen at the beam column interface (fracture at bottom flange of south beam, see *Engelhardt et al. (2000)*) was not at all captured in the ABAQUS model. Therefore, the strength degradation phenomenon in the actual test when the column was displacement in the negative direction was not captured by the ABAQUS model. Figure 3.21 shows the Von Mises stress in the specimen at column tip displacement of 5.84 inches (1^{st} cycle) which corresponds to an interstory drift angle of 0.04 radian. The contours shows that most of the yielding is concentrated in the panel zone region which corroborates observations in the experiment (*Engelhardt et al. (2000)*).The high stresses at the beam-column connection might have caused the connection failure seen in the actual test. This comparison on DBBWWPZ specimen was also done in section 3.6, Shirsat (2011), but with a monotonic material model. The comparison was not accurate with the monotonic material model. So, the comparison made in this study with a cyclic material model confirms the assumption that a reasonable cyclic material model is required to simulate the behavior of panel zone under cyclic loading accurately.

3.3.5 Yield Stress for the cyclic material model

The shear strength of the panel zone depends on the yield stress of the structural steel. The yield stress of the steel can't be found directly from the data of stress-strain pairs used in the input of ABAQUS cyclic material model. The cyclic material model developed in section 3.3 was based on the largest stabilized strain cycles in cyclic material tests by *Kaufmann et al. (2001).*

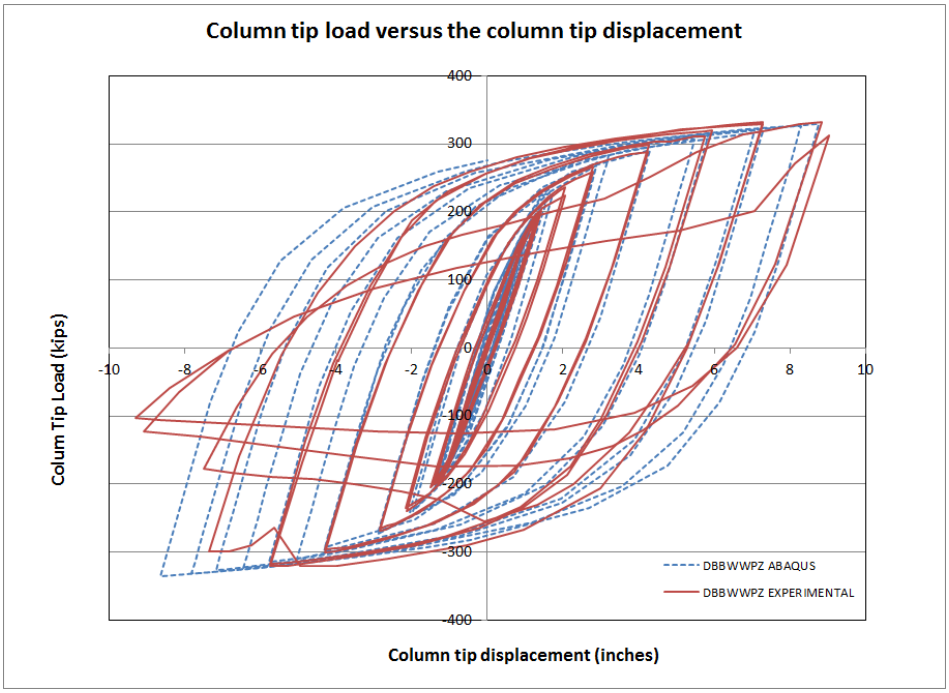

Figure 3.20: Column tip load versus column tip displacement for DBBWWPZ specimen

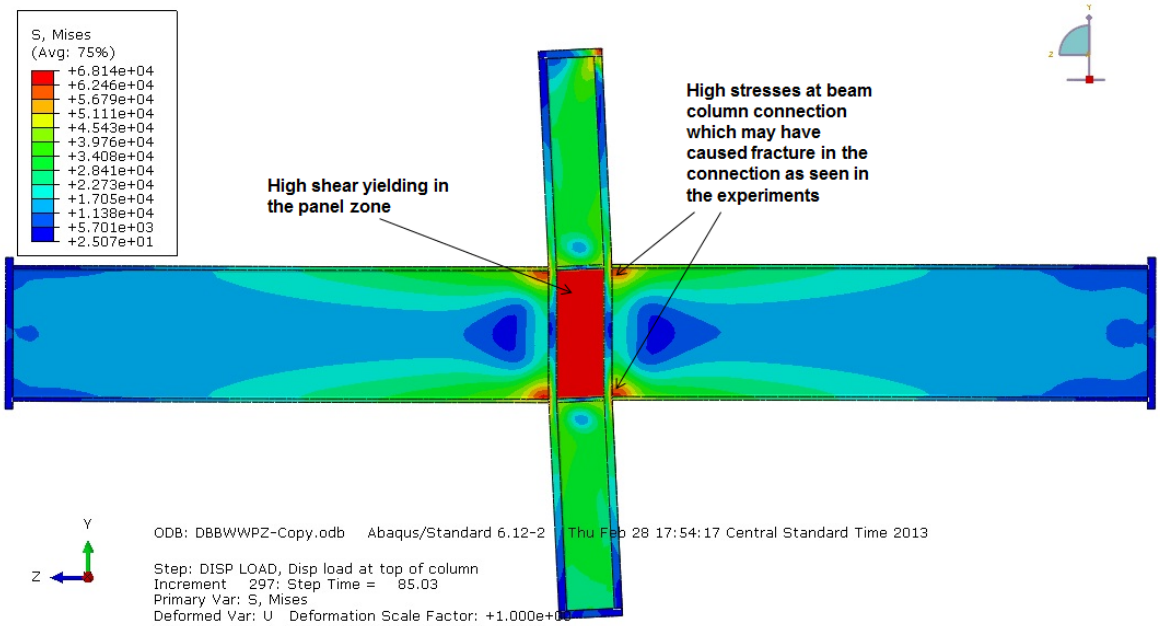

Figure 3.21: VMS in the DBBWWPZ specimen at 1st cycle of 0.04 radian interstory drift angle

In order to determine the yield stress, a tension coupon similar to the coupon used in *Kaufmann et al. (2001)* was modeled in ABAQUS 6.12 and was subjected to progressively increasing strain cycles up to strain amplitude of 0.04. A 3D finite element model view of the tension coupon is shown in Figure 3.22. The coupon had a circular cross-section with diameter of 3/8 inch at the gauge and 5/8 inch at the ends. The gauge length was 1 1/8 inches. The circular cross section of the coupon was chosen so that it has same buckling tendency in all directions when compression strains were applied at the ends.

The tension coupon had the same material model as given in Figure 3.5b. The geometric nonlinearity was considered in the analysis by activating the 'nlgeom' option in the analysis step of the simulation. The C3D8R element (mesh size of 0.088 inch) was used to model the coupon and the 'sweep' meshing technique with advancing front was used for meshing. The left end of the model was kept fixed while the right end was moved in the '–Z' direction according to the displacement amplitude 'Amp1'.The amplitude 'Amp1' varied according to the loading protocol shown in Figure 3.23. The cyclic loading at right end was increase progressively to around 0.06 inches in 72 time steps. The larger diameter portion (cross-head) at the coupon ends was restrained to move out in X and Y directions.

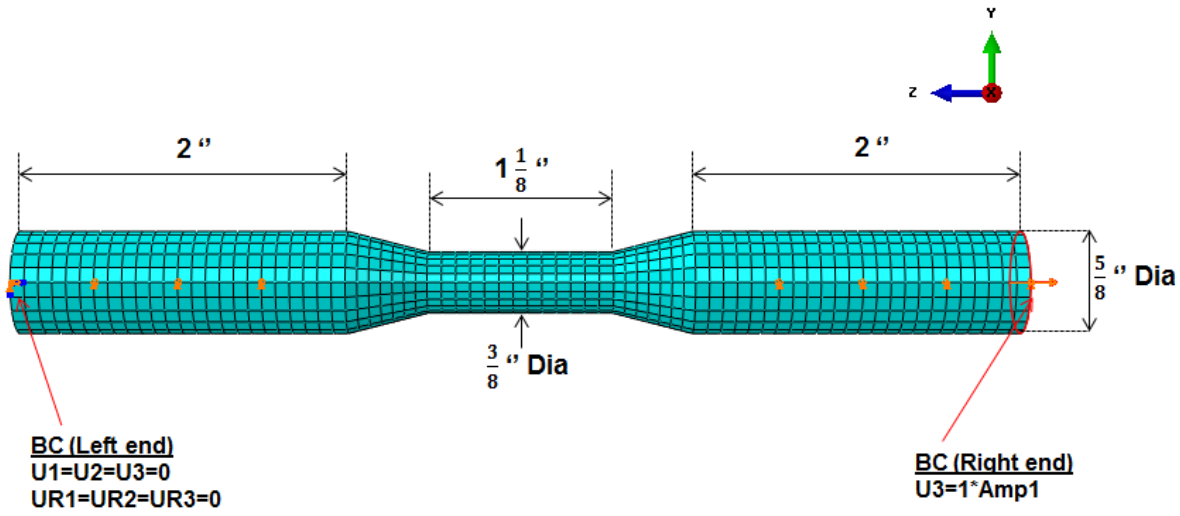

Figure 3.22: Tension coupon finite element model

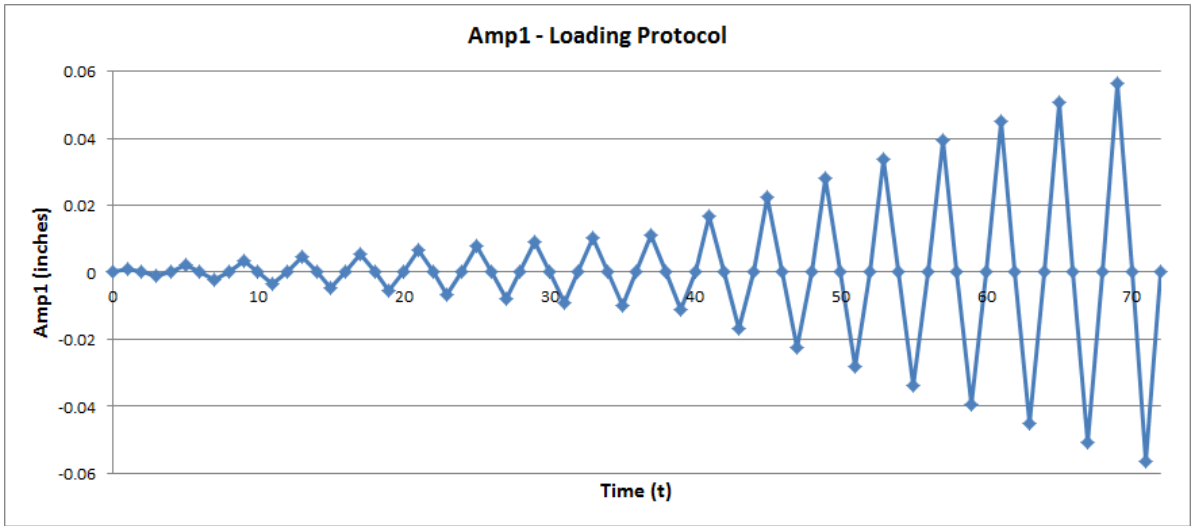

Figure 3.23: 'Amp1' displacement loading at right end of tension coupon.

The reaction at the left end and the change in the gauge length of the tension coupon was derived from the history output of the simulation. The reaction divided by the gauge cross section area and change in gauge length divided by the initial gauge length provided the engineering stress and engineering strain respectively. The contour plot for true Von Mises stress at a strain of approximately + 0.04 is shown in Figure 3.26. As expected, the stress at the gauge length remains constant. A plot of engineering stress versus engineering strain from this analysis is shown in Figure 3.24. The backbone curve is drawn as the locus of peak stresses in each cycle. This backbone curve is the cyclic stress-strain curve which means that at particular strain amplitude the stress in the material will find its way to reach the saturation stress as per this curve. The material curves of this kind do not have a well-defined yield stress point. Instead the yield stress can be determined by the 0.2 % offset rule. The rule says that if a line with initial point as (0.002, 0) and a slope of 29000 is drawn on the stress-strain curve, the intersection with the back bone curve is defined as the yield point. Figure 3.25 shows this yield point (0.003582, 47.24) and also shows the monotonic (Okazaki 2004) material model as used in Shirsat (2011) and Donkada (2012). This yield stress of 47.24 ksi is quite close to the yield stress of 52 ksi for monotonic material model. As the definition of yield point by

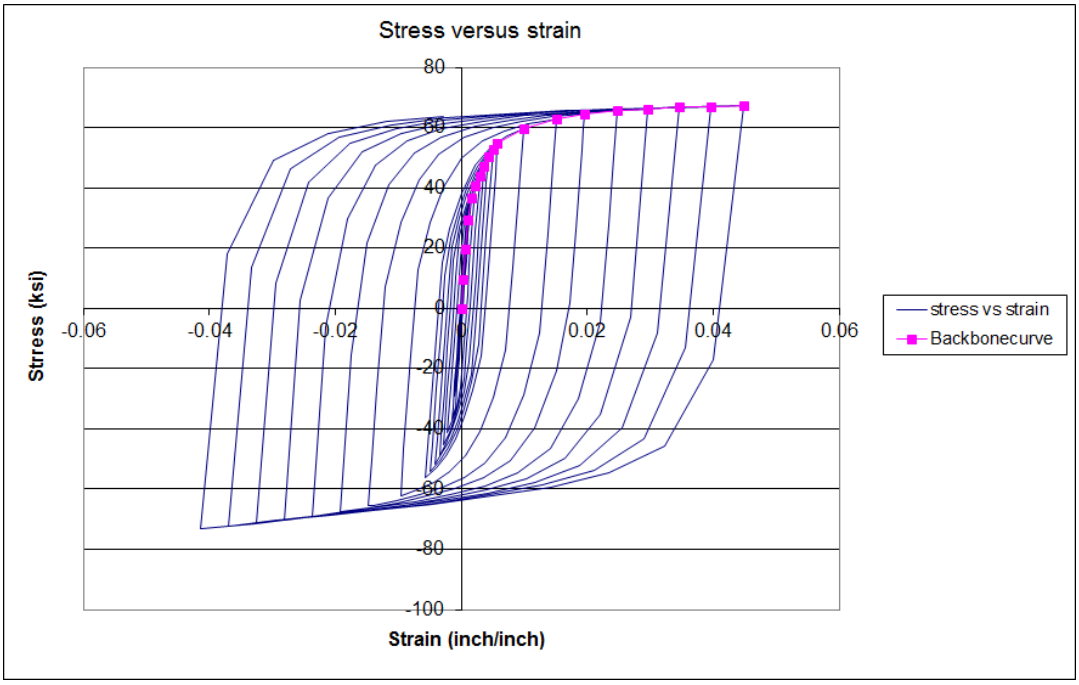

Figure 3.24: Engineering stress versus strain in the tension coupon

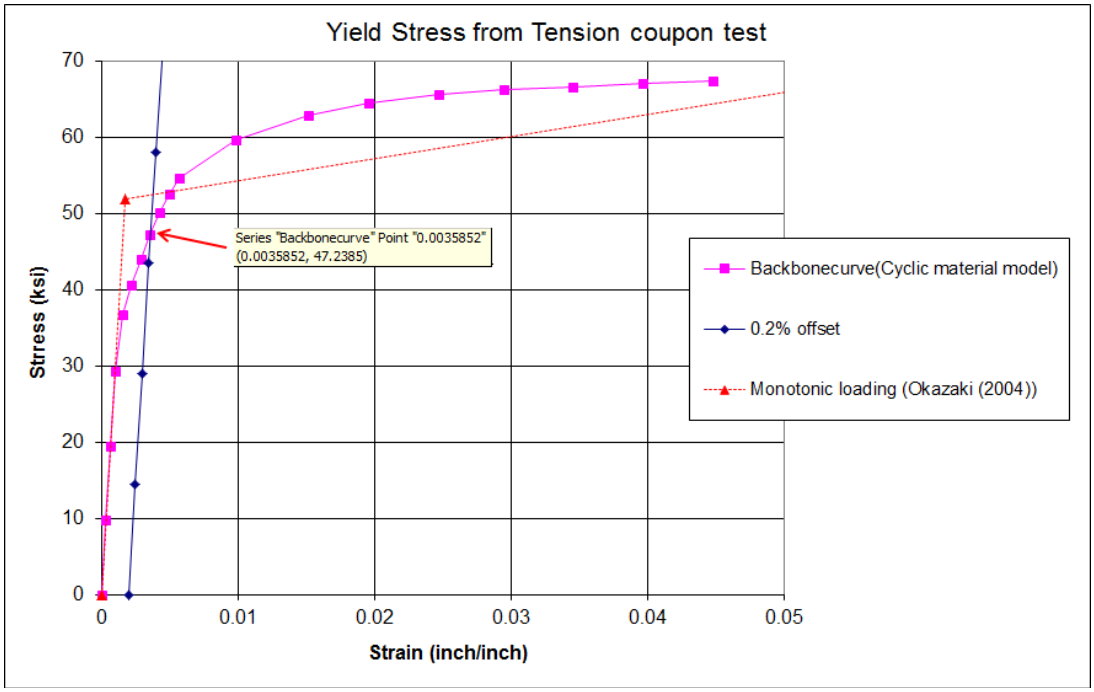

Figure 3.25: Determination of yield stress from the tension coupon test in ABAQUS

0.2% offset rule is also somewhat arbitrary, it is reasonable to assume the yield stress for the cyclic stress-strain material model is also 50 ksi for the panel zone strength calculations.

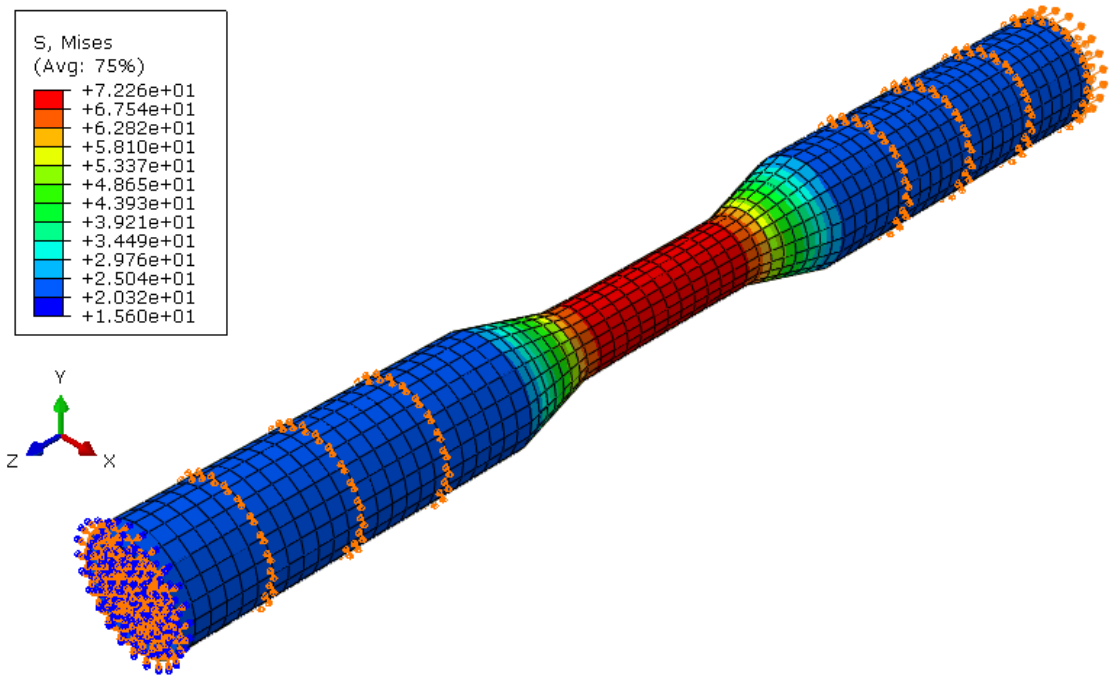

Figure 3.26: Von mises stress in the tension coupon at a strain of 0.04 in gauge length

3.3.6 Limitations of the cyclic material model

The cyclic material model developed in section 3.3.2 was validated in section 3.3.3 and 3.3.4 by comparing ABAQUS results with experimental results and they matched reasonably well. The results matched well for large strain cycles but the agreement was not as good at small strains near first yield. In order to have accuracy at both large and small levels of strains, a well calibrated isotropic component is needed in the cyclic material model. This isotropic component should play a major role at small strains but gradually diminishes to zero at larger strains. This isotropic hardening behavior at small and larger strains is in line with the physical observations in the experiments. The material model developed in this study did not have an isotropic

component as the main goal of this research is to simulate the panel zone behavior at large rotations.

At any particular rotation cycle of the panel zone, the different regions of the panel zone undergo different strain amplitude cycles but only the largest stabilized strain amplitude cycle was used as an input in ABAQUS to keep the simulation time of the model manageable. Moreover this technique was adequate to fulfill the major interest of this research which was to study panel zone behavior at large inelastic deformations.

3.4 MODEL ASSEMBLY

After the parts are modeled and the specific material properties are given to each part, these parts are assembled in the Assembly module of ABAQUS/CAE. Each part in the assembly is called an instance. The instances are a copy of the corresponding parts, so more than one instance on a part can be created in the Assembly module. These instances are translated and rotated to form an assembly as shown in Figure 3.27 (Analysis case 5A). In order to post process the quantities of interest at specific nodes and surfaces of assembly, sets and surfaces are defined. Three sets, namely top node, right node and reaction node are created in assembly to get the history output of required quantities. The horizontal displacement is requested at the top and right node (see Figure 3.27) to evaluate the panel zone rotation while the horizontal reaction is requested at the reference node (see the reference node in Figure 3.30) to evaluate the shear in the panel zone at each increment of the analysis. The surfaces in the doubler plate and continuity plate are defined in order to get section forces at these surfaces. This section forces on surfaces are required to draw free body diagrams of portions of the assembly. The surfaces defined are similar to *Donkada (2012)* (see Figure 2.8). A typical edit in the keyword of the model to request the section forces is shown in Figure 3.28. The section force command 'SOF' has some limitations as per *Abaqus 6.12 Analysis User's Manual, Section 4.1.2* (Section output from Abaqus/Standard). These limitations are as follows:

- The defined section must cut completely through the mesh, form a closed surface or be at the exterior of the body. If a section cuts only partially through the mesh, a valid free body diagram cannot be isolated.
- The total force and the total moment in the section are computed based on the internal stresses in the concerned elements. Inaccuracy may take place if distributed body forces are present in the elements. Figure 3.29 (a) shows that different forces will be obtained for a section depending on which element is chosen (1 or 2).
- Different forces may be obtained on the same section depending on which side of the section is chosen to evaluate the section forces. Figure 3.29 (b) shows that zero forces will be reported if the section is defined using element 1 while a sum of forces of concentrated loads will be reported if the section is defined using element 2.

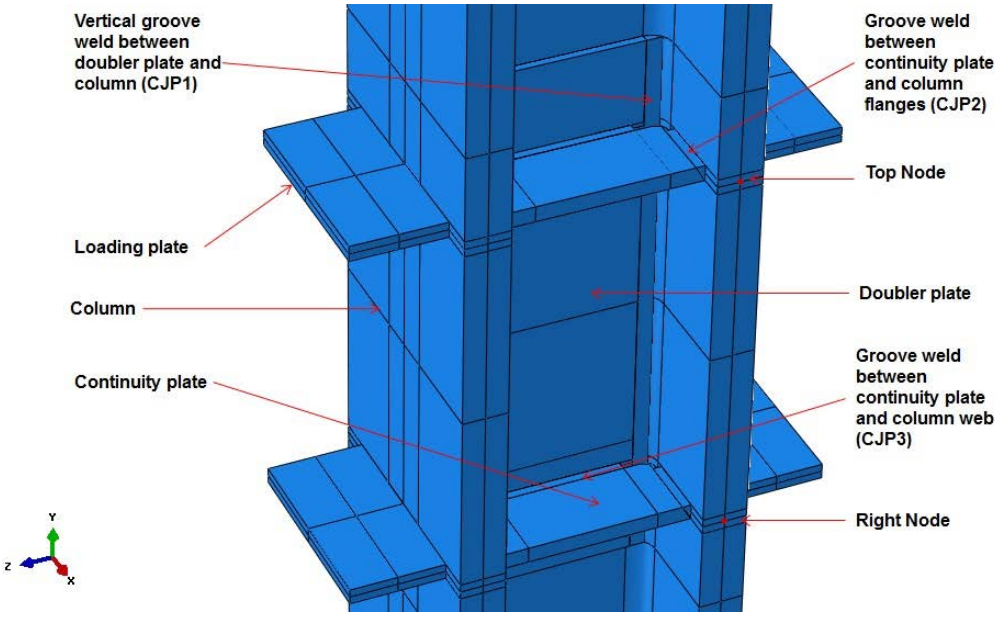

Figure 3.27: Assembly of parts (Analysis Case 5A)

```
**
** FIELD OUTPUT: F-Output-1
**
*section print,name=cp_b_front,surface=cp_b_front
SOF
*section print,name=cp_l_front,surface=cp_l_front
SOF
*section print,name=cp_r_front,surface=cp_r_front
SOF
*section print,name=cp_b_back,surface=cp_b_back
SOF
*section print,name=cp_l_back,surface=cp_l_back
SOF
*section print,name=cp_r_back,surface=cp_r_back
SOF
*section print,name=left_db,surface=left_db
SOF,SOM
*section print,name=right_db,surface=right_db
SOF,SOM
*section print,name=down_db,surface=down_db
SOF,SOM
*section print,name=up_db,surface=up_db
SOF,SOM
```

Figure 3.28: Keyword edit to request the section forces (Analysis case 5A)

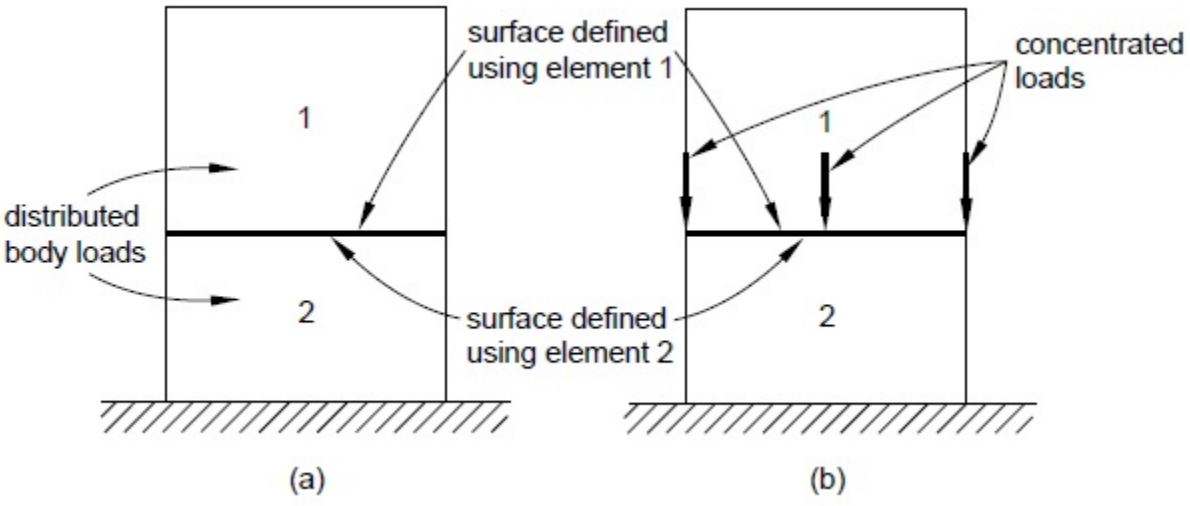

Figure 3.29: Total force in the section (*Abaqus Analysis User's Manual 6.12*)

3.5 TIME STEP

After the assembly of all the parts, an analysis step (Static, General) was created in 'Step' module of ABAQUS. This step was provided with a total time of 128 which was the number of increments defined in the loading 'Amplitude' in the loading module. The 'nlgeom' option was activated to consider geometric nonlinearity in the analysis. In a similar way as the mesh refinement, the increments in the time step are also refined to get a perfect match of output displacement amplitude and the amplitude defined in the loading module of analysis. The refined initial, minimum and the maximum increment size in the increment tab of the step was 0.1, 1E-20 and 0.2 respectively.

3.6 INTERACTION AND CONSTRAINTS

The contacts between the instances of parts in the assembly module are initialized by defining the contact pairs in this module. A part in the assembly does not get connected to other parts unless the contacts are defined. Three types of constraints were used in this study. First one is the 'tie constraint' which was used to simulate no movement of a surface of one part relative to the surface of the other part. The translations and the rotations degree of freedom for the nodes on the two surfaces become equal for 'tie constraint'. It is recommended that the surface with a coarser mesh shall be chosen as the 'master surface' and the other surface as 'slave surface' (*Abaqus 6.12 Analysis User's Manual, section 34.3.1*). A list of these surfaces pairs are tabulated in Table 3.1.

The second type of the constraint used was the 'hard contact' between the doubler plate and the column web. The 'hard contact' was realized by defining a contact property with pressure overclosure method as "hard contact" and the 'Allow separation after contact' option checked on. This contact property was given to an interaction defined in 'interaction' module. The column web (coarse mesh) and doubler plate (finer mesh) was made the master surface and the slave surface respectively. This contact allowed the separation of doubler plate and column web but didn't permit the penetration of the slave surface (doubler plate) into the master surface (column web) (*Abaqus 6.12 Analysis User's Manual, section 36.1.2*). The web of the deeper column (W40X264) was 0.96

inches thick and the doubler plate was 1 inch thick while the web of the shallow column (W14X398) was 1.77 inches thick and the doubler plate was 0.5 inches thick. So, the deeper column was more prone to buckling of both the web and DP but the shallow column did not show any buckling of its thick web. A slave adjustment to remove overclosure was provided in the interaction of the doubler plate and column web in deep column (W40X264) but no slave adjustment was provided for the shallow column (W14X398).

The third type of constraint was the 'rigid body' constraint (*Abaqus 6.12 Analysis User's Manual, section 2.4.1*). To remove the stress concentration at column ends due to the applied boundary conditions, the top and bottom surface at the column ends were made to behave as one rigid surface. This constraint was realized in the interaction module by creating a 'rigid body' constraint in which all the surface nodes were tied to the center of the surface (defined as the reference point in ABAQUS). The boundary conditions were applied at the reference point with the whole surface tied rigidly to the reference point. Figure 3.30 shows the rigid surface and the reference point at the top of column.

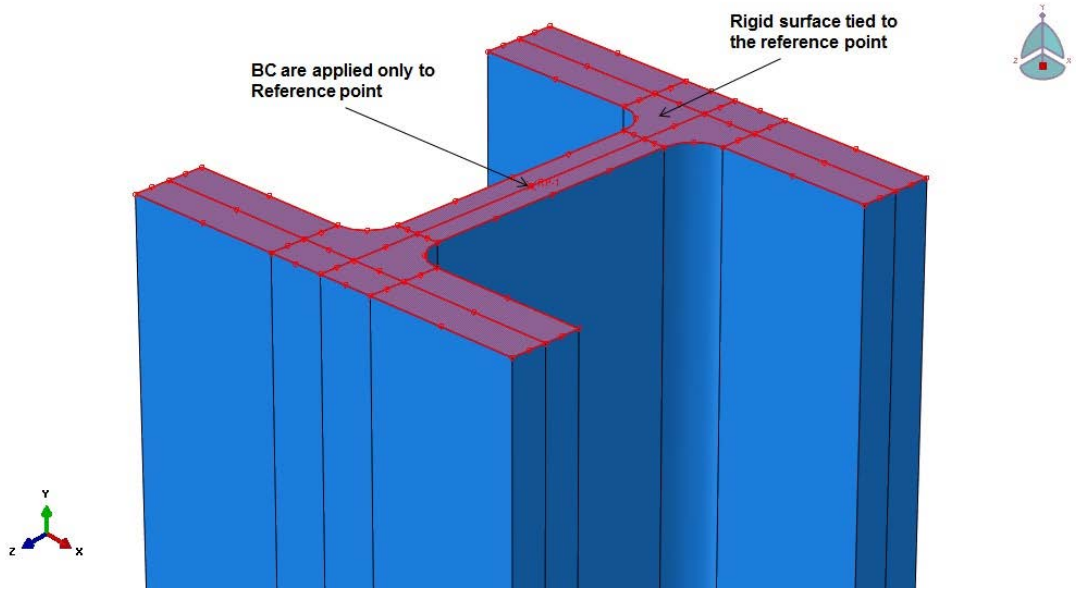

Figure 3.30: 'Rigid body constraint' in ABAQUS

Table 3.1: Master and slave surface in ABAQUS models

Type of Constraint	Master surface	Slave surface
Tie constraint	Column	Loading plate
Tie constraint	Doubler plate	Vertical groove weld (CJP1)
Tie constraint	Column	Vertical groove weld (CJP1)
Tie constraint	Continuity plate	Groove weld CJP2
Tie constraint	Continuity plate	Groove weld CJP3
Tie constraint	Column	Groove weld CJP2
Tie constraint	Column	Groove weld CJP3
Tie constraint	Doubler plate	Horizontal fillet weld
Tie constraint	Column	Horizontal fillet weld
Hard contact	Column web	Doubler plate

ABAQUS requires a node to be a part of only one constraint but in the panel zone finite element models the welds had a common node between the two constraints. Therefore, all the welds were chamfered at corners where there were boundaries of two constraints (see Figure 3.3).

3.7 Loading and Boundary Conditions

As noted in section 3.2, the columns were modeled only between the inflection points. The column top end was made a roller while the bottom end acted as pinned. The boundary points (Reference points in ABAQUS) were restrained to move in the out-of-plane direction ('X'- direction) and rotation about the axis of the column was restrained to avoid any torsion in the column. The loading in this study was displacement-control, the same as in Donkada (2012) but in contrast to load-control in Shirsat (2011). The transfer of beam load to the column was realized by applying cyclic displacement loading to the loading plates (representing flanges of the beam).

This cyclic loading on the loading plates were defined by creating a tabular type 'Amplitude' called 'Amp1'. The U3 displacement of loading plates was defined as 1 unit and the amplitude was defined by applying 'Amp1' loading protocol. This method allowed ABAQUS to use a relative loading scheme in which the total load applied at any step is the product of U3 displacement and the amplitude defined in 'Amp1'. These cycles were similar to cycles specified in Figure 3.19 which were based on the section K2

of the *Seismic Provisions for Steel Structural Buildings* (AISC 2010b). But here the rotation values given in Figure 3.19 represented panel zone rotation instead of interstory drift angle. The panel zone rotation definition in Donkada (2012) was also used in this study (Figure 2.7). The panel zone rotation was converted to displacement loading on the loading plates by multiplying the panel zone rotation by 12-inches (half of the distance between the loading plates). So, if a panel zone rotation of 0.05 was required then the displacement loading on the loading plates was 0.6 (0.05x12) inches. The loading protocol is shown in Table 3.2 and the corresponding amplitude 'Amp1' is shown in Figure 3.31. Note the total time steps in 'Amp1' are 128 which are equal to the total time input in the step module. The direction of displacement loading on the top loading plates were opposite to that on bottom loading plates (see Figure 3.32).

3.8 ELEMENT TYPE AND MESHING TECHNIQUES

All the parts in ABAQUS were meshed into elements by using 3D solid elements. The 3D element has 6 faces, 8 nodes, linear geometric order and used the ABAQUS/standard element library. It is designated as C3D8R in ABAQUS where 'C' stands for continuum solid elements,'3D' stands for 3D solid elements,'8' represents the number of nodes in the element and 'R' indicated that a reduced integration technique was used to decrease the numerical computation time. It was pointed out in Shirsat (2011) that this element has been used successfully in the past to simulate the behavior of steel members loaded well into the inelastic range.

The parts in the 'Mesh' module were meshed using the 'Mesh Controls' feature. ABAQUS tries to determine the most suitable technique by coloring the regions of the part by default as green, yellow and light orange. This default coloring can be altered by partitioning the part intelligently in the 'Part' module. The 'Hex' element shape elements can be generated by using one of the meshing techniques: Structured (green), Sweep (yellow) and Bottom-up (light orange) available in the 'Mesh Controls' feature. Table 3.3 shows the different techniques and refined mesh sizes used for the parts of the panel zone in this study. The column seed sizes were 1.5 inches globally while the panel zone region

of the column was meshed with a local seed size of 0.5 inches. Figure 3.32 shows the meshed model of W14X398 and W40X264 column.

Table 3.2: Loading protocol used in the panel zone study

Gamma	Cycles	Displacement Loading (inches)
0.00375	6	0.045
0.005	6	0.06
0.0075	6	0.09
0.01	4	0.12
0.015	2	0.18
0.02	2	0.24
0.03	2	0.36
0.04	2	0.48
0.05	2	0.6

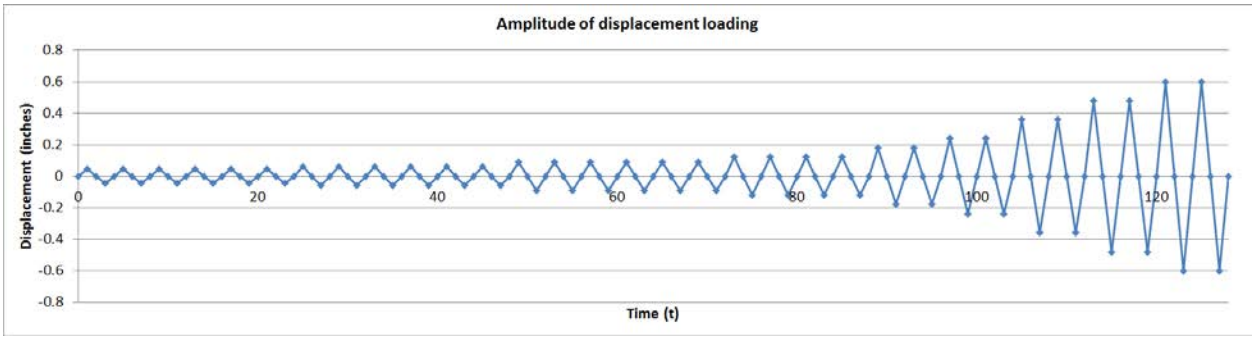

Figure 3.31: Amplitude loading ‘Amp1’ on the loading plates

Table 3.3: Meshing Technique and Mesh size for the panel zone study

Part	Meshing Technique	Mesh size W14X398)	Mesh size (W40X264)
		(inches)	(inches)
Column	'Structured'	0.5 (local)	0.5 (local)
Doubler plate	'Structured'	0.3	0.5
Continuity plate	'Sweep with advancing front algorithm'	0.3	0.5
Loading plate	'Structured'	0.25	0.25
Fillet welds	'Sweep with advancing front algorithm'	0.1	0.2
Groove welds (CJP2)	'Structured'	0.1	0.1
Groove welds (CJP3)	'Structured'	0.1	0.1
Groove welds (CJP1)	'Sweep with medial axis algorithm'	0.1	0.2

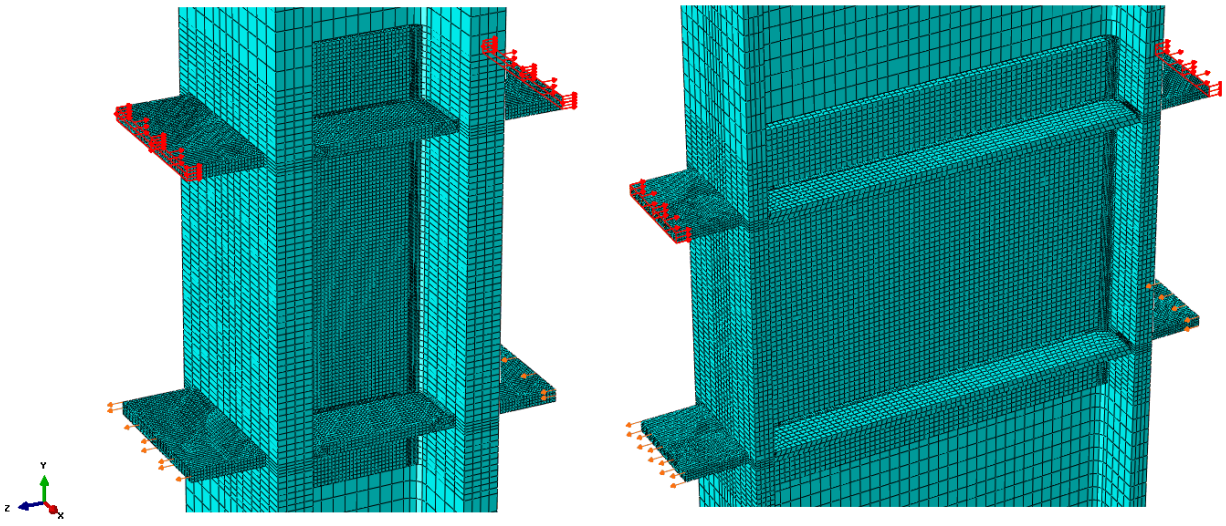

Figure 3.32: Meshed model of shallow column (W14X398) and deep column (W40X264)

3.9 JOB/POST PROCESSING

After completing all the modeling steps described from section 3.2 to section 3.8, the job (model) is ready to be submitted to ABAQUS/Standard for further analysis. The jobs were submitted via submit option in the 'Job' module of ABAQUS/CAE. Once the analysis is completed, the results can be viewed in the 'Post Processing' module. The contours showing the VMS in different parts of the assembly, reaction forces (R_f) at the column bottom (reference point) and the horizontal deflection of top (H_t) and right node

(H_r) (see Figure 3.27) were extracted from the job.odb file. The section forces at the surfaces of the doubler plate and continuity plates were extracted from the job.dat file to draw free body diagrams.

The shear (V_p) and the rotation (γ_p) in the panel zone was derived using following equations:

$$V_p = \frac{R_f\ (l-d)}{d} \qquad (Eq\ 3.1)$$

$$\gamma_p = \frac{(H_r - H_t)}{d} \qquad (Eq\ 3.2)$$

where,

R_f = Reaction at the column bottom

l = Length of the column (144 inches)

d = Distance between the loading plates (24 inches)

H_r = Horizontal displacement of the bottom flange

H_t = Horizontal displacement of the top flange

The output quantities VMS, PEEQ and PEMAG are defined in section 4.2.1 of *Abaqus 6.12 Analysis User's Manual* as follows:

VMS is the equivalent mises stress; $\text{VMS} = \sqrt{\frac{3}{2}\ S_{ij}\ S_{ij}}$ $(Eq.3.3)$

PEEQ is the cumulative equivalent plastic strain; $PEEQ = \bar{\varepsilon}^{pl}\ |_0\ + \int_0^t \bar{\varepsilon}^{\ pl}\ dt$ *(Eq. 3.4)*

PEMAG is the plastic strain magnitude; $\text{PEMAG} = \sqrt{\frac{2}{3}\ \varepsilon_{pl} : \varepsilon_{pl}}$ $(Eq.3.5)$

where,

S_{ij} = Deviatoric Stress Tensor

$\bar{\varepsilon}^{pl}\ |_0$ = Initial Equivalent Plastic Strain

In the results, the direction 1, 2 and 3 refers to the 'X', 'Y' and 'Z' directions in the global assembly model (see Figure 3.32). These post-processing results and their comparison for various analysis cases in the deep column and the shallow column are presented in subsequent chapters.

3.10 SUMMARY

The model of a column with a panel zone was developed in ABAQUS/CAE by going through the modeling process at each of the modules in ABAQUS. A cyclic material model was developed for the structural steel and the welds. The correlation of ABAQUS simulation results with the experimental results can be seen in section 3.3.3 and 3.3.4. Although some of the limitations of this model are pointed out in section 3.3.6, the overall inelastic behavior of the tested components was very well captured by the cyclic material model.

CHAPTER 4

Parametric Studies on Attachment Details of Doubler Plates in a W14X398 Column

4.1 INTRODUCTION

This chapter presents the results of the simulations performed on the shallow column (W14X398). A series of analysis cases were run to evaluate various methods for attaching the doubler plate to the column web. The results were helpful in answering the following questions of this research:

- Does the doubler plate (DP) help in increasing the shear strength of the panel zone proportional to the combined thickness of the DP and web? Does shear buckling of the DP reduce the panel zone strength?
- Is there any benefit of providing both horizontal fillet welds and vertical CJP welds to attach the doubler plate to the column or are vertical CJP welds alone sufficient?
- Is it beneficial to extend the DP above and below the loading plate (LP) levels?
- Are the continuity plates (CP's) critical elements in the assembly of the panel zone? Do the continuity plates with or without a DP help in increasing the panel zone strength and stiffness when they are placed between the column flanges?
- Do the continuity plates increase the stresses or forces in the DP substantially when the CP is welded to the DP with groove welds?
- Is web shear the only limit state when the panel zone is loaded or is there other local limit states that may govern the behavior of the panel zone region?
- Should the vertical CJP welds be designed to develop the shear strength or tensile strength of the DP?

- Are the conclusions similar as for above cases if thinner doubler plates are attached to the web in the panel zone?

All the outputs of structural response presented in this chapter at different rotations correspond to the last cycle of that rotation (See Figure 4.1). For example, the results at 0.01 radian means that results correspond to 4^{th} cycle of 0.01 radian when the panel zone rotation is +0.01 radian. All the figures in the output have a deformation scale of 5. The result for each analysis case includes one or more of the following outputs:

1. Shear (V_p) versus Gamma (γ_p) of the panel zone up to 0.05 radians according to the loading protocol described in section 3.7.
2. Shear (V_p) and force on one loading plate at the last cycle of different rotations.
3. The Von Mises Stress (VMS) and the equivalent plastic strain (PEEQ) in the column/DP at different rotations of the panel zone.
4. The out of plane displacement (U1) of the DP if the shear buckling is noticeable.
5. The VMS in the CP at different rotations of the panel zone.
6. The major stresses along the width of the DP. The top (LP level) and middle sections levels in the DP are as shown in Figure 4.5. The stresses S_{ij} (i,j=1,2,3) refers to the i j-component of the stress tensor. The directions 1, 2, 3 refer to the x, y and z directions shown in Figure 3.27.
7. The major stresses in the vertical CJP welds at the CJP1 – DP vertical interface.

Analysis case 1A to case 20A have LP's on both the sides of the column while case 21A to case 22A have LP's only on one side. The main variable parameters in this study were: (a) Colum flange thickness (t_f) – 2.85, 2.00, 1.00 and 0.50 inches (b) Doubler plate thickness (t_{dp}) – 0.50, 0.25 and 1.00 inches (c) Doubler plate extension of 6 inches above and below the loading plates, and (d) Inclusion of CP's. CP's were welded to the column or DP using groove welds.

4.2 ANALYSIS CASES

All the analysis cases are tabulated in Table 4.1.

Table 4.1: Analysis cases for the W14X398 column

Case	t_f (inches)	t_{dp} (inches)	l_{dp} (inches)	b_{dp} (inches)	CP
1A	2.85	-	-	-	No
2A		0.50	24	10	No
2A_f [2]		0.50	24	10	No
3A		0.50	36	10	No
3A_quar		0.25	36	10	No
3A_one		1.00	36	10	No
4A		-	-	-	Yes
5A		0.50	36	10	Yes
5A_quar		0.25	36	10	Yes
5A_one		1.00	36	10	Yes
6A	2.00	-	-	-	No
7A		0.50	24	10	No
8A		0.50	36	10	No
9A		-	-	-	Yes
10A		0.50	36	10	Yes
11A	1.00	-	-	-	No
12A		0.50	24	10	No
13A		0.50	36	10	No
13A_quar		0.25	36	10	No
13A_one		1.00	36	10	No
14A		-	-	-	Yes
15A		0.50	36	10	Yes
15A_quar		0.25	36	10	Yes
15A_one		1.00	36	10	Yes
16A	0.50	-	-	-	No
17A		0.50	24	10	No
18A		0.50	36	10	No
19A		-	-	-	Yes
20A		0.50	36	10	Yes
21A [4]	2.85	0.50	36	10	No
22A [4]		0.50	36	10	Yes

Note:

1. All cases with DP have vertical CJP1 groove welds.
2. Case 2A_f has horizontal fillet welds.
3. The distance between LP's is 24 inches in all cases.
4. Case 21A and 22A have LP's only on one side.

4.2.1 Analysis case 1A

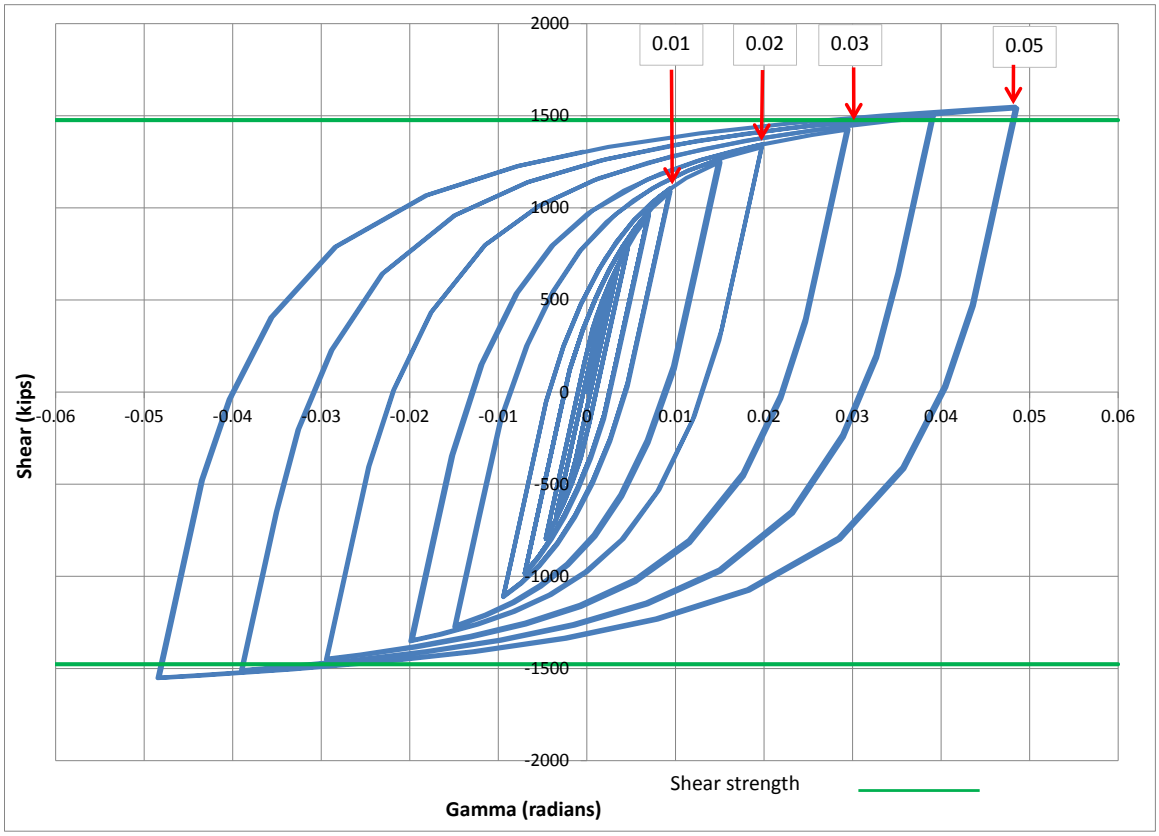

Figure 4.1: Panel zone shear versus rotation (Case 1A)

Table 4.2: Panel zone shear and force on loading plate (Case 1A)

Panel zone rotation (rad)	0.01	0.02	0.03	0.05
Panel zone shear (kips)	1107.54	1344.64	1444.26	1548.74
Force on one Loading plate (kips)	664.52	806.78	866.55	929.24

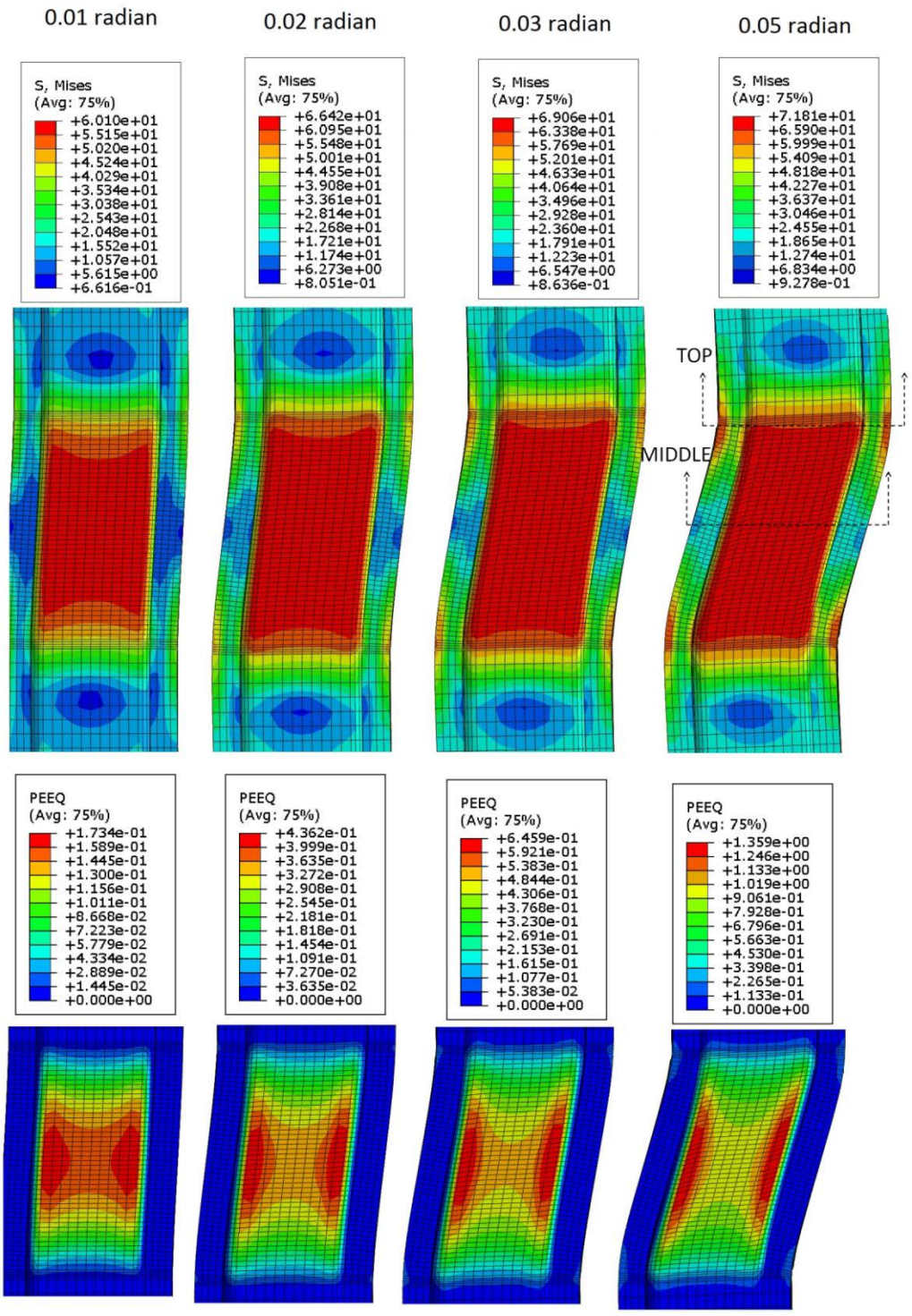

Figure 4.2: VMS and PEEQ in the column (Case 1A)

4.2.2 Analysis case 2A

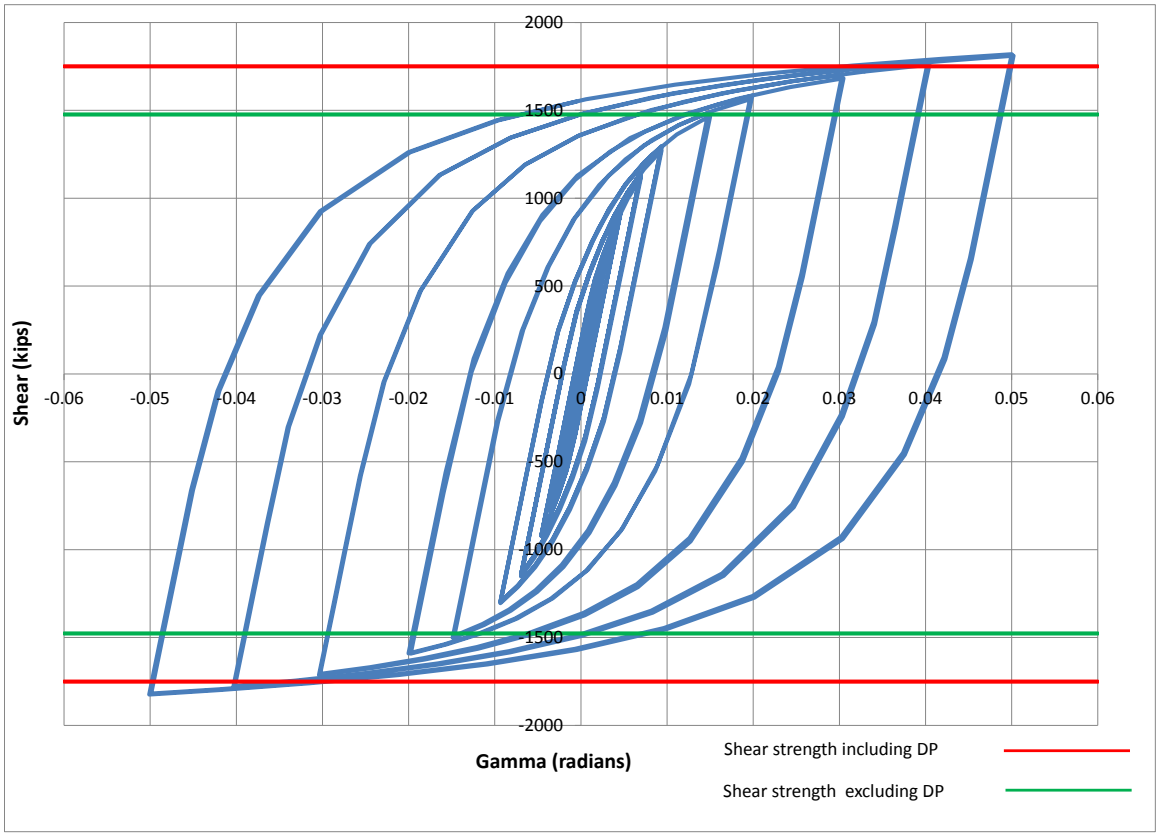

Figure 4.3: Panel zone shear versus rotation (Case 2A)

Table 4.3: Panel zone shear and force on loading plate (Case 2A)

Panel zone rotation (rad)	0.01	0.02	0.03	0.05
Panel zone shear (kips)	1296.23	1584.11	1704.65	1819.41
Force on one Loading plate (kips)	777.74	950.47	1022.79	1091.65

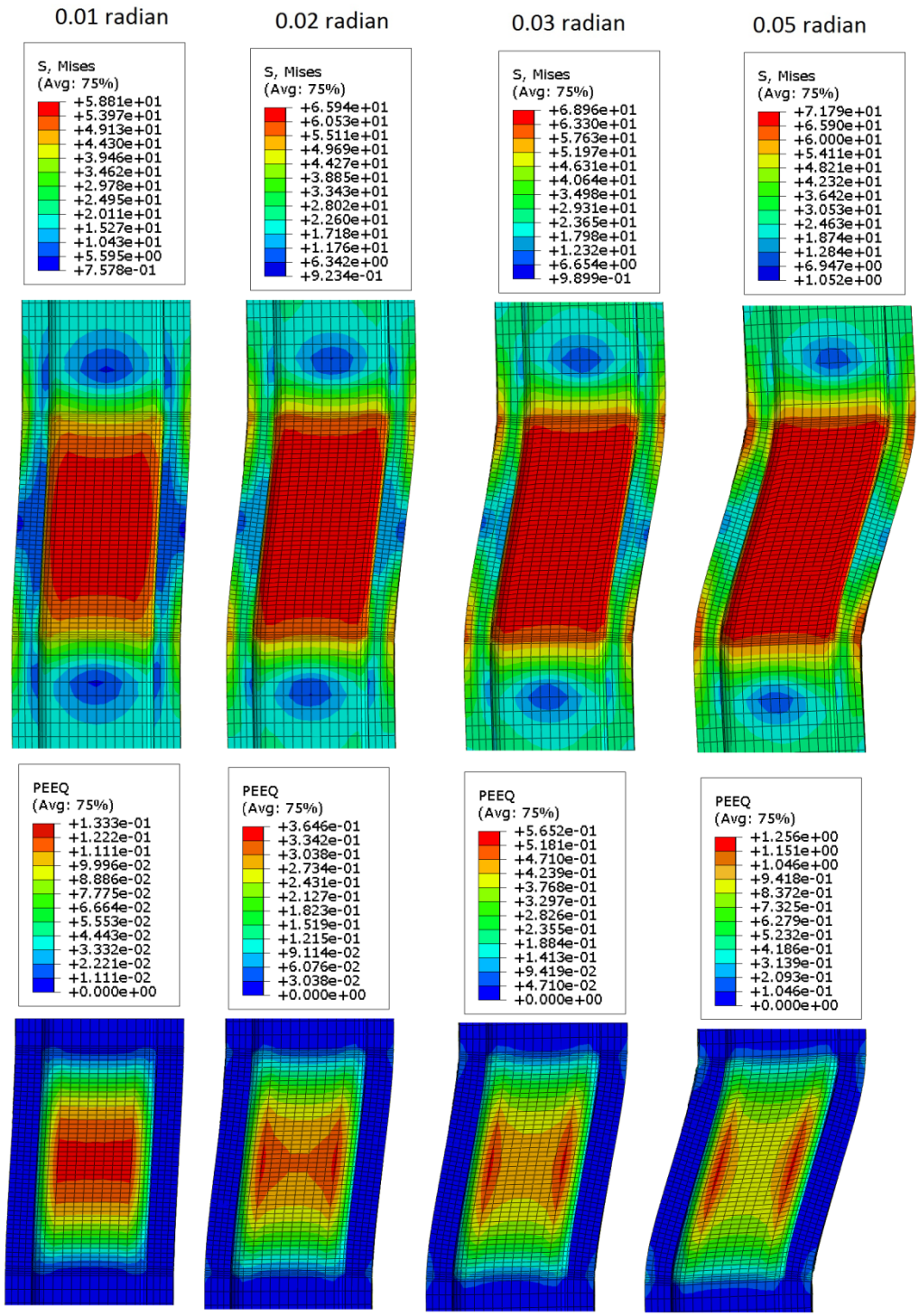

Figure 4.4: VMS and PEEQ in the column (Case 2A)

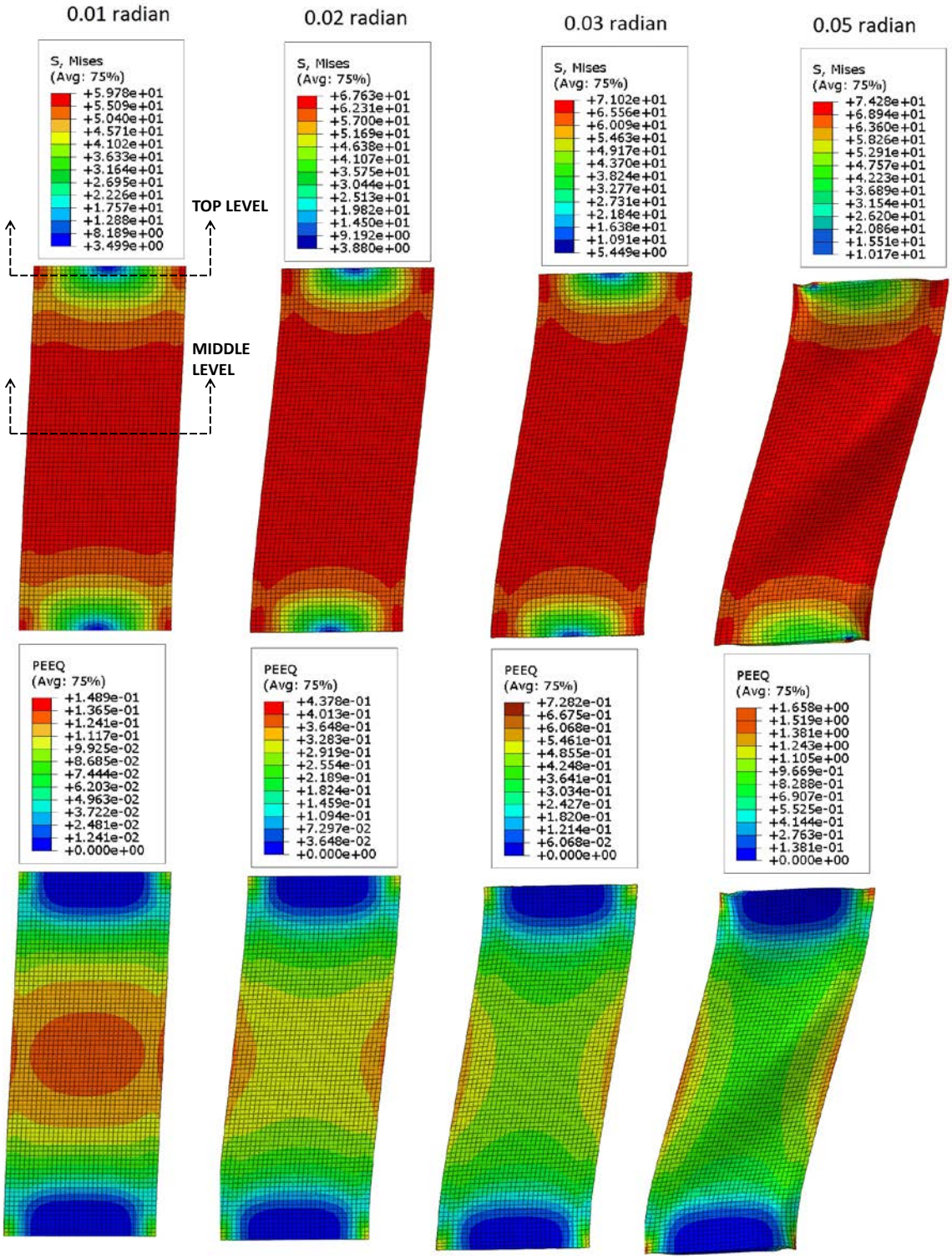

Figure 4.5: VMS and PEEQ in the DP (Case 2A)

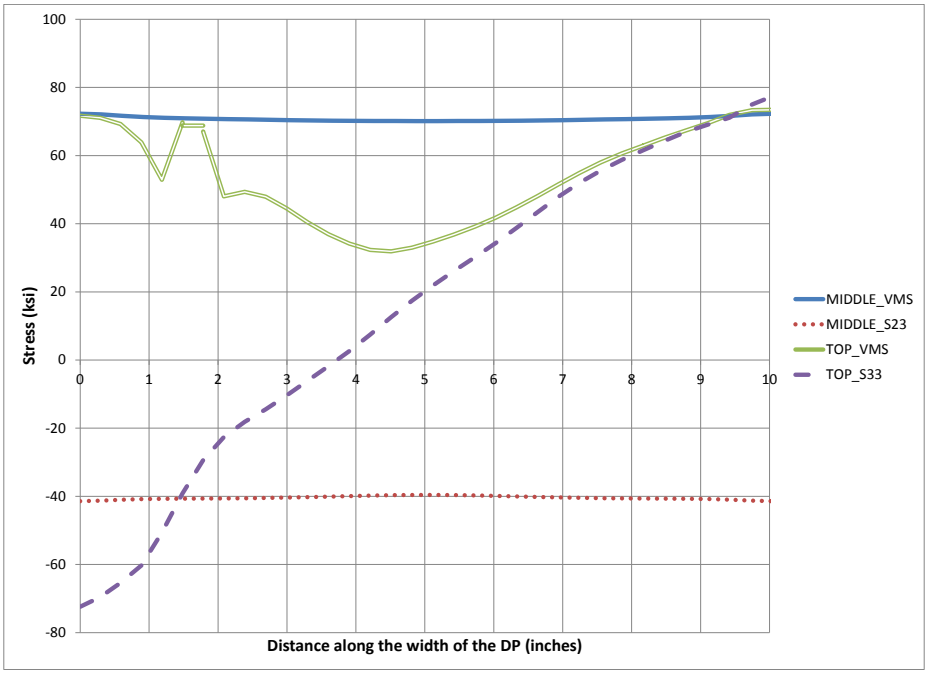

Figure 4.6: Stresses along the width of DP at 0.05 radian (Case 2A)

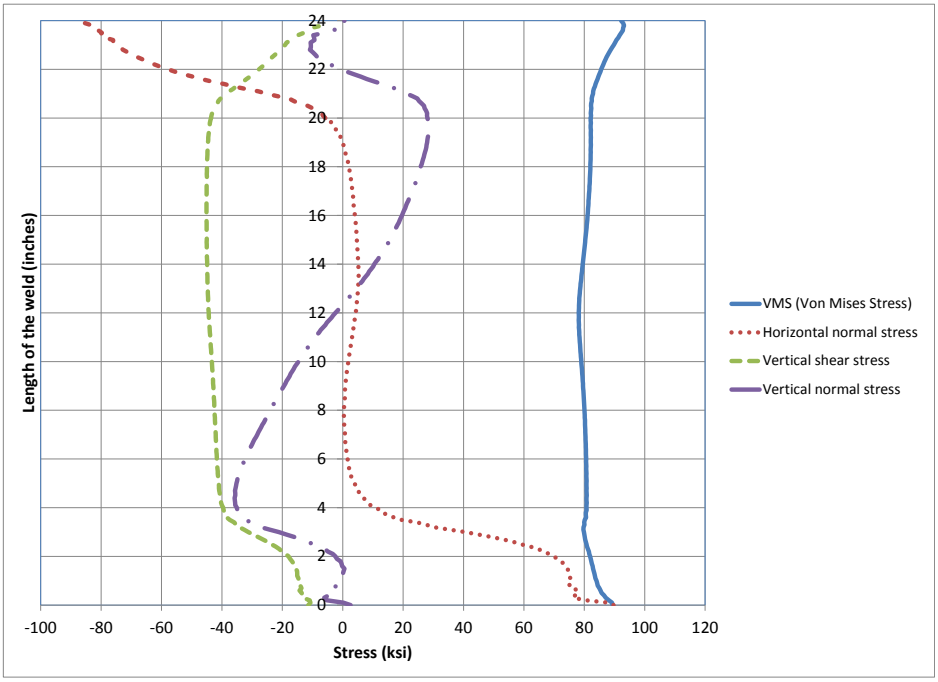

Figure 4.7: Stresses along depth of CJP1 (DP-CJP1 interface) at 0.05 radian (Case 2A)

4.2.3 Analysis case 2A_f

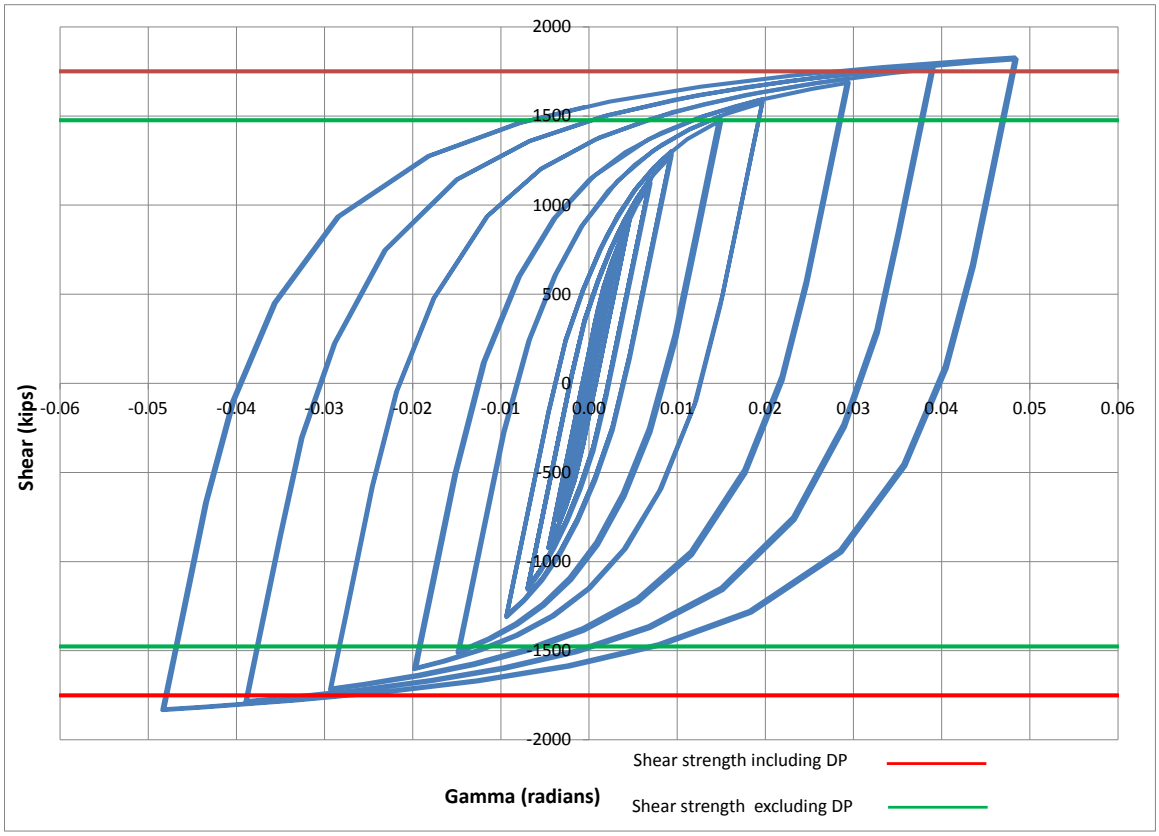

Figure 4.8: Panel zone shear versus rotation (Case 2A_f)

Table 4.4: Panel zone shear and force on loading plate (Case 2A_f)

Panel zone rotation (rad)	0.01	0.02	0.03	0.05
Panel zone shear (kips)	1304.06	1594.38	1709.24	1828.67
Force on one Loading plate (kips)	782.43	956.63	1025.54	1097.20

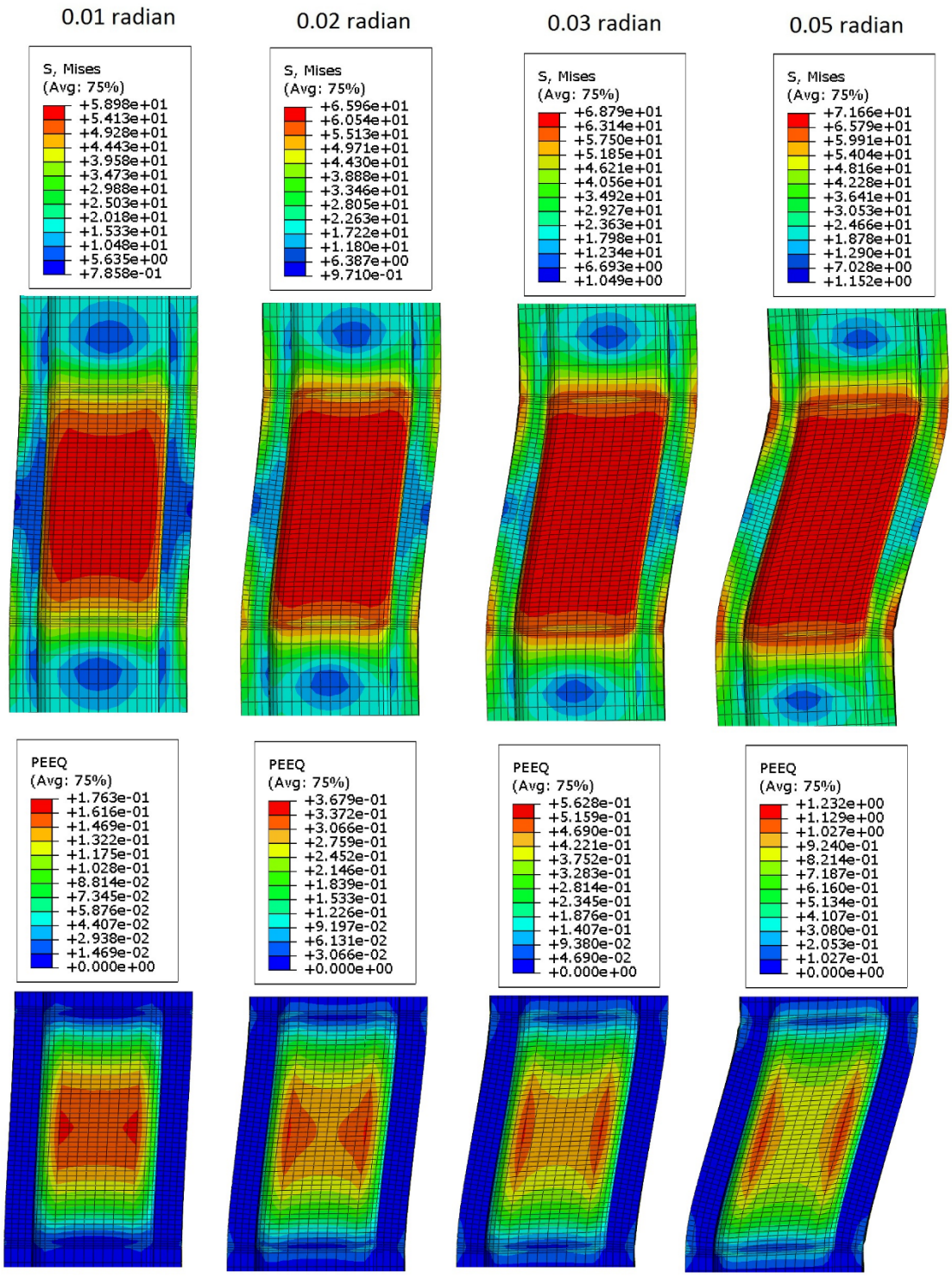

Figure 4.9: VMS and PEEQ in the column (Case 2A_f)

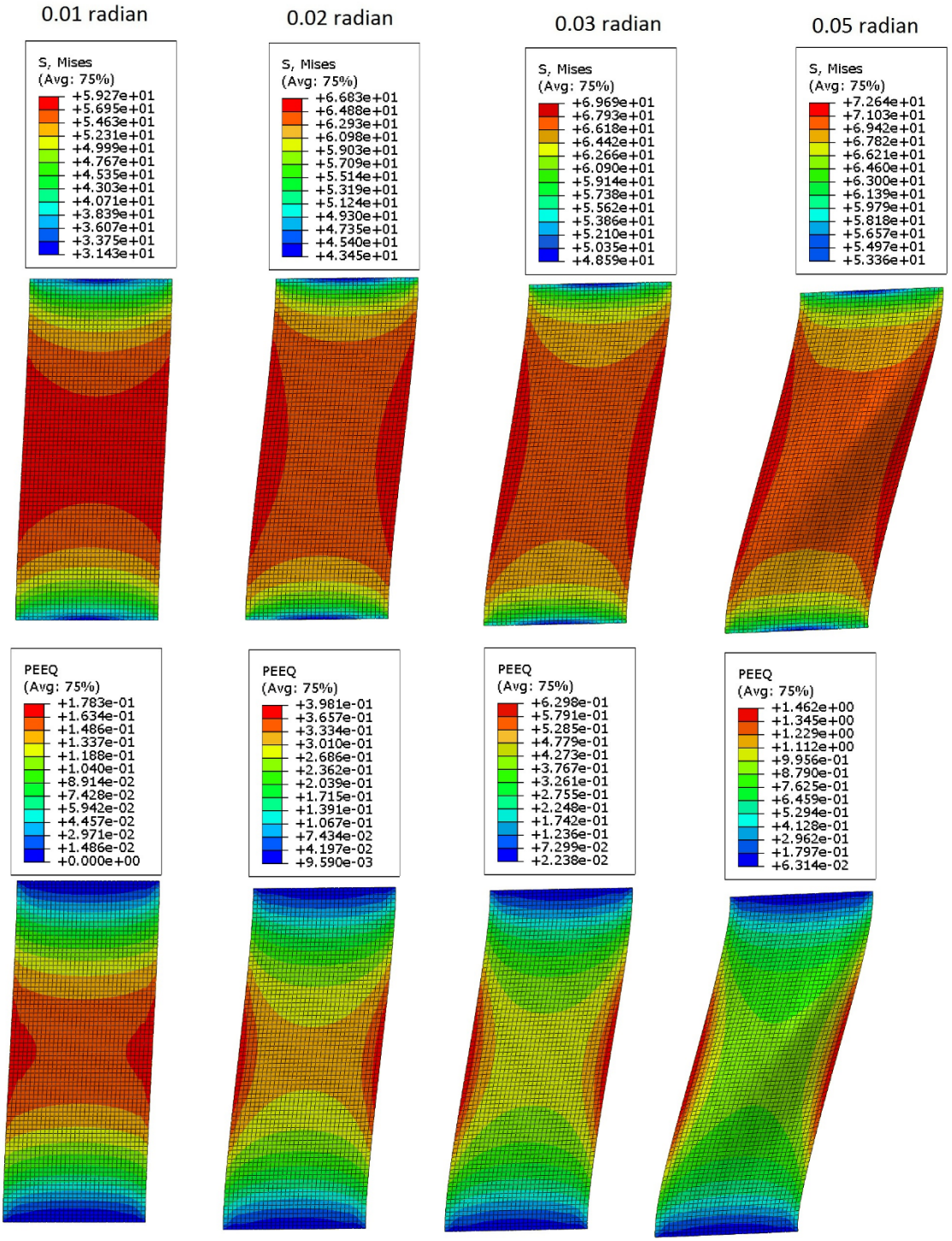

Figure 4.10: VMS and PEEQ in the DP (Case 2A_f)

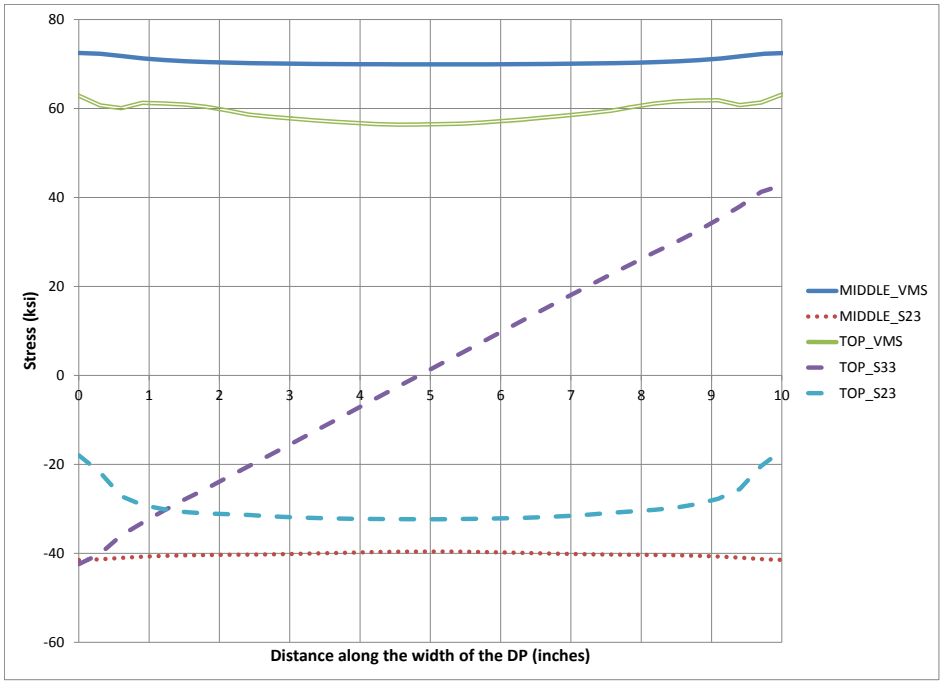

Figure 4.11: Stresses along the width of DP at 0.05 radian rotation (Case 2A_f)

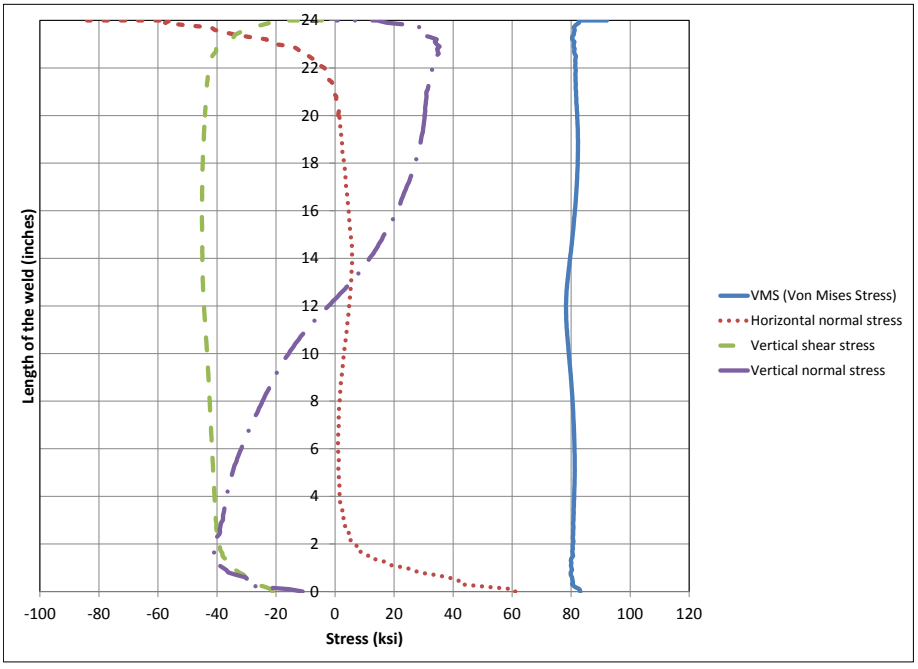

Figure 4.12: Stresses along depth of CJP1 (DP-CJP1 interface) at 0.05 radian (Case 2A_f)

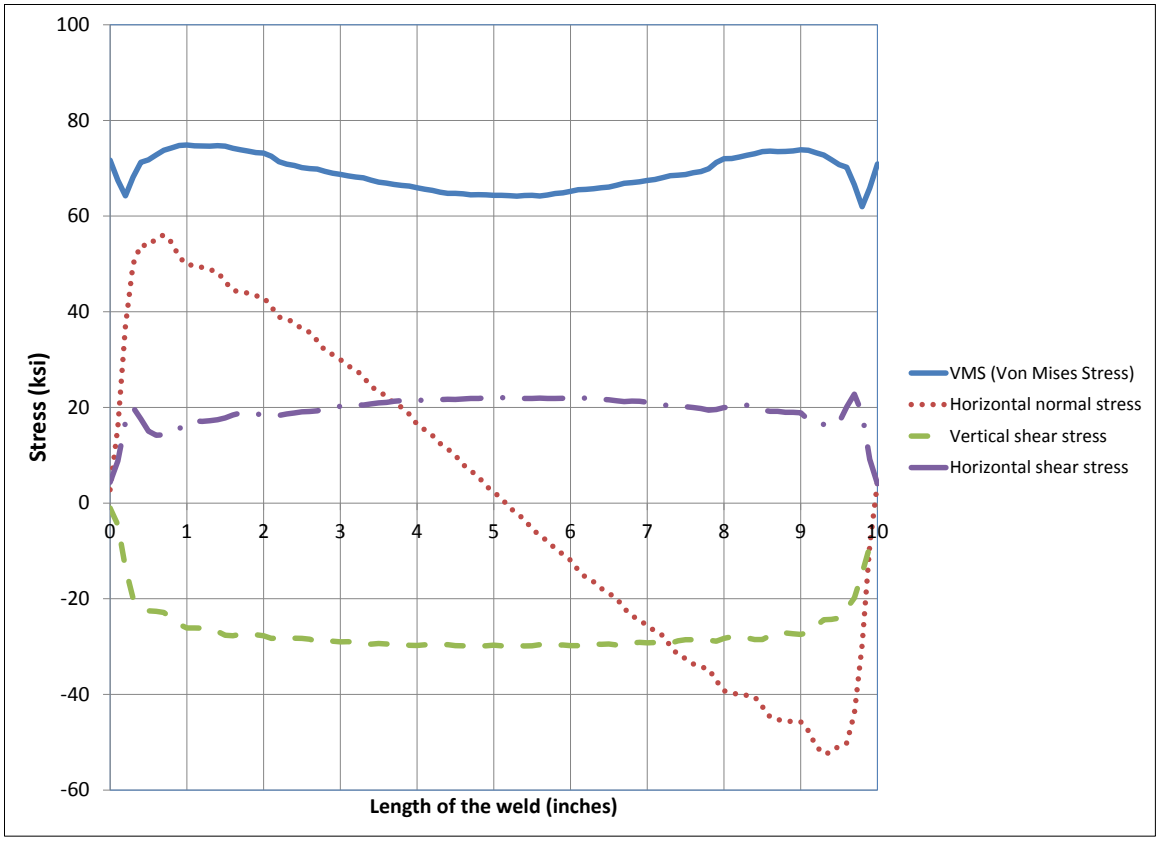

Figure 4.13: Stresses along the width of fillet weld (DP-fillet weld interface) at 0.05 radian rotation of panel zone (Case 2A_f)

4.2.4 Analysis case 3A

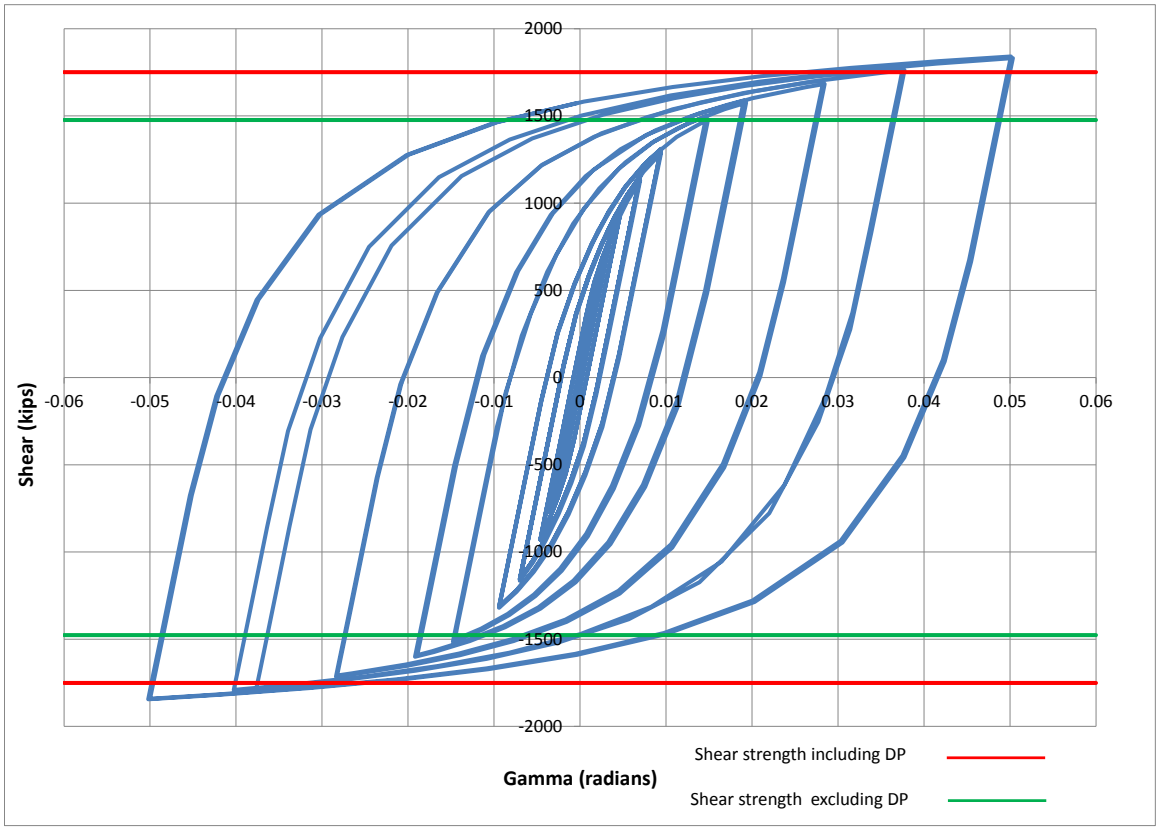

Figure 4.14: Panel zone shear versus rotation (Case 3A)

Table 4.5: Panel zone shear and force on loading plate (Case 3A)

Panel zone rotation (rad)	0.01	0.02	0.03	0.05
Panel zone shear (kips)	1311.51	1588.82	1705.02	1841.02
Force on one Loading plate (kips)	786.90	953.29	1023.01	1104.61

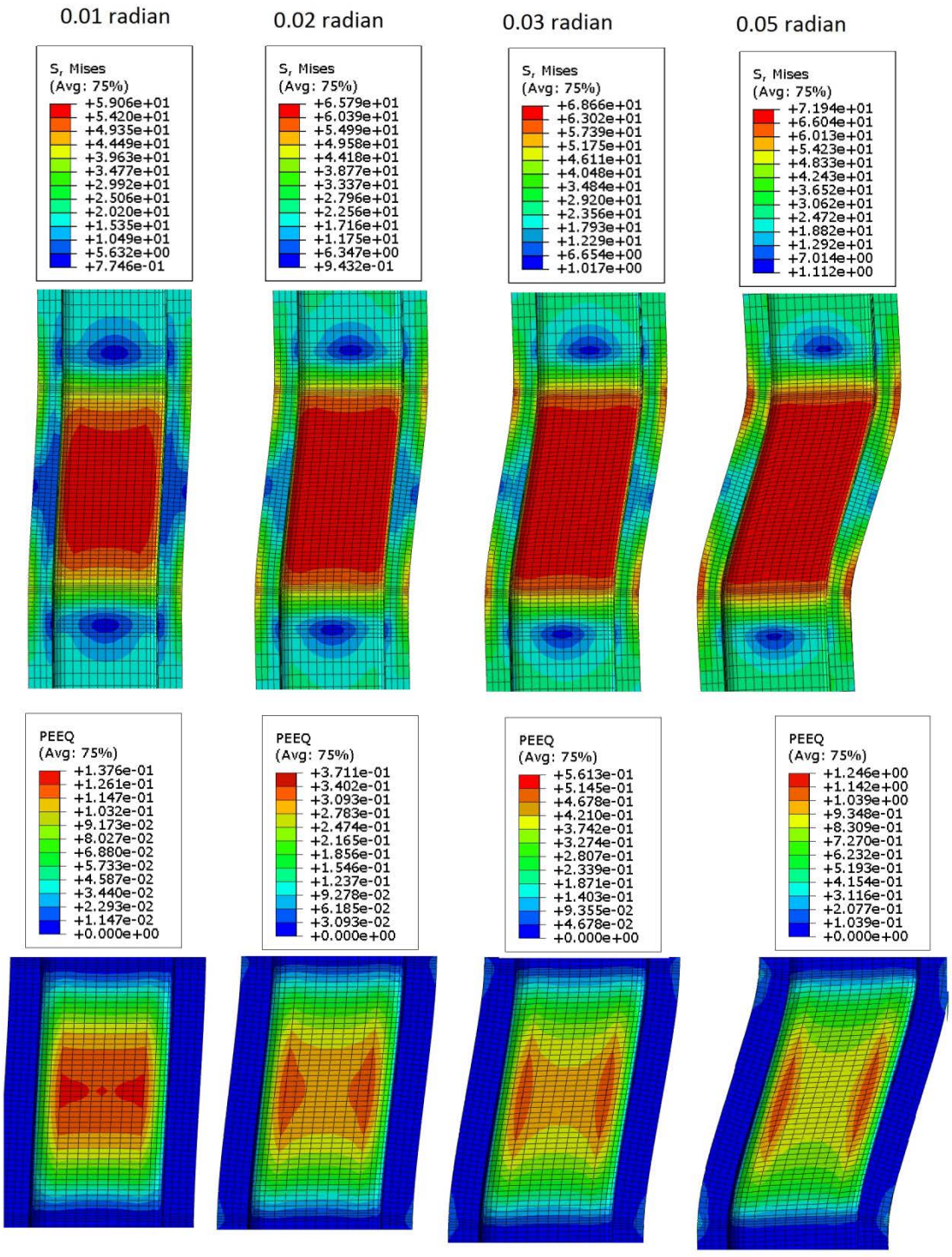

Figure 4.15: VMS and PEEQ in the column (Case 3A)

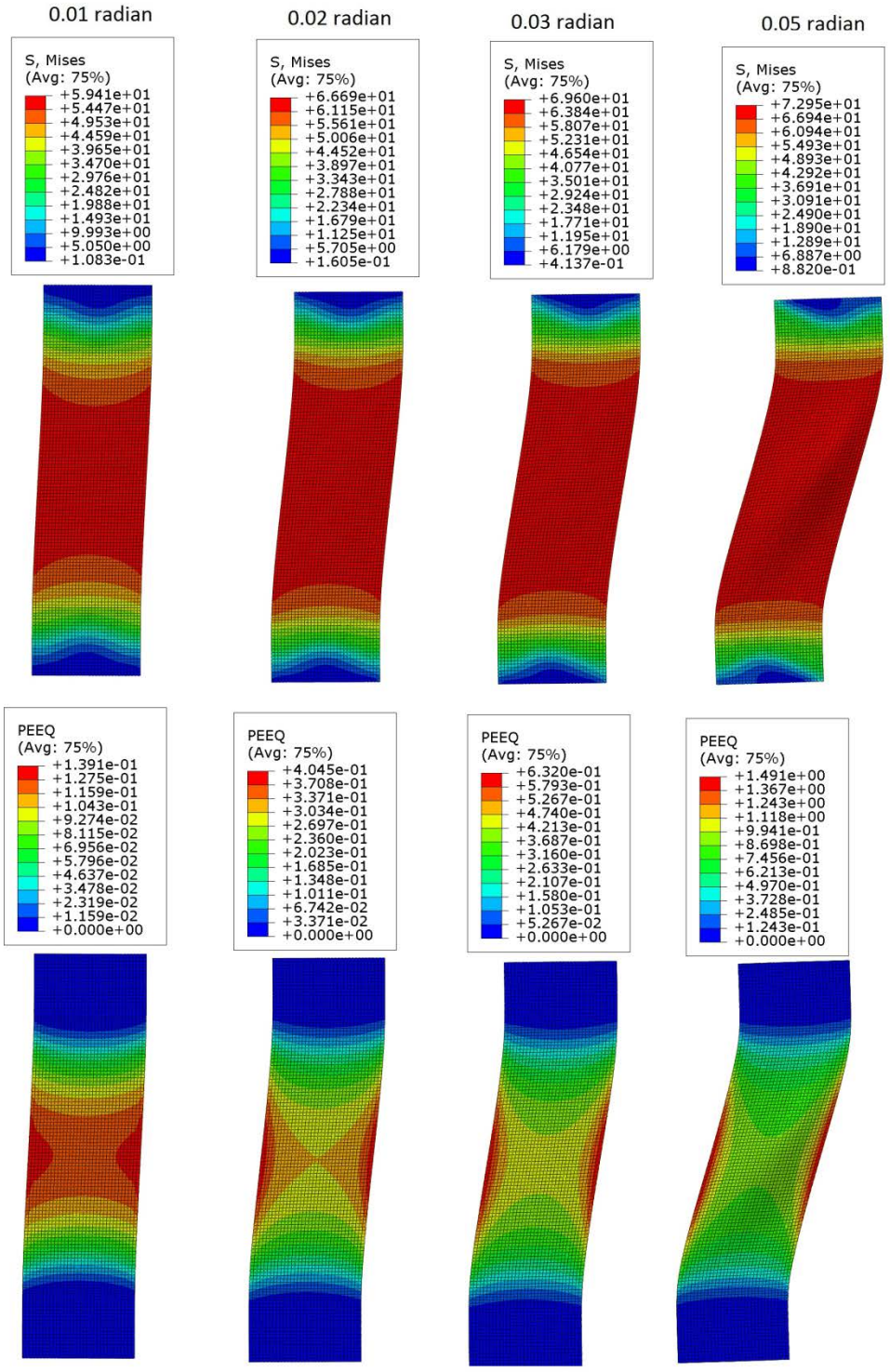

Figure 4.16: VMS and PEEQ in the DP (Case 3A)

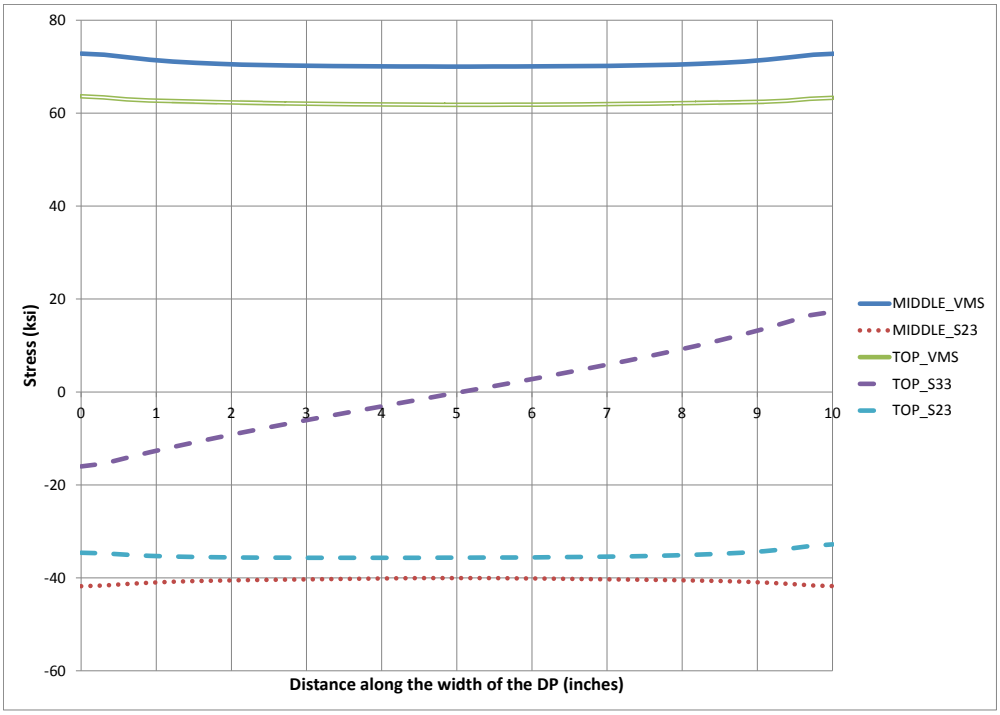

Figure 4.17: Stresses along the width of DP at 0.05 radian rotation (Case 3A)

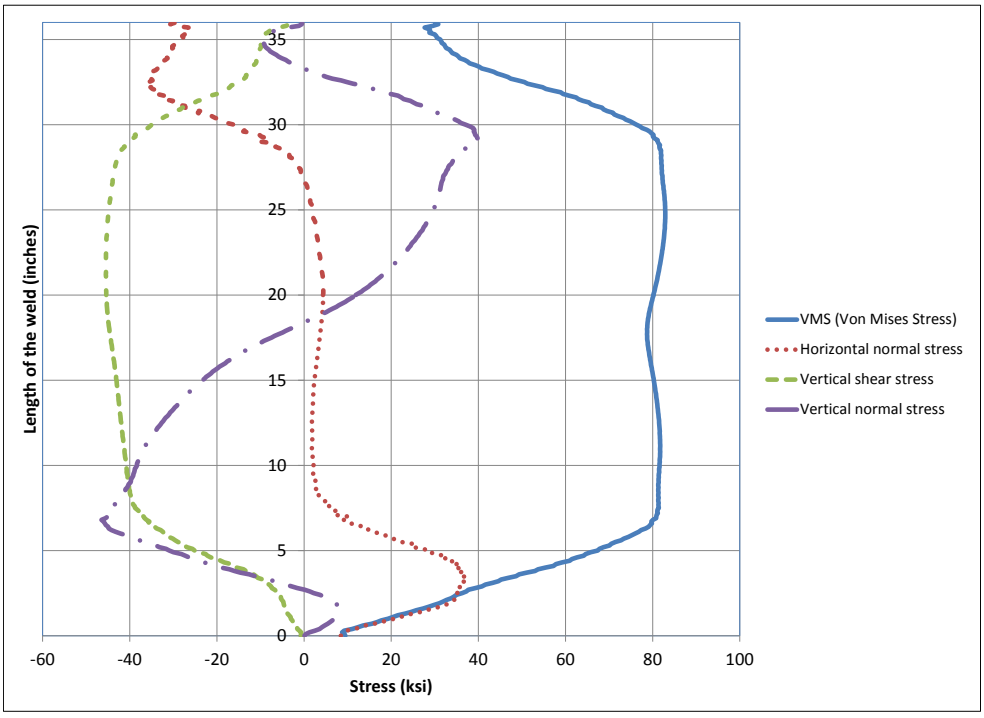

Figure 4.18: Stresses along depth of CJP1 (DP-CJP1 interface) at 0.05 radian (Case 3A)

4.2.5 Analysis case 3A_quar

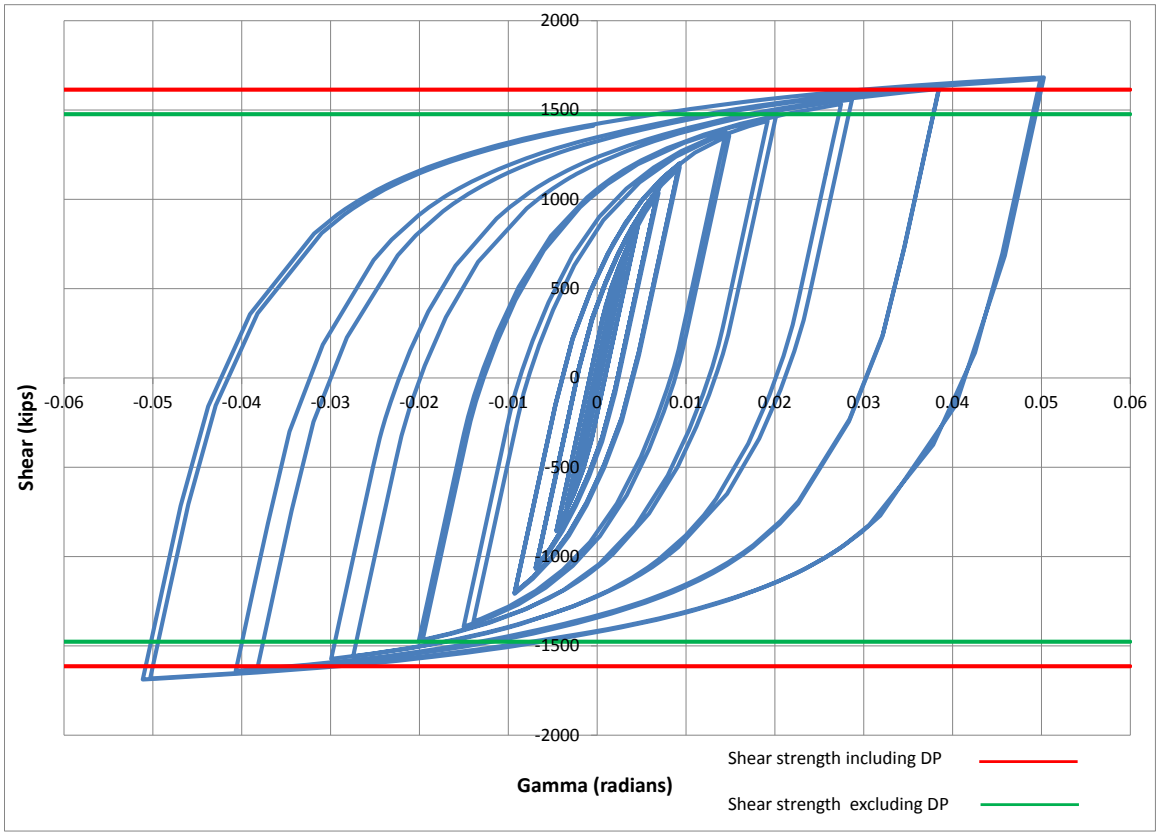

Figure 4.19: Panel zone shear versus rotation (Case 3A_quar)

Table 4.6: Panel zone shear and force on loading plate (Case 3A_quar)

Panel zone rotation (rad)	0.01	0.02	0.03	0.05
Panel zone shear (kips)	1201.19	1469.68	1558.95	1683.07
Force on one Loading plate (kips)	720.71	881.81	935.37	1009.84

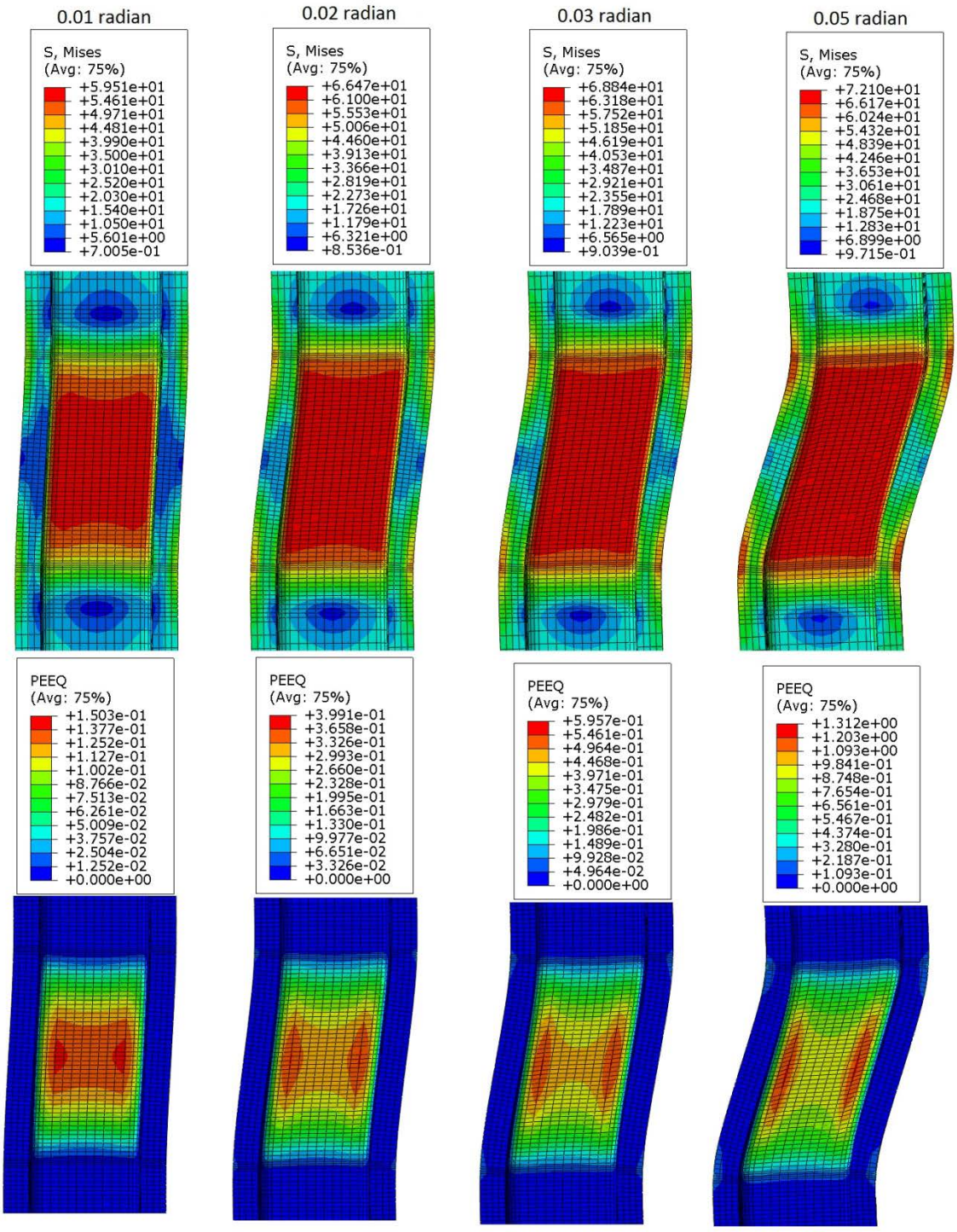

Figure 4.20: VMS and PEEQ in the column (Case 3A_quar)

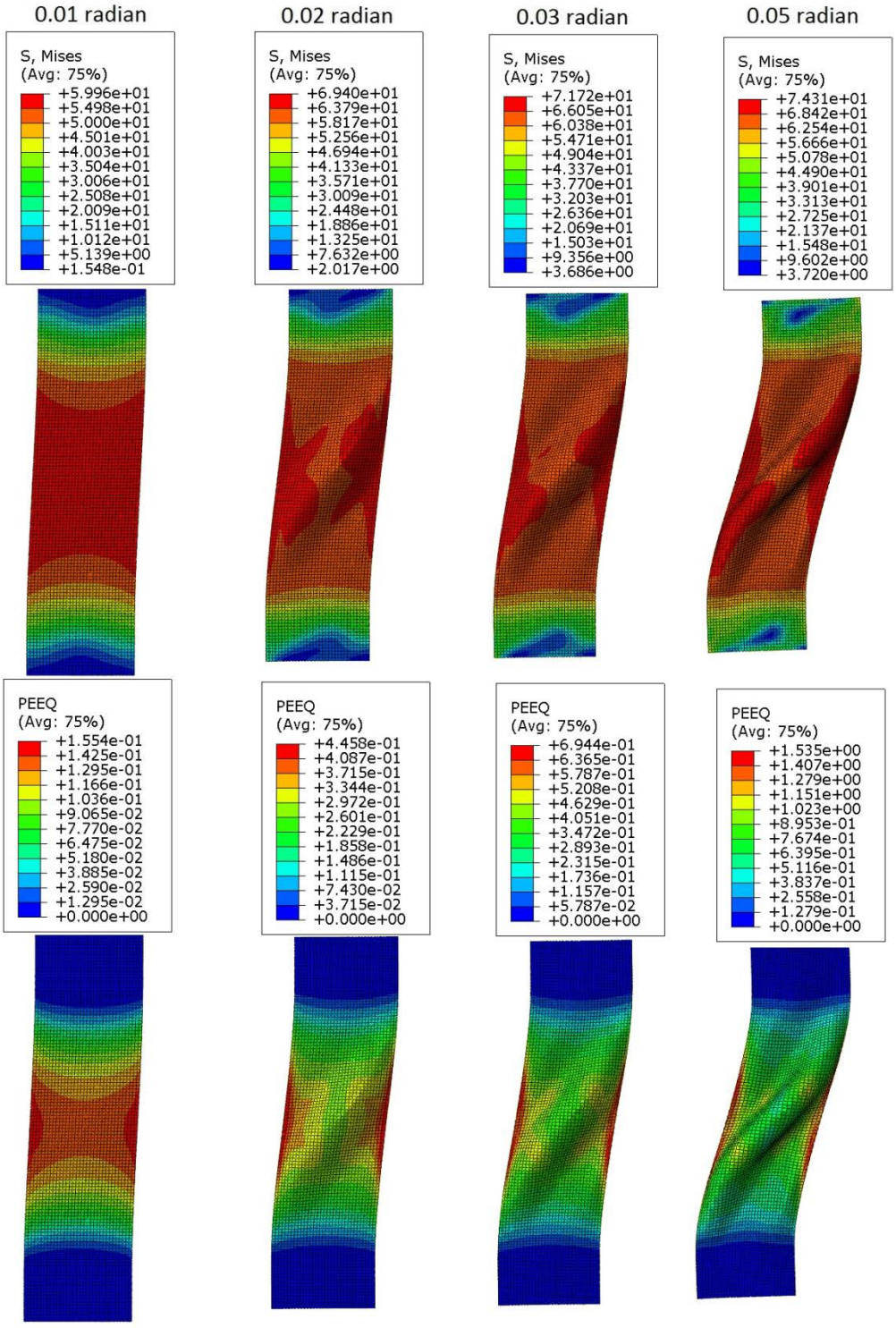

Figure 4.21: VMS and PEEQ in the DP (Case 3A_quar)

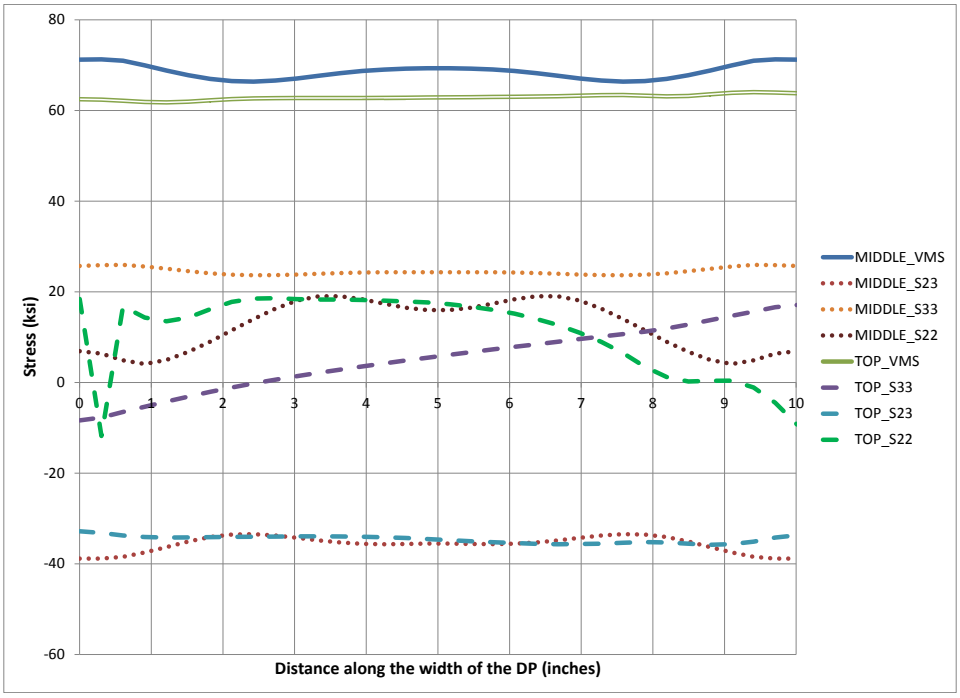

Figure 4.22: Stresses along the width of DP at 0.05 radian rotation (Case 3A_quar)

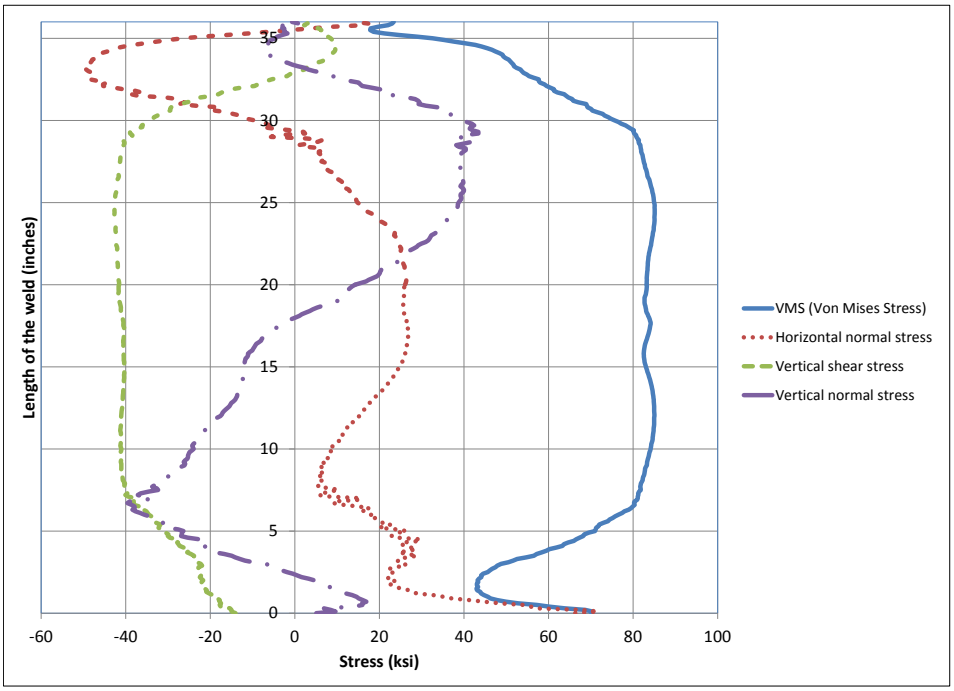

Figure 4.23: Stresses along depth of CJP1 (DP-CJP1 interface) at 0.05 radian (Case 3A_quar)

4.2.6 Analysis case 3A_one

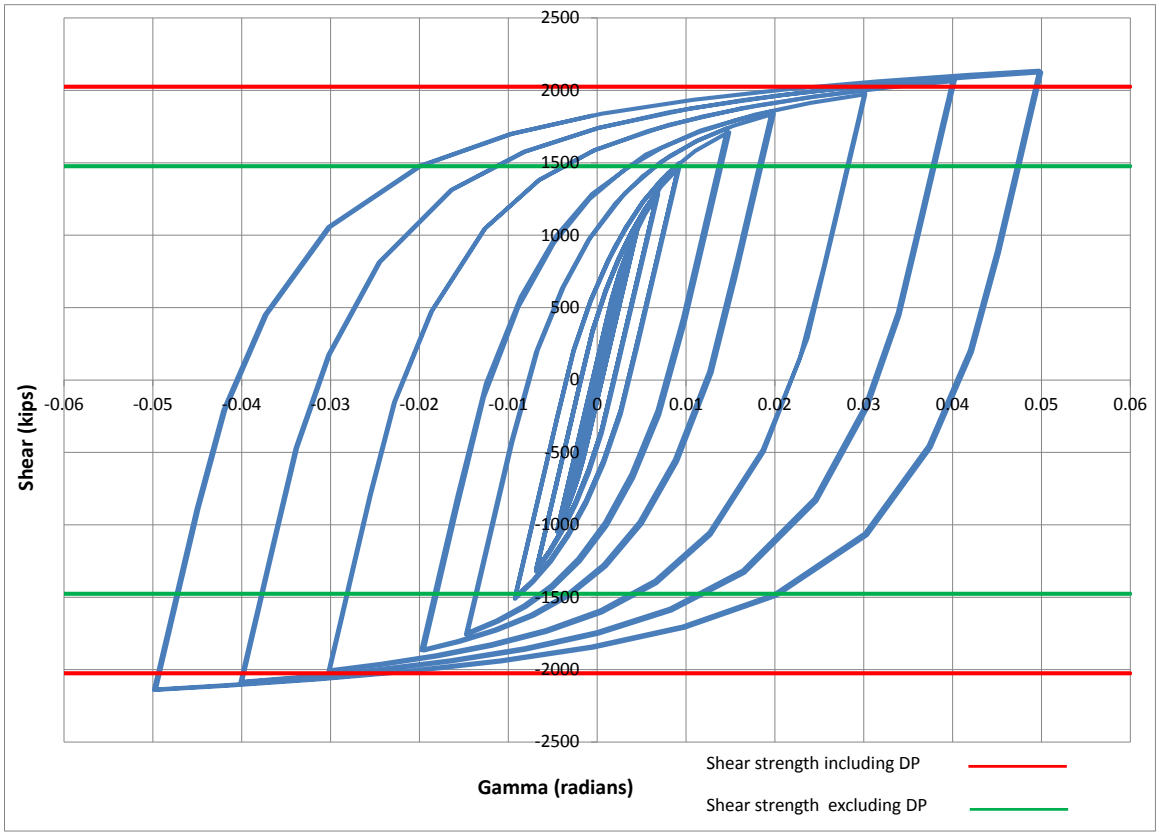

Figure 4.24: Panel zone shear versus rotation (Case 3A_one)

Table 4.7: Panel zone shear and force on loading plate (Case 3A_one)

Panel zone rotation (rad)	0.01	0.02	0.03	0.05
Panel zone shear (kips)	1499.47	1856.10	2001.20	2136.21
Force on one Loading plate (kips)	899.68	1113.66	1200.72	1281.72

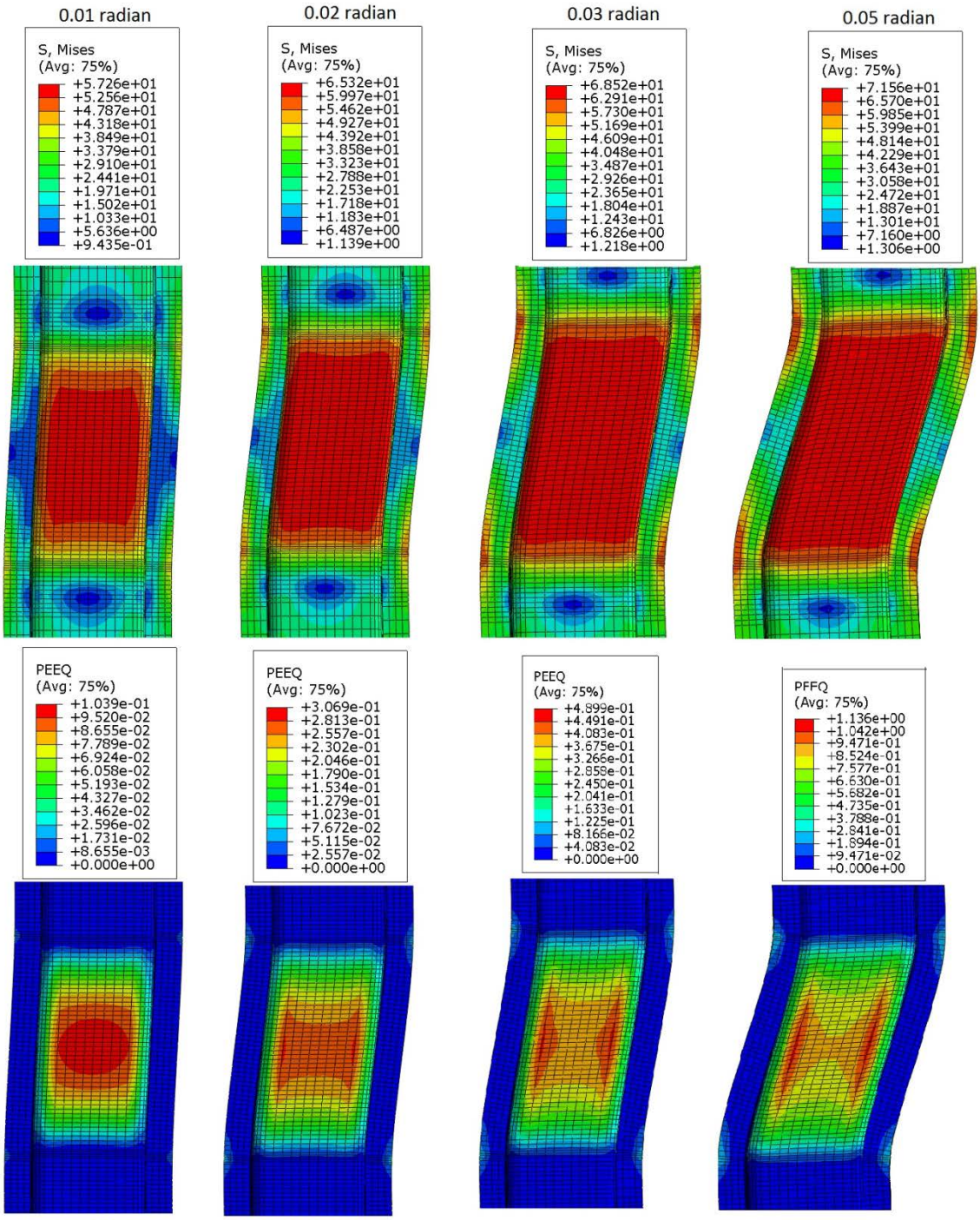

Figure 4.25: VMS and PEEQ in the column (Case 3A_one)

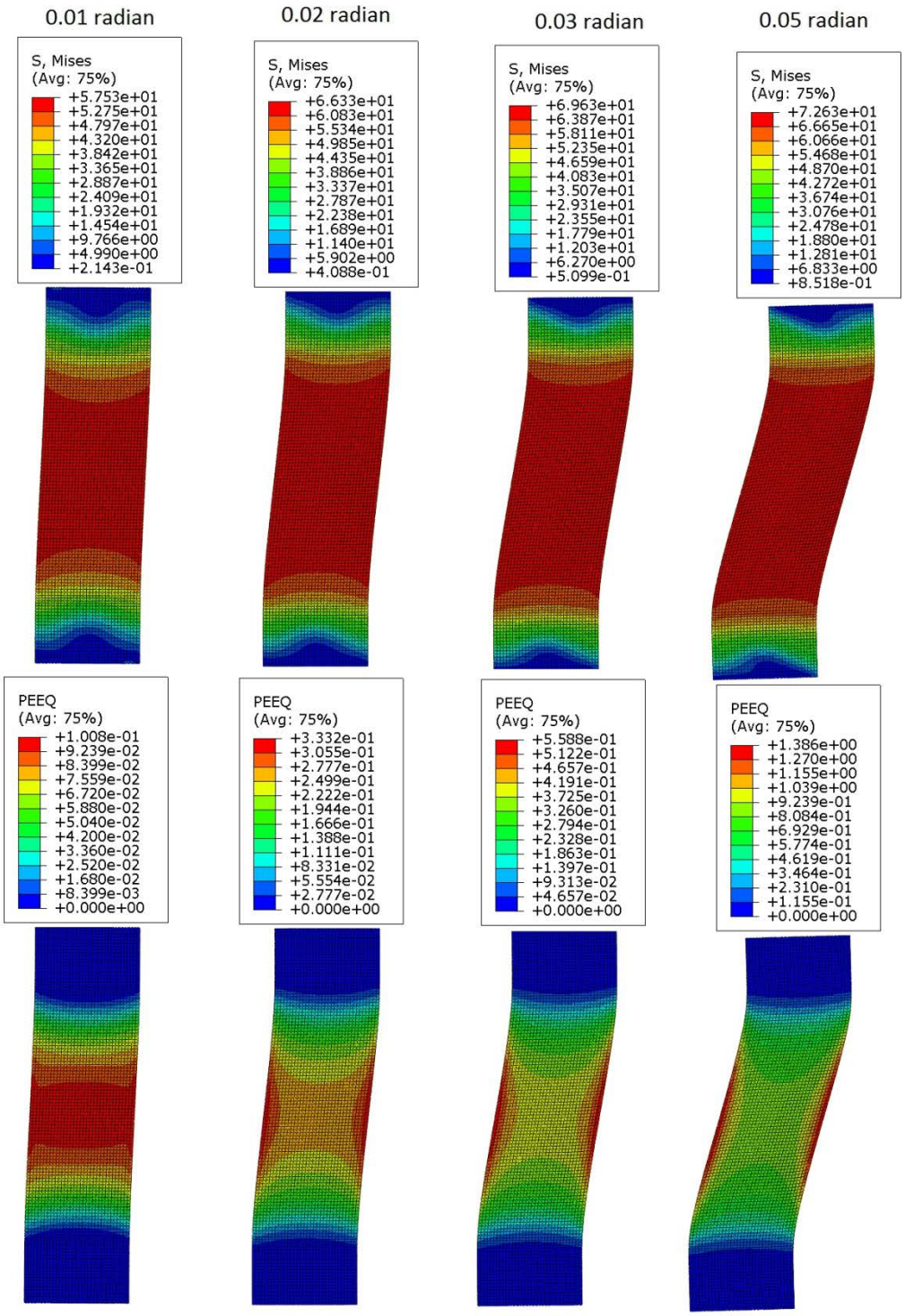

Figure 4.26: VMS and PEEQ in the DP (Case 3A_one)

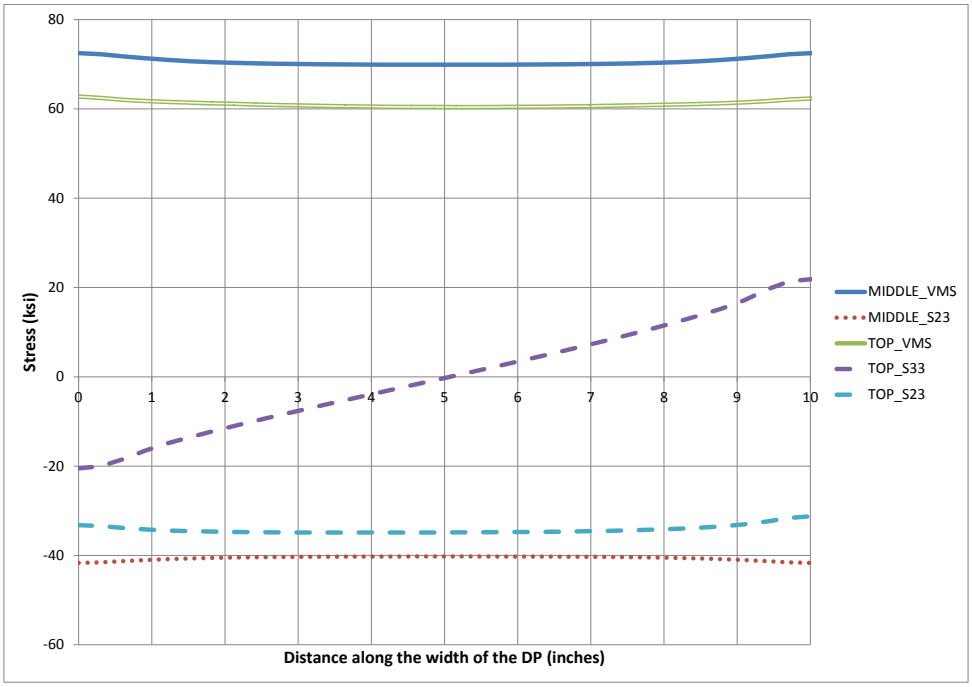

Figure 4.27: Stresses along the width of DP at 0.05 radian rotation (Case 3A_one)

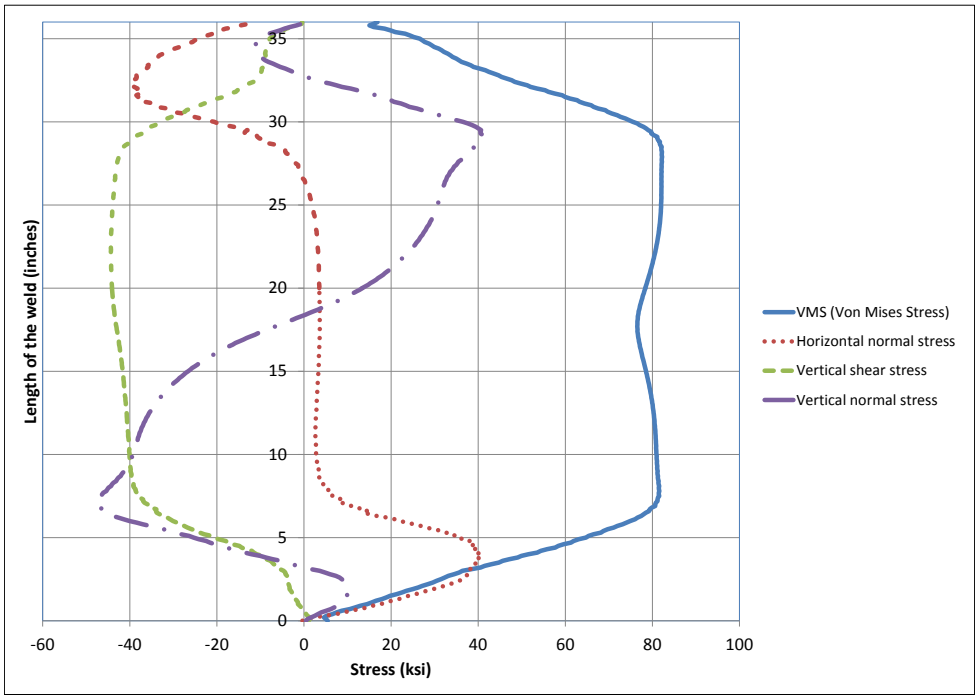

Figure 4.28: Stresses along depth of CJP1 (DP-CJP1 interface) at 0.05 radian (Case 3A_one)

4.2.7 Analysis case 4A

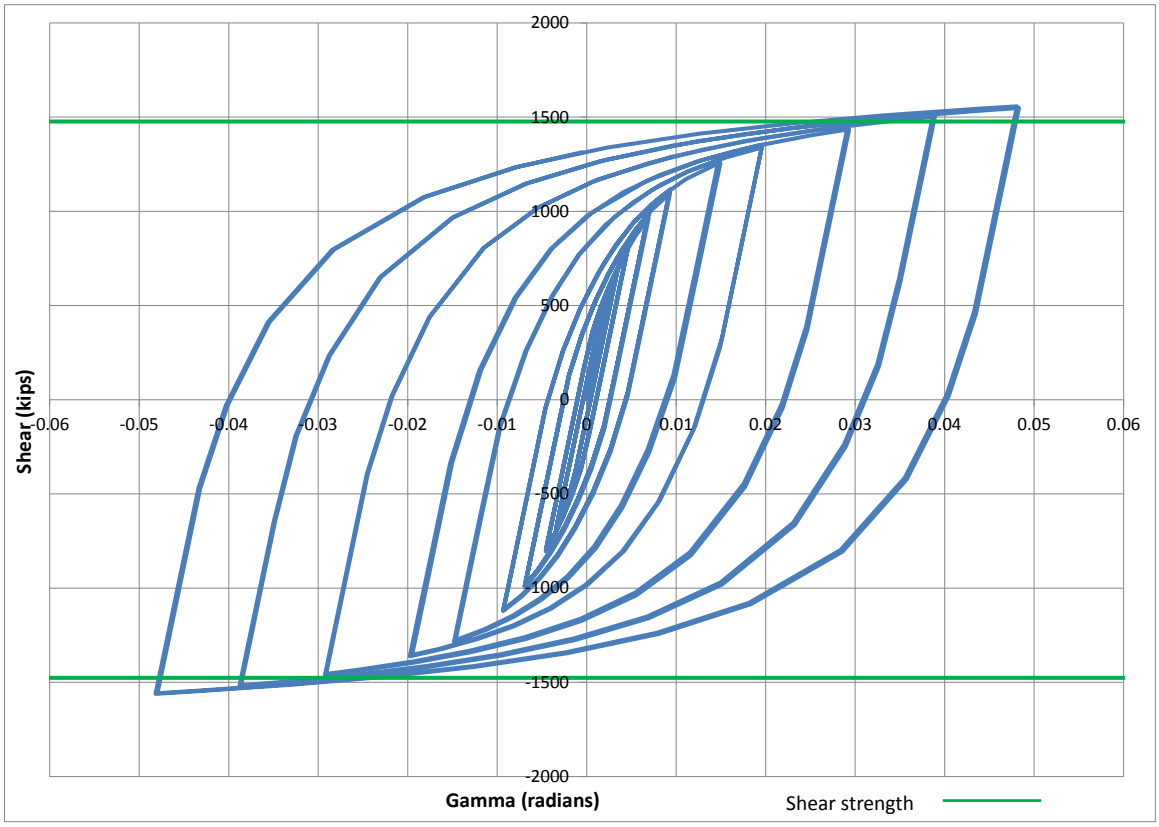

Figure 4.29: Panel zone shear versus rotation (Case 4A)

Table 4.8: Panel zone shear and force on loading plate (Case 4A)

Panel zone rotation (rad)	0.01	0.02	0.03	0.05
Panel zone shear (kips)	1115.64	1354.08	1452.98	1557.25
Force on one Loading plate (kips)	669.38	812.45	871.79	934.35

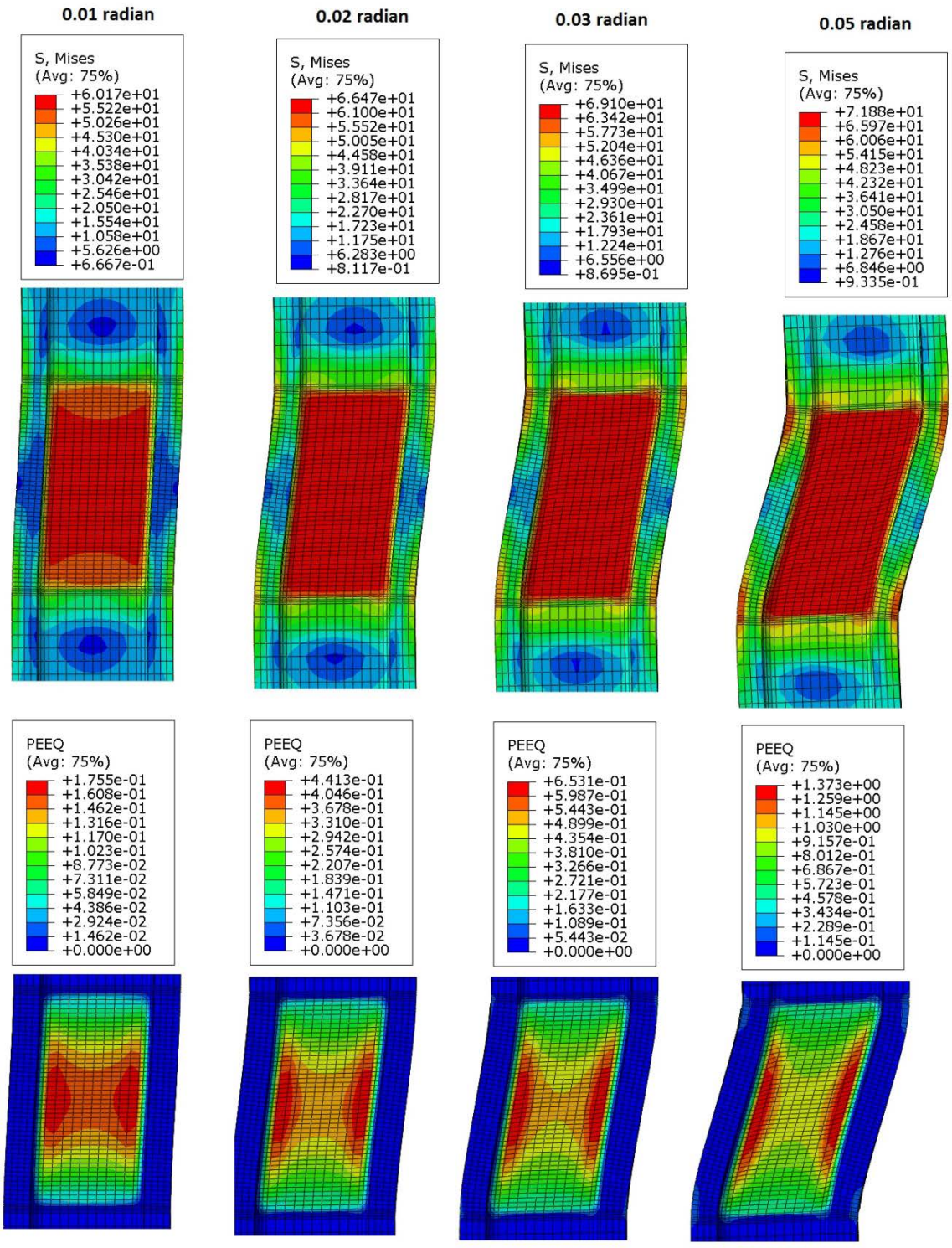

Figure 4.30: VMS and PEEQ in the column (Case 4A)

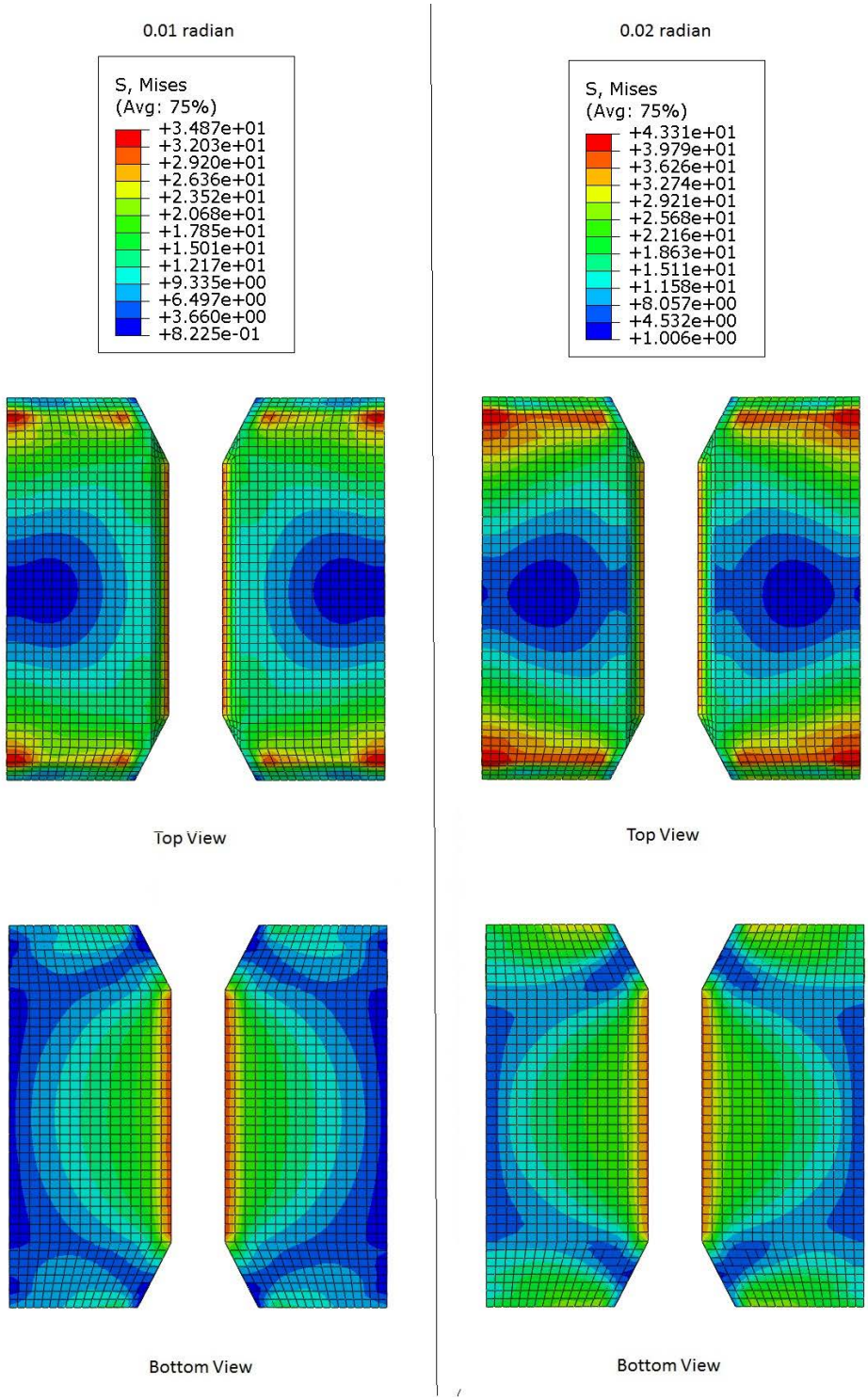

Figure 4.31: VMS in the CP at 0.01 and 0.02 radian rotation (Case 4A)

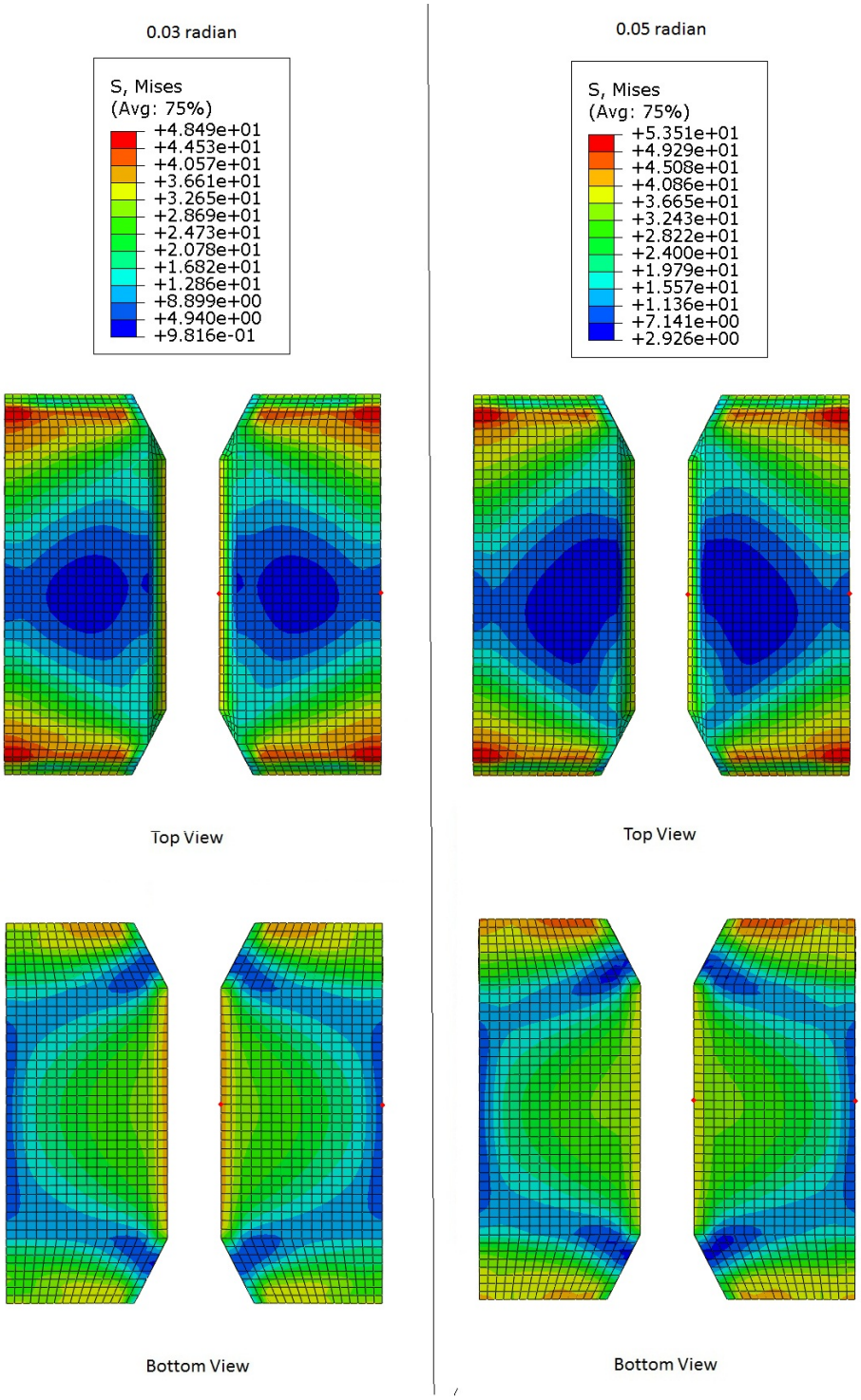

Figure 4.32: VMS in the CP at 0.03 and 0.05 radian rotation (Case 4A)

4.2.8 Analysis case 5A

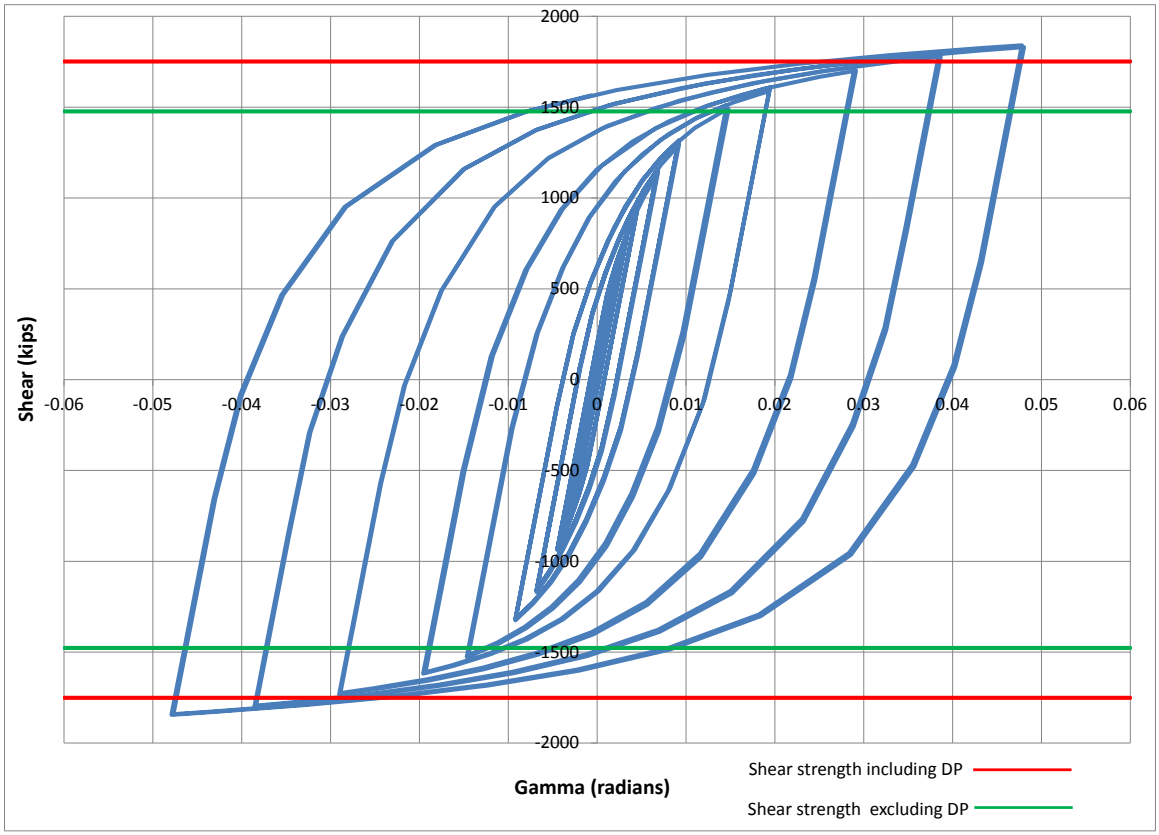

Figure 4.33: Panel zone shear versus rotation (Case 5A)

Table 4.9: Panel zone shear and force on loading plate (Case 5A)

Panel zone rotation (rad)	0.01	0.02	0.03	0.05
Panel zone shear (kips)	1316.93	1608.75	1722.16	1840.69
Force on one Loading plate (kips)	790.16	965.25	1033.30	1104.41

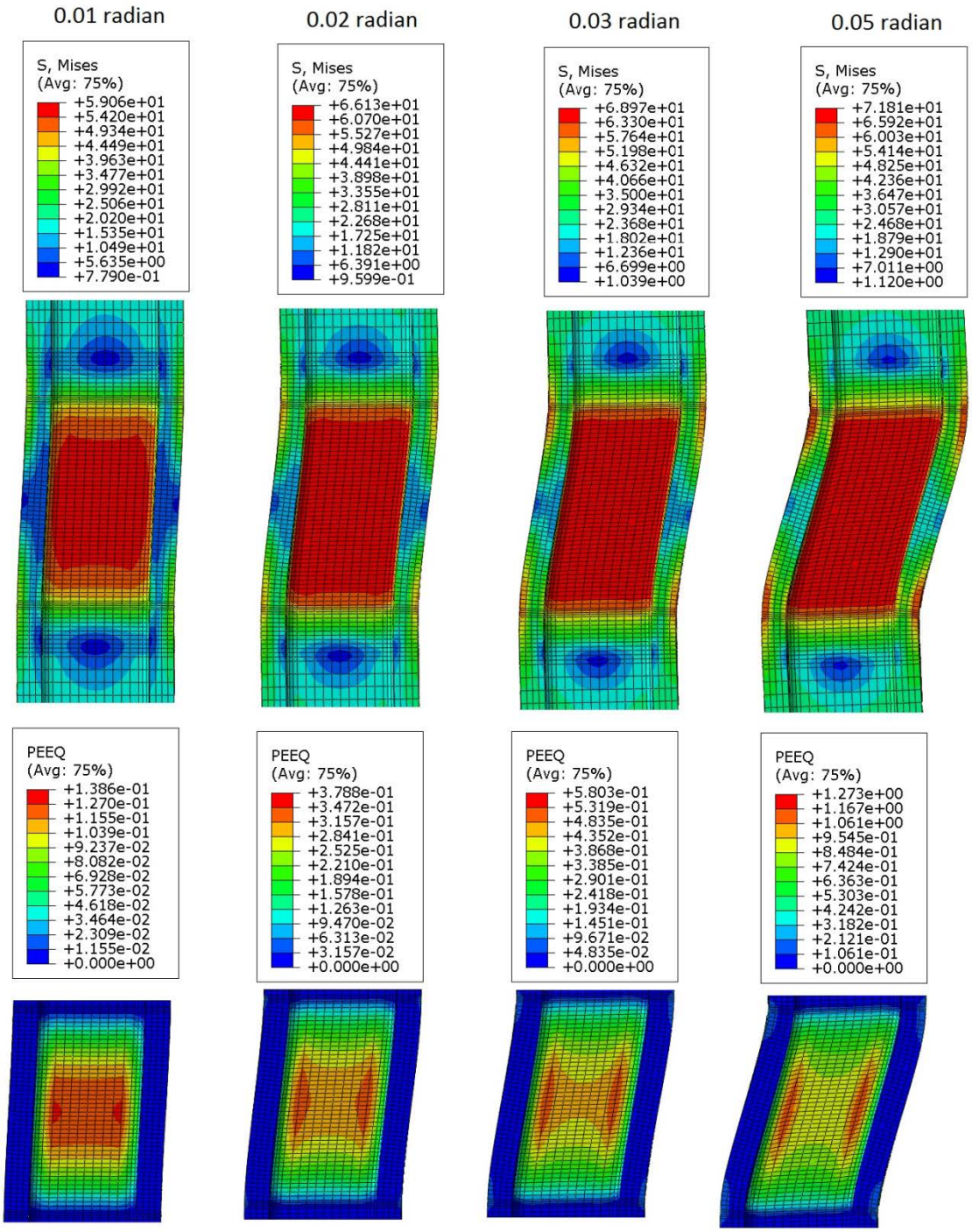

Figure 4.34: VMS and PEEQ in the column (Case 5A)

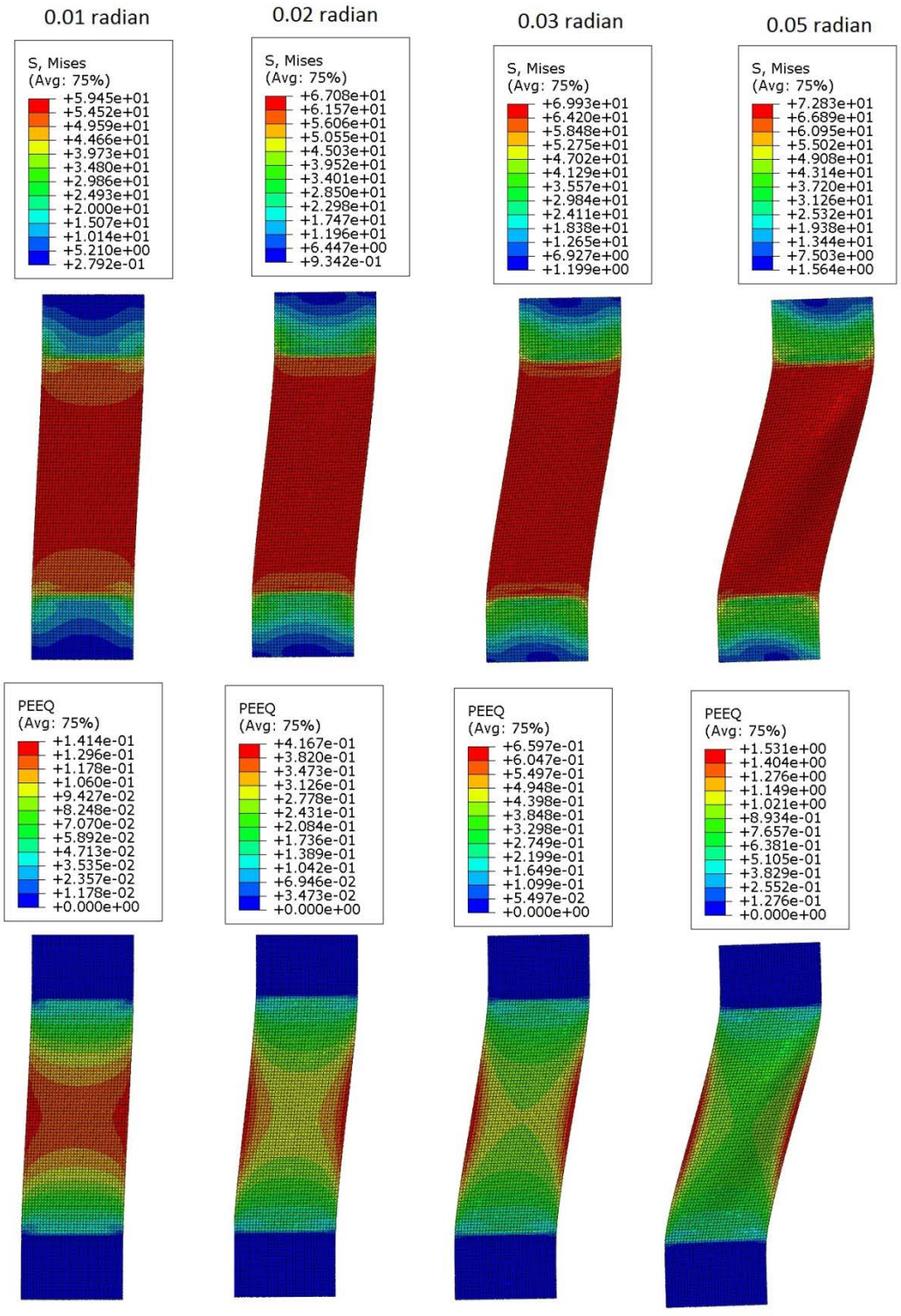

Figure 4.35: VMS and PEEQ in the DP (Case 5A)

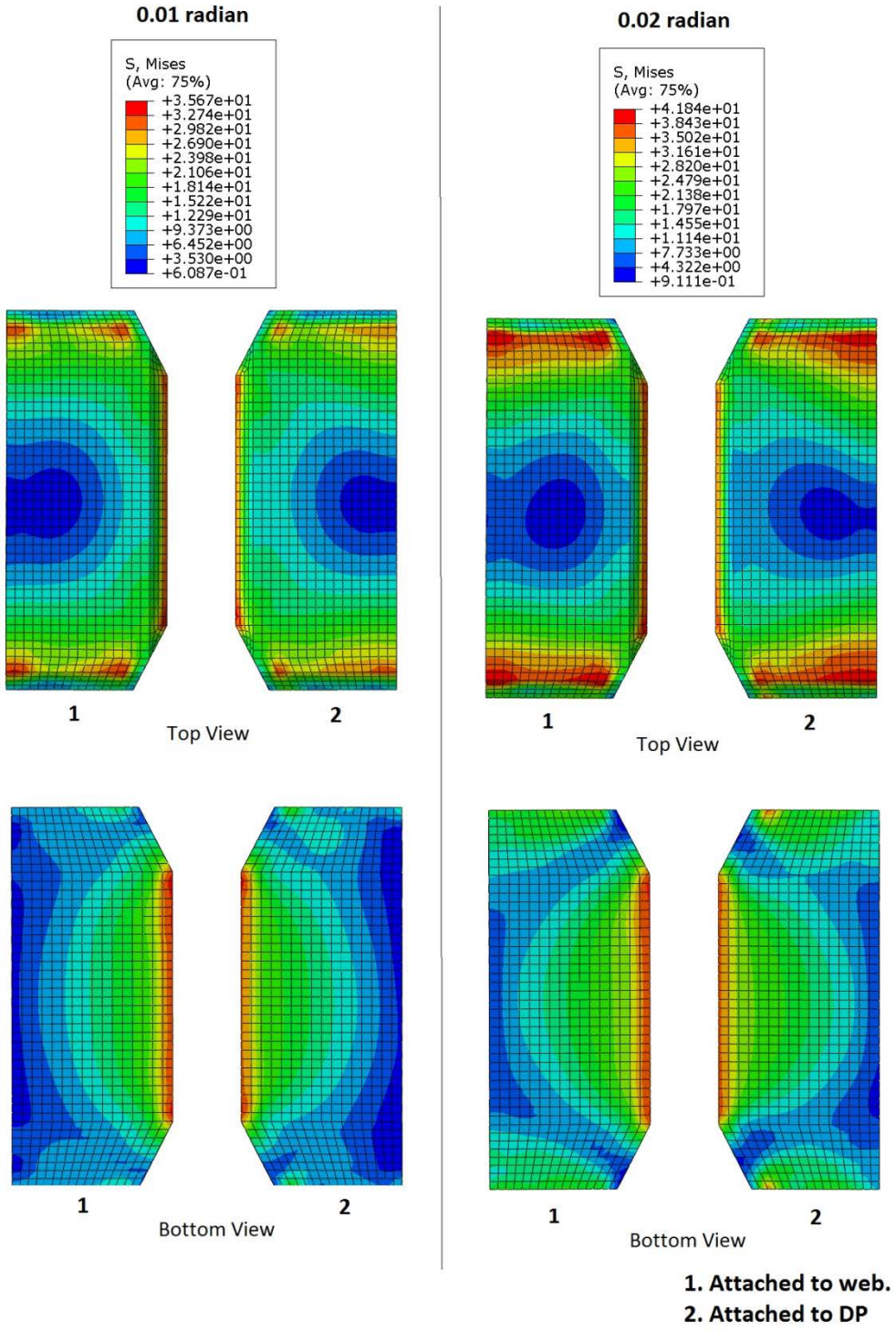

Figure 4.36: VMS in the CP at 0.01 and 0.02 radian rotation (Case 5A)

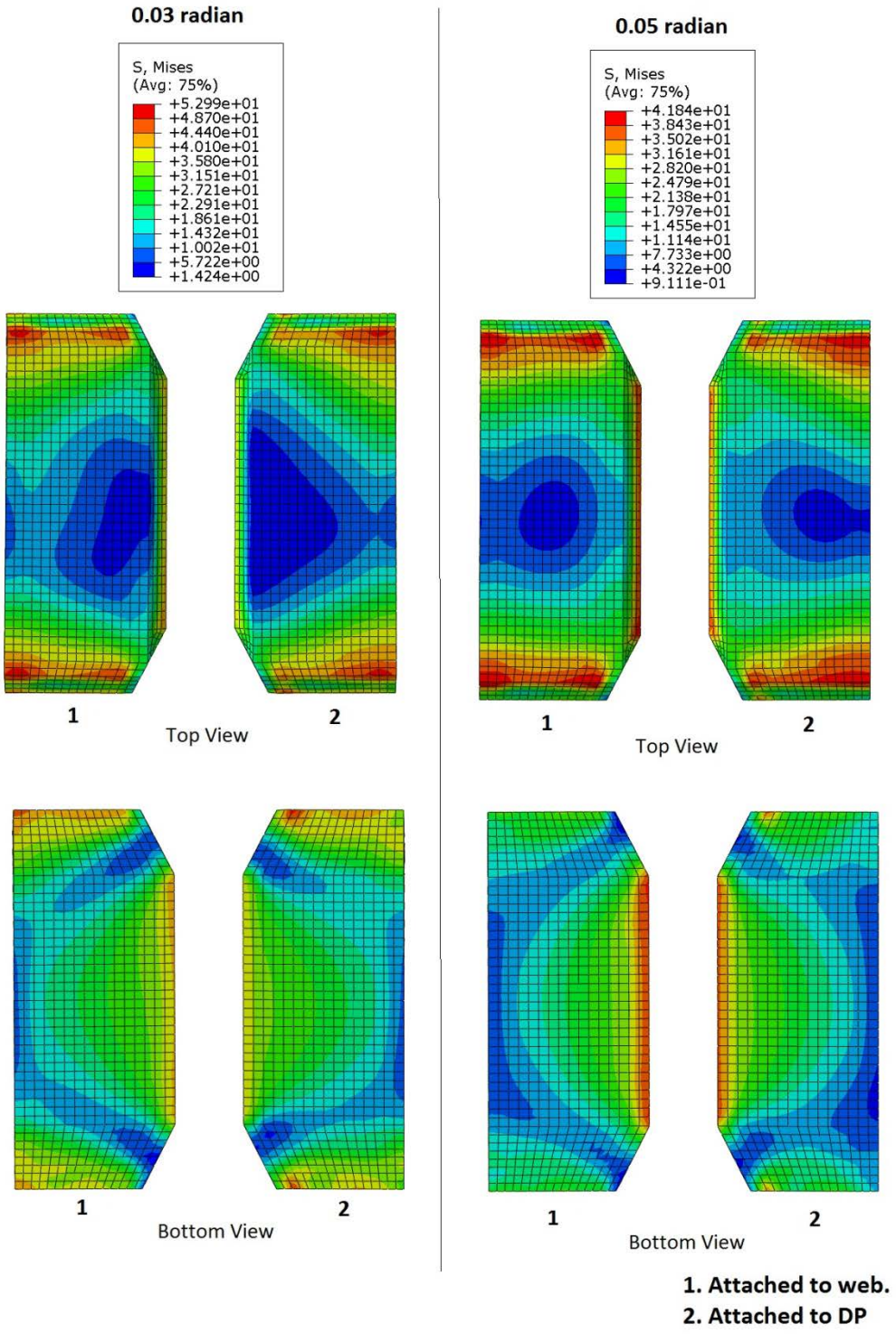

Figure 4.37: VMS in the CP at 0.03 and 0.05 radian rotation (Case 5A)

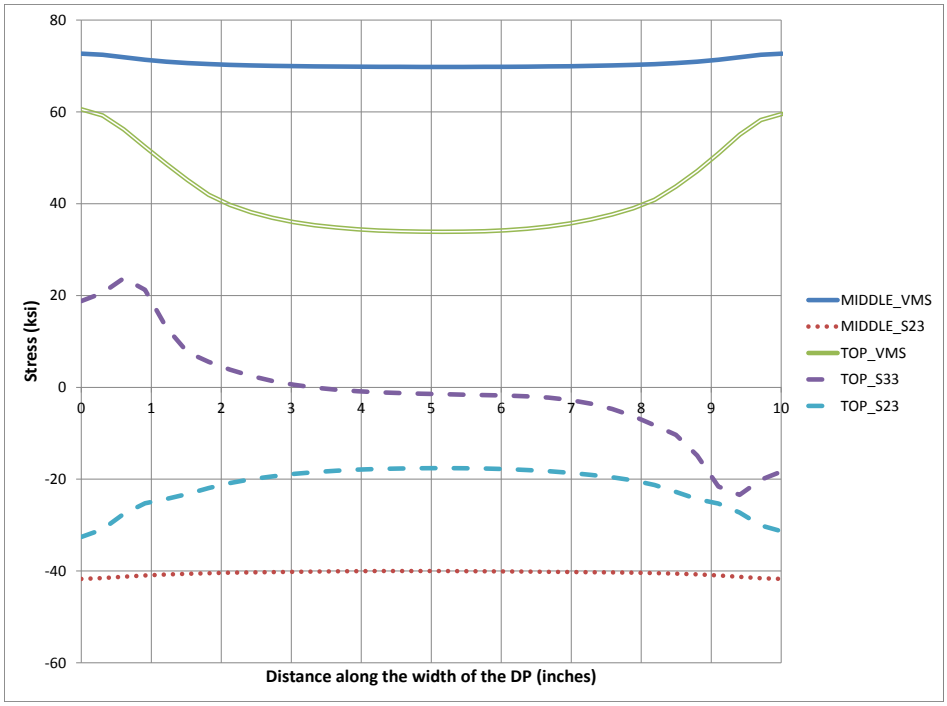

Figure 4.38: Stresses along the width of DP at 0.05 radian rotation (Case 5A)

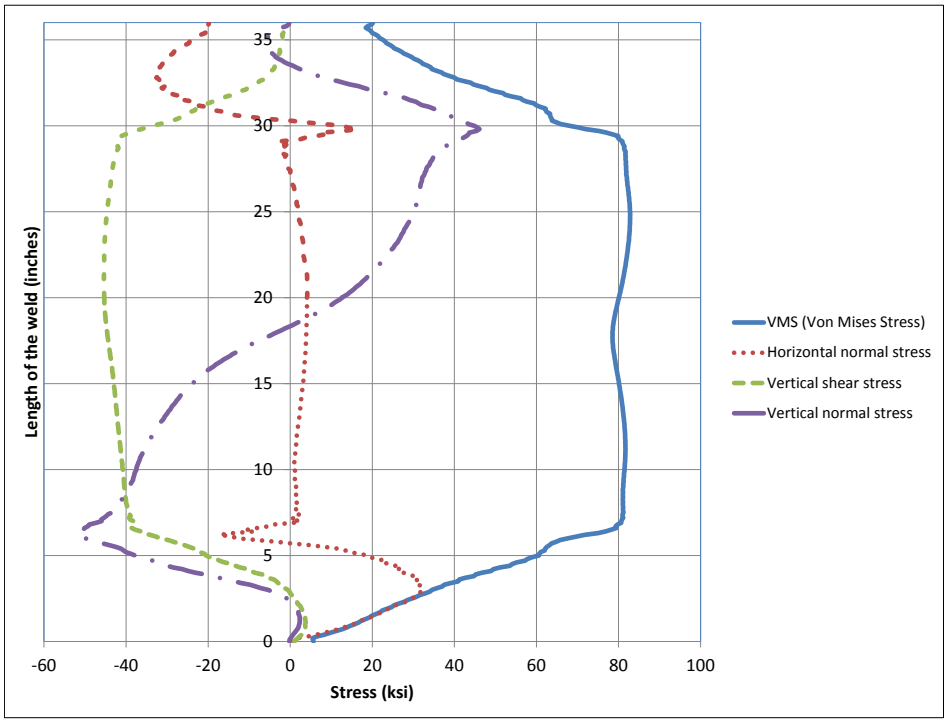

Figure 4.39: Stresses along depth of CJP1 (DP-CJP1 interface) at 0.05 radian (Case 5A)

4.2.9 Analysis case 5A_quar

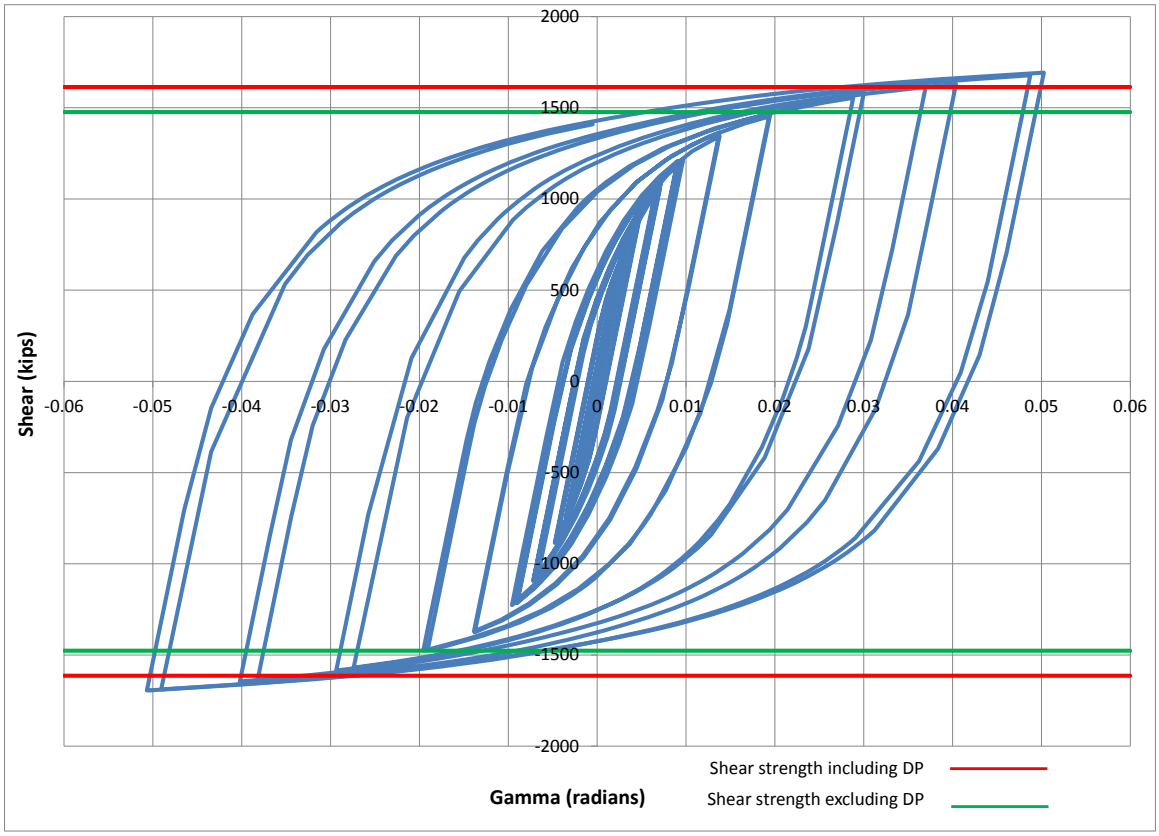

Figure 4.40: Panel zone shear versus rotation (Case 5A_quar)

Table 4.10: Panel zone shear and force on loading plate (Case 5A_quar)

Panel zone rotation (rad)	0.01	0.02	0.03	0.05
Panel zone shear (kips)	1208.93	1468.02	1581.98	1692.71
Force on one Loading plate (kips)	725.36	880.81	949.19	1015.62

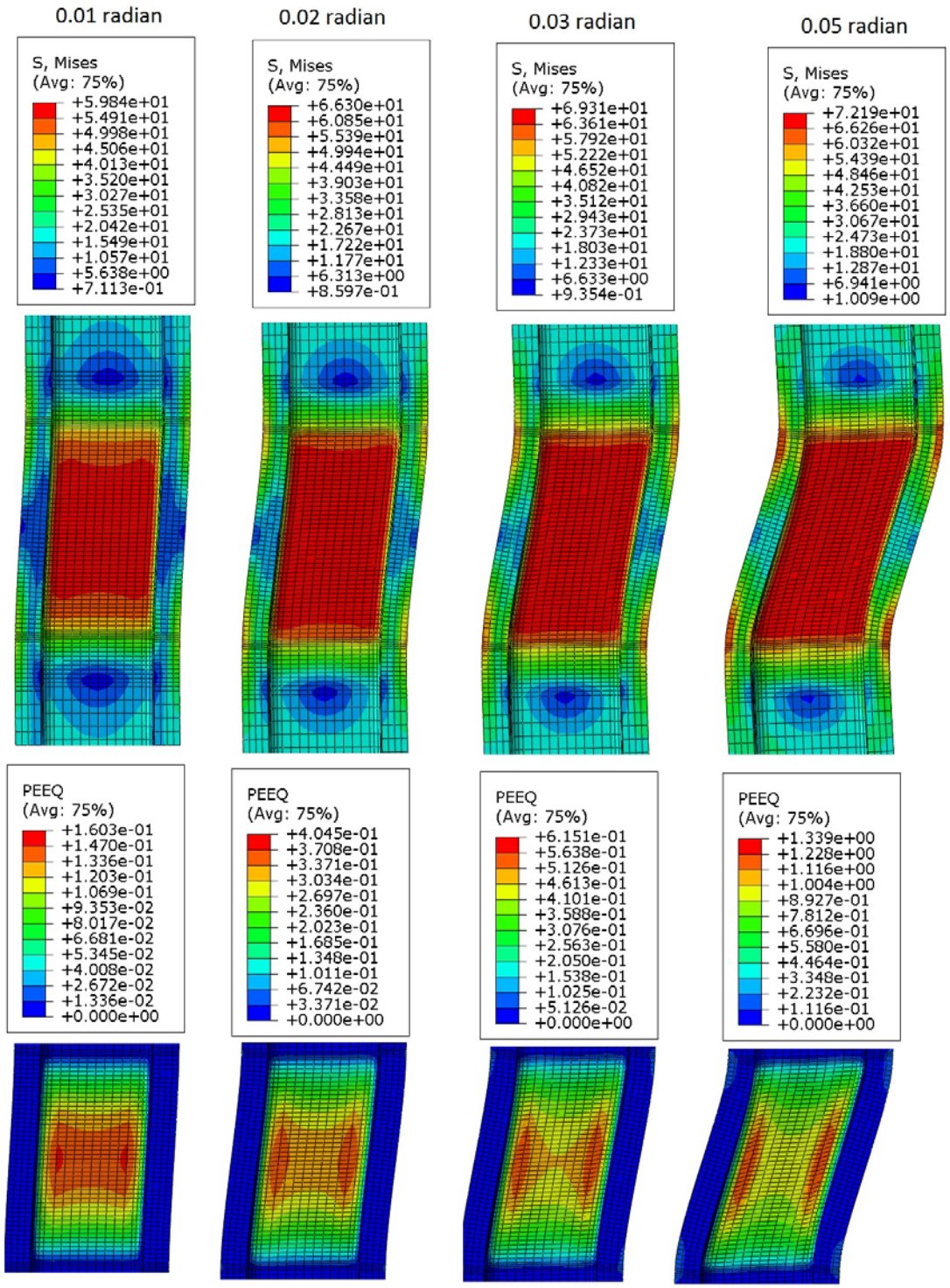

Figure 4.41: VMS and PEEQ in the column at different rotation (Case 5A_quar)

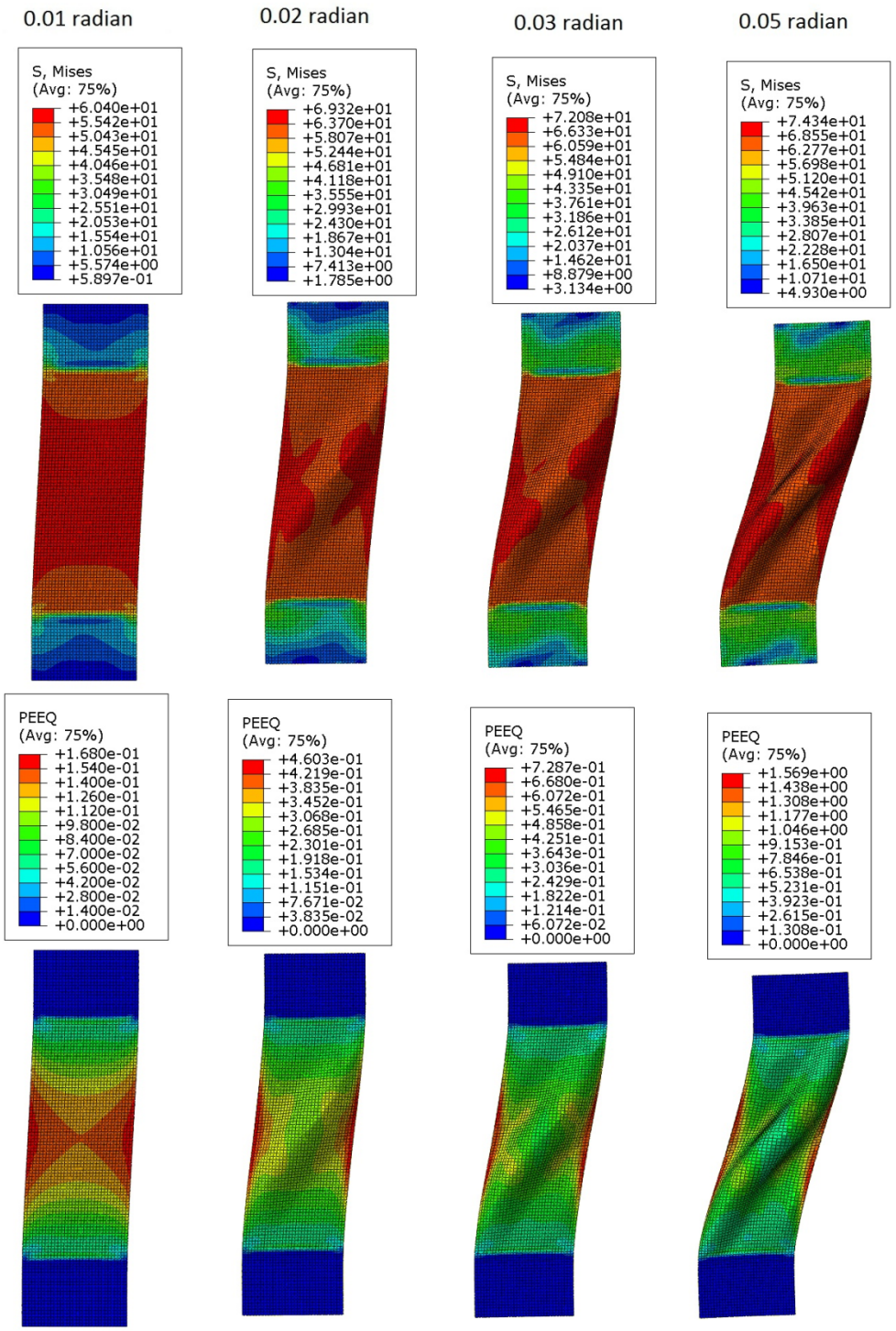

Figure 4.42: VMS and PEEQ in the DP at different rotations (Case 5A_quar)

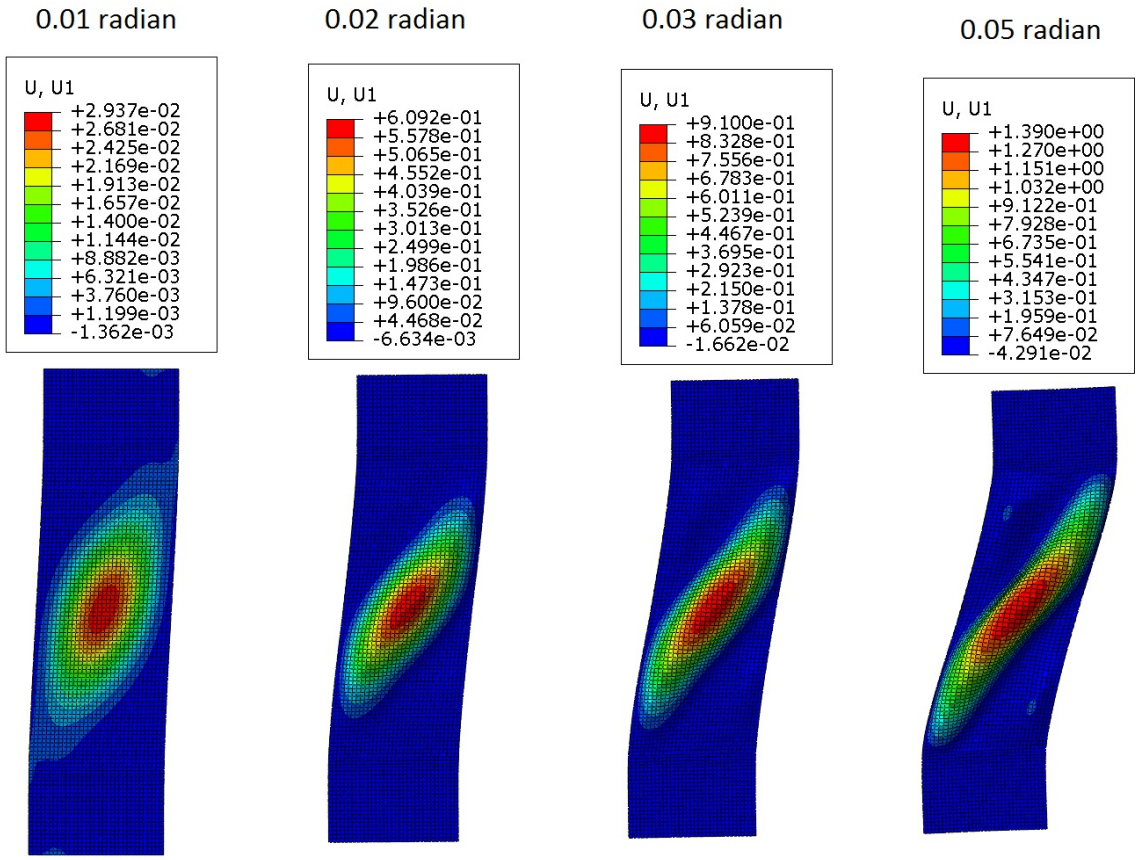

Figure 4.43: Out of plane displacement (U1) in the DP (Case 5A_quar)

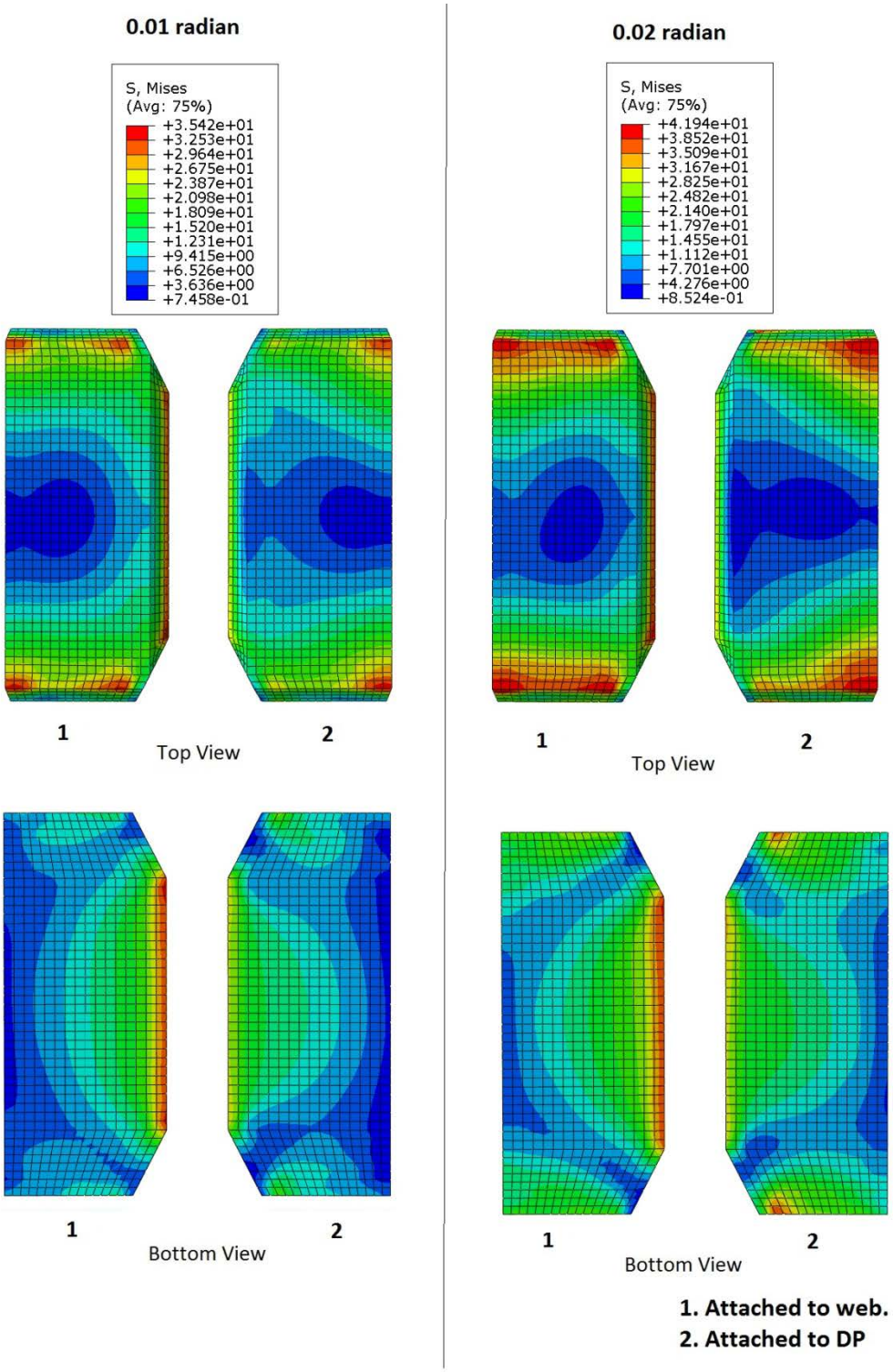

Figure 4.44: VMS in the CP at 0.01 and 0.02 radian rotation (Case 5A_quar)

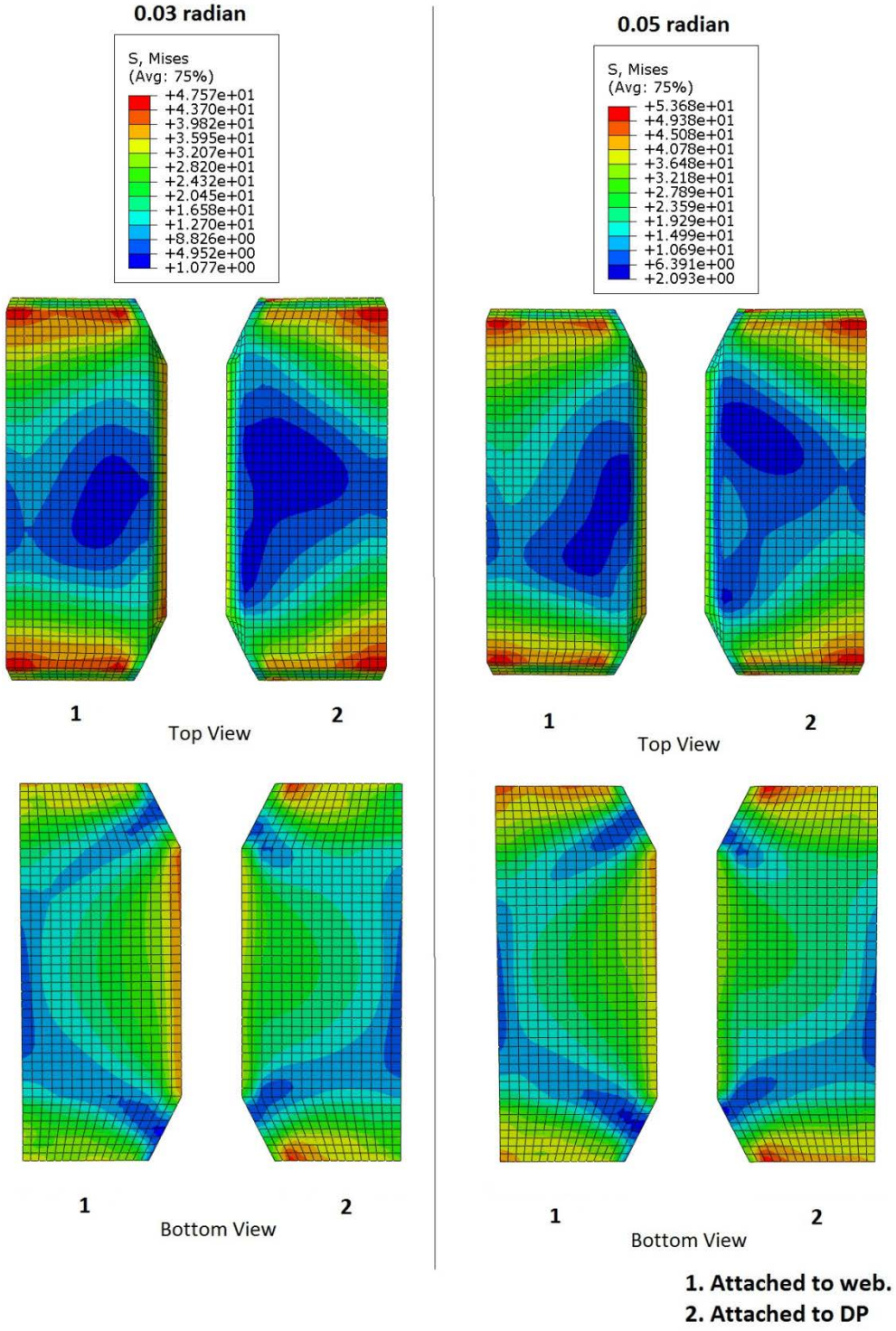

Figure 4.45: VMS in the CP at 0.03 and 0.05 radian rotation (Case 5A_quar)

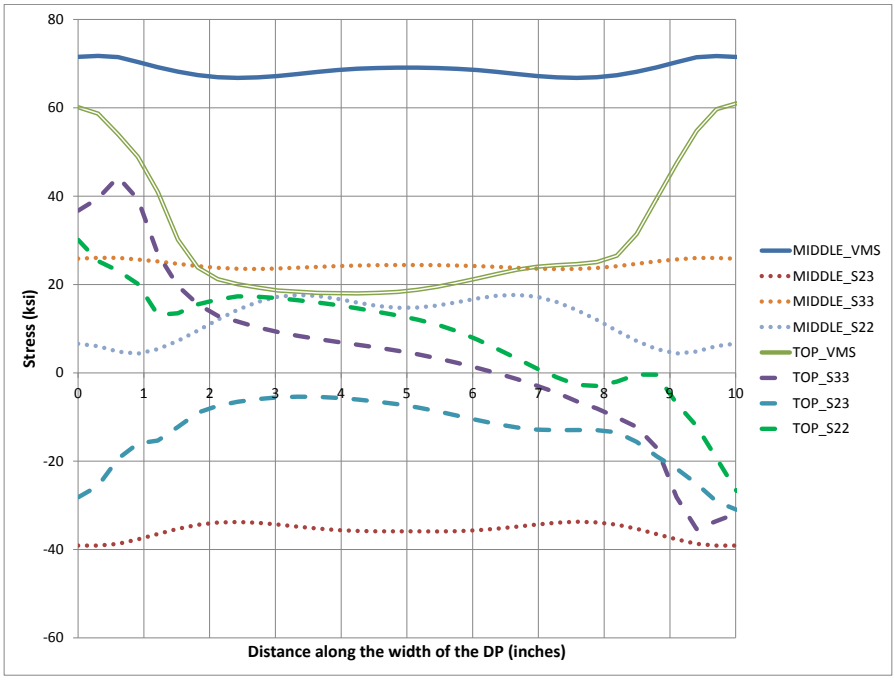

Figure 4.46: Stresses along the width of DP at 0.05 radian rotation (Case 5A_quar)

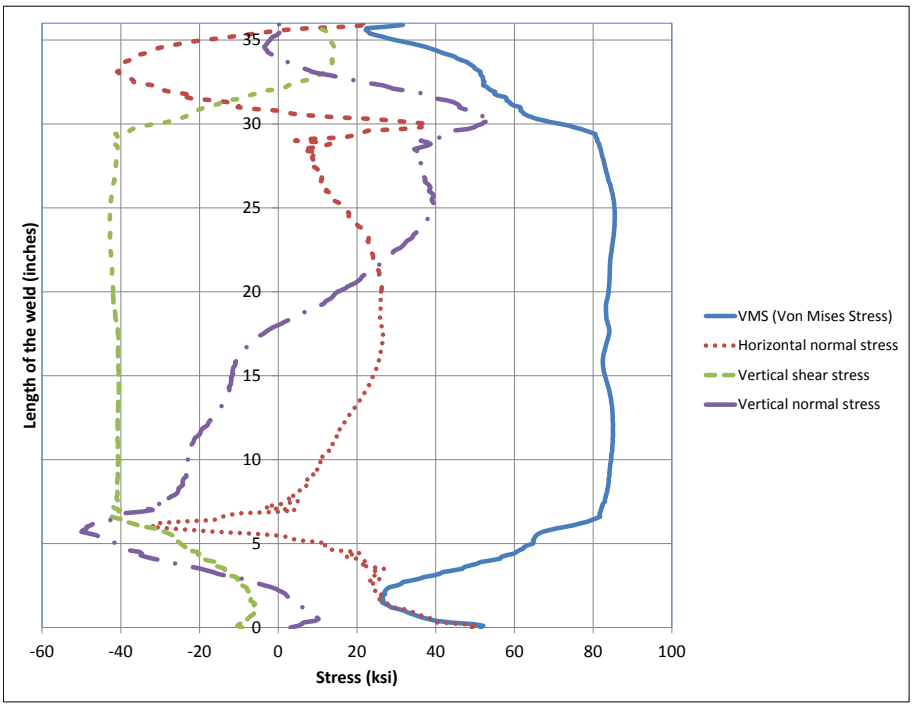

Figure 4.47: Stresses along depth of CJP1 (DP-CJP1 interface) at 0.05 radian (Case 5A_quar)

4.2.10 Analysis case 5A_one

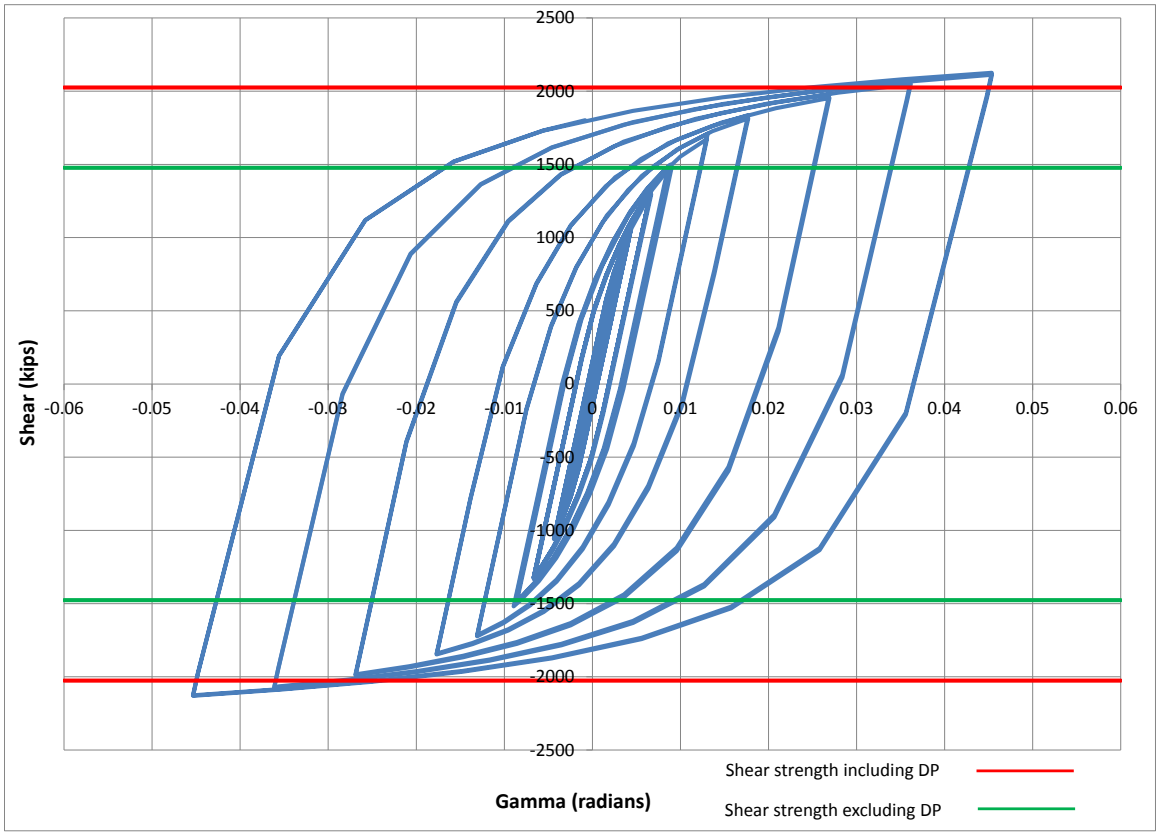

Figure 4.48: Panel zone shear versus rotation (Case 5A_one)

Table 4.11: Panel zone shear and force on loading plate (Case 5A_one)

Panel zone rotation (rad)	0.01	0.02	0.03	0.05
Panel zone shear (kips)	1485.81	1836.19	1979.67	2125.12
Force on one Loading plate (kips)	891.48	1101.71	1187.80	1275.07

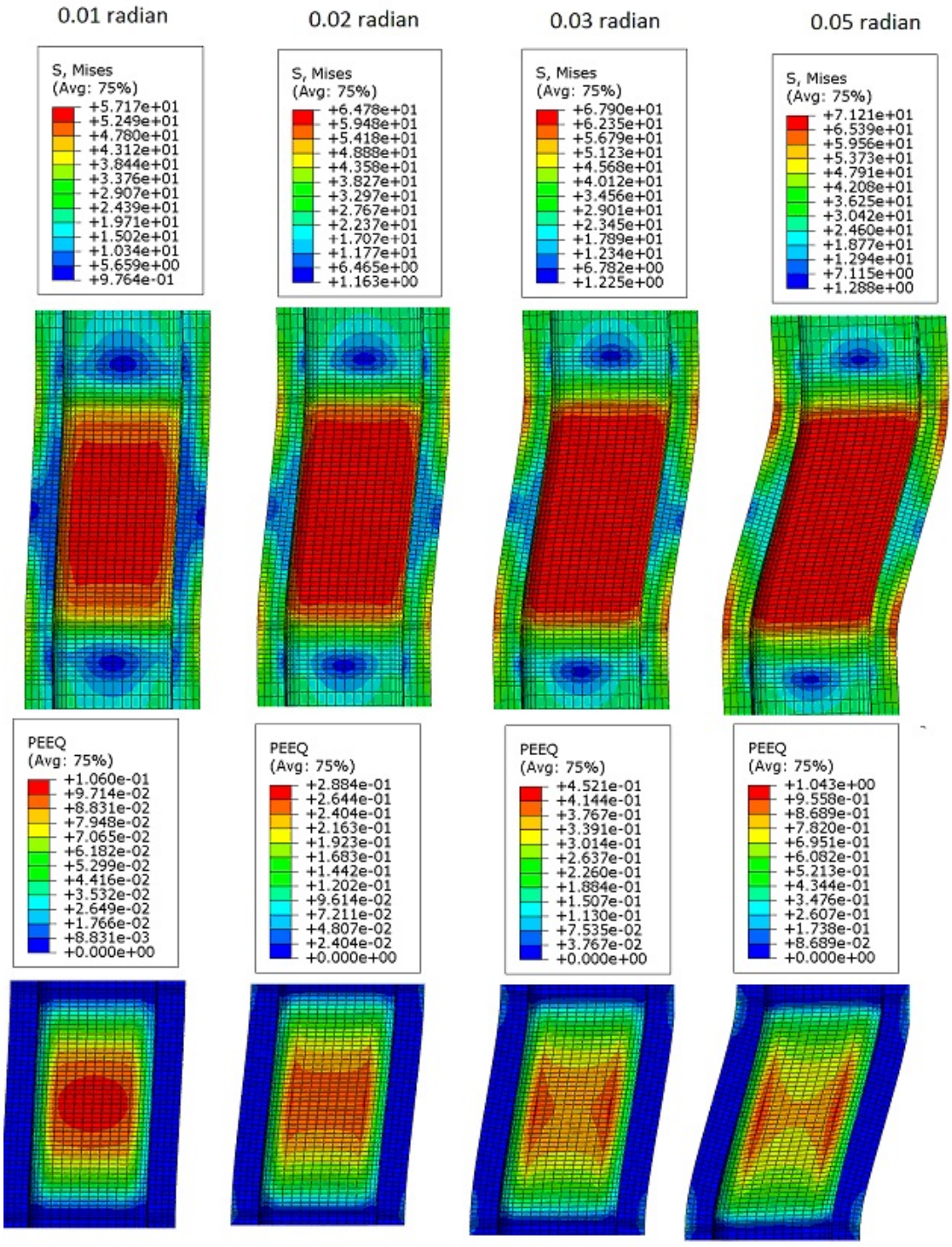

Figure 4.49: VMS and PEEQ in the column (Case 5A_one)

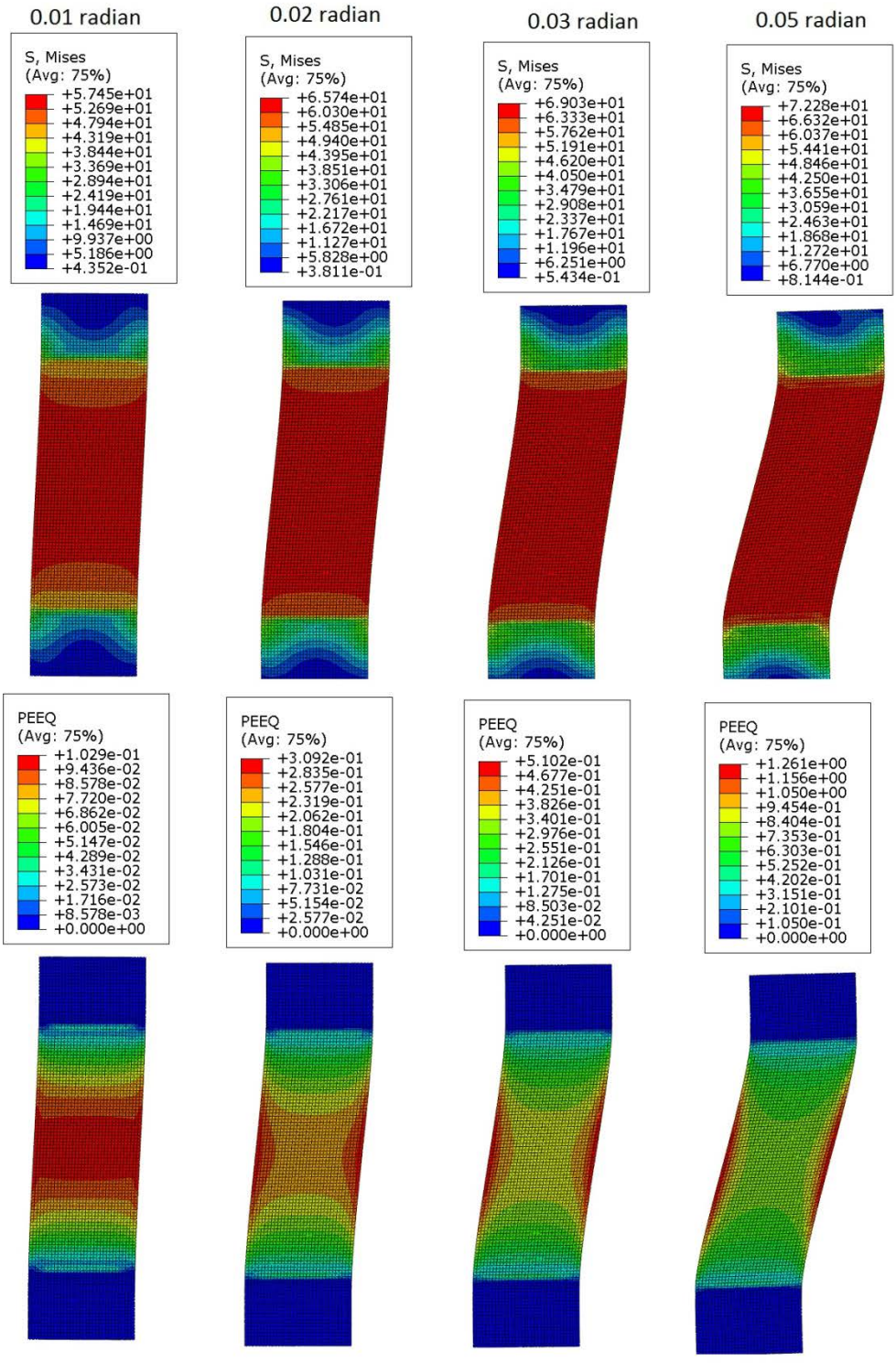

Figure 4.50: VMS and PEEQ in the DP (Case 5A_one)

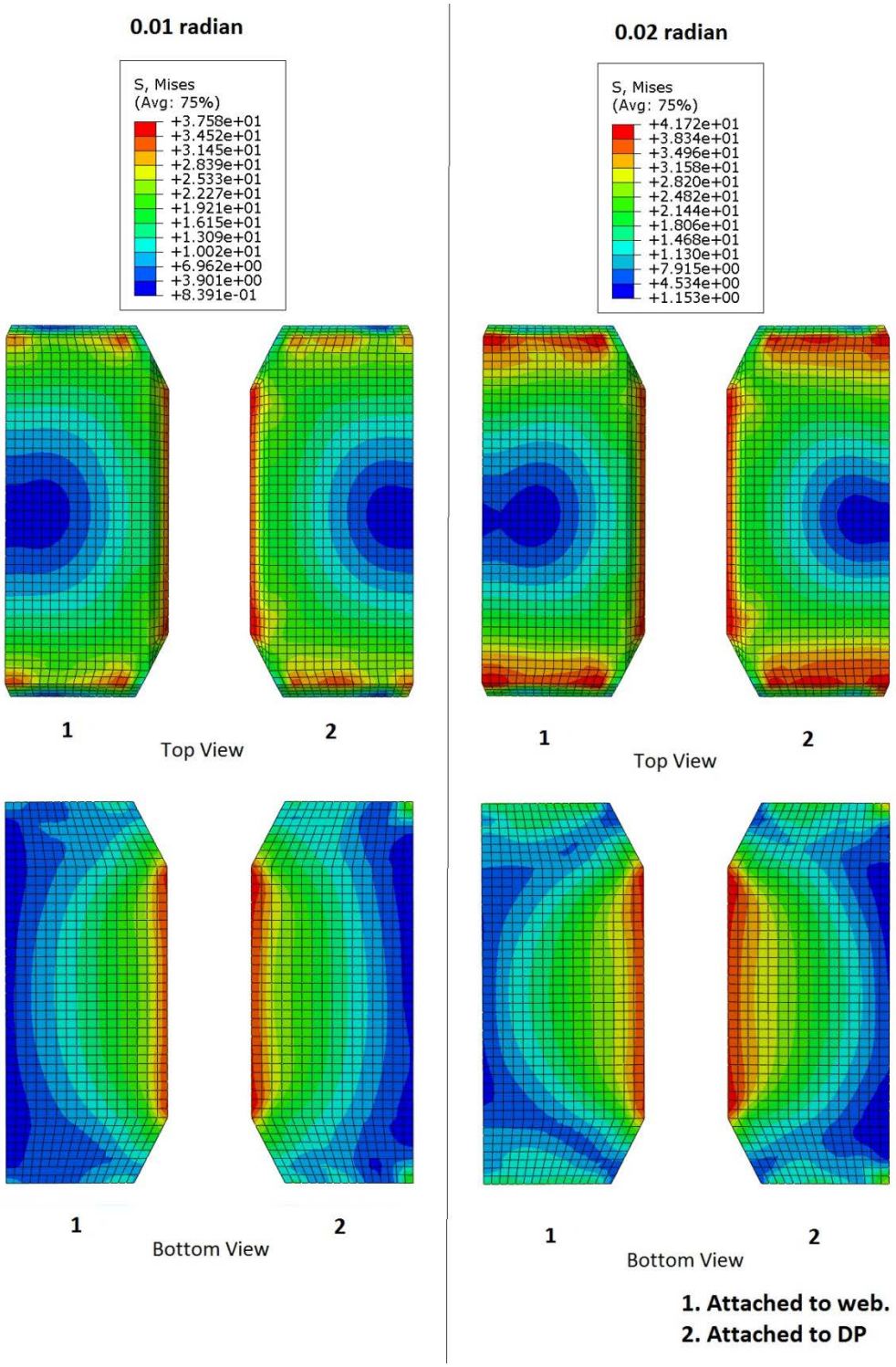

Figure 4.51: VMS in the CP at 0.01 and 0.02 radian rotation (Case 5A_one)

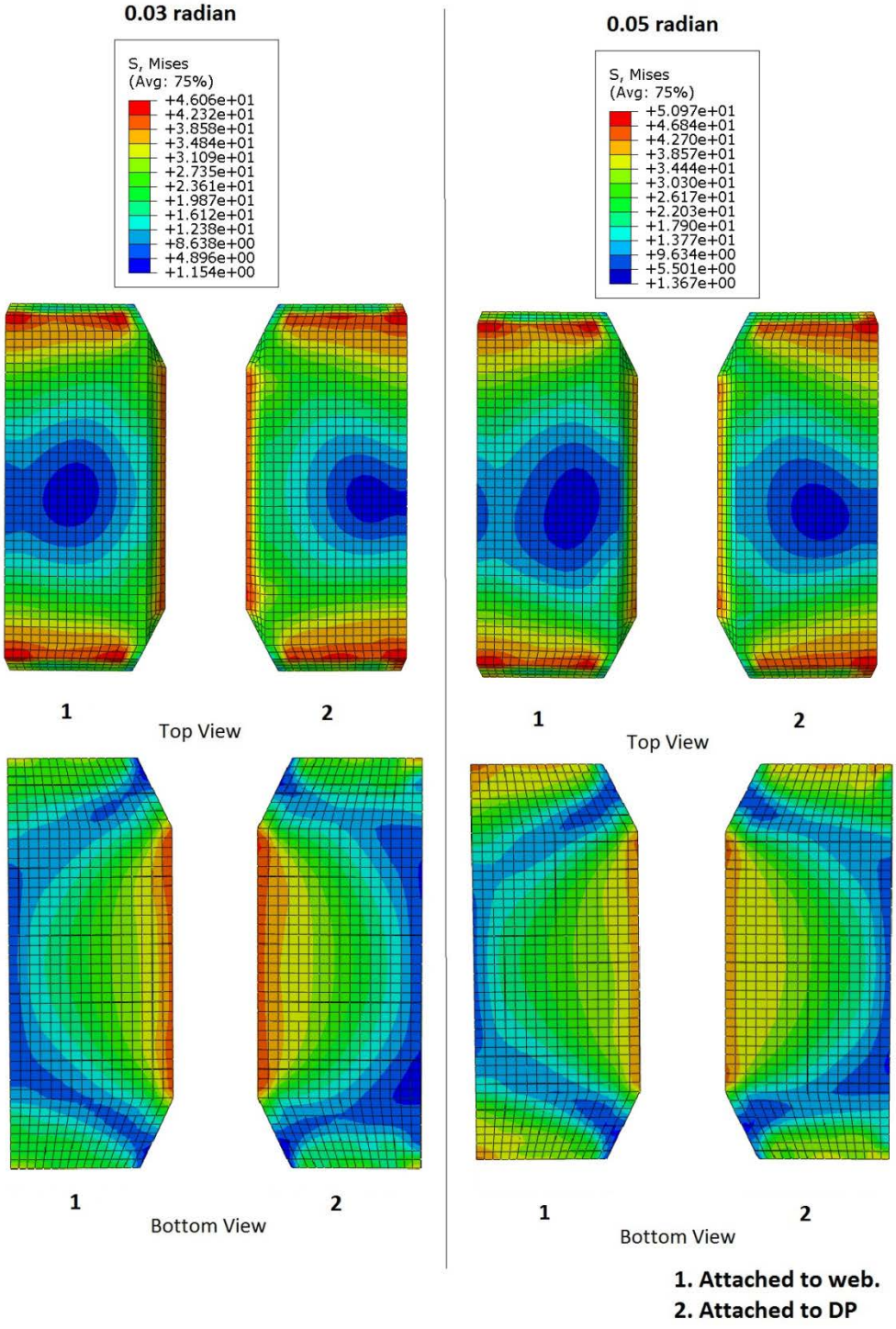

Figure 4.52: VMS in the CP at 0.03 and 0.05 radian rotation (Case 5A_one)

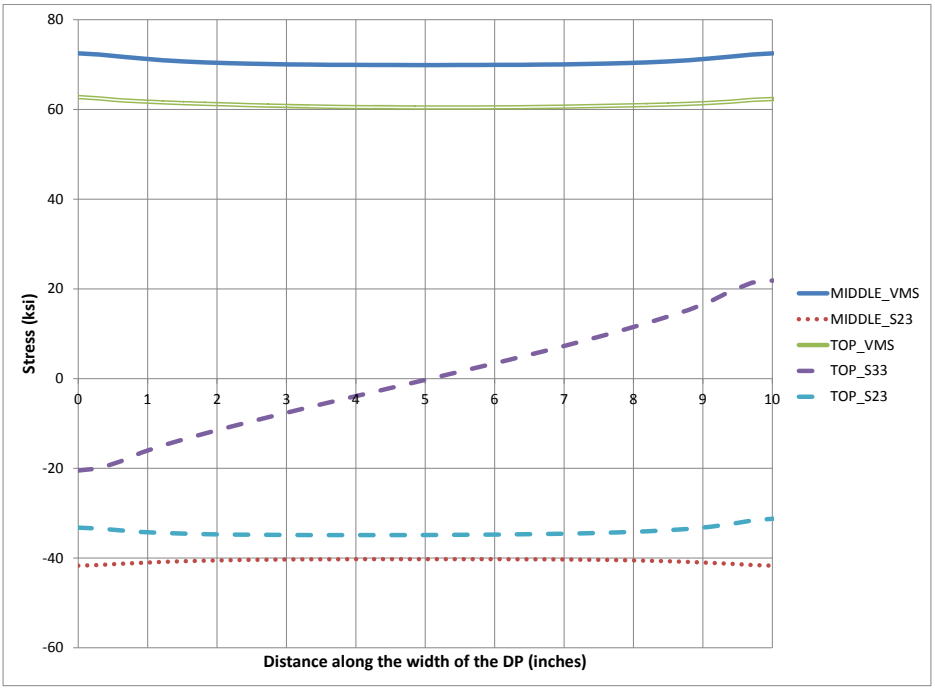

Figure 4.53: Stresses along the width of DP at 0.05 radian rotation (Case 5A_one)

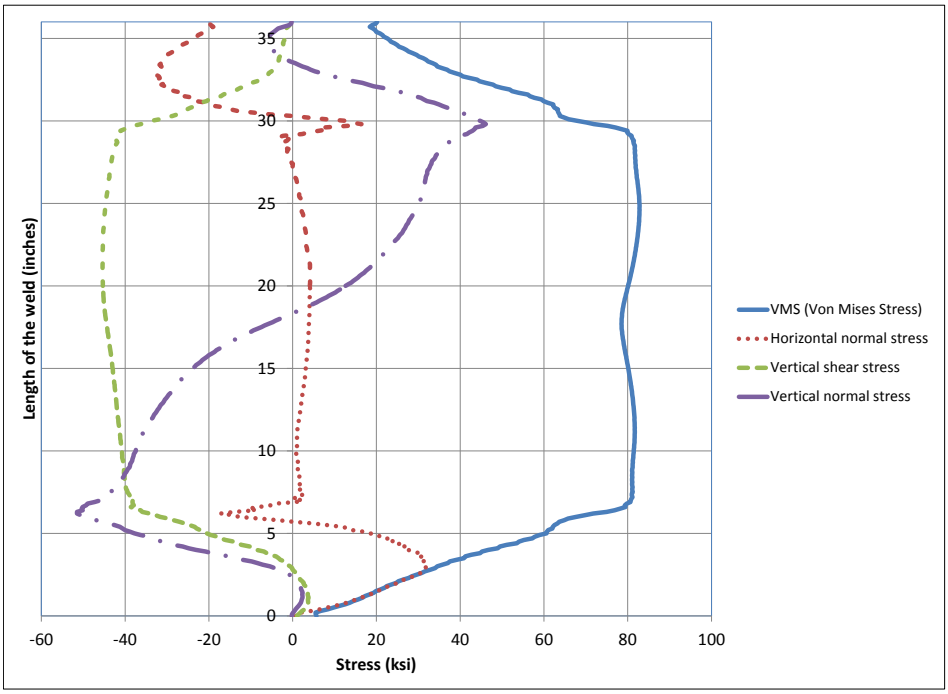

Figure 4.54: Stresses along depth of CJP1 (DP-CJP1 interface) at 0.05 radian (Case 5A_one)

4.2.11 Analysis case 6A

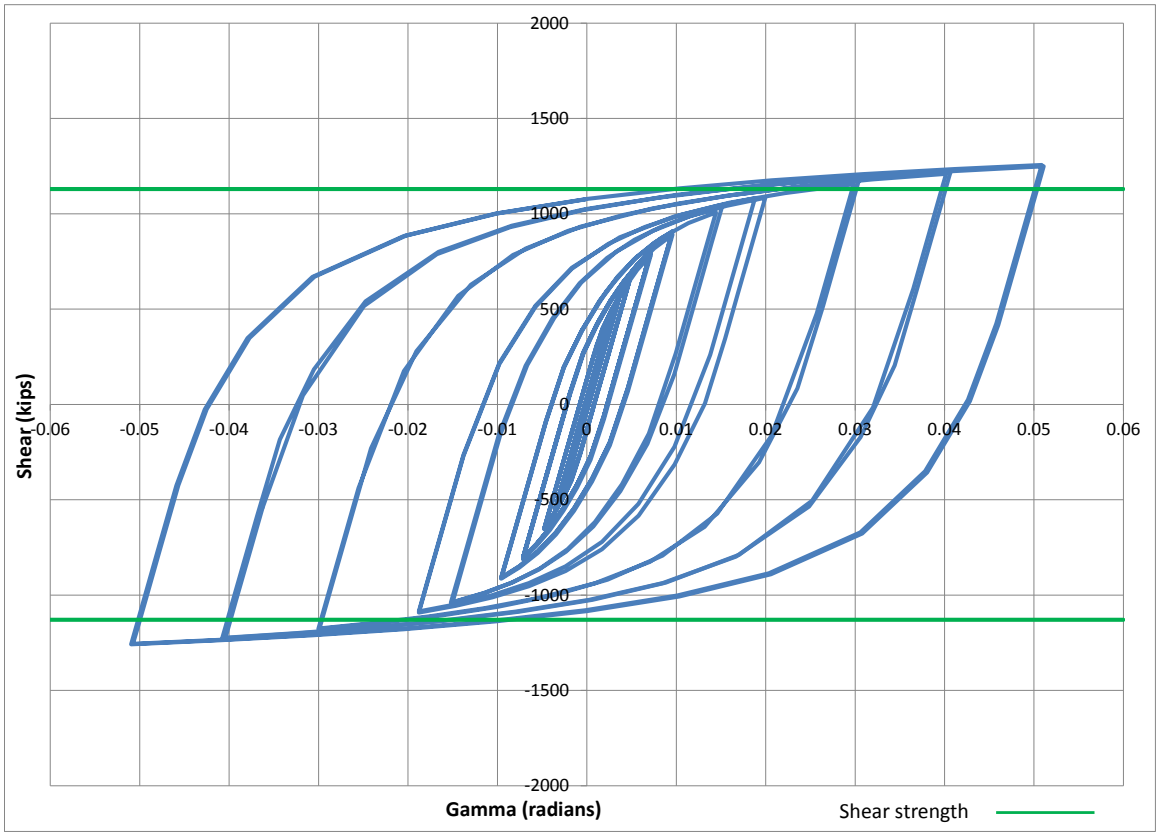

Figure 4.55: Panel zone shear versus rotation (Case 6A)

Table 4.12: Panel zone shear and force on loading plate (Case 6A)

Panel zone rotation (rad)	0.01	0.02	0.03	0.05
Panel zone shear (kips)	908.34	1081.53	1173.80	1255.65
Force on one Loading plate (kips)	545.00	648.92	704.28	753.39

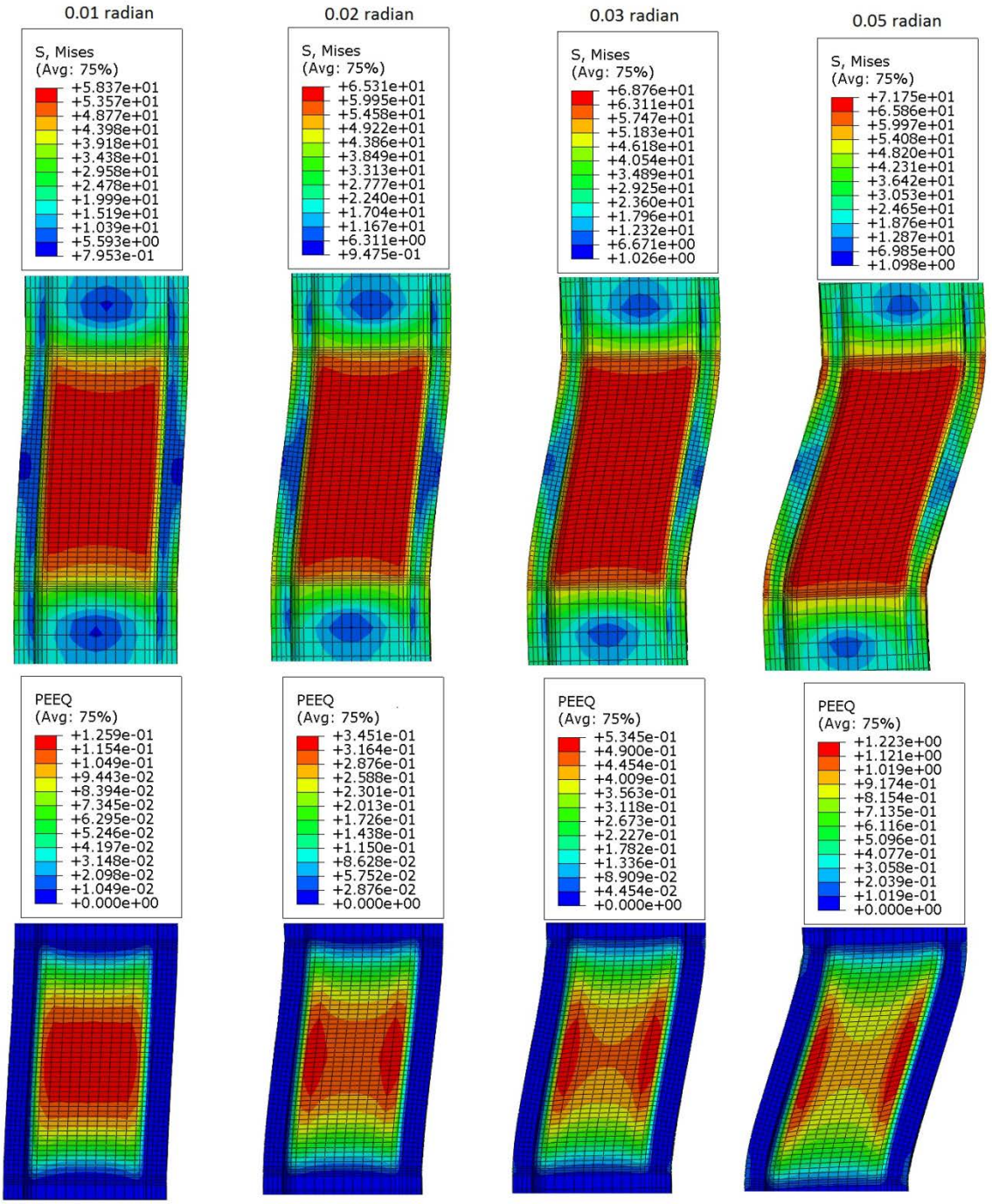

Figure 4.56: VMS and PEEQ in the column (Case 6A)

4.2.12 Analysis case 7A

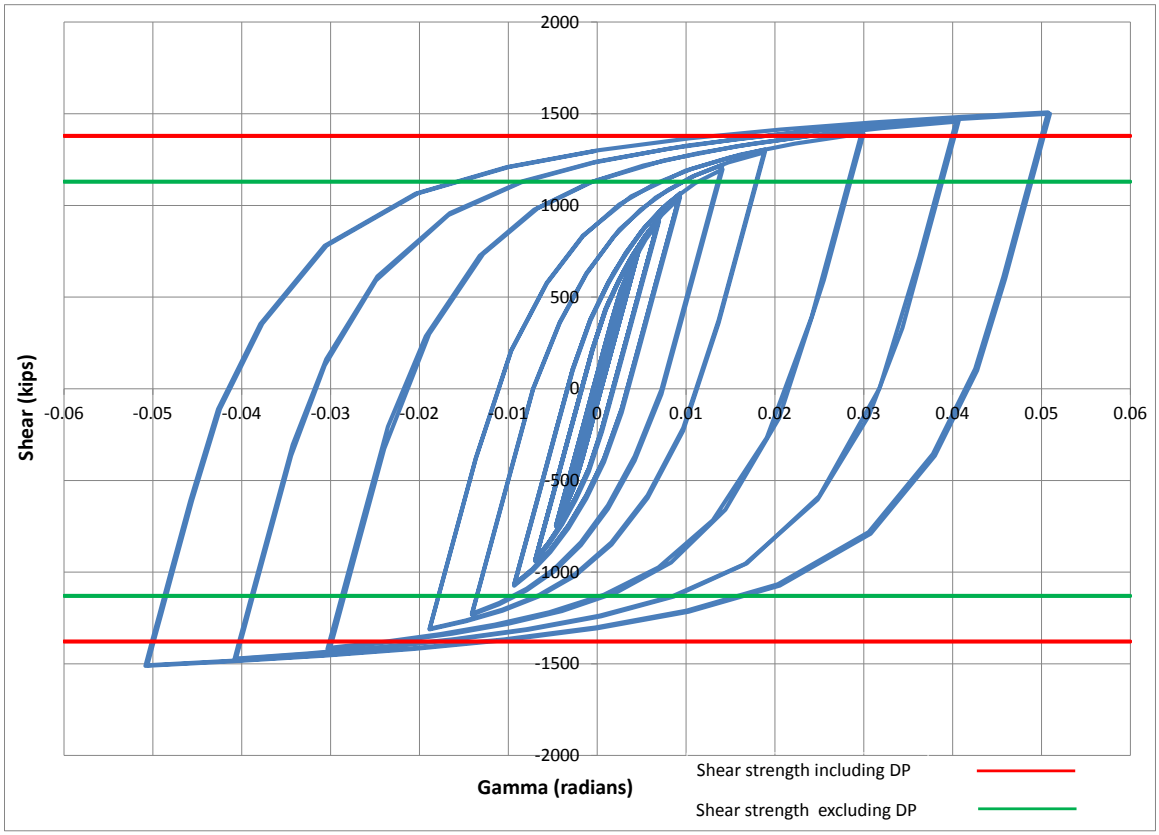

Figure 4.57: Panel zone shear versus rotation (Case 7A)

Table 4.13: Panel zone shear and force on loading plate (Case 7A)

Panel zone rotation (rad)	0.01	0.02	0.03	0.05
Panel zone shear (kips)	1066.09	1305.43	1410.57	1507.61
Force on one Loading plate (kips)	639.65	783.26	846.34	904.56

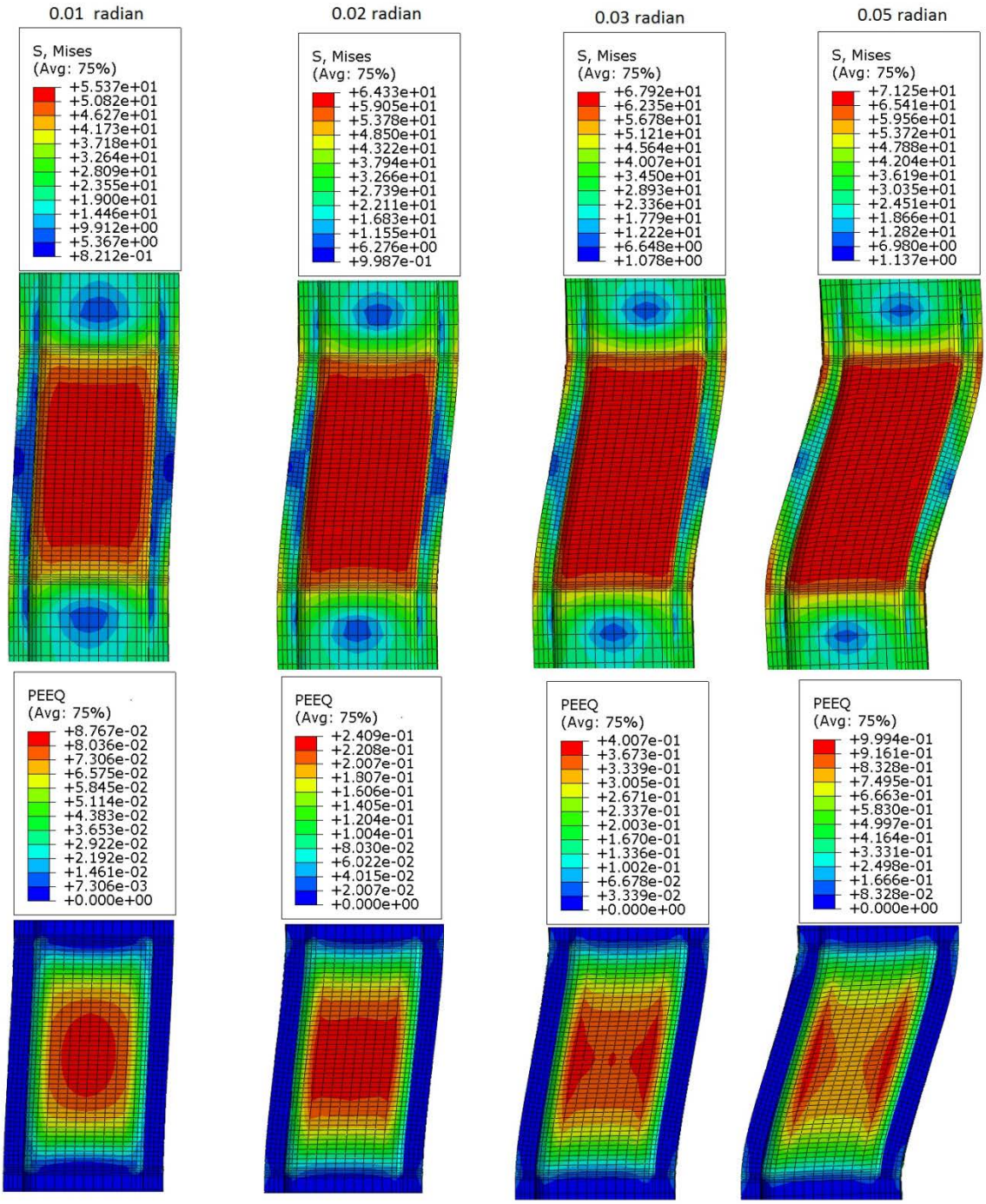

Figure 4.58: VMS and PEEQ in the column (Case 7A)

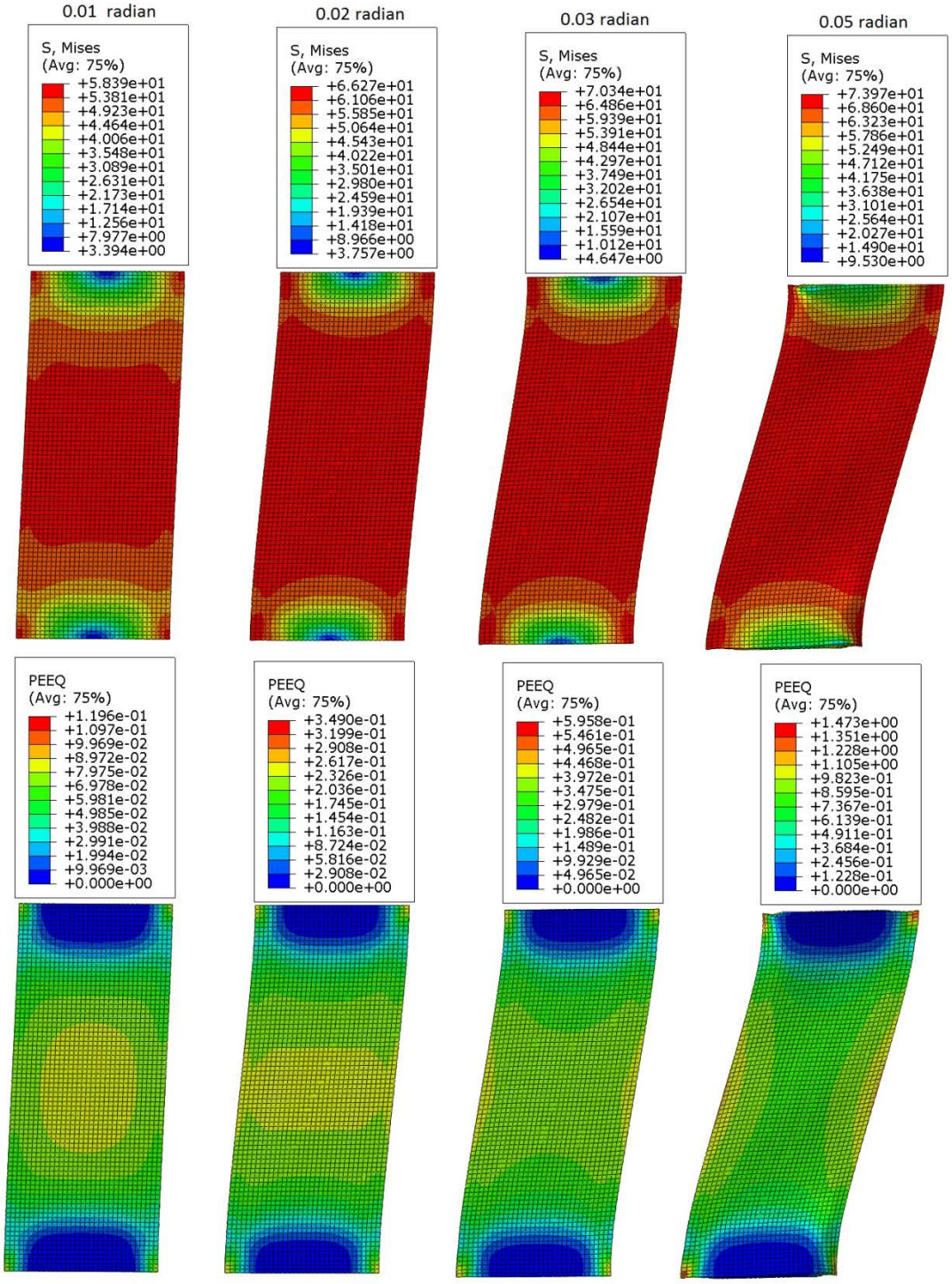

Figure 4.59: VMS and PEEQ in the DP (Case 7A)

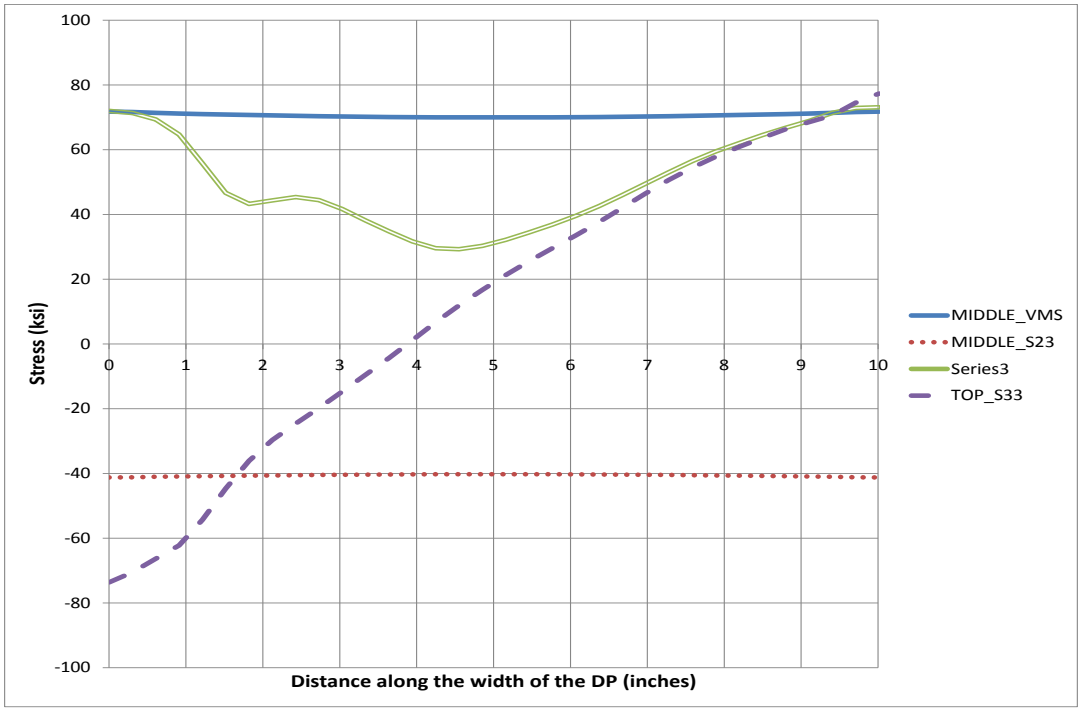

Figure 4.60: Stresses along the width of DP at 0.05 radian rotation (Case 7A)

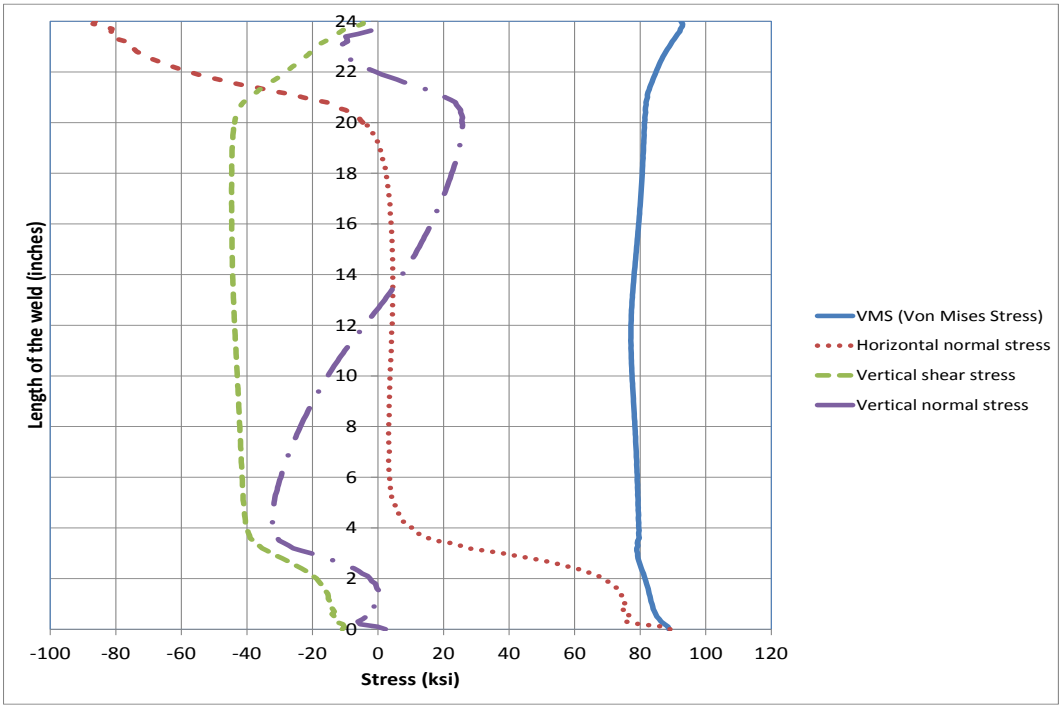

Figure 4.61: Stresses along depth of CJP1 (DP-CJP1 interface) at 0.05 radian (Case 7A)

4.2.13 Analysis case 8A

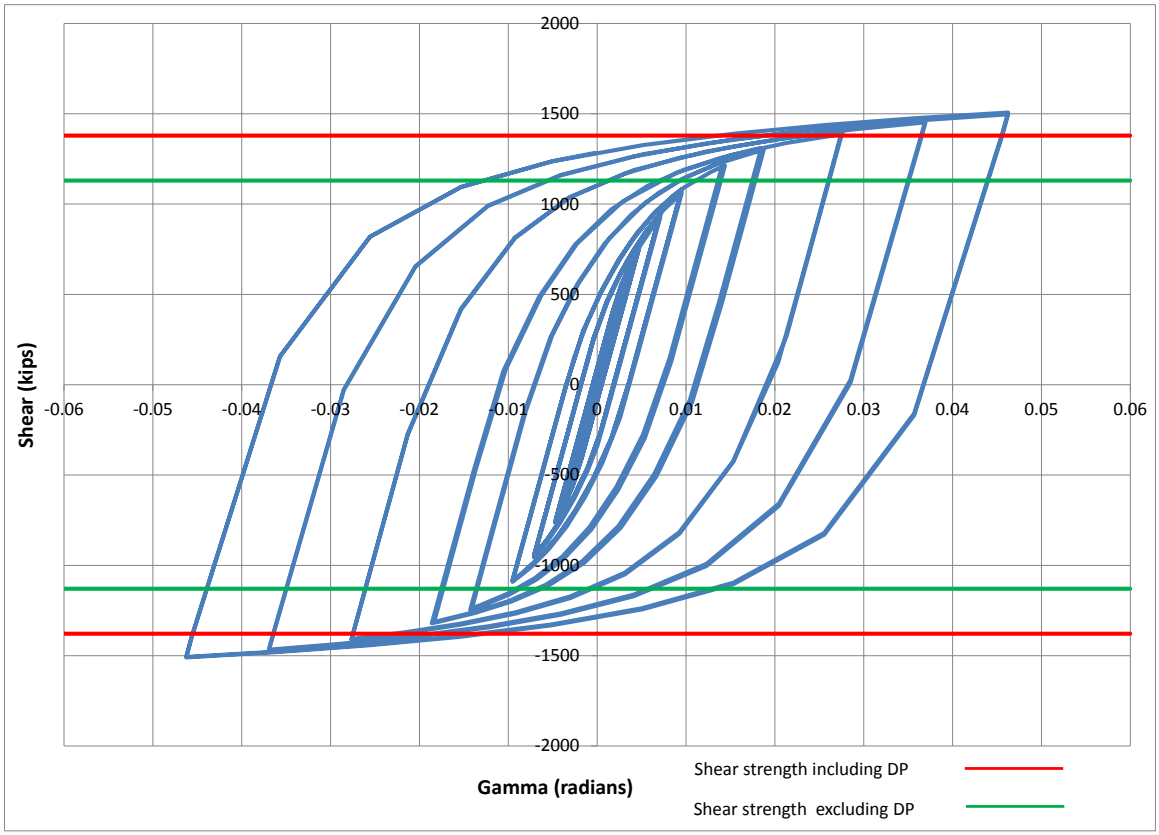

Figure 4.62: Panel zone shear versus rotation (Case 8A)

Table 4.14: Panel zone shear and force on loading plate (Case 8A)

Panel zone rotation (rad)	0.01	0.02	0.03	0.05
Panel zone shear (kips)	1082.55	1310.85	1405.44	1506.38
Force on one Loading plate (kips)	649.53	786.51	843.26	903.83

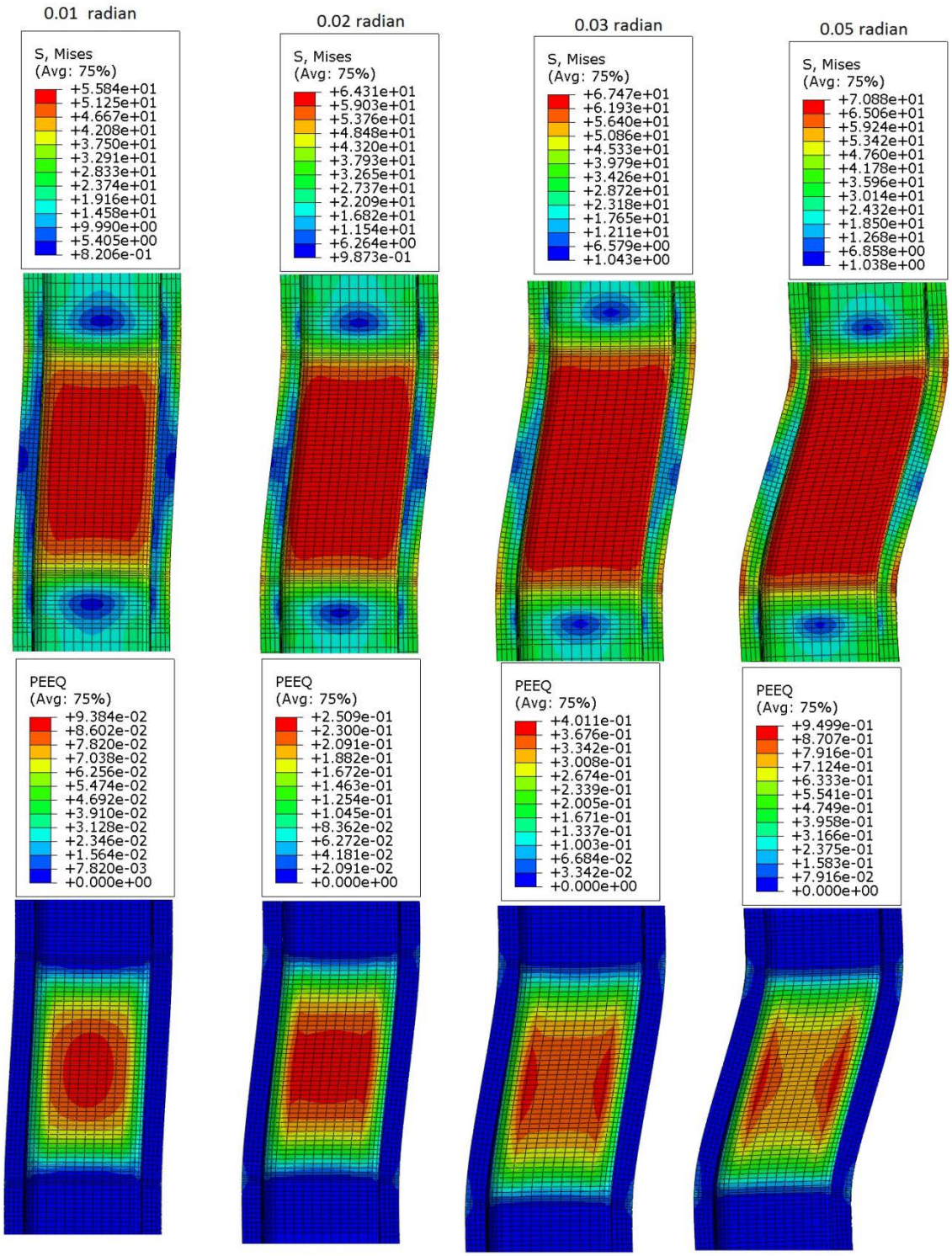

Figure 4.63: VMS and PEEQ in the column (Case 8A)

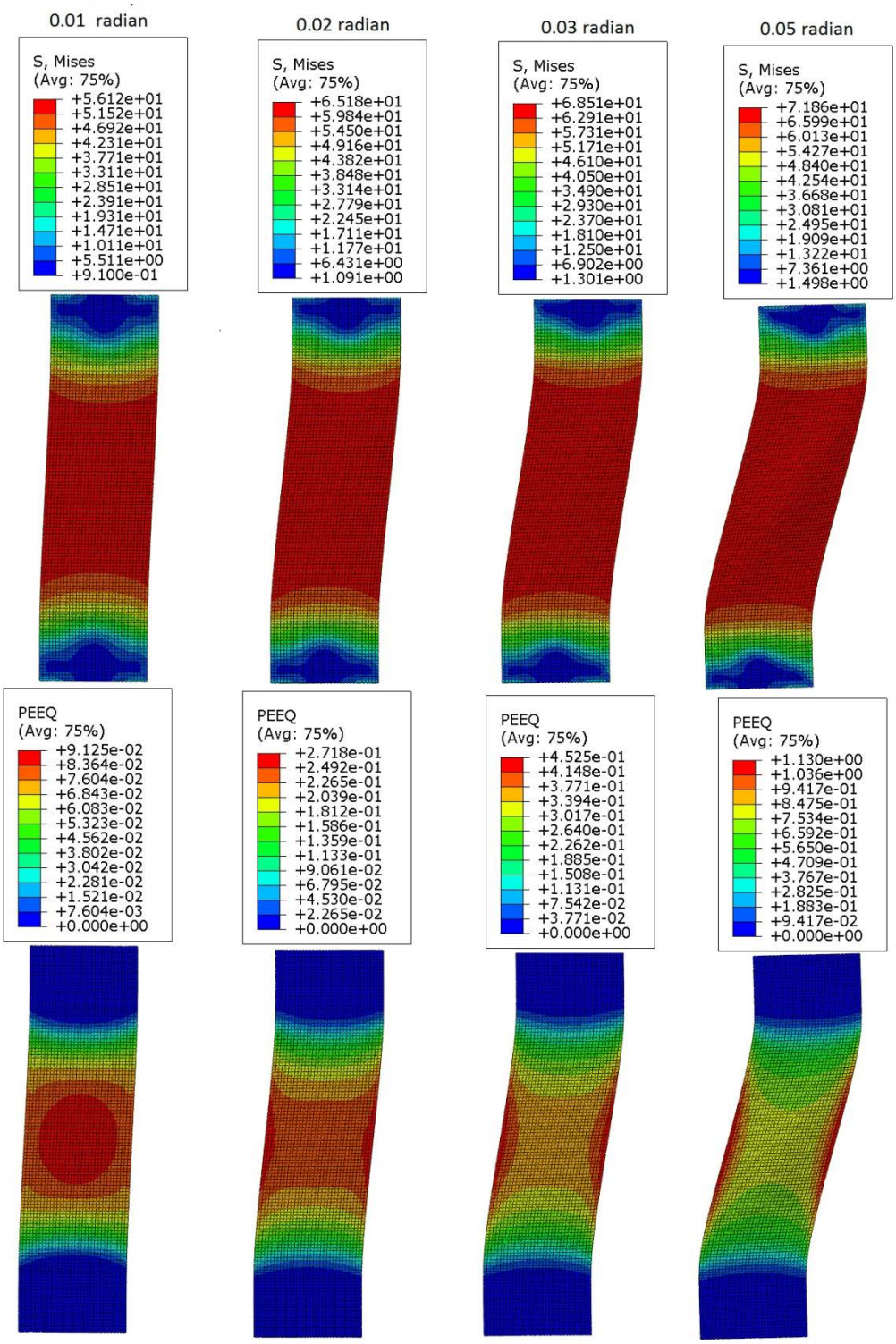

Figure 4.64: VMS and PEEQ in the DP (Case 8A)

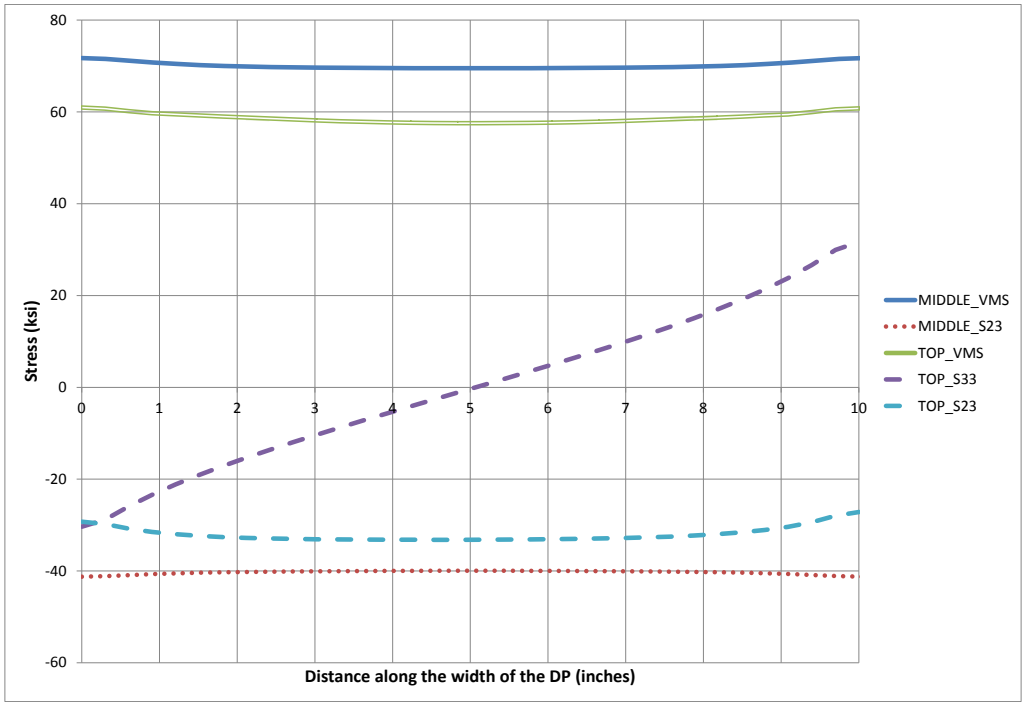

Figure 4.65: Stresses along the width of DP at 0.05 radian rotation (Case 8A)

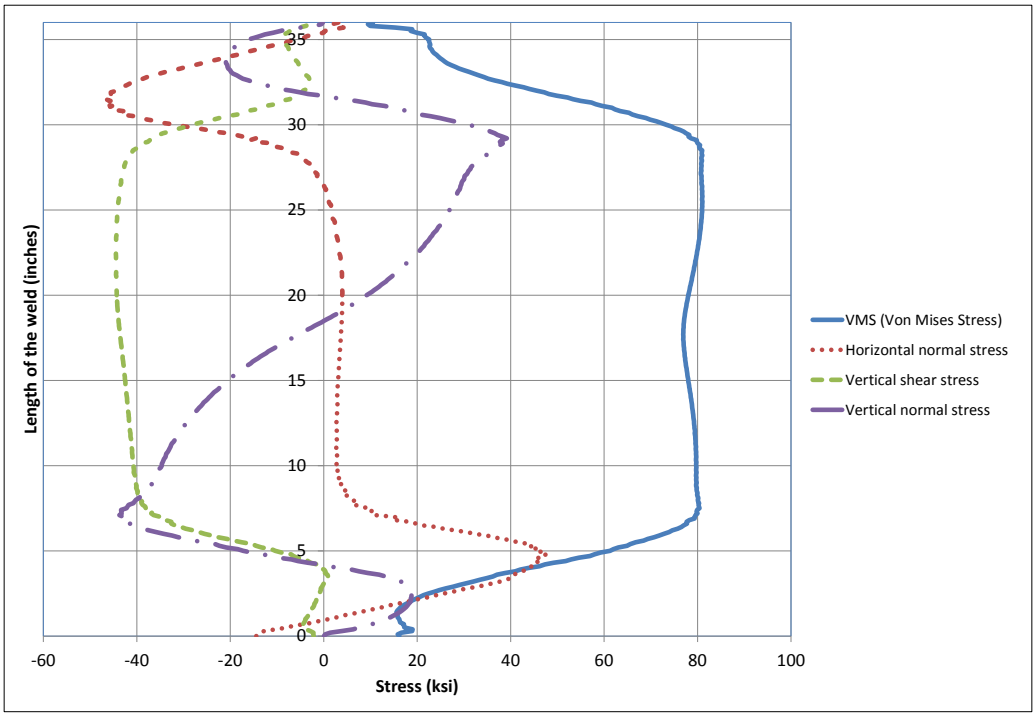

Figure 4.66: Stresses along depth of CJP1 (DP-CJP1 interface) at 0.05 radian (Case 8A)

4.2.14 Analysis case 9A

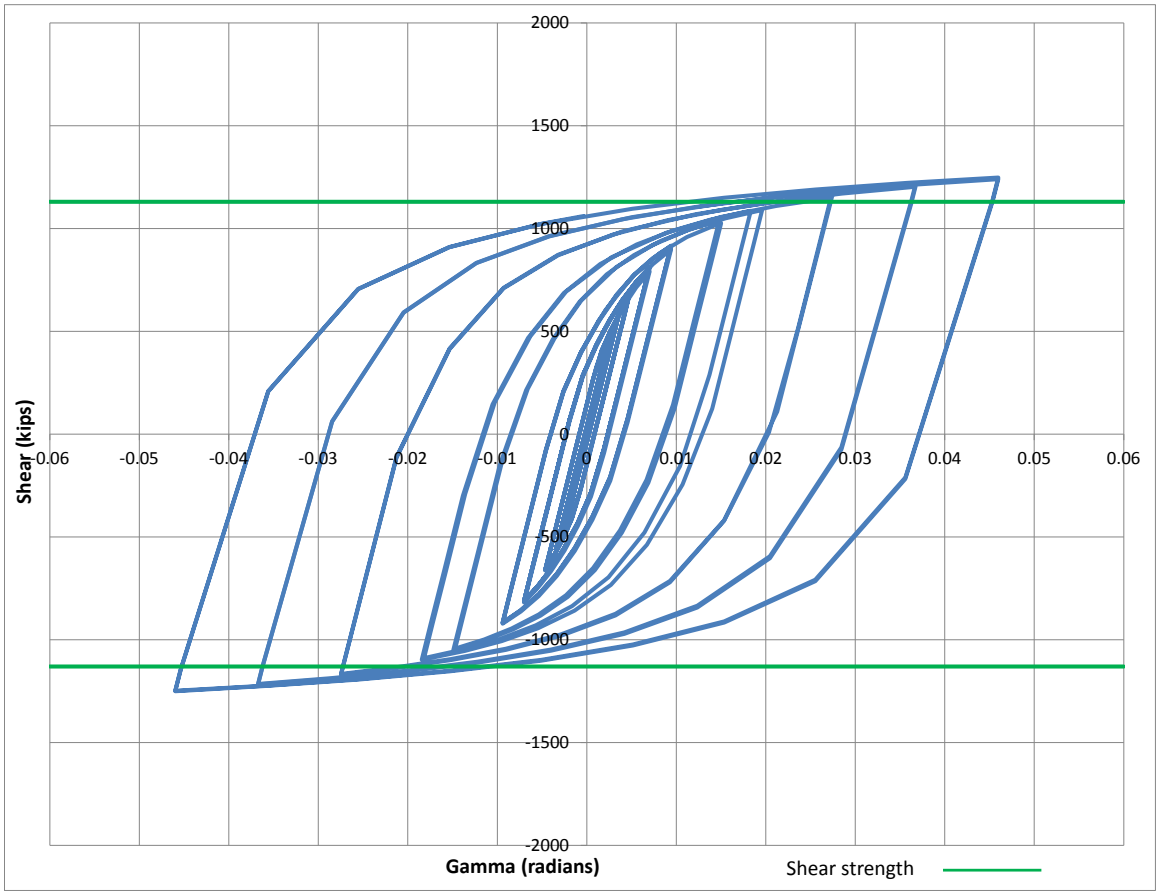

Figure 4.67: Panel zone shear versus rotation (Case 9A)

Table 4.15: Panel zone shear and force on loading plate (Case 9A)

Panel zone rotation (rad)	0.01	0.02	0.03	0.05
Panel zone shear (kips)	916.24	1086.13	1163.96	1247.56
Force on one Loading plate (kips)	549.74	651.68	698.38	748.53

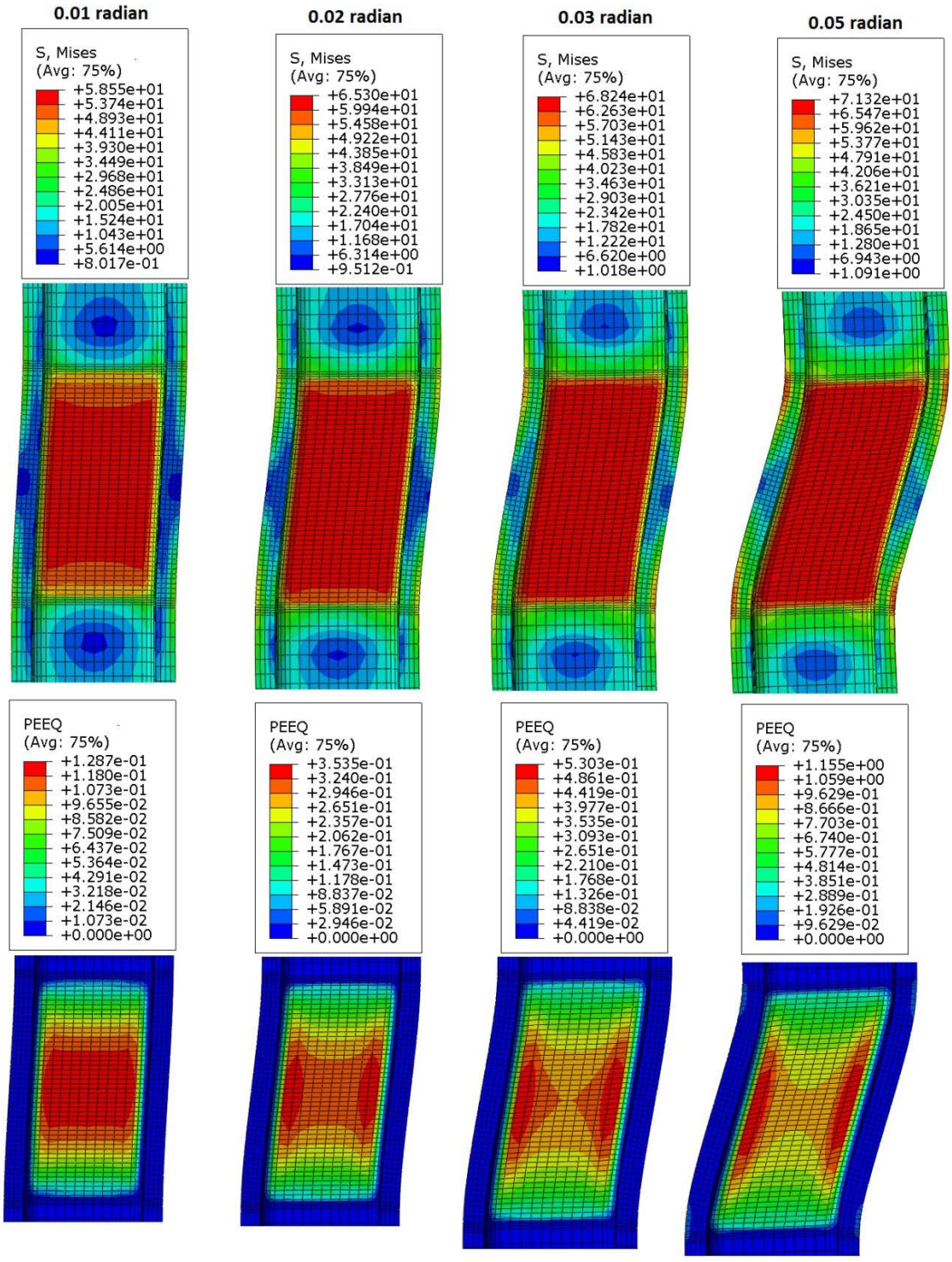

Figure 4.68: VMS and PEEQ in the column (Case 9A)

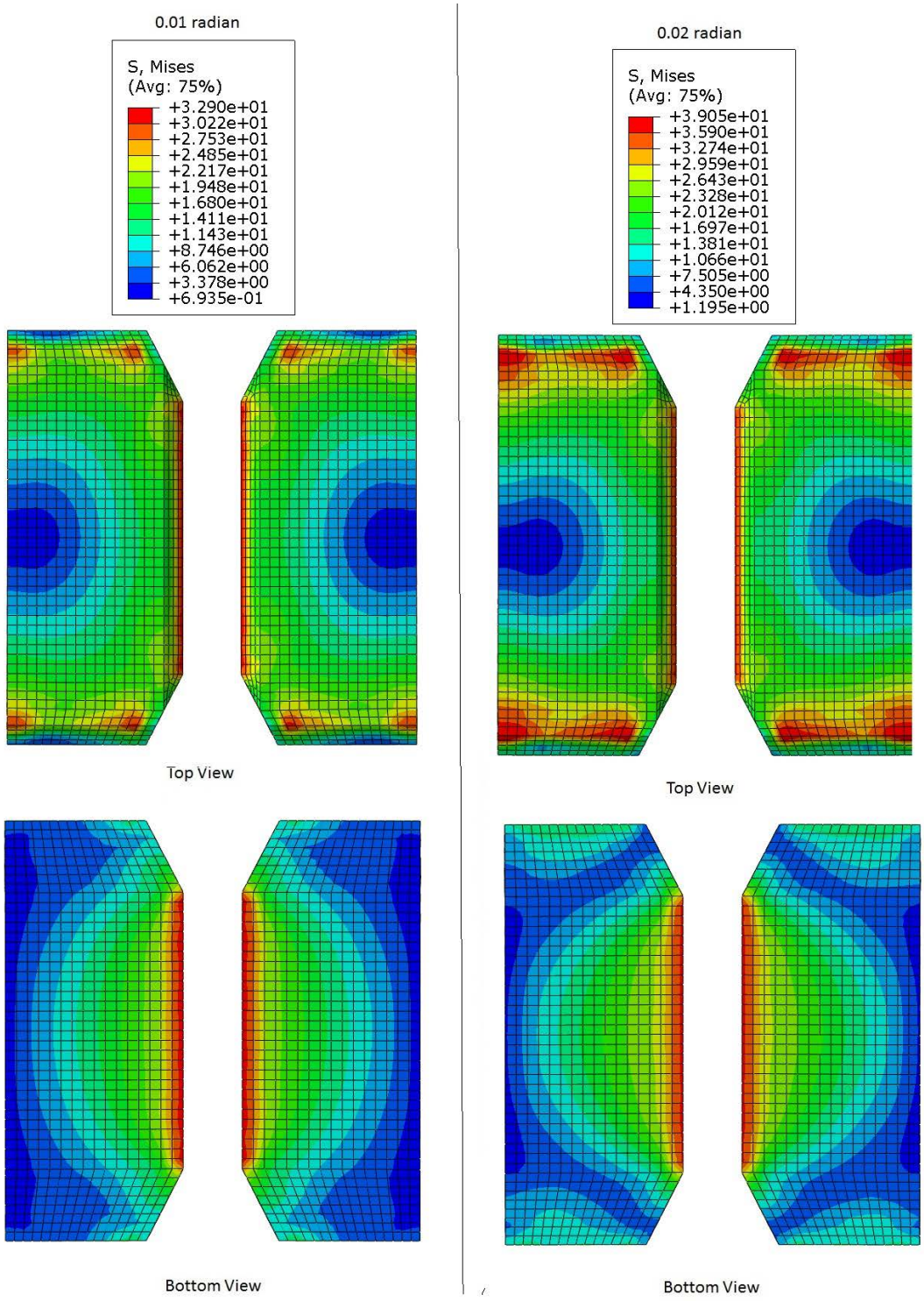

Figure 4.69: VMS in the CP at 0.01 and 0.02 radian rotation (Case 9A)

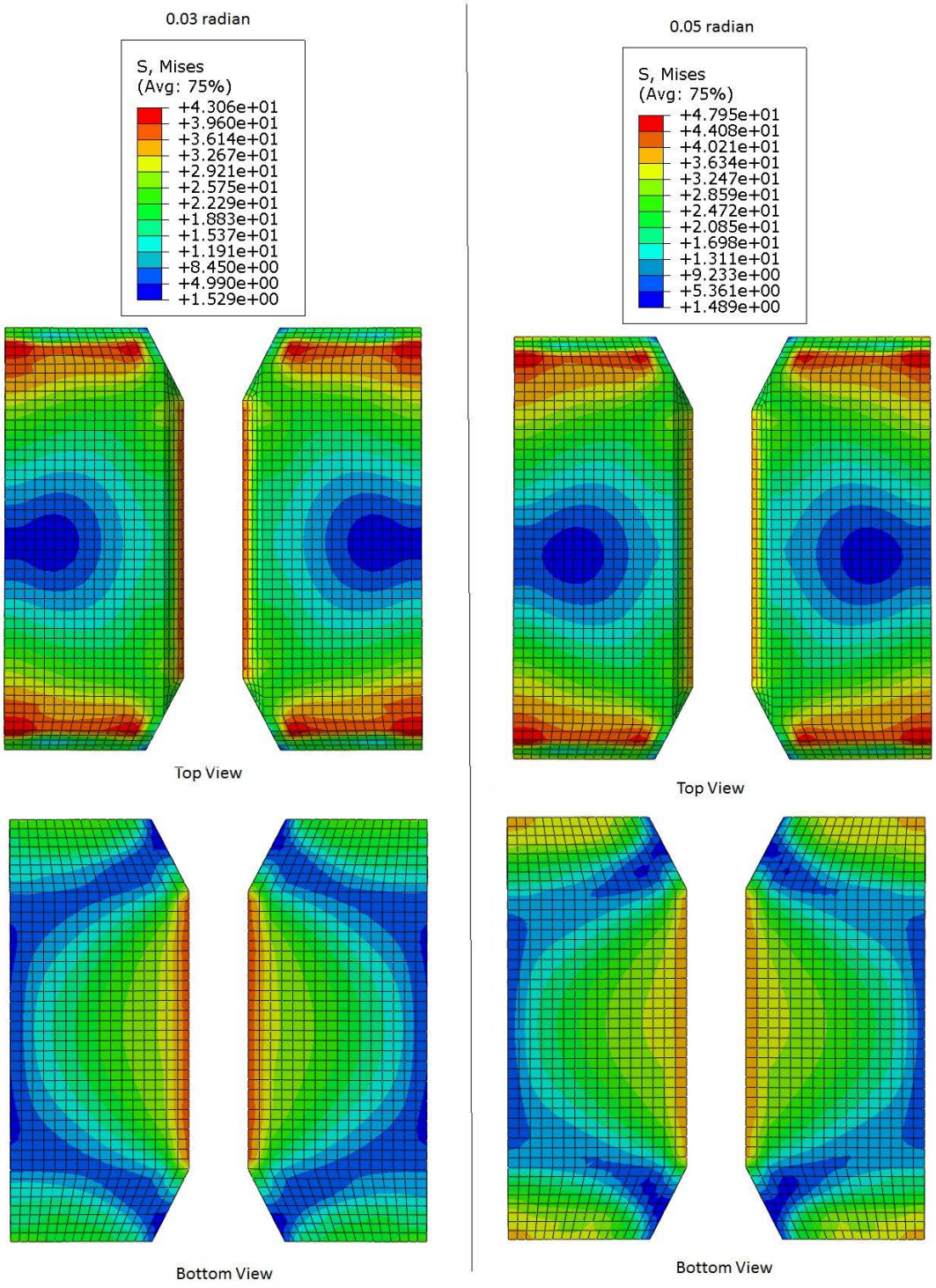

Figure 4.70: VMS in the CP at 0.03 and 0.05 radian rotation (Case 9A)

4.2.15 Analysis case 10A

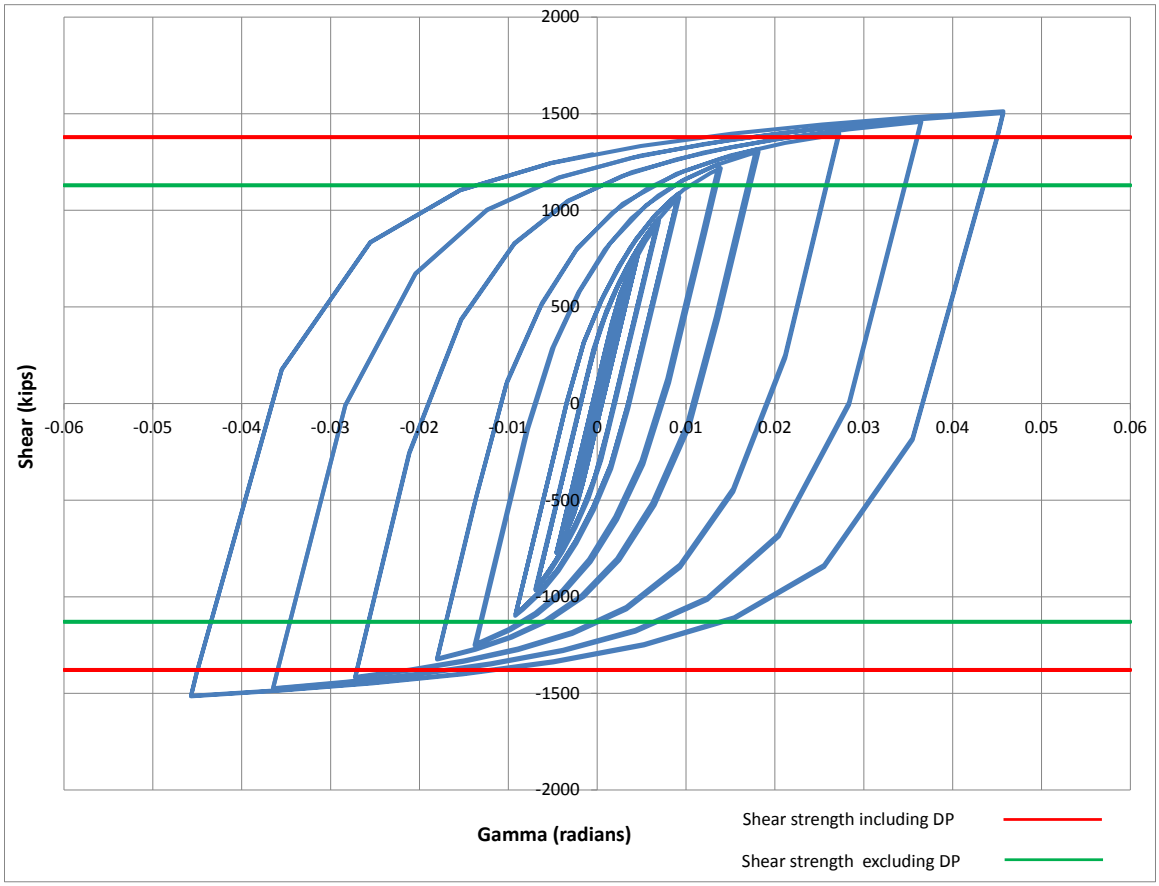

Figure 4.71: Panel zone shear versus rotation (Case 10A)

Table 4.16: Panel zone shear and force on loading plate (Case 10A)

Panel zone rotation (rad)	0.01	0.02	0.03	0.05
Panel zone shear (kips)	1087.18	1315.60	1412.36	1512.27
Force on one Loading plate (kips)	652.31	789.36	847.41	907.36

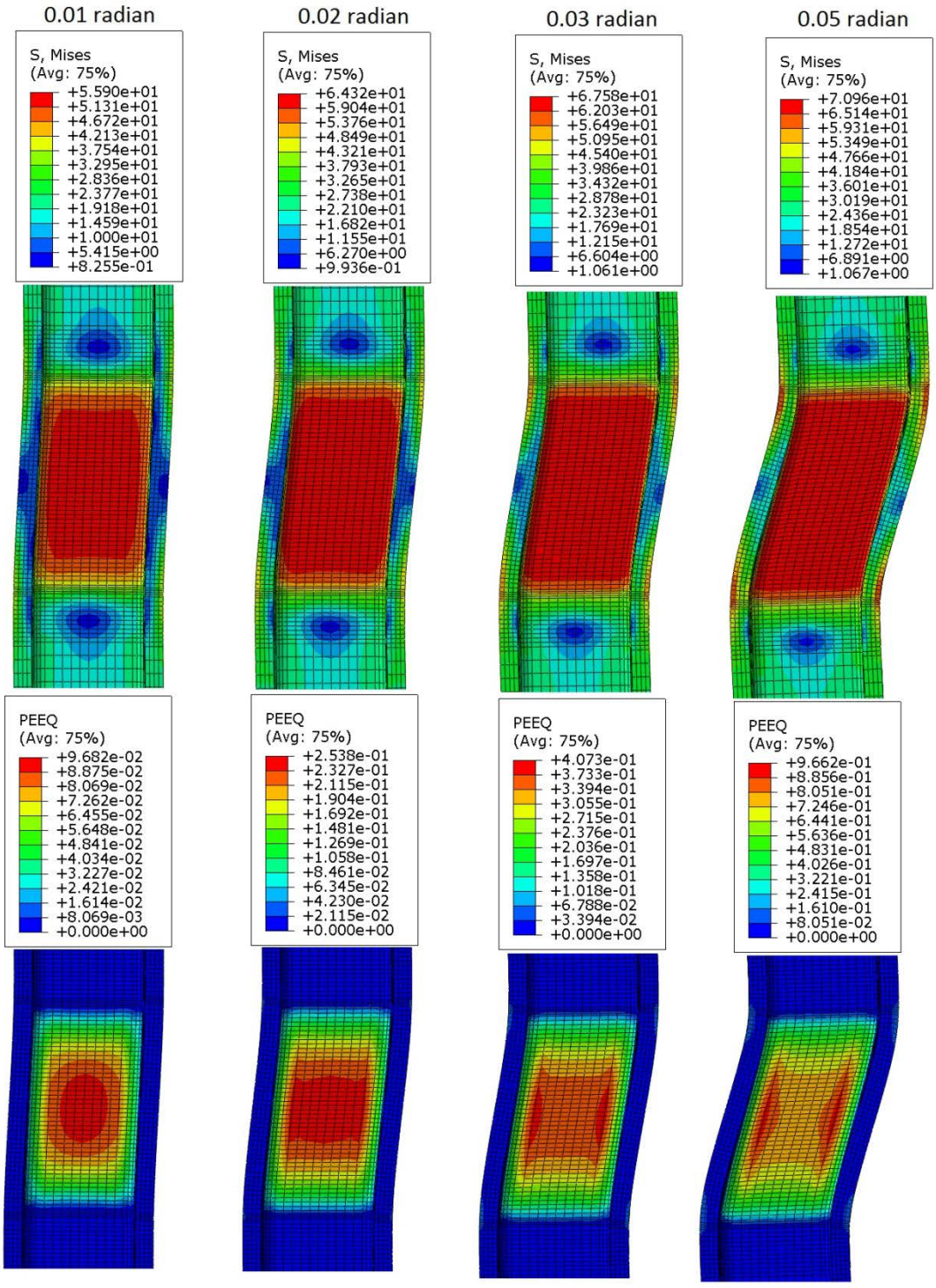

Figure 4.72: VMS and PEEQ in the column (Case 10A)

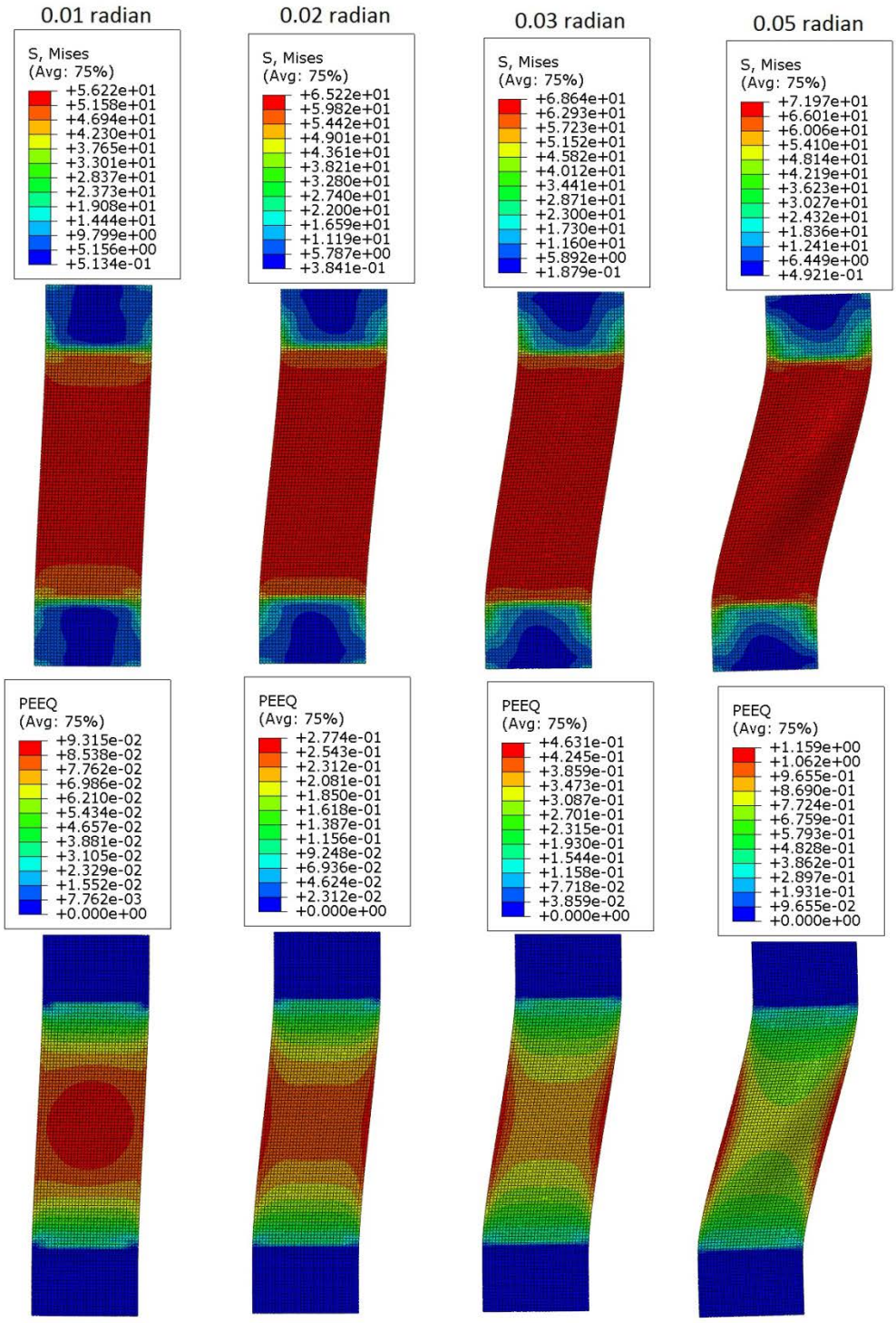

Figure 4.73: VMS and PEEQ in the DP (Case 10A)

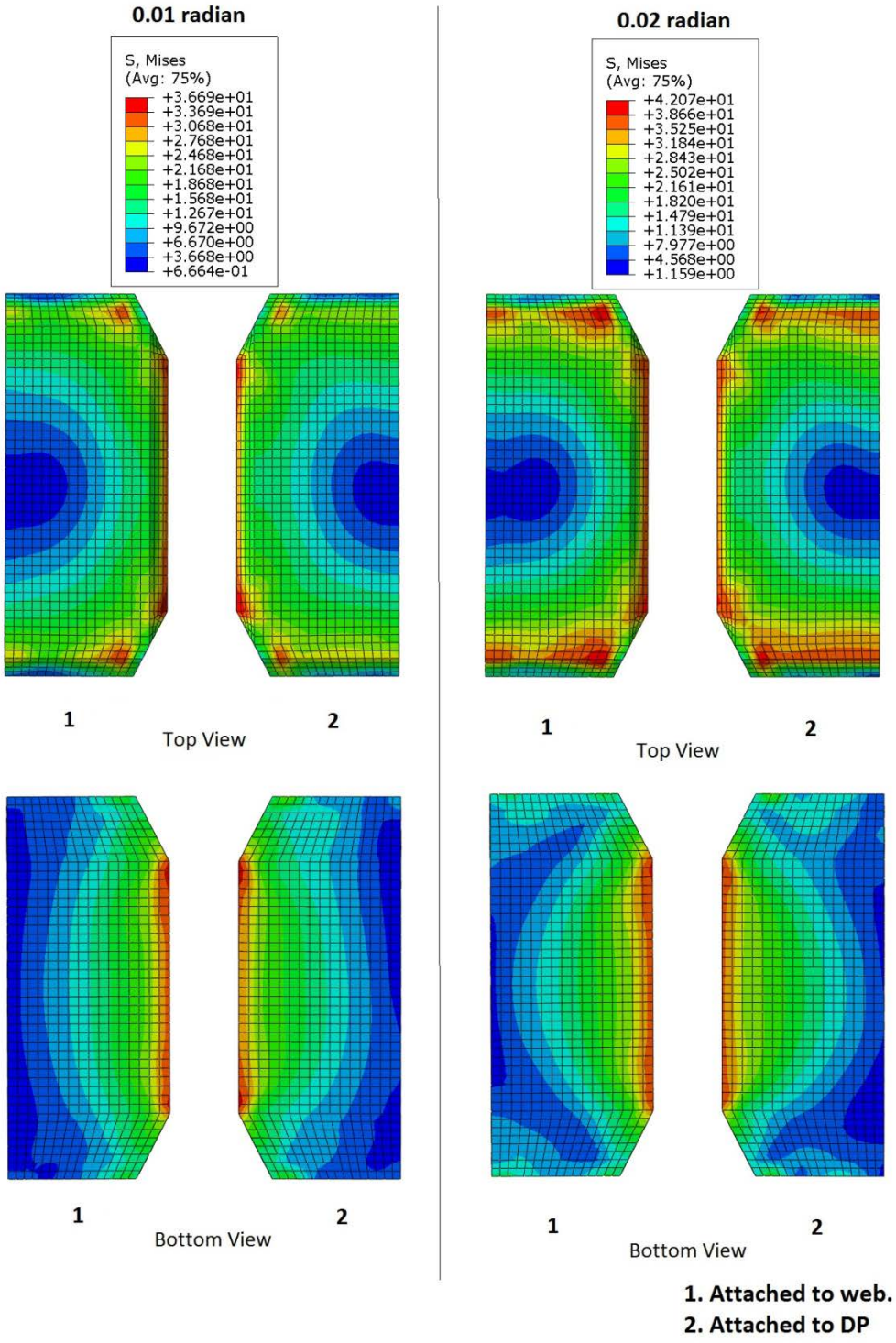

Figure 4.74: VMS in the CP at 0.01 and 0.02 radian rotation (Case 10A)

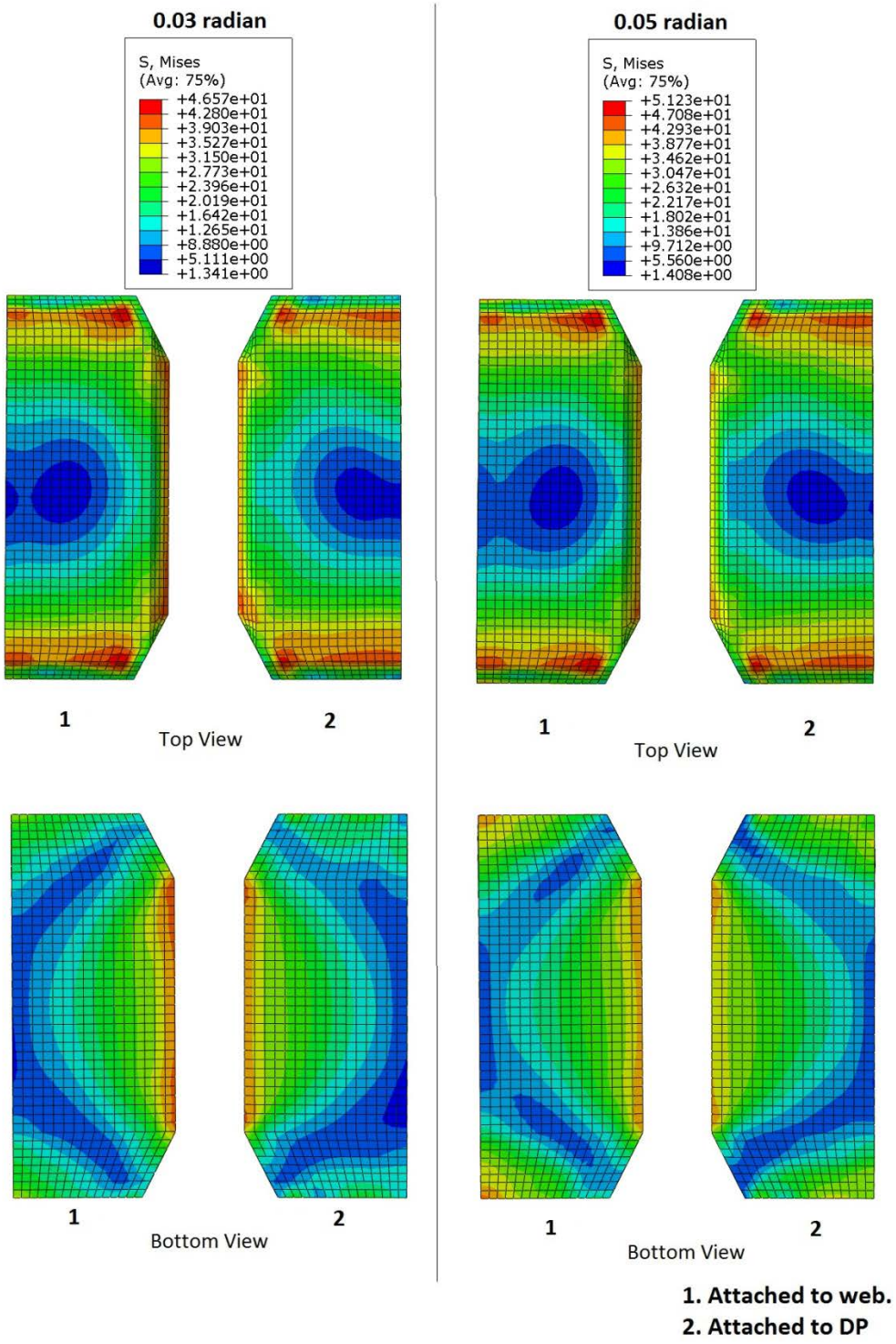

Figure 4.75: VMS in the CP at 0.03 and 0.05 radian rotation (Case 10A)

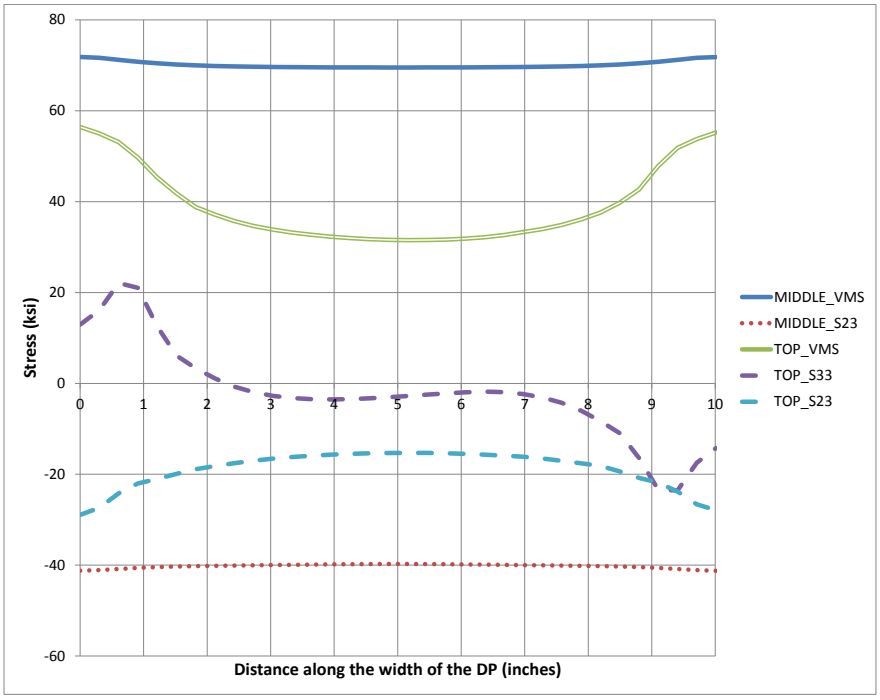

Figure 4.76: Stresses along the width of DP at 0.05 radian rotation (Case 10A)

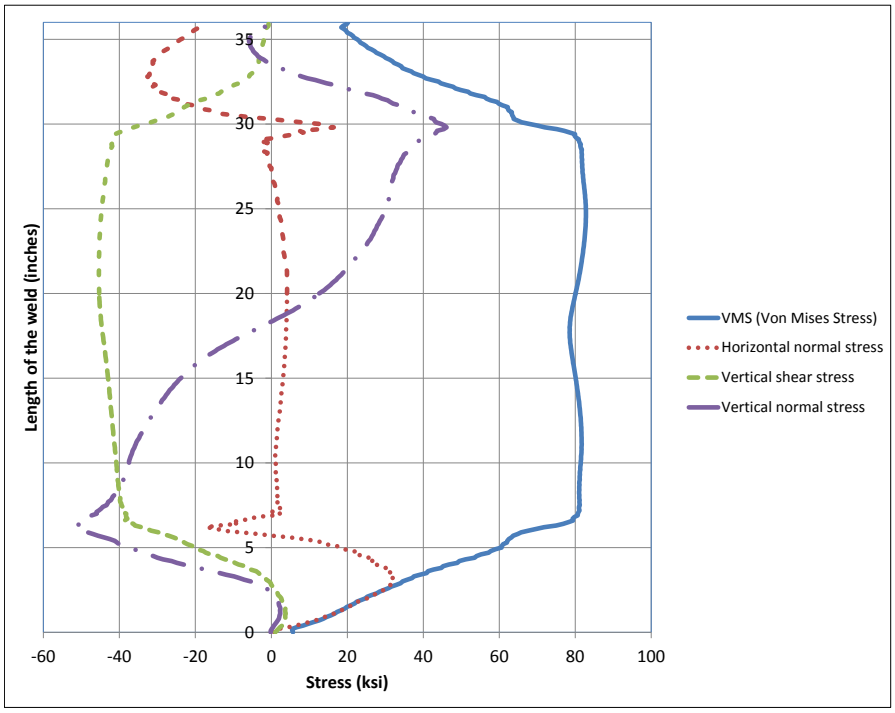

Figure 4.77: Stresses along depth of CJP1 (DP-CJP1 interface) at 0.05 radian (Case 10A)

4.2.16 Analysis case 11A

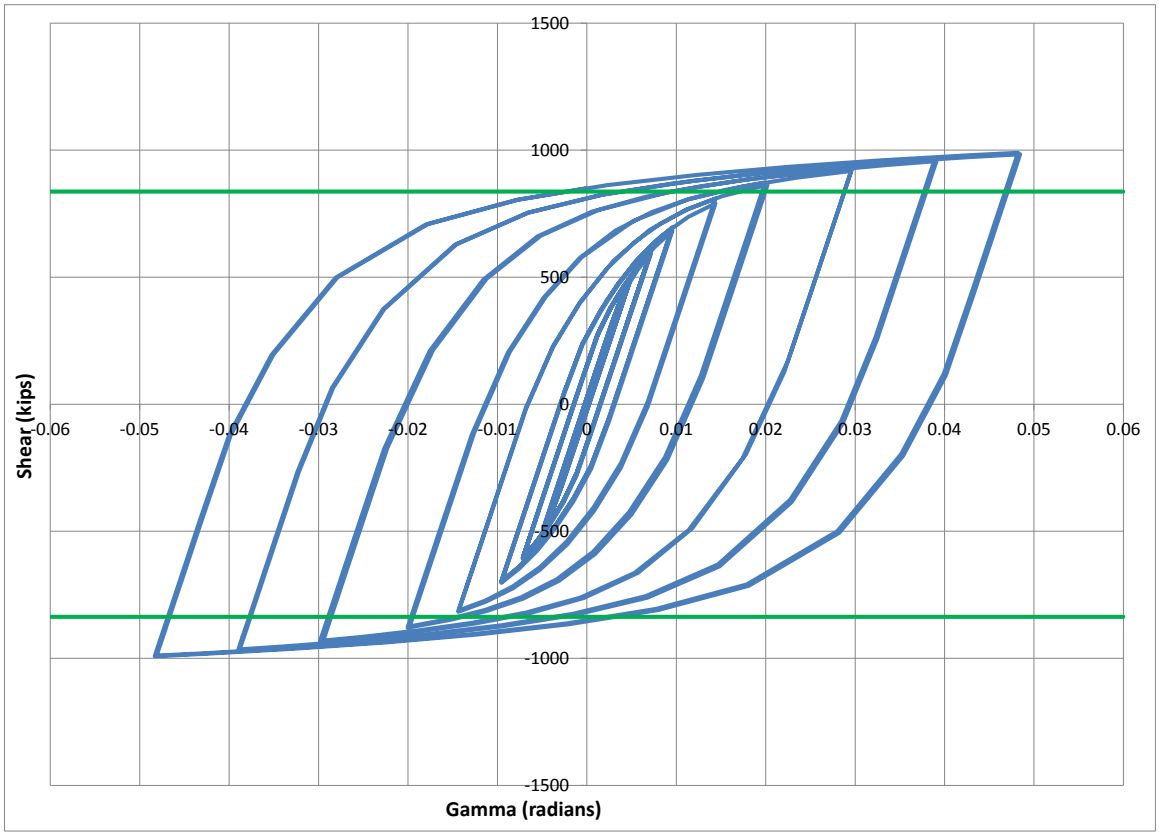

Figure 4.78: Panel zone shear versus rotation (Case 11A)

Table 4.17: Panel zone shear and force on loading plate (Case 11A)

Panel zone rotation (rad)	0.01	0.02	0.03	0.05
Panel zone shear (kips)	696.24	872.89	929.79	989.57
Force on one Loading plate (kips)	417.74	523.73	557.87	593.74

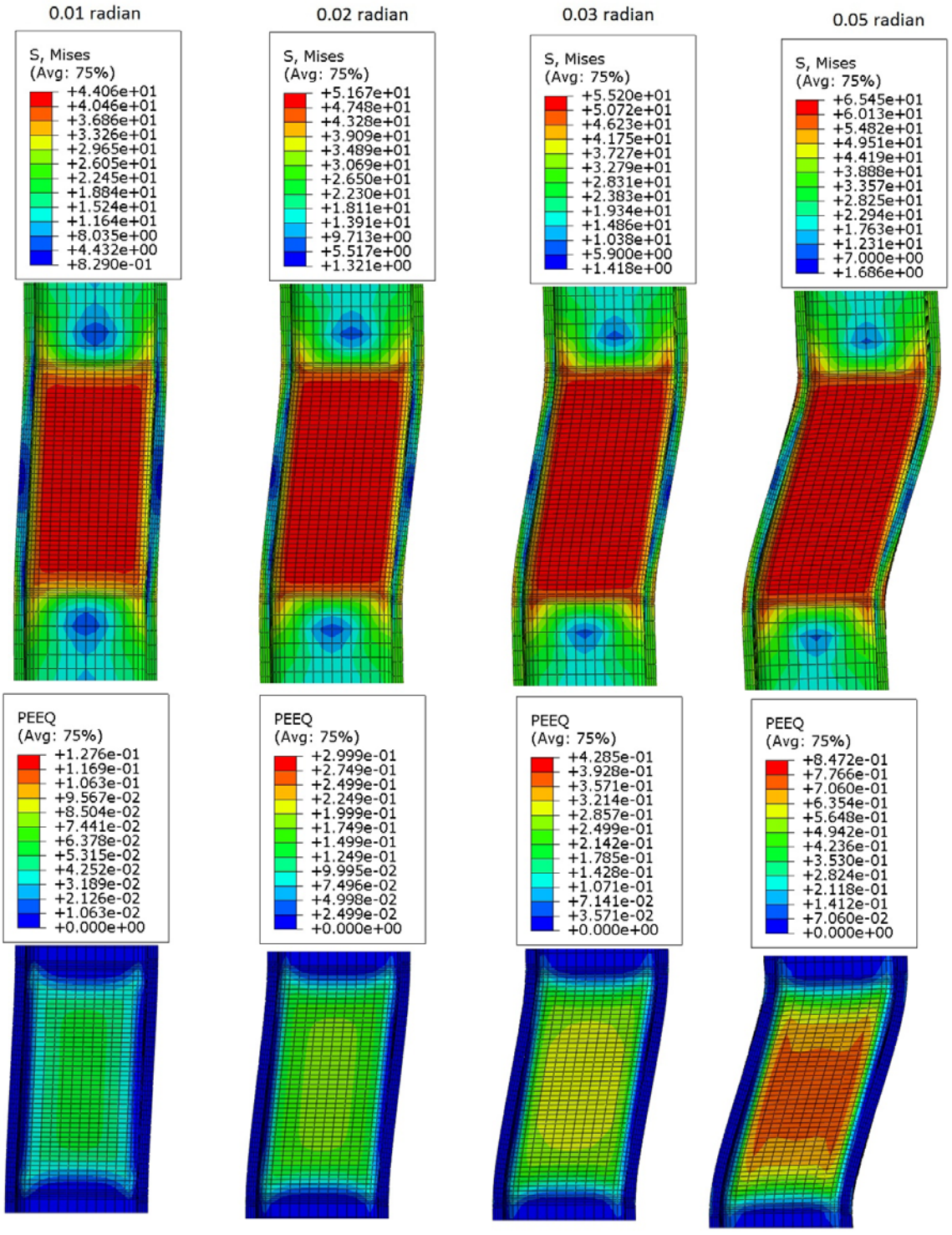

Figure 4.79: VMS and PEEQ in the column (Case 11A)

4.2.17 Analysis case 12A

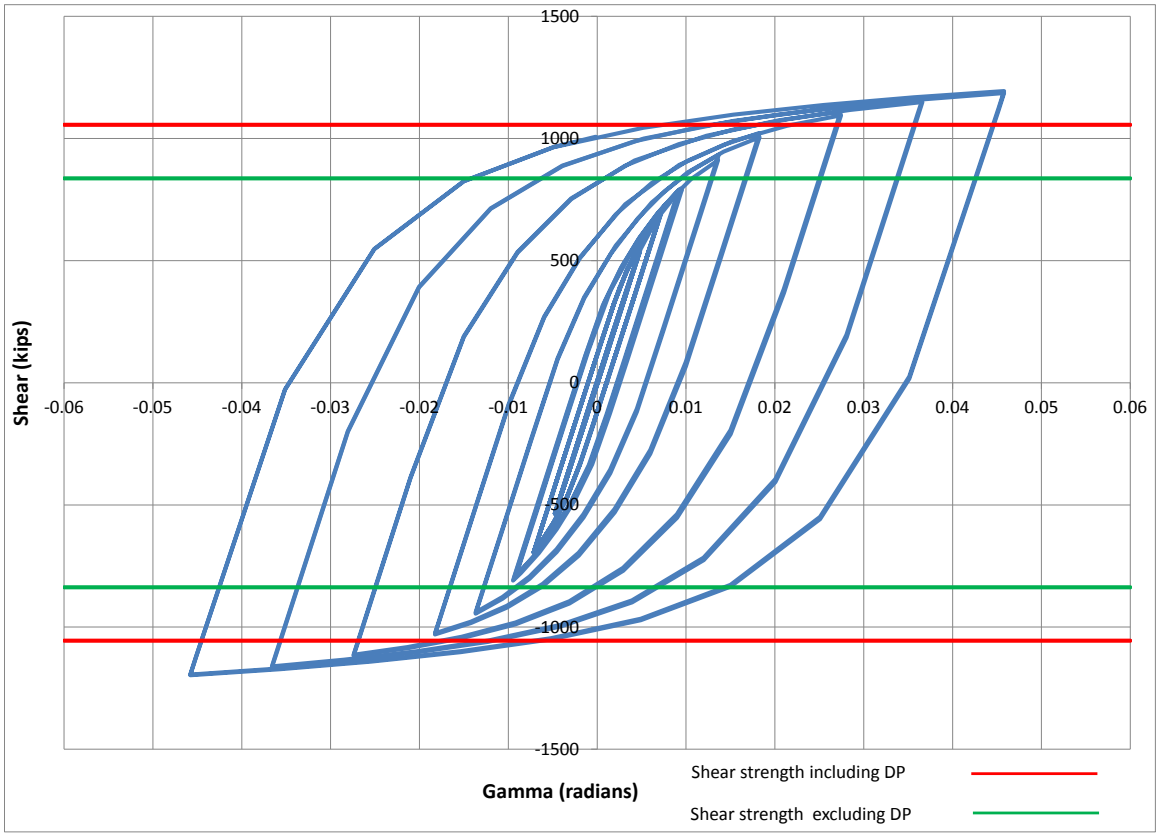

Figure 4.80: Panel zone shear versus rotation (Case 12A)

Table 4.18: Panel zone shear and force on loading plate (Case 12A)

Panel zone rotation (rad)	0.01	0.02	0.03	0.05
Panel zone shear (kips)	787.90	1022.24	1110.79	1194.05
Force on one Loading plate (kips)	472.74	613.34	666.47	716.43

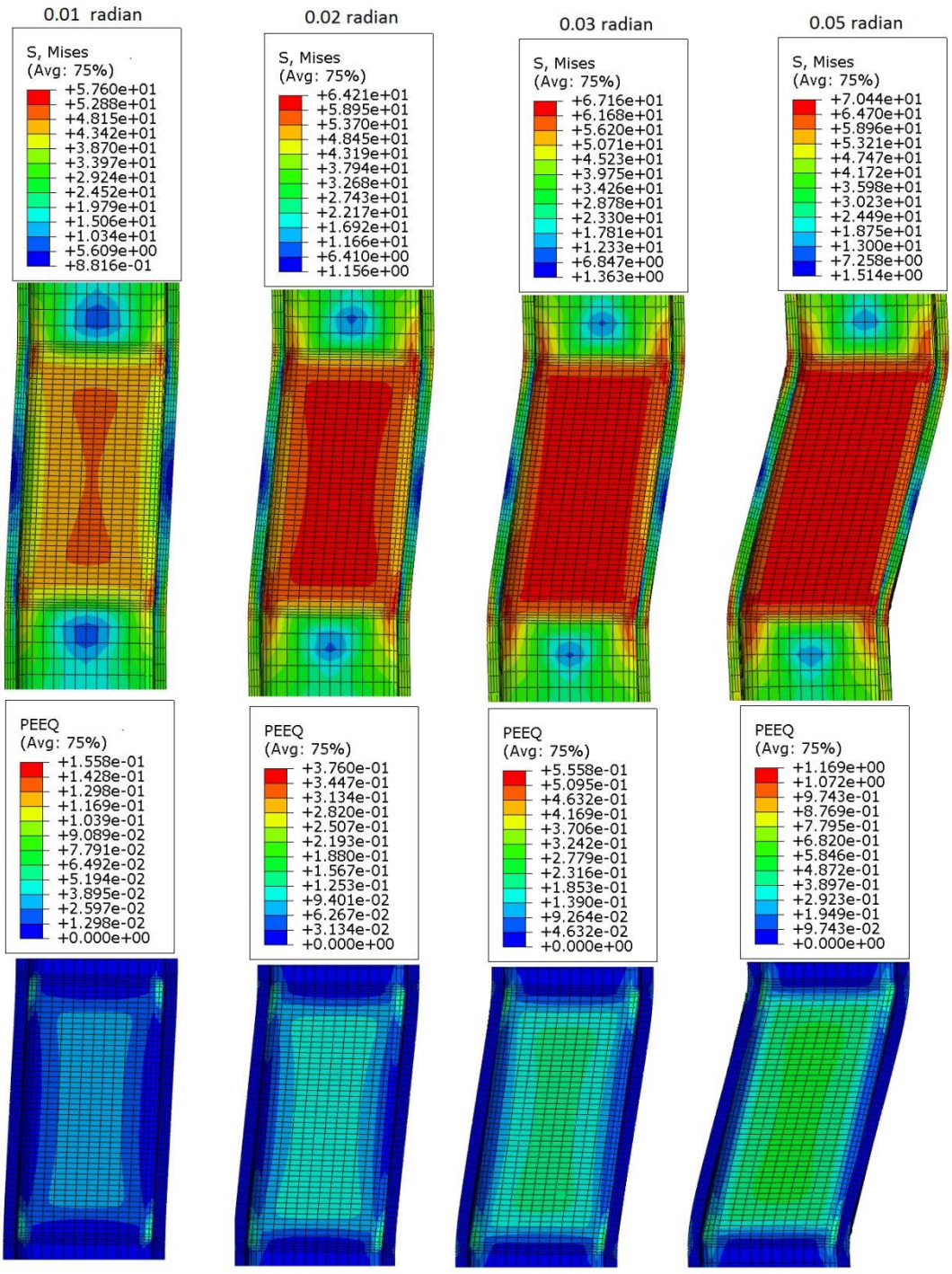

Figure 4.81: VMS and PEEQ in the column (Case 12A)

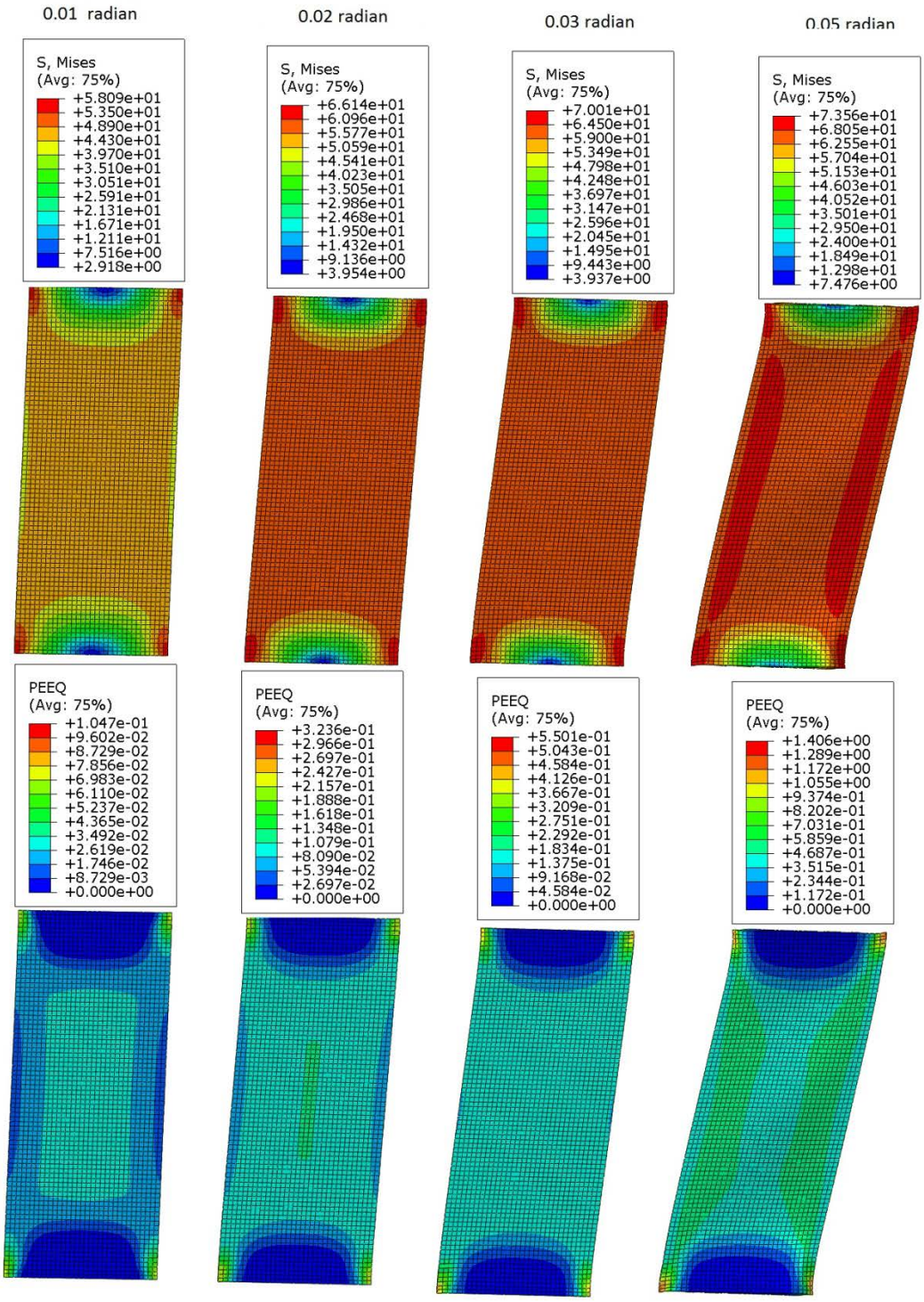

Figure 4.82: VMS and PEEQ in the DP (Case 12A)

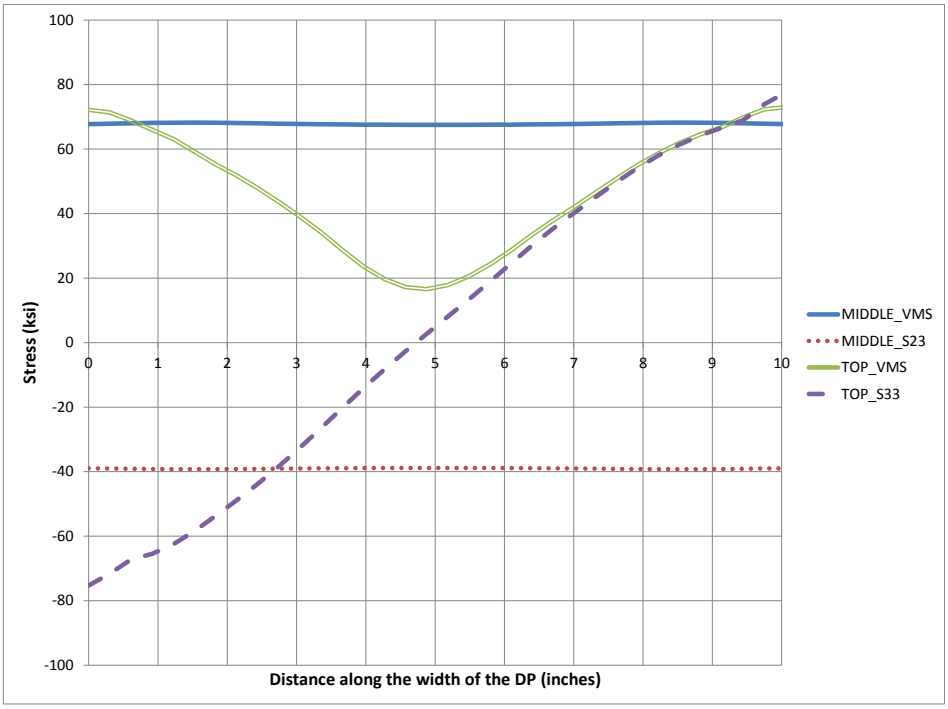

Figure 4.83: Stresses along the width of DP at 0.05 radian rotation (Case 12A)

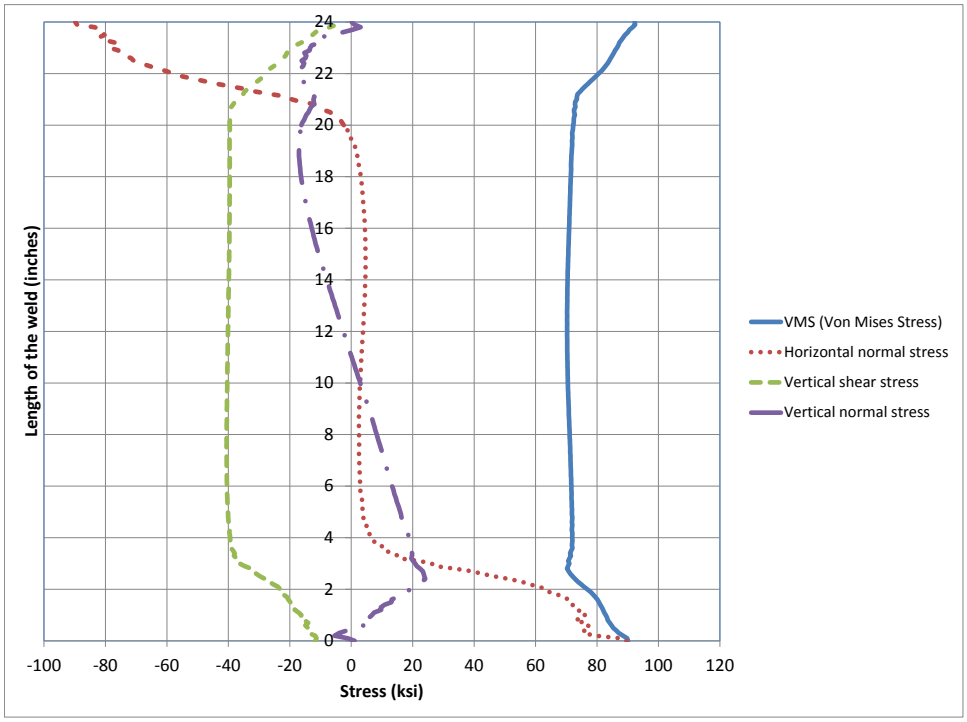

Figure 4.84: Stresses along depth of CJP1 (DP-CJP1 interface) at 0.05 radian (Case 12A)

4.2.18 Analysis case 13A

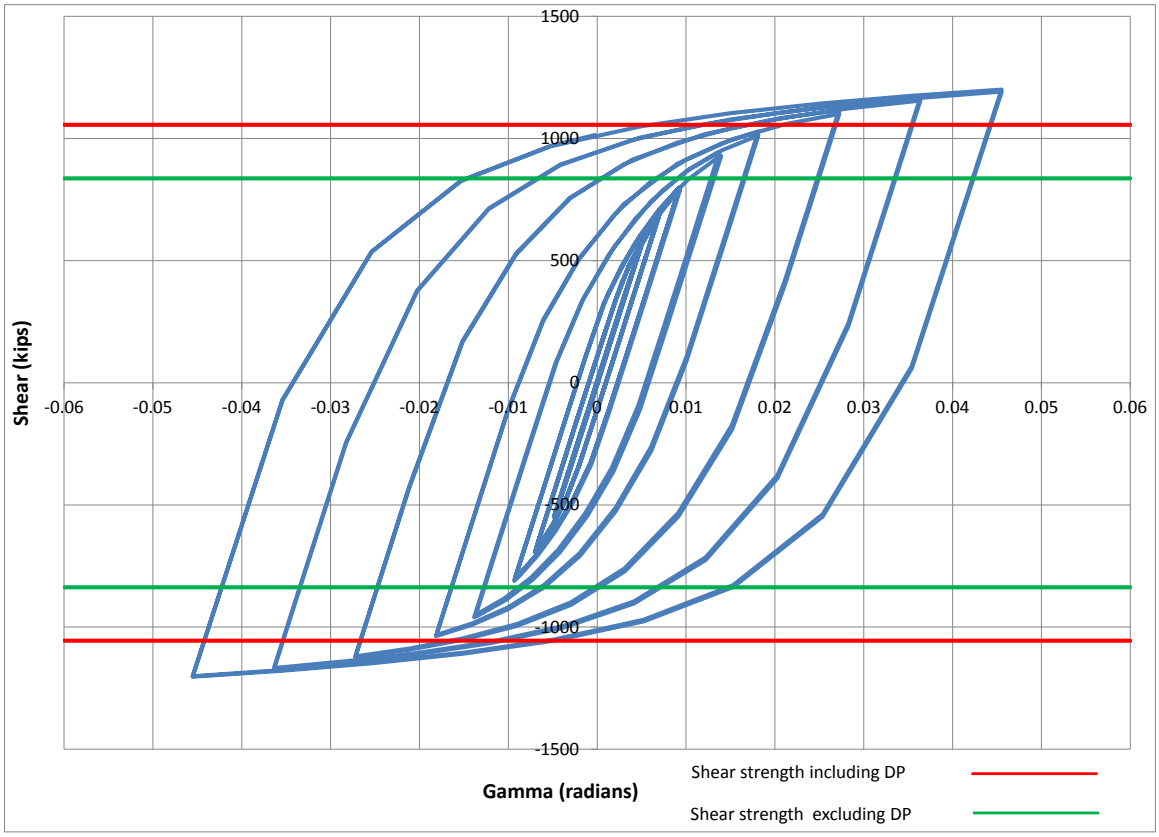

Figure 4.85: Panel zone shear versus rotation (Case 13A)

Table 4.19: Panel zone shear and force on loading plate (Case 13A)

Panel zone rotation (rad)	0.01	0.02	0.03	0.05
Panel zone shear (kips)	800.32	1029.23	1117.03	1200.25
Force on one Loading plate (kips)	480.19	617.54	670.22	720.15

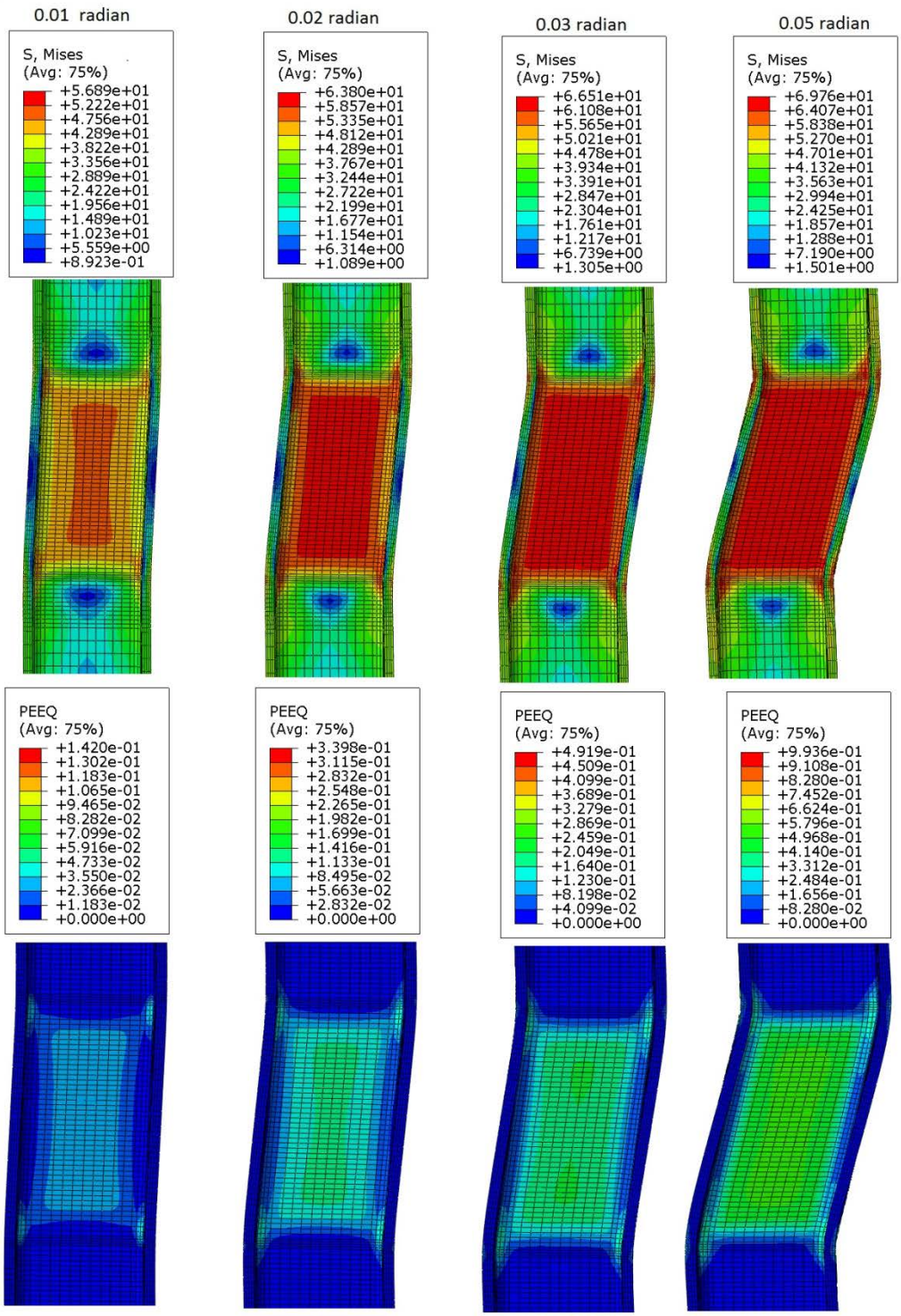

Figure 4.86: VMS and PEEQ in the column (Case 13A)

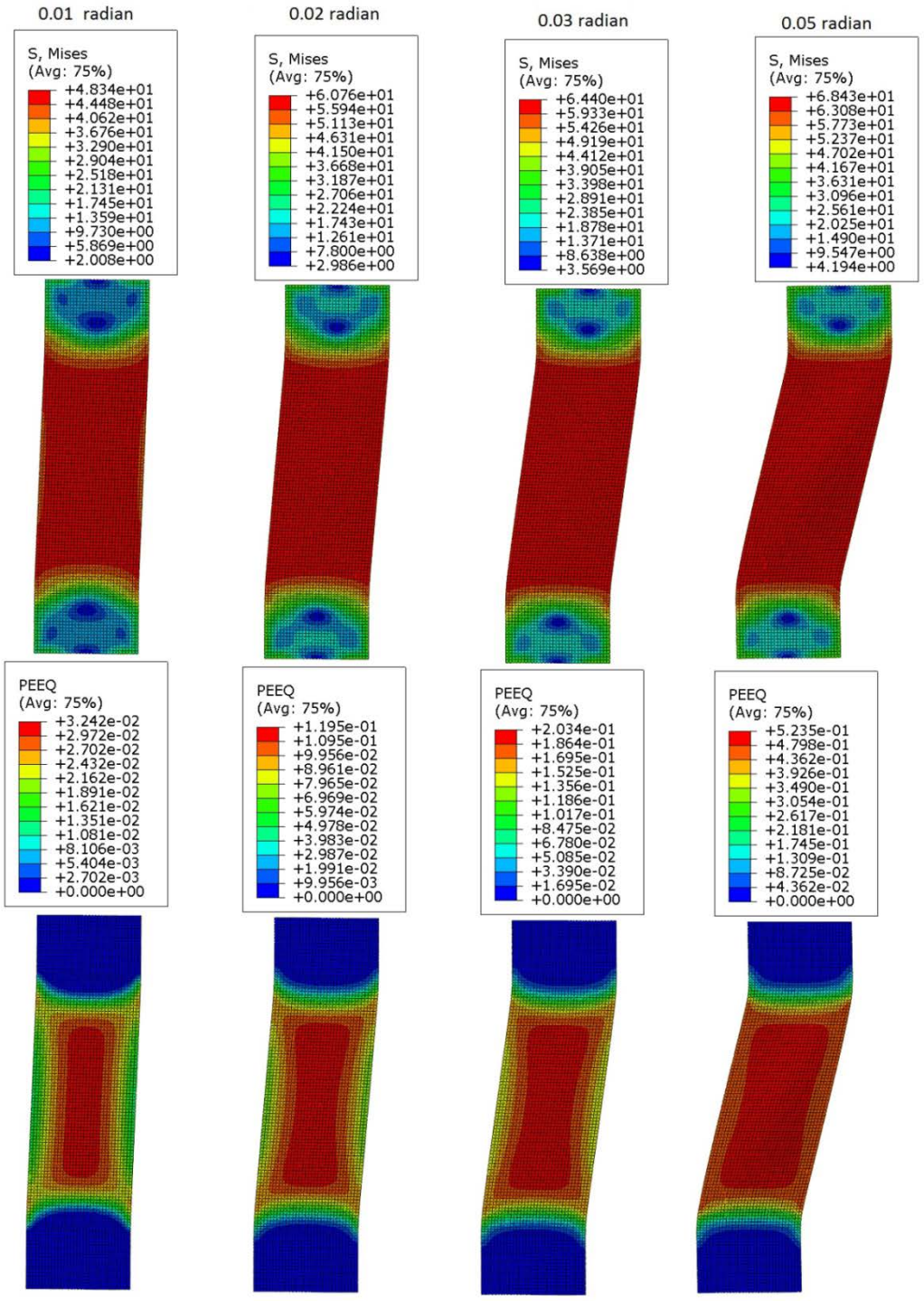

Figure 4.87: VMS and PEEQ in the DP (Case 13A)

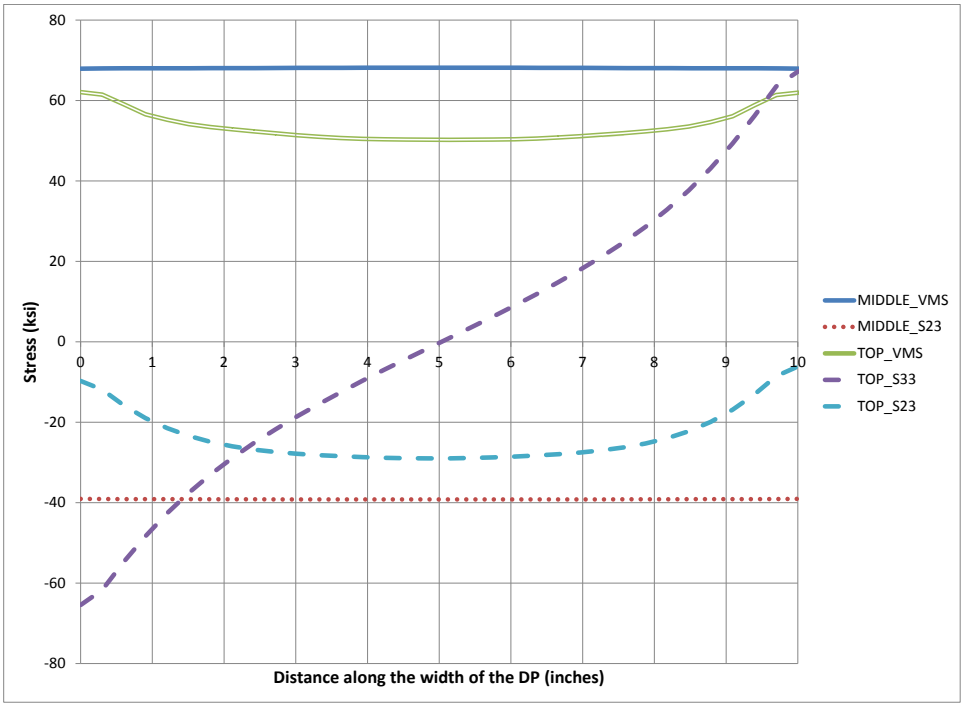

Figure 4.88: Stresses along the width of DP at 0.05 radian rotation (Case 13A)

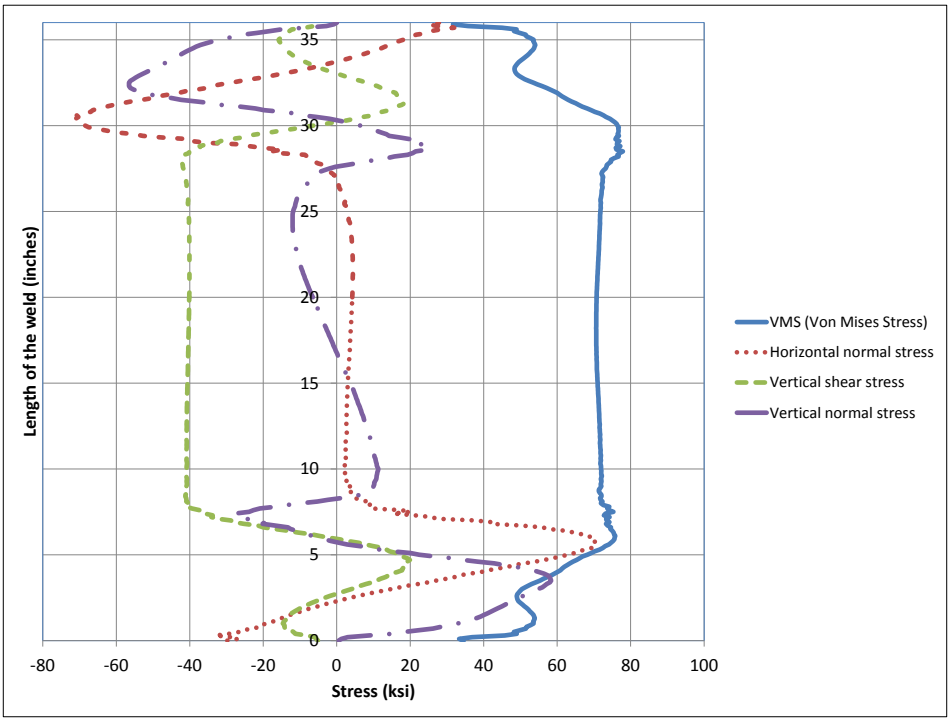

Figure 4.89: Stresses along depth of CJP1 (DP-CJP1 interface) at 0.05 radian (Case 13A)

4.2.19 Analysis case 13A_quar

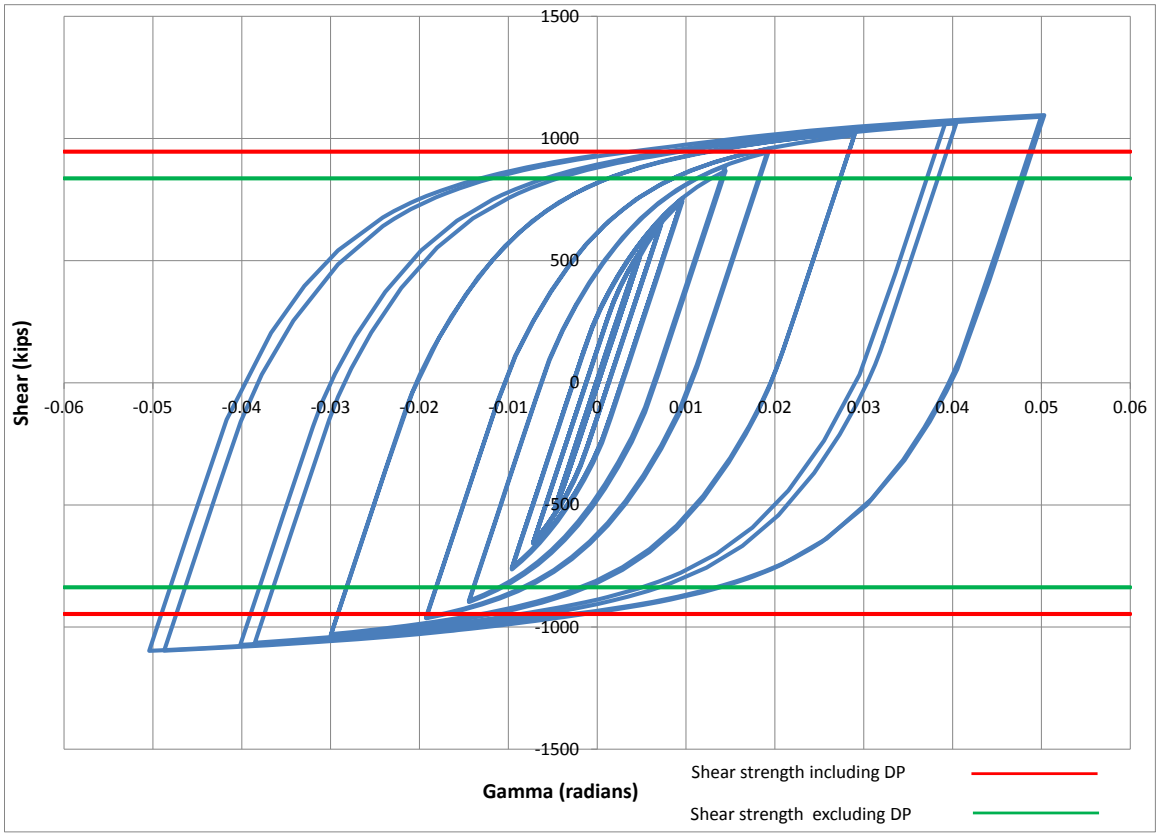

Figure 4.90: Panel zone shear versus rotation (Case 13A_quar)

Table 4.20: Panel zone shear and force on loading plate (Case 13A_quar)

Panel zone rotation (rad)	0.01	0.02	0.03	0.05
Panel zone shear (kips)	756.45	958.26	1027.04	1095.51
Force on one Loading plate (kips)	453.87	574.96	616.22	657.31

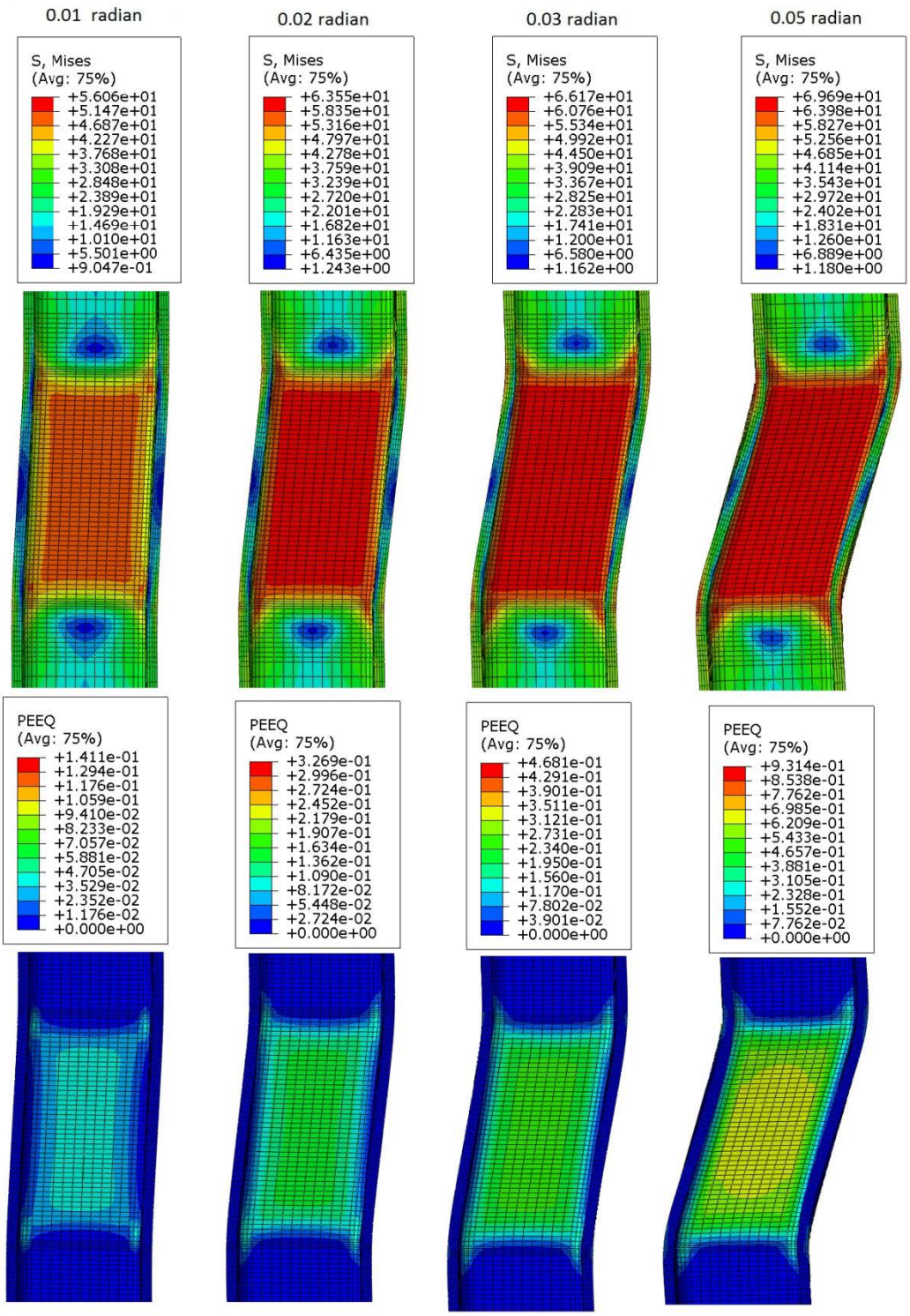

Figure 4.91: VMS and PEEQ in the column (Case 13A_quar)

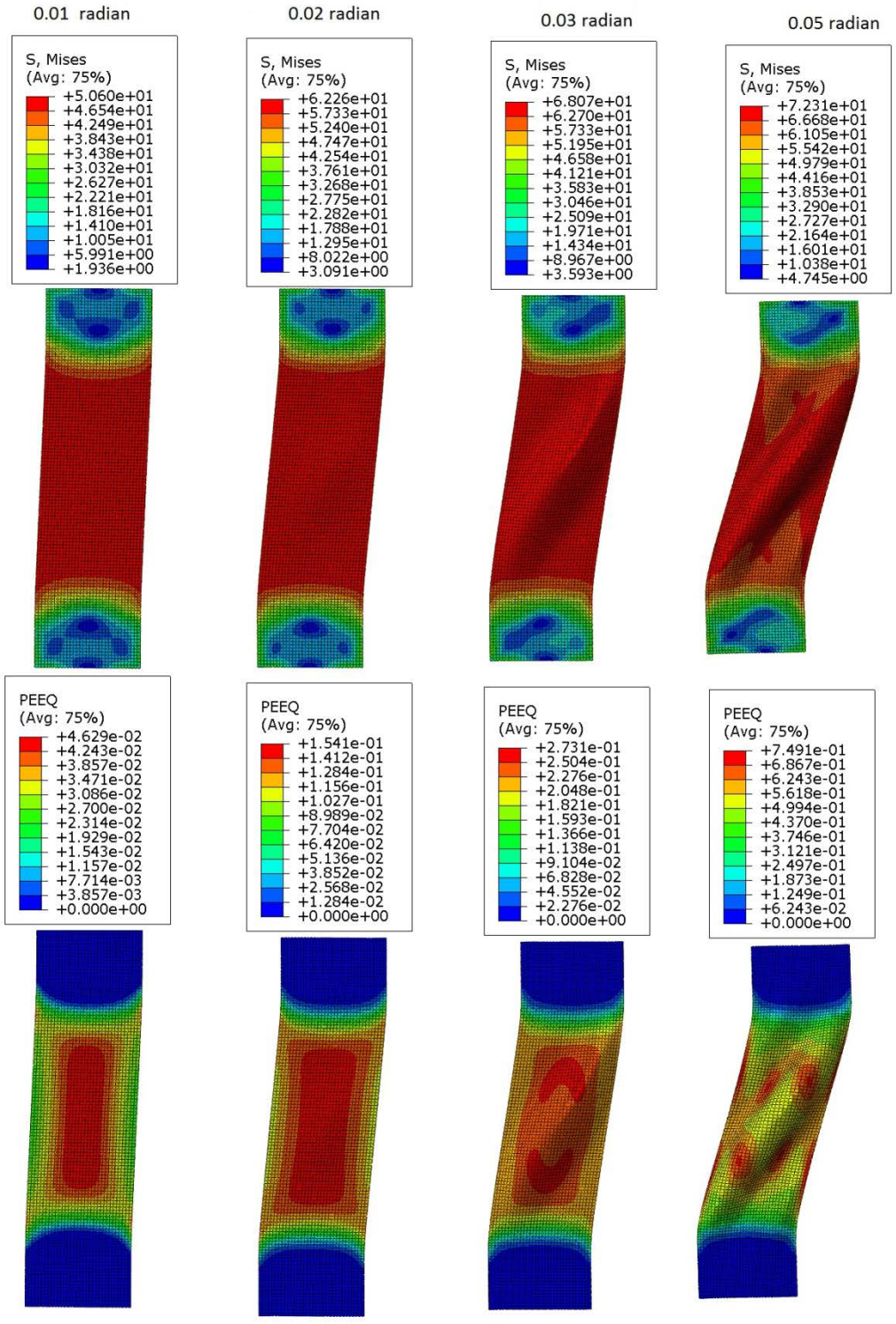

Figure 4.92: VMS and PEEQ in the DP (Case 13A_quar)

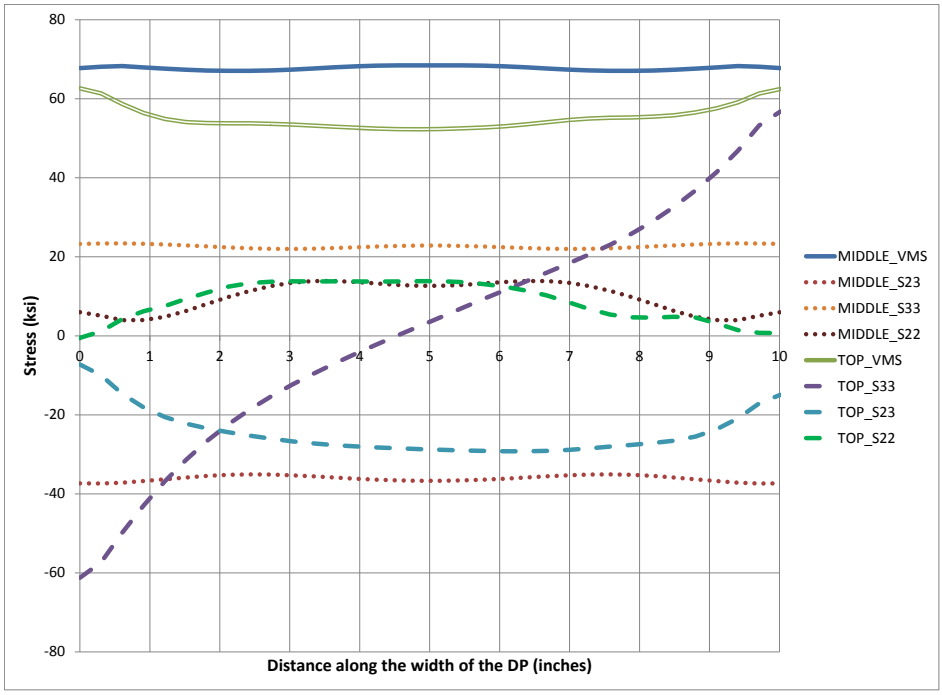

Figure 4.93: Stresses along the width of DP at 0.05 radian rotation (Case 13A_quar)

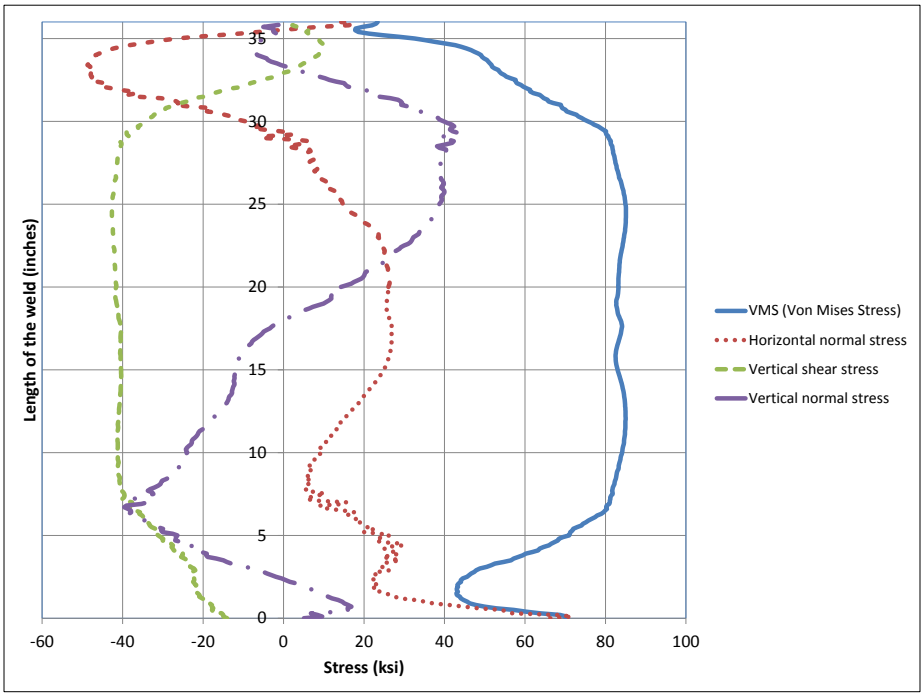

Figure 4.94: Stresses along depth of CJP1 (DP-CJP1 interface) at 0.05 radian (Case 13A_quar)

4.2.20 Analysis case 13A_one

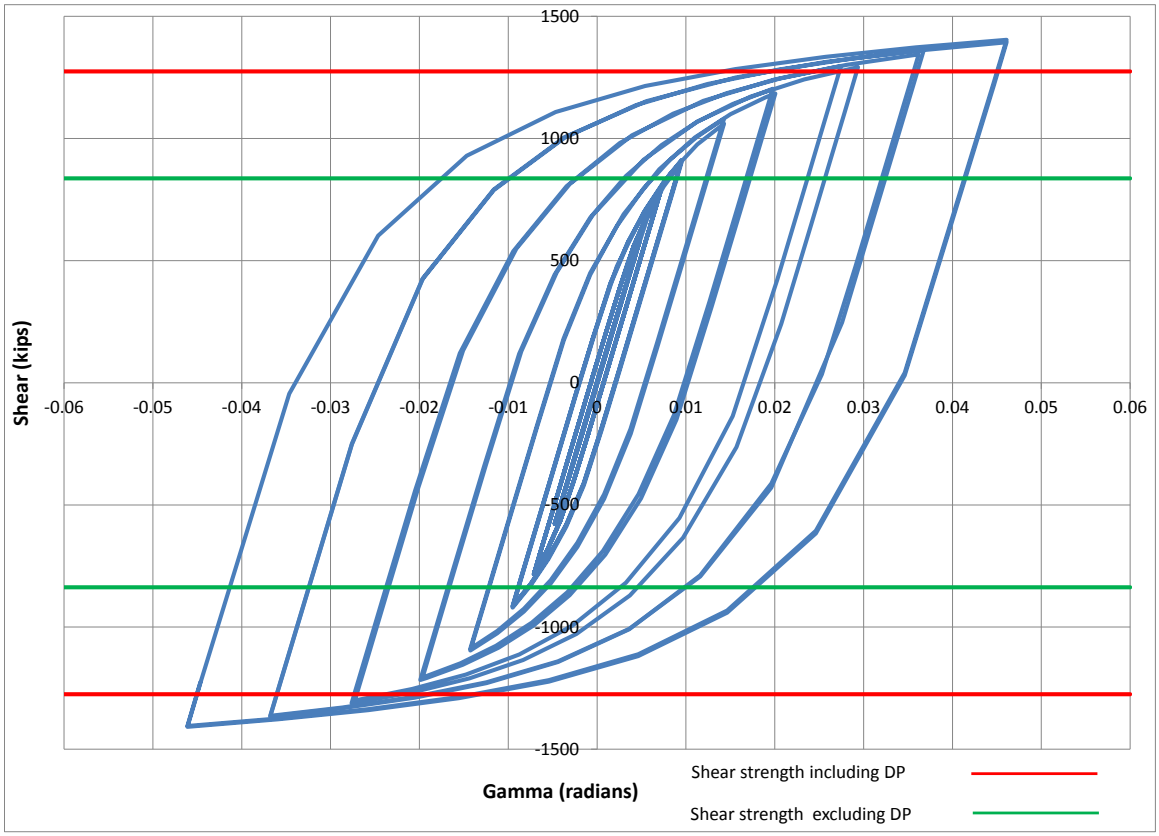

Figure 4.95: Panel zone shear versus rotation (Case 13A_one)

Table 4.21: Panel zone shear and force on loading plate (Case 13A_one)

Panel zone rotation (rad)	0.01	0.02	0.03	0.05
Panel zone shear (kips)	911.81	1203.20	1295.88	1404.12
Force on one Loading plate (kips)	547.08	721.92	777.53	842.47

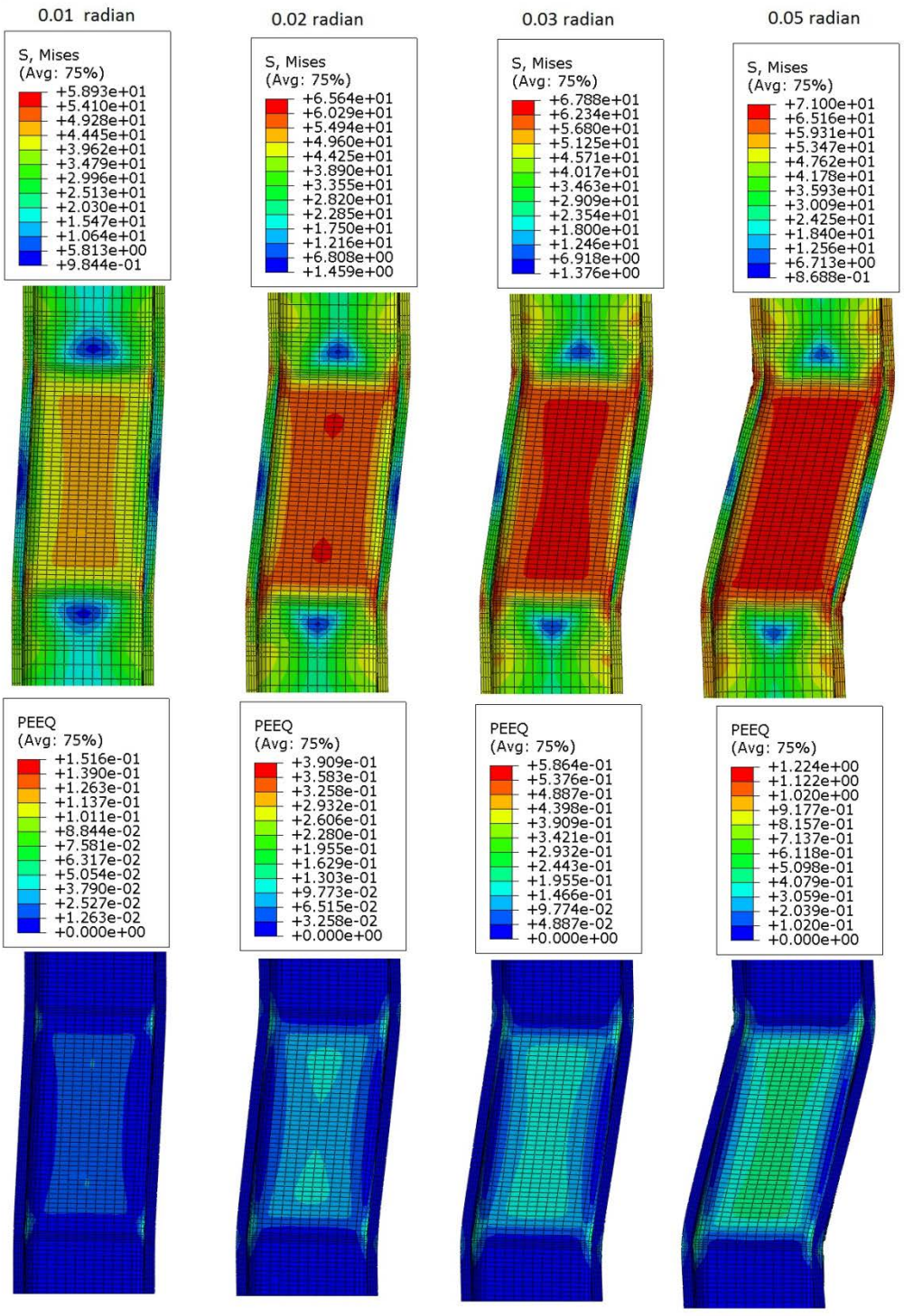

Figure 4.96: VMS and PEEQ in the column (Case 13A_one)

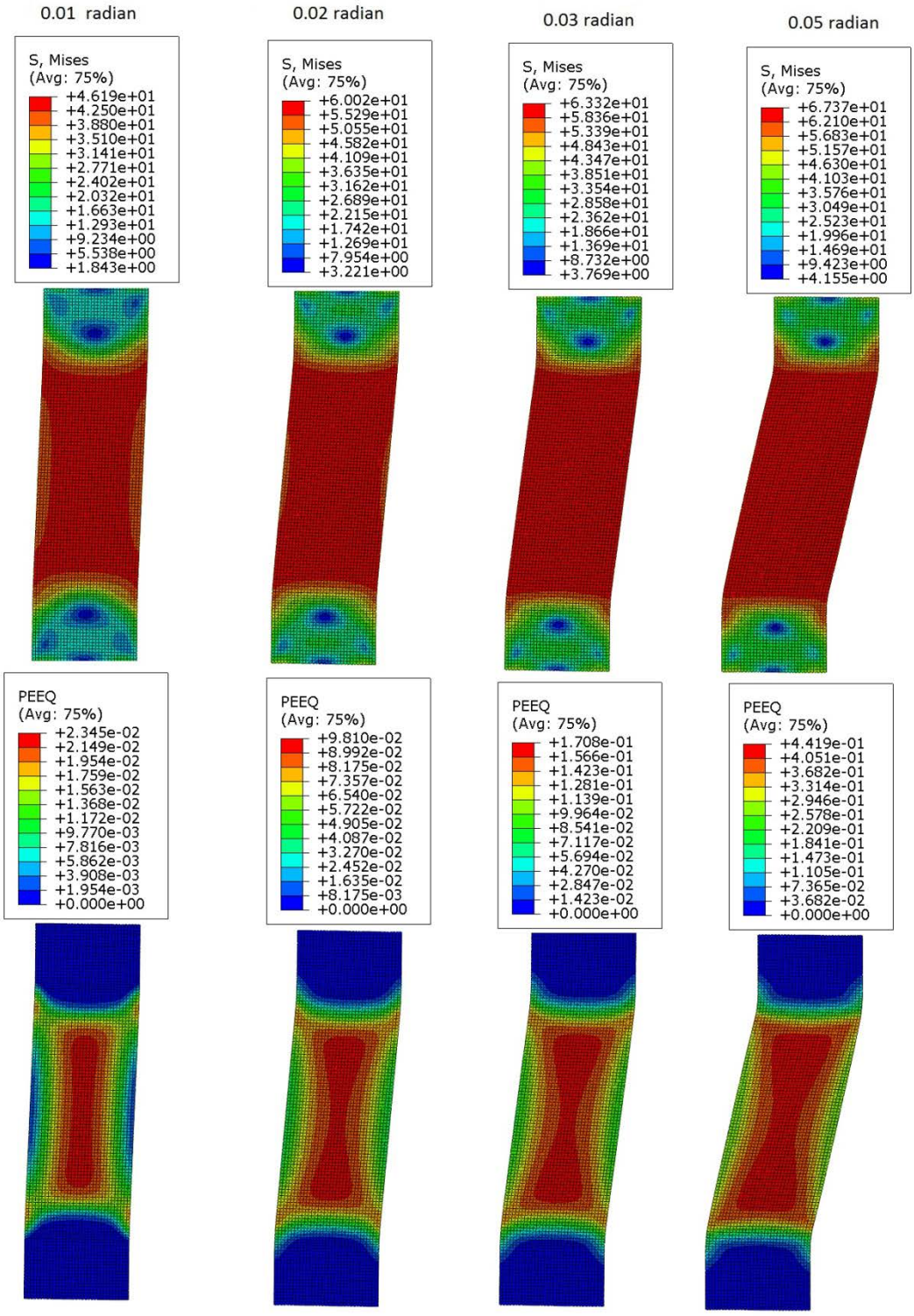

Figure 4.97: VMS and PEEQ in the DP (Case 13A_one)

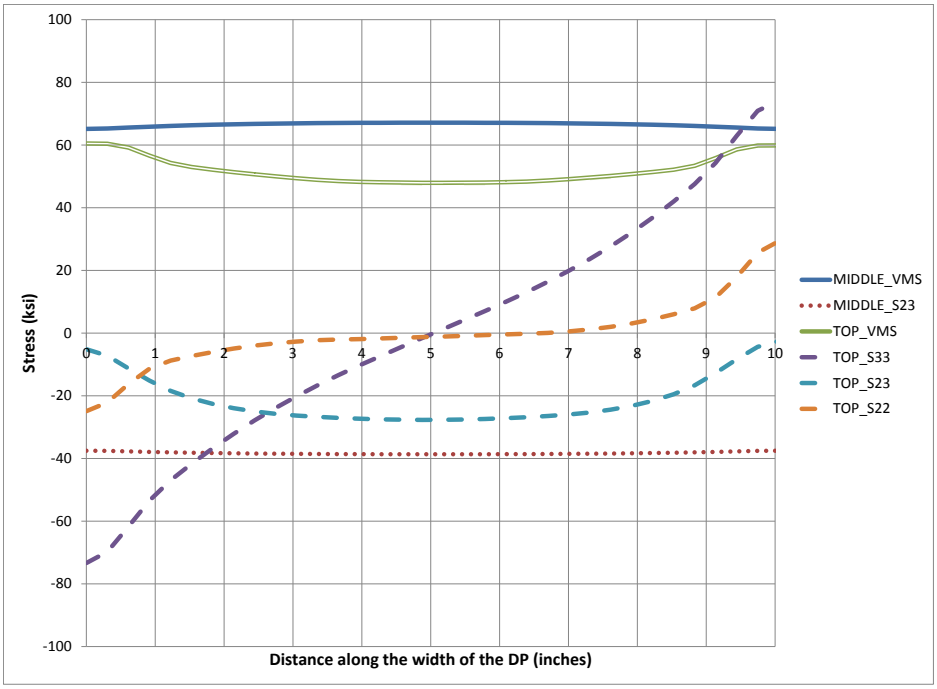

Figure 4.98: Stresses along the width of DP at 0.05 radian rotation (Case 13A_one)

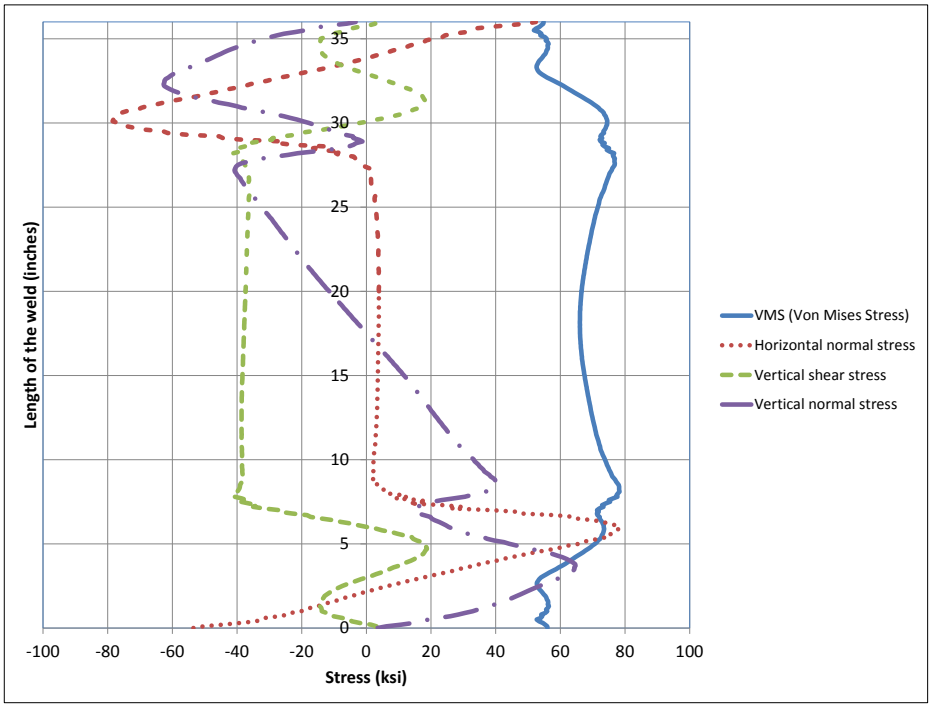

Figure 4.99: Stresses along depth of CJP1 (DP-CJP1 interface) at 0.05 radian (Case 13A_one)

4.2.21 Analysis case 14A

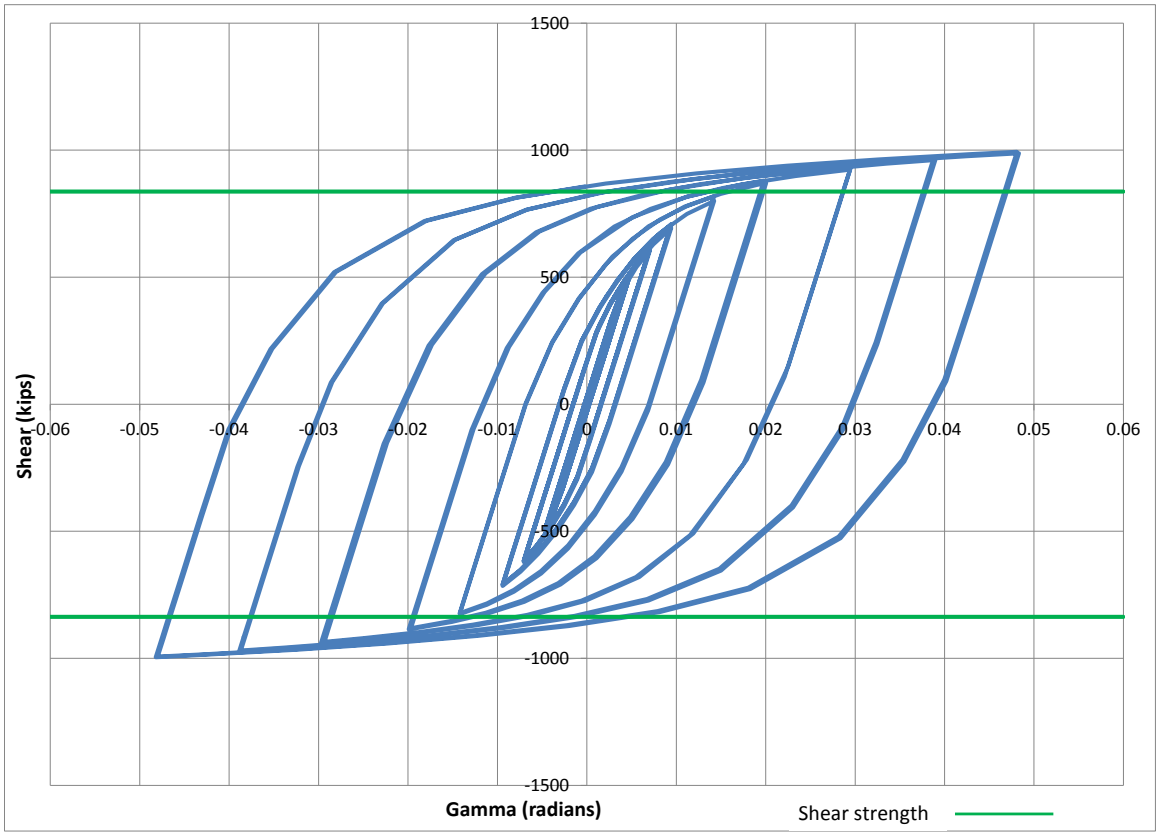

Figure 4.100: Panel zone shear versus rotation (Case 14A)

Table 4.22: Panel zone shear and force on loading plate (Case 14A)

Panel zone rotation (rad)	0.01	0.02	0.03	0.05
Panel zone shear (kips)	708.38	880.00	935.06	993.38
Force on one Loading plate (kips)	425.03	528.00	561.03	596.03

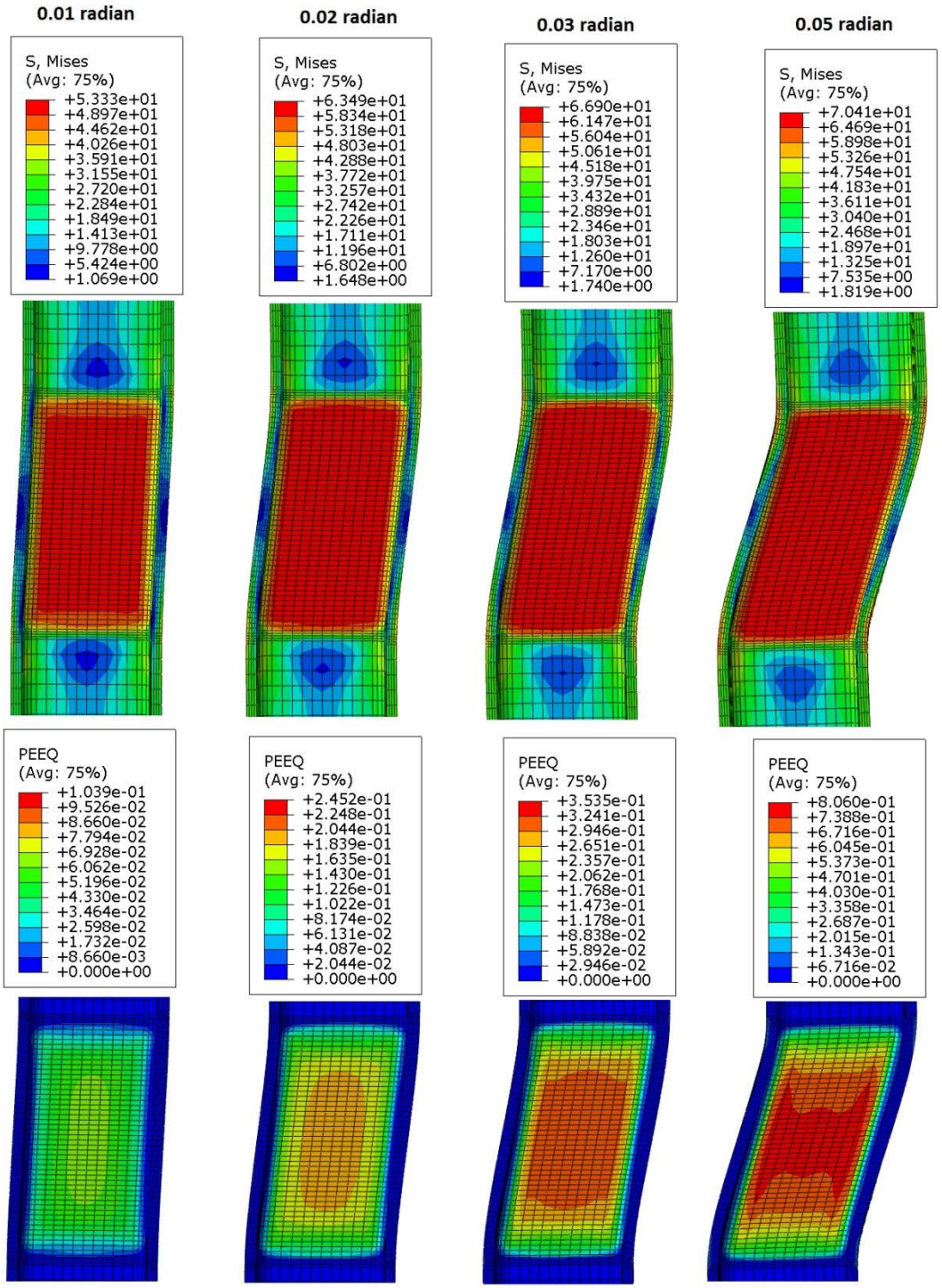

Figure 4.101: VMS and PEEQ in the column (Case 14A)

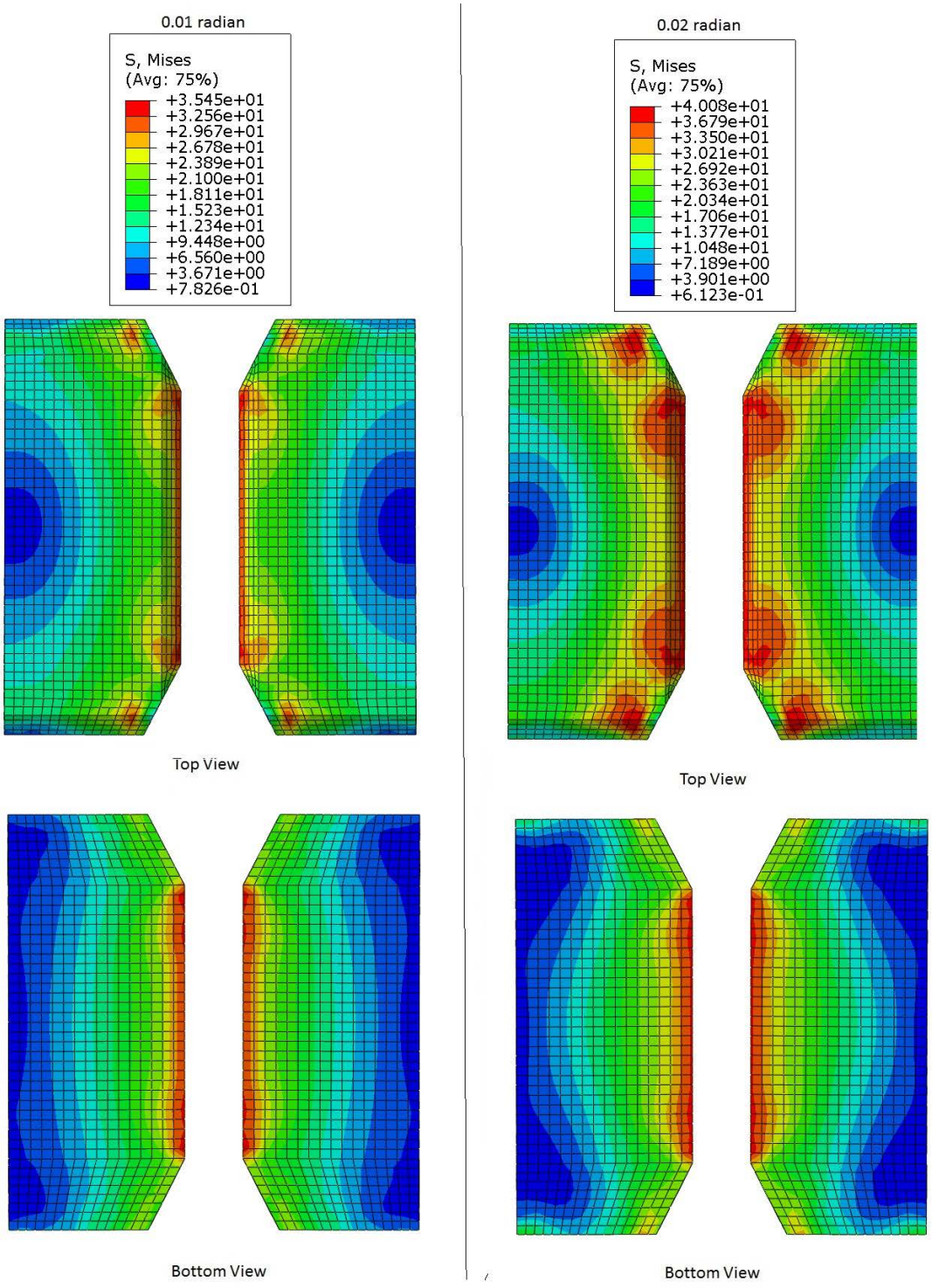

Figure 4.102: VMS in the CP at 0.01 and 0.02 radian rotation (Case 14A)

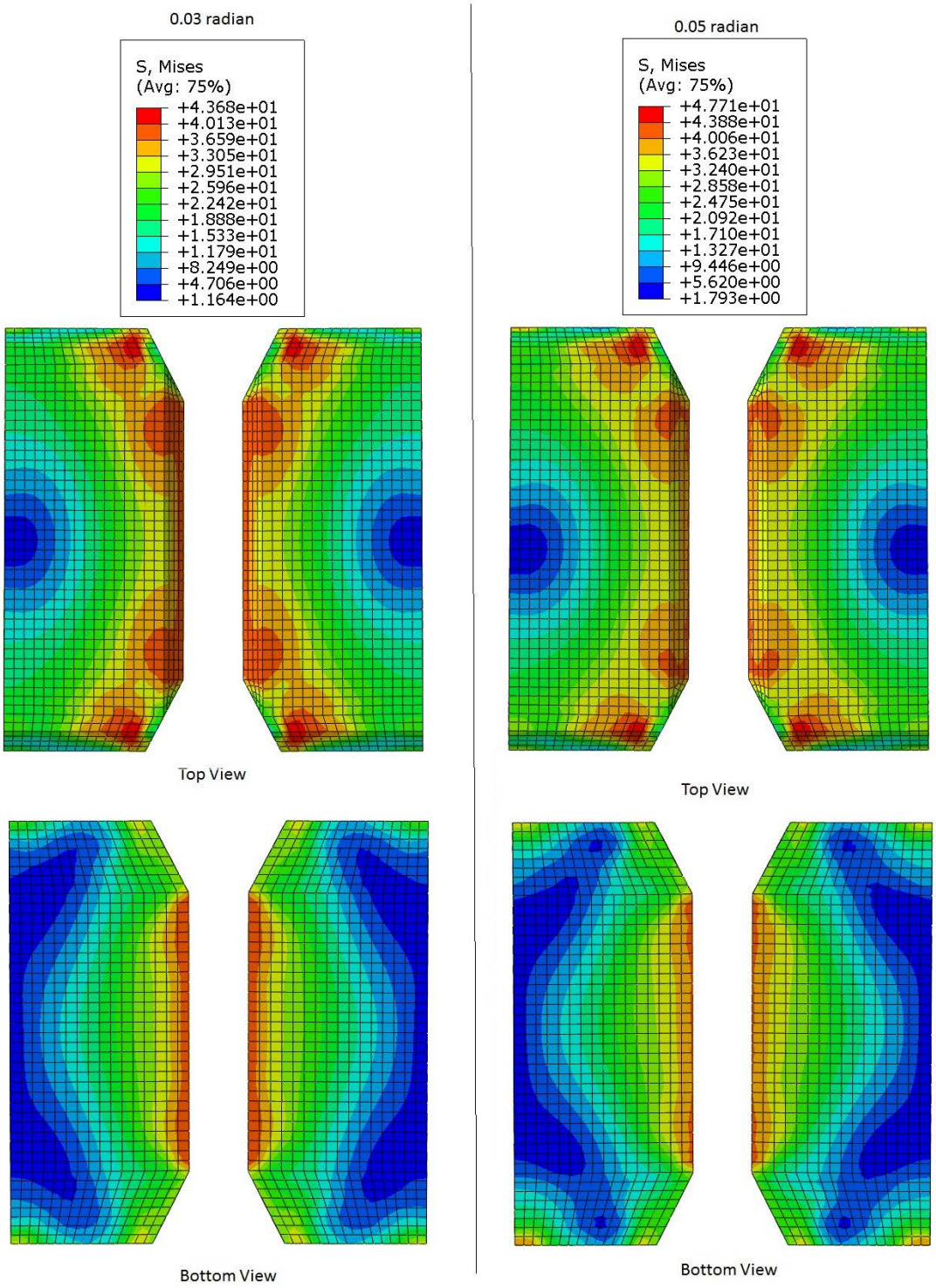

Figure 4.103: VMS in the CP at 0.03 and 0.05 radian rotation (Case 14A)

4.2.22 Analysis case 15A

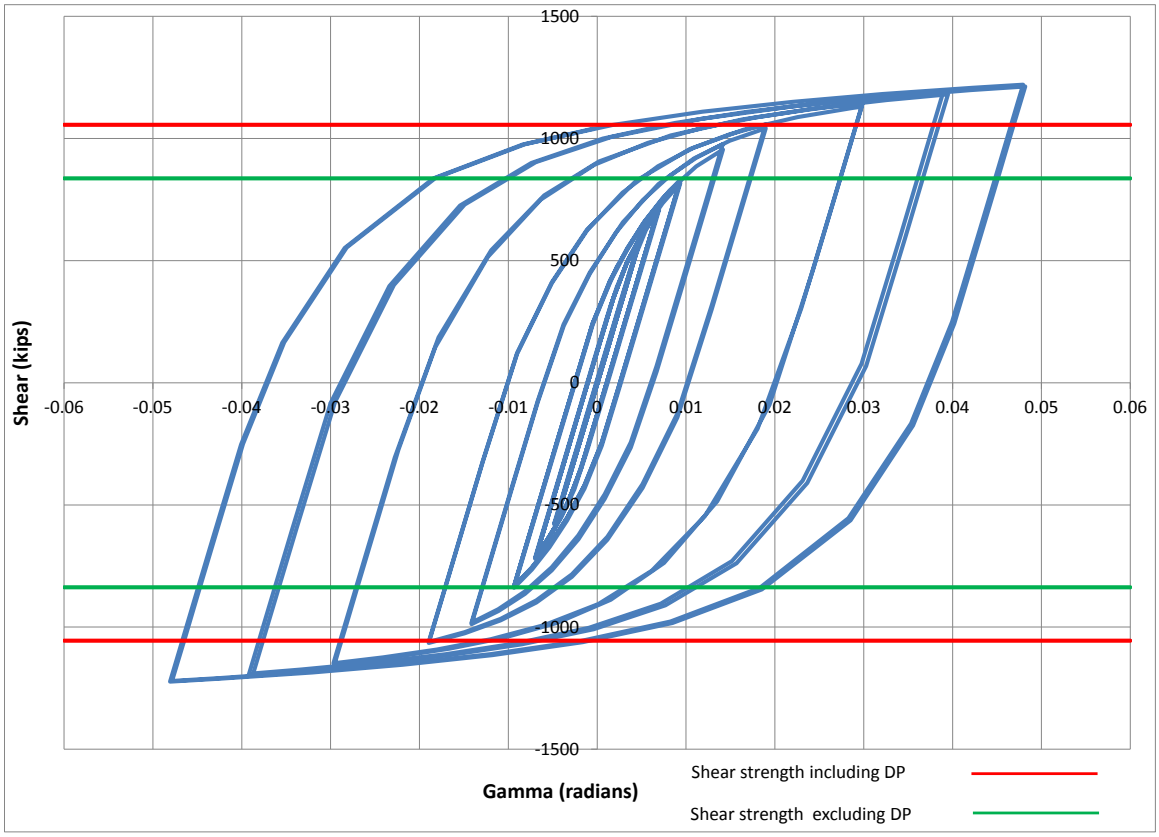

Figure 4.104: Panel zone shear versus rotation (Case 15A)

Table 4.23: Panel zone shear and force on loading plate (Case 15A)

Panel zone rotation (rad)	0.01	0.02	0.03	0.05
Panel zone shear (kips)	830.76	1057.97	1145.82	1220.37
Force on one Loading plate (kips)	498.45	634.78	687.49	732.22

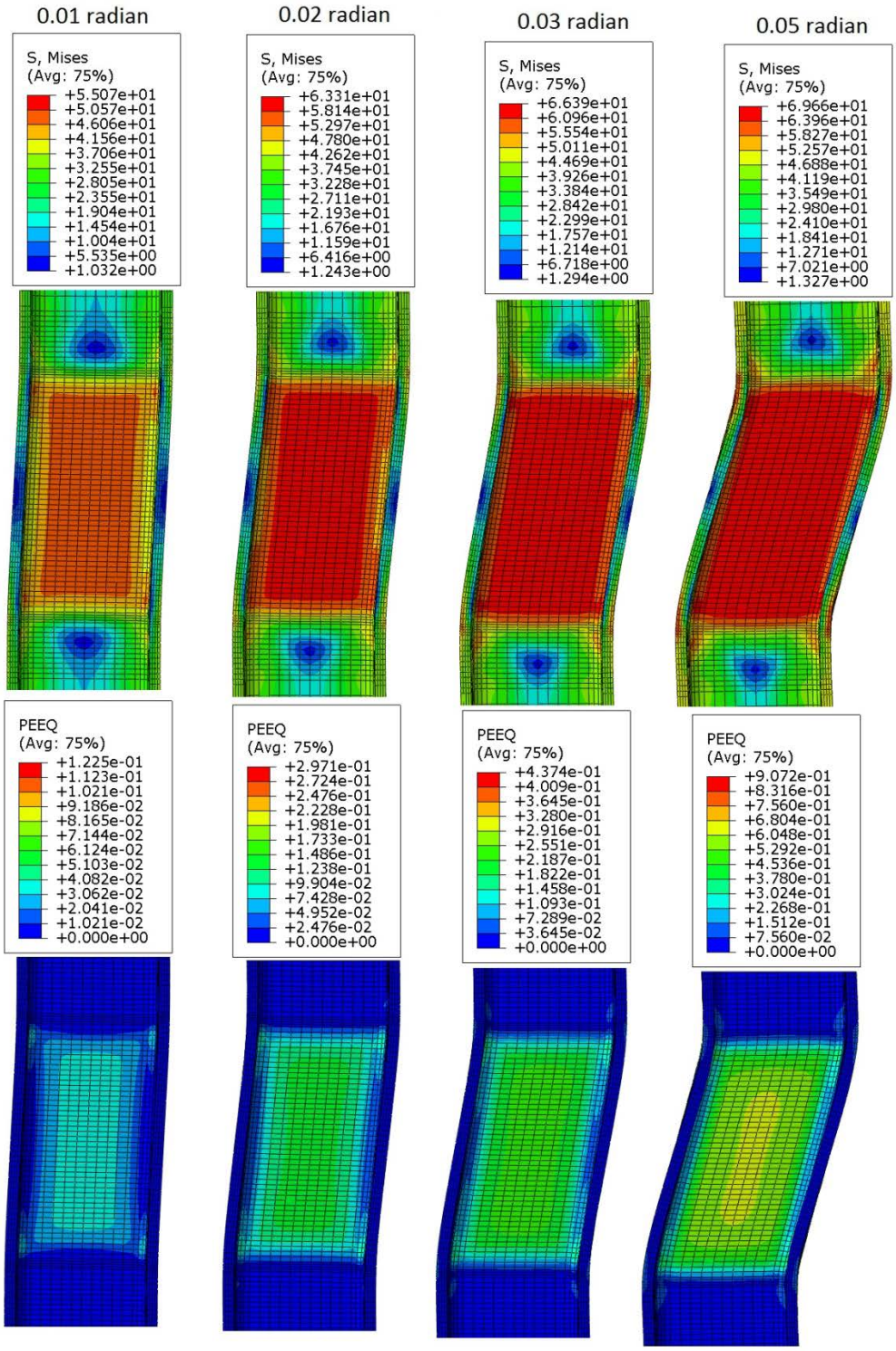

Figure 4.105: VMS and PEEQ in the column (Case 15A)

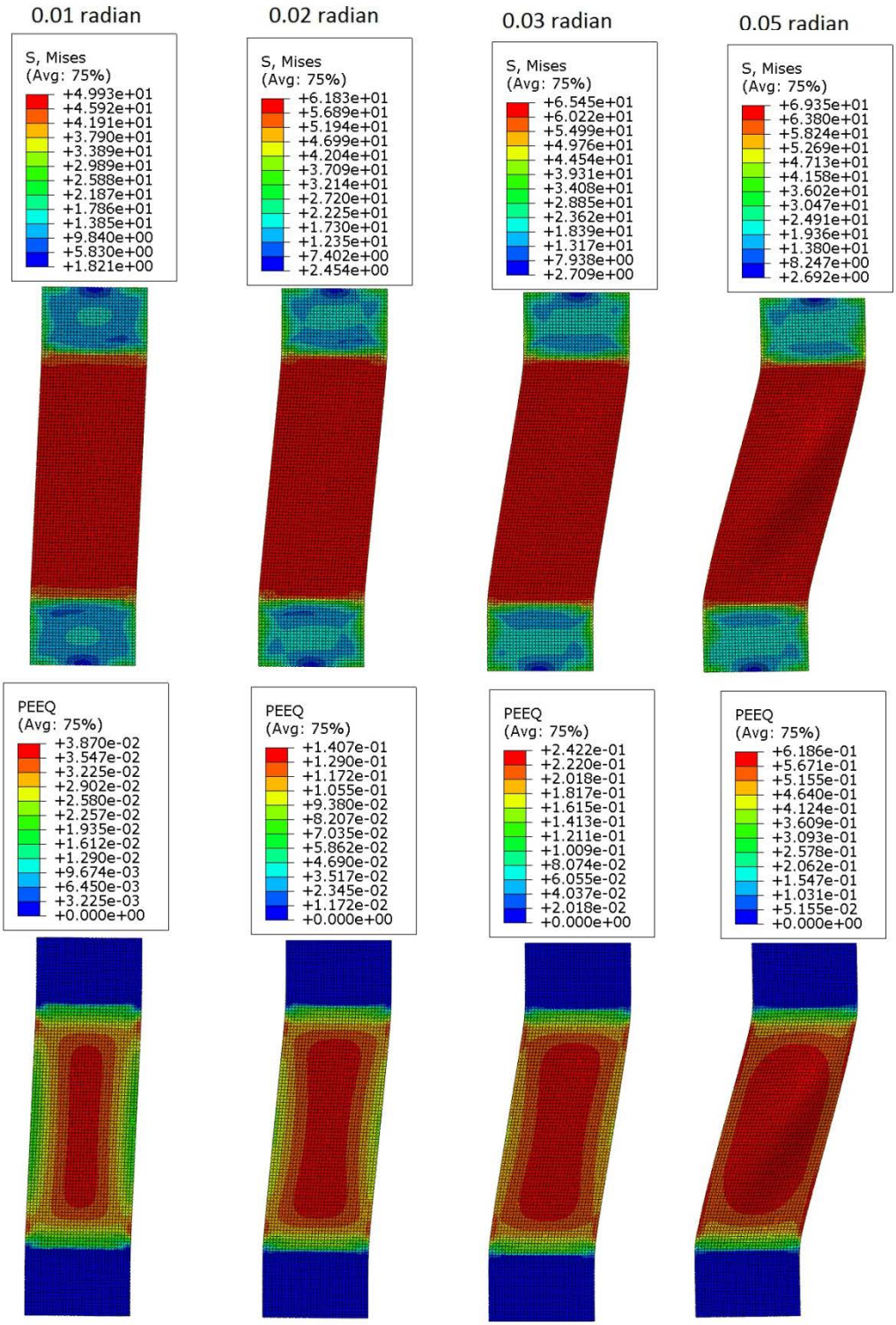

Figure 4.106: VMS and PEEQ in the DP (Case 15A)

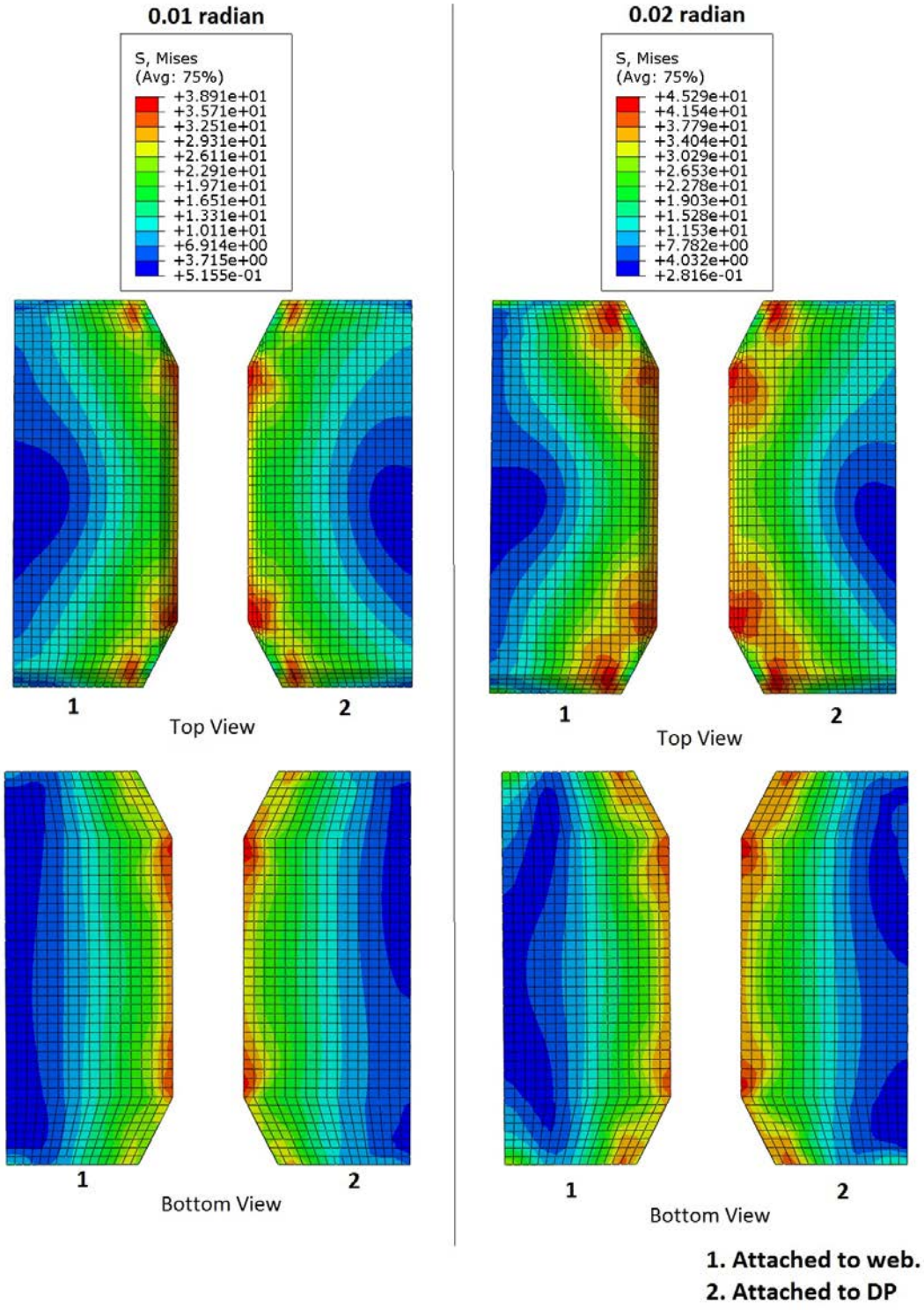

Figure 4.107: VMS in the CP at 0.01 and 0.02 radian rotation (Case 15A)

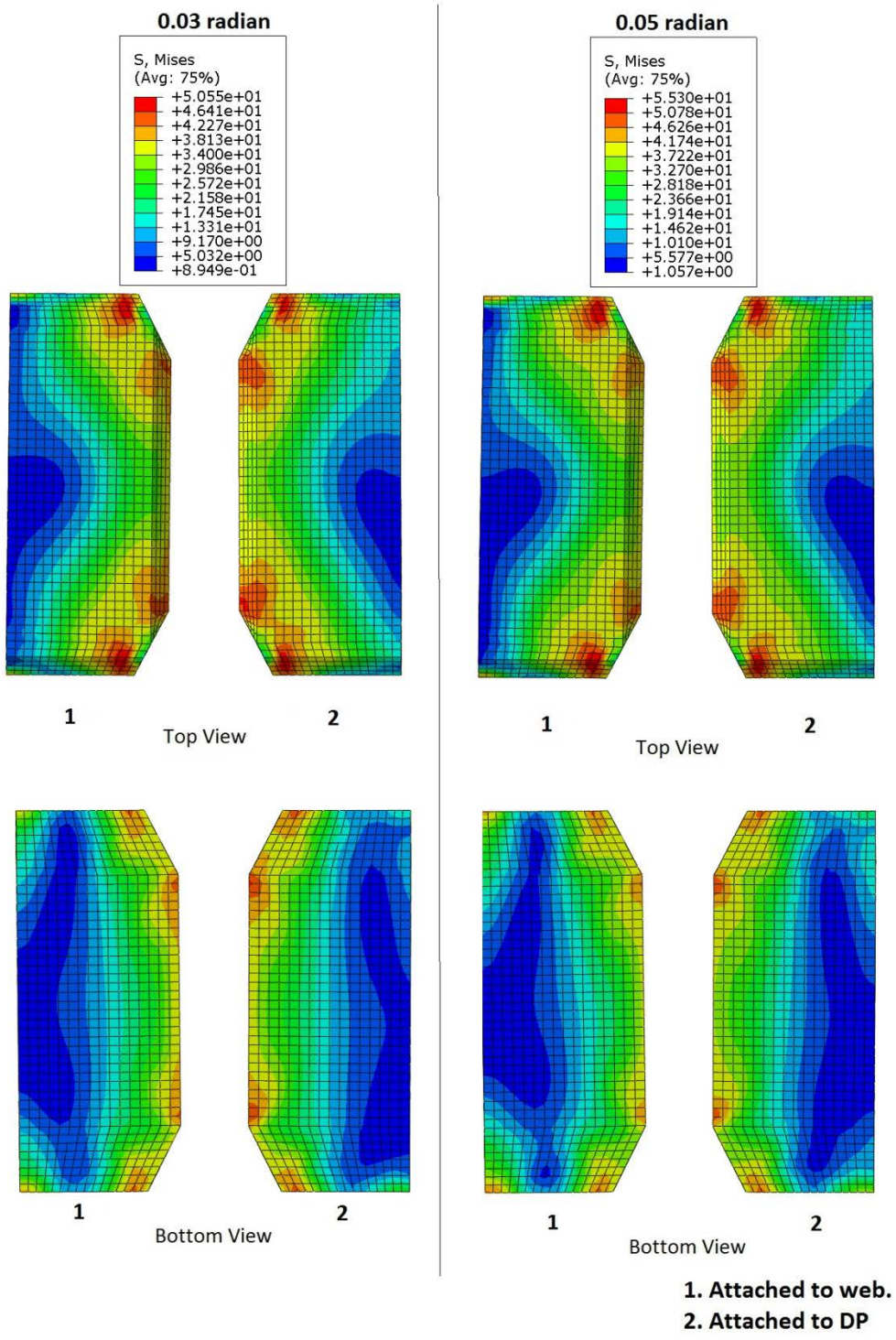

Figure 4.108: VMS in the CP at 0.03 and 0.05 radian rotation (Case 15A)

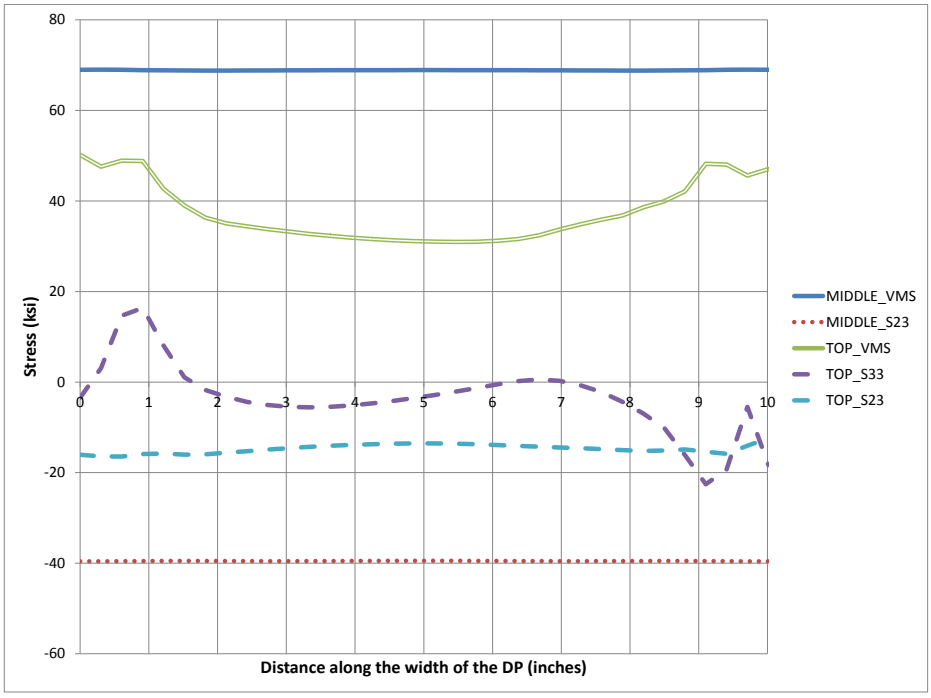

Figure 4.109: Stresses along the width of DP at 0.05 radian rotation (Case 15A)

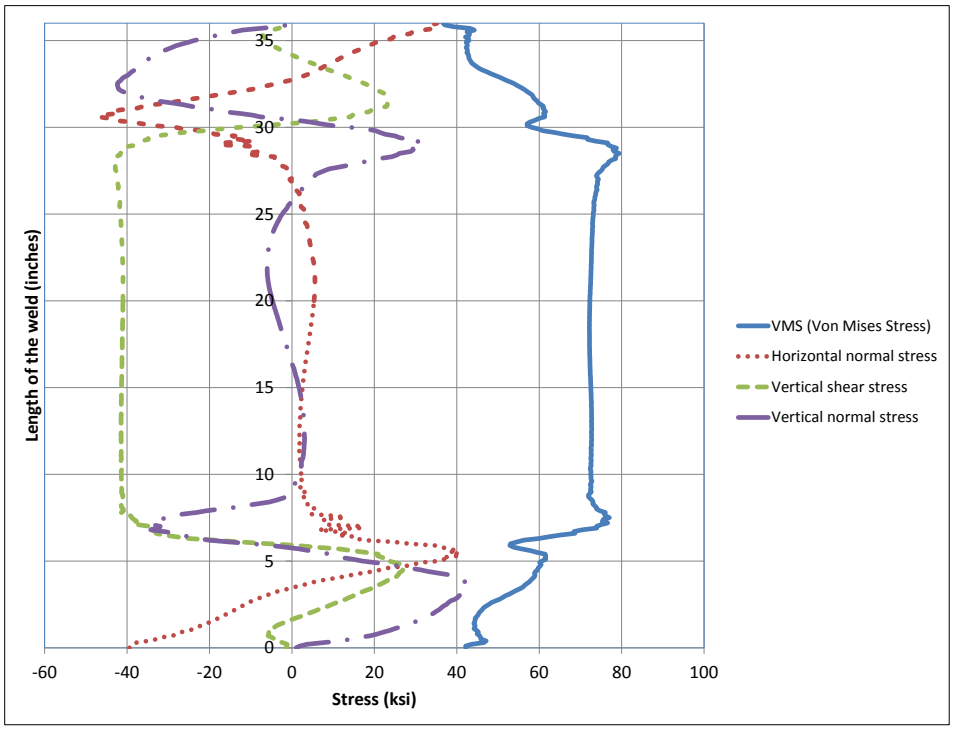

Figure 4.110: Stresses along depth of CJP1 (DP-CJP1 interface) at 0.05 radian(Case 15A)

4.2.23 Analysis case 15A_quar

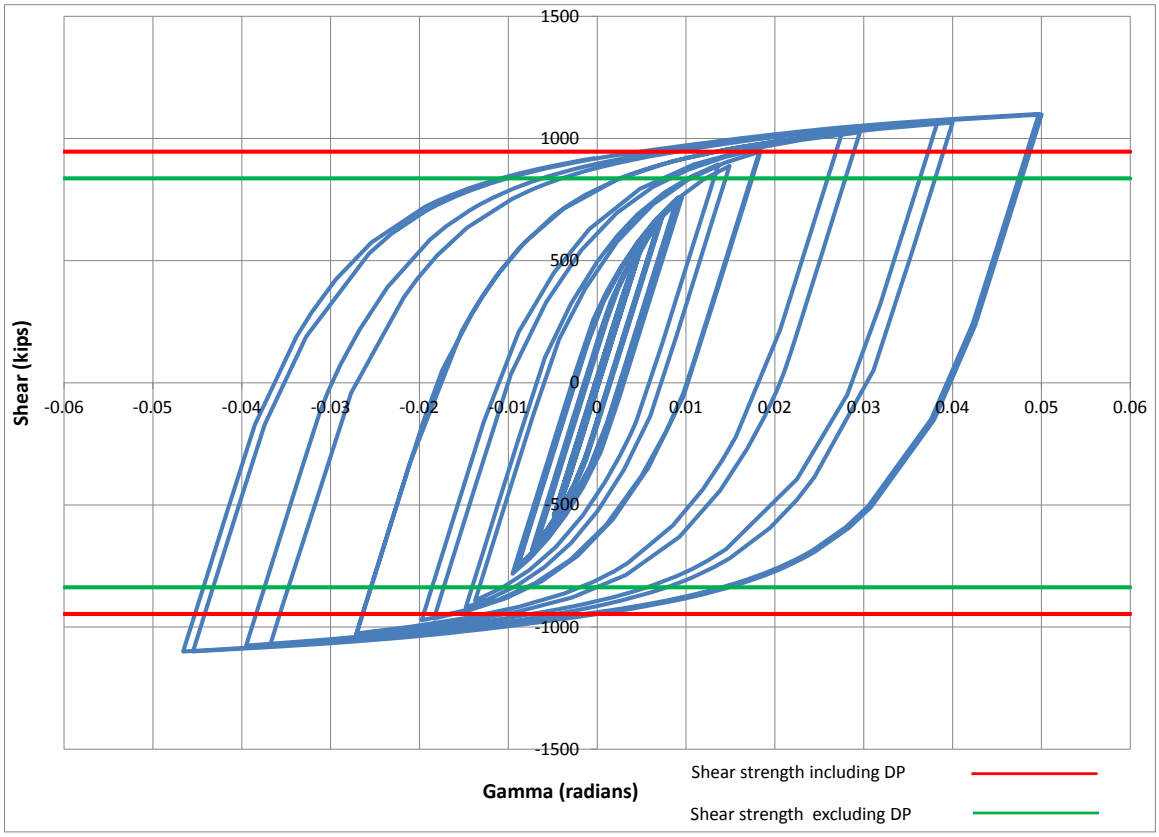

Figure 4.111: Panel zone shear versus rotation (Case 15A_quar)

Table 4.24: Panel zone shear and force on loading plate (Case 15A_quar)

Panel zone rotation (rad)	0.01	0.02	0.03	0.05
Panel zone shear (kips)	752.51	959.51	1023.30	1100.17
Force on one Loading plate (kips)	451.50	575.71	613.98	660.10

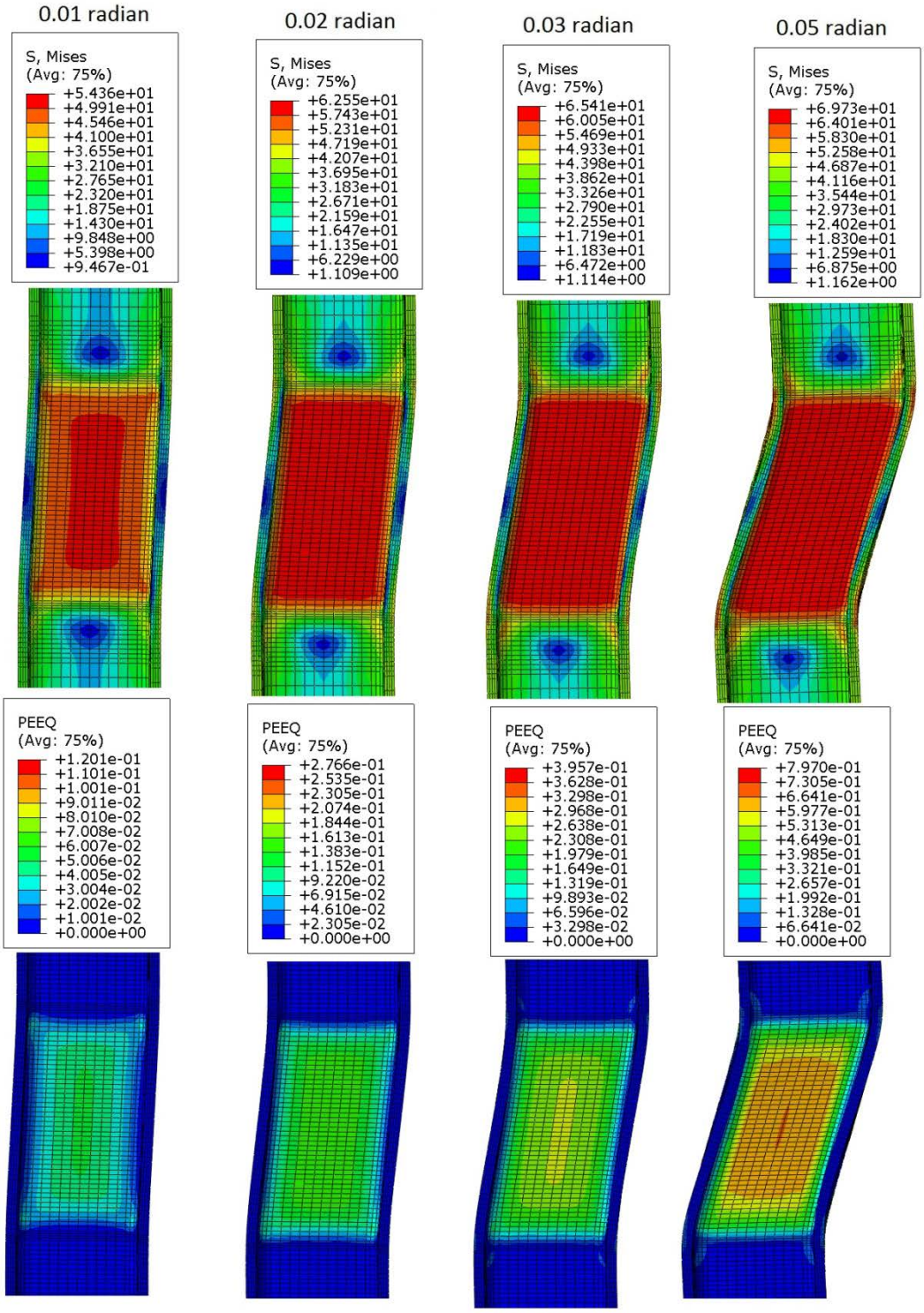

Figure 4.112: VMS and PEEQ in the column (Case 15A_quar)

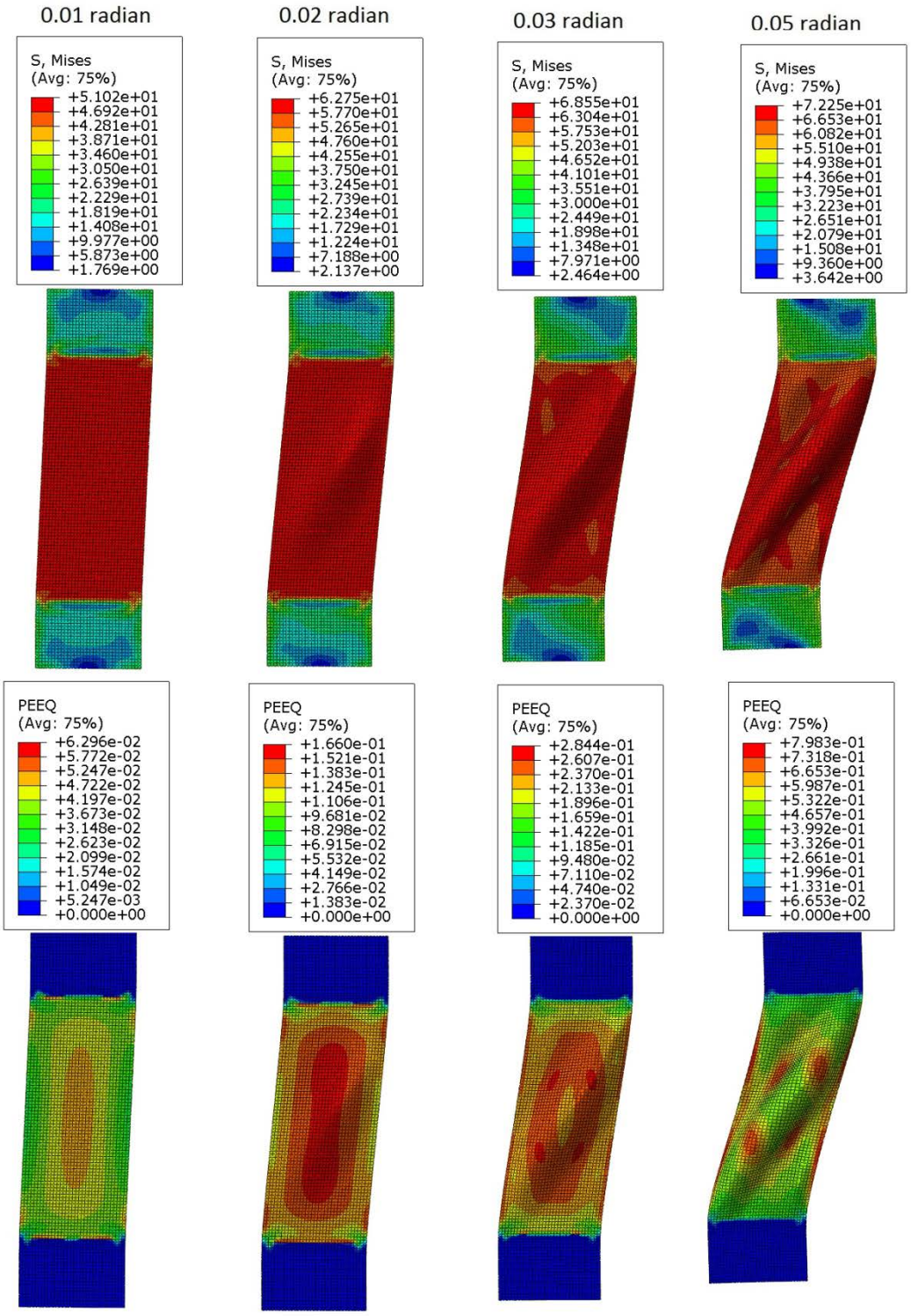

Figure 4.113: VMS and PEEQ in the DP (Case 15A_quar)

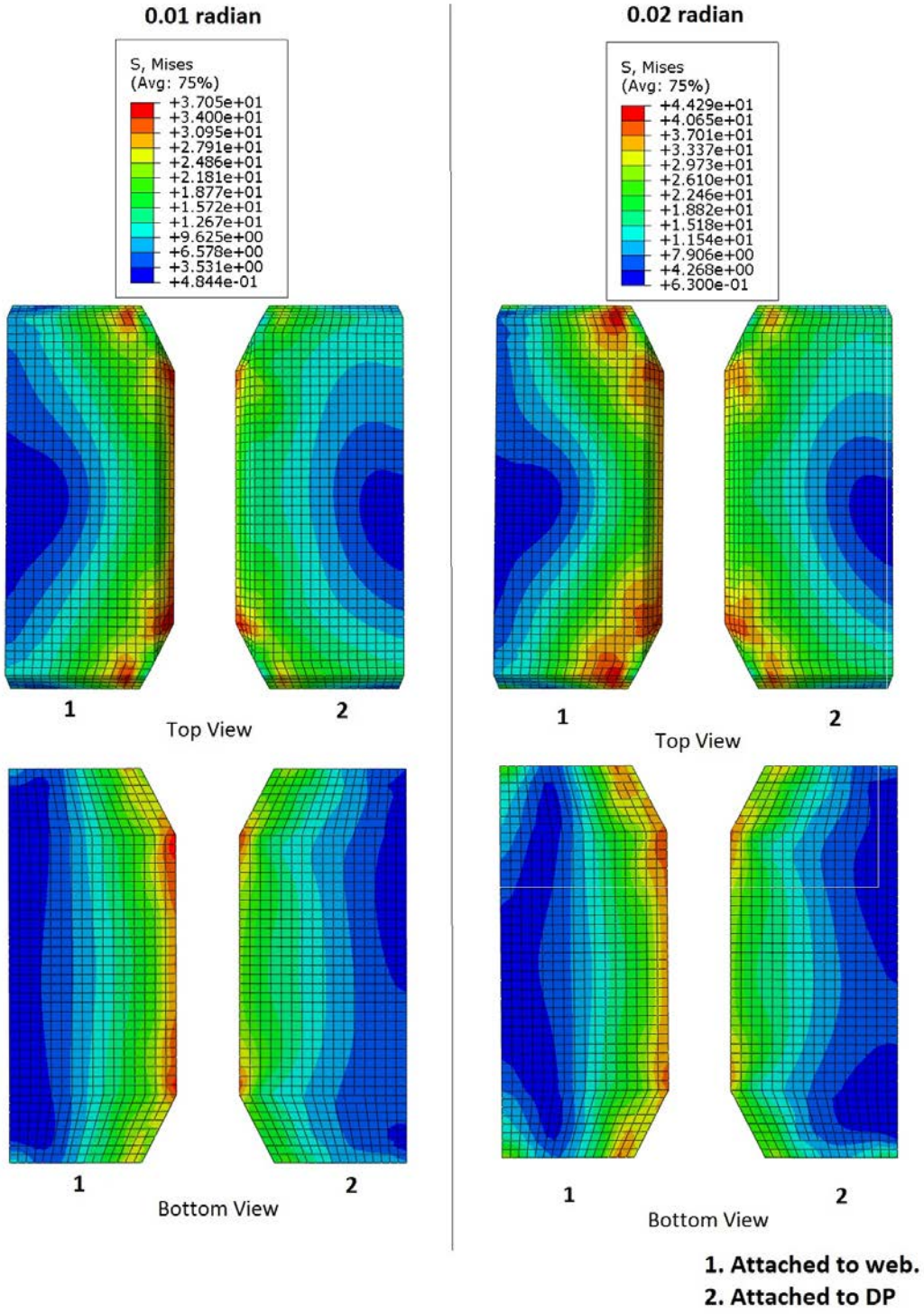

Figure 4.114: VMS in the CP at 0.01 and 0.02 radian rotation (Case 15A_quar)

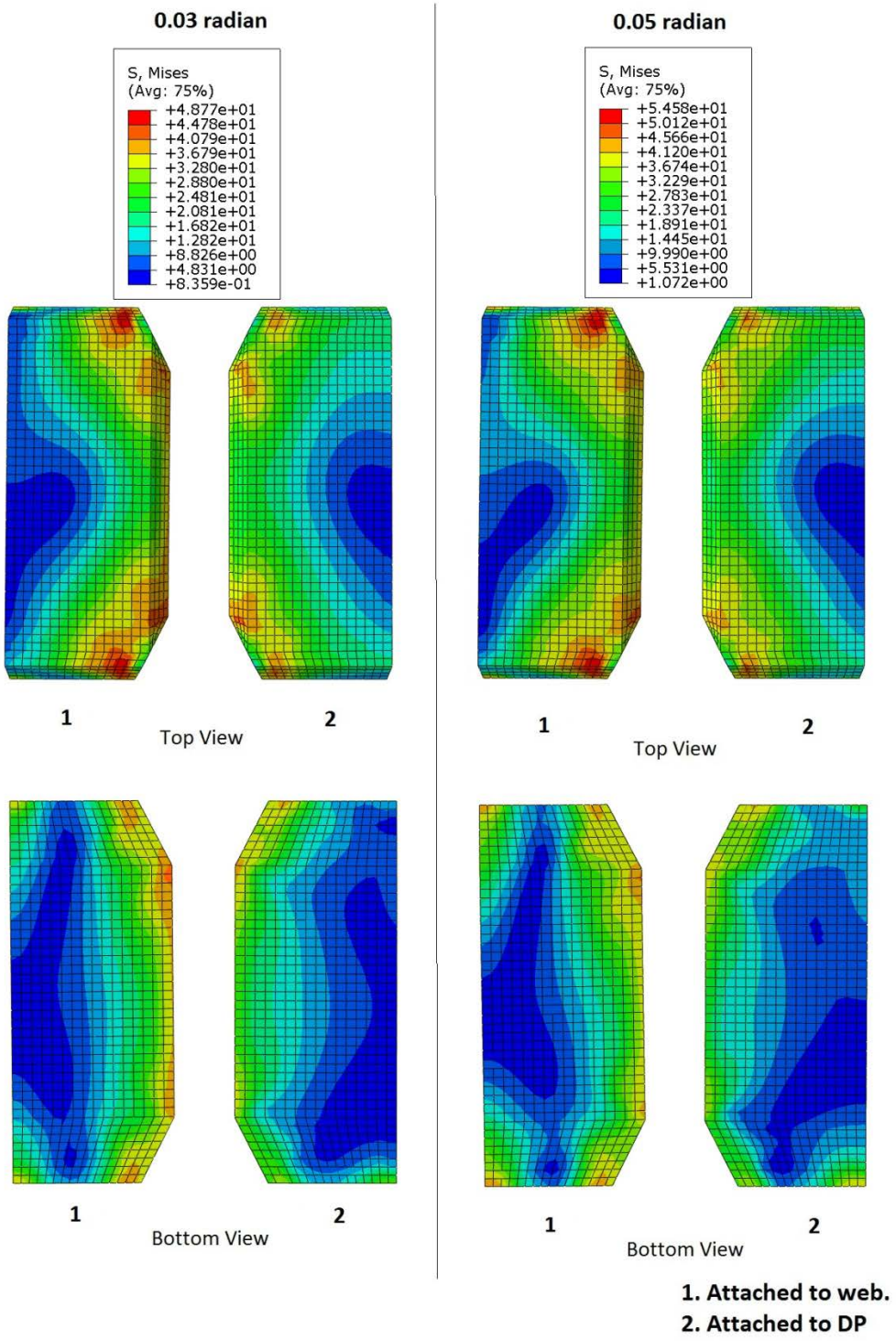

Figure 4.115: VMS in the CP at 0.03 and 0.05 radian rotation (Case 15A_quar)

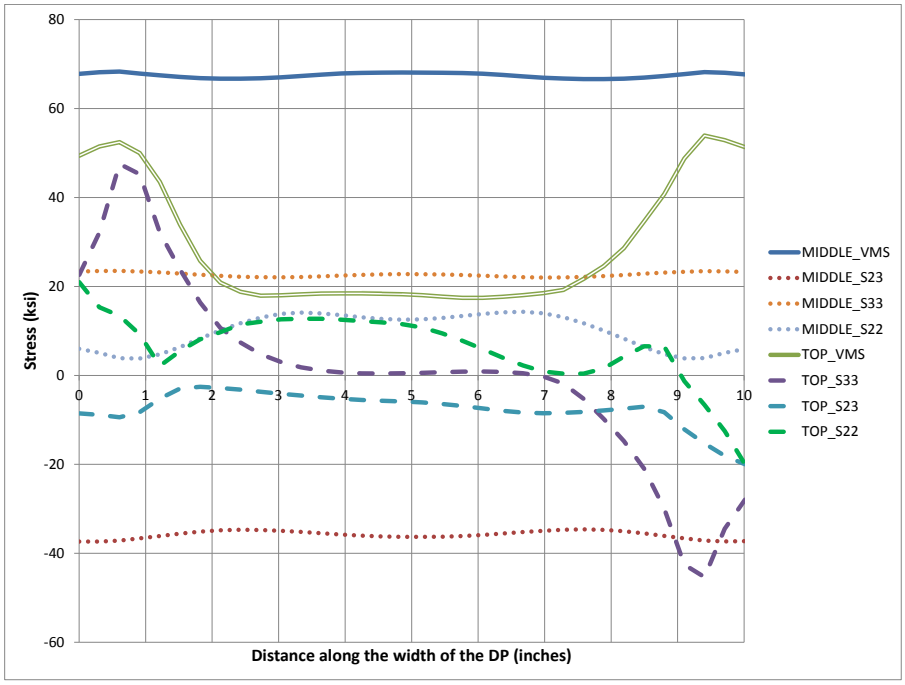

Figure 4.116: Stresses along the width of DP at 0.05 radian rotation (Case 15A_quar)

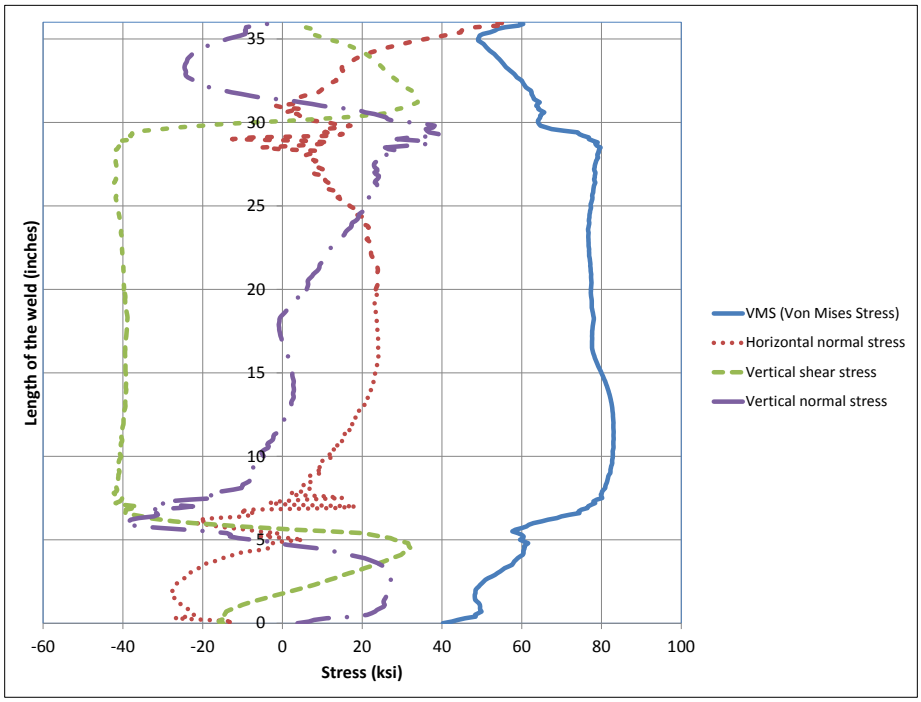

Figure 4.117: Stresses along depth of CJP1 (DP-CJP1 interface) at 0.05 radian (Case 15A_quar)

4.2.24 Analysis case 15A_one

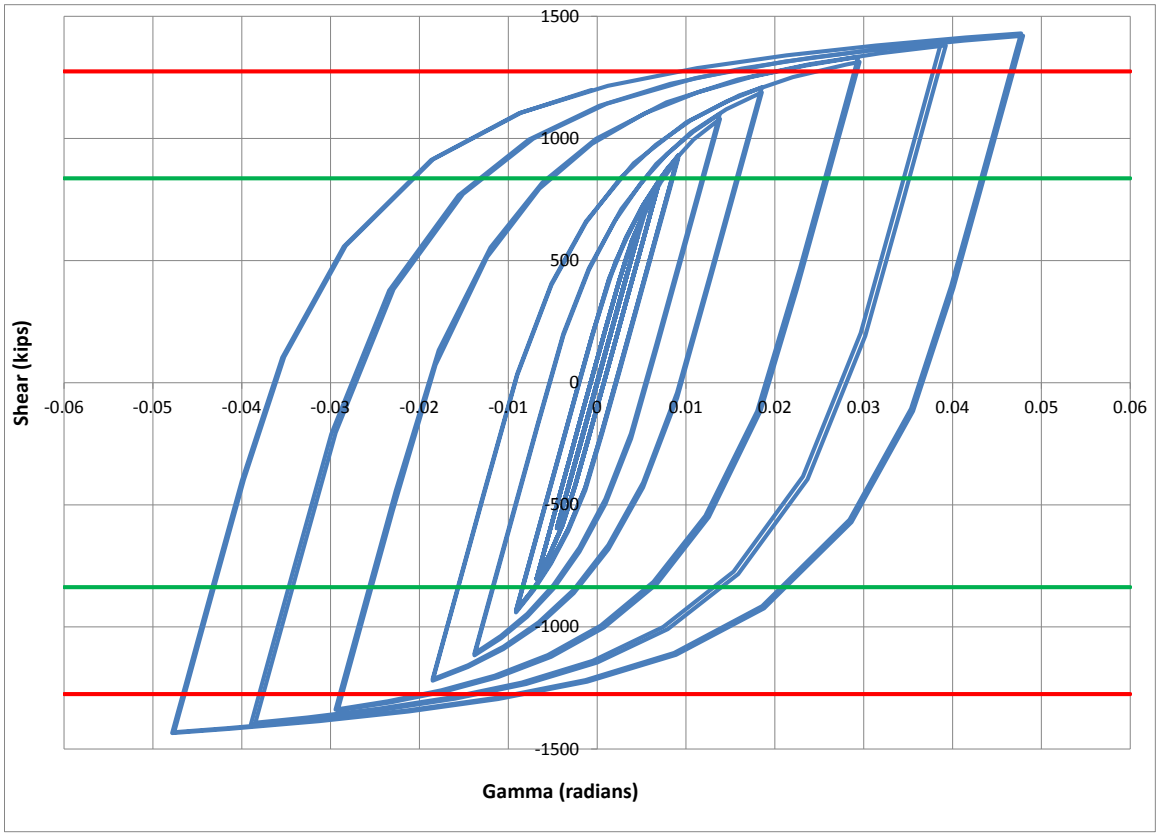

Figure 4.118: Panel zone shear versus rotation (Case 15A_one)

Table 4.25: Panel zone shear and force on loading plate (Case 15A_one)

Panel zone rotation (rad)	0.01	0.02	0.03	0.05
Panel zone shear (kips)	931.50	1209.39	1333.98	1430.41
Force on one Loading plate (kips)	558.90	725.63	800.39	858.24

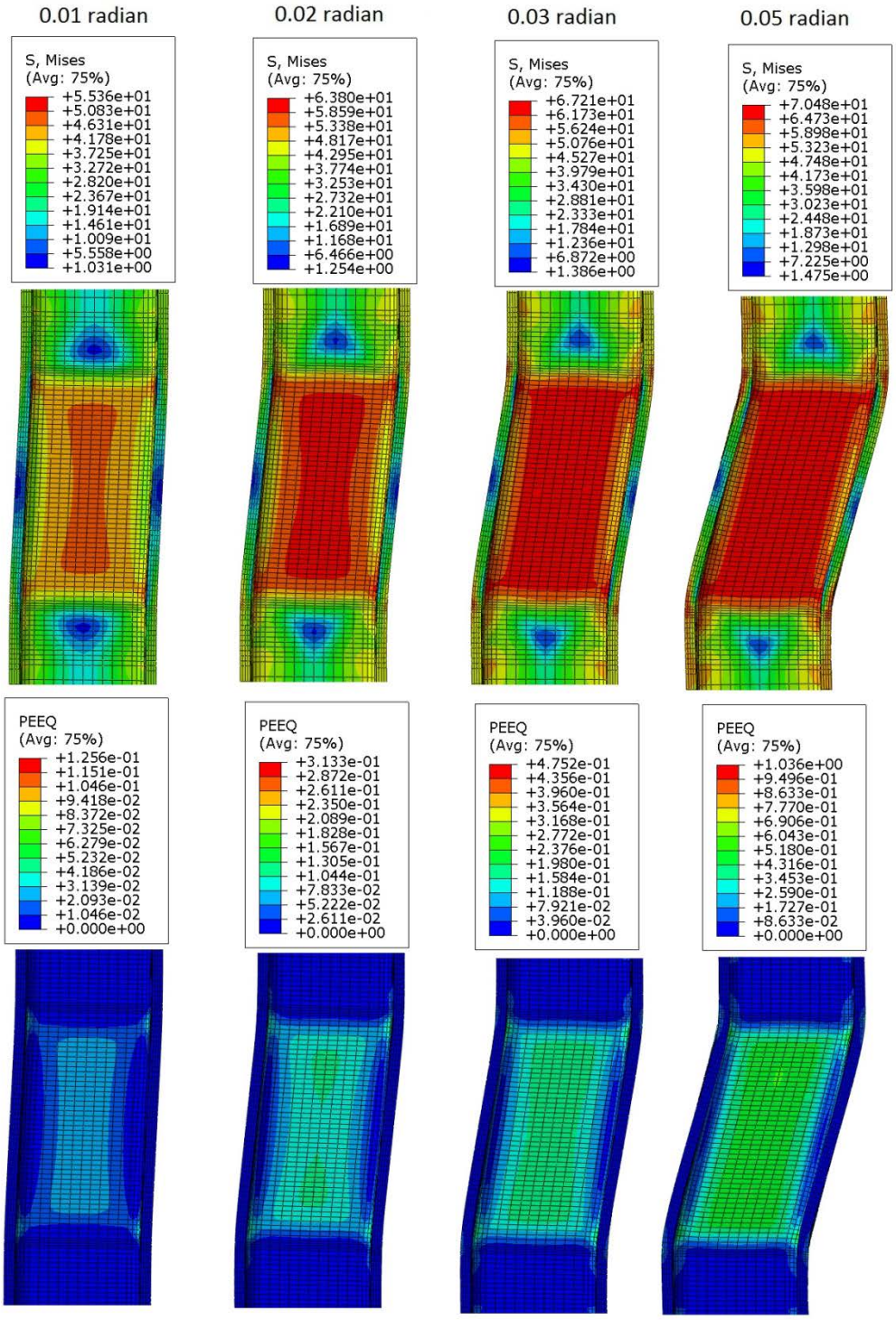

Figure 4.119: VMS and PEEQ in the column (Case 15A_one)

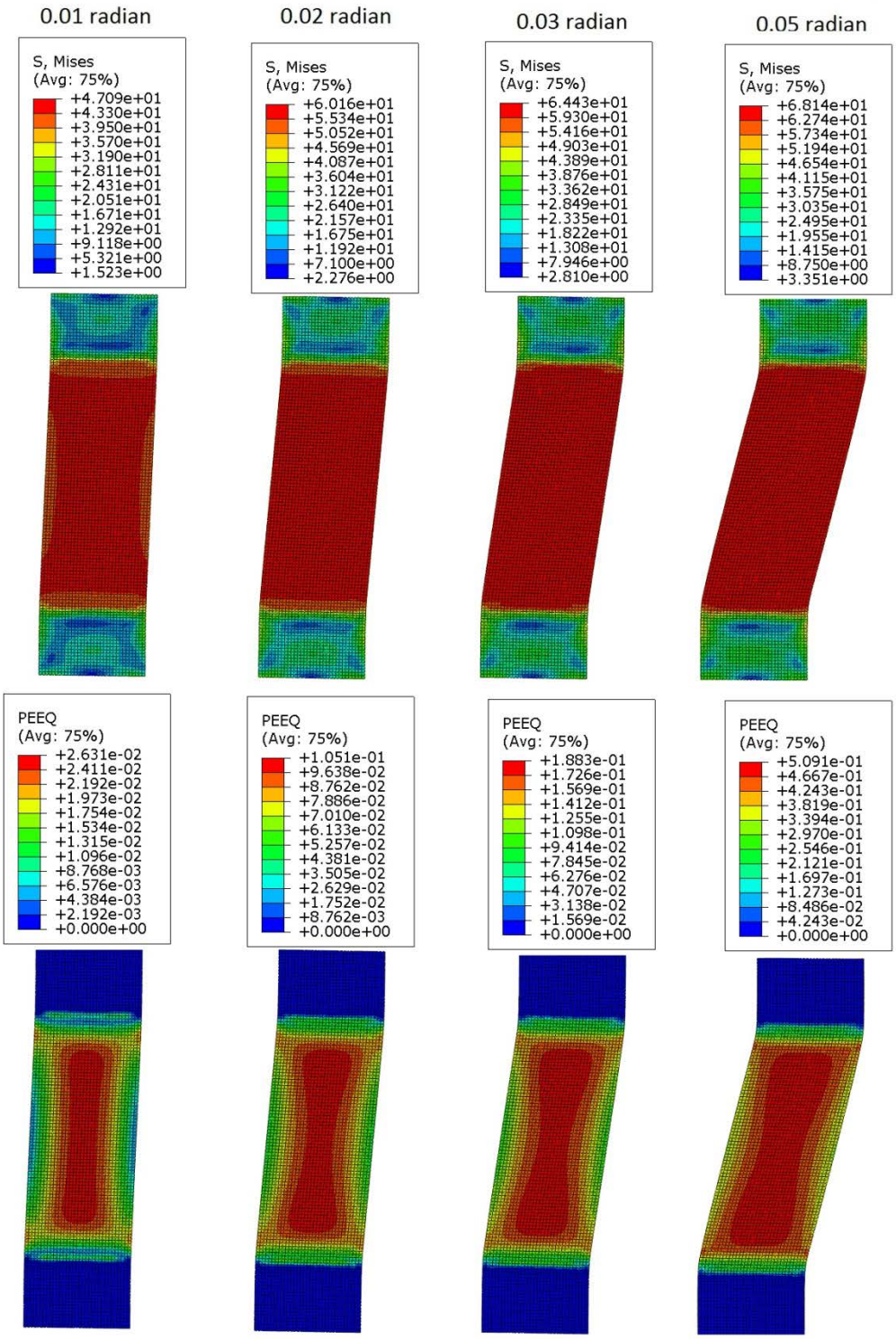

Figure 4.120: VMS and PEEQ in the DP (Case 15A_one)

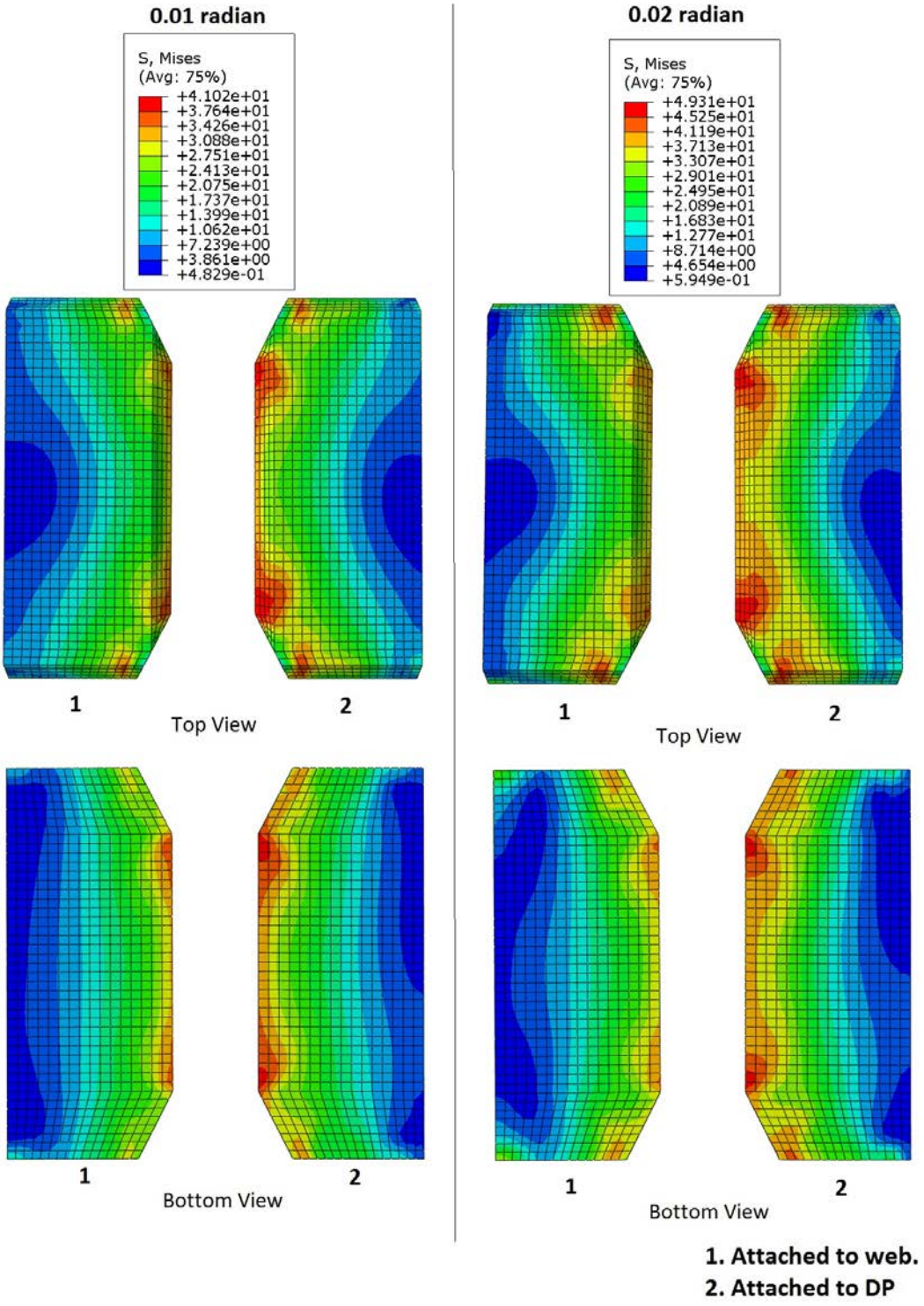

Figure 4.121: VMS in the CP at 0.01 and 0.02 radian rotation (Case 15A_one)

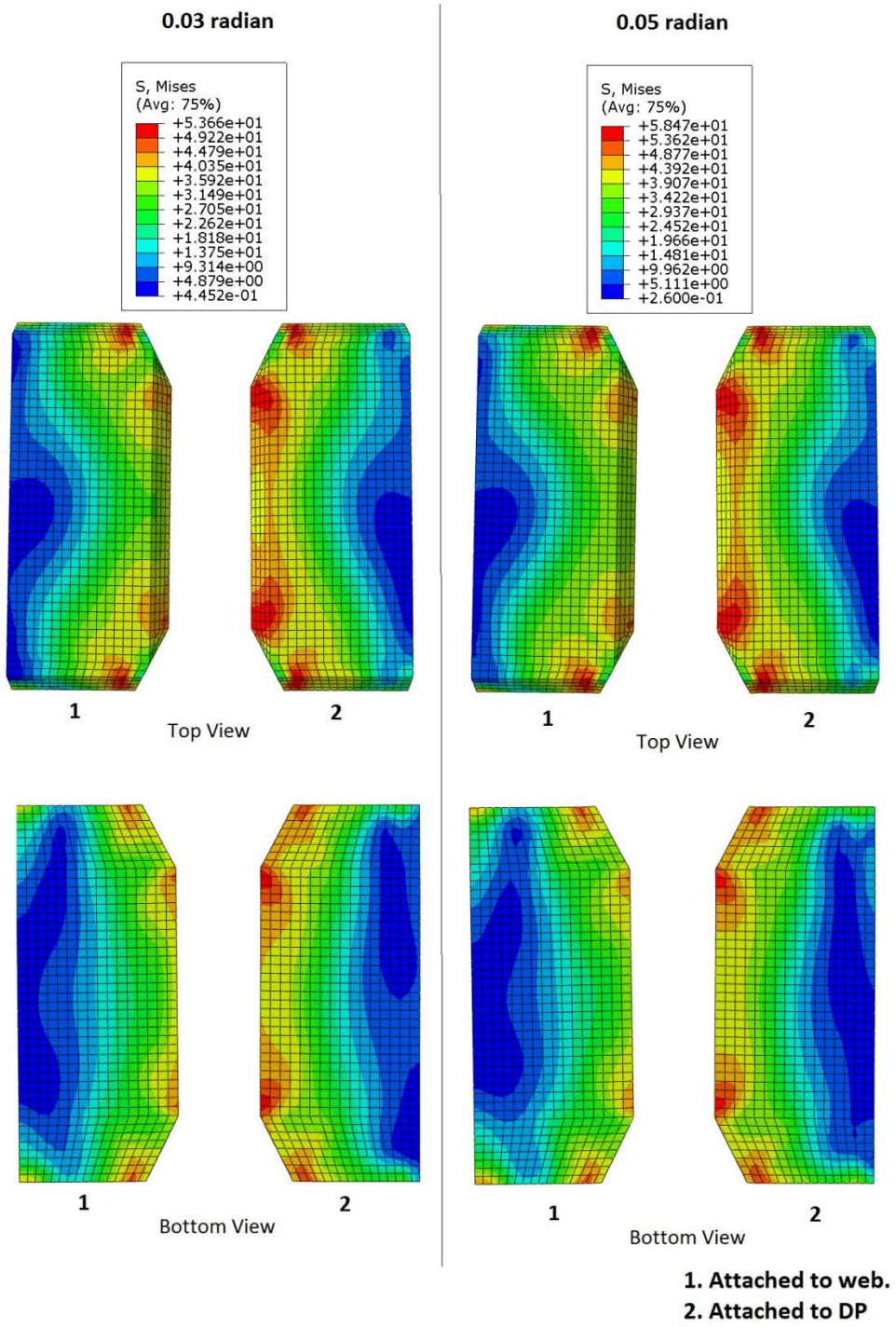

Figure 4.122: VMS in the CP at 0.03 and 0.05 radian rotation (Case 15A_one)

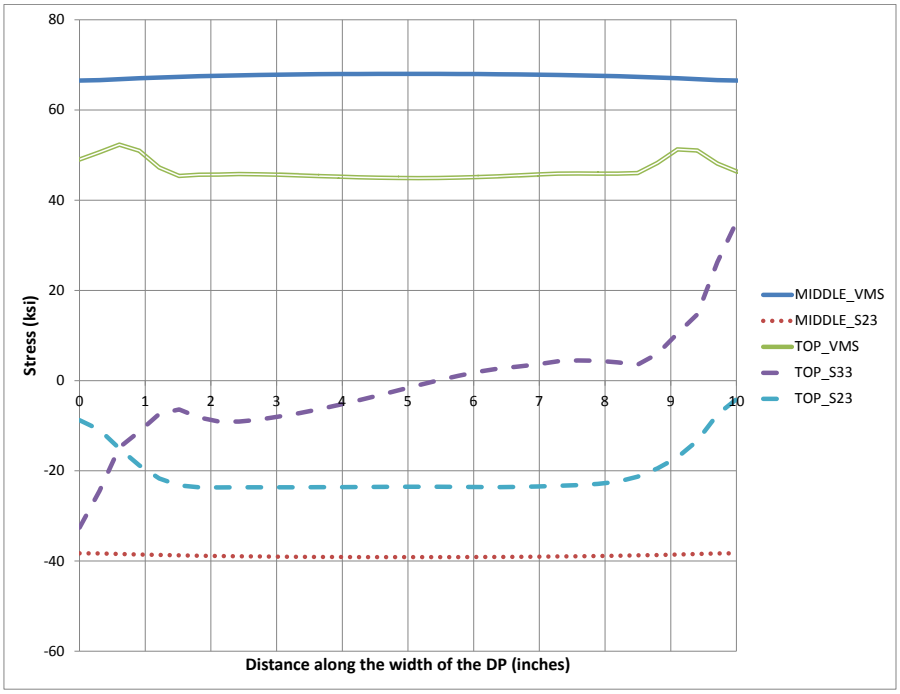

Figure 4.123: Stresses along the width of DP at 0.05 radian rotation (Case 15A_one)

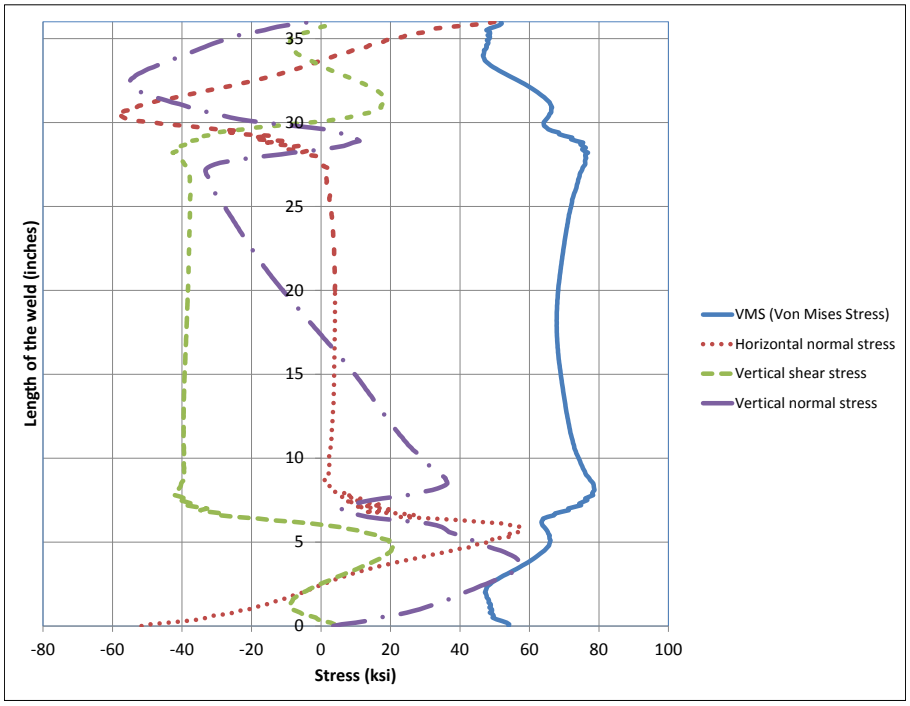

Figure 4.124: Stresses along depth of CJP1 (DP-CJP1 interface) at 0.05 radian (Case 15A_one)

4.2.25 Analysis case 16A

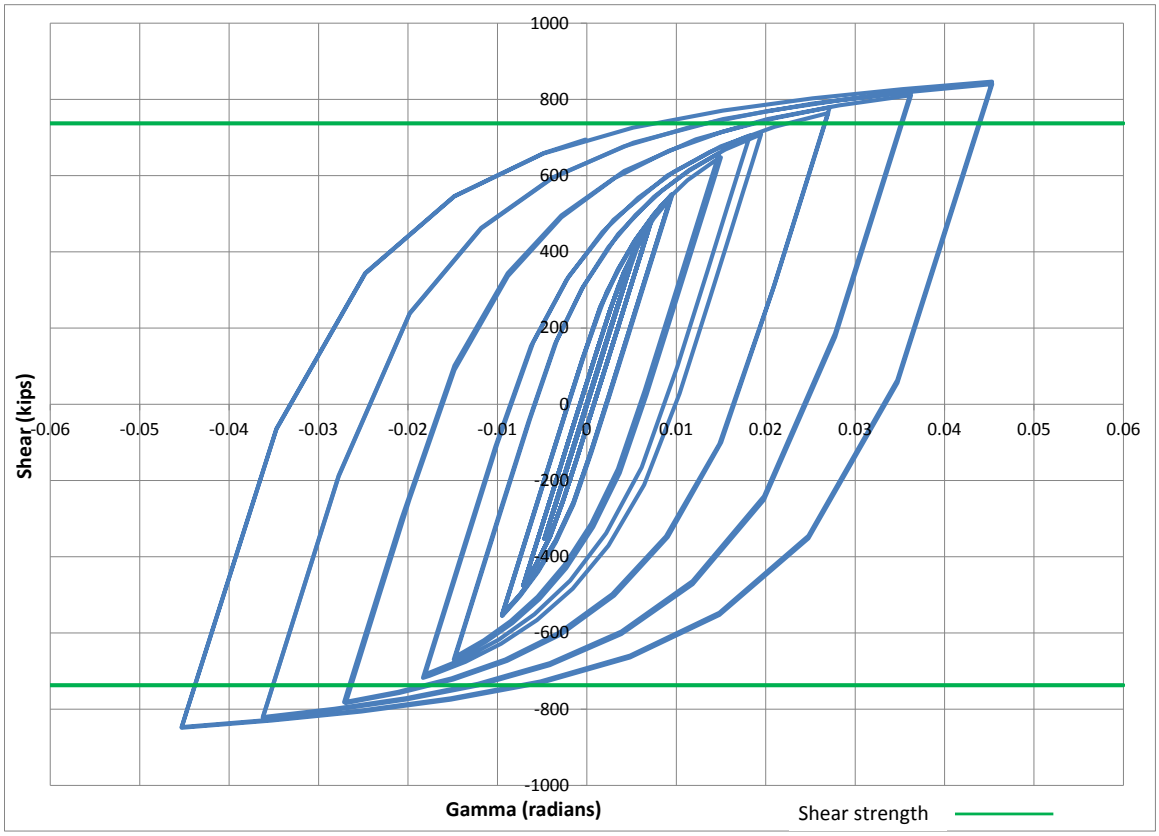

Figure 4.125: Panel zone shear versus rotation (Case 16A)

Table 4.26: Panel zone shear and force on loading plate (Case 16A)

Panel zone rotation (rad)	0.01	0.02	0.03	0.05
Panel zone shear (kips)	550.89	705.44	778.96	846.37
Force on one Loading plate (kips)	330.53	423.26	467.38	507.82

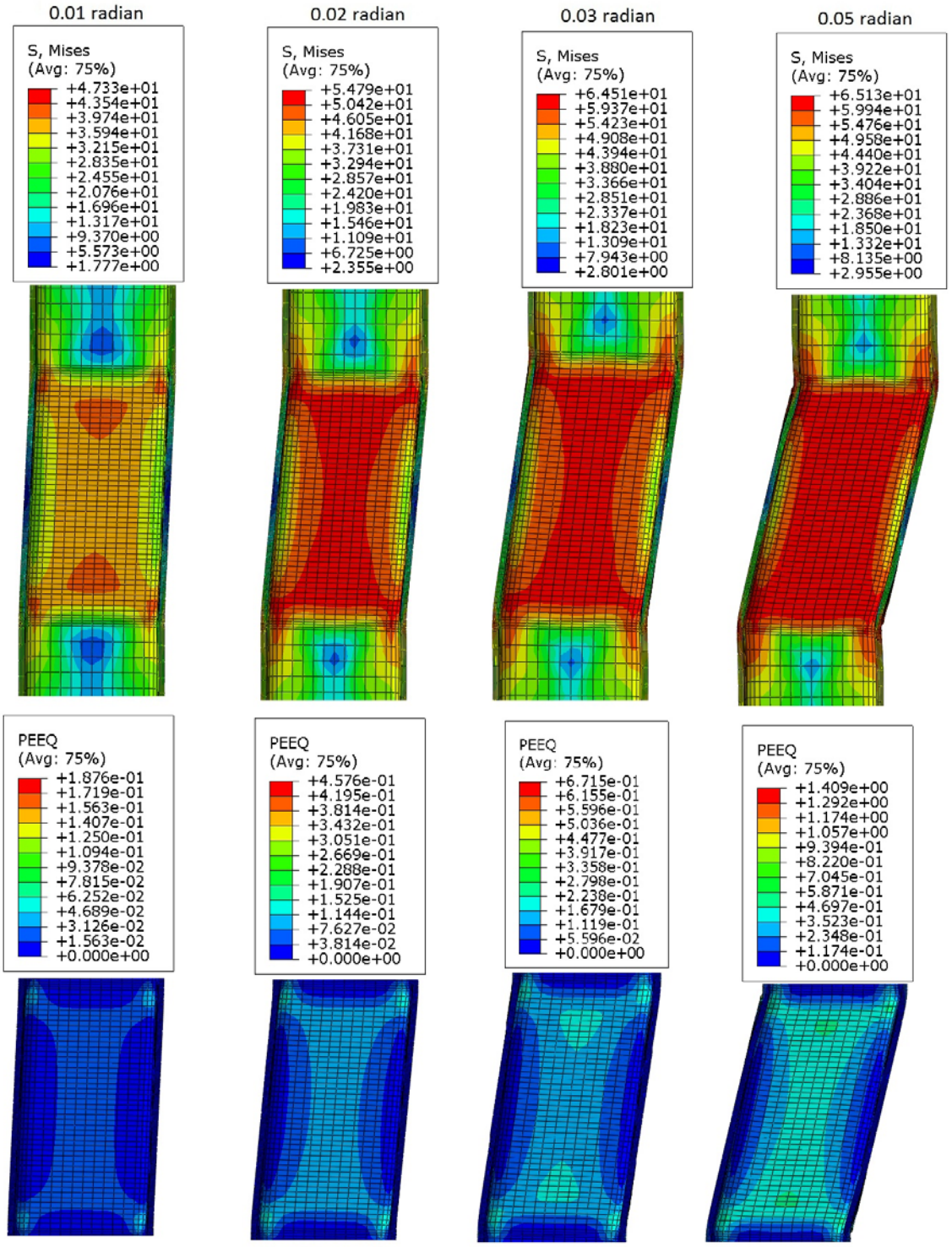

Figure 4.126: VMS and PEEQ in the column (Case 16A)

4.2.26 Analysis case 17A

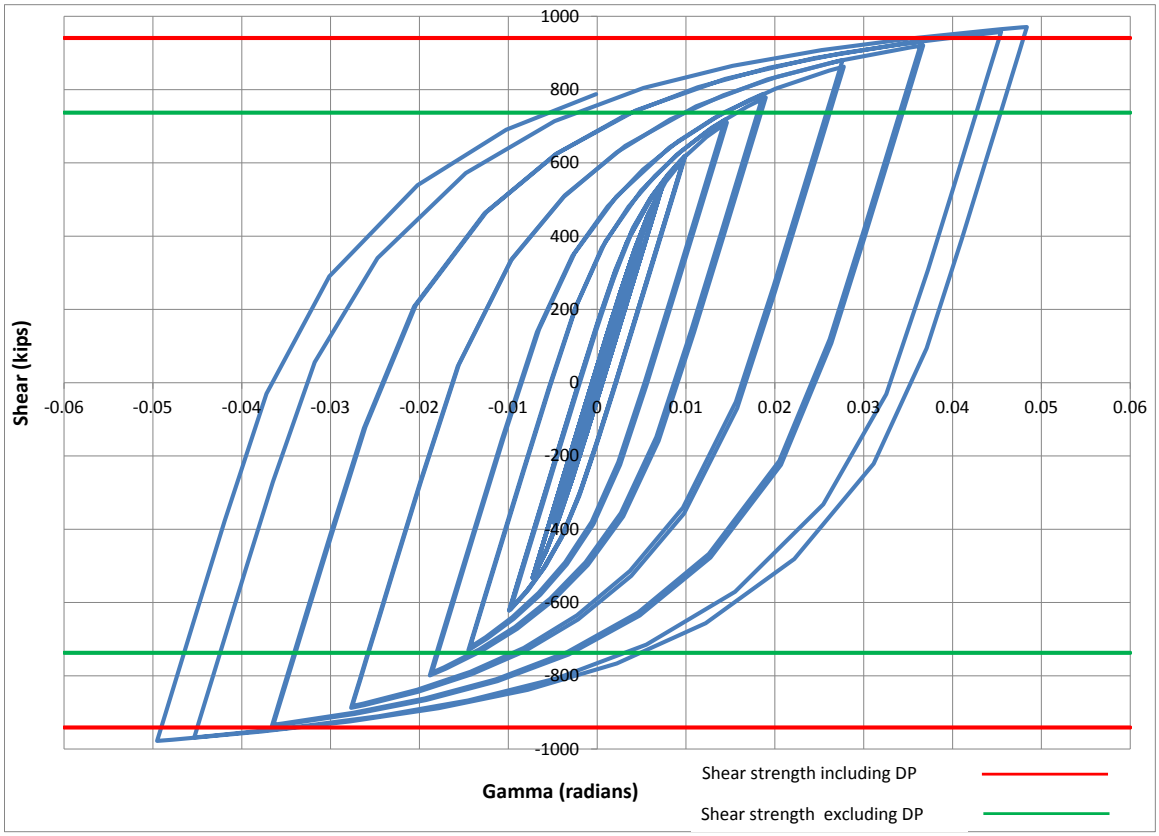

Figure 4.127: Panel zone shear versus rotation (Case 17A)

Table 4.27: Panel zone shear and force on loading plate (Case 17A)

Panel zone rotation (rad)	0.01	0.02	0.03	0.05
Panel zone shear (kips)	618.40	788.61	879.91	971.03
Force on one Loading plate (kips)	371.04	473.17	527.95	582.62

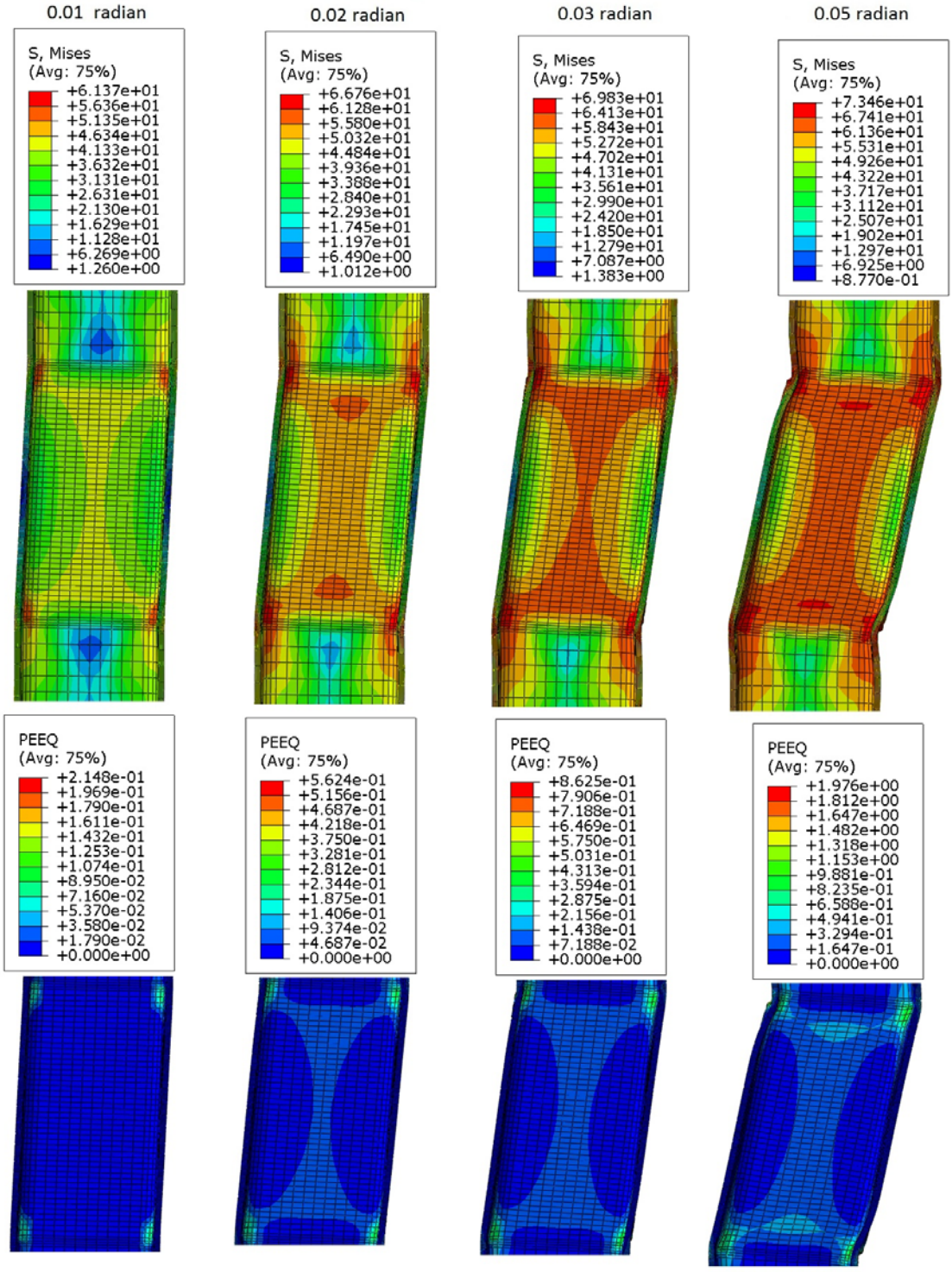

Figure 4.128: VMS and PEEQ in the column (Case 17A)

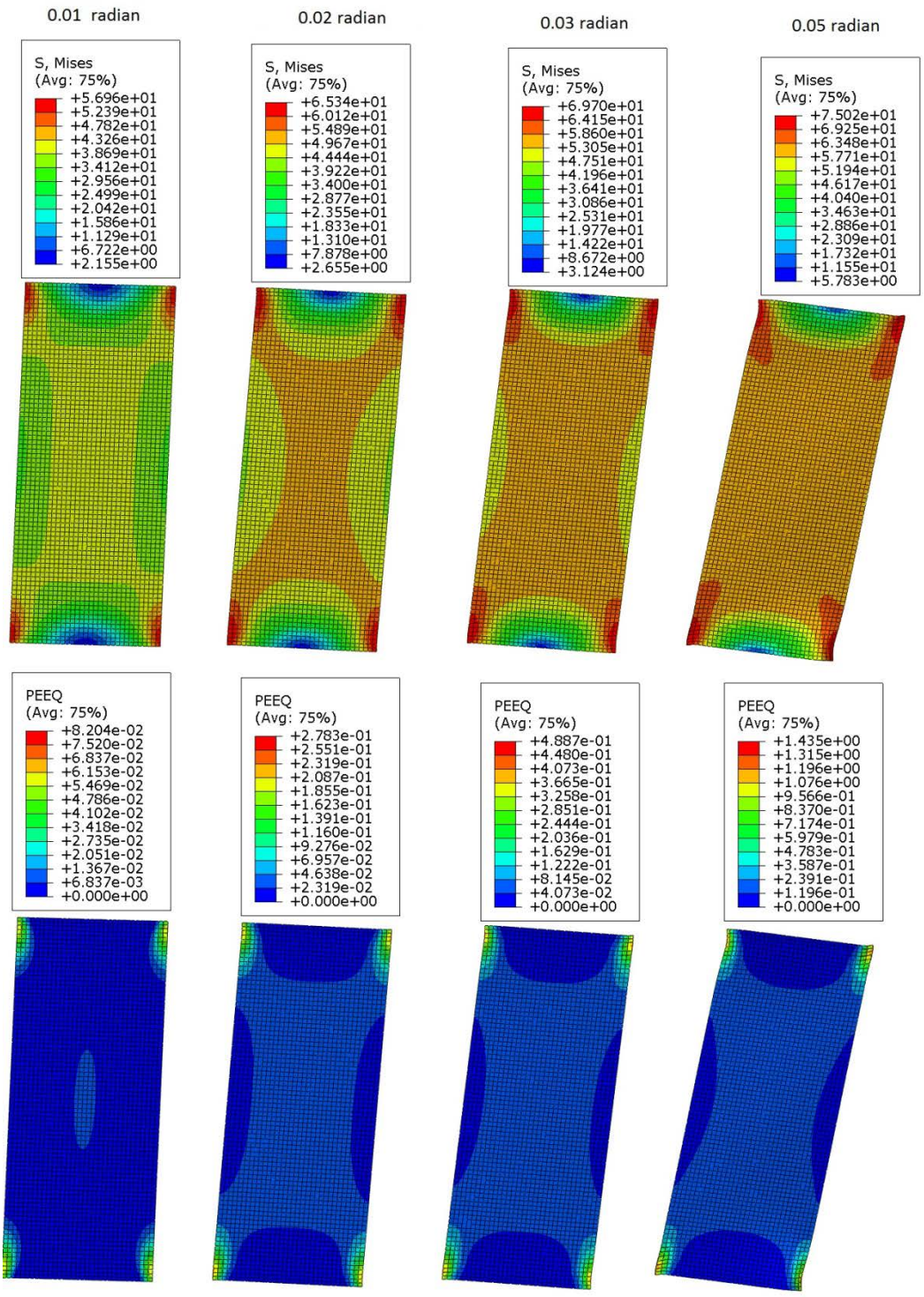

Figure 4.129: VMS and PEEQ in the DP (Case 17A)

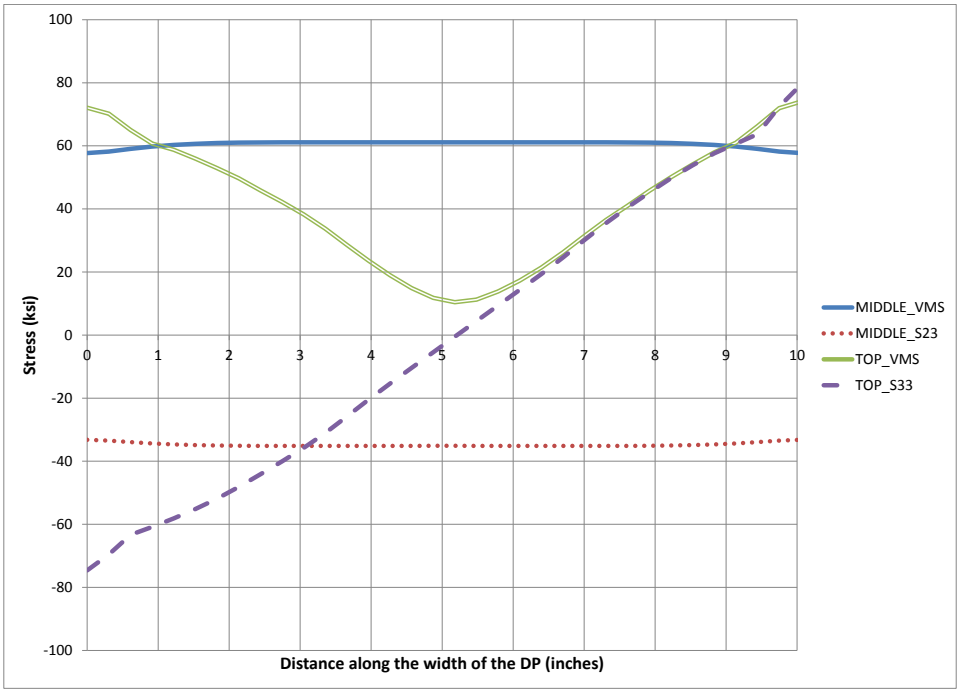

Figure 4.130: Stresses along the width of DP at 0.05 radian rotation (Case 17A)

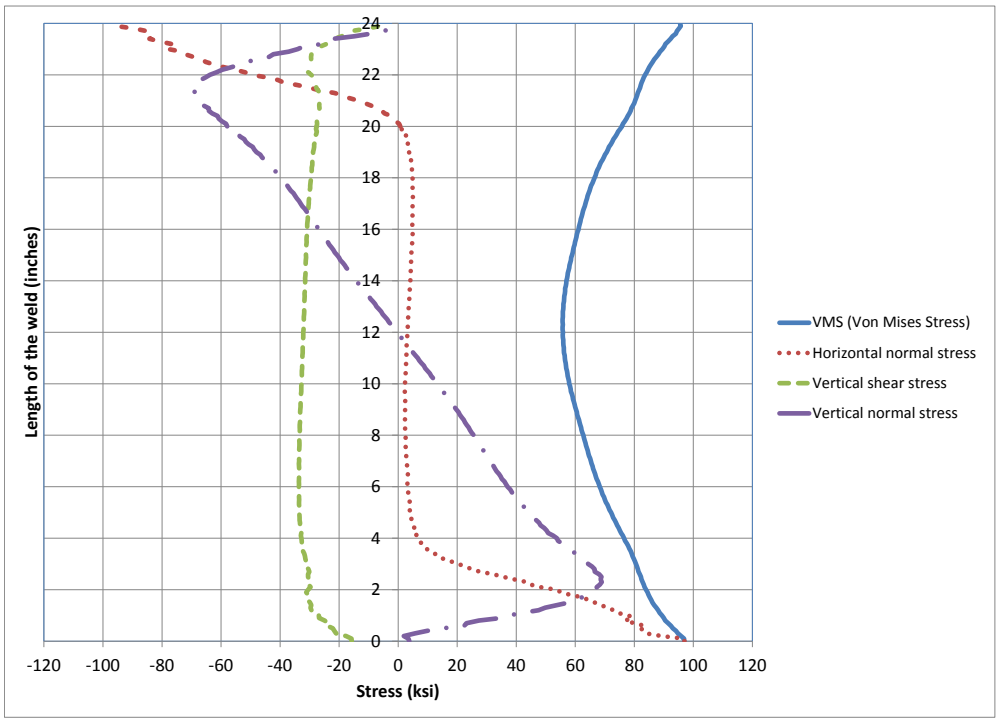

Figure 4.131: Stresses along depth of CJP1 (DP-CJP1 interface) at 0.05 radian(Case 17A)

4.2.27 Analysis case 18A

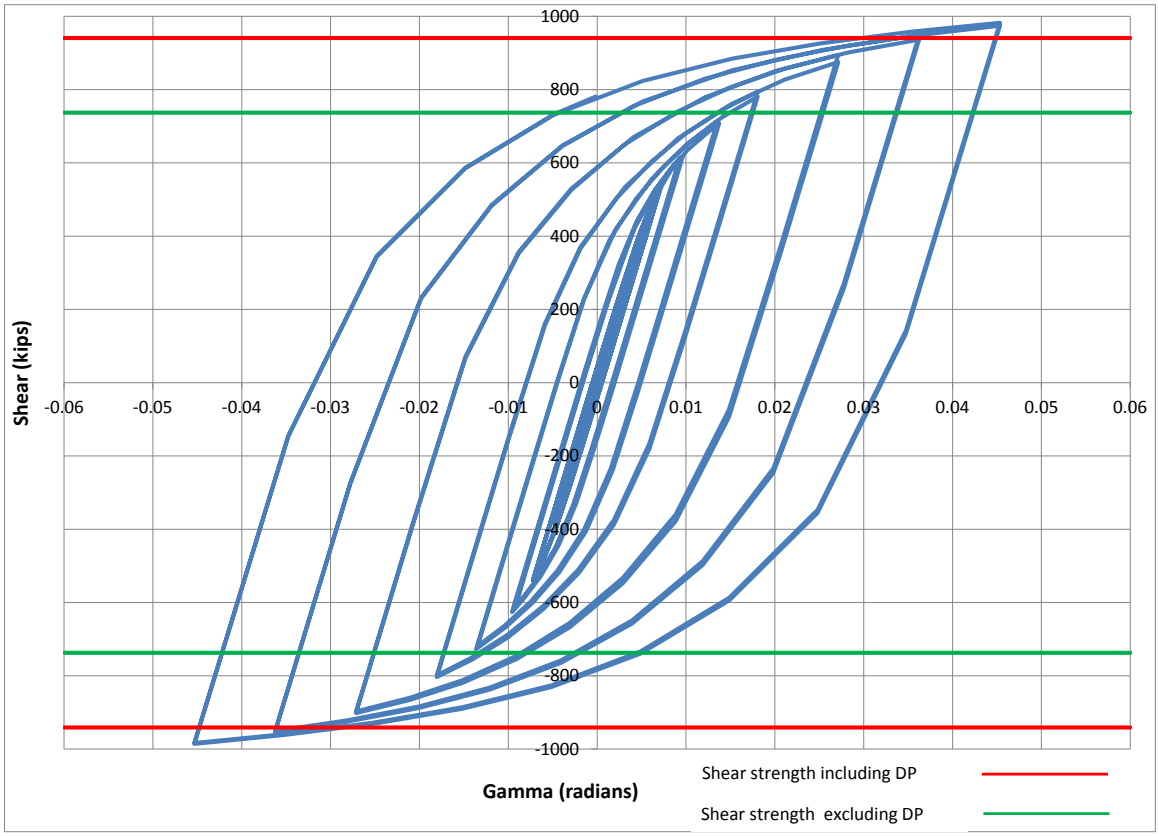

Figure 4.132: Panel zone shear versus rotation (Case 18A)

Table 4.28: Panel zone shear and force on loading plate (Case 18A)

Panel zone rotation (rad)	0.01	0.02	0.03	0.05
Panel zone shear (kips)	612.55	794.34	894.26	982.37
Force on one Loading plate (kips)	367.53	476.60	536.55	589.42

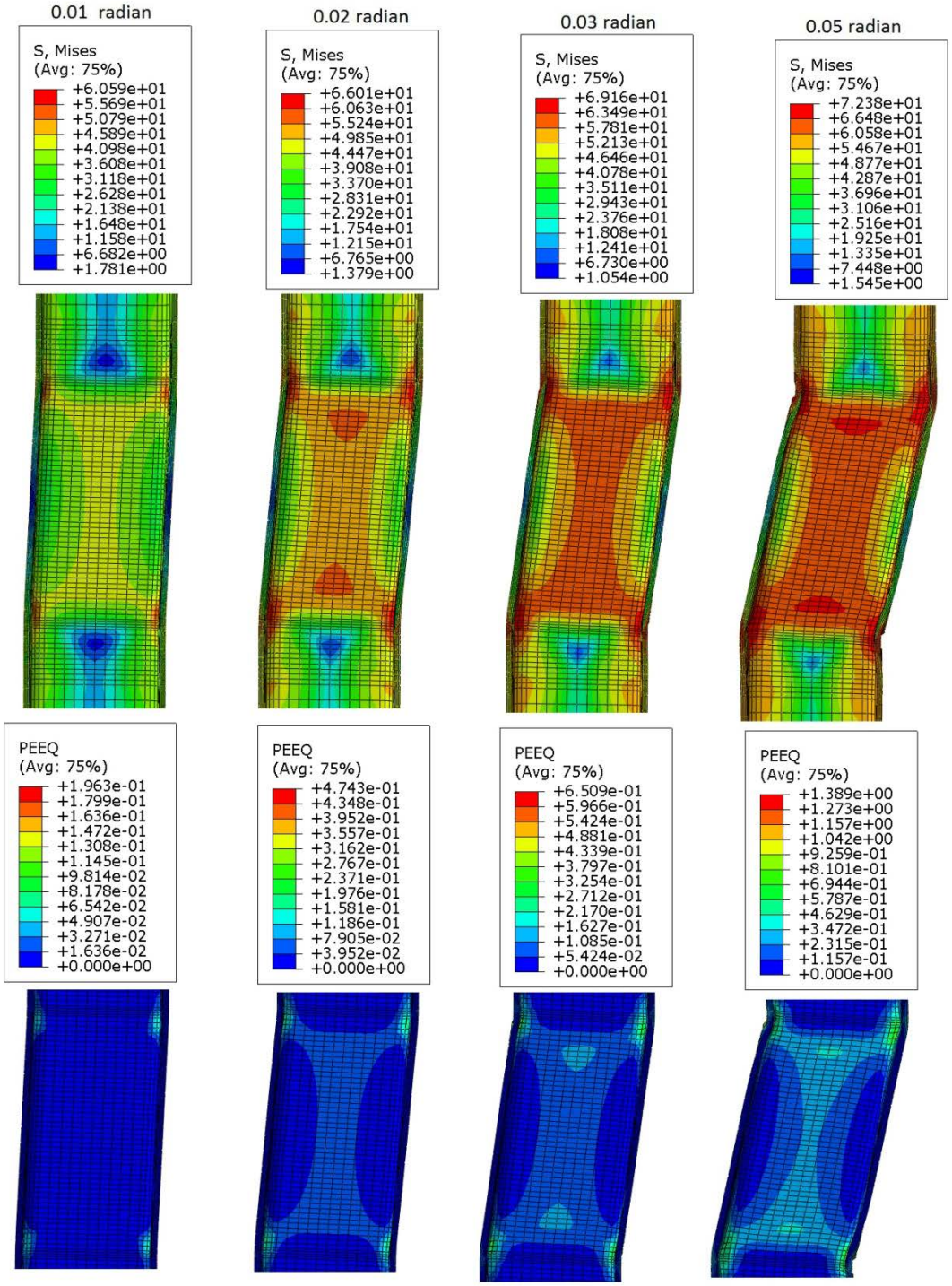

Figure 4.133: VMS and PEEQ in the column (Case 18A)

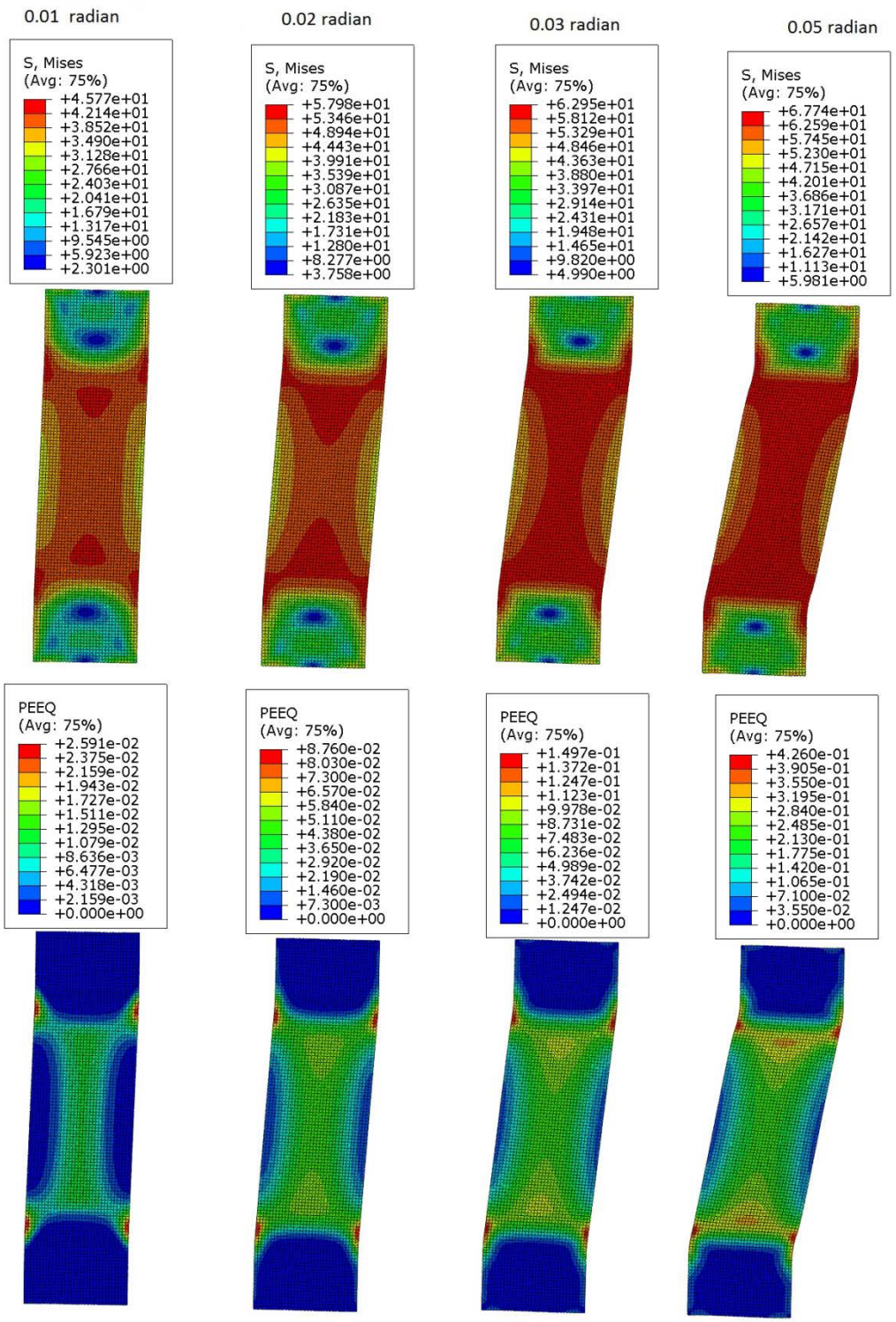

Figure 4.134: VMS and PEEQ in the DP (Case 18A)

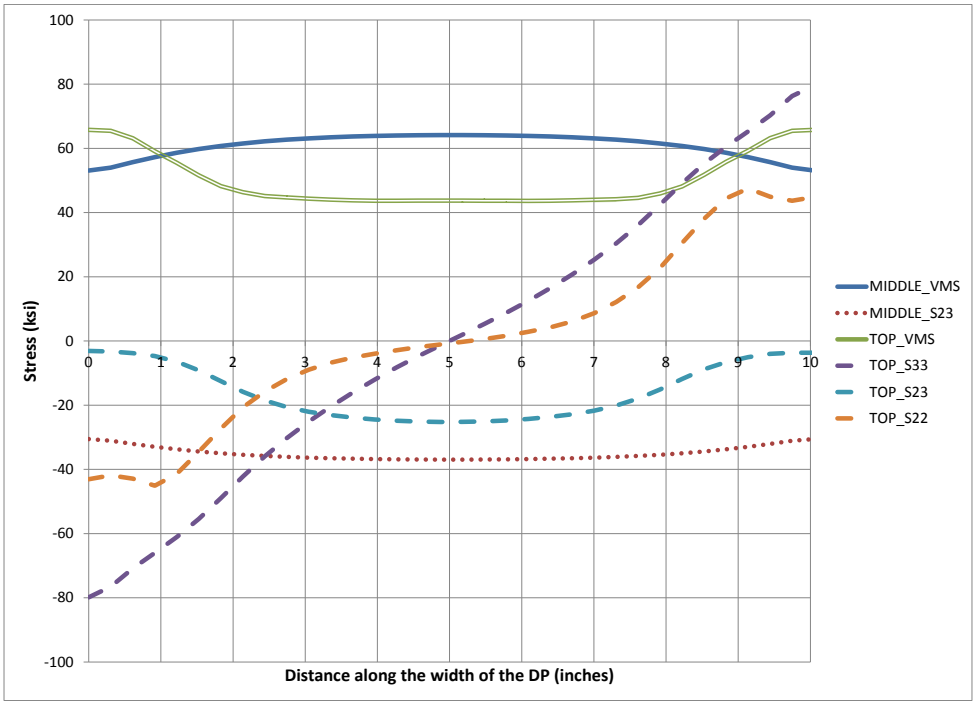

Figure 4.135: Stresses along the width of DP at 0.05 radian rotation (Case 18A)

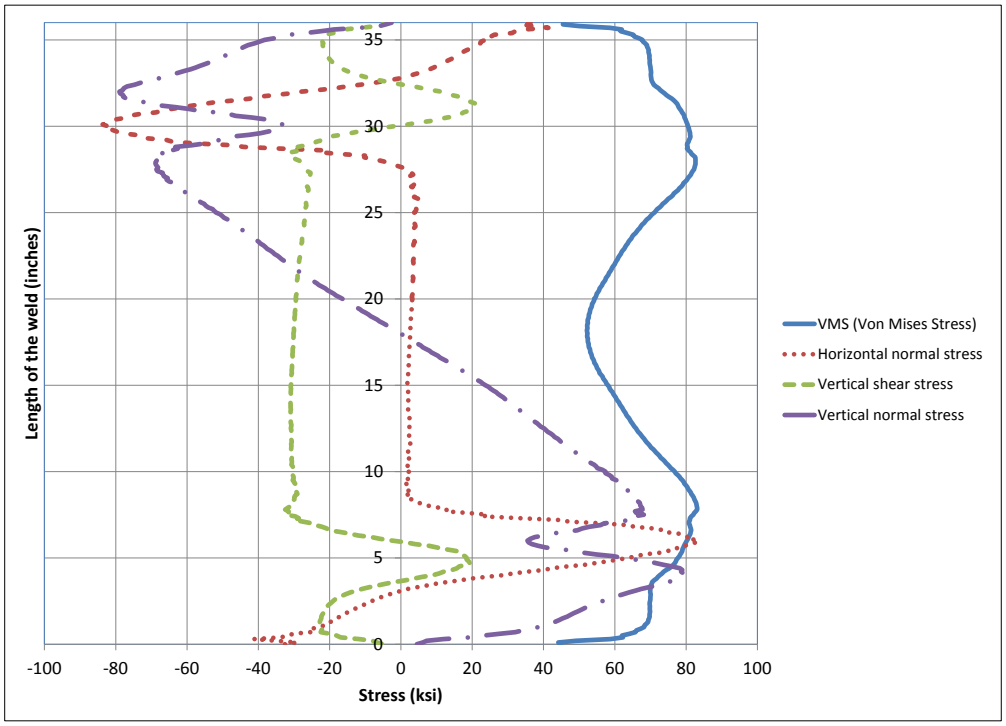

Figure 4.136: Stresses along depth of CJP1 (DP-CJP1 interface) at 0.05 radian(Case 18A)

4.2.28 Analysis case 19A

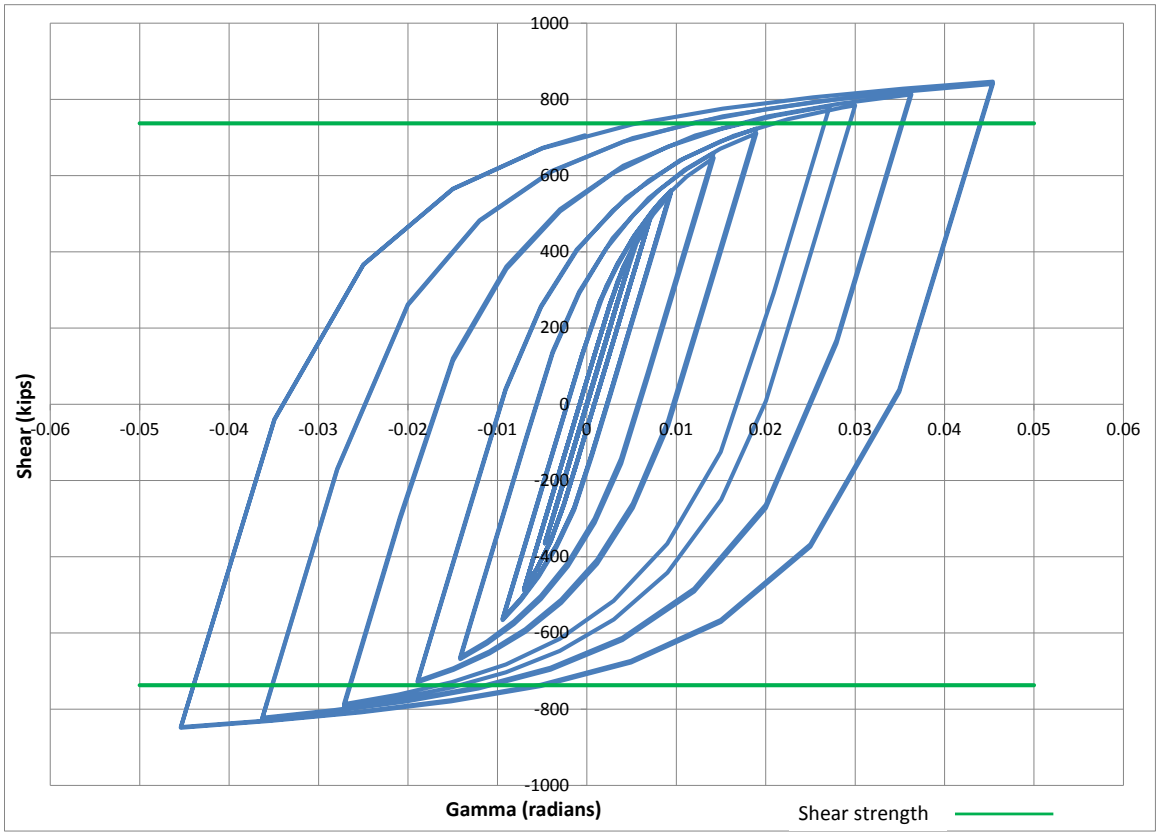

Figure 4.137: Panel zone shear versus rotation (Case 19A)

Table 4.29: Panel zone shear and force on loading plate (Case 19A)

Panel zone rotation (rad)	0.01	0.02	0.03	0.05
Panel zone shear (kips)	561.22	723.50	782.64	846.48
Force on one Loading plate (kips)	336.73	434.10	469.58	507.89

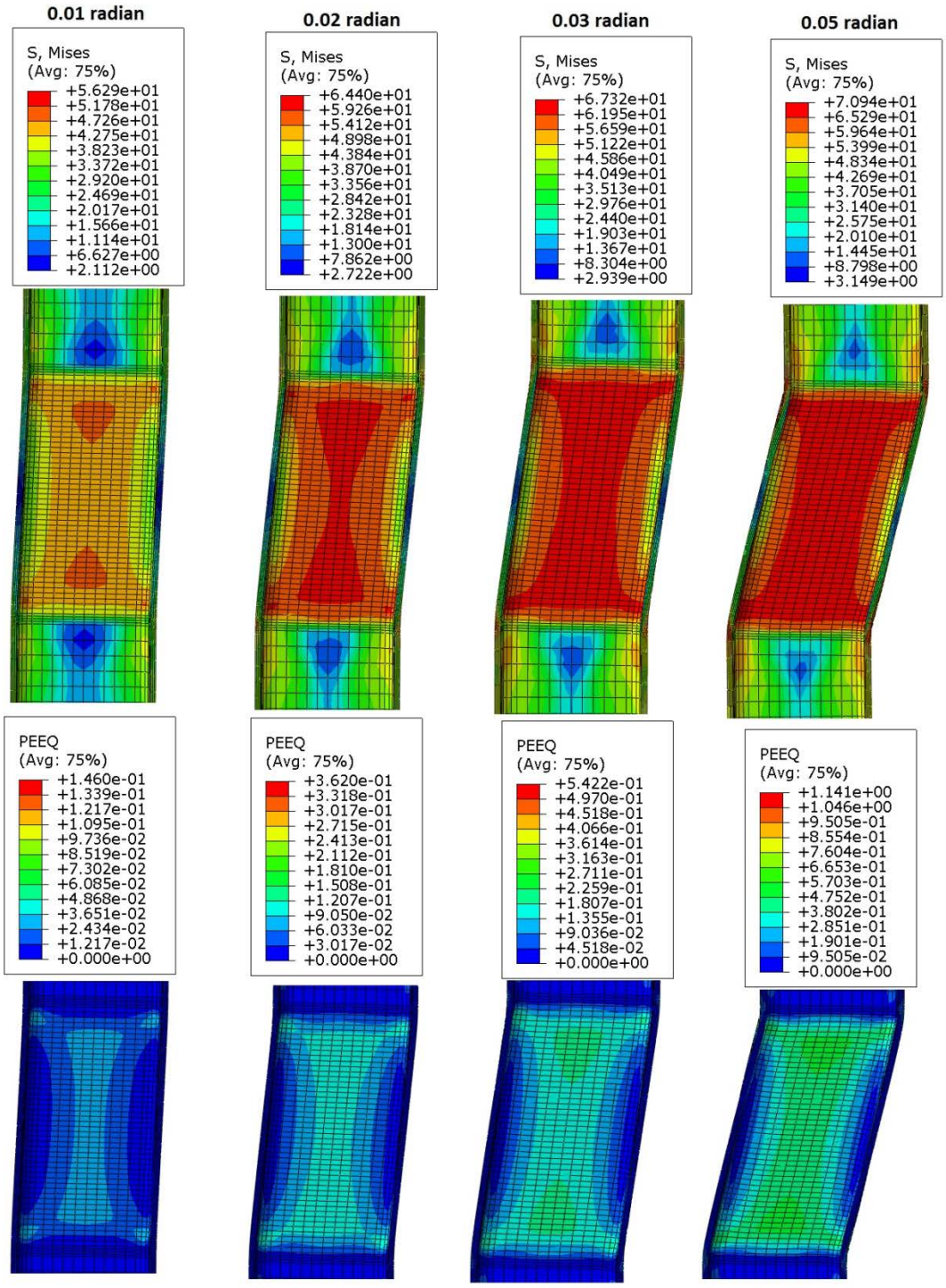

Figure 4.138: VMS and PEEQ in the column (Case 19A)

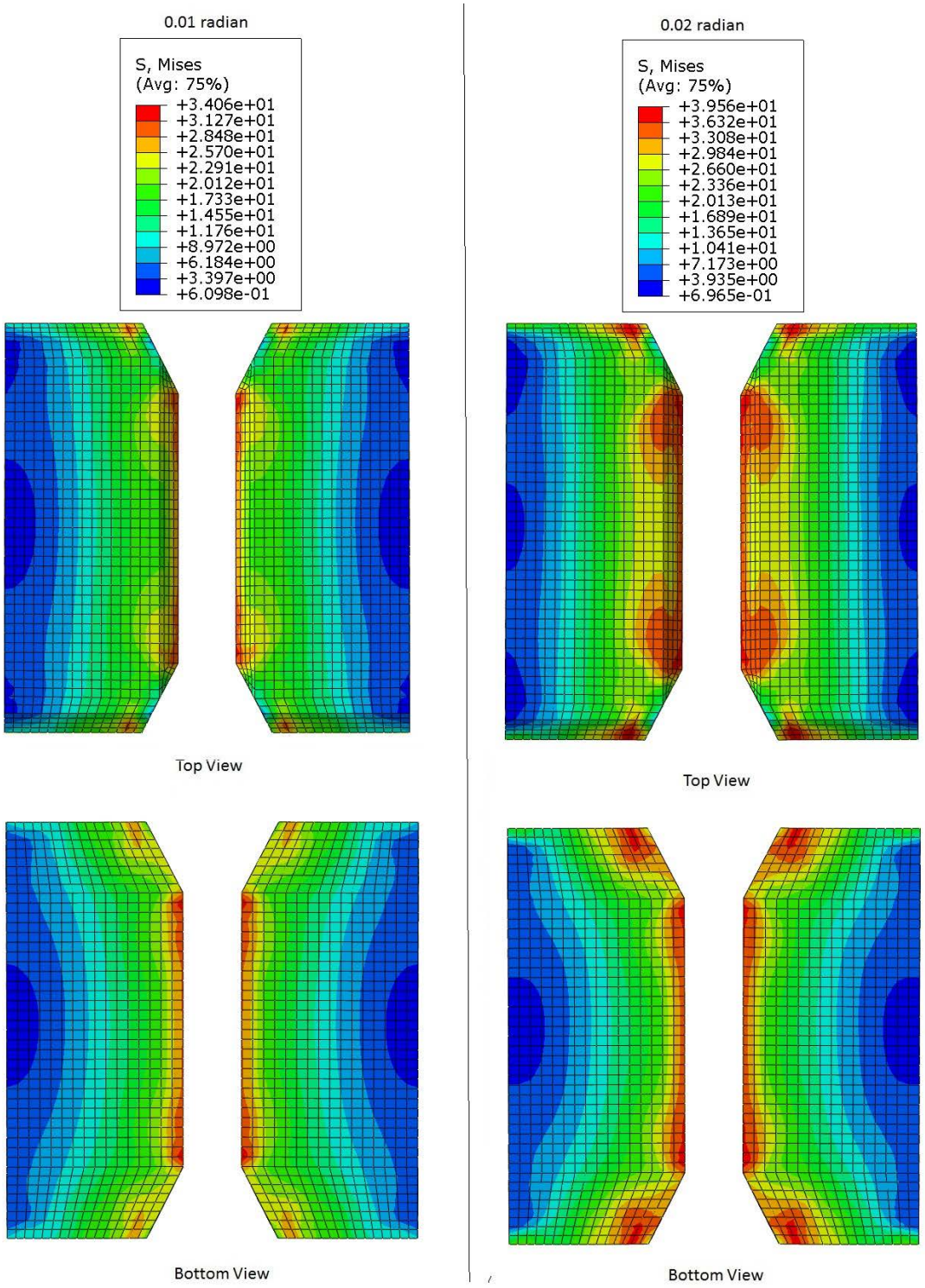

Figure 4.139: VMS in the CP at 0.01 and 0.02 radian rotation (Case 19A)

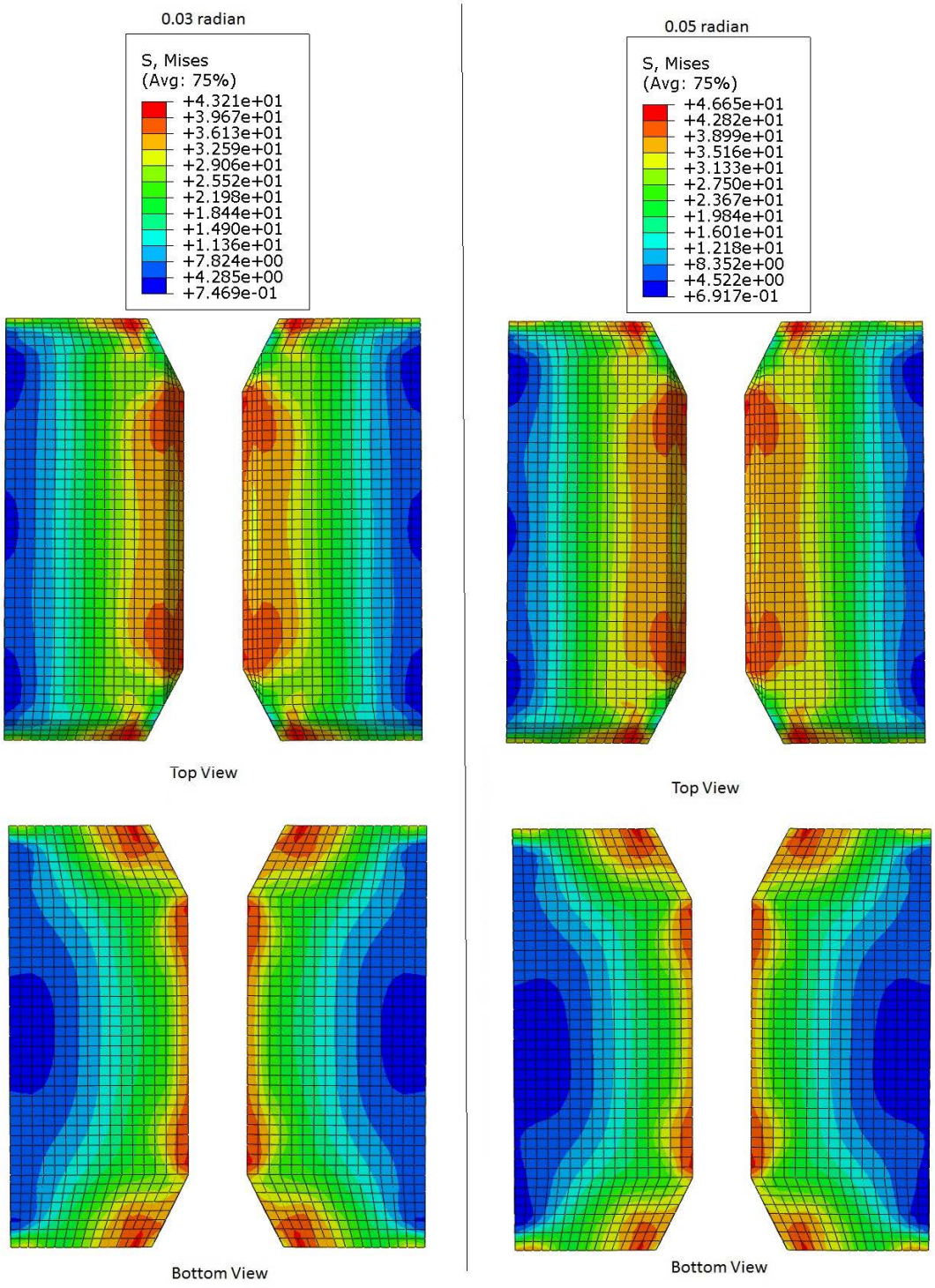

Figure 4.140: VMS in the CP at 0.03 and 0.05 radian rotation (Case 19A)

4.2.29 Analysis case 20A

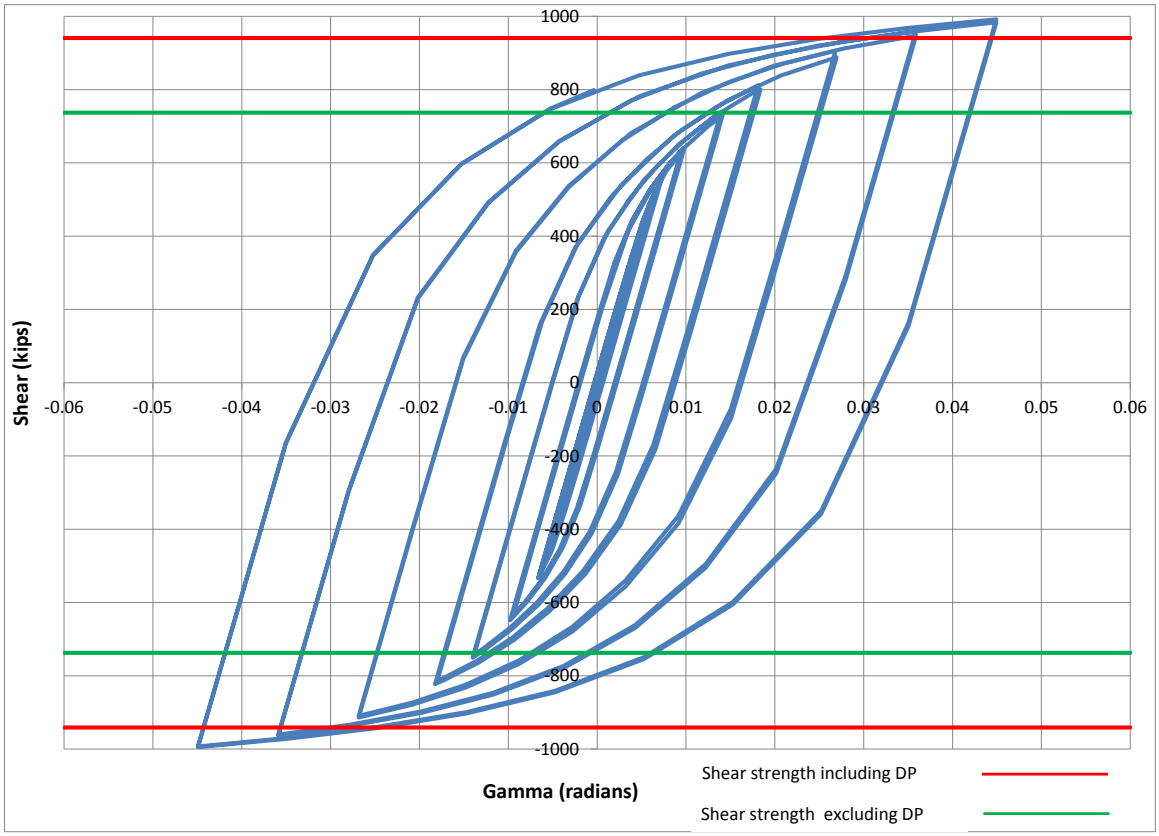

Figure 4.141: Panel zone shear versus rotation (Case 20A)

Table 4.30: Panel zone shear and force on loading plate (Case 20A)

Panel zone rotation (rad)	0.01	0.02	0.03	0.05
Panel zone shear (kips)	634.36	811.58	906.39	991.63
Force on one Loading plate (kips)	380.62	486.95	543.83	594.98

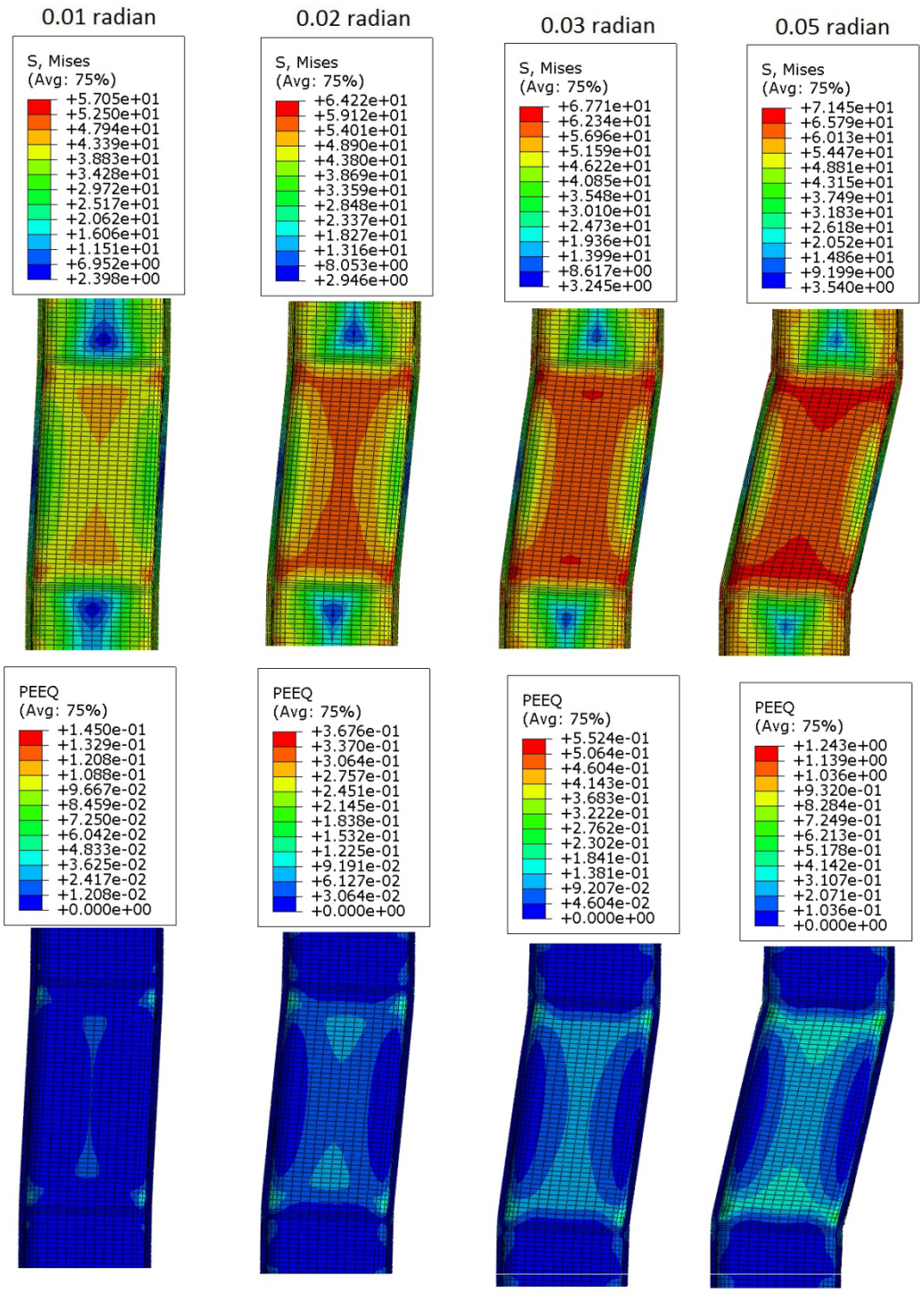

Figure 4.142: VMS and PEEQ in the column (Case 20A)

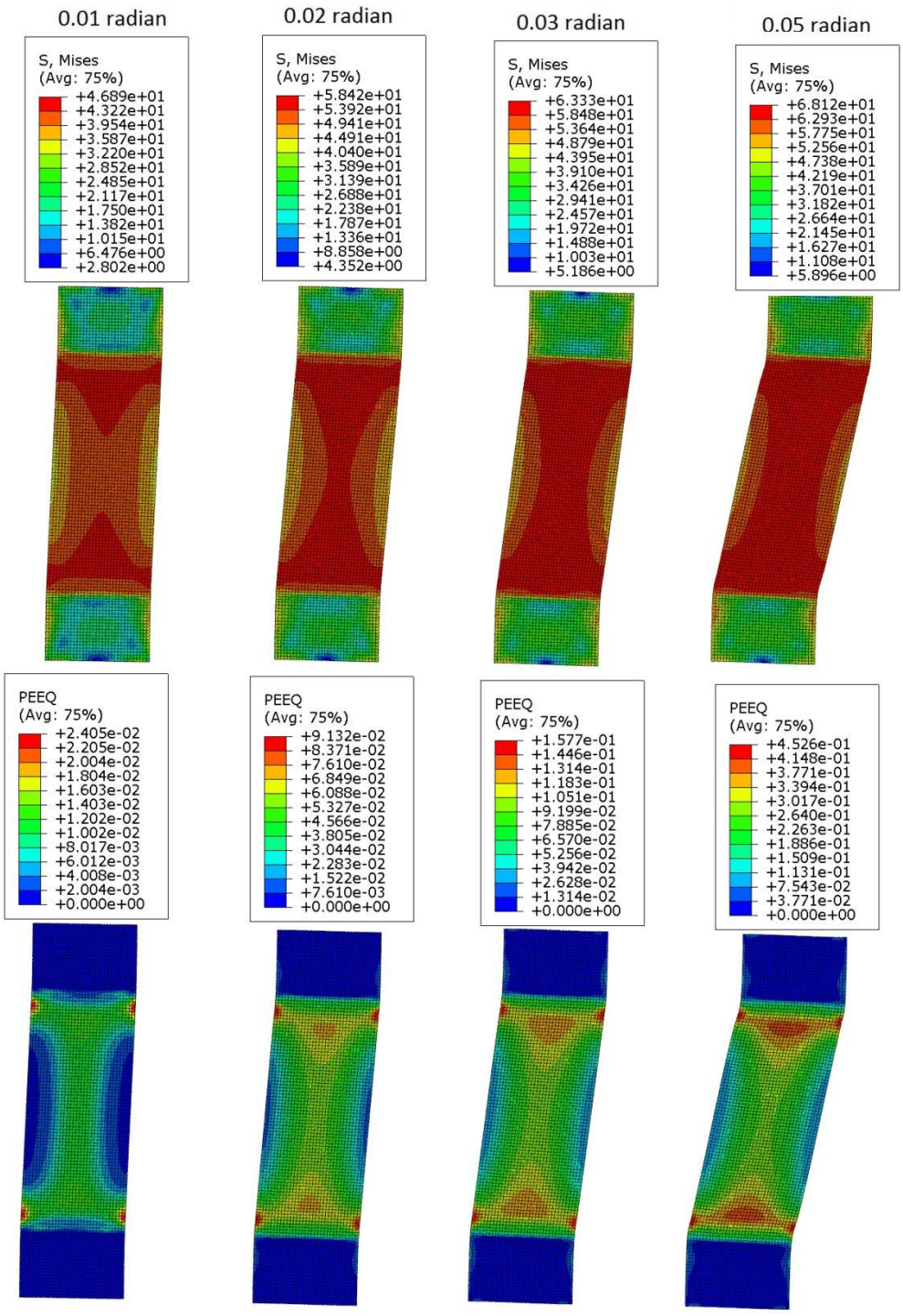

Figure 4.143: VMS and PEEQ in the DP (Case 20A)

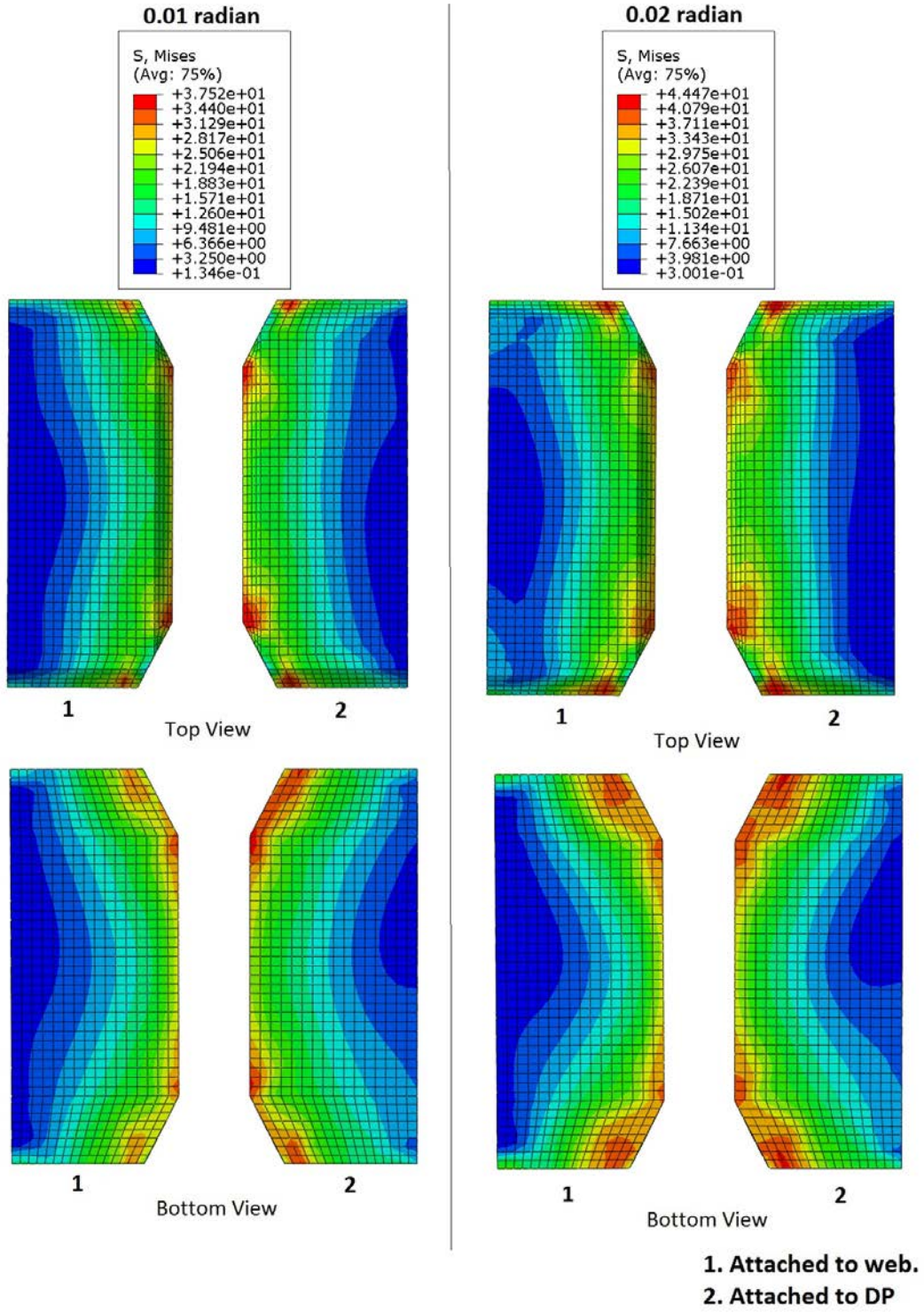

Figure 4.144: VMS in the CP at 0.01 and 0.02 radian rotation (Case 20A)

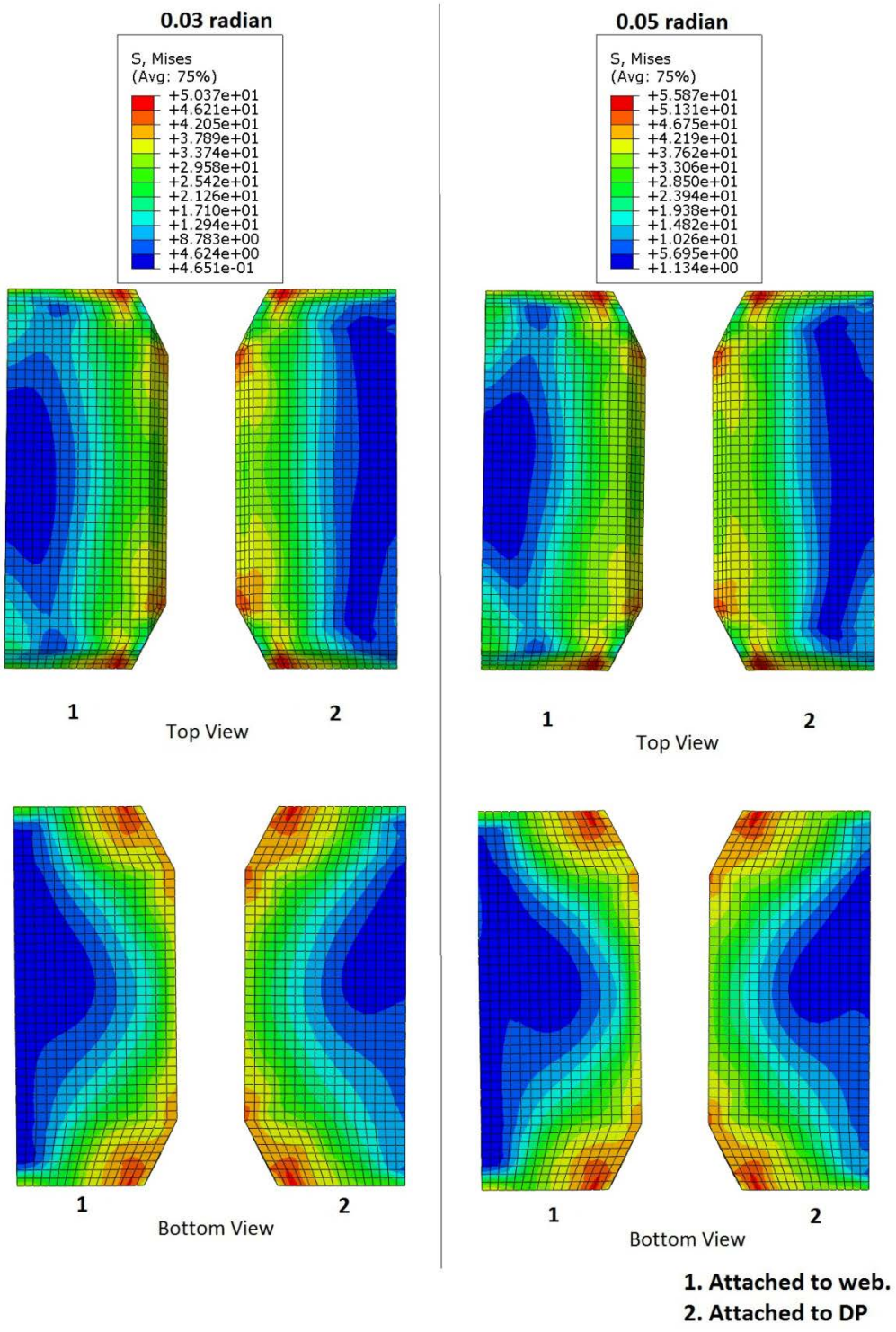

Figure 4.145: VMS in the CP at 0.03 and 0.05 radian rotation (Case 20A)

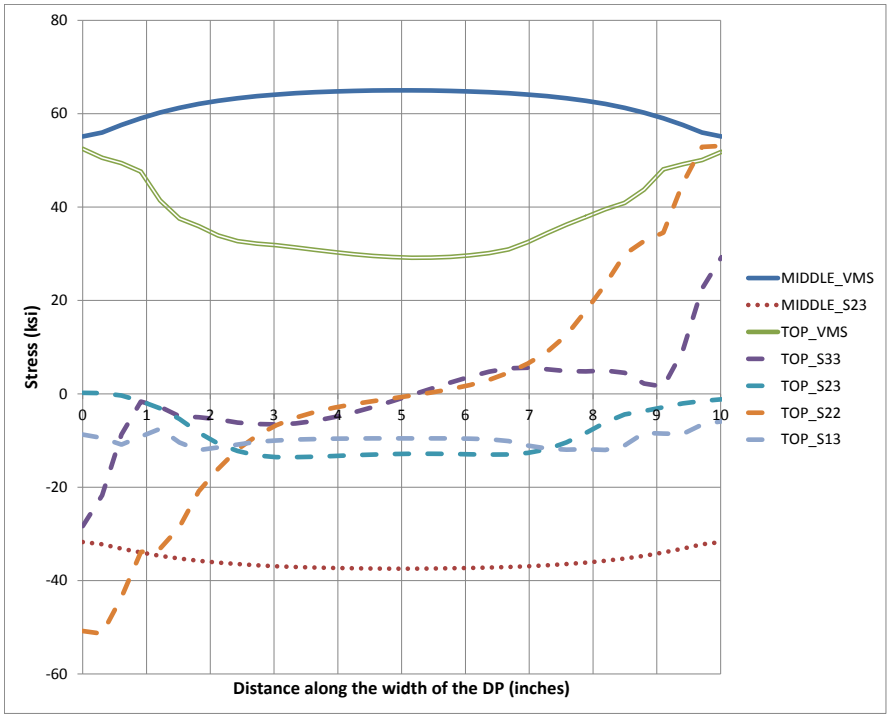

Figure 4.146: Stresses along the width of DP at 0.05 radian rotation (Case 20A)

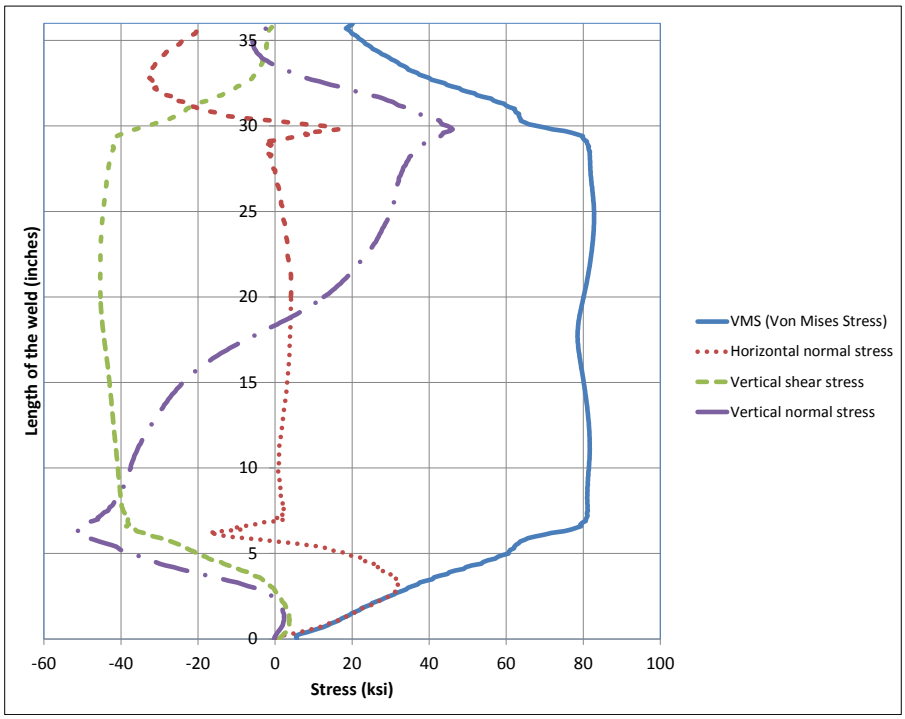

Figure 4.147: Stresses along depth of CJP1 (DP-CJP1 interface) at 0.05 radian(Case 20A)

4.2.30 Analysis case 21A

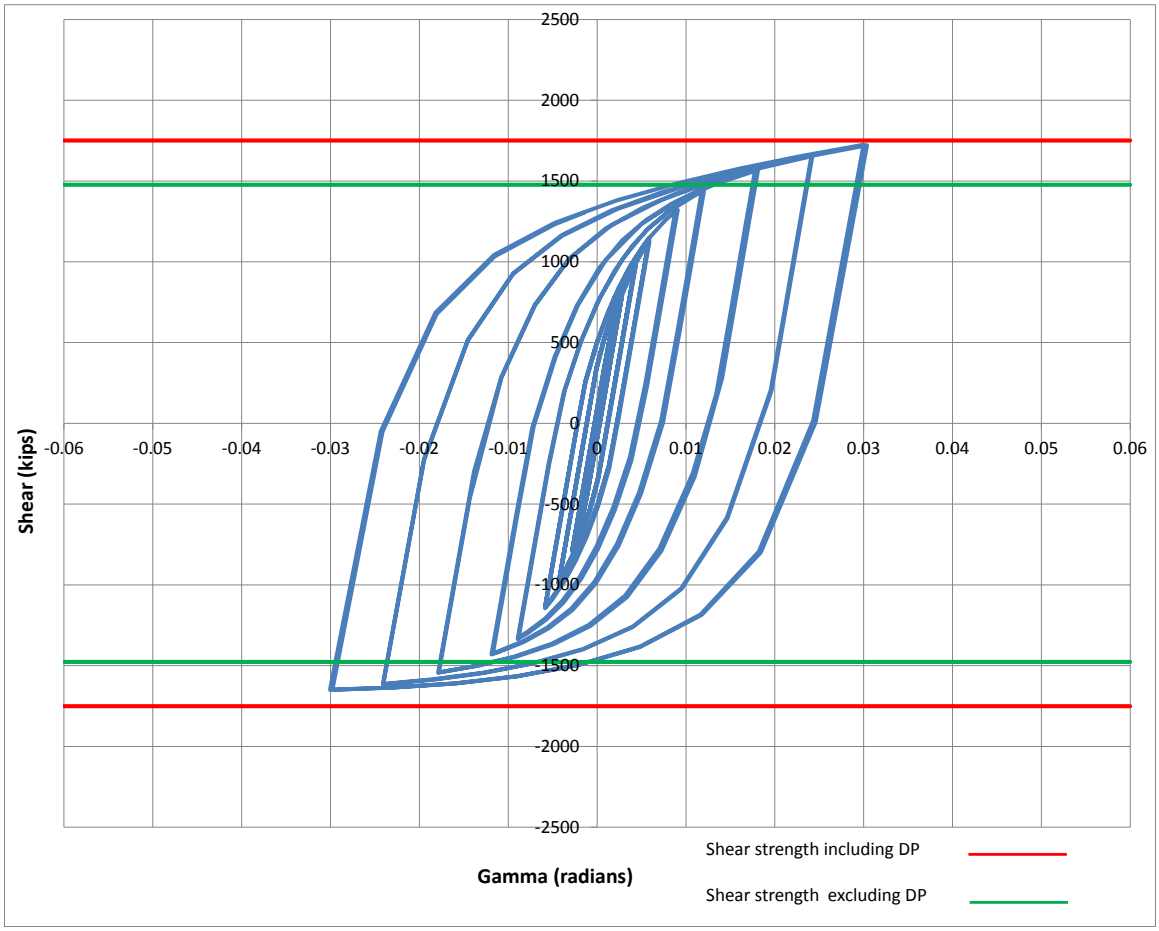

Figure 4.148: Panel zone shear versus rotation (Case 21A)

Table 4.31: Panel zone shear and force on loading plate (Case 21A)

Panel zone rotation (rad)	0.01	0.02	0.024	0.03
Panel zone shear (kips)	1342.93	1574.66	1659.11	1724.89
Force on one Loading plate (kips)	1611.51	1889.59	1990.93	2069.87

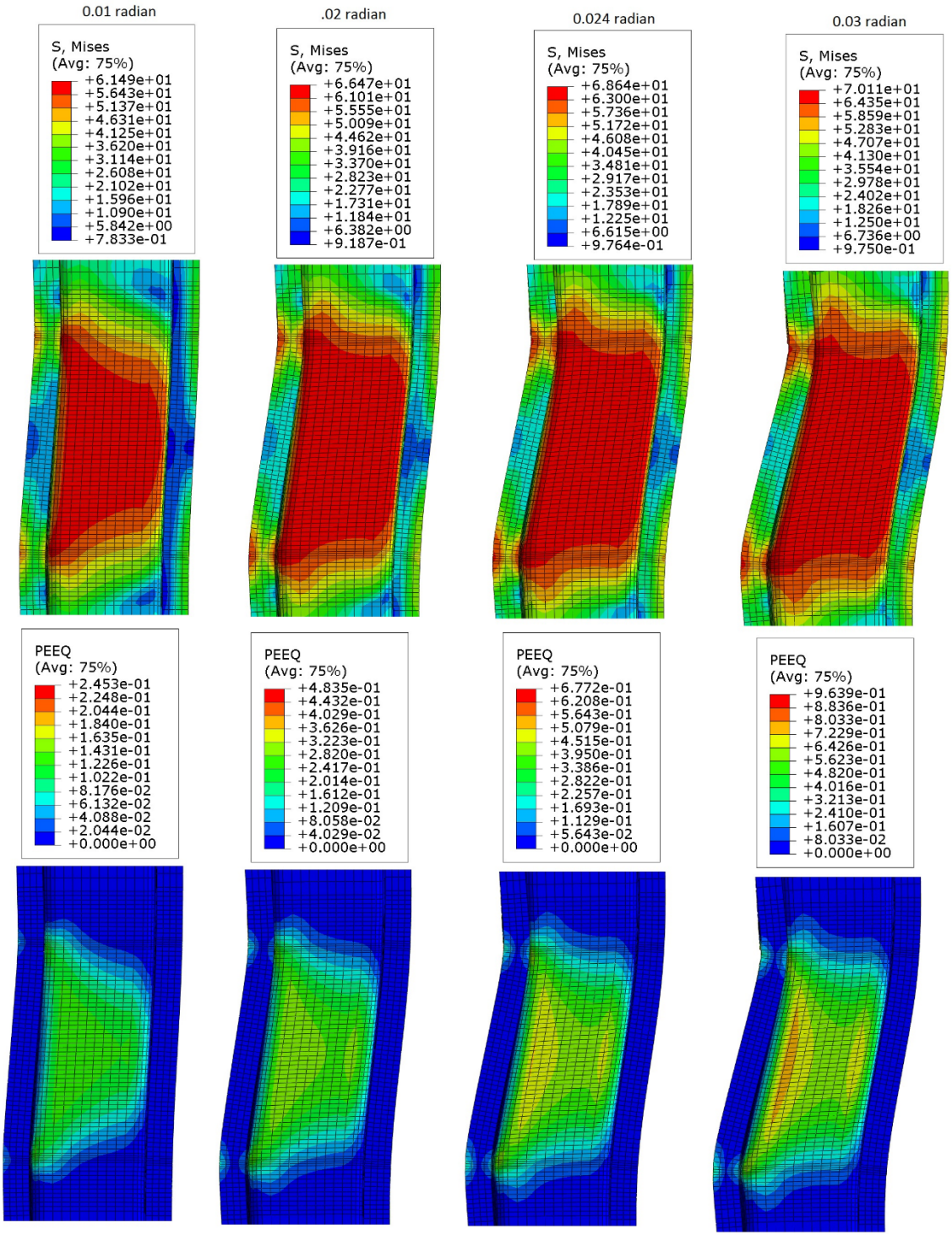

Figure 4.149: VMS and PEEQ in the column at different rotation (Case 21A)

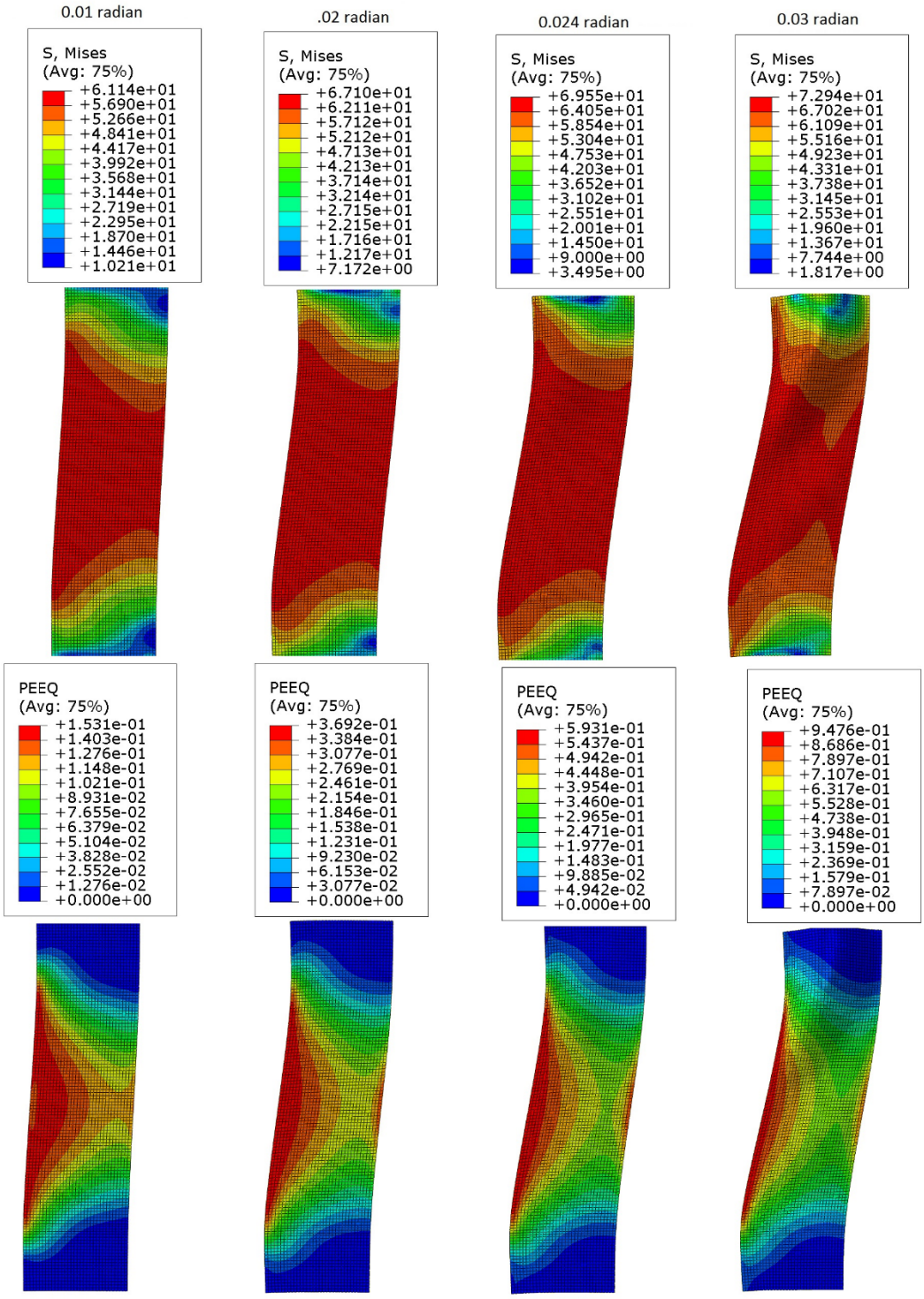

Figure 4.150: VMS and PEEQ in the DP at different rotations (Case 21A)

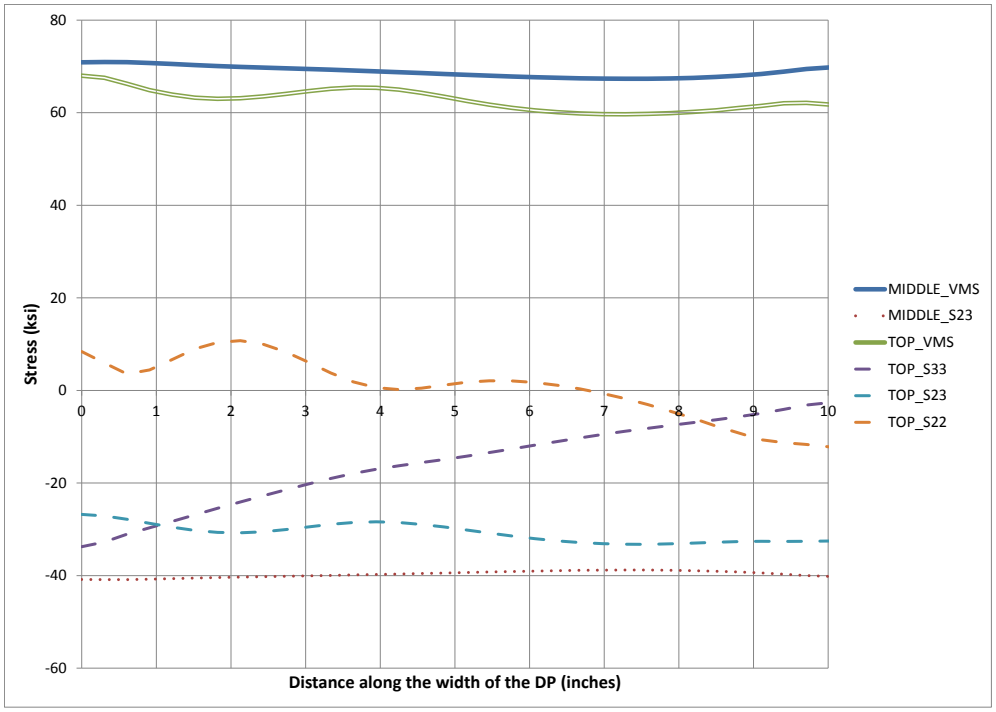

Figure 4.151: Stresses along the width of DP at 0.05 radian rotation (Case 21A)

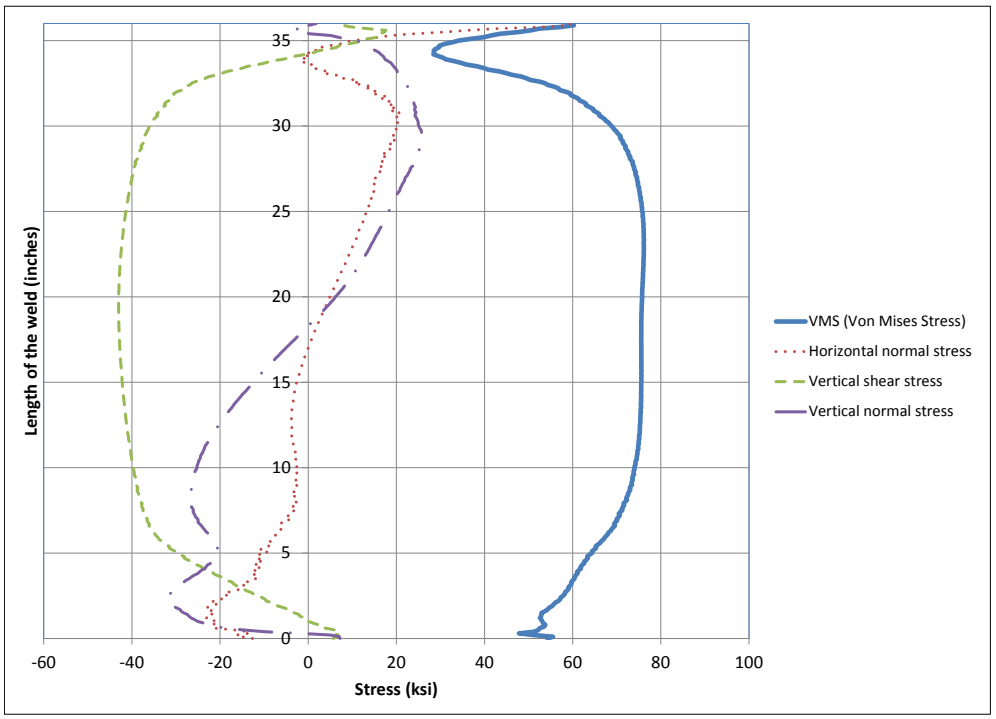

Figure 4.152: Stresses along depth of CJP1 (DP-CJP1 interface) at 0.05 radian(Case 21A)

4.2.31 Analysis case 22A

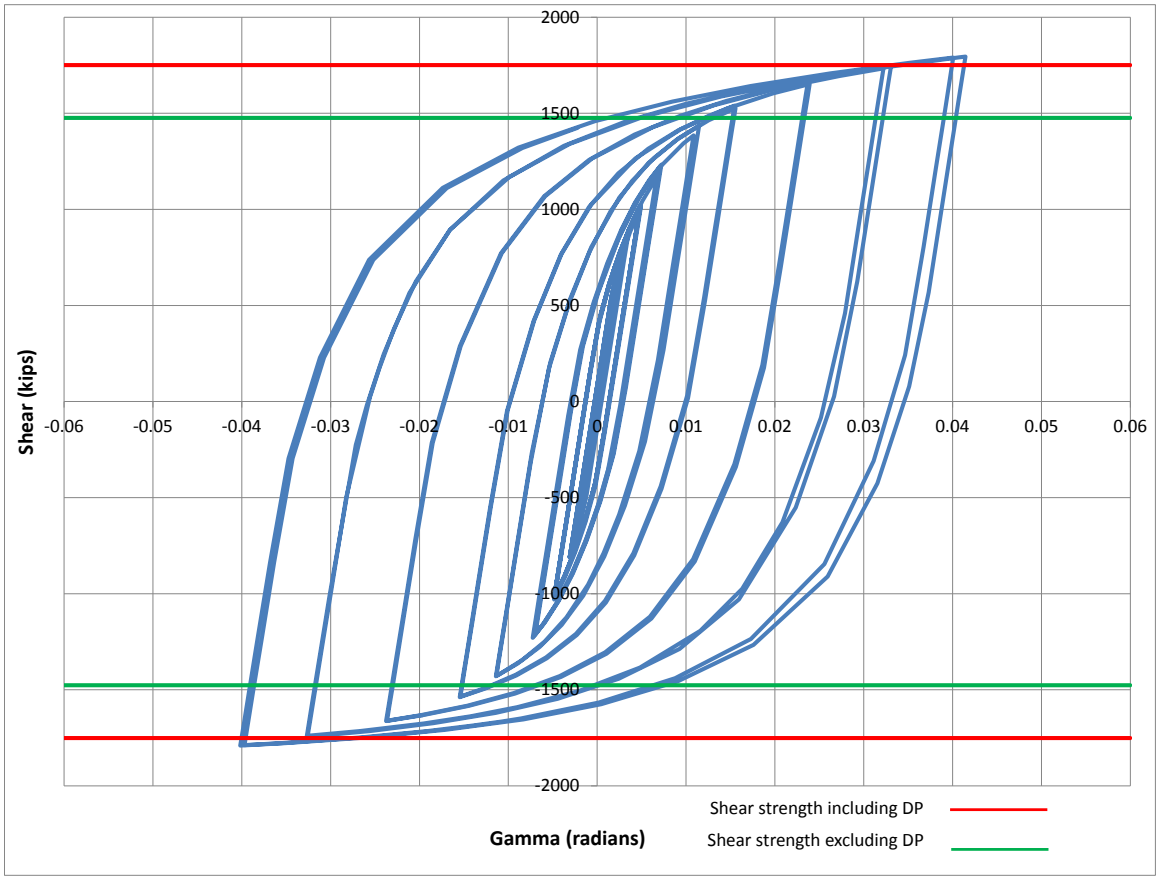

Figure 4.153: Panel zone shear versus rotation (Case 22A)

Table 4.32: Panel zone shear and force on loading plate (Case 22A)

Panel zone rotation (rad)	0.01	0.02	0.03	0.04
Panel zone shear (kips)	1218.51	1539.91	1666.03	1790.27
Force on one Loading plate (kips)	1462.21	1847.89	1999.24	2148.32

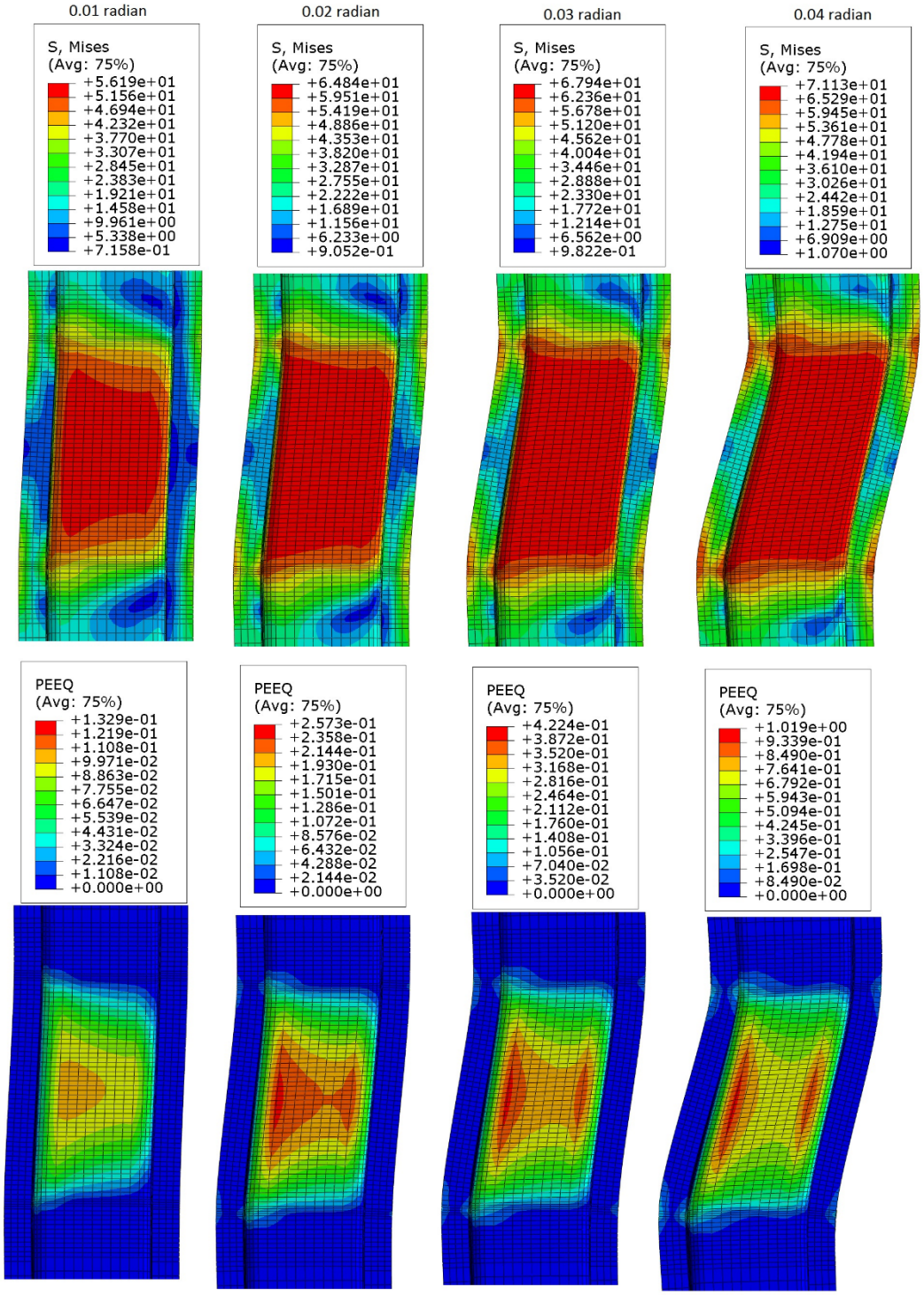

Figure 4.154: VMS and PEEQ in the column at different rotation (Case 22A)

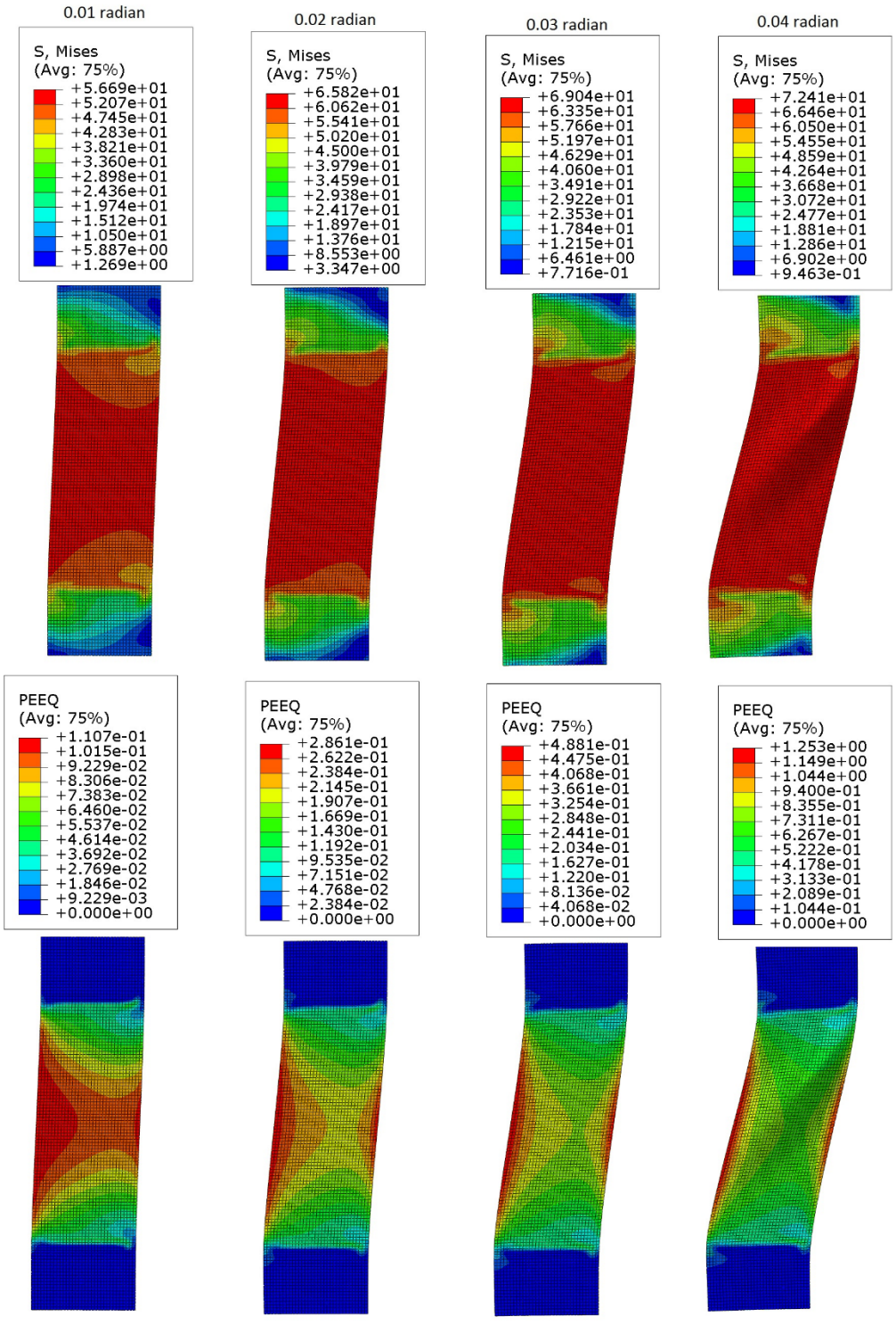

Figure 4.155: VMS and PEEQ in the DP at different rotations (Case 22A)

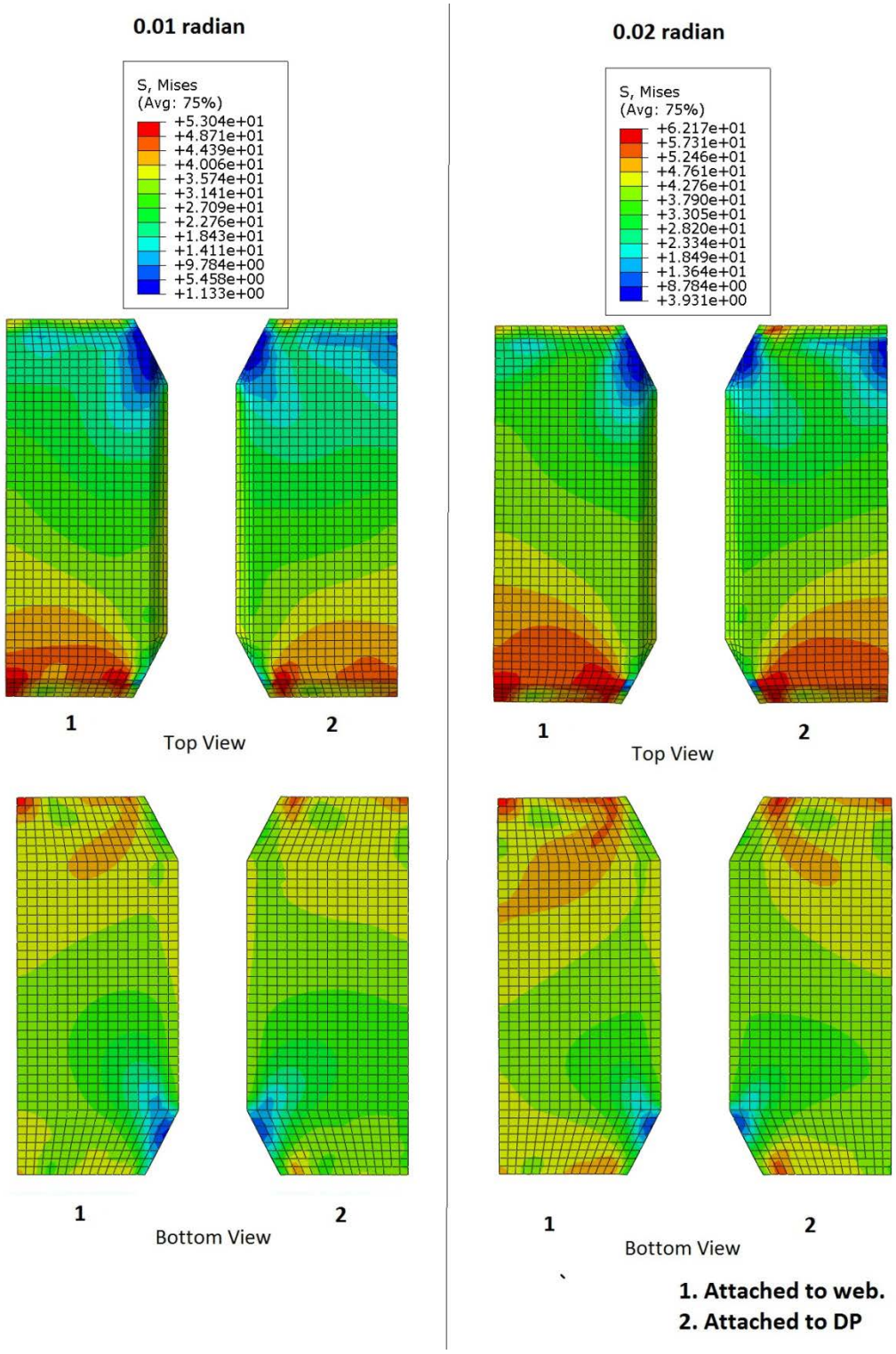

Figure 4.156: VMS in the CP at 0.01 and 0.02 radian rotation (Case 22A)

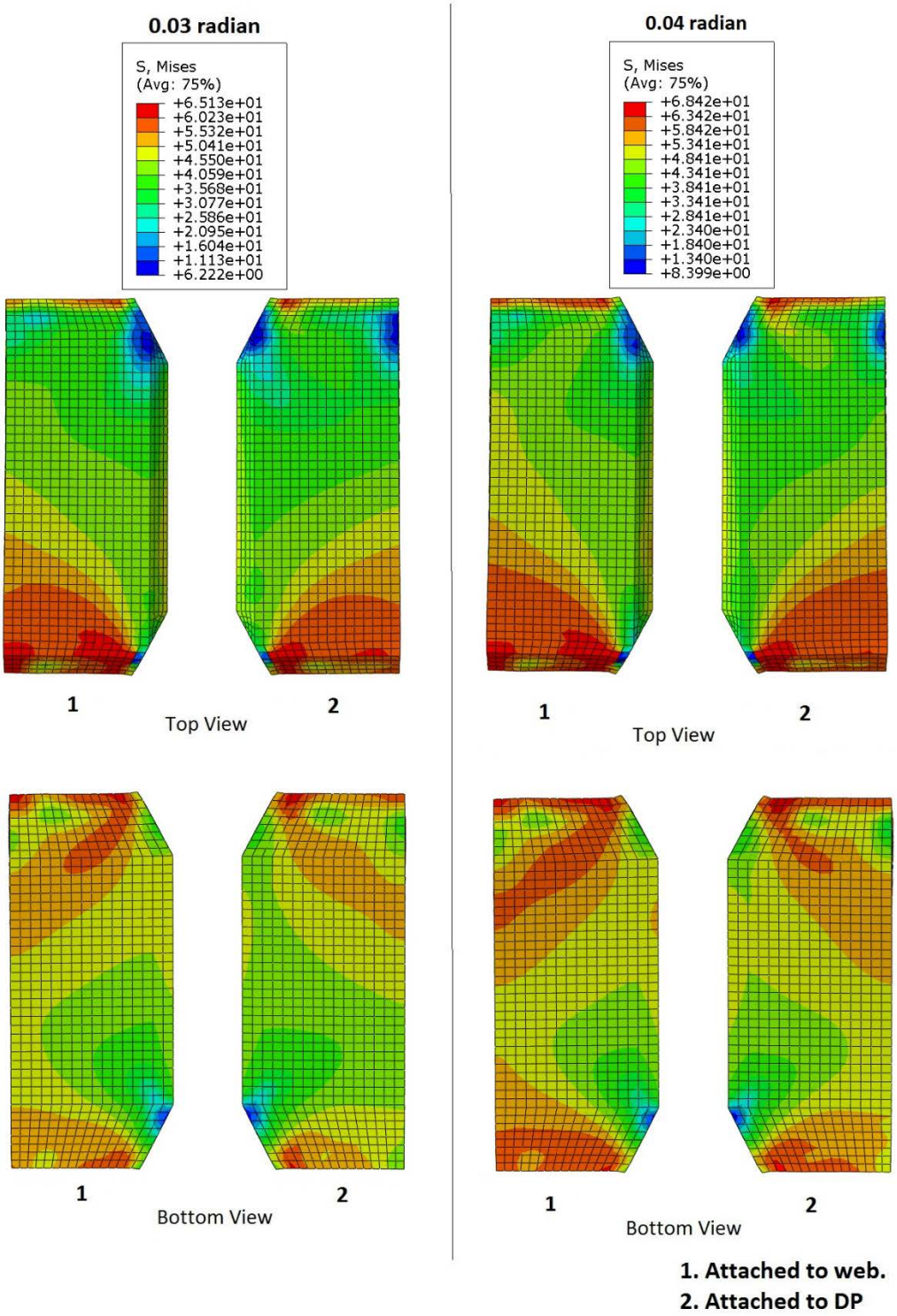

Figure 4.157: VMS in the CP at 0.03 and 0.05 radian rotation (Case 22A)

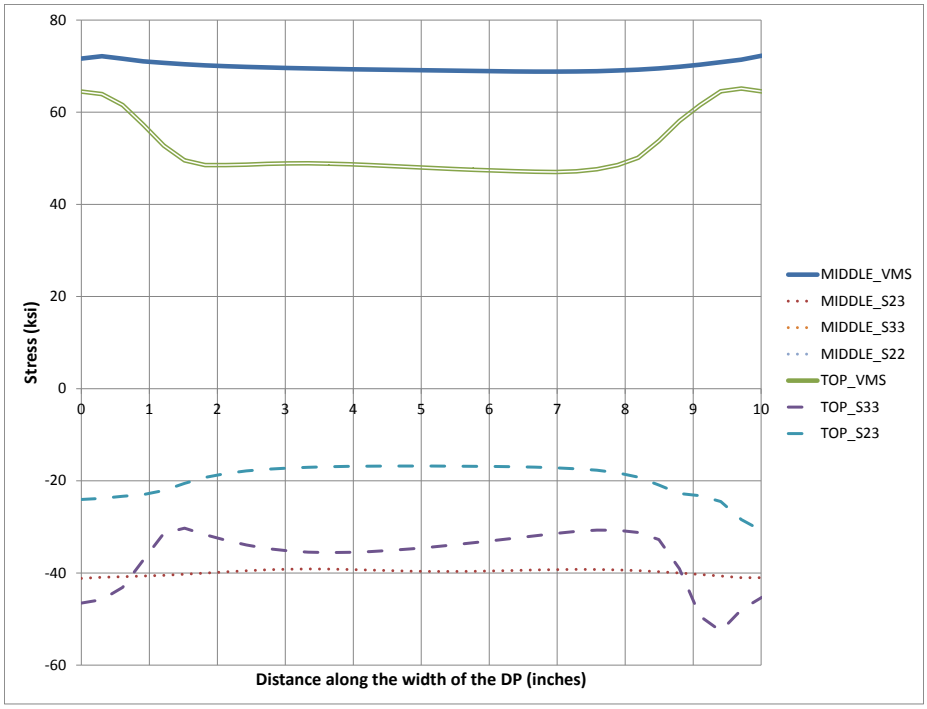

Figure 4.158: Stresses along the width of DP at 0.05 radian rotation (Case 22A)

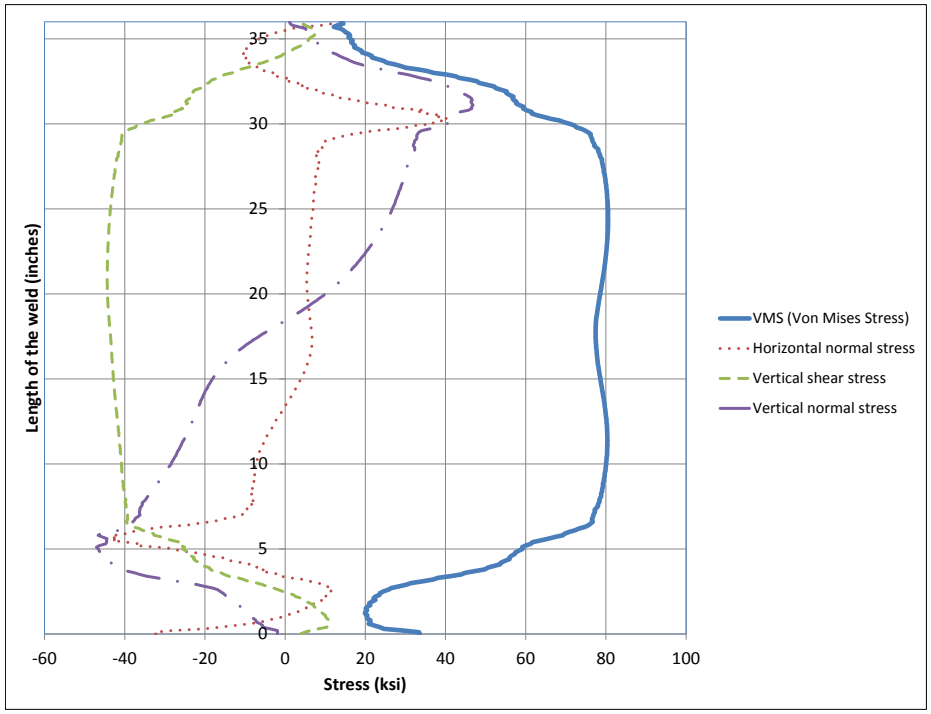

Figure 4.159: Stresses along depth of CJP1 (DP-CJP1 interface) at 0.05 radian(Case 22A)

4.3 PANEL ZONE SHEAR STRENGTH

A comparative study of the panel zone shear strength in the shallow column (W14X398) is made in this section. The shear in the panel zone may be altered by the presence of DP and CP in the assembly. To investigate their contribution, the panel zone shear versus rotation is plotted for case 1A-5A, 6A-10A, 11A-15A, and 16A-20A in Figure 4.160, 4.161, 4.162 and 4.163 respectively. The figures only show the last cycle of 0.05 radian in each case. As expected, the panel zone shear increases proportionally when the DP is attached to the column. No increase in shear is noticed when CP's are introduced between the flanges of column and there is no DP in the assembly. There is no increase in the strength of the panel zone when the DP is extended 6 inches beyond the LP level as compared to cases where the DP is terminated at the LP level. In each case, the panel zone shear is greater than the nominal panel zone shear strength. This implies that the limit state for each case in the shallow columns is web panel zone shear. No local limit states like flange local bending and web/DP crippling are observed in these cases. The nominal shear strength is calculated using Eq. J10-11 in *Specification for Steel Structural Buildings* (AISC 2010a). A yield stress of 50 ksi is considered to evaluate the strength (See section 3.3.5).

$$V_n = 0.6\, F_y d_c t_w \left(1 + \frac{3 b_{cf} t_{cf}^2}{d_b d_c t_w}\right) \qquad (Eq.\ 4.1)$$

Where,

F_y: Minimum specified yield stress of column web (ksi)

d_c: Column depth (in)

d_b: Beam depth (Center to center distance between LP's) (in)

t_{cf}: Thickness of the column flange (in)

t_w: Combined thickness of column web and DP (in)

b_{cf}: Width of the column flange (in)

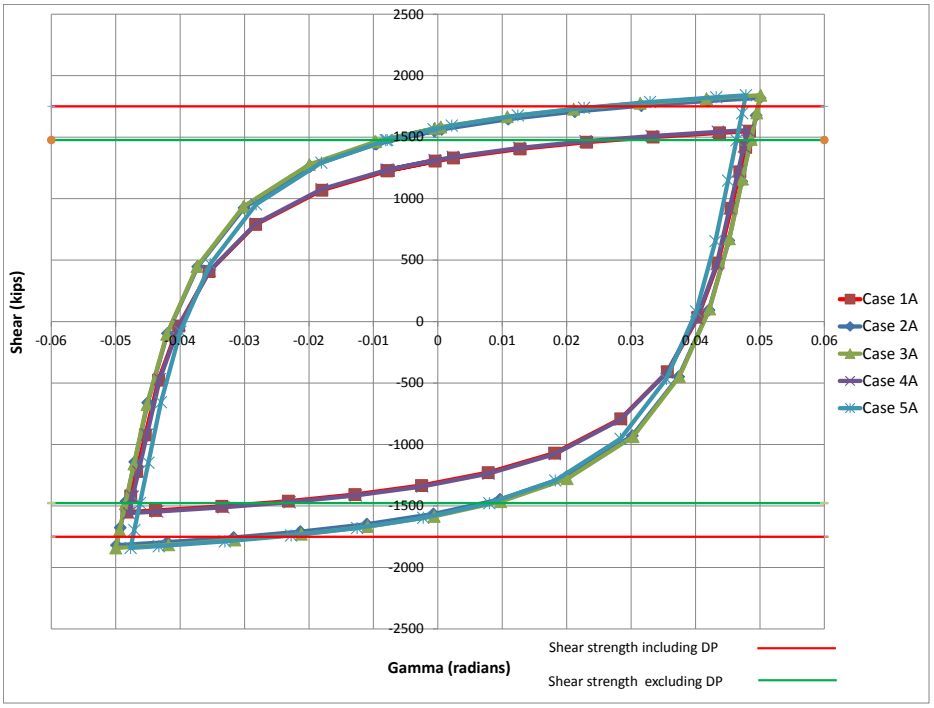

Figure 4.160: Panel zone shear comparison (Case 1A – 5A)

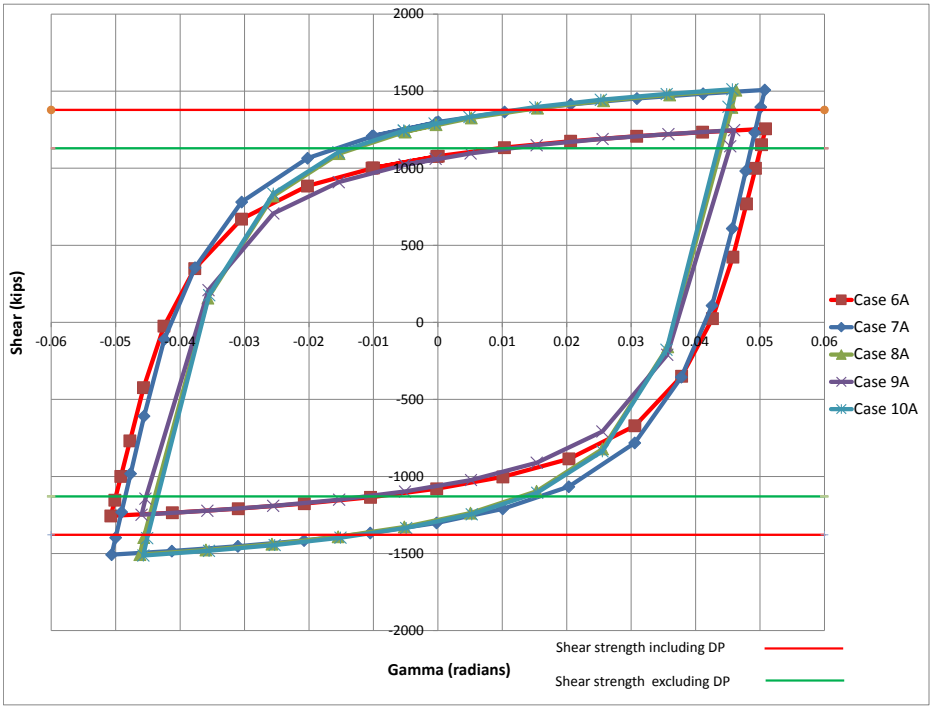

Figure 4.161: Panel zone shear comparison (Case 6A – 10A)

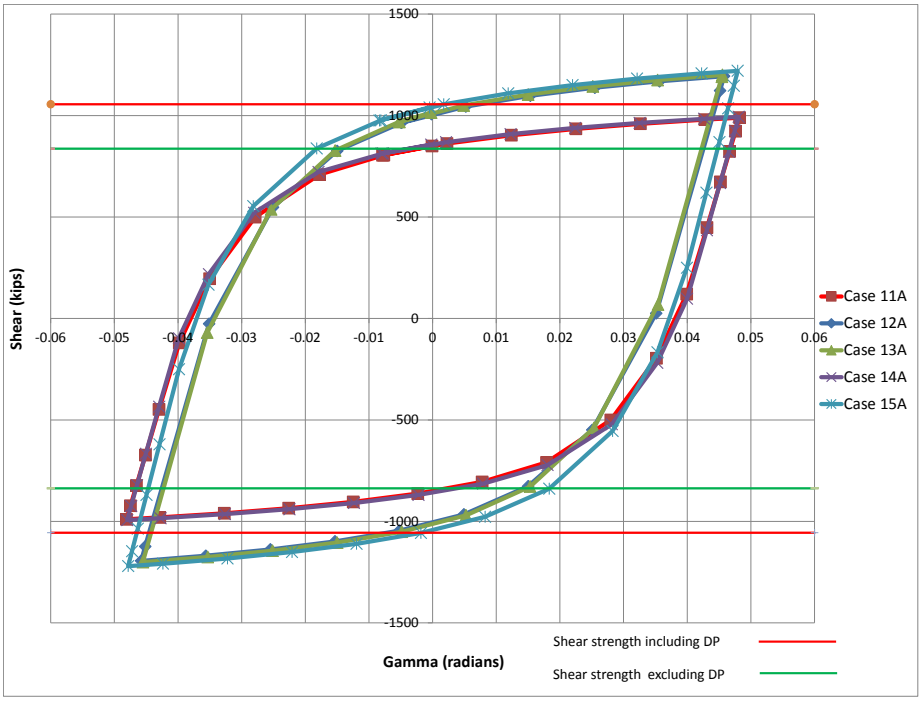

Figure 4.162: Panel zone shear comparison (Case 11A – 15A)

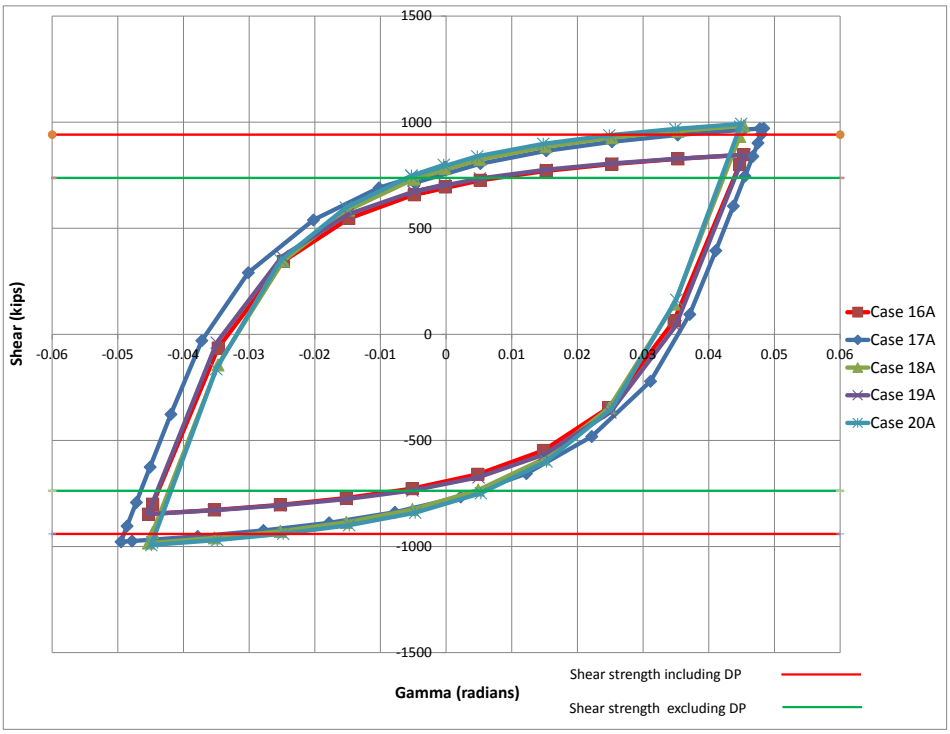

Figure 4.163: Panel zone shear comparison (Case 16A – 20A)

4.4 MAXIMUM VON MISES STRESS, PEEQ AND PEMAG

The maximum Von Mises Stresses, PEEQ and plastic strain magnitude (PEMAG) in the different parts of the panel zone assembly are listed in Table 4.33 – Table 4.38. These quantities are reported at +0.01 radian (last cycle) and +0.05 radian (last cycle).The quantities at +0.05 radian suggests the structural behavior at target rotation while the quantities at +0.01 radian suggests behavior near first yield of the panel zone shear versus gamma curve. The PEEQ and PEMAG provide information about the strain demands in the panel zone. At large inelastic deformations, the stress-strain curve is quite flat, so very small changes in stress may result in large changes in strain (see Figure 4.164).

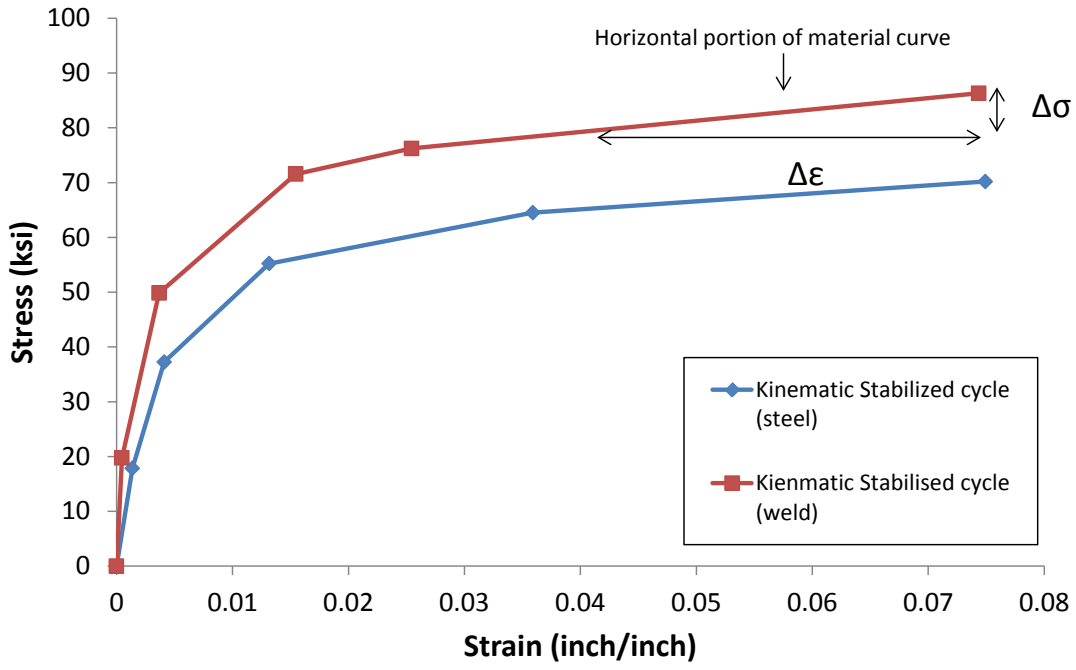

Figure 4.164: Stress versus strain (material curve)

The main observations from these tabulated values (Table 4.33 – 4.38) are as follows:

- The maximum VMS, PEEQ and PEMAG in the column at +0.05 radian are similar in all the cases irrespective of the presence of DP and CP's. This suggests that column ultimately shares the same load though different load paths. The load passes from column flanges directly to column web in cases without CP's while a portion of load passes through CP's and finds it way ultimately to the column web in cases with CP's. The same conclusions can be drawn at +0.01 radian.
- The maximum VMS, PEEQ and PEMAG in the DP are similar to those in the column for each case. So, the DP acts as a web in the column and thus increases the panel zone shear strength proportional to the combined thickness of DP and web of the column. This also suggests that web panel zone shear is the limit state governing the strength of the panel zone.
- The maximum VMS in vertical CJP1 weld reduces by around 10% in cases where the DP is extended 6 inches or the DP is also welded horizontally or the continuity plate is welded to the DP as compared to the case where the DP is between LP's. This reduction is around 30% in cases 16A-20A (t_f = 0.50 inch) But the extension of the DP did not help in reducing the stress in CJP1 weld in case 13A_one (thin flange = 1.00 inch, t_{dp} = 1.00 inch).
- The maximum VMS in CJP2, CJP3 and CP at +0.05 radian are almost similar in all the cases. Except in case 22A (LP's on one side), these stresses are higher as the force on one LP in case 22A is around double than the force in case 5A.
- The thickness of column web is around 3 times the thickness of the DP. But the stresses in the CJP2, CJP3 and CP are similar at the front and back side of the panel zone. The front side (F) is the side where the CP is welded to the DP while the back side (B) is the side where the CP is welded to the web of column.

Table 4.33: Maximum Von Mises stress at 0.05 radian rotation

Case	Column	DB	CJP1	CJP2	CJP3	CP
1A	71.81					
2A	71.79	72.48	104.50			
2A_f	71.66	72.64	88.09	88.32 (horizontal fillet weld)		
3A	72.10	74.31	90.93			
3A_quar	71.94	72.95	89.00			
3A_one	71.56	72.63	93.71			
4A	71.88			90.03	96.72	53.51
5A	72.04	74.05	91.07	90.04 (F)	93.56 (F)	52.92 (F)
				89.30 (B)	95.88 (B)	51.75 (B)
5A_quar	71.81	72.83	88.99	92.93 (F)	97.10 (F)	52.99 (F)
				89.34 (B)	94.61 (B)	51.59 (B)
5A_one	71.21	72.28	92.97	88.32 (F)	97.96 (F)	50.97 (F)
				88.02 (B)	93.76 (B)	50.61 (B)
6A	71.75					
7A	71.25	73.97	101.50			
8A	70.88	71.86	86.10			
9A	71.32			84.69	91.61	59.82
10A	70.96	71.97	86.52	87.02 (F)	94.52 (F)	48.88 (F)
				82.46 (B)	91.39 (B)	51.23 (B)
11A	65.45					
12A	70.44	73.56	104.40			
13A	69.69	72.31	85.33			
13A_quar	69.76	68.43	88.70			
13A_one	71.00	67.37	101.00			
14A	70.41			84.34	88.03	48.27
15A	69.73	72.25	84.65	86.47 (F)	94.04 (F)	47.11 (F)
				85.36 (B)	90.74 (B)	54.58 (B)
15A_quar	69.66	69.35	84.54	87.95 (F)	94.97 (F)	55.28 (F)
				87.96 (B)	89.62 (B)	55.30 (B)
15A_one	70.48	68.14	88.96	91.39 (F)	93.70 (F)	58.47 (F)
				90.04 (B)	88.59 (B)	57.37 (B)
16A	65.13					
17A	73.46	75.02	135.60			
18A	72.38	67.74	97.31			
19A	70.94			85.15	85.13	46.65
20A	71.45	68.12	87.50	90.11 (F)	88.48 (F)	55.87 (F)
				87.39 (B)	85.49 (B)	55.23 (B)
21A	70.11	72.94	90.78			
22A	71.13	72.41	88.41	115.20 (F)	108.60 (F)	68.42 (F)
				107.60 (B)	110.50 (B)	68.40 (B)

Table 4.34: Maximum Von Mises stress at 0.01 radian rotation

Case	Column	DB	CJP1	CJP2	CJP3	CP
1A	60.18					
2A	58.90	59.78	79.70			
2A_f	58.95	59.27	74.22	67.40 (horizontal fillet weld)		
3A	59.59	60.08	76.71			
3A_quar	59.15	59.51	74.41			
3A_one	57.37	57.66	78.88			
4A	60.24			69.78	78.79	40.75
5A	59.78	60.47	77.02	69.83 (F)	80.80 (F)	32.88 (F)
				59.77 (B)	79.00 (B)	35.46 (B)
5A_quar	59.14	59.55	74.49	70.40 (F)	80.47 (F)	35.11 (F)
				59.33 (B)	78.34 (B)	35.73 (B)
5A_one	56.80	57.07	78.50	66.97 (F)	80.31 (F)	37.37 (F)
				56.05 (B)	77.47 (B)	36.15 (B)
6A	58.47					
7A	55.48	58.39	78.15			
8A	55.98	56.27	70.39			
9A	58.64			68.83	76.17	37.27
10A	55.98	56.34	70.51	70.41 (F)	80.99 (F)	36.63 (F)
				59.24 (B)	77.05 (B)	36.26 (B)
11A	44.20					
12A	57.30	57.62	80.42			
13A	56.16	50.78	73.31			
13A_quar	56.95	48.51	77.79			
13A_one	59.02	46.38	82.01			
14A	53.45			70.60	74.90	35.49
15A	53.83	50.40	69.68	63.33 (F)	81.72 (F)	34.89 (F)
				67.95 (B)	76.61 (B)	36.80 (B)
15A_quar	55.20	50.12	70.78	72.86 (F)	81.74 (F)	38.75 (F)
				70.11 (B)	76.93 (B)	37.38 (B)
15A_one	55.49	47.29	77.53	78.20 (F)	80.69 (F)	40.99 (F)
				71.37 (B)	76.16 (B)	37.41 (B)
16A	47.43					
17A	61.52	57.10	81.62			
18A	60.35	45.44	78.99			
19A	56.42			68.31	71.44	34.18
20A	56.79	46.55	71.42	75.95 (F)	78.68 (F)	37.08 (F)
				71.25 (B)	72.10 (B)	35.13 (B)
21A	61.49	61.14	82.11			
22A	56.07	56.57	73.24	83.02 (F)	84.36 (F)	51.75 (F)
				82.00 (B)	82.91 (B)	52.81 (B)

Table 4.35: Maximum PEEQ at 0.05 radian rotation

Case	Column	DB	CJP1	CJP2	CJP3	CP
1A	1.359					
2A	1.256	1.658	2.802			
2A_f	1.232	1.426	1.045	1.015 (horizontal fillet weld)		
3A	1.312	1.535	1.335			
3A_quar	1.246	1.491	0.965			
3A_one	1.136	1.386	1.712			
4A	1.373			0.995	2.133	0.226
5A	1.339	1.569	1.413	1.209 (F)	2.175 (F)	0.061 (F)
				0.908 (B)	2.026 (B)	0.060 (B)
5A_quar	1.273	1.531	1.020	1.227 (F)	2.351 (F)	0.051 (F)
				0.874 (B)	1.950 (B)	0.059 (B)
5A_one	1.043	1.261	1.560	0.740 (F)	2.350 (F)	0.049 (F)
				0.709 (B)	1.848 (B)	0.064 (B)
6A	1.223					
7A	0.999	1.473	2.385			
8A	0.950	1.130	0.677			
9A	1.155			0.642	1.547	0.110
10A	0.966	1.159	0.699	0.713 (F)	2.127 (F)	0.055 (F)
				0.353 (B)	1.617 (B)	0.069 (B)
11A	0.847					
12A	1.169	1.406	2.667			
13A	0.931	0.749	0.812			
13A_quar	0.994	0.524	1.426			
13A_one	1.224	0.442	2.980			
14A	0.806			0.573	1.178	0.059
15A	0.797	0.798	0.667	0.321 (F)	2.466 (F)	0.043 (F)
				0.720 (B)	1.396 (B)	0.091 (B)
15A_quar	0.907	0.619	0.713	1.047 (F)	2.258 (F)	0.109 (F)
				0.875 (B)	1.410 (B)	0.097 (B)
15A_one	1.036	0.509	1.305	1.695 (F)	2.012 (F)	0.157 (F)
				1.108 (B)	1.260 (B)	0.113 (B)
16A	1.409					
17A	1.976	1.435	4.207			
18A	1.389	0.426	2.094			
19A	1.141			0.556	0.808	0.050
20A	1.243	0.453	0.882	1.249 (F)	1.406 (F)	0.120 (F)
				0.854 (B)	0.830 (B)	0.093 (B)
21A	0.964	0.948	1.711			
22A	1.019	1.253	1.016	4.652 (F)	4.524 (F)	0.747 (F)
				3.699 (B)	4.149 (B)	0.723 (B)

Table 4.36: Maximum PEEQ at 0.01 radian rotation

Case	Column	DB	CJP1	CJP2	CJP3	CP
1A	0.222					
2A	0.175	0.195	0.355			
2A_f	0.176	0.178	0.189	0.07954 (horizontal fillet weld)		
3A	0.195	0.203	0.246			
3A_quar	0.180	0.184	0.177			
3A_one	0.139	0.137	0.313			
4A	0.225			0.118	0.310	0.014
5A	0.207	0.218	0.263	0.082 (F)	0.488 (F)	0.008 (F)
				0.018 (B)	0.349 (B)	0.013 (B)
5A_quar	0.181	0.187	0.179	0.094 (F)	0.485 (F)	0.000 (F)
				0.015 (B)	0.316 (B)	0.002 (B)
5A_one	0.139	0.137	0.315	0.083 (F)	0.485 (F)	0.006 (F)
				0.011 (B)	0.313 (B)	0.003 (B)
6A	0.164					
7A	0.116	0.158	0.289			
8A	0.124	0.121	0.109			
9A	0.169			0.108	0.251	0.005
10A	0.127	0.123	0.104	0.114 (F)	0.530 (F)	0.002 (F)
				0.020 (B)	0.293 (B)	0.003 (B)
11A	0.162					
12A	0.199	0.141	0.497			
13A	0.176	0.065	0.167			
13A_quar	0.181	0.047	0.304			
13A_one	0.196	0.035	0.613			
14A	0.133			0.125	0.222	0.003
15A	0.151	0.083	0.114	0.045 (F)	0.625 (F)	0.001 (F)
				0.081 (B)	0.287 (B)	0.005 (B)
15A_quar	0.157	0.056	0.124	0.139 (F)	0.540 (F)	0.009 (F)
				0.092 (B)	0.270 (B)	0.006 (B)
15A_one	0.162	0.039	0.302	0.270 (F)	0.460 (F)	0.018 (F)
				0.104 (B)	0.248 (B)	0.007 (B)
16A	0.242					
17A	0.282	0.116	0.517			
18A	0.252	0.037	0.335			
19A	0.188			0.078	0.140	0.001
20A	0.190	0.037	0.123	0.184 (F)	0.336 (F)	0.008 (F)
				0.098 (B)	0.155 (B)	0.003 (B)
21A	0.245	0.153	0.476			
22A	0.140	0.119	0.178	0.736 (F)	0.817 (F)	0.106 (F)
				0.469 (B)	0.630 (B)	0.104 (B)

Table 4.37: Maximum PEMAG at 0.05 radian rotation

Case	Column	DB	CJP1	CJP2	CJP3	CP
1A	0.0555					
2A	0.0545	0.1023	0.1373			
2A_f	0.0527	0.0666	0.0467	0.0569 (horizontal fillet weld)		
3A	0.0582	0.1211	0.0621			
3A_quar	0.0563	0.0721	0.0515			
3A_one	0.0514	0.0666	0.0769			
4A	0.0557			0.0570	0.0936	0.0124
5A	0.0602	0.1244	0.0654	0.0605 (F)	0.0839 (F)	0.0034 (F)
				0.0553 (B)	0.0956 (B)	0.0036 (B)
5A_quar	0.0545	0.0701	0.0514	0.0727 (F)	0.0955 (F)	0.0045 (F)
				0.0533 (B)	0.0826 (B)	0.0033 (B)
5A_one	0.0473	0.0609	0.0729	0.0486 (F)	0.1005 (F)	0.0034 (F)
				0.0464 (B)	0.0781 (B)	0.0032 (B)
6A	0.0543					
7A	0.0485	0.0957	0.1208			
8A	0.0443	0.0548	0.0362			
9A	0.0492			0.0288	0.0661	0.0071
10A	0.0451	72.8800	0.0383	0.0423 (F)	0.0819 (F)	0.0026 (F)
				0.0265 (B)	0.0653 (B)	0.0032 (B)
11A	0.0384					
12A	0.0490	0.0860	0.1351			
13A	0.0368	0.0859	0.0324			
13A_quar	0.0382	0.0311	0.0506			
13A_one	0.0528	0.0251	0.1163			
14A	0.0397			0.0278	0.0470	0.0027
15A	0.0358	0.7983	0.0374	0.3210 (F)	0.0786 (F)	0.0034 (F)
				0.0325 (B)	0.0609 (B)	0.0041 (B)
15A_quar	0.0371	0.0352	0.0284	0.0466 (F)	0.0837 (F)	0.0047 (F)
				0.0462 (B)	0.0055 (B)	0.0462 (B)
15A_one	0.0433	0.0301	0.0516	0.0654 (F)	0.0768 (F)	0.0066 (F)
				0.0572 (B)	0.0495 (B)	0.0055 (B)
16A	0.0573					
17A	0.1113	0.1152	0.3027			
18A	0.0708	0.0241	0.0958			
19A	0.0470			0.0313	0.0317	0.0024
20A	0.0564	0.0268	0.0437	0.0587 (F)	0.0521 (F)	0.0055 (F)
				0.0434 (B)	0.0356 (B)	0.0047 (B)
21A	0.0544	0.0775	0.0613			
22A	0.0470	0.0633	0.0486	0.1980 (F)	0.1634 (F)	0.0334 (F)
				0.1556 (B)	0.1717 (B)	0.0304 (B)

Table 4.38: Maximum PEMAG at 0.01 radian rotation

Case	Column	DB	CJP1	CJP2	CJP3	CP
1A	0.0061					
2A	0.0051	0.0068	0.0119			
2A_f	0.0052	0.0054	0.0054	0.003704 (horizontal fillet weld)		
3A	0.0056	0.0059	0.0071			
3A_quar	0.0053	0.0055	0.0055			
3A_one	0.0043	0.0044	0.0093			
4A	0.0061			0.0034	0.0092	0.0007
5A	0.0055	0.0061	0.0070	0.0042 (F)	0.0120 (F)	0.0000 (F)
				0.0014 (B)	0.0094 (B)	0.0002 (B)
5A_quar	0.0053	0.0055	0.0055	0.0049 (F)	0.0119 (F)	0.0001 (F)
				0.0013 (B)	0.0088 (B)	0.0002 (B)
5A_one	0.0040	0.0041	0.0088	0.0034 (F)	0.0120 (F)	0.0004 (F)
				0.0009 (B)	0.0079 (B)	0.0002 (B)
6A	0.0049					
7A	0.0036	0.0058	0.0095			
8A	0.0038	0.0038	0.0036			
9A	0.0050			0.0032	0.0067	0.0004
10A	0.0038	0.0039	0.0036	0.0051 (F)	0.0139 (F)	0.0003 (F)
				0.0013 (B)	0.0077 (B)	0.0002 (B)
11A	0.0043					
12A	0.0053	0.0053	0.0118			
13A	0.0049	0.0023	0.0049			
13A_quar	0.0050	0.0019	0.0083			
13A_one	0.0057	0.0015	0.0164			
14A	0.0036			0.0039	0.0059	0.0002
15A	0.0038	0.0029	0.0033	0.0030 (F)	0.0156 (F)	0.0004 (F)
				0.0029 (B)	0.0080 (B)	0.0004 (B)
15A_quar	0.0044	0.0022	0.0038	0.0054 (F)	0.0164 (F)	0.0008 (F)
				0.0037 (B)	0.0085 (B)	0.0004 (B)
15A_one	0.0047	0.0017	0.0079	0.0093 (F)	0.0142 (F)	0.0010 (F)
				0.0043 (B)	0.0081 (B)	0.0004 (B)
16A	0.0066					
17A	0.0088	0.0050	0.0152			
18A	0.0071	0.0014	0.0098			
19A	0.0053			0.0029	0.0041	0.0000
20A	0.0057	0.0017	0.0042	0.0075 (F)	0.0104 (F)	0.0006 (F)
				0.0042 (B)	0.0054 (B)	0.0003 (B)
21A	0.0091	0.0071	0.0166			
22A	0.0038	0.0040	0.0049	0.0204 (F)	0.0273 (F)	0.0033 (F)
				0.0162 (B)	0.0206 (B)	0.0034 (B)

4.5 FORCE FLOW THROUGH CONTINUITY PLATE

The amount of force entering the CP's depends on the flange thickness of the column. In the cases considered, the column flange thickness was progressively decreased to ascertain the load path when CP's are critical elements in the system. The amount of force on one LP in each case has been tabulated in Table 4.2 - 4.32. The force entering each CP is derived using the section forces command as described in section 3.4. The force passing through the CP's is the summation of the forces passing through front (attached to DP) and back (attached to column web) CP's at a LP location. The percentage of force flow though CP for each case having CP's is listed in Table 4.39 – 4.51. The major observations from these data are as follows:

- As the column flange thickness decreases, the percentage of force flow through CP's increases which make CP'S a more critical element in columns with thin flanges. The thinner flanges have a higher tendency to bend and thus transfer higher forces to the CP's in order to resist bending. The percentage force flow is 30% in case 19A - 20A.
- The amount of force passing through front and back CP's is similar in cases where the CP is welded to the DP.
- The percentage of force flowing through CP's is similar when different DP thickness is used in the panel zone assembly (Case 5A, 5A_quar, 5A_one).See Table 4.43, 4.44 and 4.45.
- The percentage of force through CP's in each case decreases as the loading progresses from 0.01 radian to 0.05 radian but reverse is true for cases 19A, 20A (very thin flanges, t_f = 0.50 inches).

• The percentage of force flow is 25 % when the LP's are only on one side as compared to around 10 % when LP's are on both the sides (Case 5A, 22A). See Table 4.43 and Table 4.51.

Table 4.39: Force flow through continuity plate (Case 4A)

γ_p (radians)	Force on one LP (kips)	SOF3 through CP's (kips)	% of Force through CP's
0.01	669.38	80.90	12.09
-0.01	669.85	83.52	12.47
0.02	812.45	85.46	10.52
-0.02	813.41	93.58	11.50
0.03	871.79	79.52	9.12
-0.03	873.29	94.10	10.78
0.04	909.17	70.96	7.80
-0.04	910.04	92.86	10.20
0.05	934.35	62.96	6.74
-0.05	934.84	92.58	9.90

Table 4.40: Force flow through continuity plate (Case 9A)

γ_p (radians)	Force on one LP (kips)	SOF3 through CP (kips)	% of Force through CP's
0.01	549.74	101.84	18.53
-0.01	550.13	102.38	18.61
0.02	651.68	116.32	17.85
-0.02	653.54	117.94	18.05
0.03	698.38	117.90	16.88
-0.03	699.67	120.16	17.17
0.04	728.18	116.08	15.94
-0.04	728.95	119.44	16.39
0.05	748.53	114.54	15.30
-0.05	749.00	118.86	15.87

Table 4.41: Force flow through continuity plate (Case 14A)

γ_p (radians)	Force on one LP (kips)	SOF3 through CP's (kips)	% of Force through CP's
0.01	425.03	120.50	28.35
-0.01	425.57	119.84	28.16
0.02	528.00	155.84	29.52
-0.02	528.84	151.30	28.61
0.03	561.03	167.76	29.90
-0.03	561.33	159.88	28.48
0.04	581.29	173.96	29.93
-0.04	581.56	163.82	28.17
0.05	596.03	177.84	29.84
-0.05	596.09	166.14	27.87

Table 4.42: Force flow through continuity plate (Case 19A)

γ_p (radians)	Force on one LP (kips)	SOF3 through CP (kips)	% of Force through CP's
0.01	336.73	108.40	32.19
-0.01	337.50	109.62	32.48
0.02	434.10	142.80	32.90
-0.02	435.75	144.64	33.19
0.03	469.58	156.62	33.35
-0.03	472.26	157.36	33.32
0.04	492.82	166.00	33.68
-0.04	493.67	162.96	33.01
0.05	507.89	172.36	33.94
-0.05	508.34	165.96	32.65

Table 4.43: Force flow through continuity plate (Case 5A)

γ_p (radians)	Force on one LP (kips)	SOF3 through CP's (kips)	% of Force through CP's
0.01	790.16	95.39	12.07
-0.01	790.82	95.90	12.13
0.02	965.25	102.96	10.67
-0.02	966.33	108.96	11.28
0.03	1033.30	95.94	9.28
-0.03	1034.94	107.93	10.43
0.04	1075.85	87.32	8.12
-0.04	1076.66	105.43	9.79
0.05	1104.41	79.66	7.21
-0.05	1104.83	103.55	9.37

Table 4.44: Force flow through continuity plate (Case 5A_quarter)

γ_p (radians)	Force on one LP (kips)	SOF3 through CP's (kips)	% of Force through CP's
0.01	725.36	76.89	10.60
-0.01	721.17	76.49	10.61
0.02	880.81	82.94	9.42
-0.02	885.17	82.95	9.37
0.03	949.19	77.71	8.19
-0.03	942.00	80.62	8.56
0.04	978.61	72.18	7.38
-0.04	986.96	78.87	7.99
0.05	1007.30	62.74	6.23
-0.05	1016.84	78.41	7.71

Table 4.45: Force flow through continuity plate (Case 5A_one)

γ_p (radians)	Force on one LP (kips)	SOF3 through CP's (kips)	% of Force through CP's
0.01	891.48	117.45	13.17
-0.01	889.85	117.16	13.17
0.02	1101.71	136.20	12.36
-0.02	1104.96	140.11	12.68
0.03	1187.80	134.53	11.33
-0.03	1190.28	142.21	11.95
0.04	1239.76	127.32	10.27
-0.04	1241.08	139.47	11.24
0.05	1275.07	120.52	9.45
-0.05	1275.82	136.62	10.71

Table 4.46: Force flow through continuity plate (Case 10A)

γ_p (radians)	Force on one LP (kips)	SOF3 through CP's (kips)	% of Force through CP's
0.01	652.31	114.85	17.61
-0.01	652.90	112.56	17.24
0.02	789.36	137.84	17.46
-0.02	792.05	135.96	17.17
0.03	847.41	143.23	16.90
-0.03	849.04	141.48	16.66
0.04	883.01	142.82	16.17
-0.04	883.87	141.94	16.06
0.05	907.36	140.57	15.49
-0.05	907.73	140.95	15.53

Table 4.47: Force flow through continuity plate (Case 15A)

γ_p (radians)	Force on one LP (kips)	SOF3 through CP's (kips)	% of Force through CP's
0.01	498.45	129.41	25.96
-0.01	499.40	126.01	25.23
0.02	634.78	166.18	26.18
-0.02	636.76	161.05	25.29
0.03	687.49	181.60	26.41
-0.03	689.05	173.20	25.14
0.04	713.90	189.91	26.60
-0.04	713.99	178.97	25.07
0.05	732.22	196.06	26.78
-0.05	732.25	183.46	25.05

Table 4.48: Force flow through continuity plate (Case 15A_quarter)

γ_p (radians)	Force on one LP (kips)	SOF3 through CP's (kips)	% of Force through CP's
0.01	451.50	109.37	24.22
-0.01	450.59	104.81	23.26
0.02	575.71	142.43	24.74
-0.02	583.05	135.63	23.26
0.03	613.98	154.15	25.11
-0.03	615.51	142.86	23.21
0.04	641.07	162.70	25.38
-0.04	645.47	149.88	23.22
0.05	660.10	167.94	25.44
-0.05	659.81	153.72	23.30

Table 4.49: Force flow through continuity plate (Case 15A_one)

γ_p (radians)	Force on one LP (kips)	SOF3 through CP's (kips)	% of Force through CP's
0.01	558.90	140.02	25.05
-0.01	560.32	138.52	24.72
0.02	725.63	179.86	24.79
-0.02	728.51	179.39	24.62
0.03	800.39	198.43	24.79
-0.03	803.32	195.54	24.34
0.04	835.11	208.93	25.02
-0.04	835.50	202.15	24.20
0.05	858.24	217.04	25.29
-0.05	858.57	207.21	24.13

Table 4.50: Force flow through continuity plate (Case 20A)

γ_p (radians)	Force on one LP (kips)	SOF3 through CP's (kips)	% of Force through CP's
0.01	380.62	108.65	28.55
-0.01	380.65	108.71	28.56
0.02	486.95	139.55	28.66
-0.02	488.52	144.11	29.50
0.03	543.83	158.02	29.06
-0.03	545.73	164.90	30.22
0.04	575.36	170.35	29.61
-0.04	576.51	175.97	30.52
0.05	594.98	179.27	30.13
-0.05	595.70	182.35	30.61

Table 4.51: Force flow through continuity plate (Case 22A)

γ_p (radians)	Force on one LP (kips)	SOF3 through CP's (kips)	% of Force through CP's
0.01	1462.21	378.70	25.90
-0.01	1451.78	376.80	25.95
0.02	1847.89	468.70	25.36
-0.02	1842.10	466.60	25.33
0.03	1999.24	506.60	25.34
-0.03	1993.70	503.10	25.23
0.04	2099.53	529.70	25.23
-0.04	2094.53	525.50	25.09
0.05	2148.32	540.70	25.17
-0.05	2145.47	536.90	25.02

4.6 FREE BODY DIAGRAM OF A DOUBLER PLATE CUT AND CONTINUITY PLATE

The force on the LP's in the panel zone assembly is transferred to the DP, CP, column and the welds. The load can be transferred to web/DP by two paths: (1) LP -> Column flange -> Vertical CJP1 weld -> Column web/DP (2) LP -> Column flange -> CP -> Column web/DP. The free body diagram (FBD) of the DP and CP can be drawn to investigate the load path in different analysis cases. Figures 4.165 to 4.179 shows the FBD for case 3A, case 4A and case 5A while Figures 4.180 to 4.194 shows FBD of case 18A, case 19A and case 20A at approximately 0.01, 0.02 and 0.05 radian rotation of panel zone. The following observations can be made by comparing theses FBD's:

- The shear force at a cut 2 inches below the LP level remains similar in case 3A and case 5A at 0.01, 0.02 and 0.05 radian rotation. This essentially means that shear force in the DP doesn't change by the presence of the CP. At 0.05 radian in case 3A, the push force and pull force at the ends of the DP are 100.40 kips and 95.33 kips respectively leading to a shear of 195.70 kips at the cut whereas in case 5A, the push

and pull force at the ends of DP reduces to 60.78 and 50.79 respectively but the CP pushes the DP with a force of 84.53 kips leading to a shear of 196.00 kips at the cut. Similar conclusions can be drawn for case 18A and case 20A. These analysis cases suggest that the continuity plate, when welded to the doubler plate, does not significantly change the shear force in the doubler plate.

- The forces entering through the left end of the DP increases progressively as the loading increases from 0.01 radian to 0.05 radian in case 3A, case 5A and case 18A. But in case 20A, the force entering through the groove weld is negligible and all the force is flowing via the CP to the DP due to the very thin flanges (t_f = 0.50 inches) of the column.
- In case 5A,the shear force transmitted by the CP to the DP increases slightly from 0.01 radian to 0.02 radian but decreases again as loading reaches to 0.05 radian. While in case 20A, this transmitted force increases monotonically. This reconfirms the observation made in section 4.5 that the percentage of force passing through CP's decreases as the loading increases for the sections with thick flanges (case 5A) while this percentage increases with loading for the section with thin flanges (case 20A).
- In case 5A and case 20A, the CP's attached to the DP and the column web transmit comparable shear forces to the DP and the column web respectively. The slight difference in the transmitted force increases as the loading advances towards 0.05 radian. At 0.05 radian, around 15 - 20 kips more force is transferred via the CP to the web than via CP to DP in case 5A while opposite is true for case 20A.

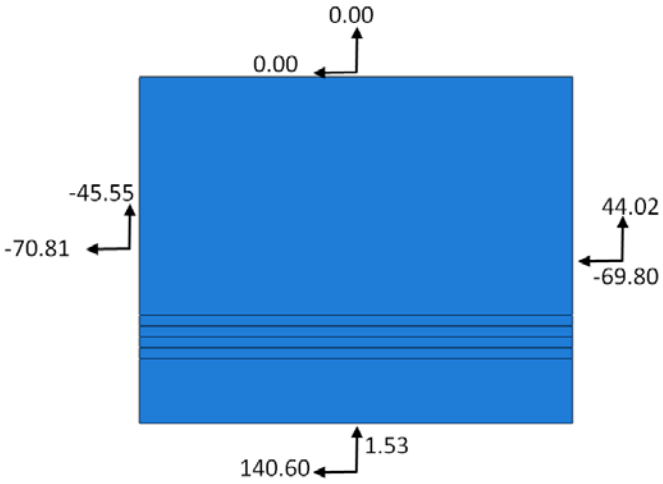

Figure 4.165: FBD of DP at 0.01 radian (case 3A)

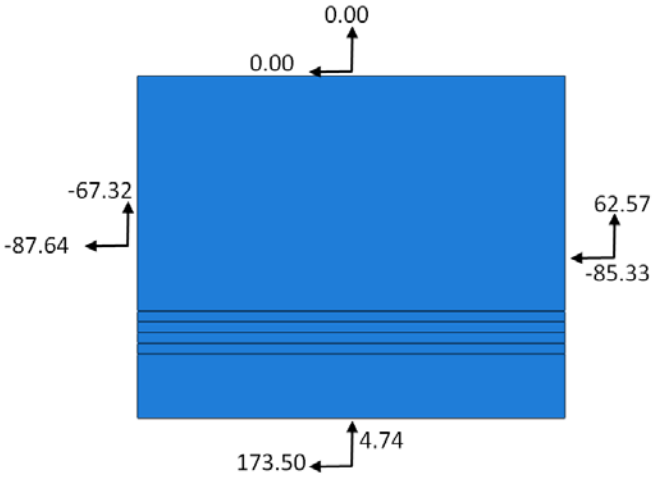

Figure 4.166: FBD of DP at 0.02 radian (case 3A)

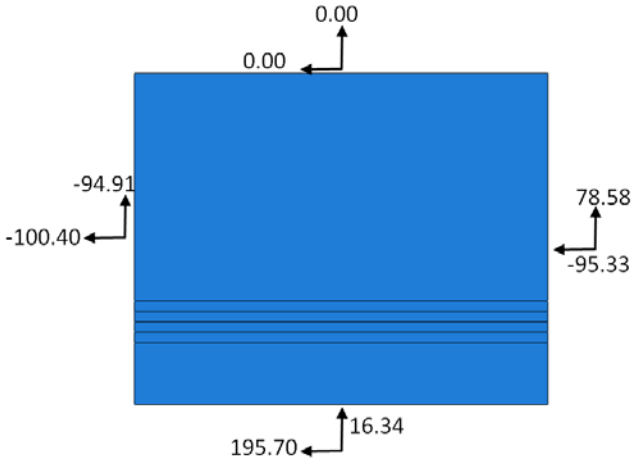

Figure 4.167: FBD of DP at 0.05 radian (case 3A)

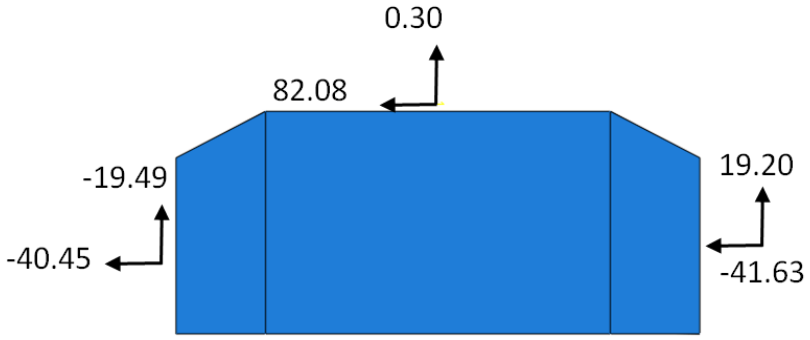

Figure 4.168: FBD of CP at 0.01 radian (case 4A)

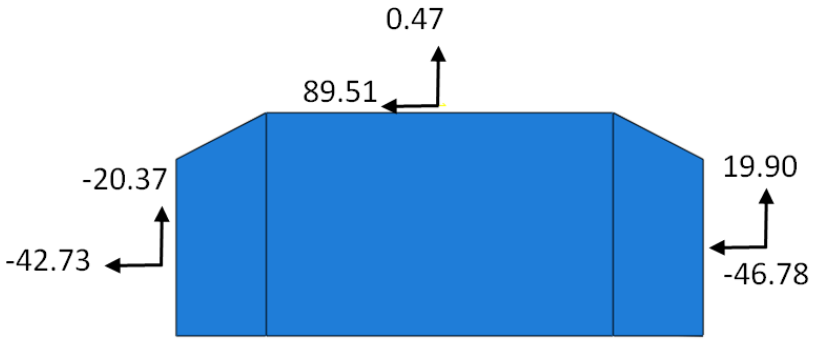

Figure 4.169: FBD of CP at 0.02 radian (case 4A)

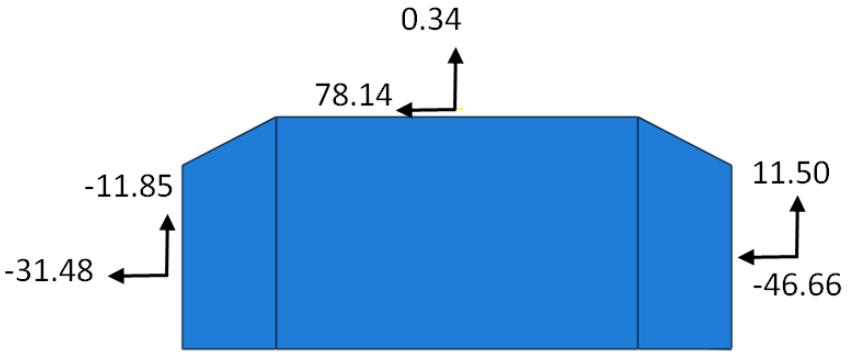

Figure 4.170: FBD of CP at 0.05 radian (case 4A)

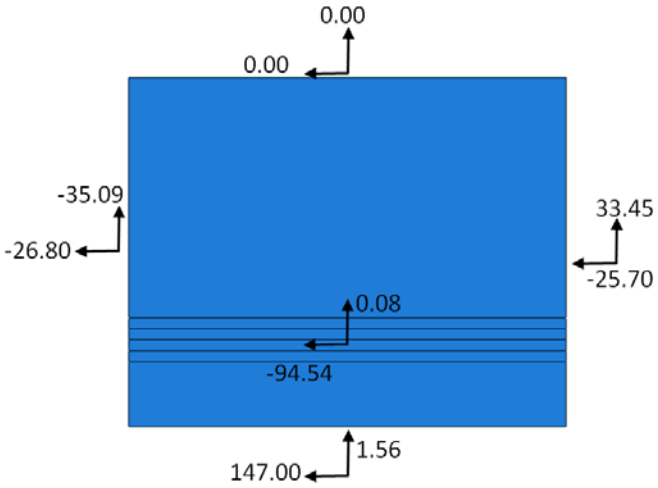

Figure 4.171: FBD of DP at 0.01 radian (case 5A)

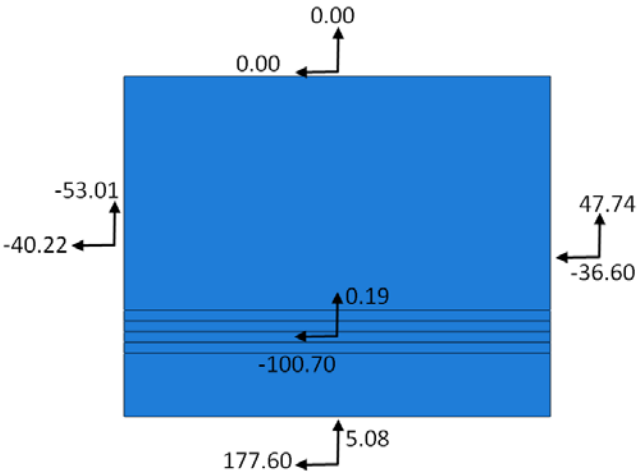

Figure 4.172: FBD of DP at 0.02 radian (case 5A)

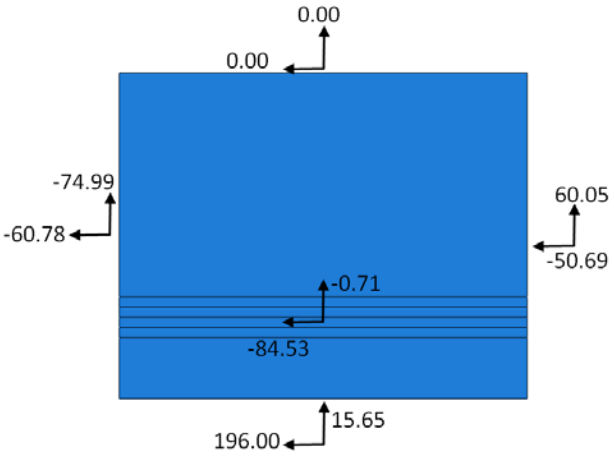

Figure 4.173: FBD of DP at 0.05 radian (case 5A)

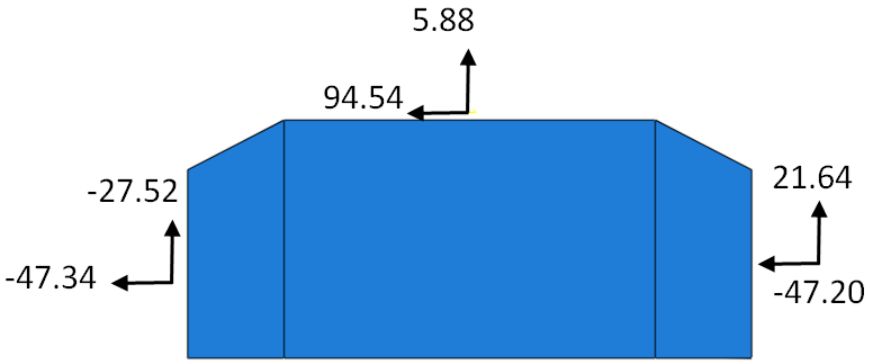

Figure 4.174: FBD of CP attached to DP at 0.01 radian (case 5A)

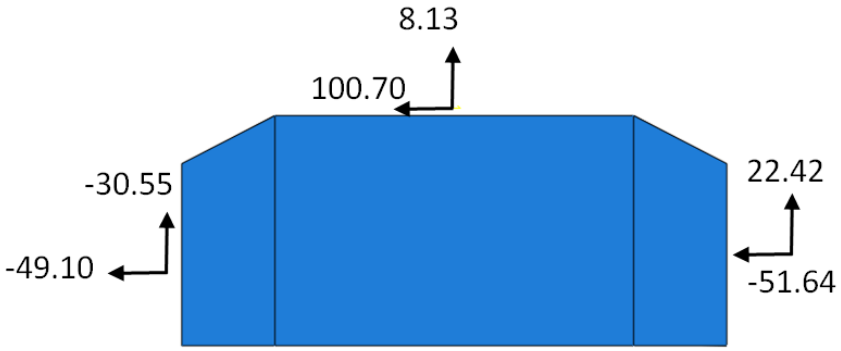

Figure 4.175: FBD of CP attached to DP at 0.02 radian (case 5A)

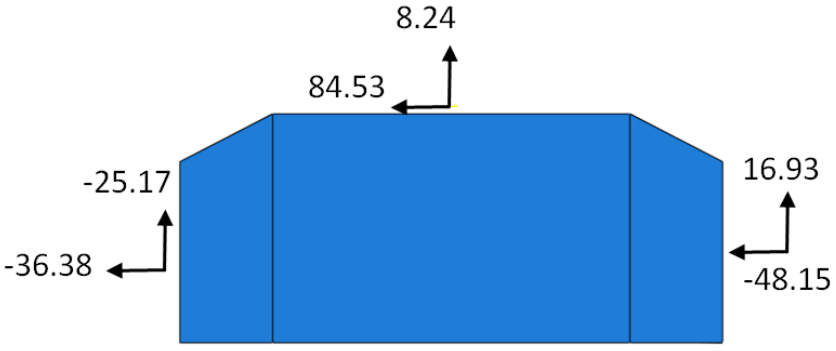

Figure 4.176: FBD of CP attached to DP at 0.05 radian (case 5A)

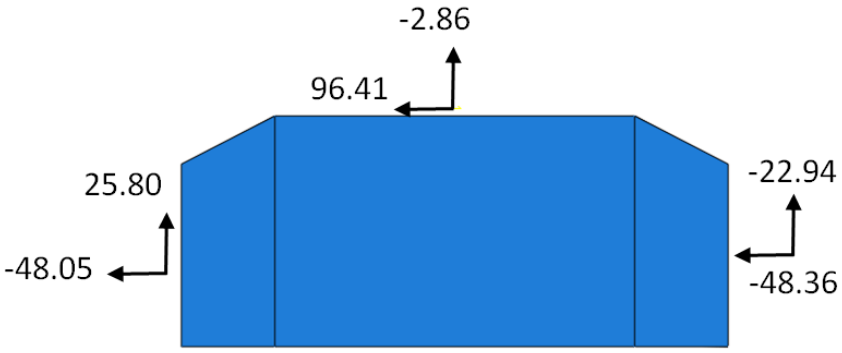

Figure 4.177: FBD of CP attached to column web at 0.01 radian (case 5A)

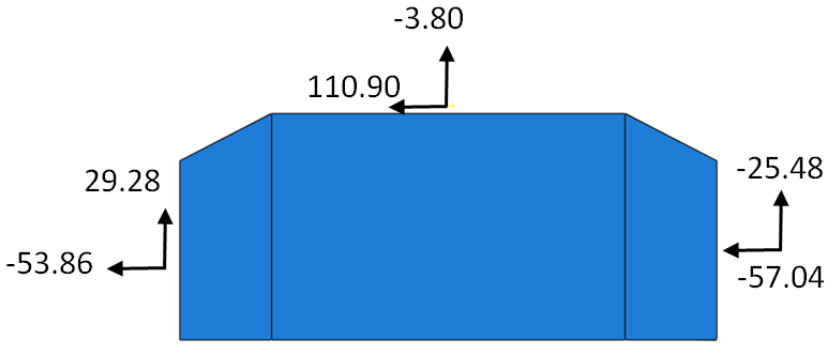

Figure 4.178: FBD of CP attached to column web at 0.02 radian (case 5A)

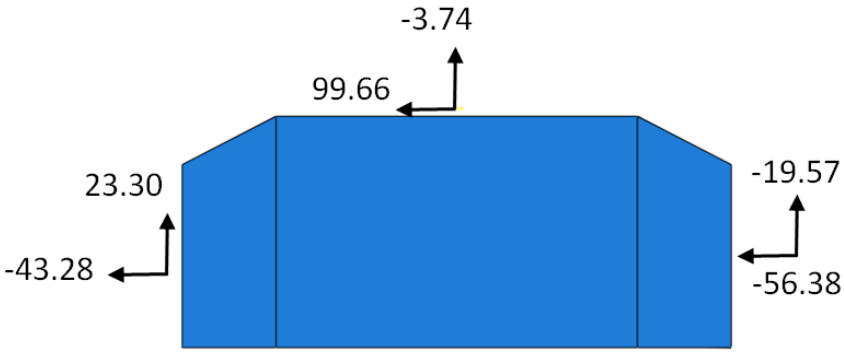

Figure 4.179: FBD of CP attached to column web at 0.05 radian (case 5A)

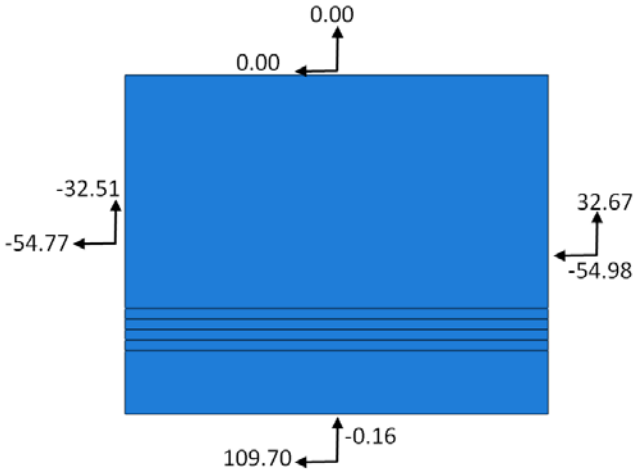

Figure 4.180: FBD of DP at 0.01 radian (case 18A)

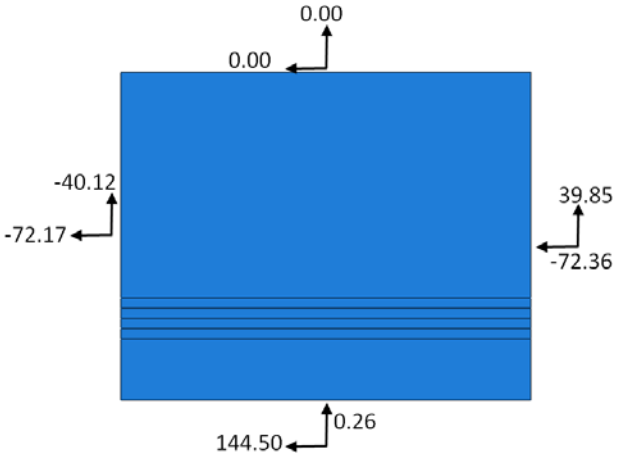

Figure 4.181: FBD of DP at 0.02 radian (case 18A)

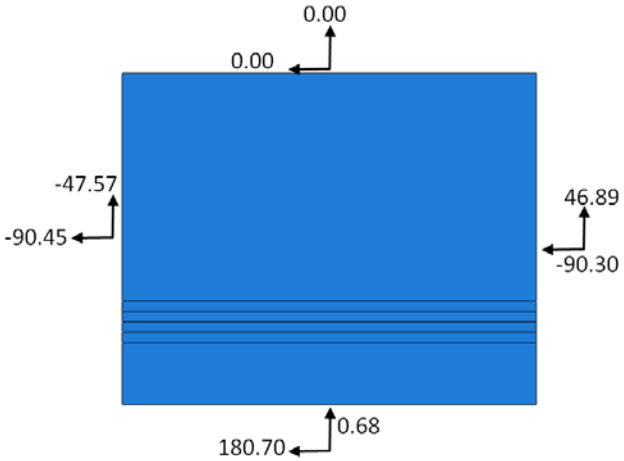

Figure 4.182: FBD of DP at 0.05 radian (case 18A)

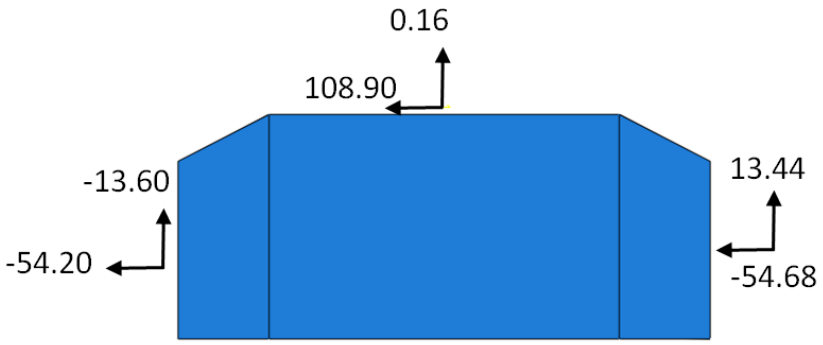

Figure 4.183: FBD of CP at 0.01 radian (case 19A)

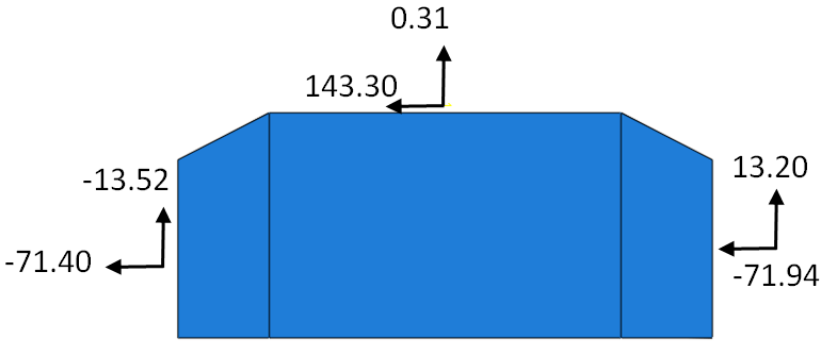

Figure 4.184: FBD of CP at 0.02 radian (case 19A)

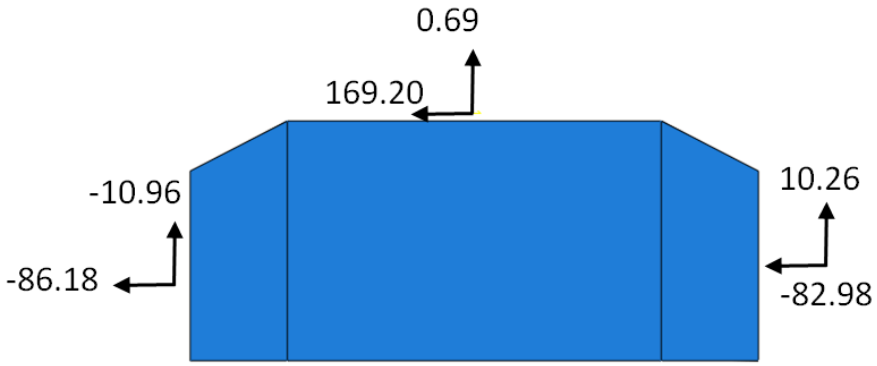

Figure 4.185: FBD of CP at 0.05 radian (case 19A)

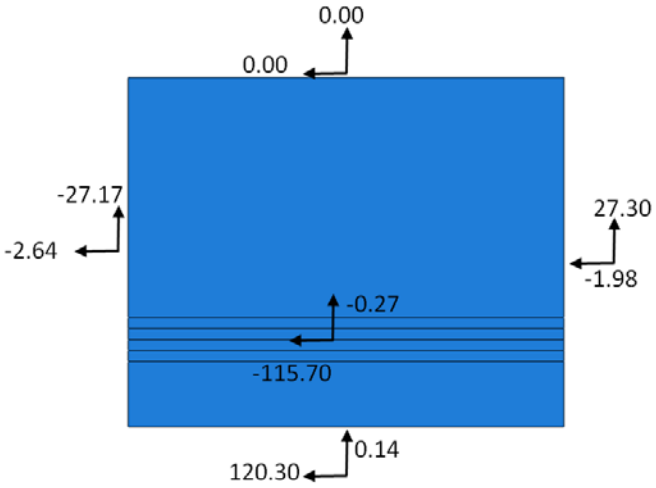

Figure 4.186: FBD of DP at 0.01 radian (case 20A)

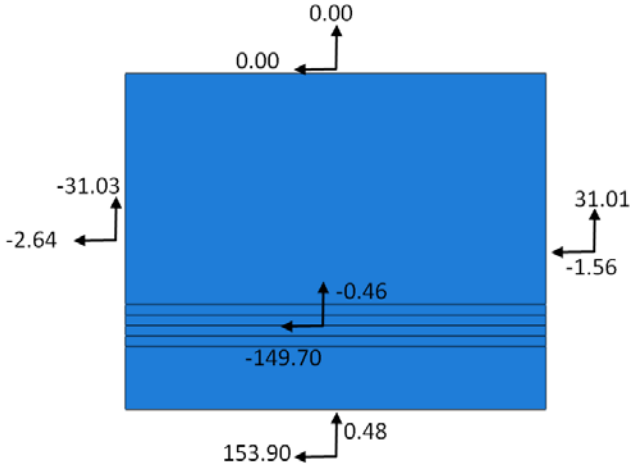

Figure 4.187: FBD of DP at 0.02 radian (case 20A)

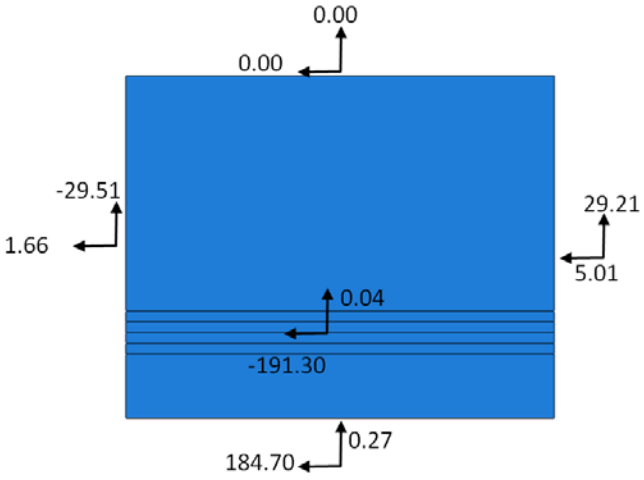

Figure 4.188: FBD of DP at 0.05 radian (case 20A)

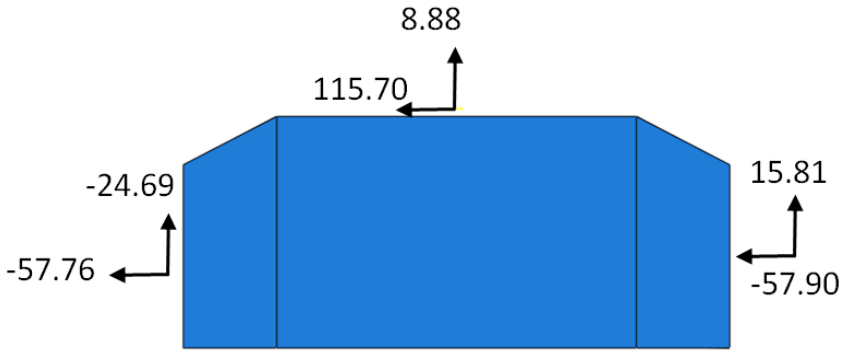

Figure 4.189: FBD of CP attached to DP at 0.01 radian (case 20A)

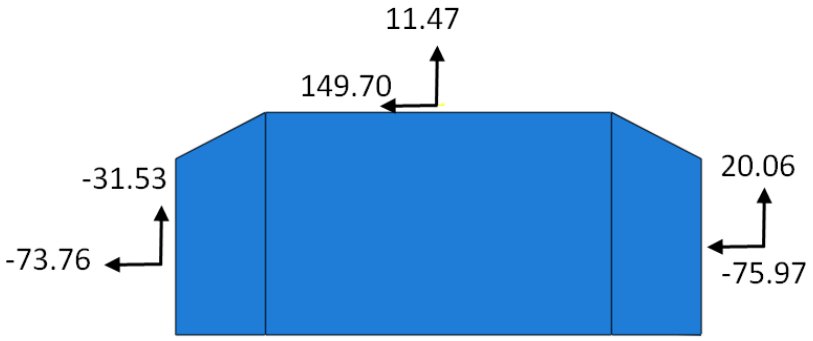

Figure 4.190: FBD of CP attached to DP at 0.02 radian (case 20A)

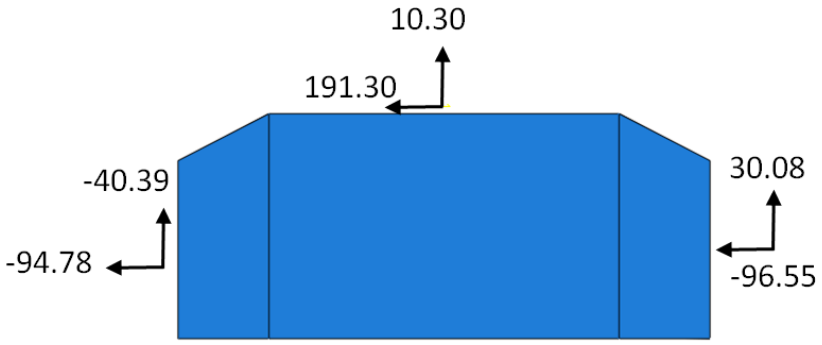

Figure 4.191: FBD of CP attached to DP at 0.05 radian (case 20A)

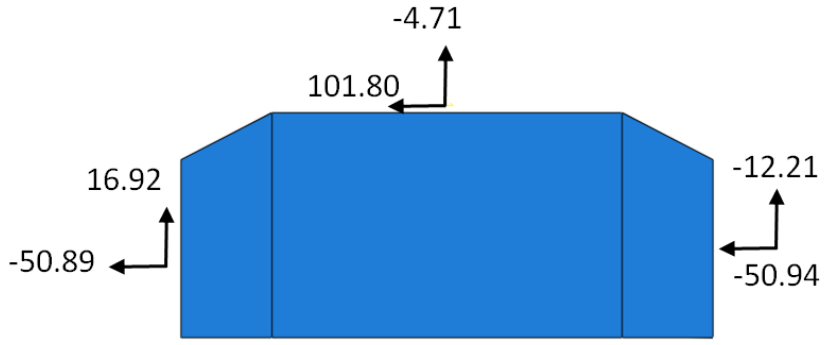

Figure 4.192: FBD of CP attached to column web at 0.01 radian (case 20A)

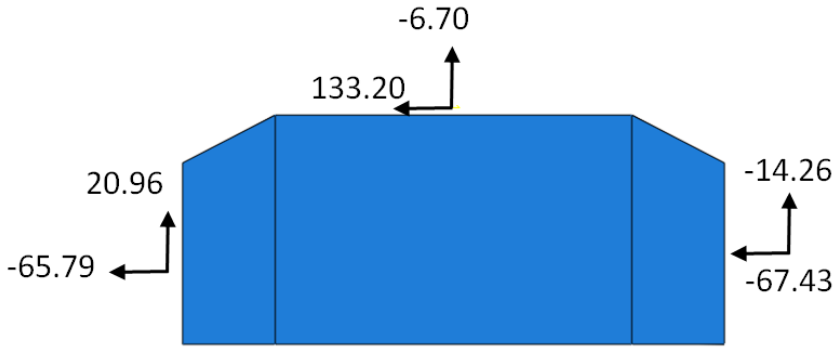

Figure 4.193: FBD of CP attached to column web at 0.02 radian (case 20A)

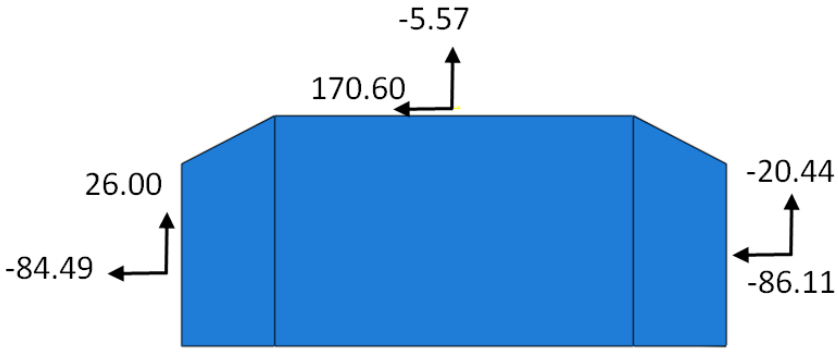

Figure 4.194: FBD of CP attached to column web at 0.05 radian (case 20A)

4.7 SUMMARY AND DISCUSSIONS

All of the simulations performed on the shallow column (W14X398) were able to reach the nominal shear strength of the panel zone. The yielding in the column web/DP started at the middle depth and spread towards the top and bottom as the loading progresses to 0.05 radian rotation. The stresses at the middle depth of the DP are predominantly horizontal shear stress (S23) while stresses at the LP level are a combination of horizontal shear stress (S23) and horizontal normal stress (S33). The stresses in the vertical CJP1 weld at the DP-CJP1 weld interface are predominantly vertical shear (S23) at the middle region of the weld and horizontal normal stress (S33) at the LP level. Thus the vertical weld should be designed to develop both the shear strength and tensile strength of the DP. The VMS in different parts of the panel zone may be similar at 0.05 radian rotation but the strain parameters like PEEQ and PEMAG may be slightly different. This is due to the fact that the change in strain is large with small changes in stress near the ultimate stress point in the material model. The major conclusions from section 4.3, 4.4, 4.5 and 4.6 shows that there is no increase in the shear strength by extending the DP and it is safe to weld the CP to the DP. The CP's are critical elements in the column sections having thinner flanges.

CHAPTER 5

Parametric Studies on Attachment Details of Doubler Plates in a W40x264 Column

5.1 INTRODUCTION

This chapter presents the results of the simulations performed on the deep column (W40X264). A series of analysis cases were run to evaluate various methods for attaching the doubler plate to the column web. The results were intended to investigate the same issues described in chapter 4 for the W14x398 column.

Analysis cases 1B to case 10B have LP's on both sides of the column. The main variable parameters in this study were: (a) Colum flange thickness (t_f) – 1.75 and 0.75 inches (b) Doubler plate extension of 6 inches (c) Inclusion of CP's.

5.2 ANALYSIS CASES

All the analysis cases are tabulated in Table 5.1.

Table 5.1: Analysis cases for the W40X264 column

Case	t_f (inches)	t_{dp} (inches)	l_{dp} (inches)	b_{dp} (inches)	CP
1B	1.75	-	-	-	No
2B		1.00	24	34	No
2B _f [2]		1.00	24	34	No
3B		1.00	36	34	No
4B		-	-	-	Yes
5B		1.00	36	34	Yes
6B	0.75	-	-	-	No
7B		1.00	24	34	No
8B		1.00	36	34	No
9B		-	-	-	Yes
10B		1.00	36	34	Yes

Note:

5. All cases with DP have vertical CJP1 groove welds.
6. Case 2B_f has both horizontal fillet welds and vertical CJP1 groove welds.
7. The distance between LP's is 24 inches in all cases.

5.2.1 Analysis case 1B

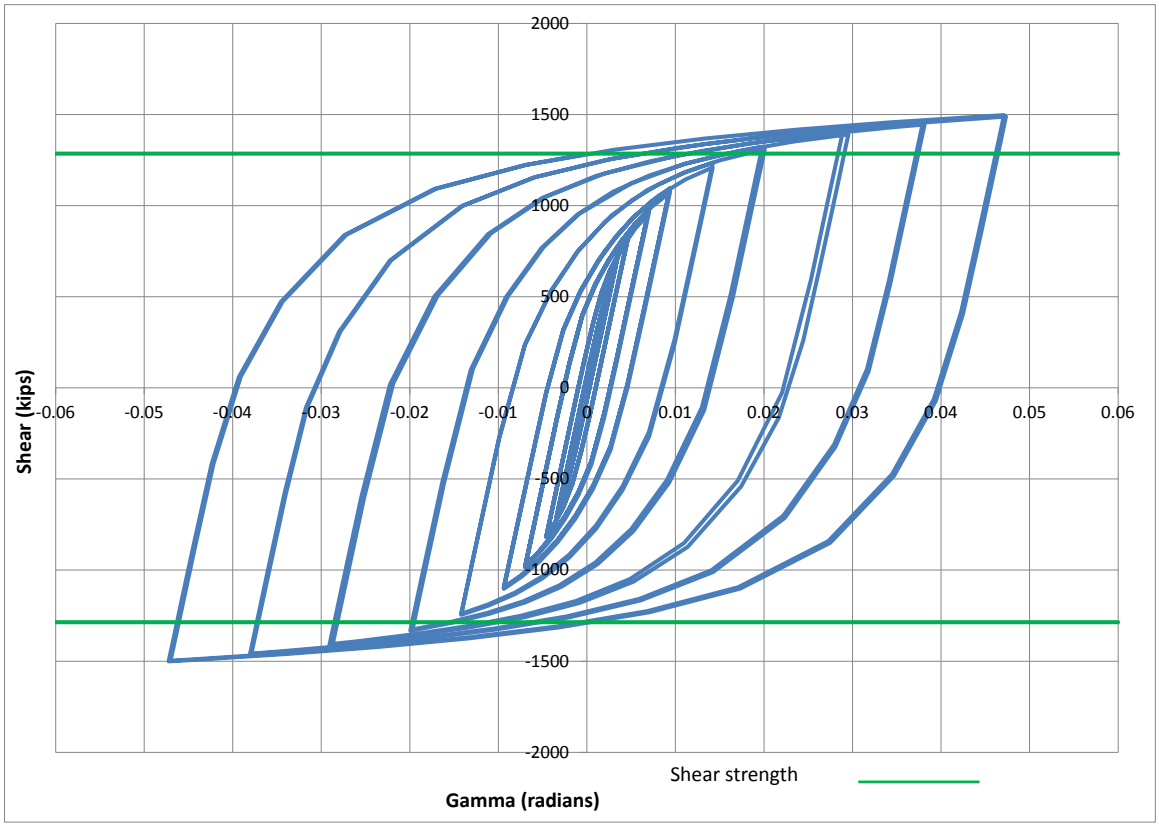

Figure 5.1: Panel zone shear versus rotation (Case 1B)

Table 5.2: Panel zone shear and force on loading plate (Case 1B)

Panel zone rotation (rad)	0.01	0.02	0.03	0.05
Panel zone shear (kips)	1094.83	1323.29	1403.23	1496.66
Force on one Loading plate (kips)	656.90	793.97	841.94	898.00

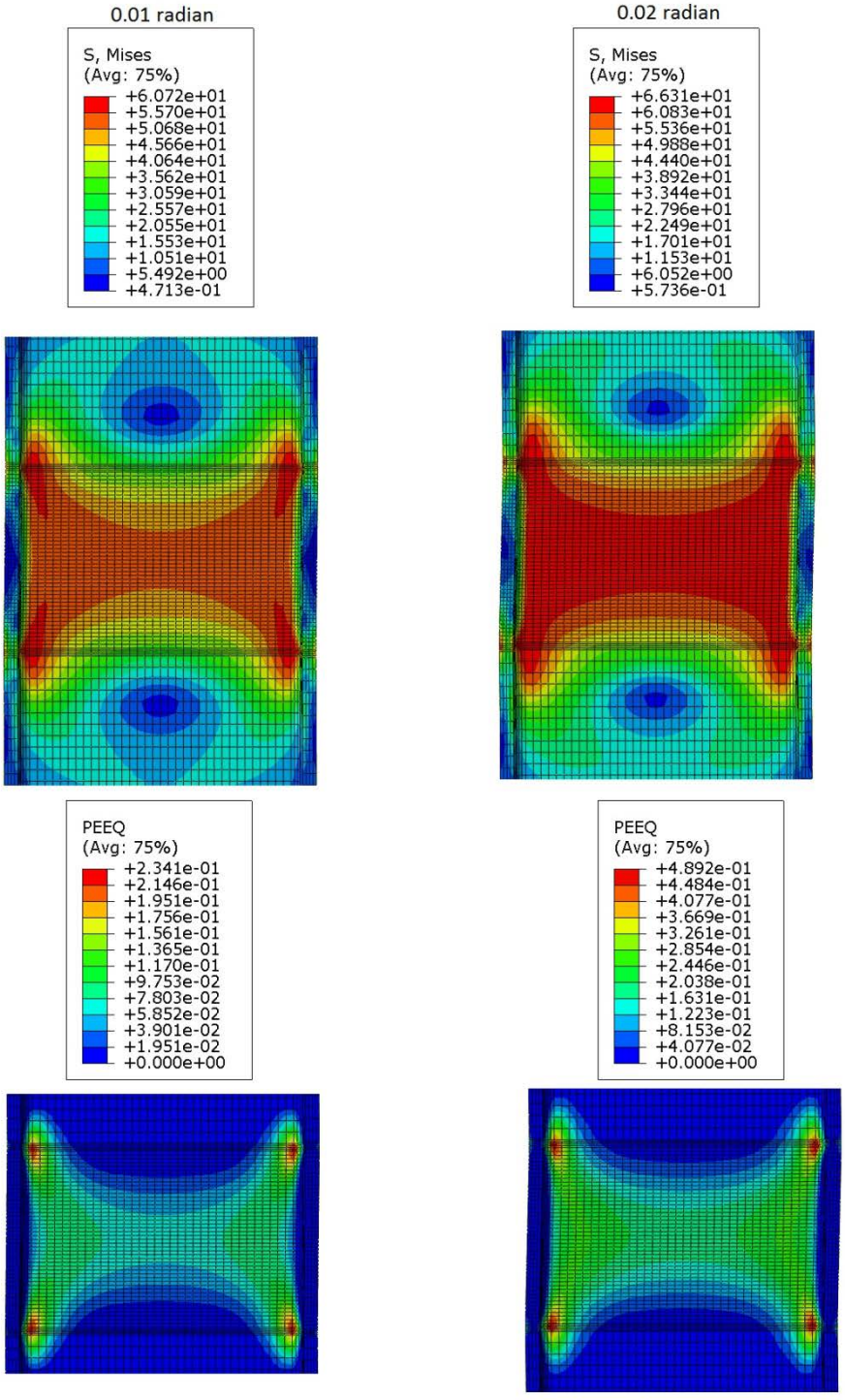

Figure 5.2: VMS and PEEQ in the column (Case 1B)

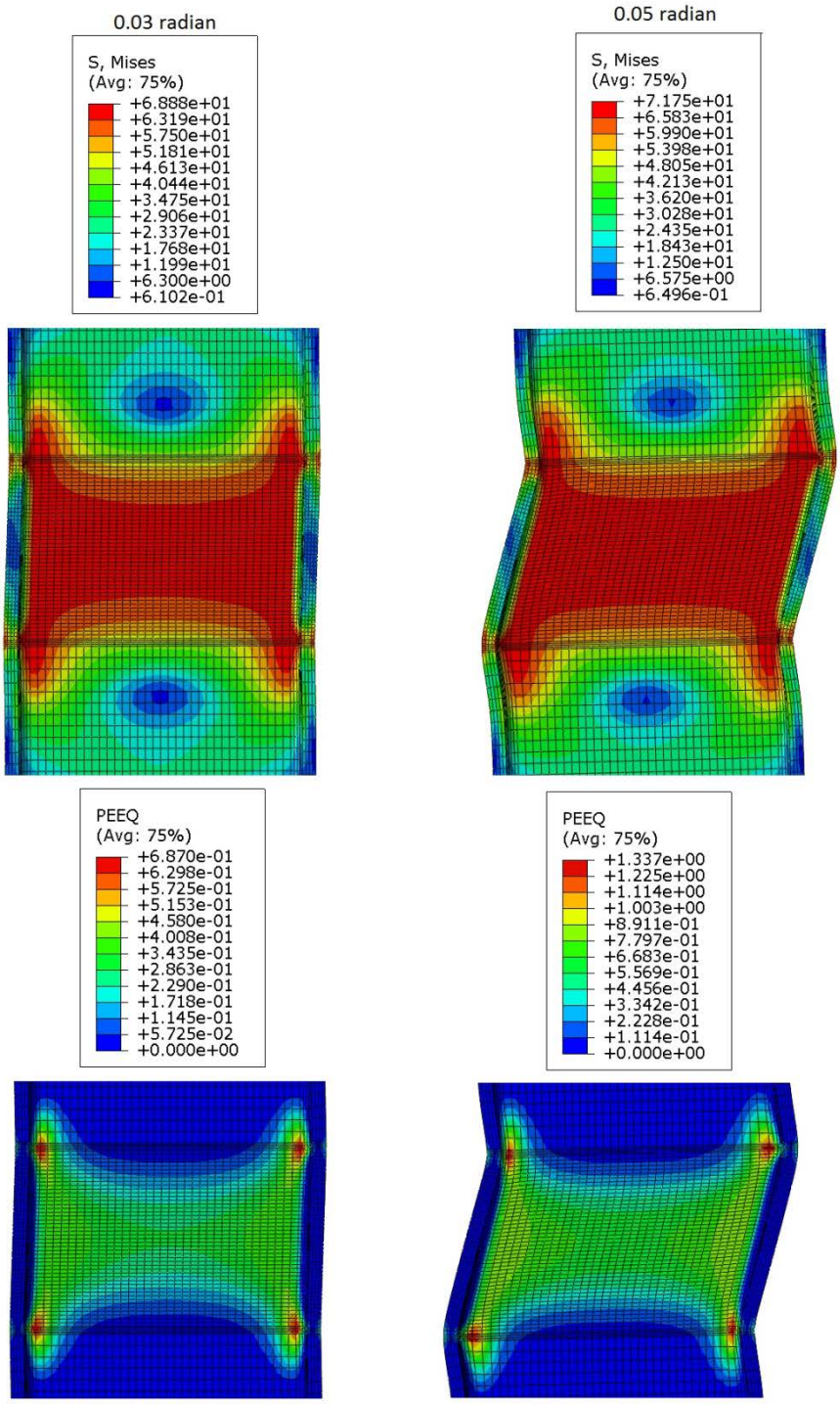

Figure 5.3: VMS and PEEQ in the column (Case 1B)

5.2.2 Analysis case 2B

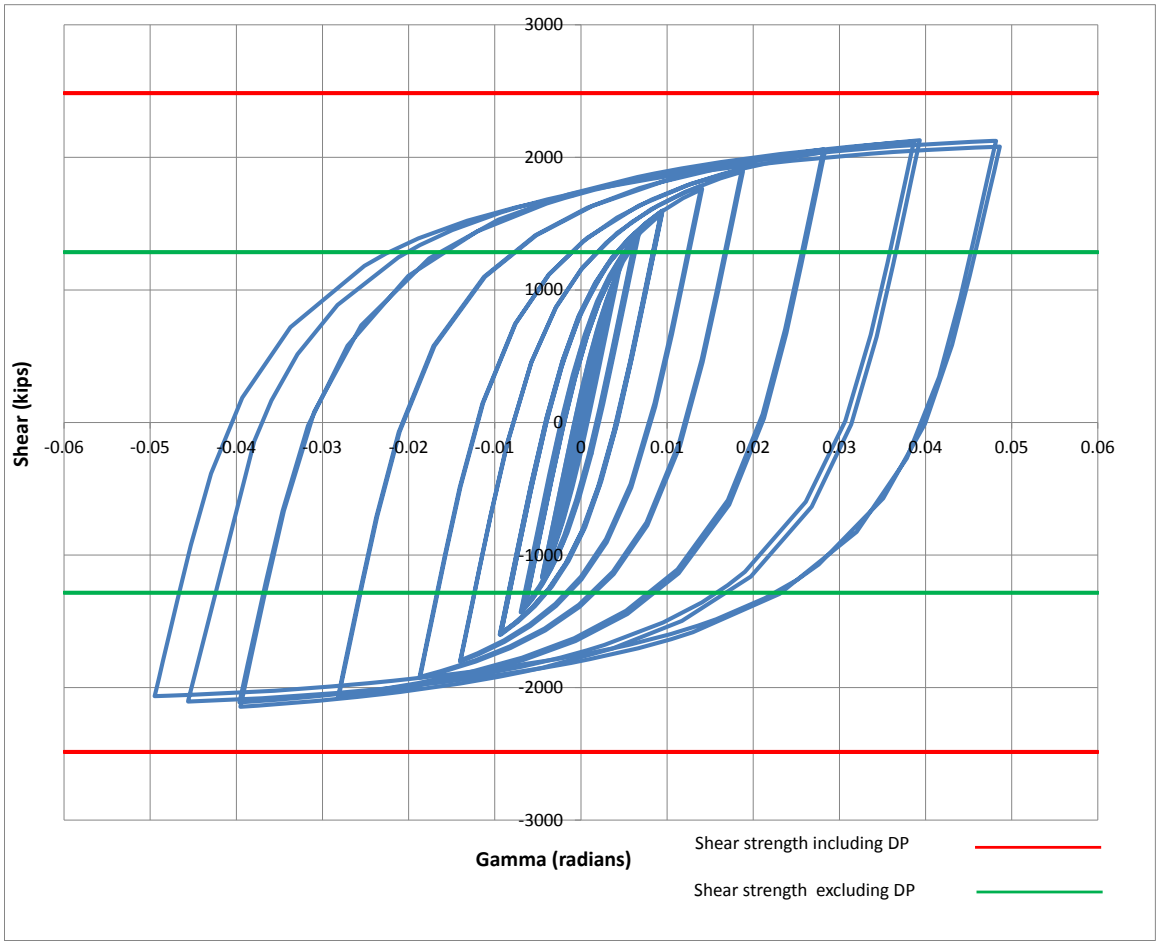

Figure 5.4: Panel zone shear versus rotation (Case 2B)

Table 5.3: Panel zone shear and force on loading plate (Case 2B)

Panel zone rotation (rad)	0.01	0.02	0.03	0.05
Panel zone shear (kips)	1592.76	1914.74	2060.26	2080.86
Force on one Loading plate (kips)	955.65	1148.84	1236.15	1248.52

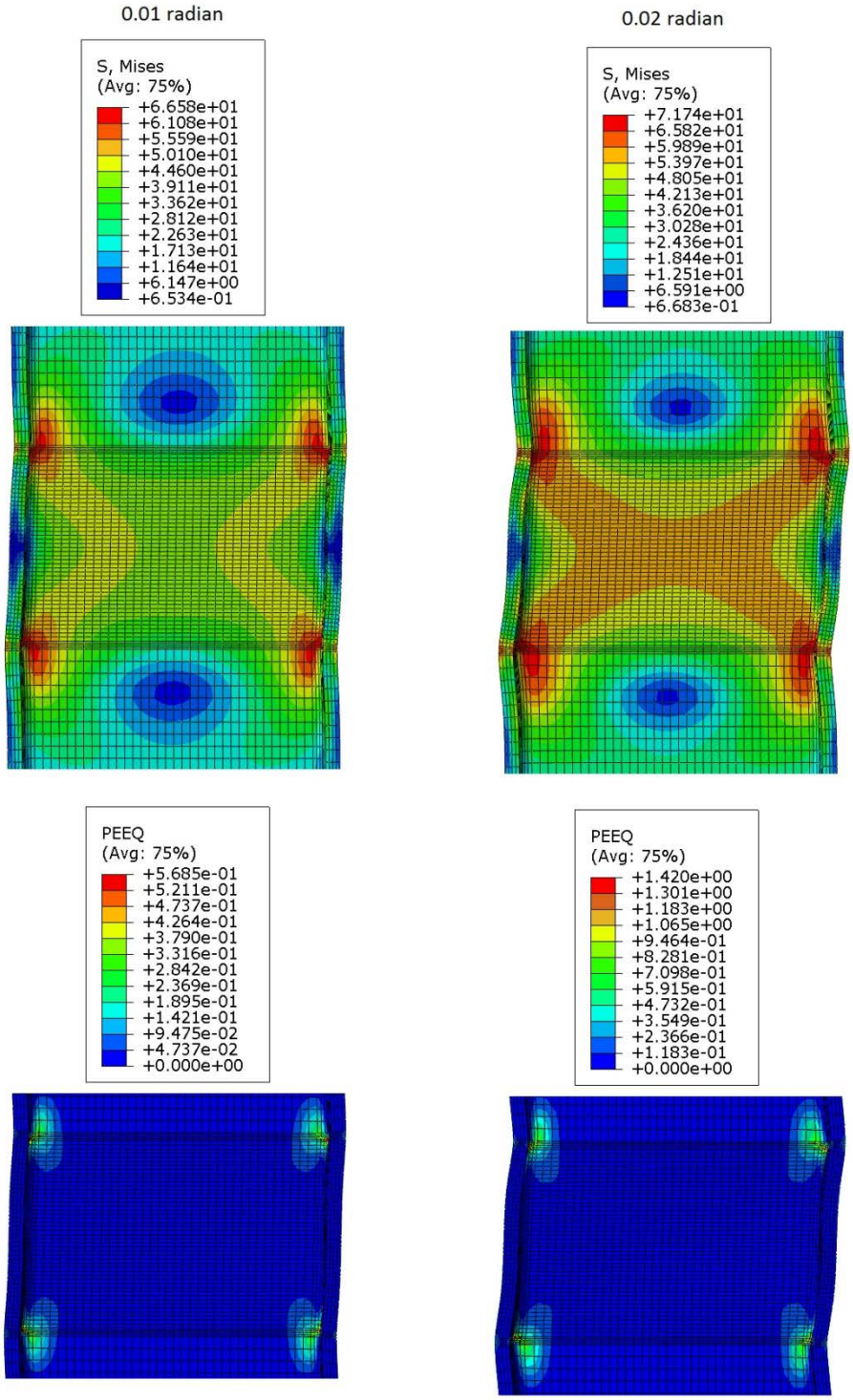

Figure 5.5: VMS and PEEQ in the column (Case 2B)

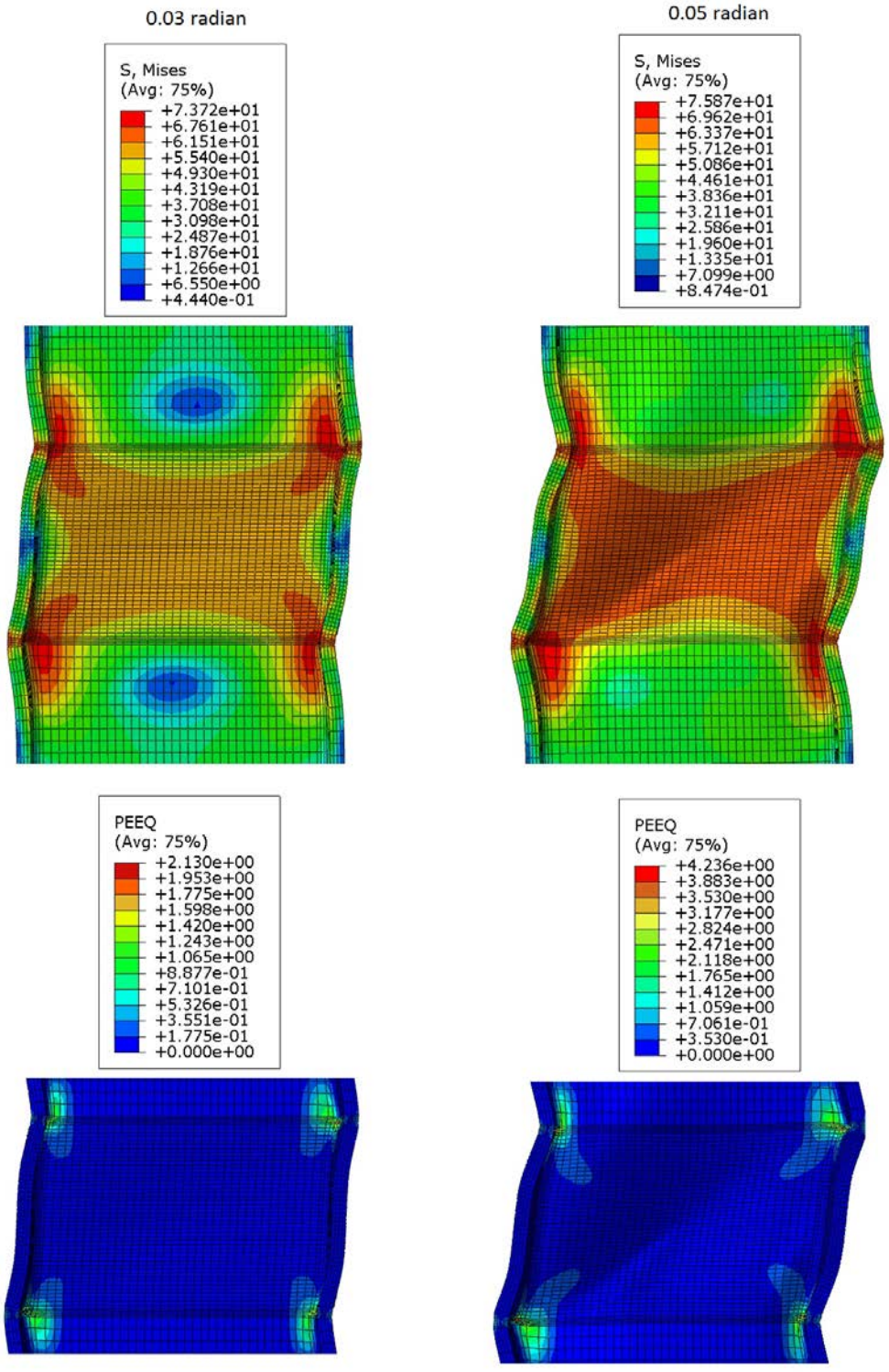

Figure 5.6: VMS and PEEQ in the column (Case 2B)

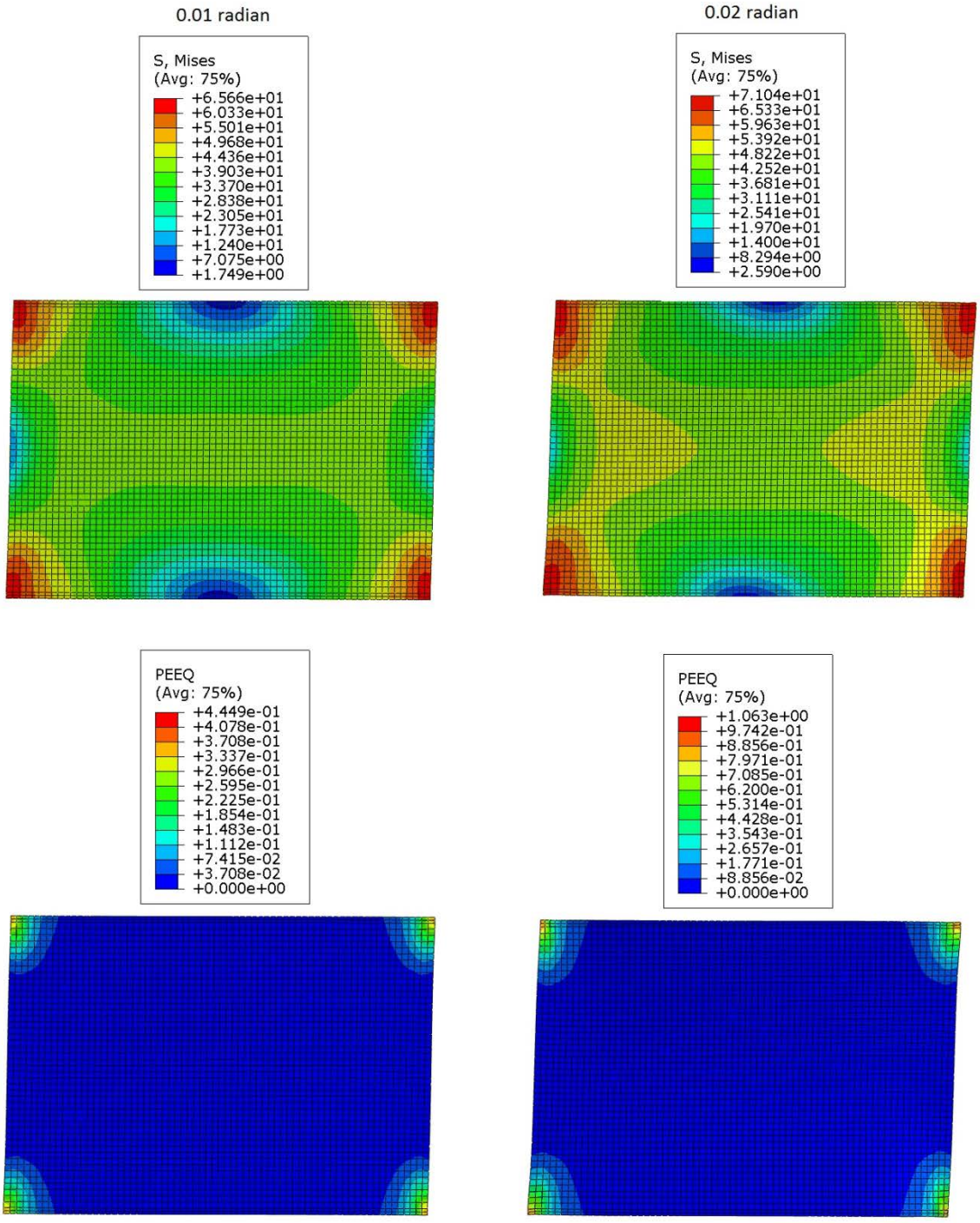

Figure 5.7: VMS and PEEQ in the DP (Case 2B)

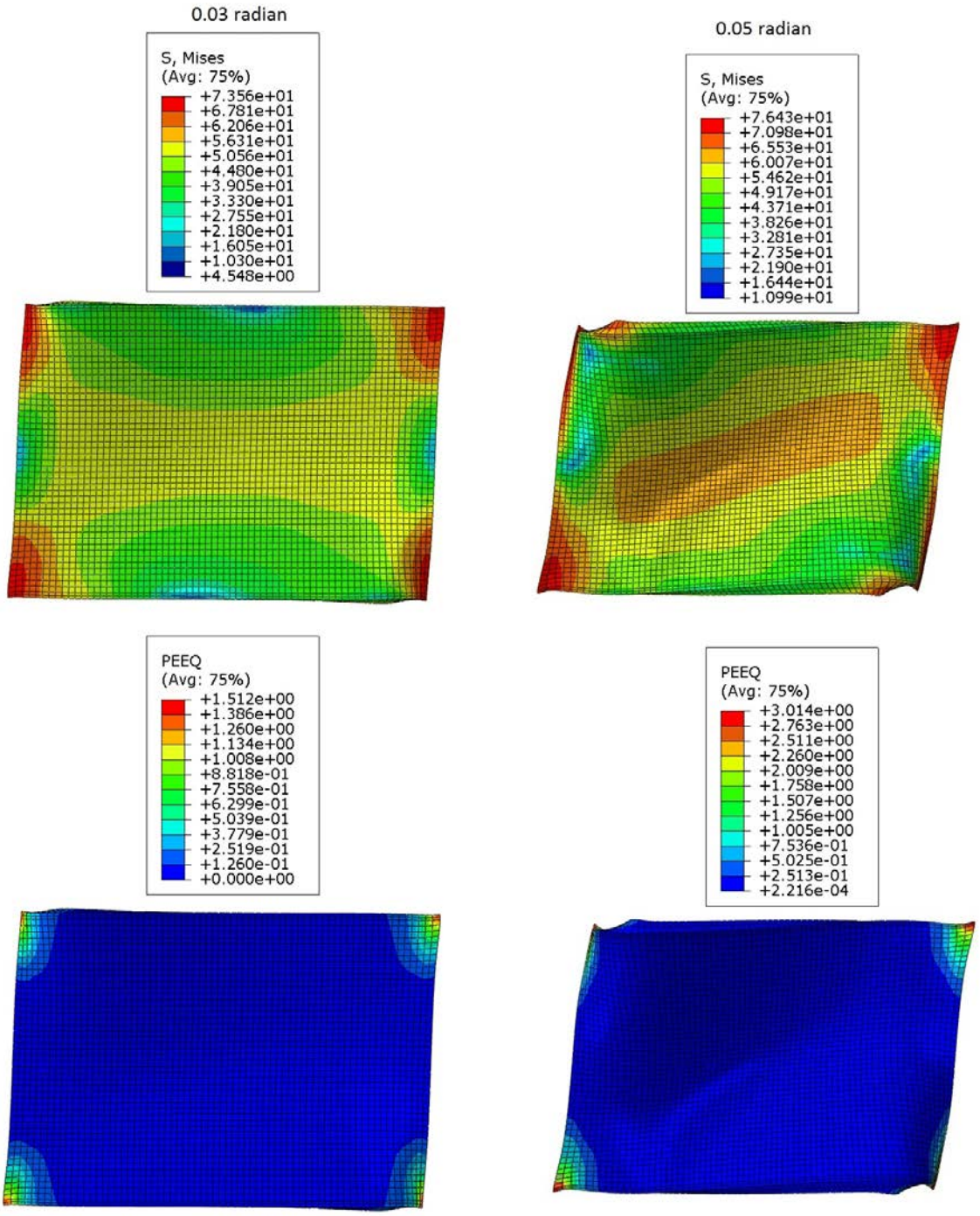

Figure 5.8: VMS and PEEQ in the DP (Case 2B)

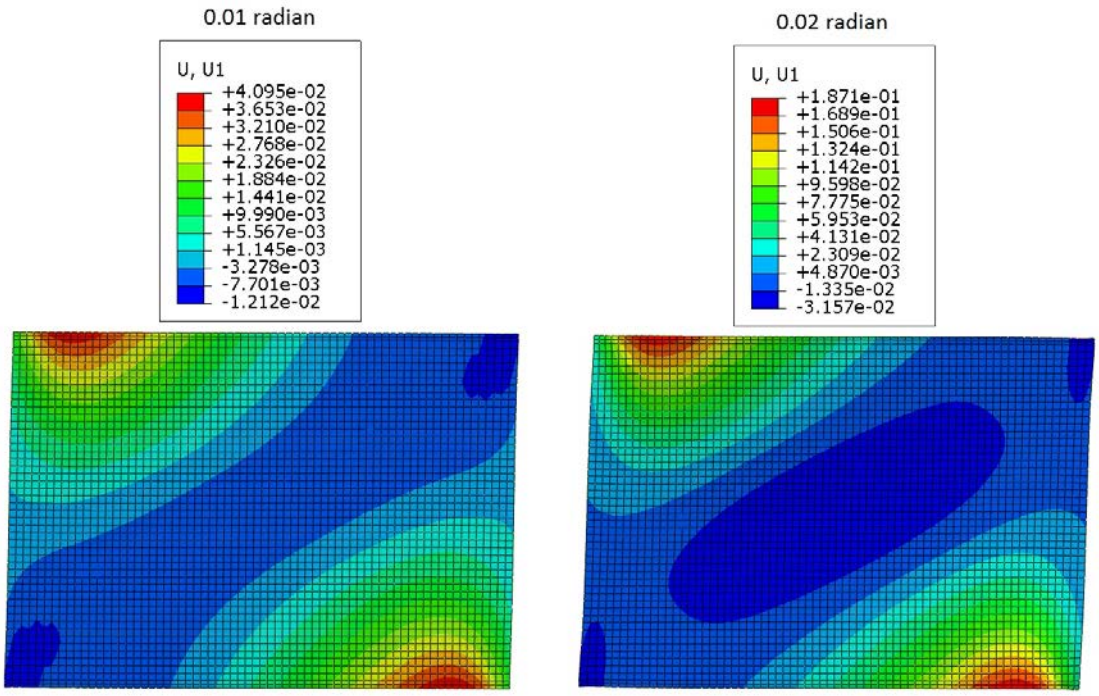

Figure 5.9: U1 displacement in the DP (Case 2B)

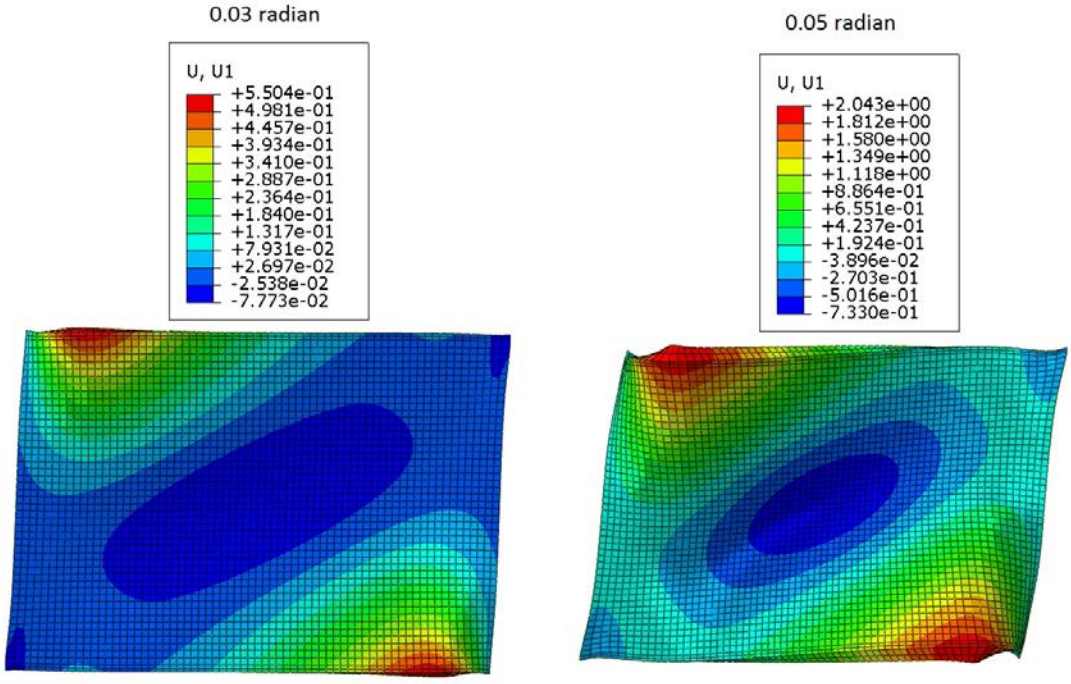

Figure 5.10: U1 displacement in the DP (Case 2B)

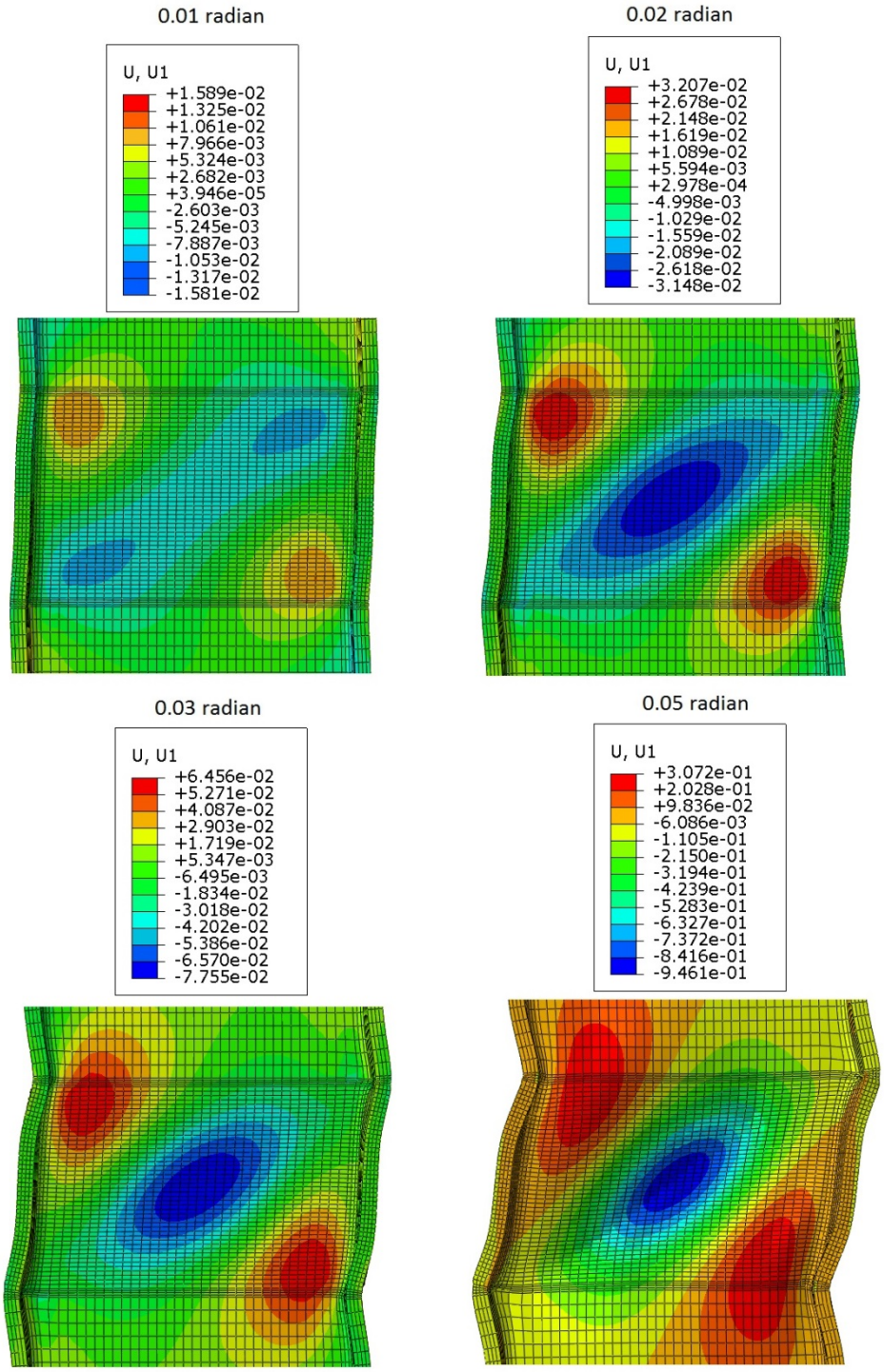

Figure 5.11: U1 displacement in the column (Case 2B)

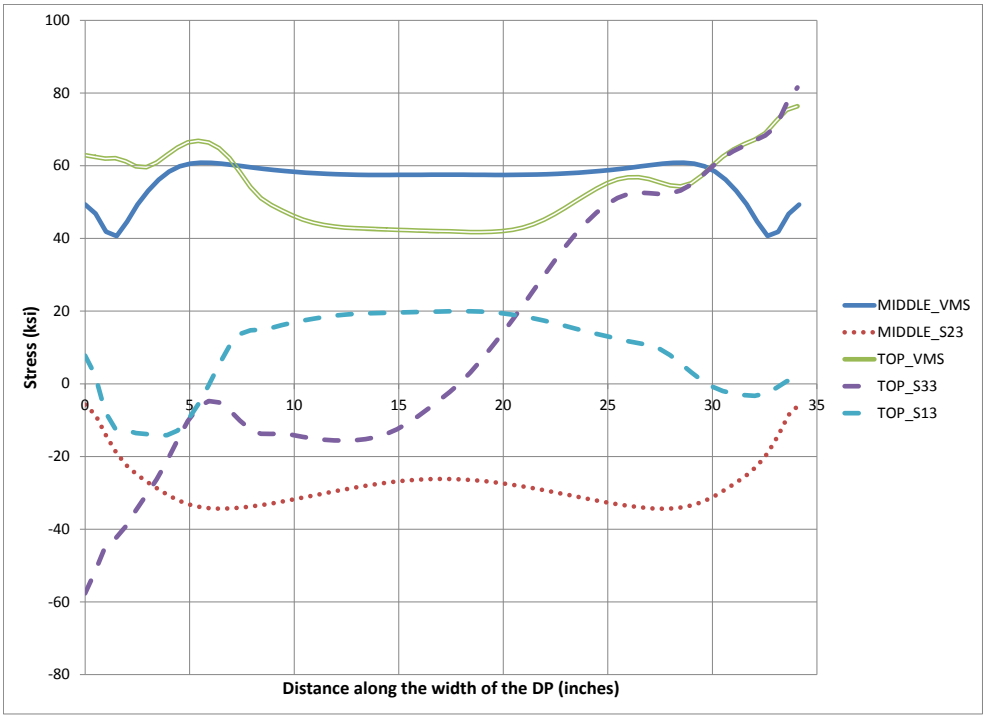

Figure 5.12: Stresses along the width of DP at 0.05 radian rotation (Case 2B)

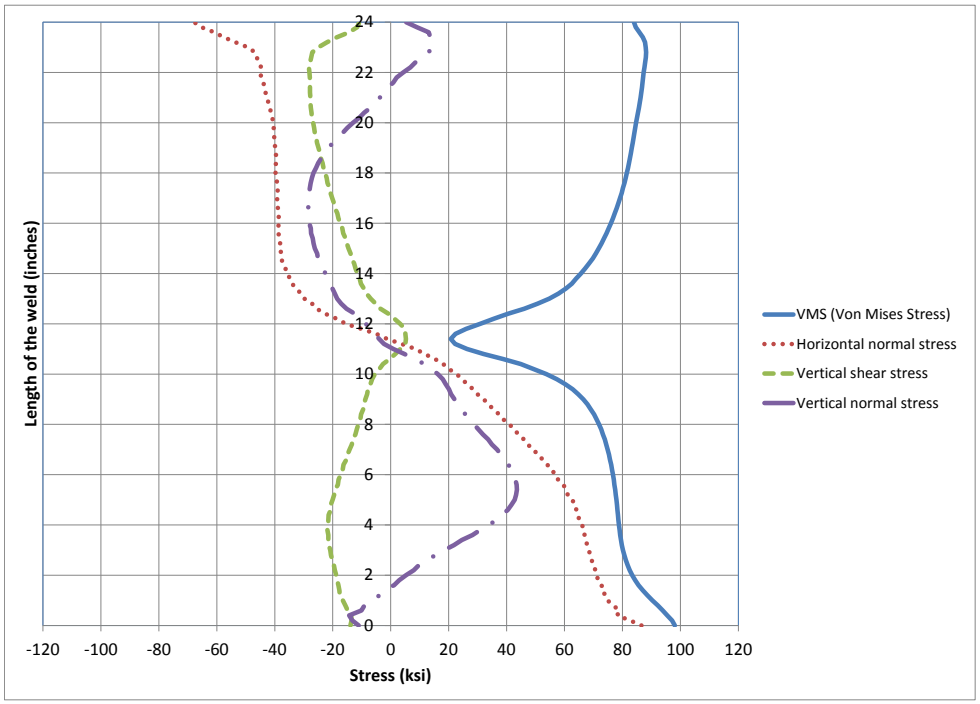

Figure 5.13: Stresses along depth of CJP1 (DP-CJP1 interface) at 0.05 radian (Case 2B)

5.2.3 Analysis case 2B_f

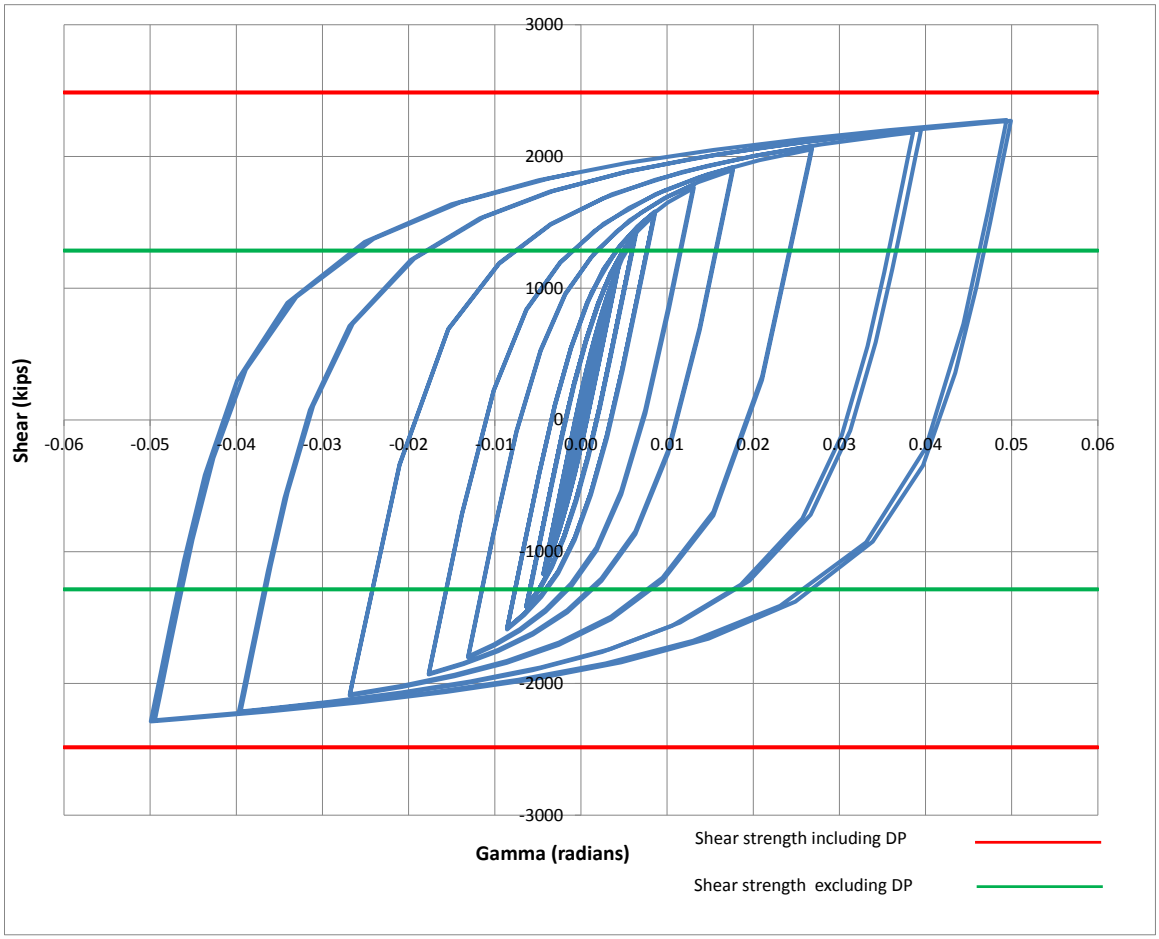

Figure 5.14: Panel zone shear versus rotation (Case 2B_f)

Table 5.4: Panel zone shear and force on loading plate (Case 2B_f)

Panel zone rotation (rad)	0.01	0.02	0.03	0.05
Panel zone shear (kips)	1581.02	1919.83	2079.67	2277.29
Force on one Loading plate (kips)	948.61	1151.90	1247.80	1366.37

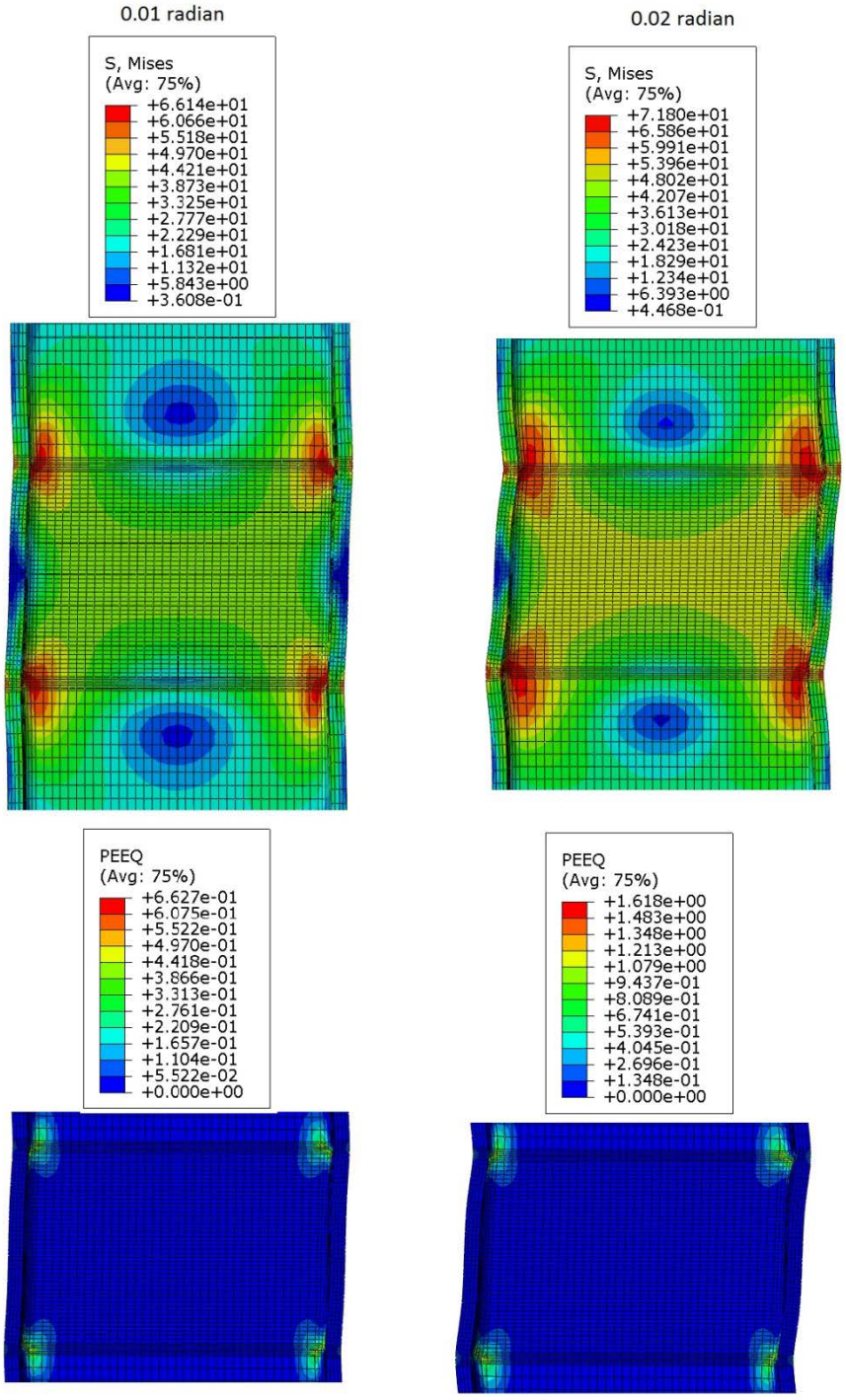

Figure 5.15: VMS and PEEQ in the column (Case 2B_f)

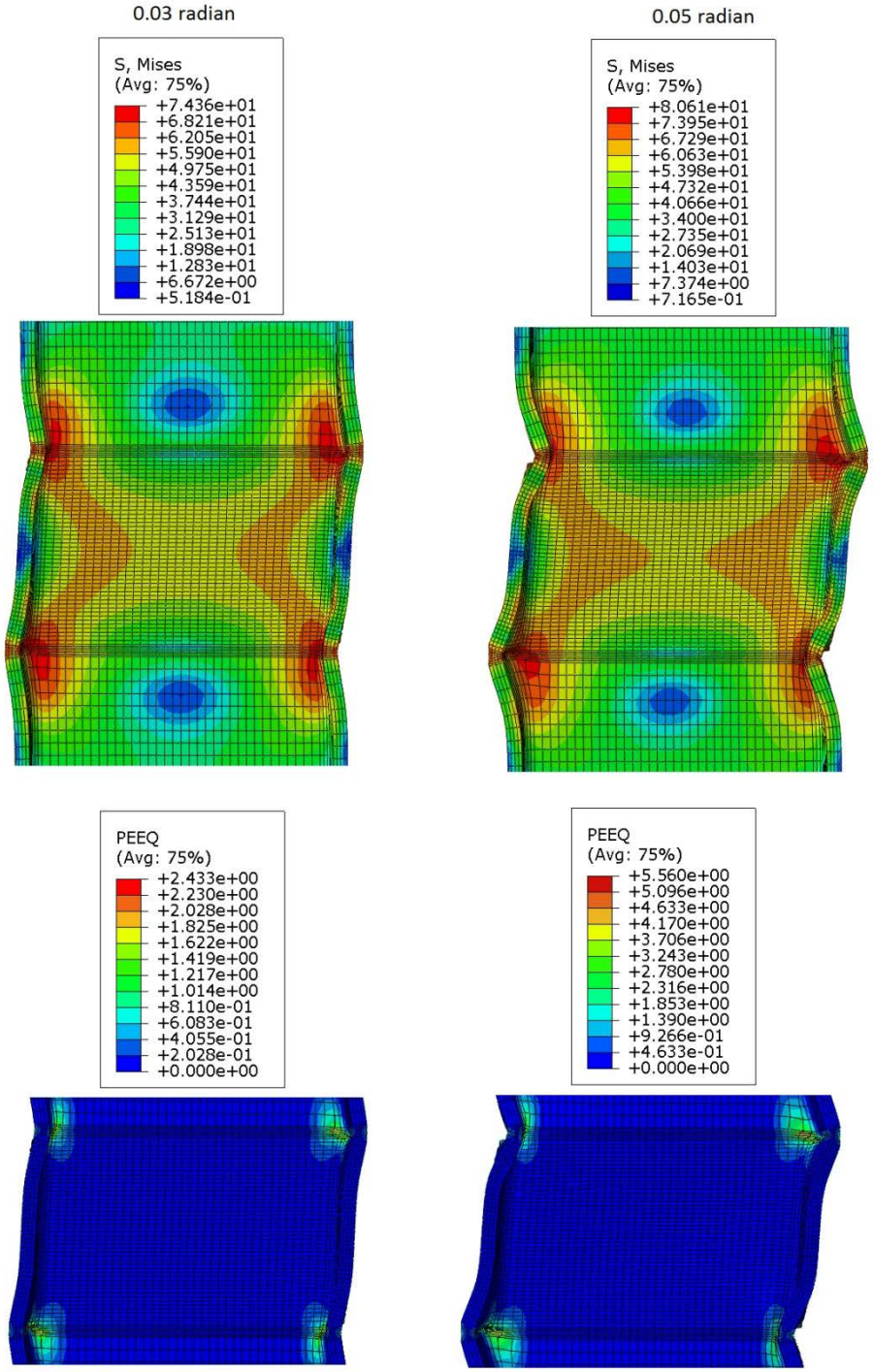

Figure 5.16: VMS and PEEQ in the column (Case 2B_f)

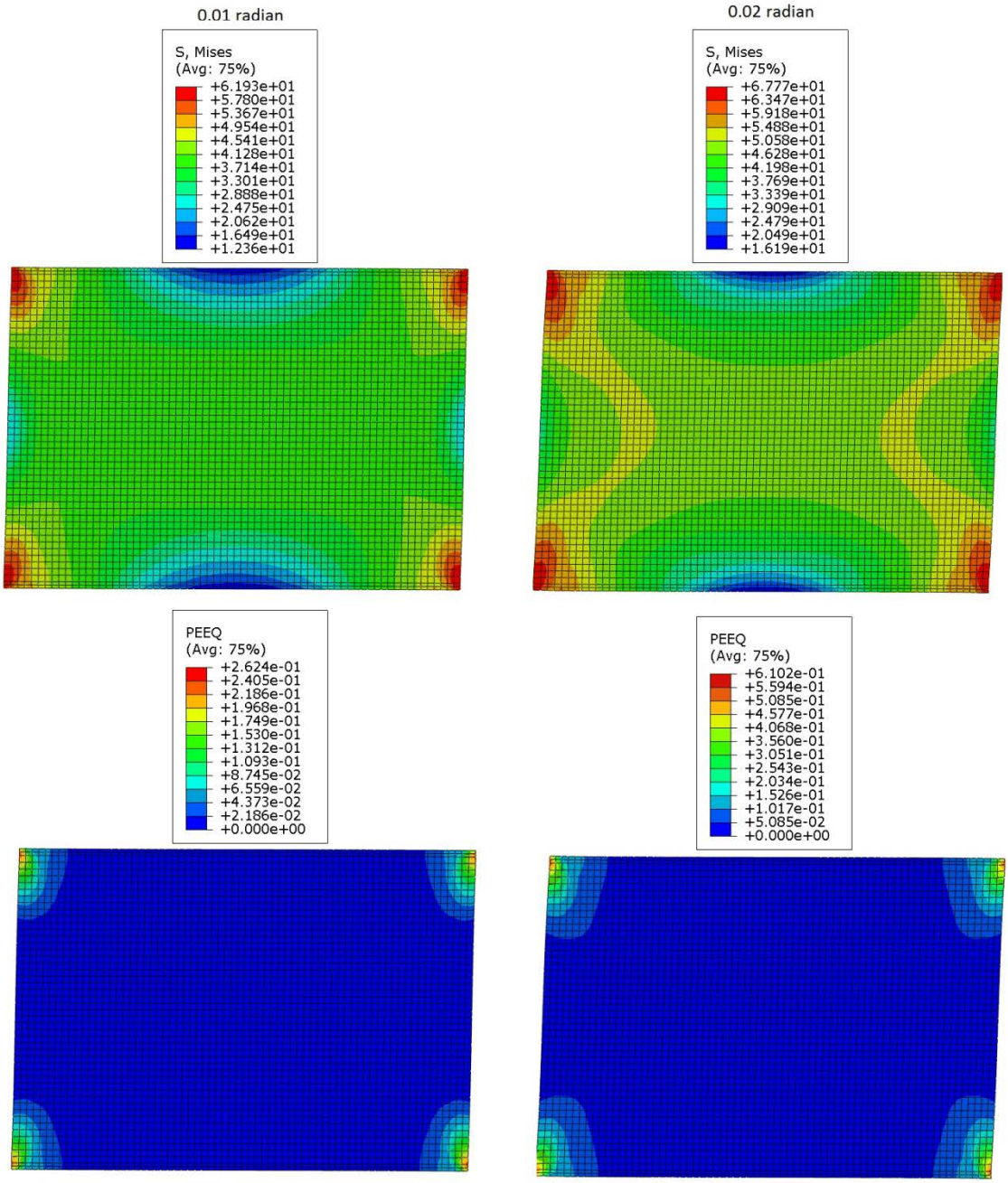

Figure 5.17: VMS and PEEQ in the DP (Case 2B_f)

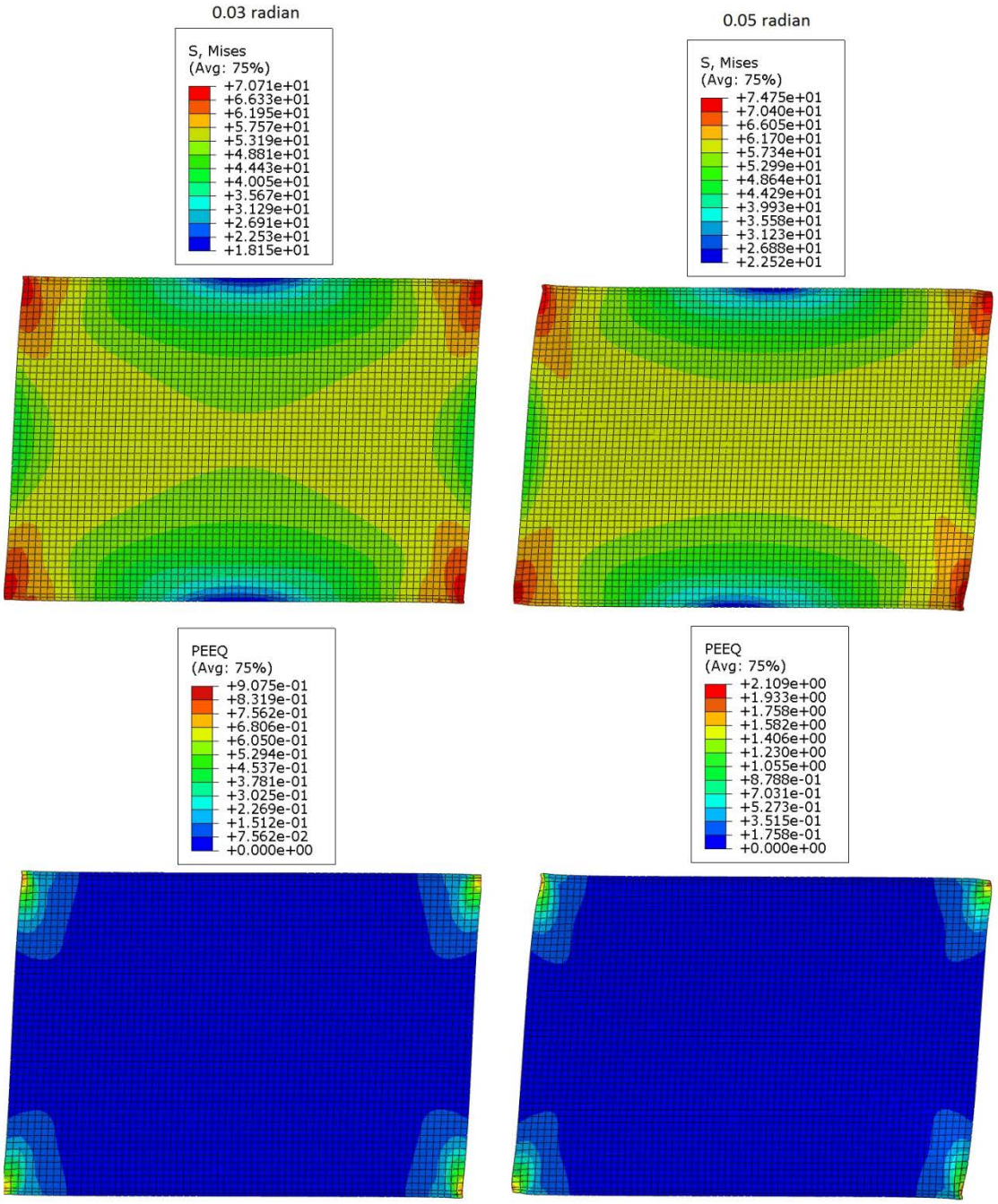

Figure 5.18: VMS and PEEQ in the DP (Case 2B_f)

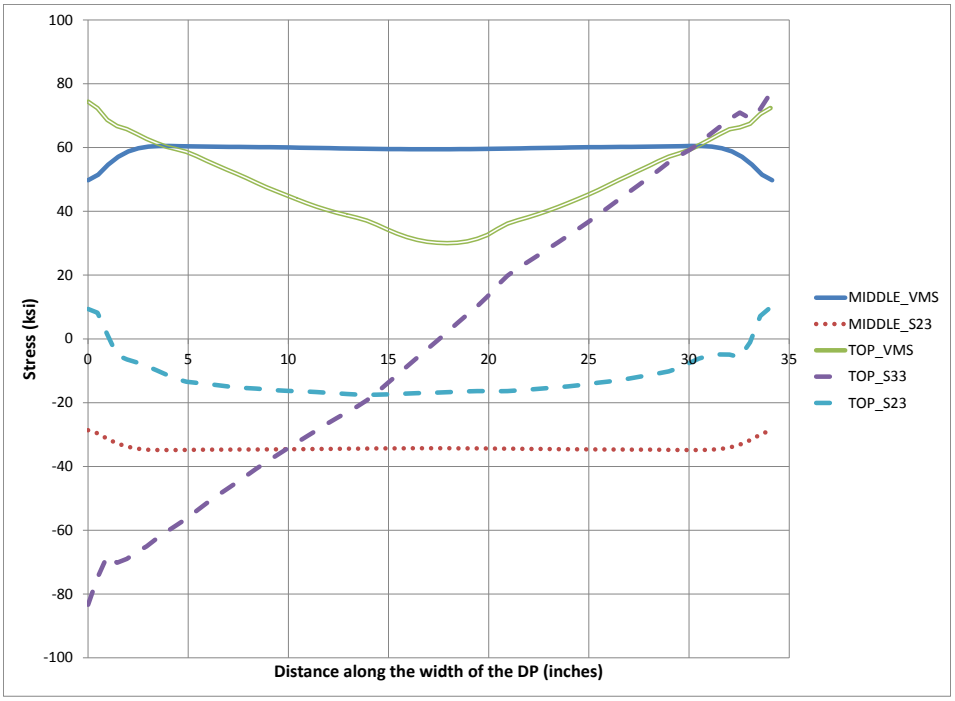

Figure 5.19: Stresses along the width of DP at 0.05 radian rotation (Case 2B_f)

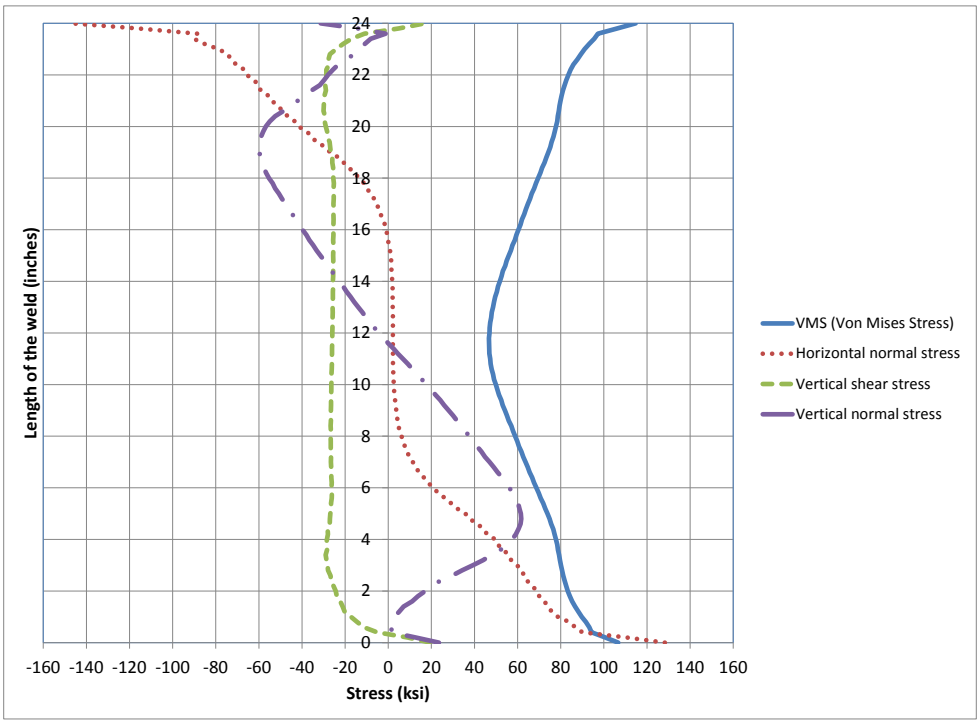

Figure 5.20: Stresses along depth of CJP1 (DP-CJP1 interface) at 0.05 radian (Case 2B_f)

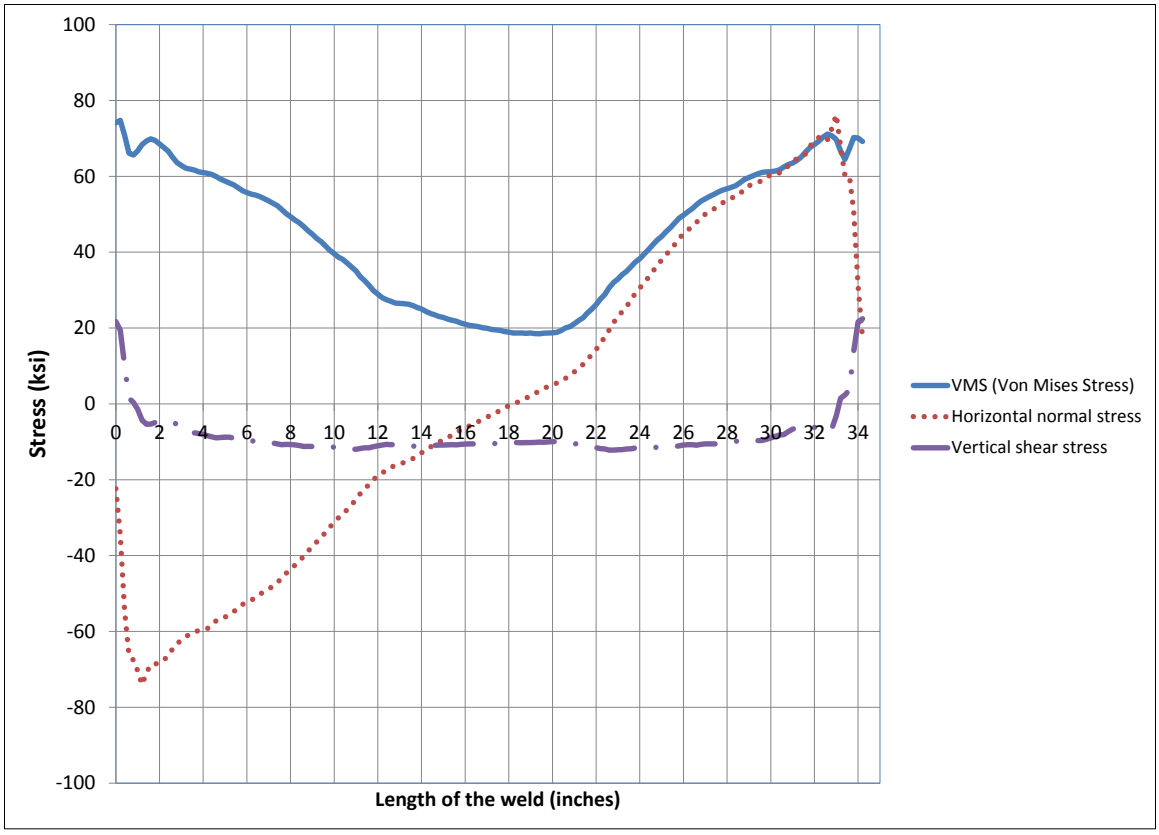

Figure 5.21: Stresses along the width of fillet weld (DP-fillet weld interface) at 0.05 radian rotation of panel zone (Case 2B_f)

5.2.4 Analysis case 3B

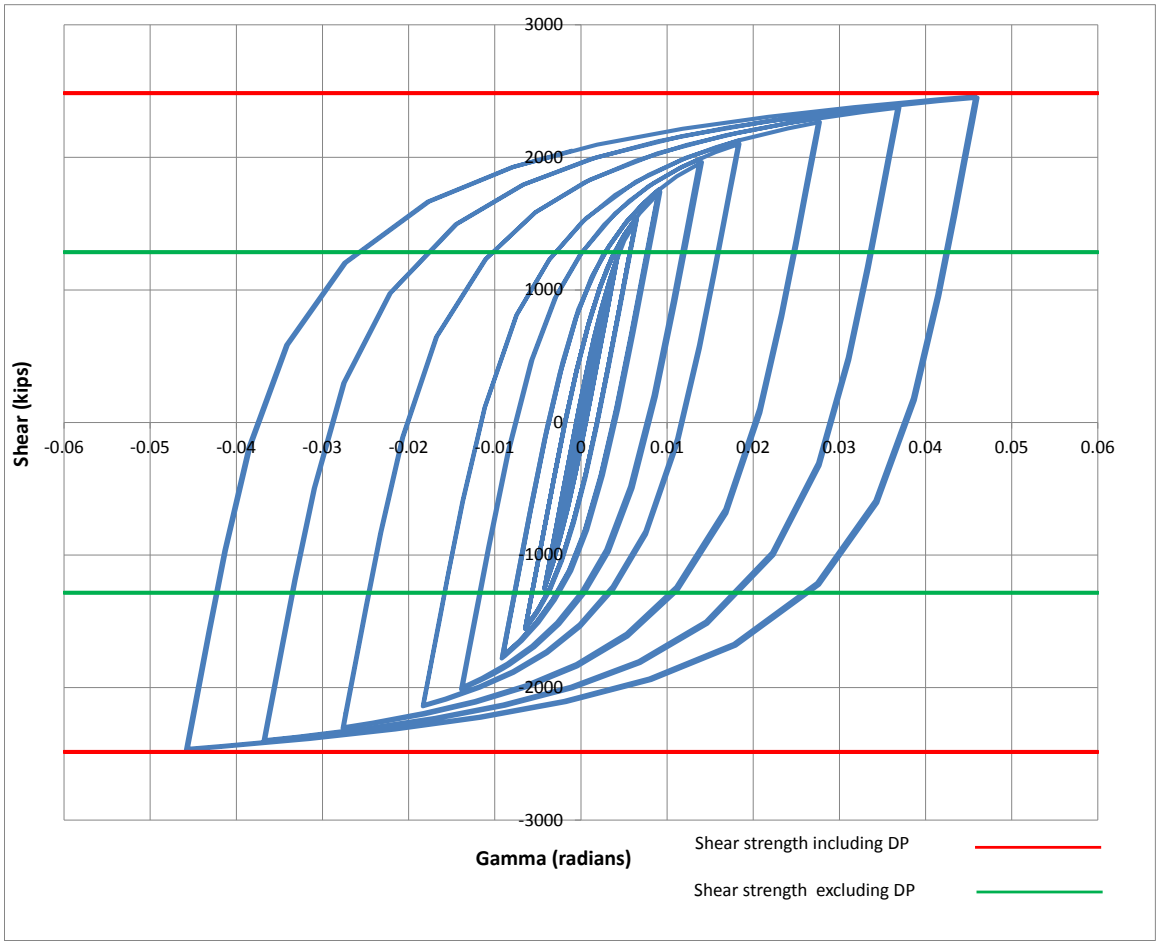

Figure 5.22: Panel zone shear versus rotation (Case 3B)

Table 5.5: Panel zone shear and force on loading plate (Case 3B)

Panel zone rotation (rad)	0.01	0.02	0.03	0.05
Panel zone shear (kips)	1760.27	2127.41	2295.10	2460.77
Force on one Loading plate (kips)	1056.16	1276.45	1377.06	1476.46

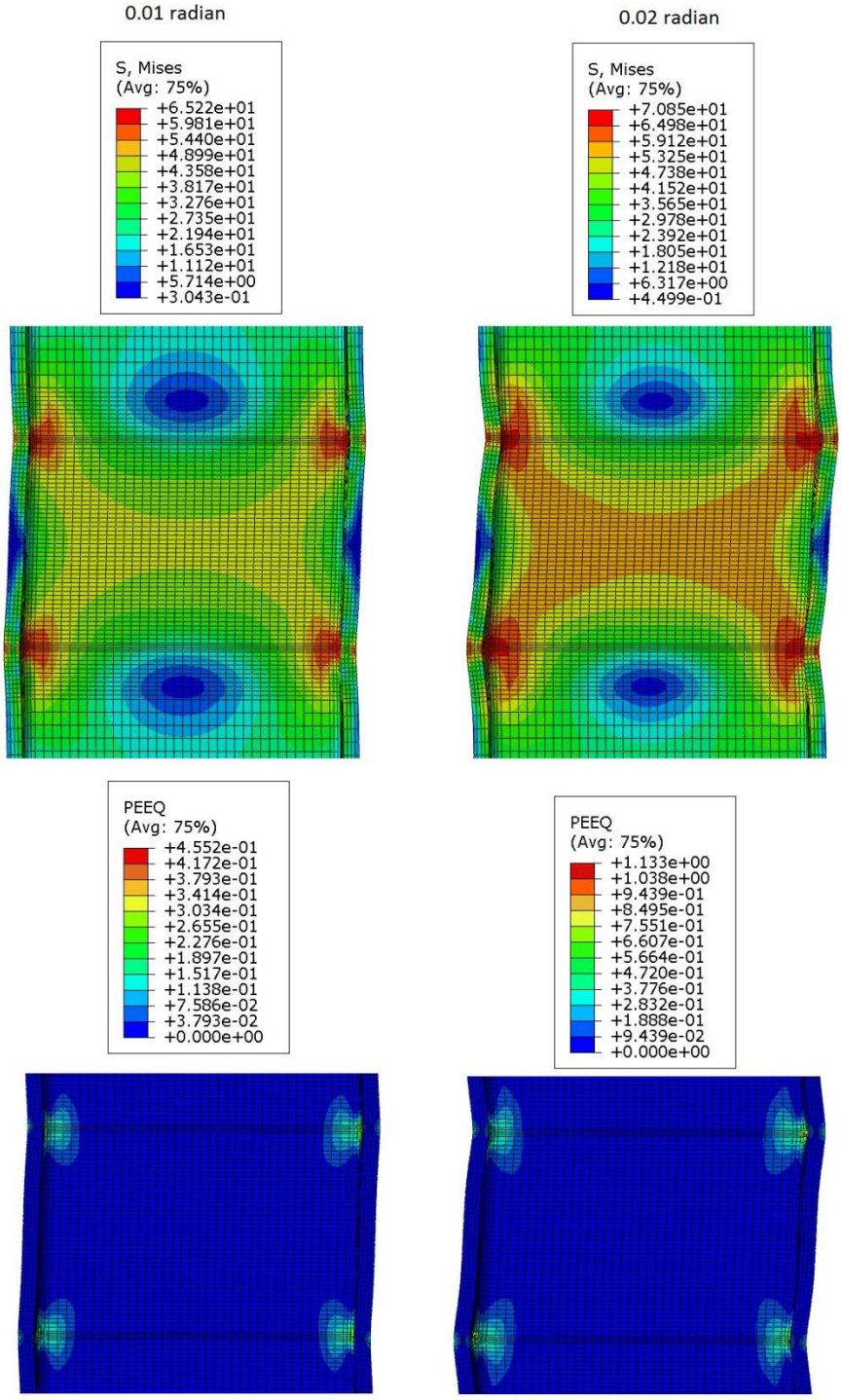

Figure 5.23: VMS and PEEQ in the column (Case 3B)

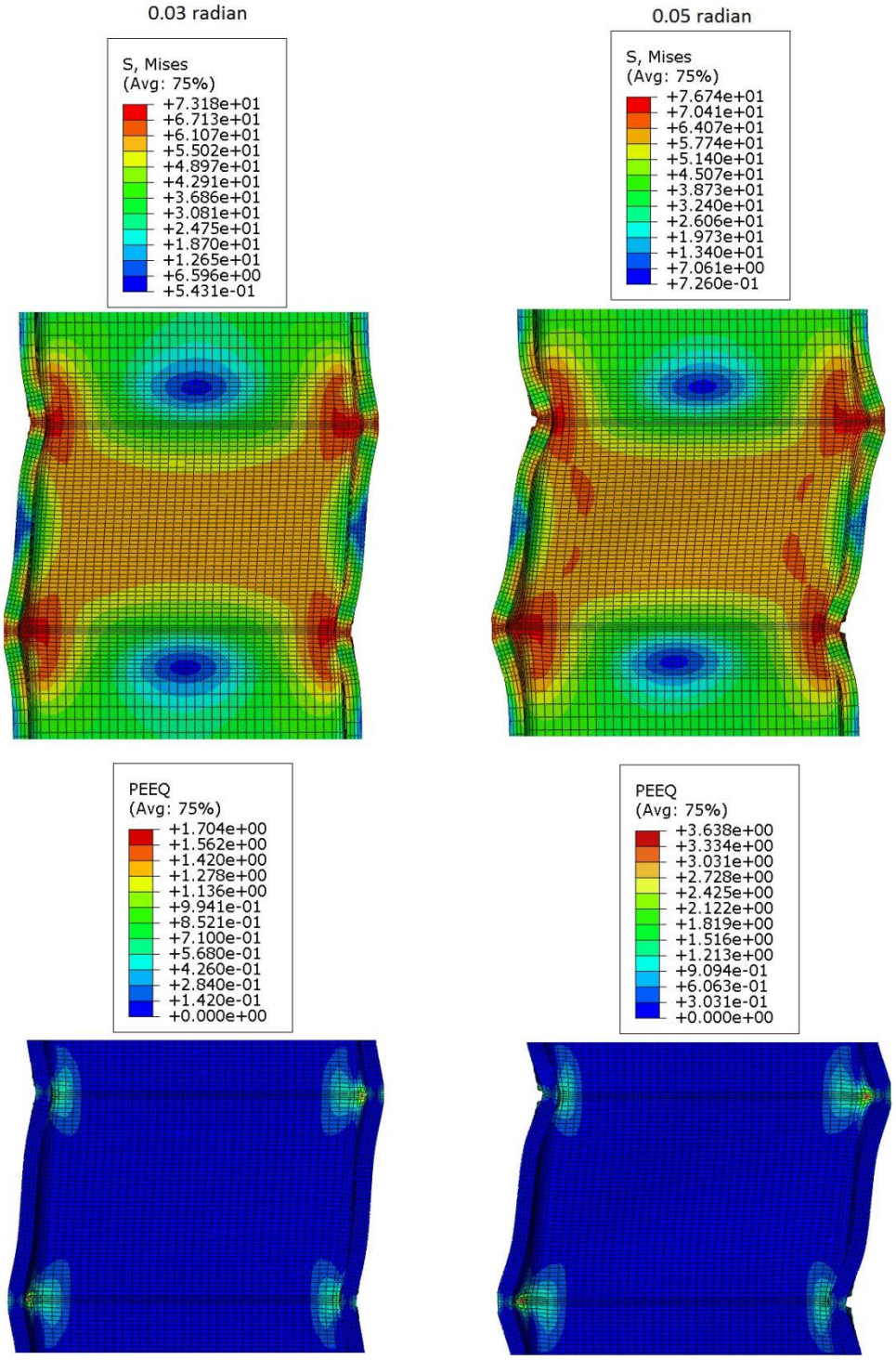

Figure 5.24: VMS and PEEQ in the column (Case 3B)

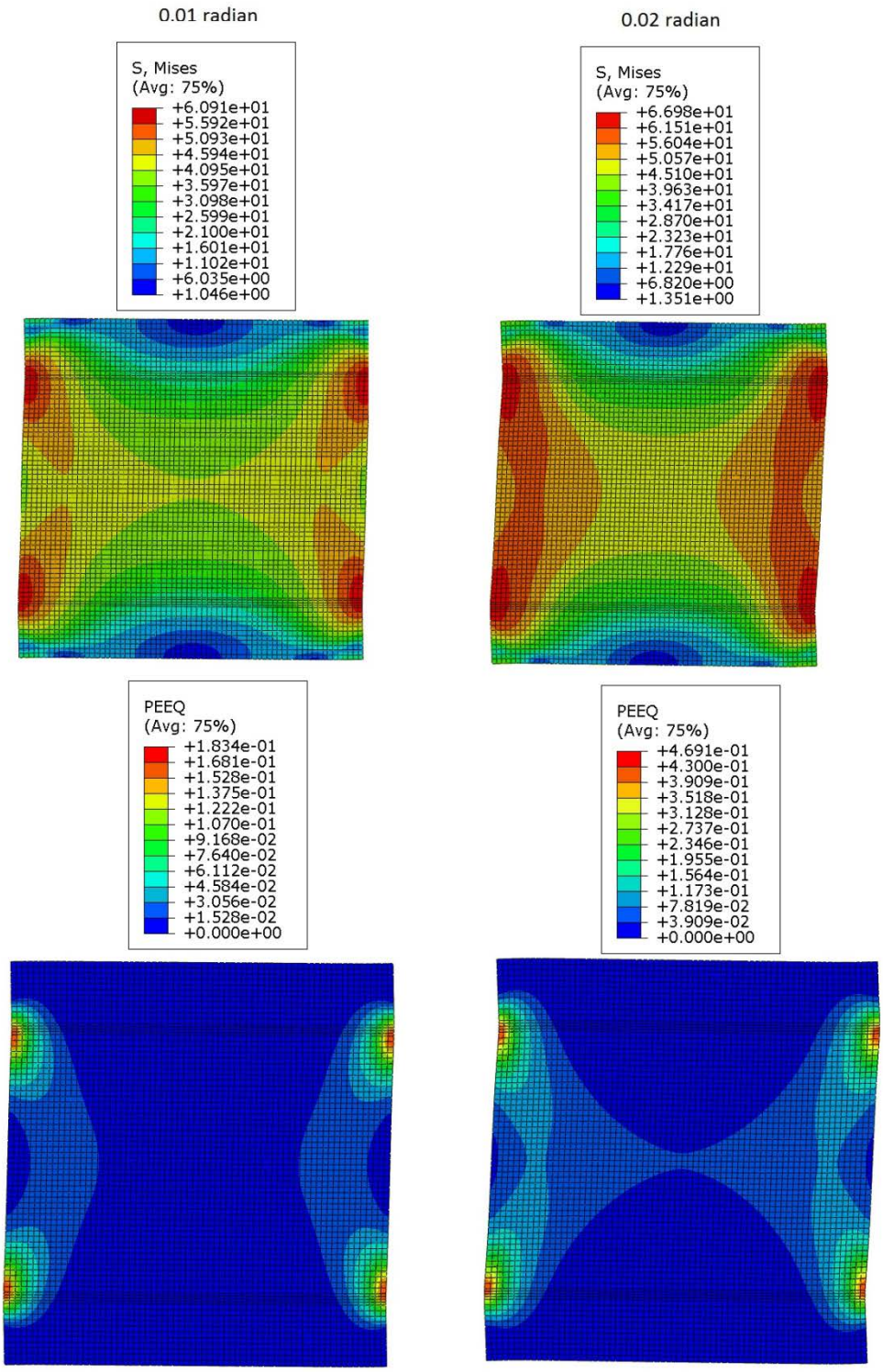

Figure 5.25: VMS and PEEQ in the DP (Case 3B)

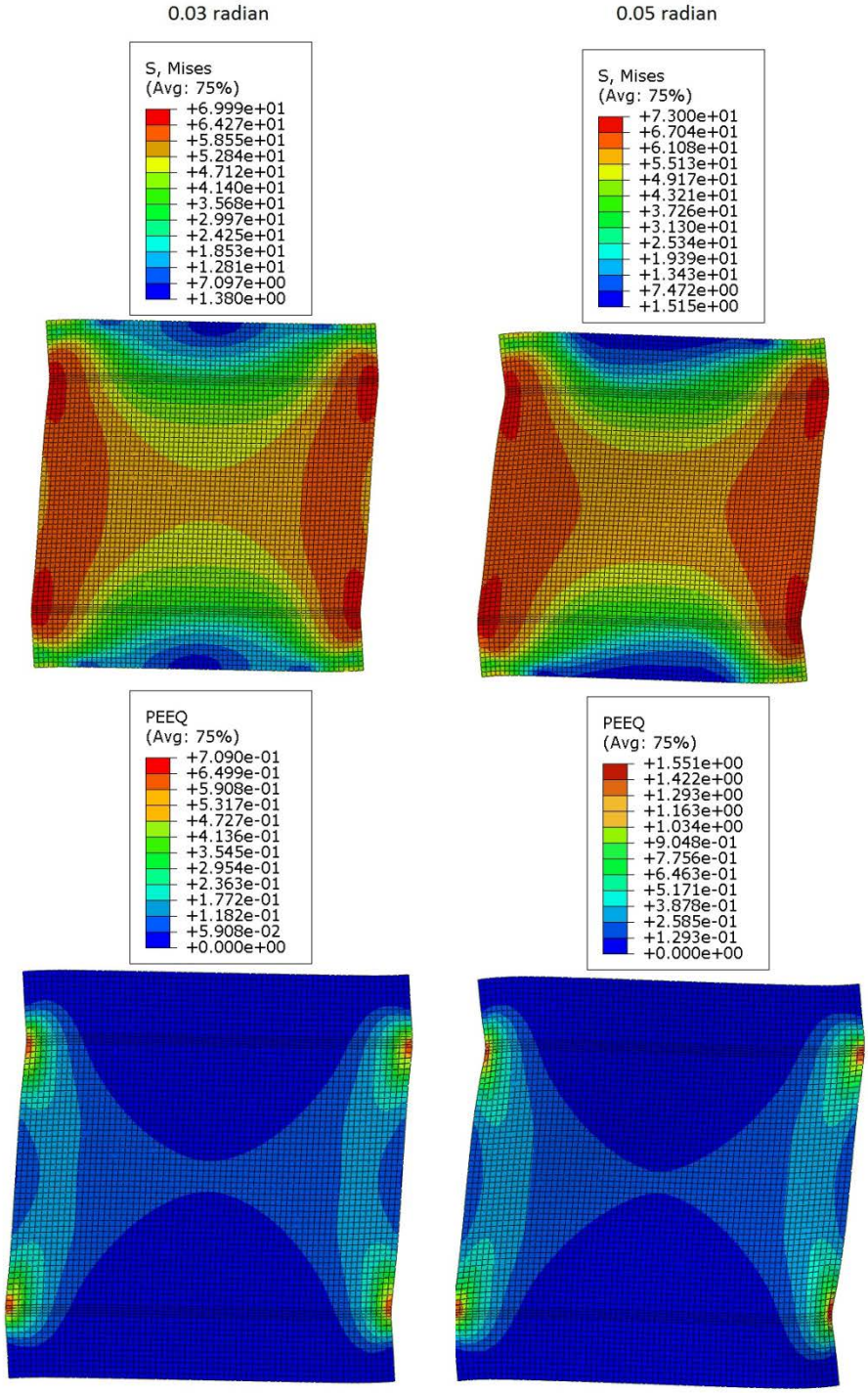

Figure 5.26: VMS and PEEQ in the DP (Case 3B)

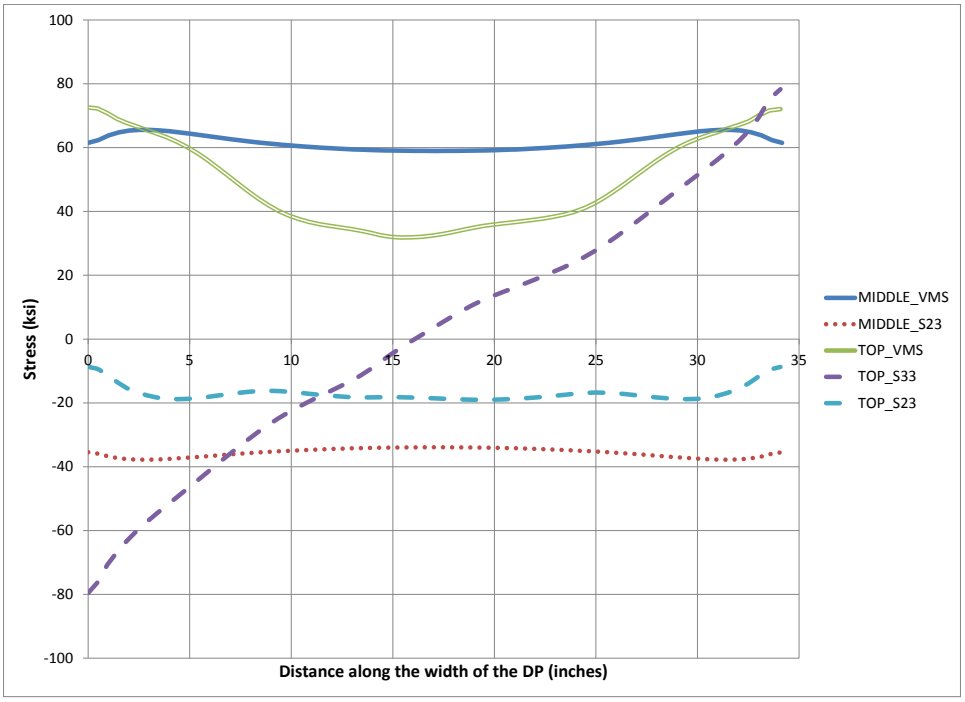

Figure 5.27: Stresses along the width of DP at 0.05 radian rotation (Case 3B)

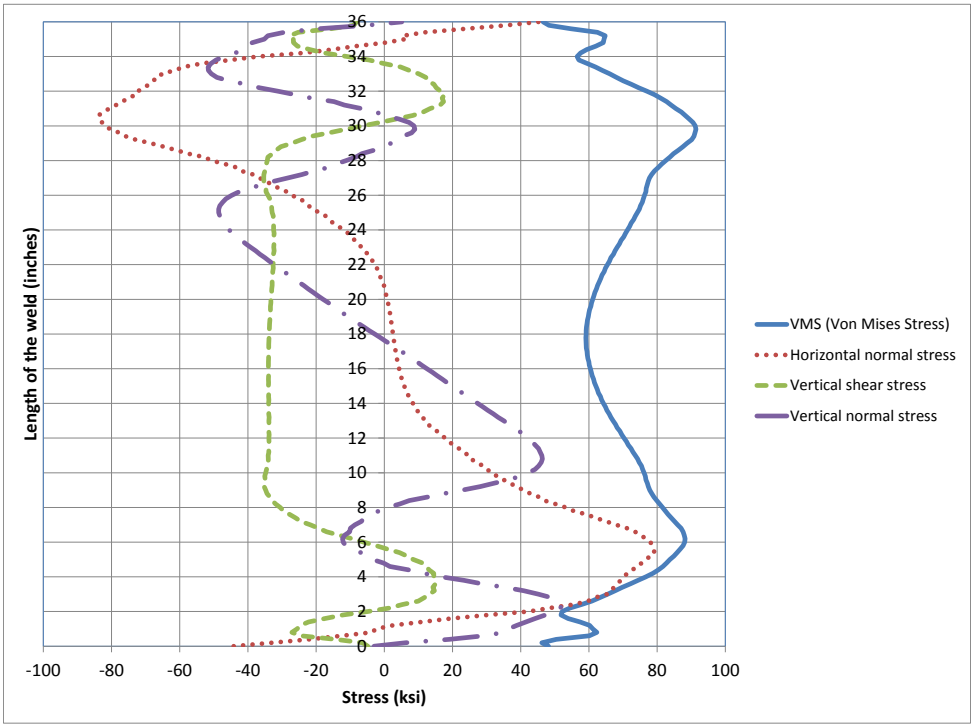

Figure 5.28: Stresses along depth of CJP1 (DP-CJP1 interface) at 0.05 radian (Case 3B)

5.2.5 Analysis case 4B

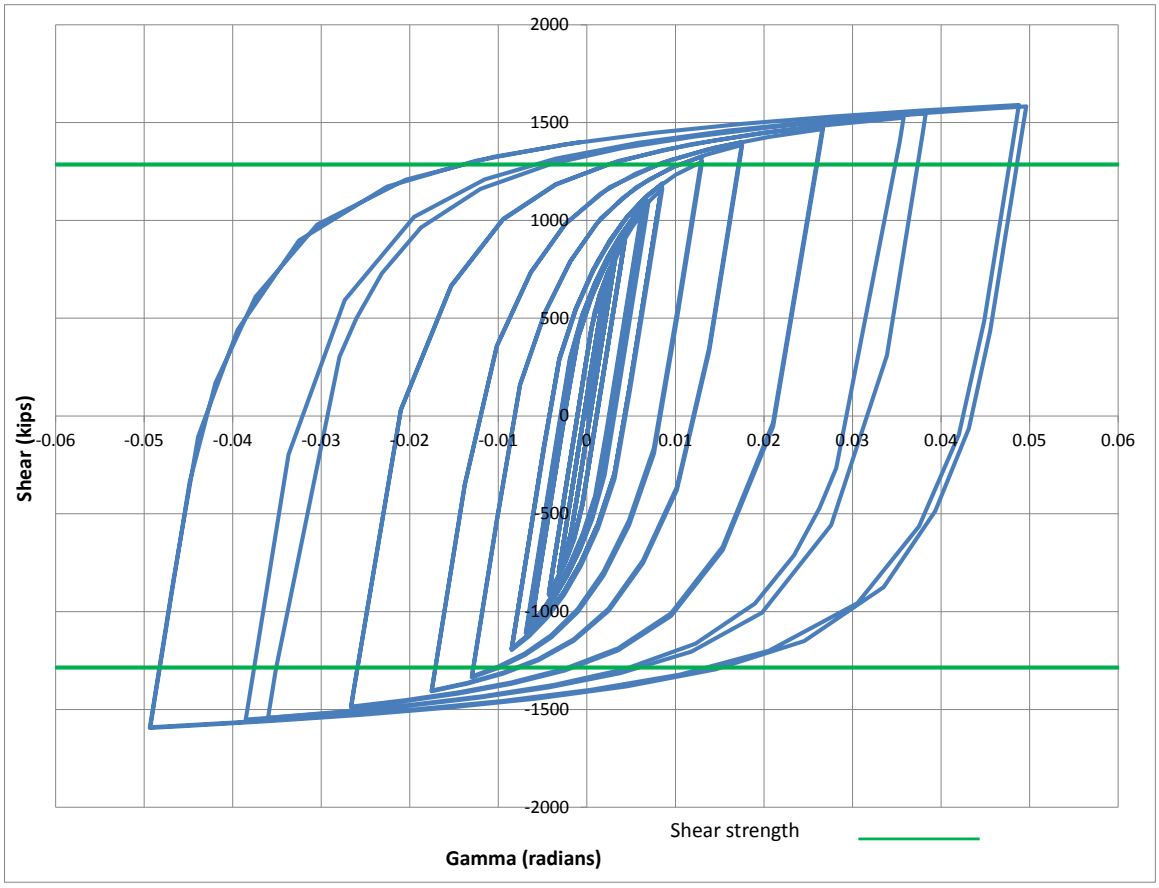

Figure 5.29: Panel zone shear versus rotation (Case 4B)

Table 5.6: Panel zone shear and force on loading plate (Case 4B)

Panel zone rotation (rad)	0.01	0.02	0.03	0.05
Panel zone shear (kips)	1188.21	1400.77	1483.61	1590.08
Force on one Loading plate (kips)	712.92	840.46	890.16	954.05

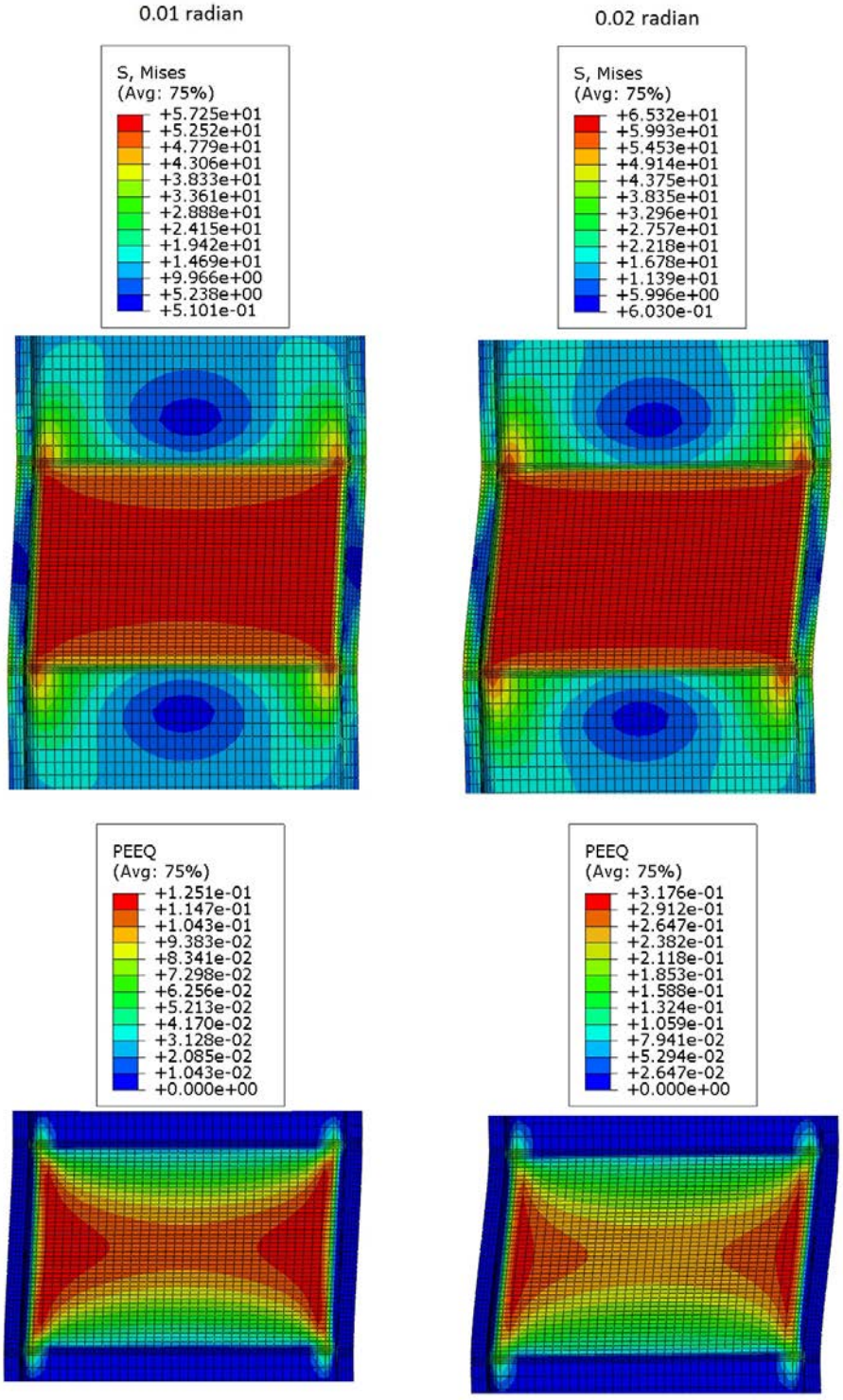

Figure 5.30: VMS and PEEQ in the column (Case 4B)

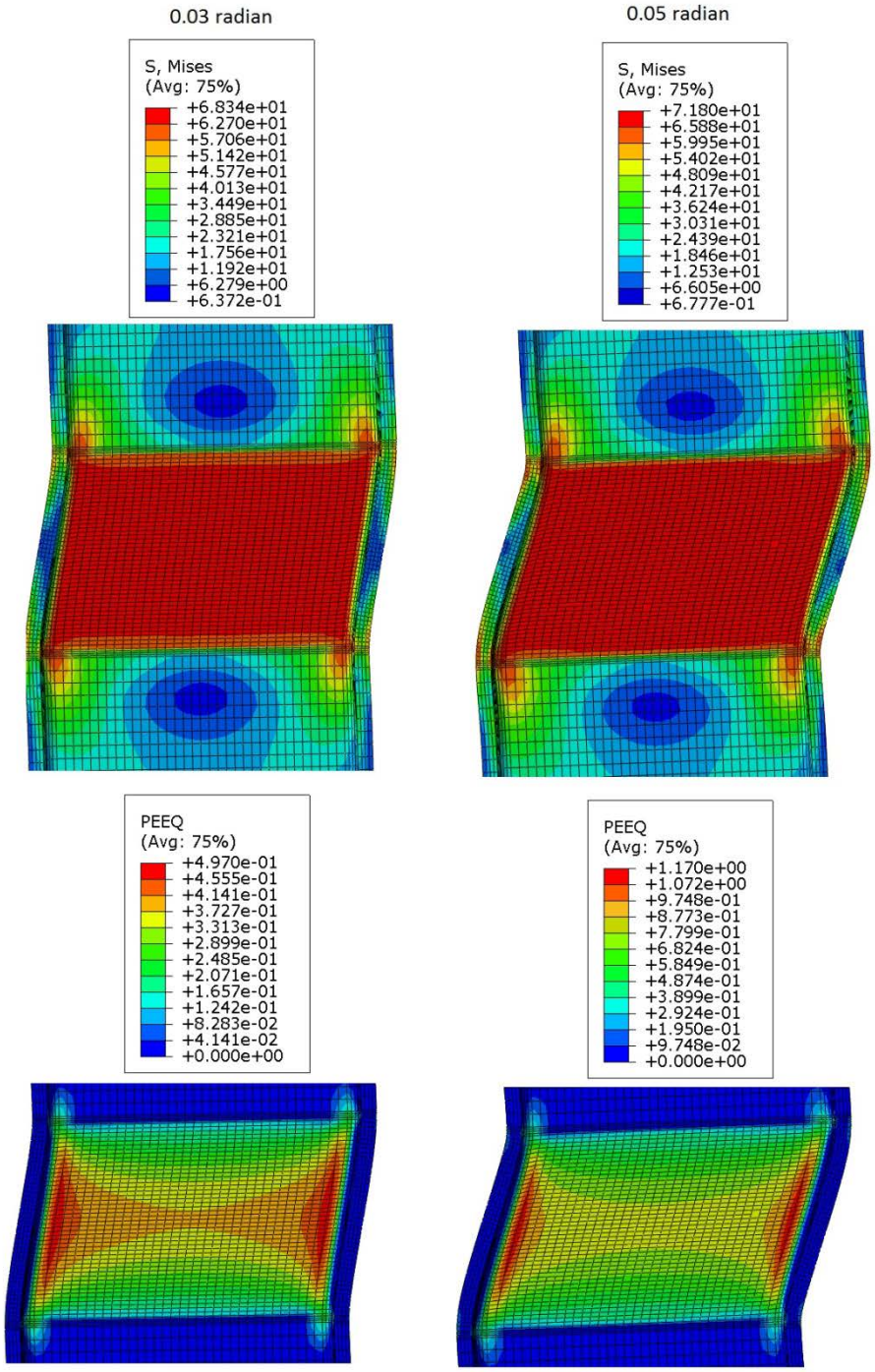

Figure 5.31: VMS and PEEQ in the column (Case 4B)

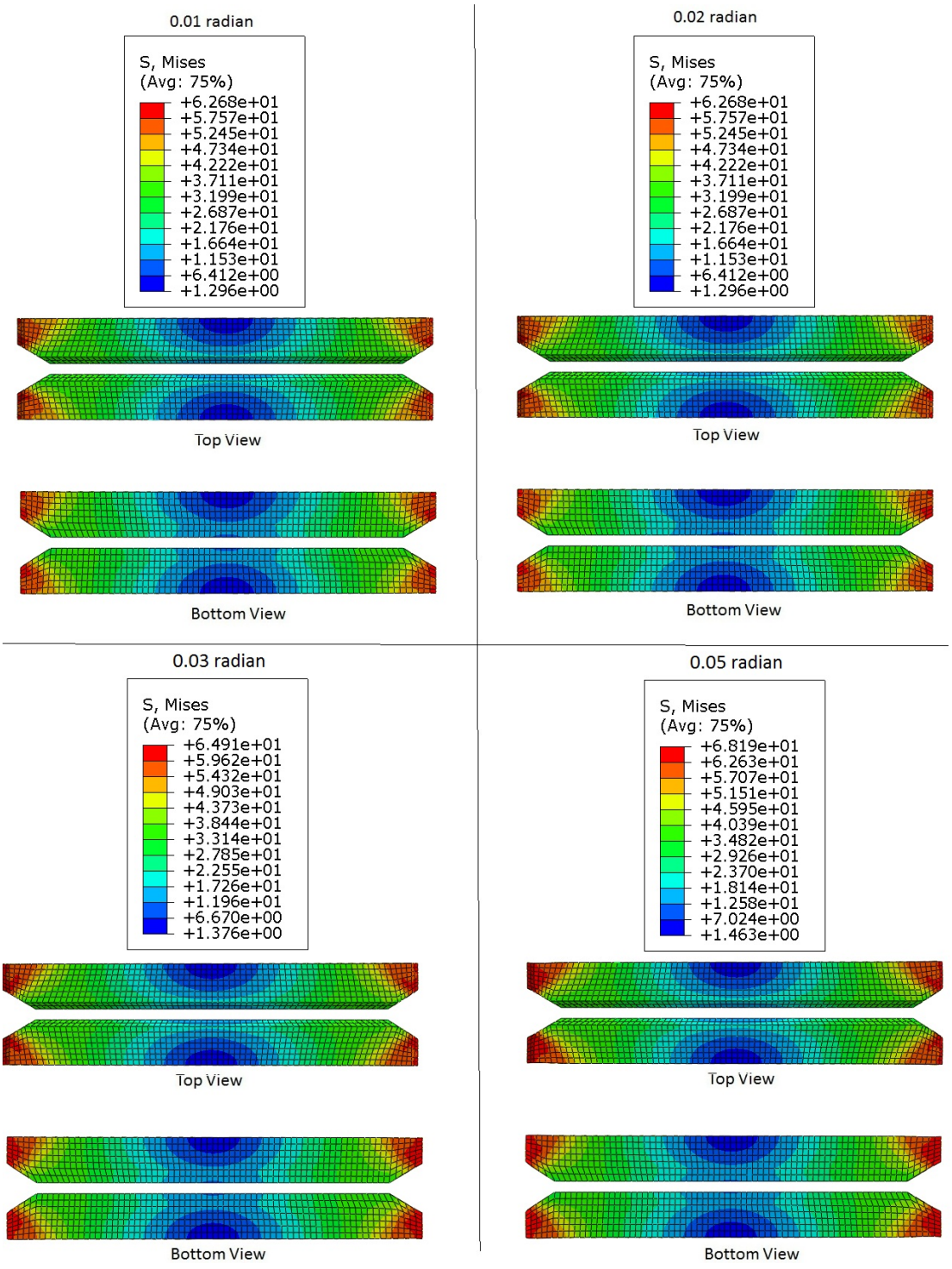

Figure 5.32: VMS in the CP at different rotations (Case 4B)

5.2.6 Analysis case 5B

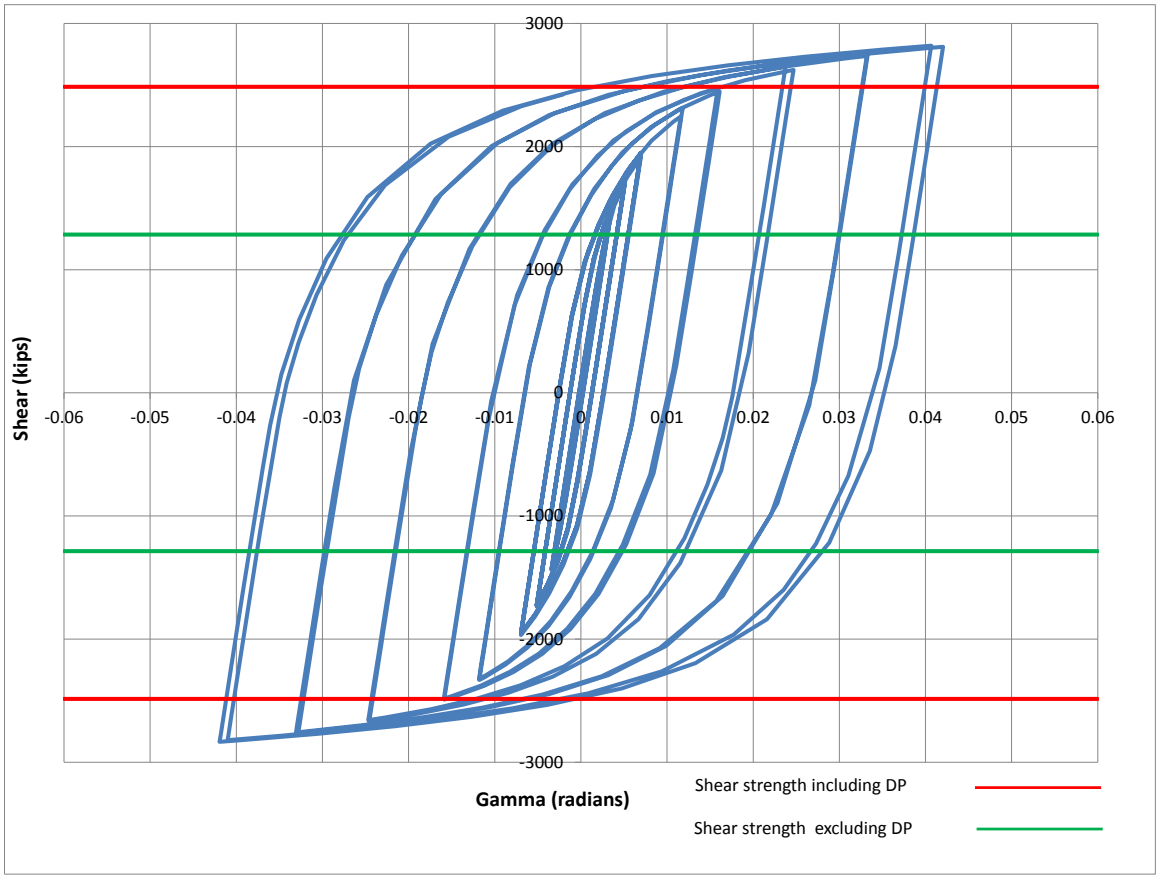

Figure 5.33: Panel zone shear versus rotation (Case 5B)

Table 5.7: Panel zone shear and force on loading plate (Case 5B)

Panel zone rotation (rad)	0.01	0.02	0.03	0.05
Panel zone shear (kips)	1950.41	2475.53	2646.68	2819.45
Force on one Loading plate (kips)	1170.25	1485.32	1588.01	1691.67

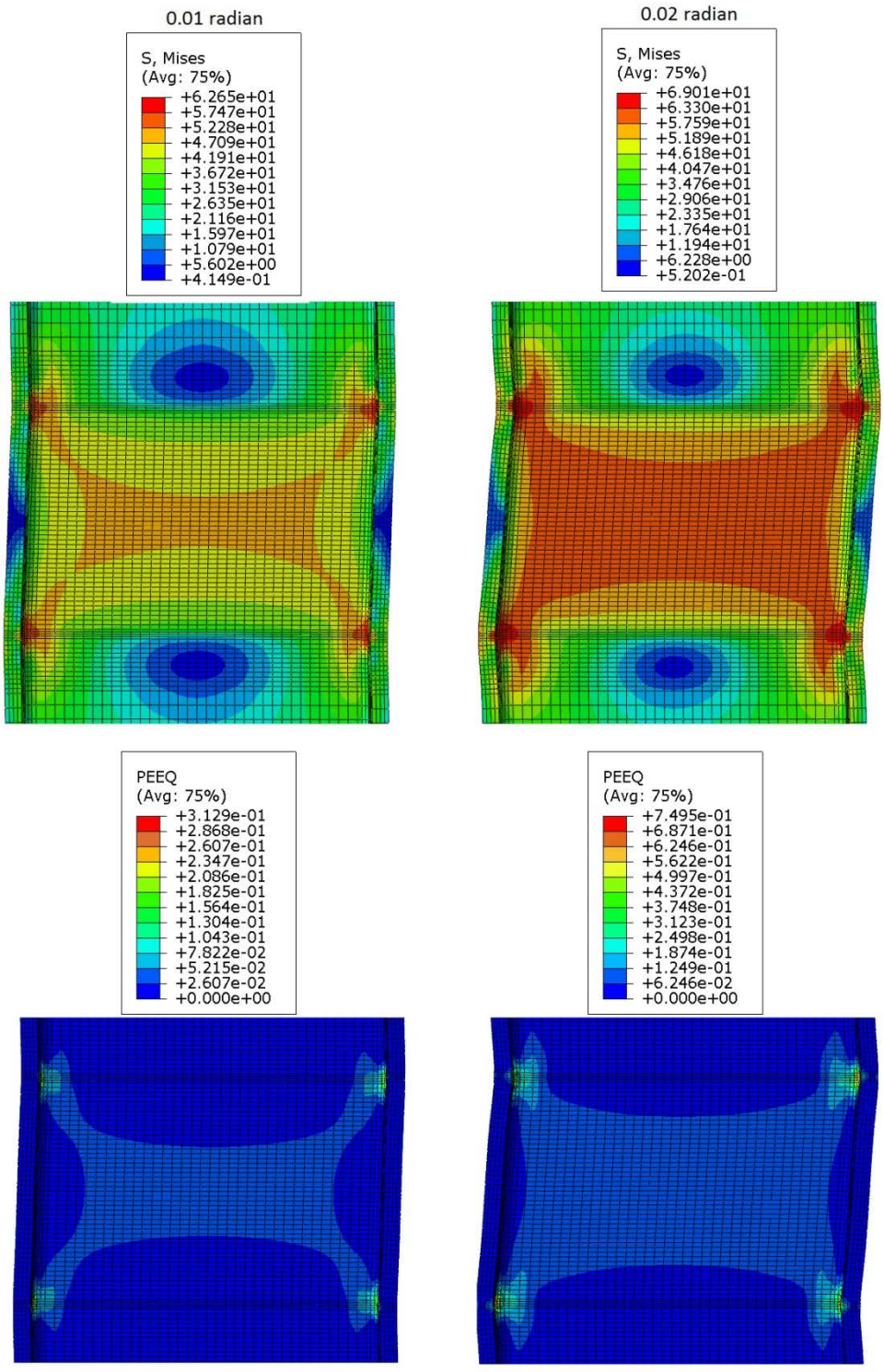

Figure 5.34: VMS and PEEQ in the column (Case 5B)

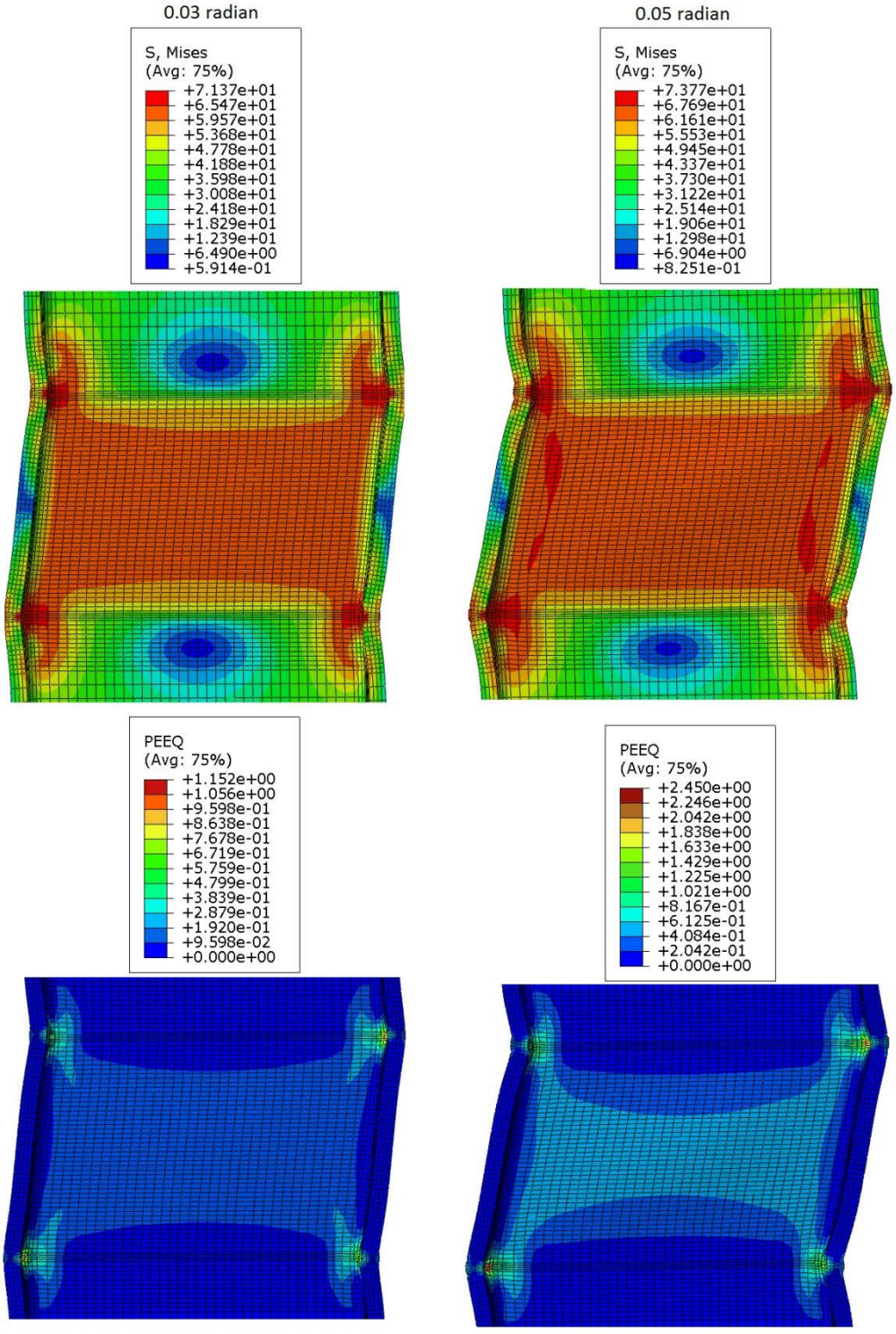

Figure 5.35: VMS and PEEQ in the column (Case 5B)

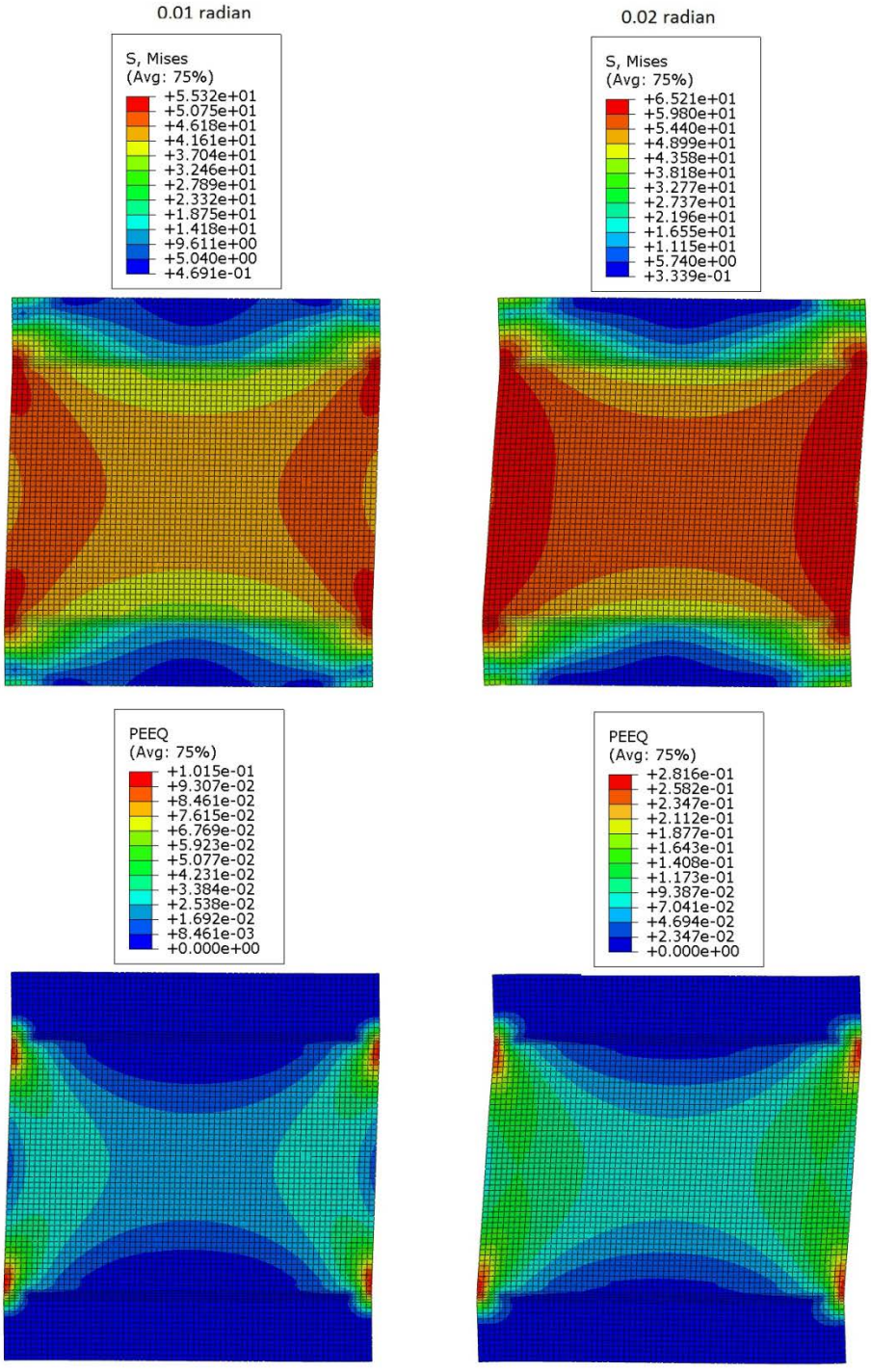

Figure 5.36: VMS and PEEQ in the DP at different rotations (Case 5B)

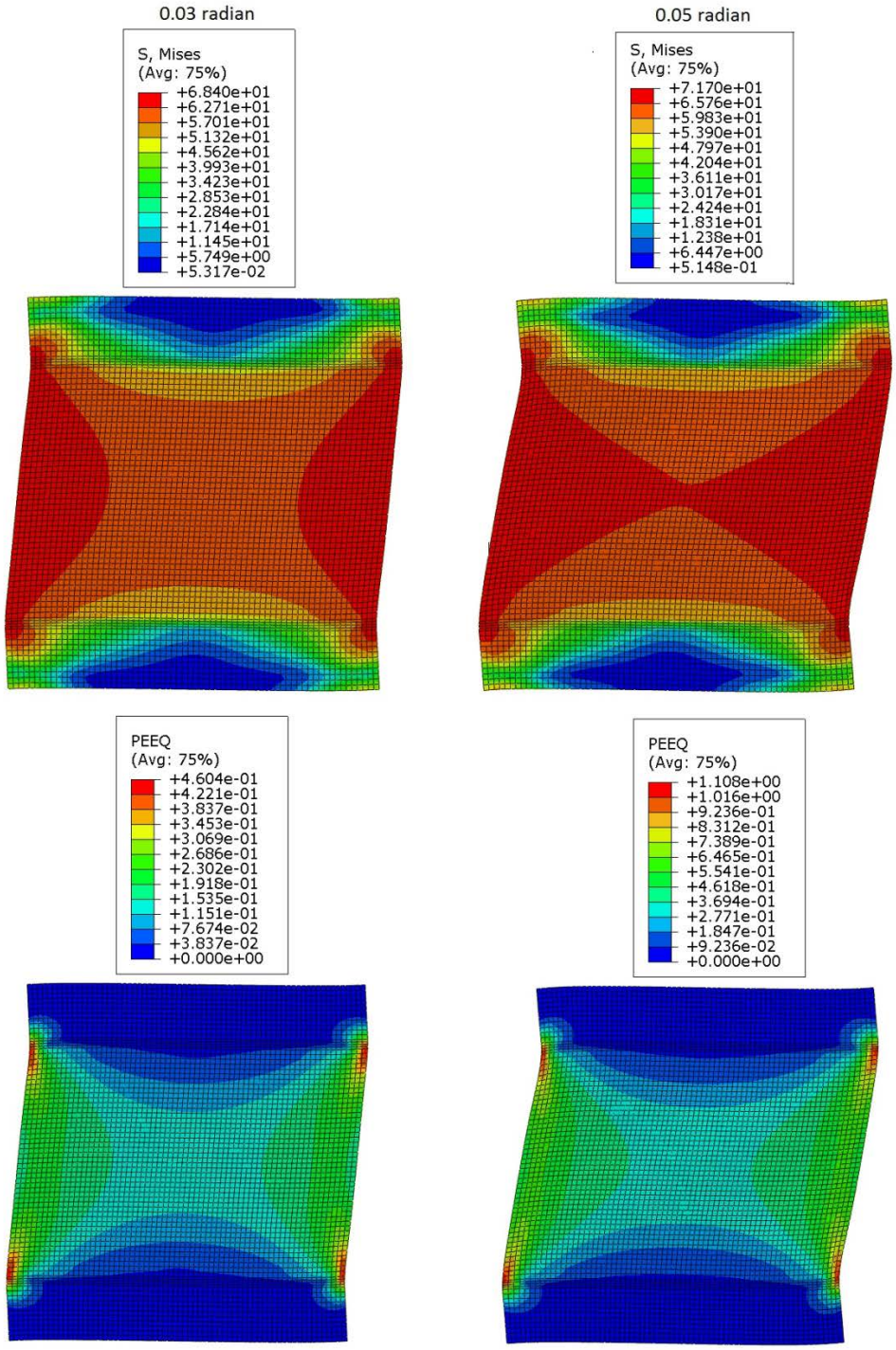

Figure 5.37: VMS and PEEQ in the DP (Case 5B)

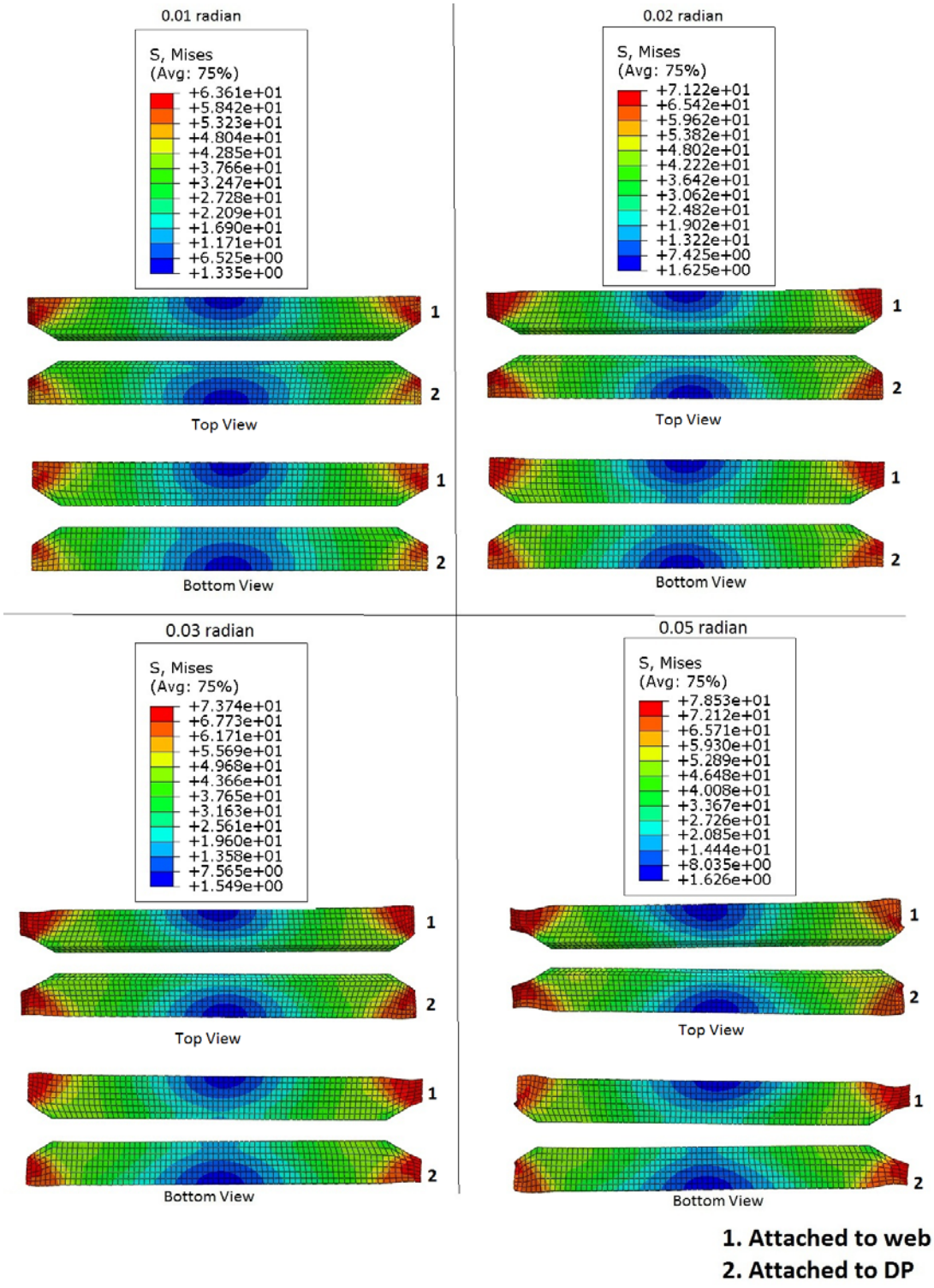

Figure 5.38: VMS in the CP at different rotations (Case 5B)

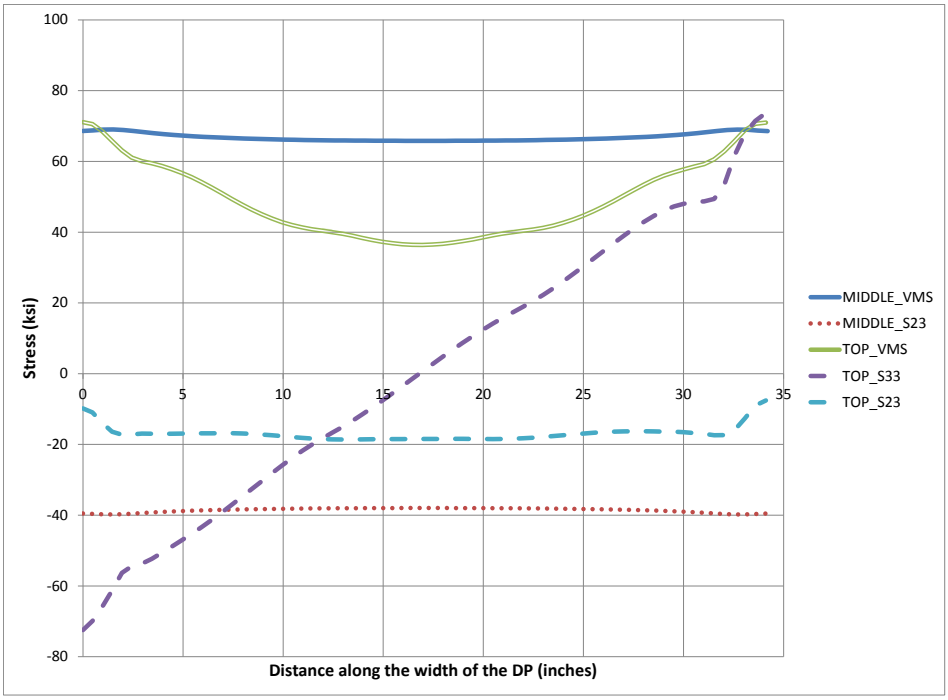

Figure 5.39: Stresses along the width of DP at 0.05 radian rotation (Case 5B)

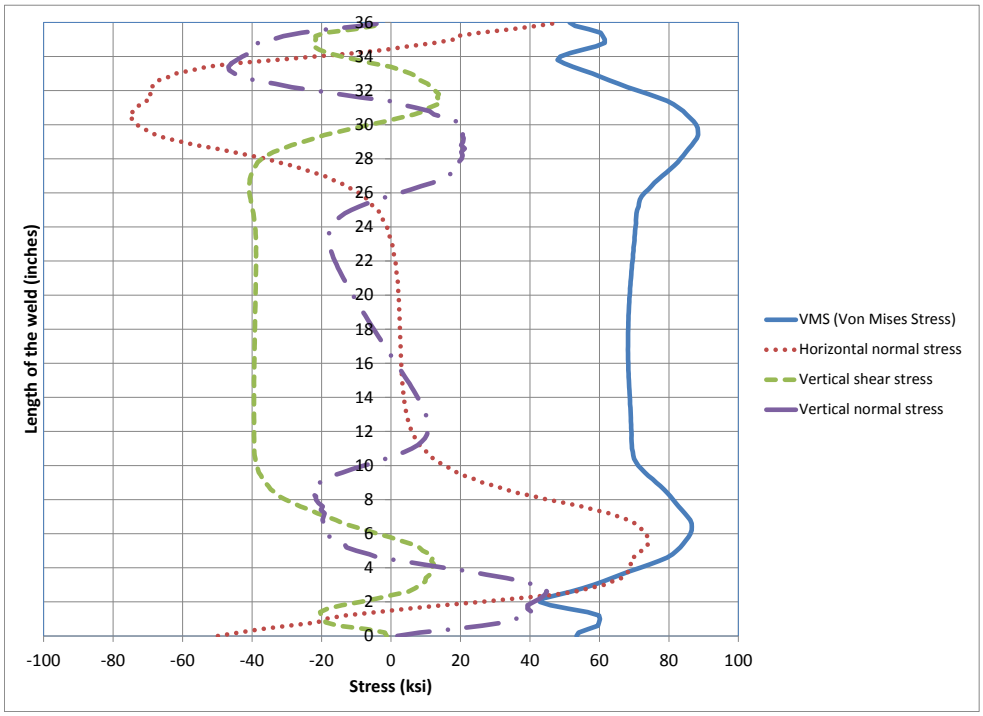

Figure 5.40: Stresses along depth of CJP1 (DP-CJP1 interface) at 0.05 radian (Case 5B)

5.2.7 Analysis case 6B

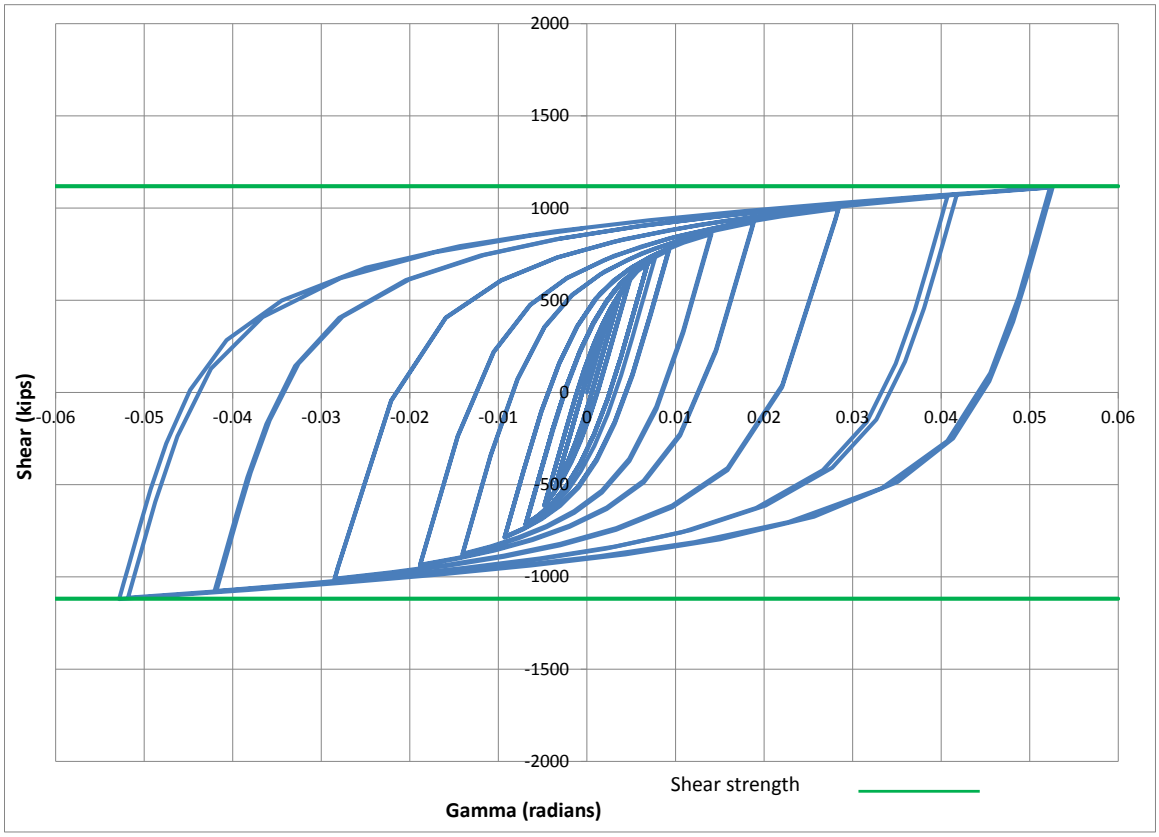

Figure 5.41: Panel zone shear versus rotation (Case 6B)

Table 5.8: Panel zone shear and force on loading plate (Case 6B)

Panel zone rotation (rad)	0.01	0.02	0.03	0.05
Panel zone shear (kips)	782.76	931.39	1007.02	1112.58
Force on one Loading plate (kips)	469.65	558.83	604.21	667.55

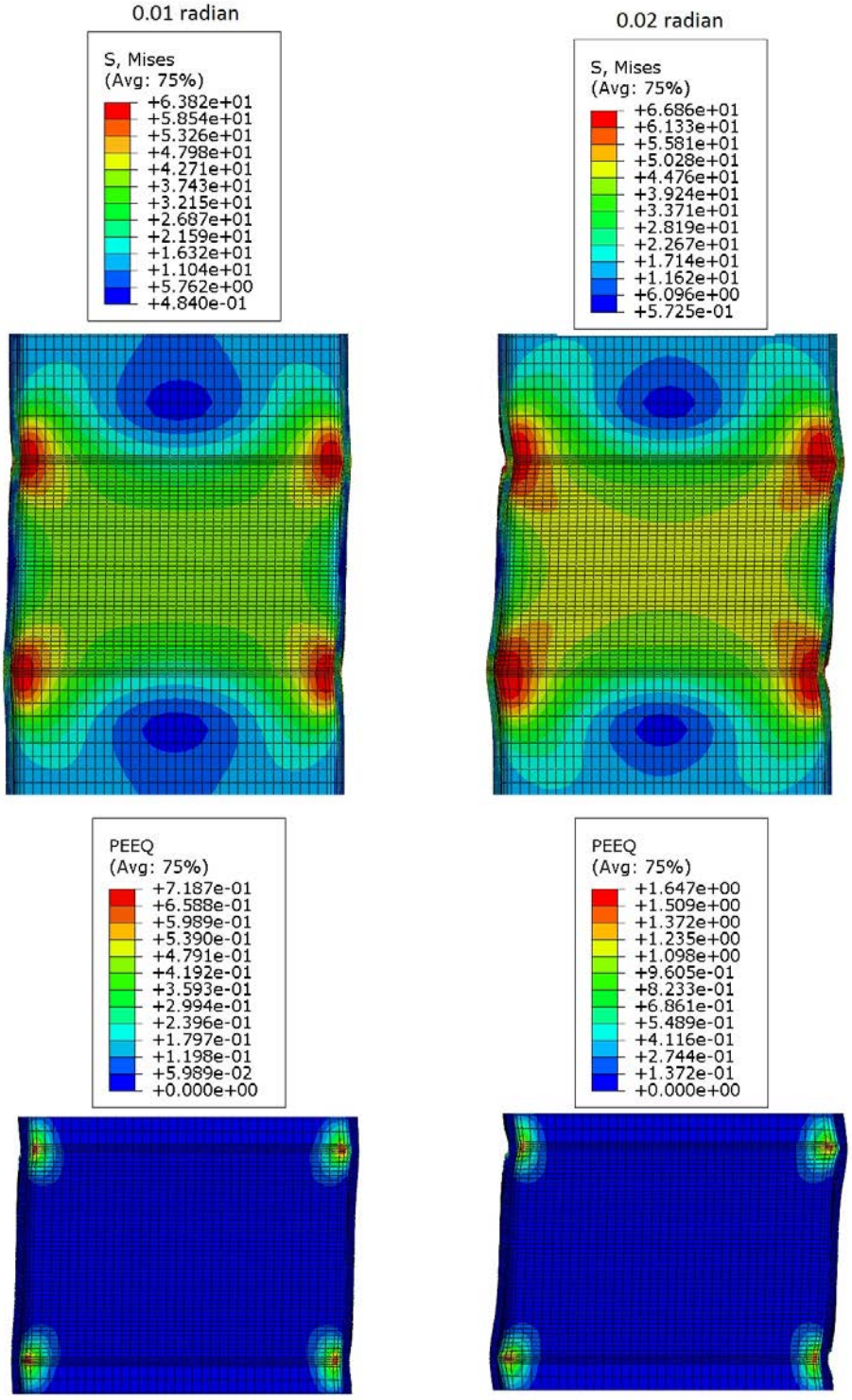

Figure 5.42: VMS and PEEQ in the column (Case 6B)

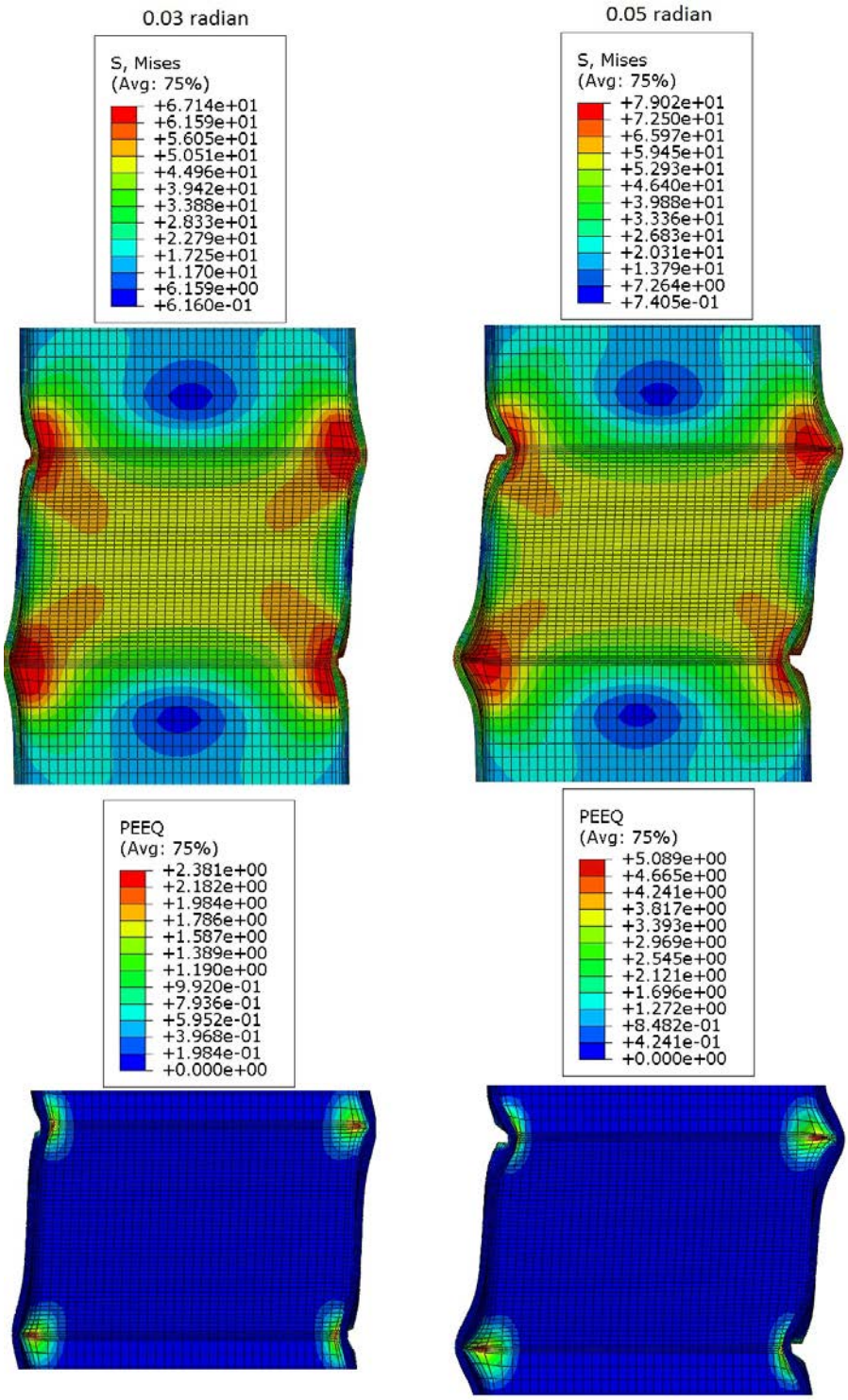

Figure 5.43: VMS and PEEQ in the column (Case 6B)

5.2.8 Analysis case 7B

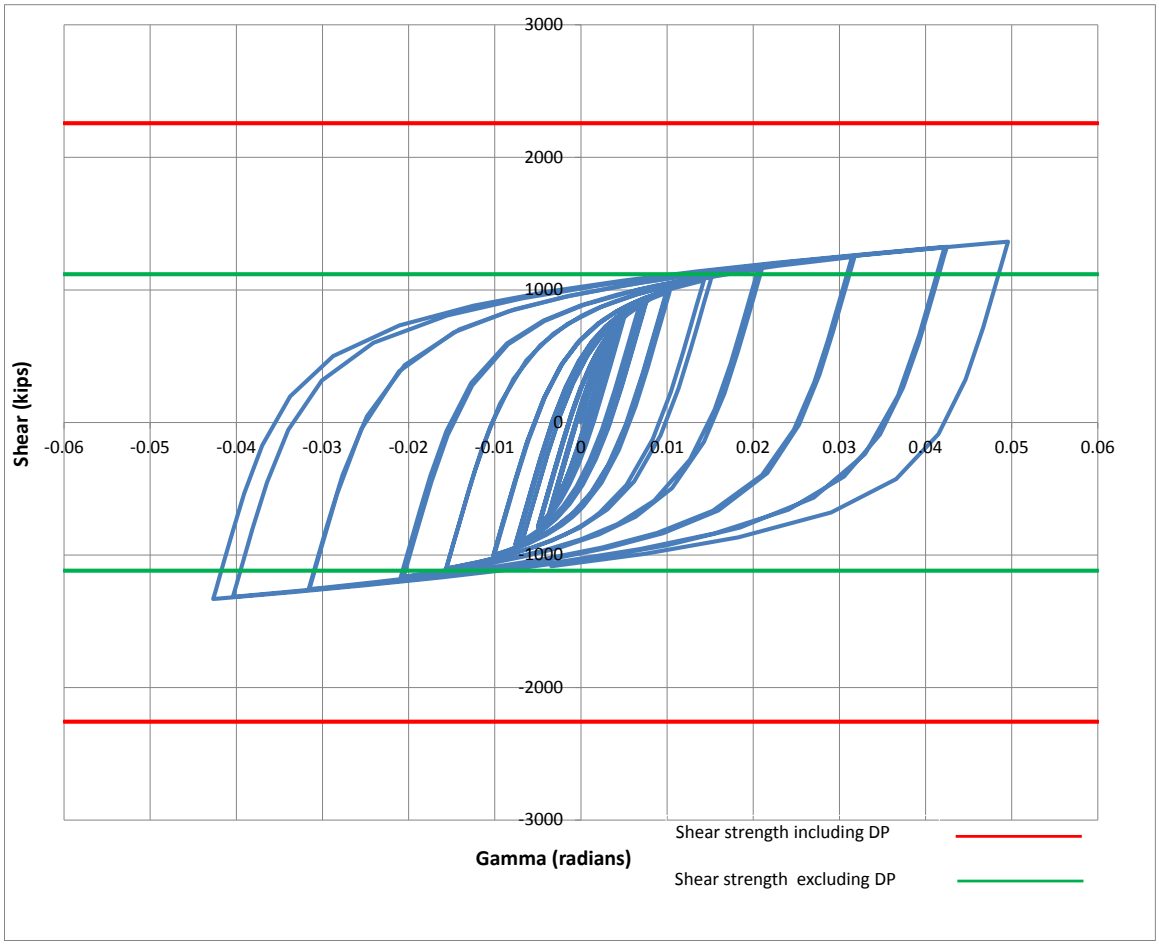

Figure 5.44: Panel zone shear versus rotation (Case 7B)

Table 5.9: Panel zone shear and force on loading plate (Case 7B)

Panel zone rotation (rad)	0.01	0.02	0.03	0.05
Panel zone shear (kips)	999.37	1162.58	1254.60	1366.04
Force on one Loading plate (kips)	599.62	697.55	752.76	819.62

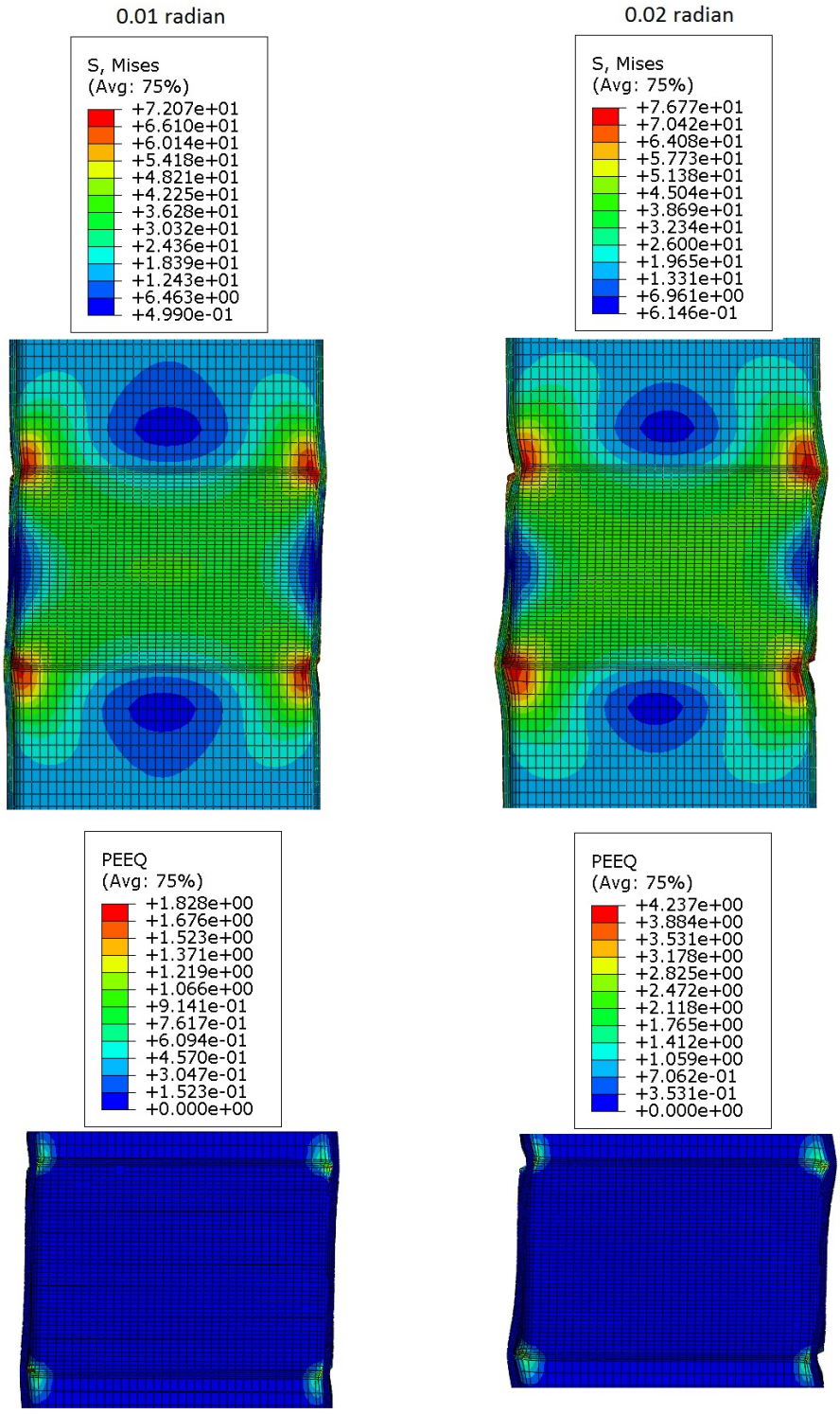

Figure 5.45: VMS and PEEQ in the column (Case 7B)

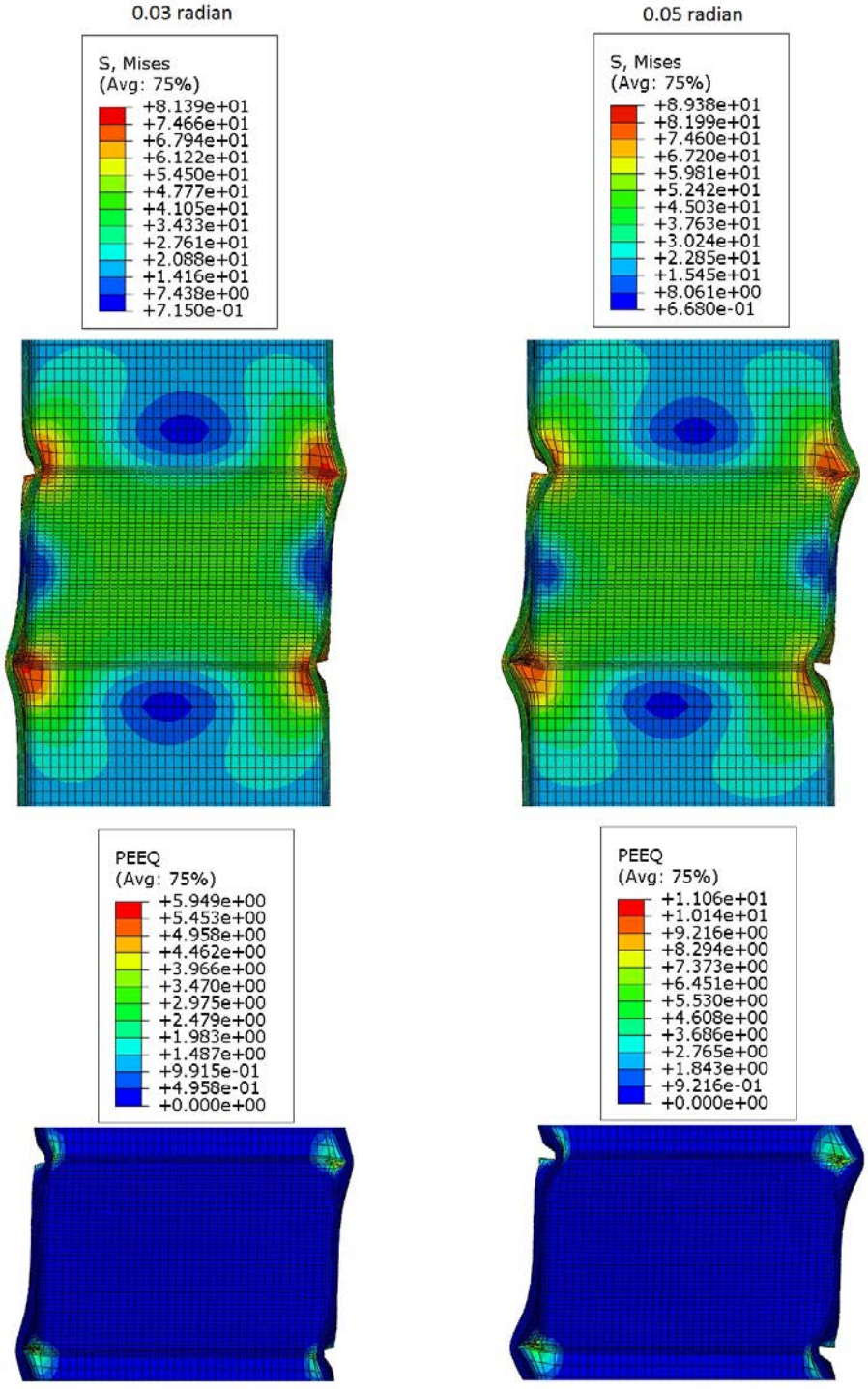

Figure 5.46: VMS and PEEQ in the column (Case 7B)

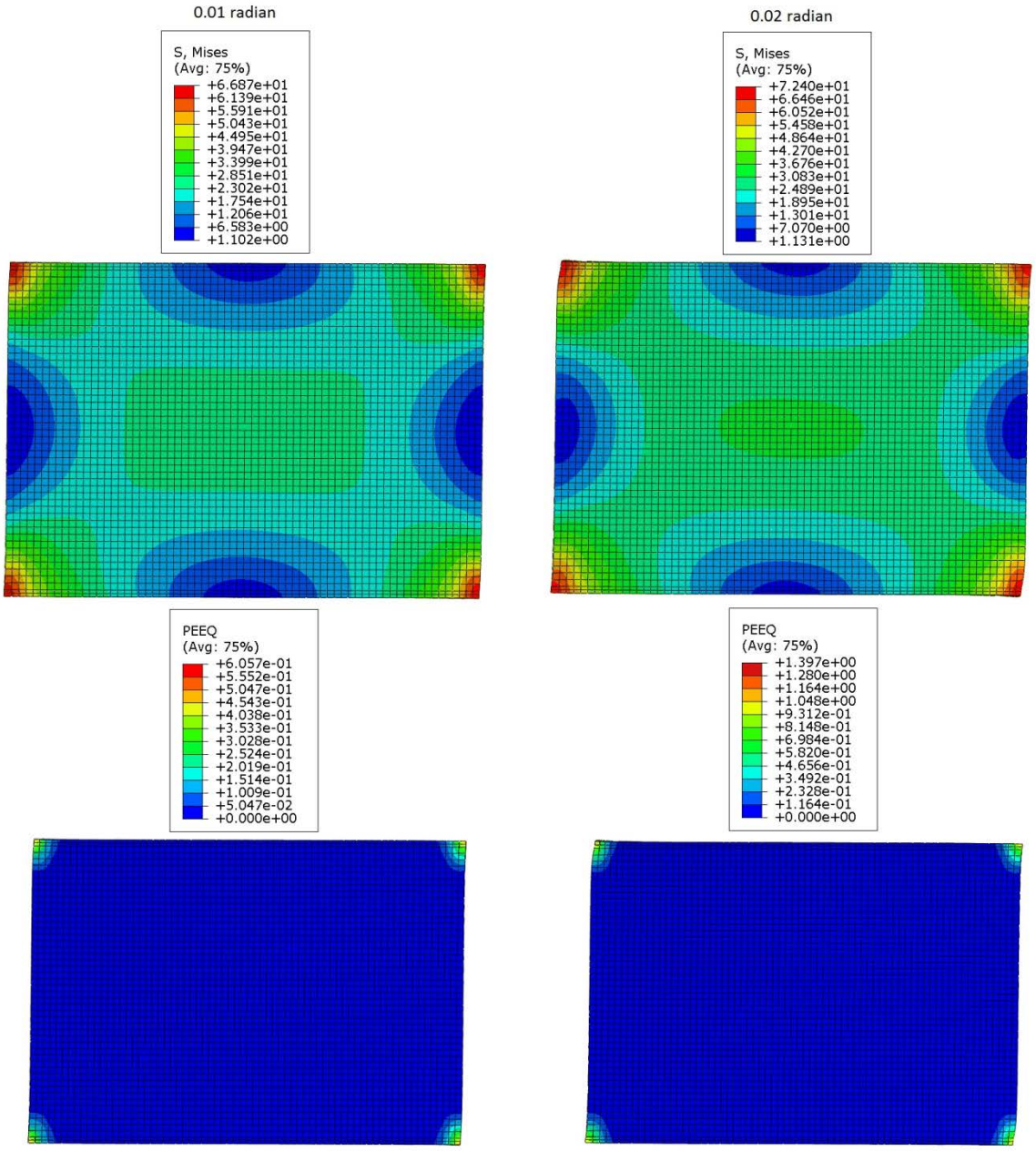

Figure 5.47: VMS and PEEQ in the DP (Case 7B)

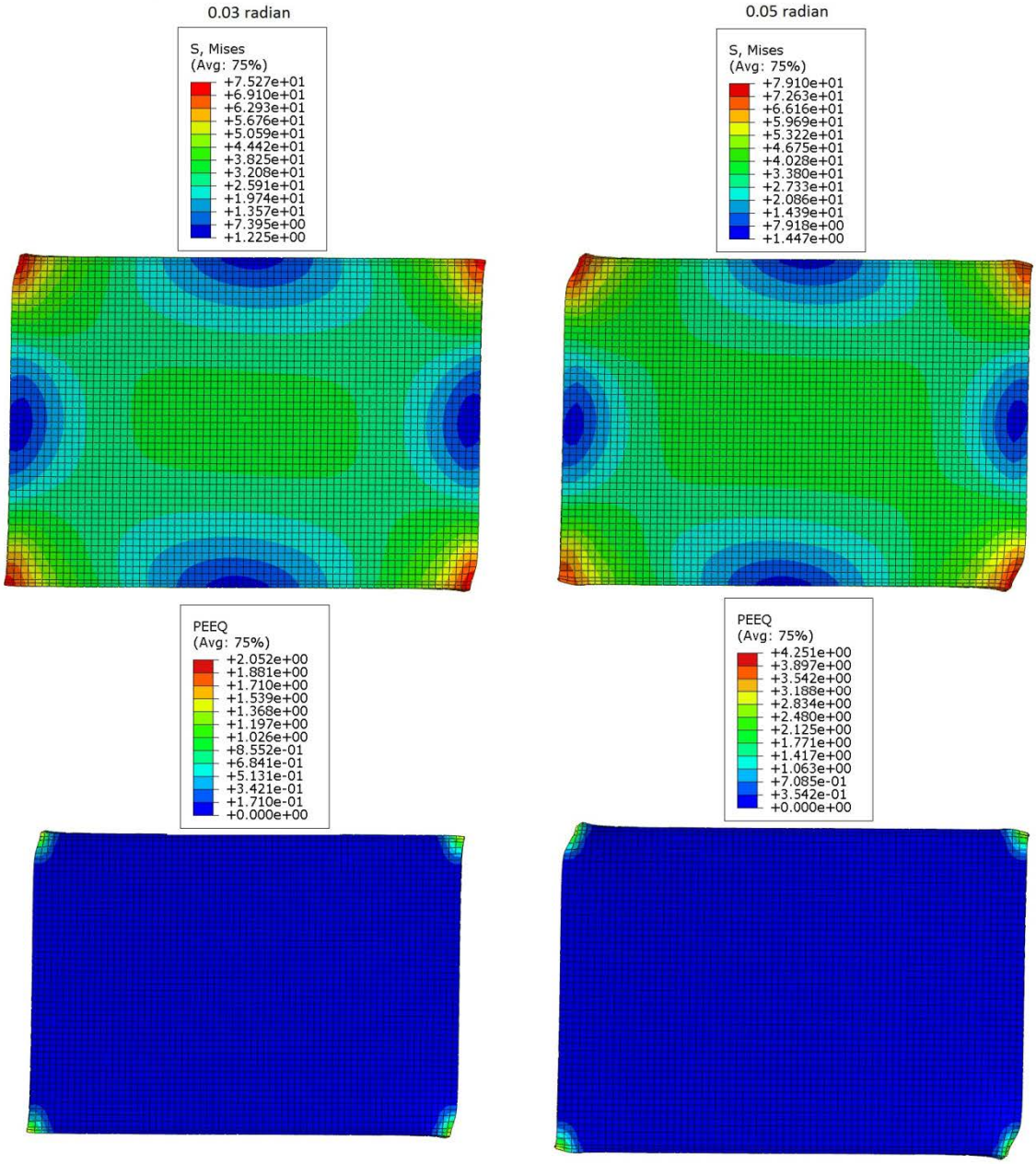

Figure 5.48: VMS and PEEQ in the DP (Case 7B)

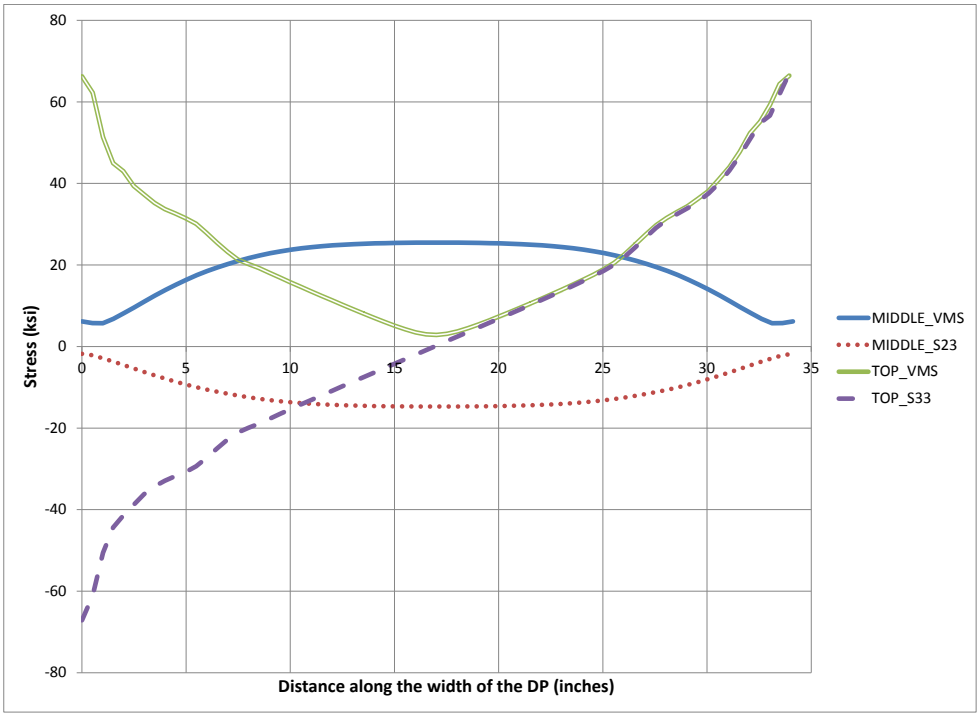

Figure 5.49: Stresses along the width of DP at 0.05 radian rotation (Case 7B)

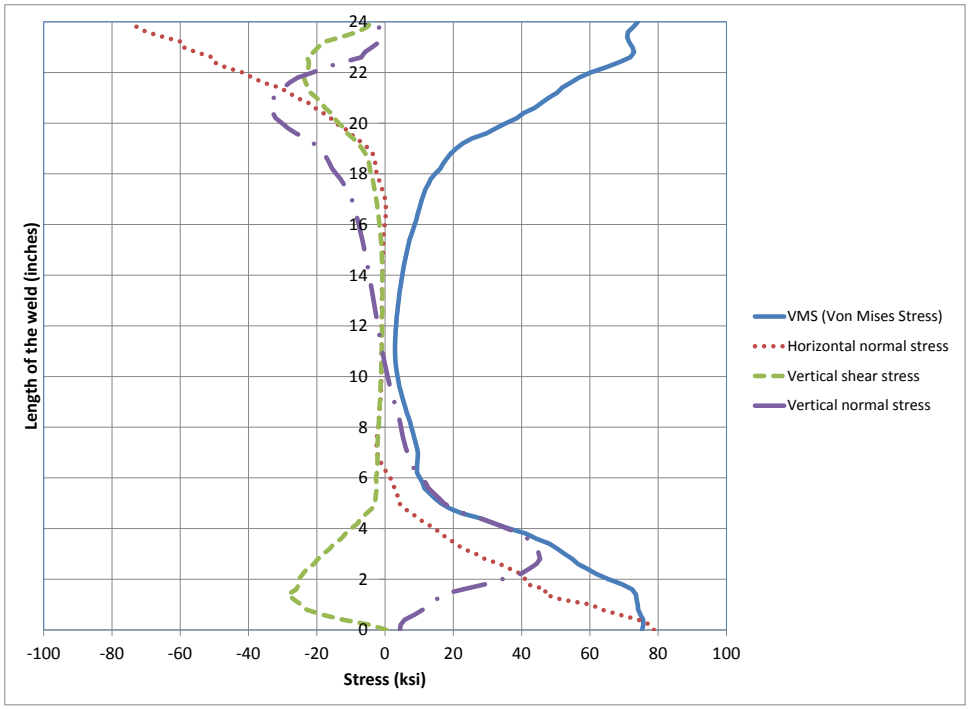

Figure 5.50: Stresses along depth of CJP1 (DP-CJP1 interface) at 0.05 radian (Case 7B)

5.2.9 Analysis case 8B

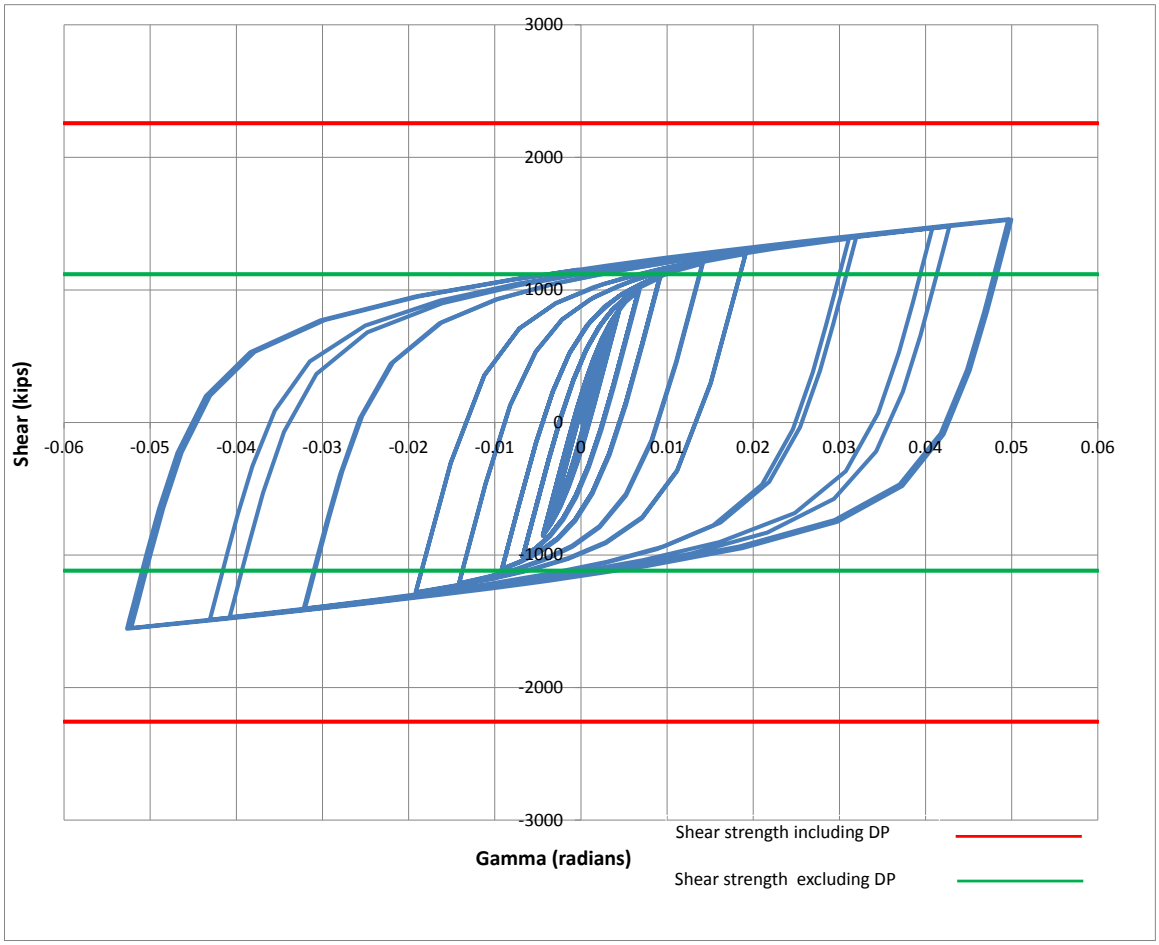

Figure 5.51: Panel zone shear versus rotation (Case 8B)

Table 5.10: Panel zone shear and force on loading plate (Case 8B)

Panel zone rotation (rad)	0.01	0.02	0.03	0.05
Panel zone shear (kips)	1105.17	1278.04	1399.95	1533.18
Force on one Loading plate (kips)	663.10	766.82	839.97	919.91

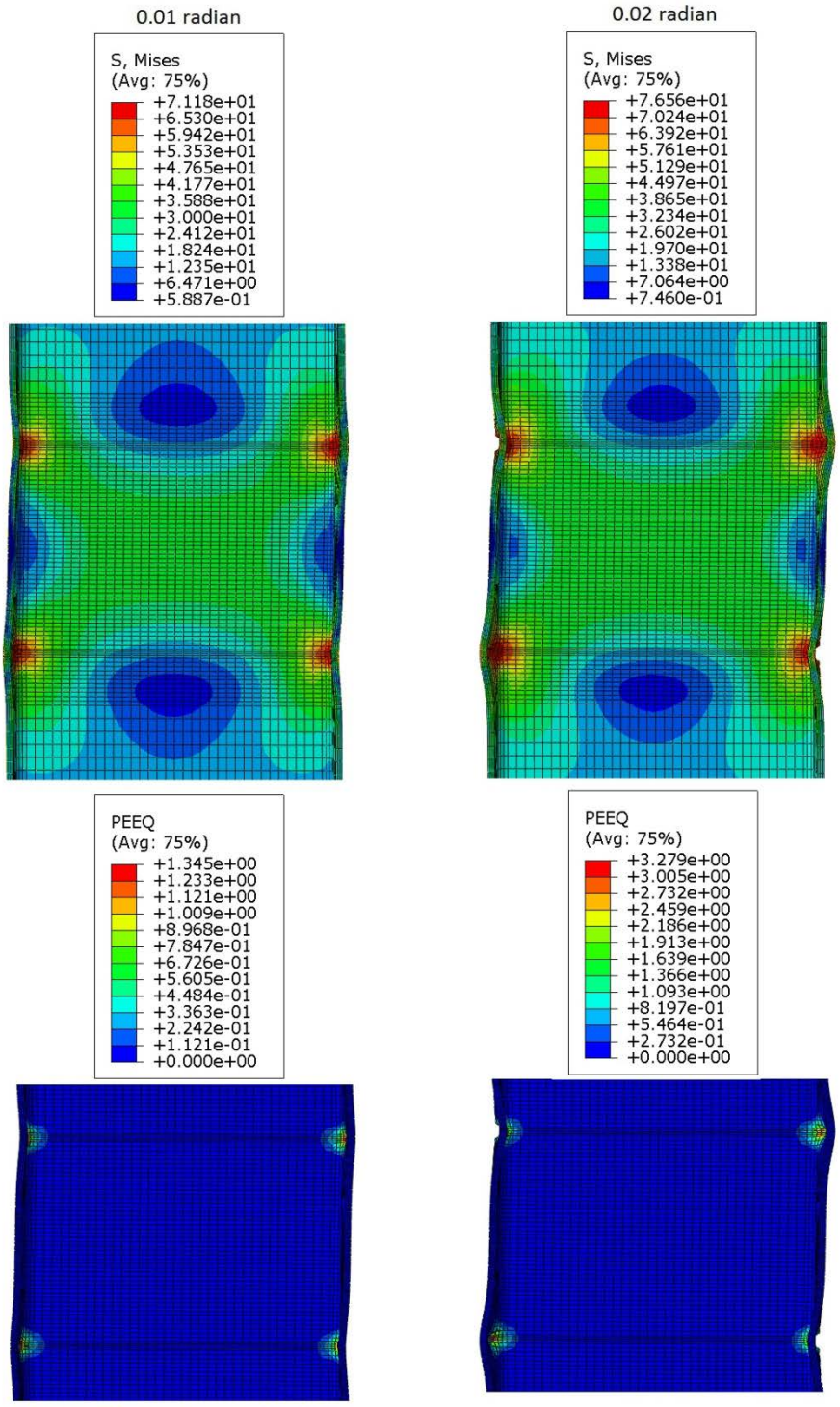

Figure 5.52: VMS and PEEQ in the column (Case 8B)

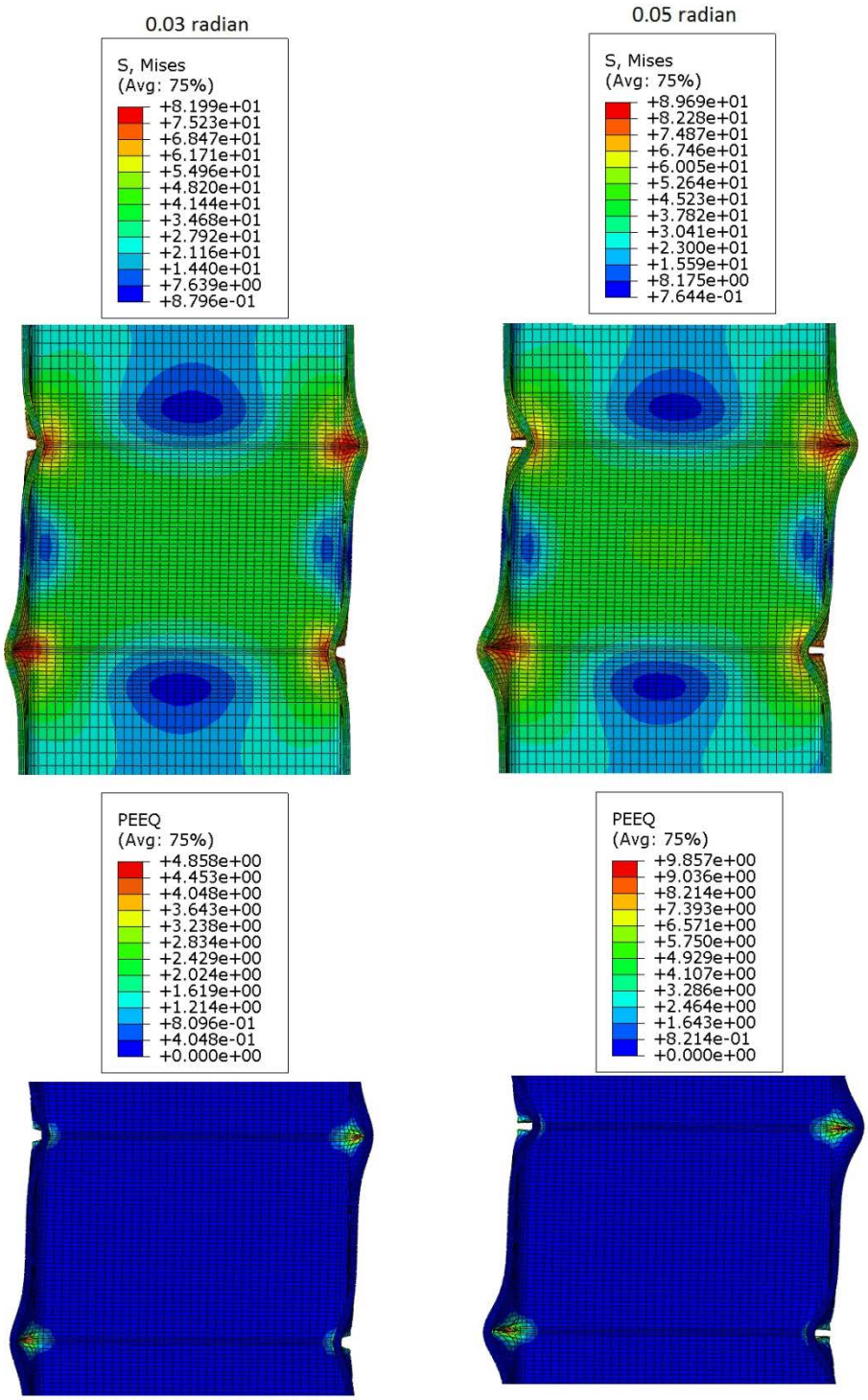

Figure 5.53: VMS and PEEQ in the column (Case 8B)

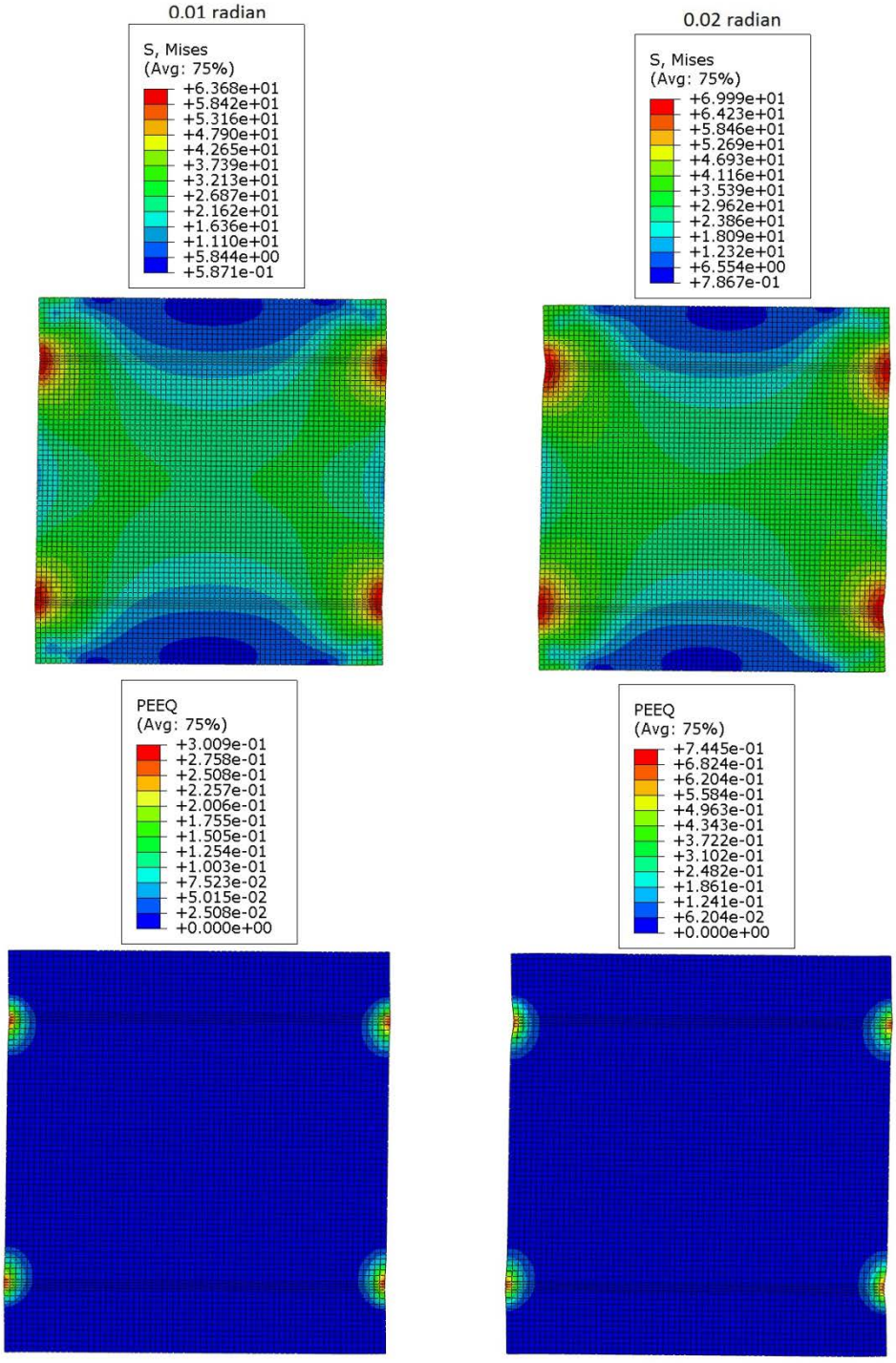

Figure 5.54: VMS and PEEQ in the DP (Case 8B)

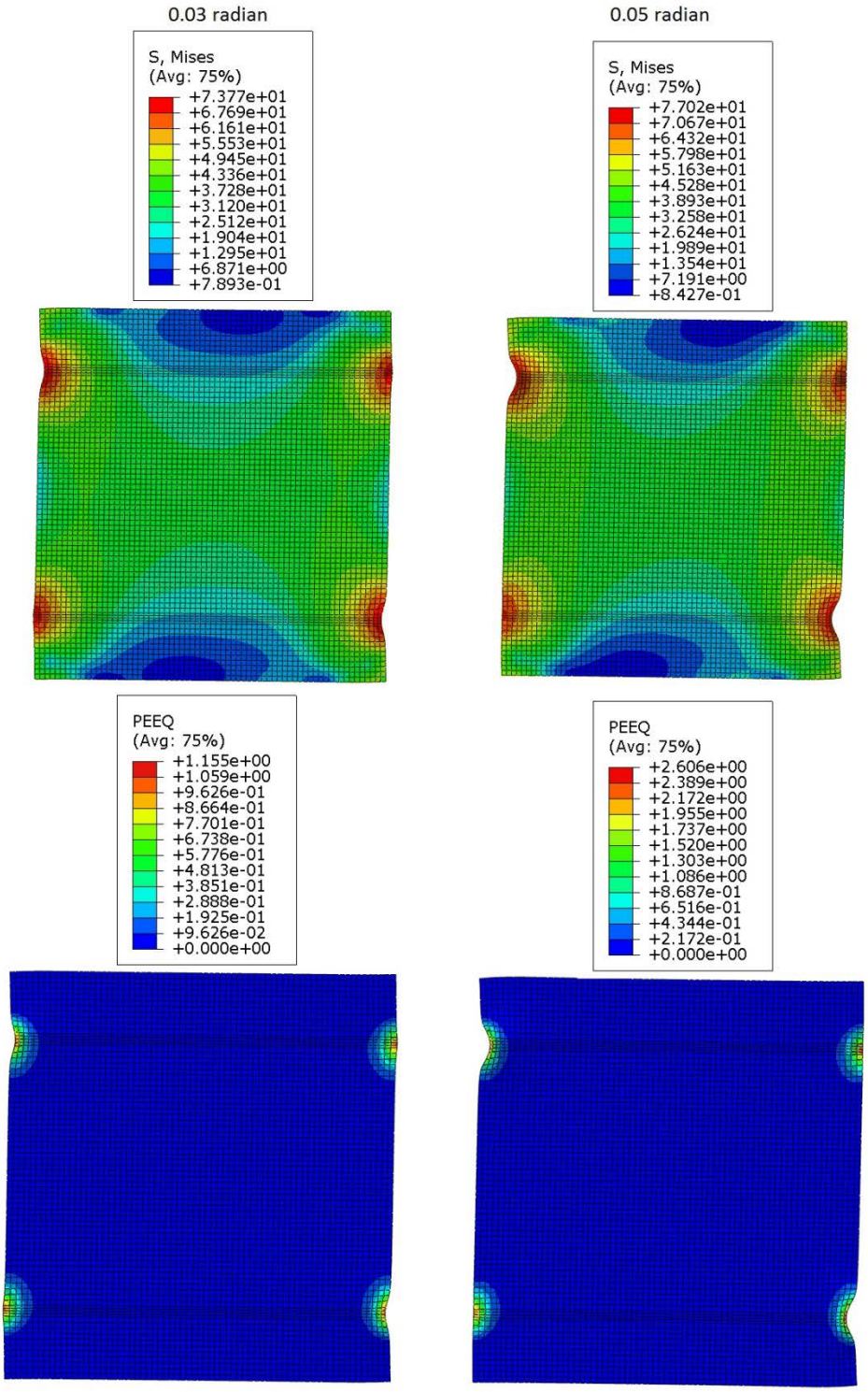

Figure 5.55: VMS and PEEQ in the DP (Case 8B)

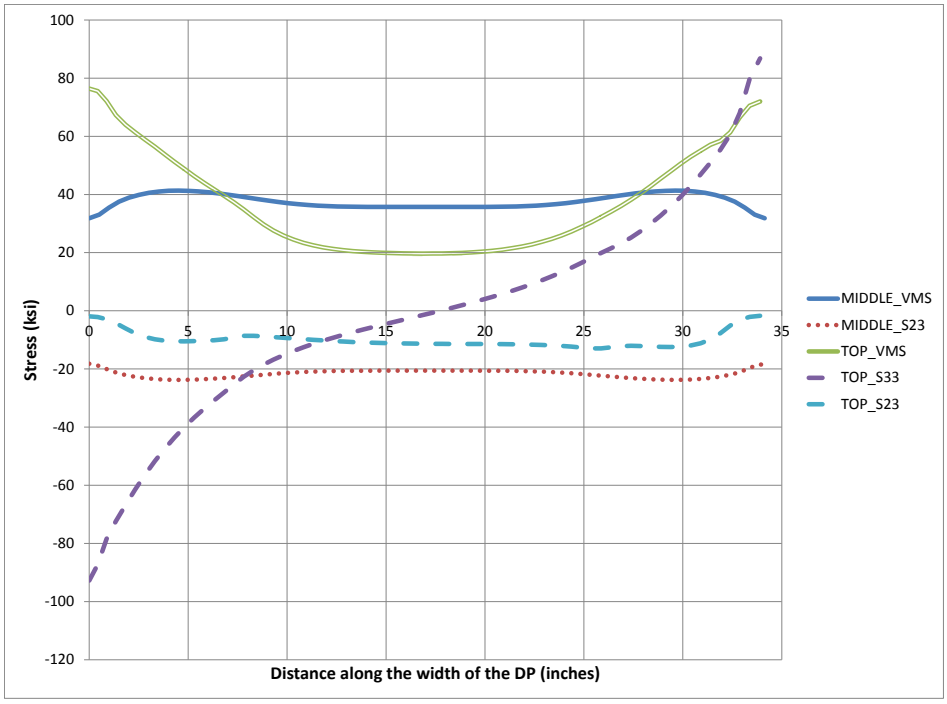

Figure 5.56: Stresses along the width of DP at 0.05 radian rotation (Case 8B)

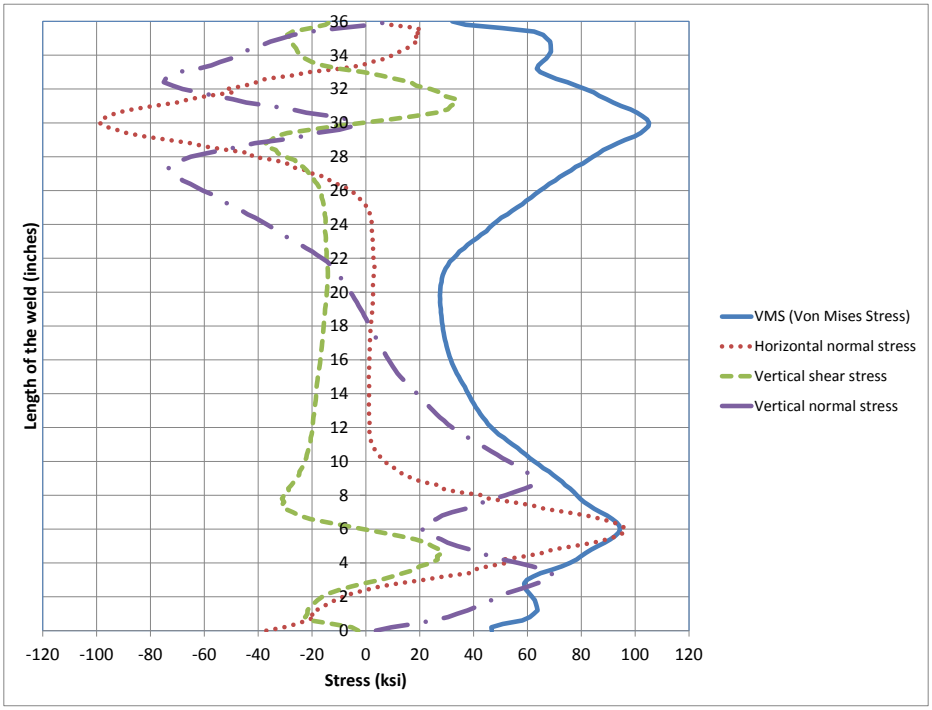

Figure 5.57: Stresses along depth of CJP1 (DP-CJP1 interface) at 0.05 radian (Case 8B)

5.2.10 Analysis case 9B

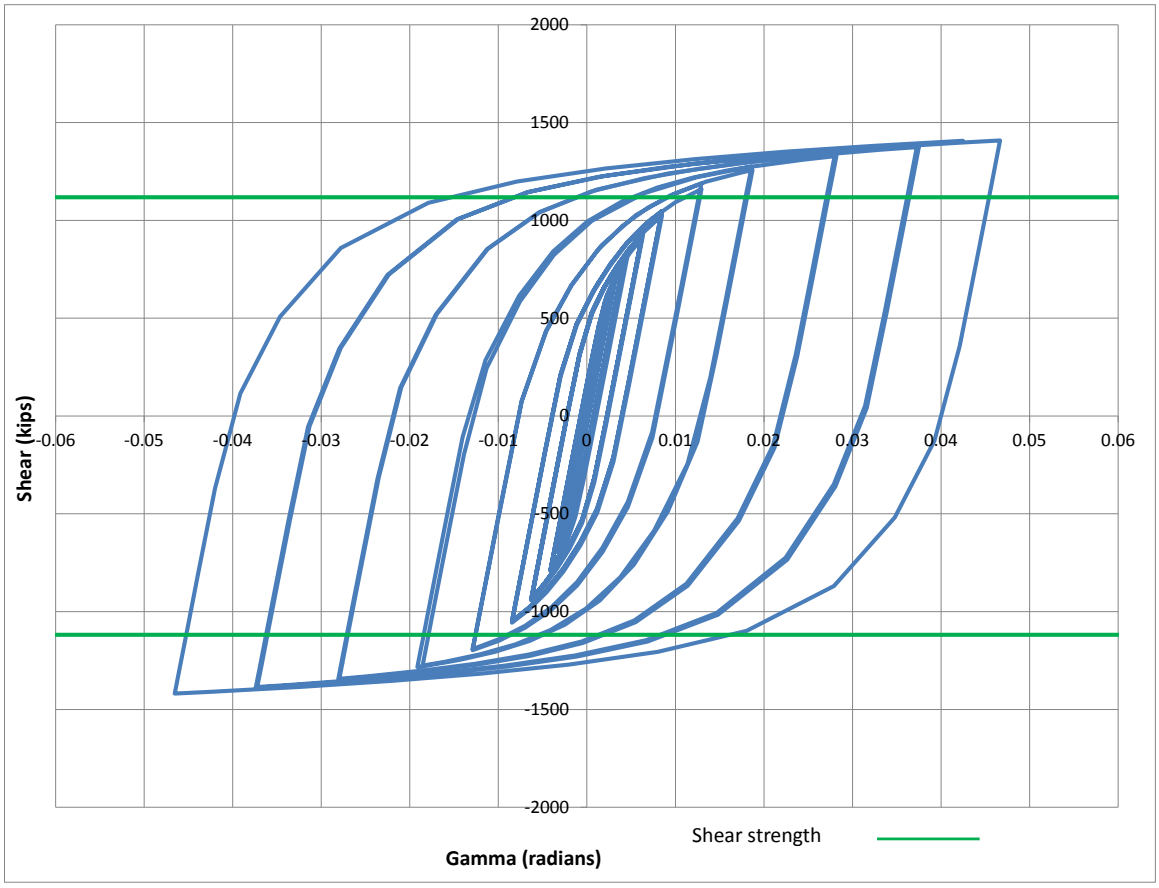

Figure 5.58: Panel zone shear versus rotation (Case 9B)

Table 5.11: Panel zone shear and force on loading plate (Case 9B)

Panel zone rotation (rad)	0.01	0.02	0.03	0.05
Panel zone shear (kips)	1048.21	1275.61	1341.41	1416.13
Force on one Loading plate (kips)	628.93	765.36	804.84	849.68

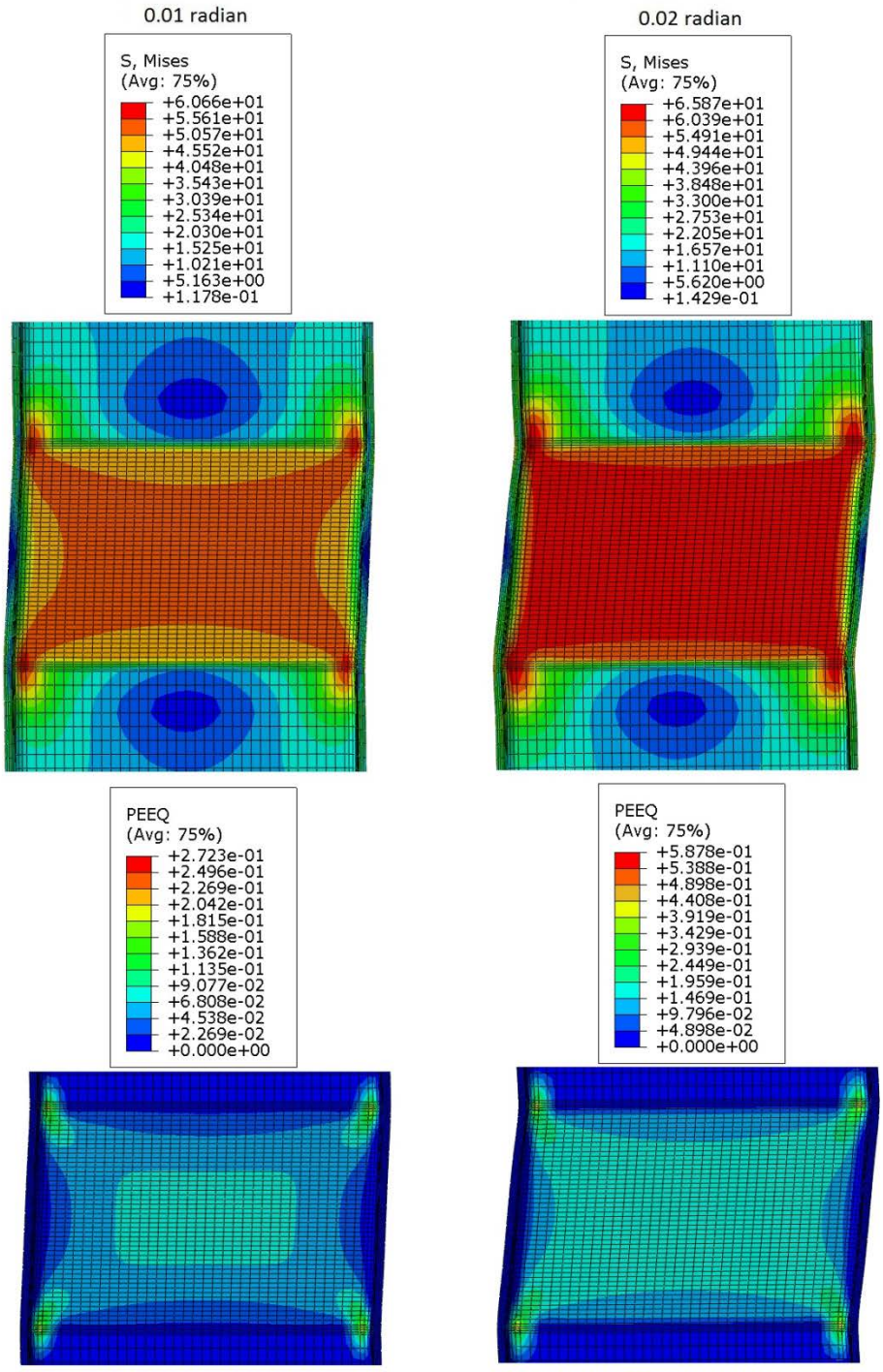

Figure 5.59: VMS and PEEQ in the column (Case 9B)

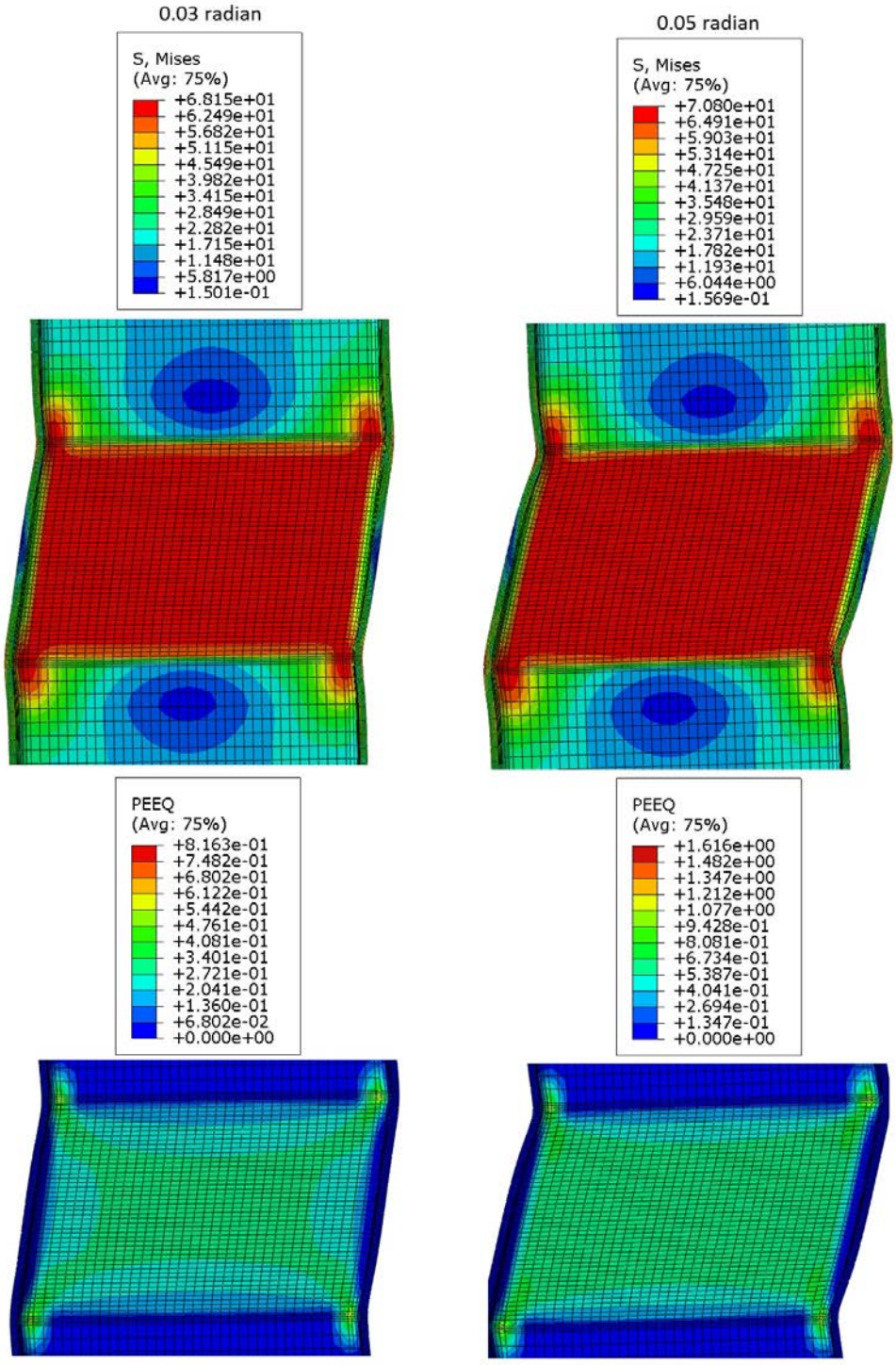

Figure 5.60: VMS and PEEQ in the column (Case 9B)

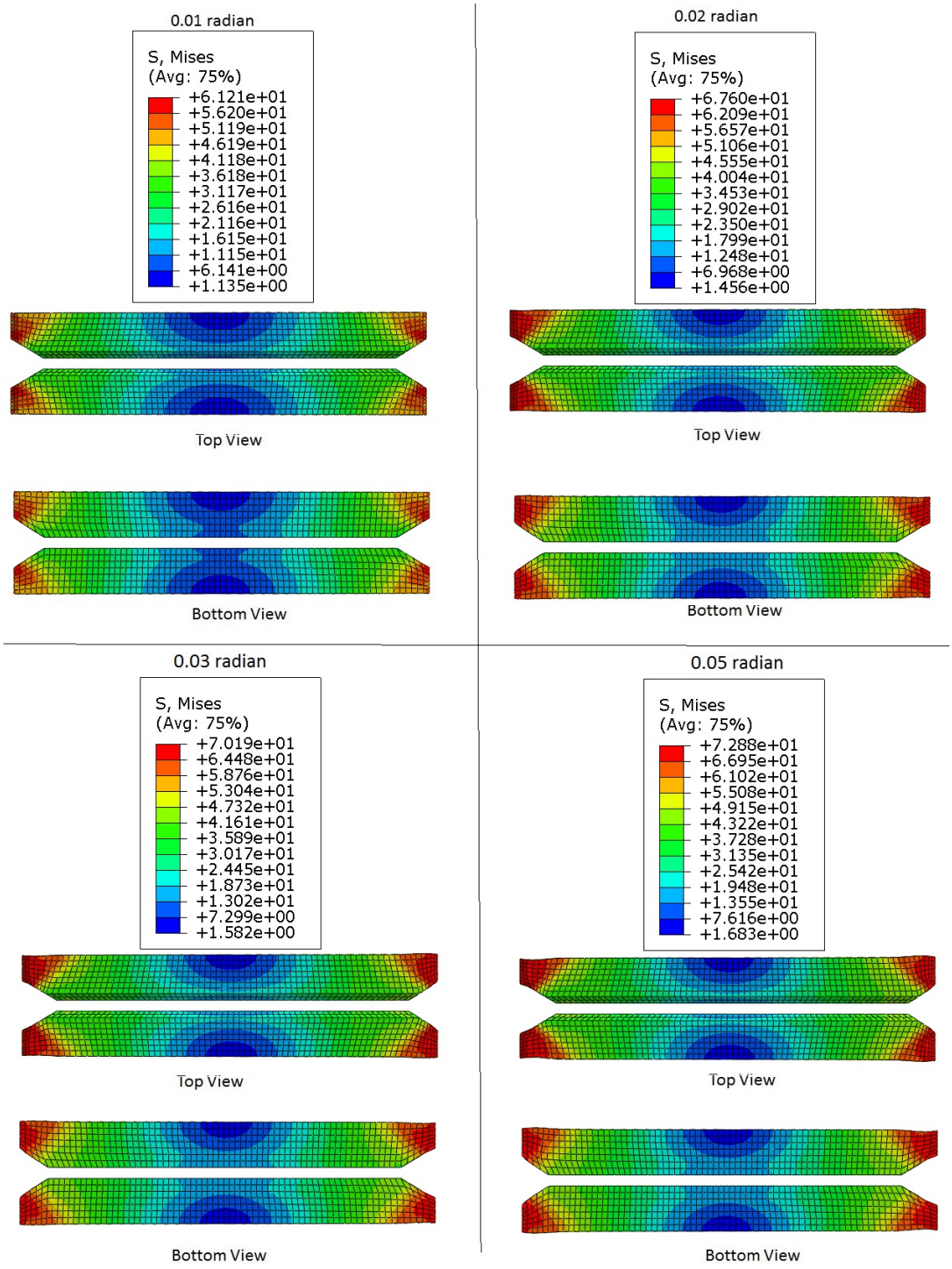

Figure 5.61: VMS in the CP at different rotations (Case 9B)

5.2.11 Analysis case 10B

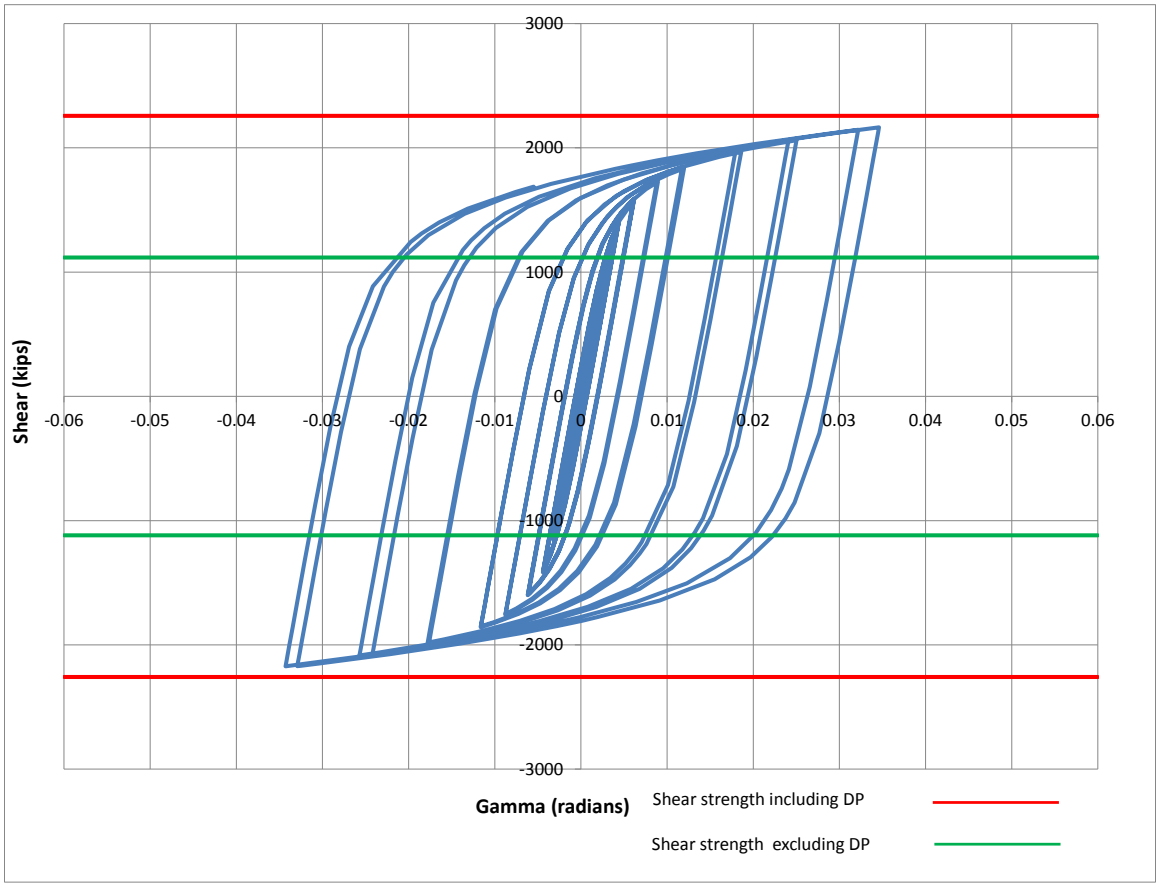

Figure 5.62: Panel zone shear versus rotation (Case 10B)

Table 5.12: Panel zone shear and force on loading plate (Case 10B)

Panel zone rotation (rad)	0.01	0.02	0.03	0.05
Panel zone shear (kips)	1590.89	1846.77	1975.44	2145.93
Force on one Loading plate (kips)	954.53	1108.06	1185.26	1287.56

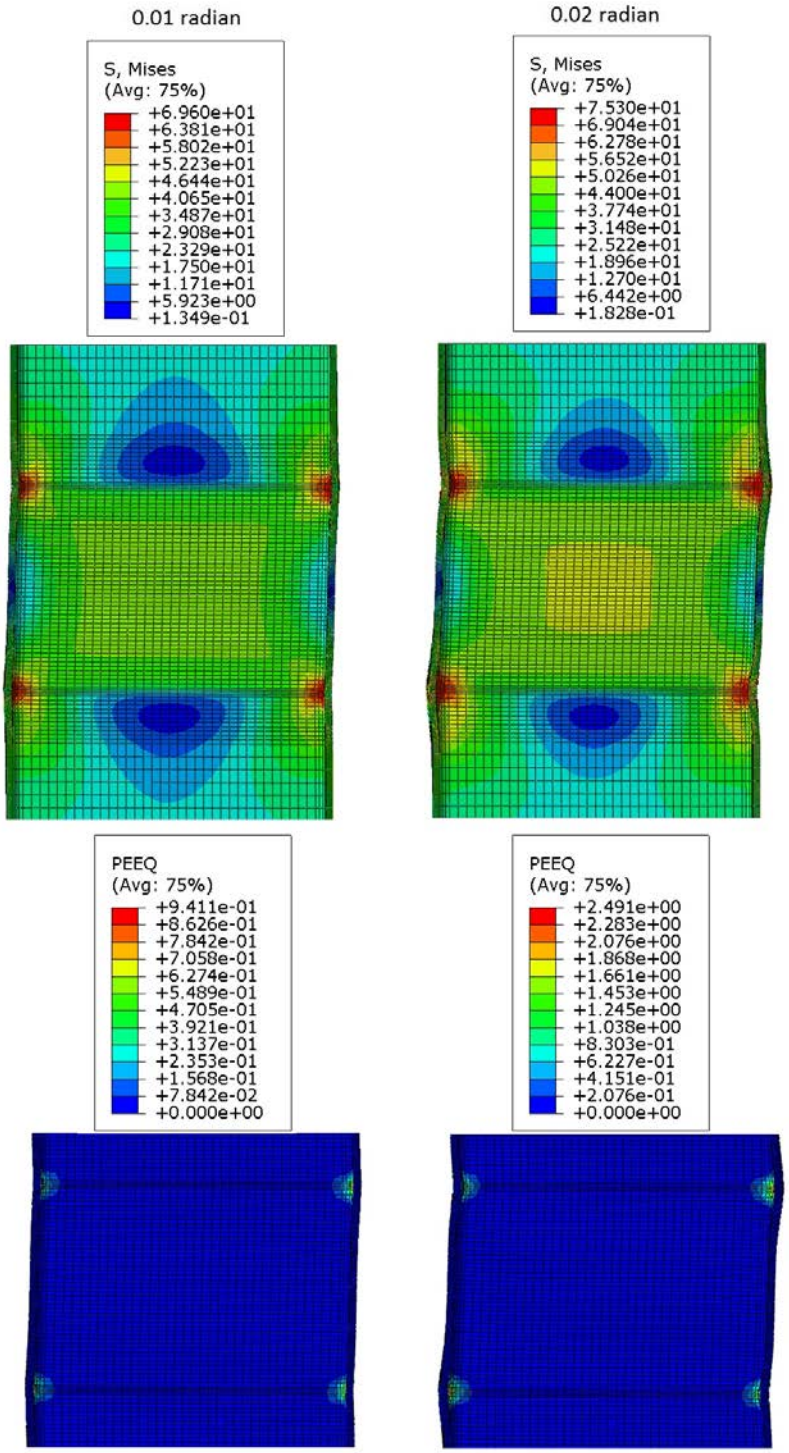

Figure 5.63: VMS and PEEQ in the column (Case 10B)

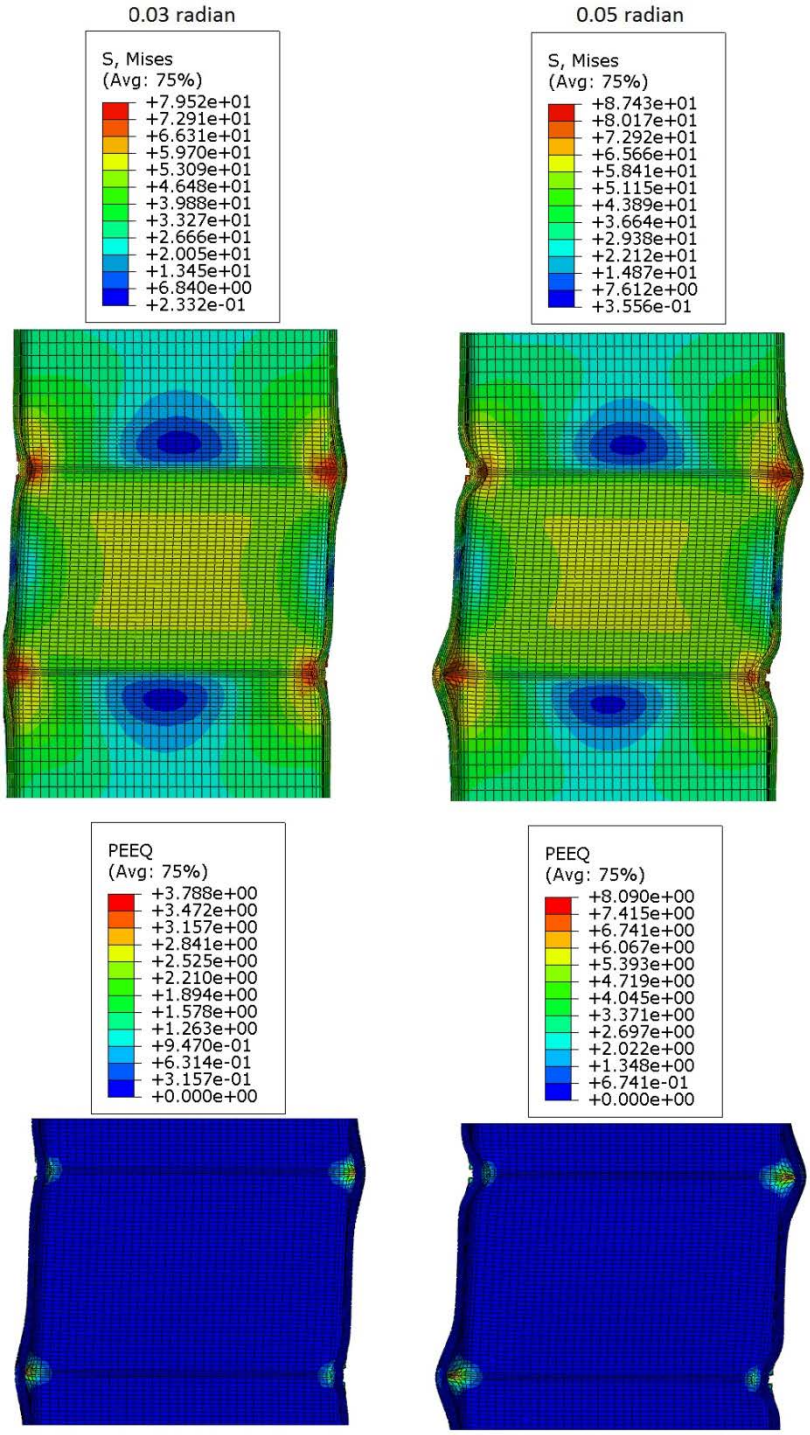

Figure 5.64: VMS and PEEQ in the column (Case 10B)

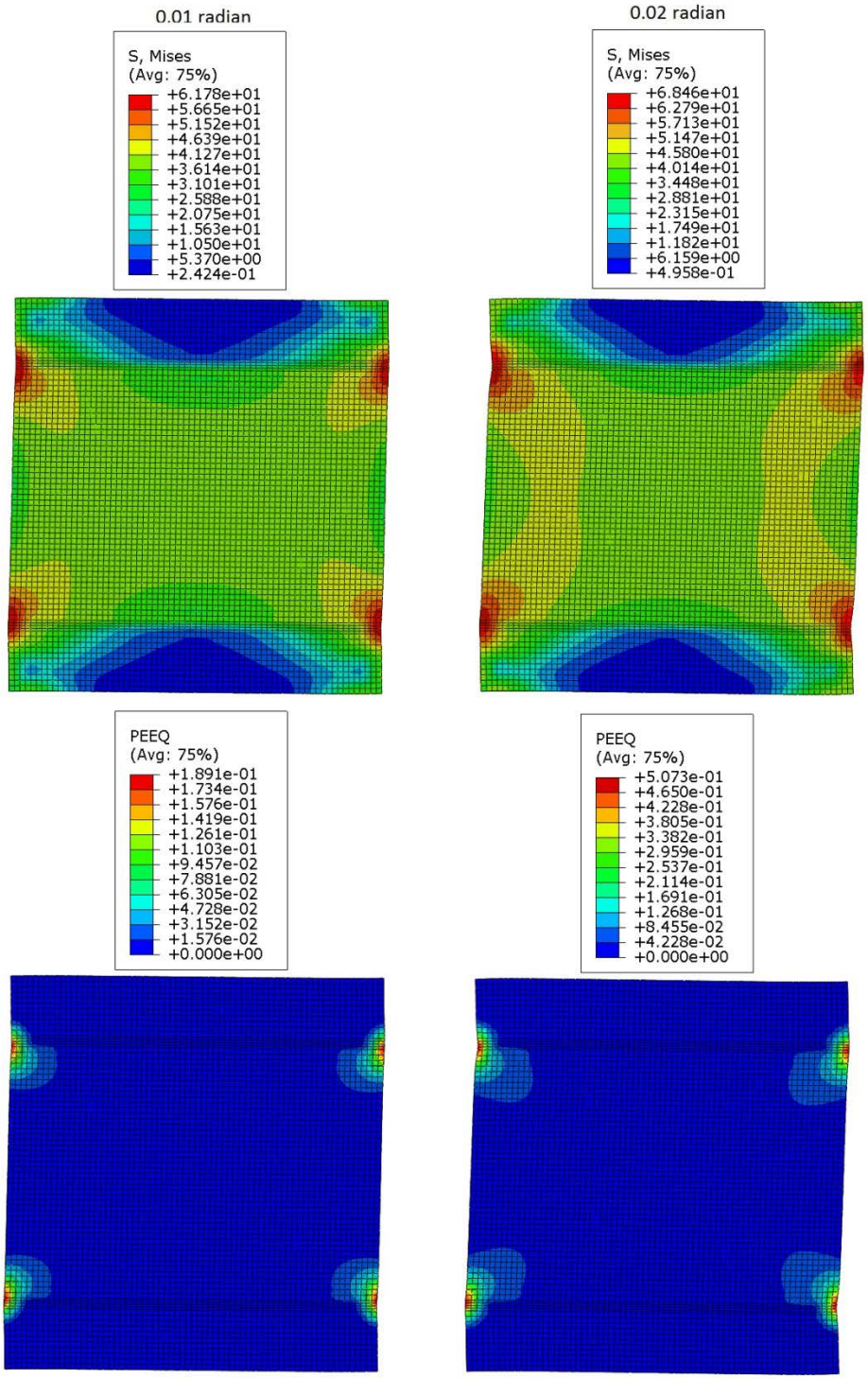

Figure 5.65: VMS and PEEQ in the DP (Case 10B)

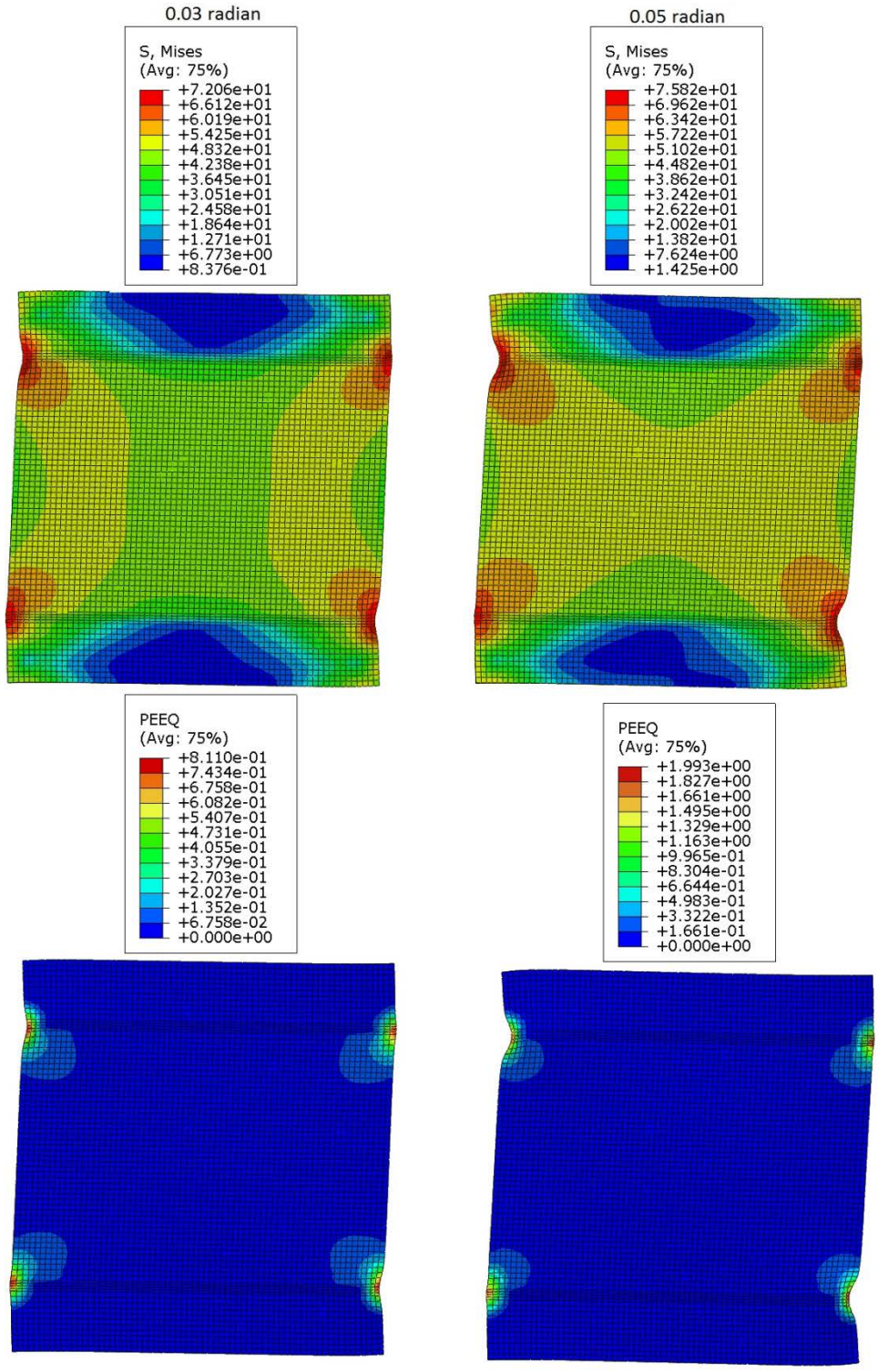

Figure 5.66: VMS and PEEQ in the DP (Case 10B)

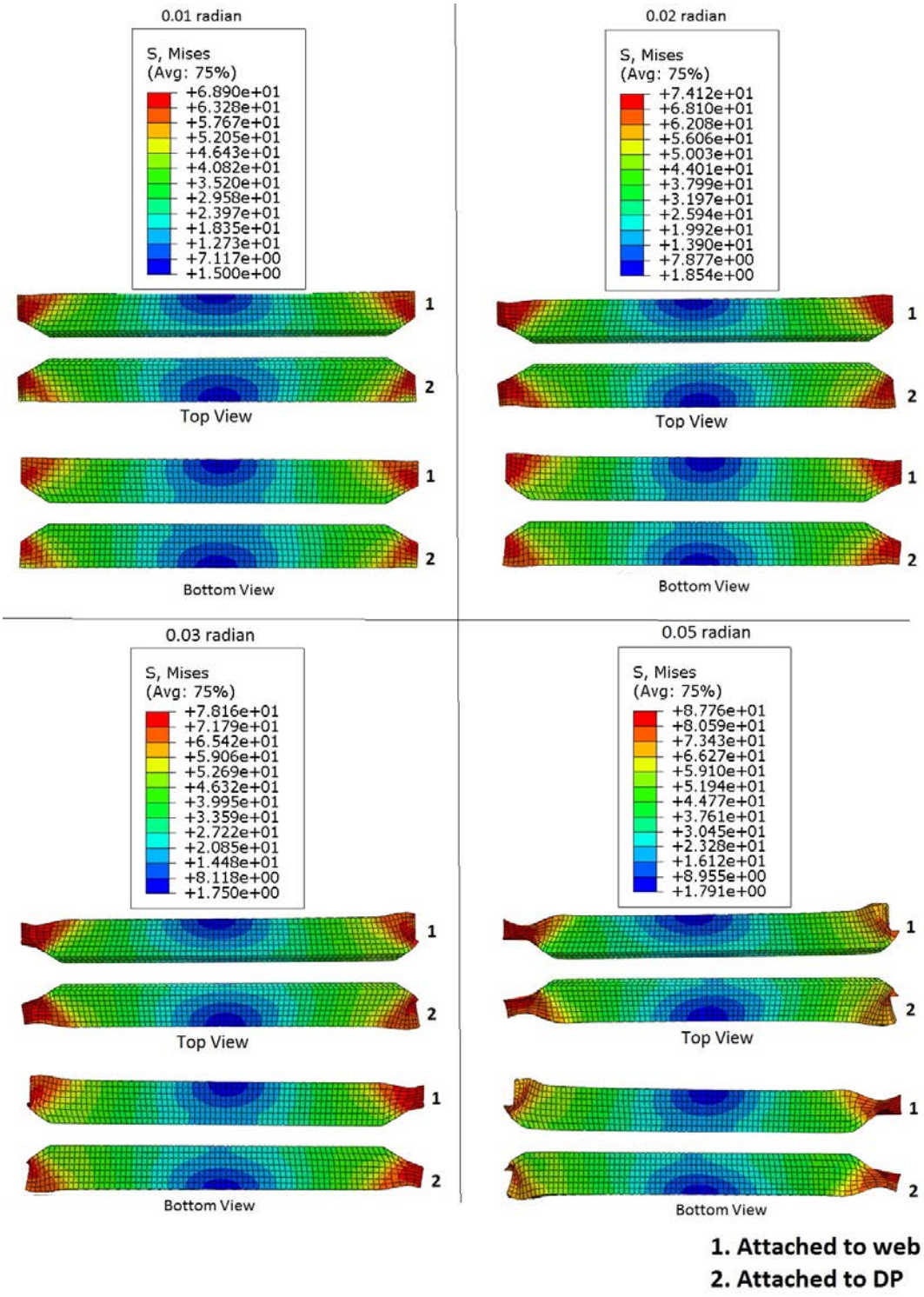

Figure 5.67: VMS in the CP at different radian rotation (Case 10B)

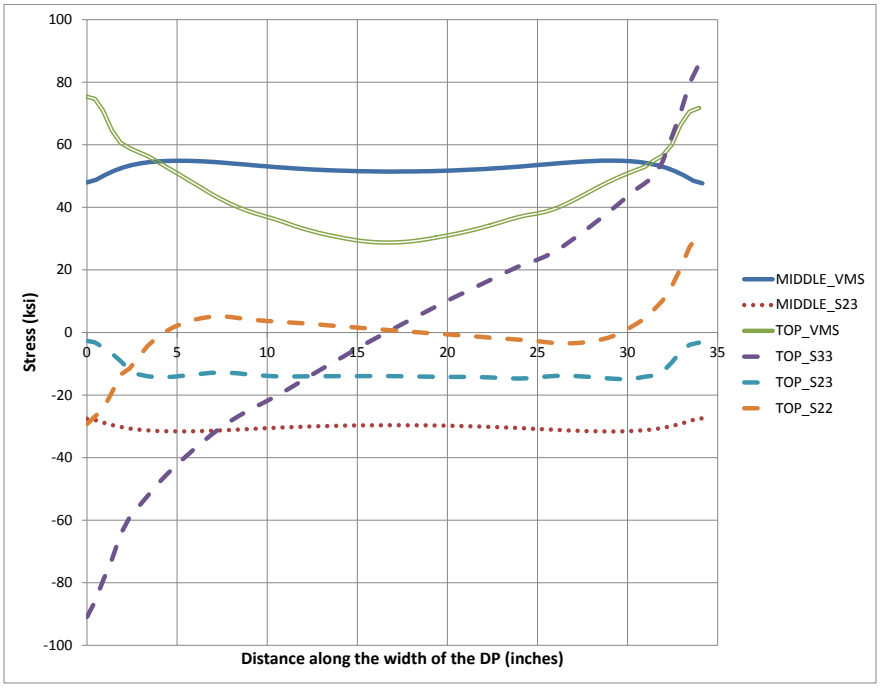

Figure 5.68: Stresses along the width of DP at 0.05 radian rotation (Case 10B)

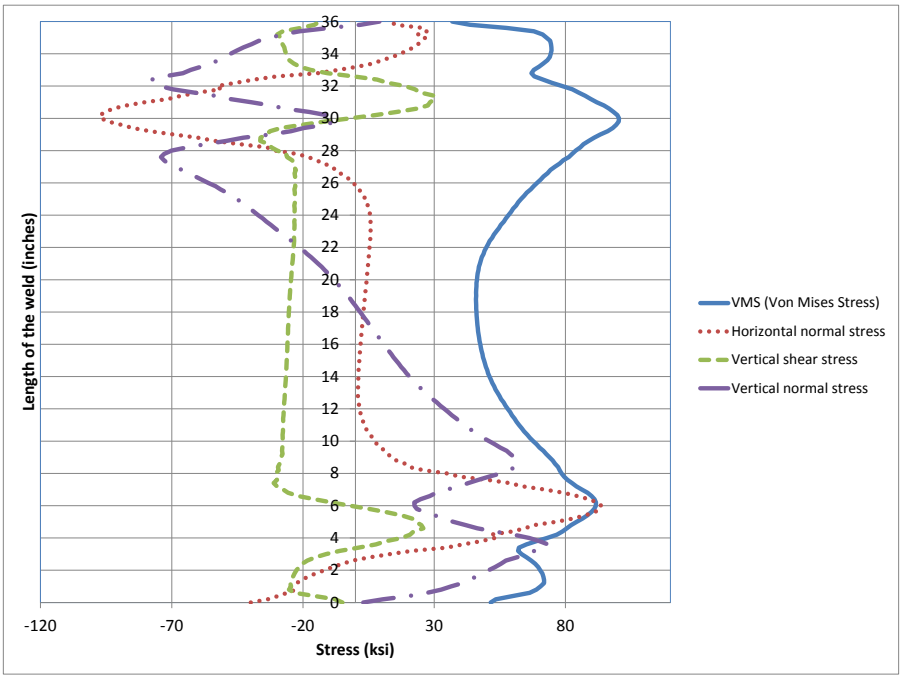

Figure 5.69: Stresses along depth of CJP1 (DP-CJP1 interface) at 0.05 radian (Case 10B)

5.3 PANEL ZONE SHEAR STRENGTH

A comparative study of the panel zone shear strength developed in the deep column (W40x264) is made in this section. The shear in the panel zone may be altered by the presence of the DP and CP's in the assembly. To investigate their contribution, the panel zone shear versus rotation is plotted for case 1B-5B and 6B-10B in Figure 5.70 and 5.71 respectively. The figures only show the last cycle of 0.05 radian in each case. The panel zone shear strength, as defined by the AISC Specification was achieved only in cases 1B, 4B, 5B and 9B. In other cases (2B, 3B, 6B, 7B, 8B and 10B), local limit states like flange local bending and web/DP crippling were dominant.

An increase in strength of the panel zone was noticed when CP's were introduced between the flanges of the deep column. The amounts of increase were: (a) 6 % (94 kips, case 1B and 4B) (b) 27 % (304 kips, case 6B and 9B) (c) 15 % (359 kips, case 3B and 5B) and (d) 40 % (613 kips, case 8B and 10B). The cases with the largest increase in strength correspond with the cases of the most severe localized flange bending in the column when CP's were not provided.

There was an increase in the strength of the panel zone when the DP is extended 6 inches beyond the LP level as compared to cases where the DP is terminated at the LP level. The amounts of increase were: (a) 18 % (380 kips, case 2B and 3B) and (b) 12 % (167 kips, case 7B and 8B). There was an increase in the strength of the panel zone (196 kips, 10 %) when the DP was welded on all 4 sides compared to when the DP had only vertical CJP welds (case 2B and 2B_f). The extension of the DP or welding the DP on all 4 sides in deeper columns increases the panel zone strength because it stiffens the DP/web against crippling/buckling in the out-of-plane direction.

The attachment of the DP to the column web did not increase the shear strength of the panel zone proportional to the total thickness of web and DP (case 1B and 2B, case

6B and 7B). This was due to the fact that localized flange bending or web/DP crippling initiated in the column before the reaching the shear strength limit.

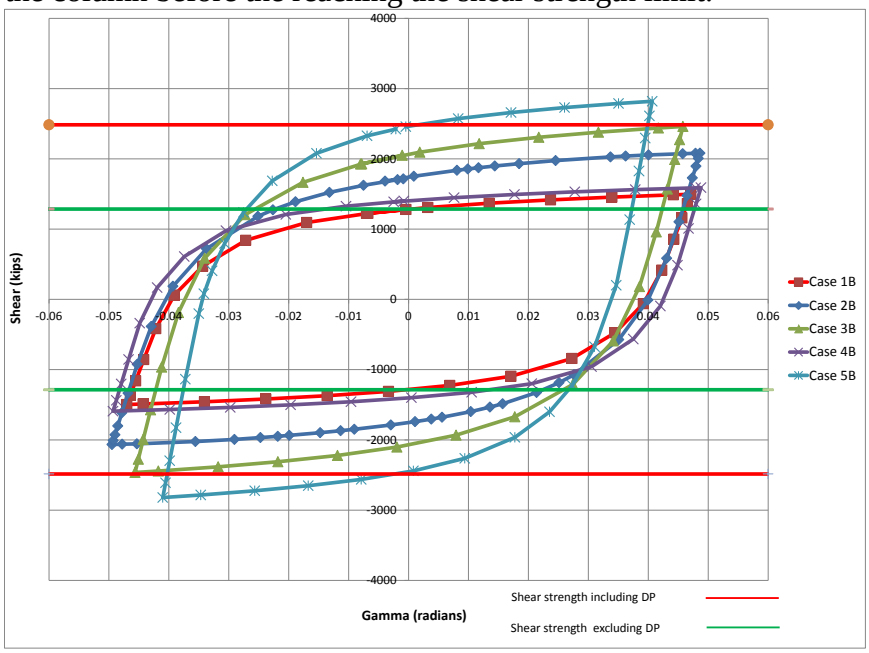

Figure 5.70: Panel zone shear comparison (Case 1B – 5B)

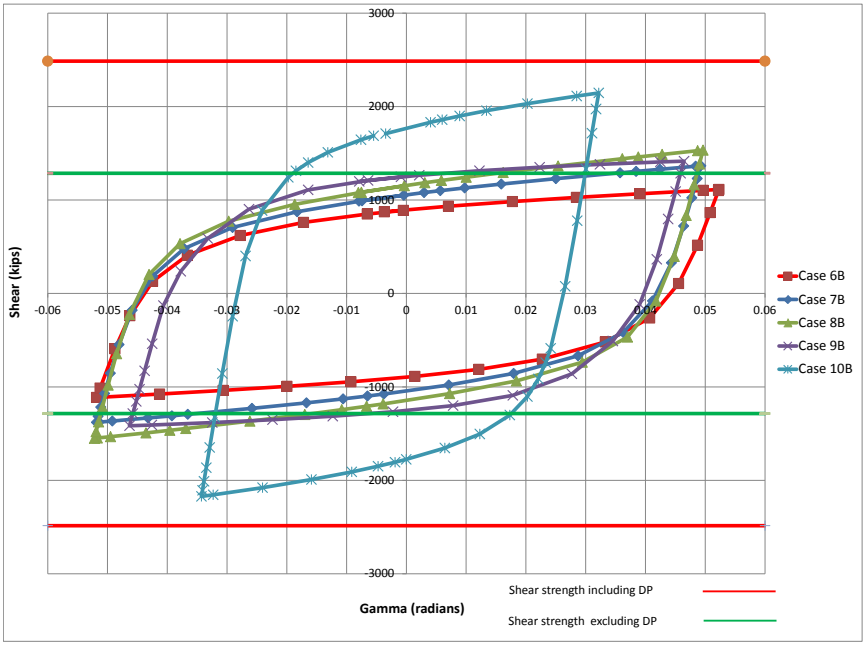

Figure 5.71: Panel zone shear comparison (Case 6B – 10B)

The strength for the different limit states are calculated according to the relevant equations provided in *Specification for Steel Structural Buildings* (AISC 2010a). A yield stress of 50 ksi is considered to evaluate the strength (See section 3.3.5).

The nominal shear strength is calculated using Eq. J10-11:

$$R_n = 0.6\, F_y d_c t_p \left(1 + \frac{3 b_{cf} t_f^2}{d_b d_c t_p}\right) \qquad (Eq. 5.1)$$

The nominal localized flange bending strength is calculated using Eq. J10-1:

$$R_n = 6.25\, F_y t_f^2$$

The nominal web crippling strength is calculated using Eq. J10-4:

$$R_n = 0.8\, t_w^2 \left[1 + 3\left(\frac{l_b}{d_c}\right)\left(\frac{t_w}{t_f}\right)^{1.5}\right] \sqrt{\frac{E F_y t_f}{t_w}} \qquad (Eq. 5.2)$$

The nominal DP crippling strength is calculated using Eq. J10-5a:

$$R_n = 0.4\, t_{dp}^2 \left[1 + 3\left(\frac{l_b}{d_c}\right)\left(\frac{t_{dp}}{t_f}\right)^{1.5}\right] \sqrt{\frac{E F_y t_f}{t_{dp}}} \qquad (Eq. 5.3)$$

The nominal web local yielding strength is calculated using Eq. J10-2:

$$R_n = F_y t_w (5k + l_b) \qquad (Eq. 5.4)$$

Where,

F_y: Minimum specified yield stress of column web (ksi)

E : Young modulus (ksi)

d_c: Column depth (in)

d_b: Beam depth (Center to center distance between LP's) (in)

t_f: Thickness of the column flange (in)

t_p: Combined thickness of column web and DP (in)

b_{cf}: Width of the column flange (in)

t_w: Thickness of column web (in)

t_{dp}: Thickness of DP (in)

l_b: Length of bearing (in)

k: Distance from the outer face of the flange to the web toe of the fillet (in)

Table 5.13: Limit states for the W40X264 column

Case	Panel zone nominal shear strength (kips)	Flange bending nominal strength (kips)	Web crippling nominal strength (kips)	DP crippling nominal strength (kips)	Local web yielding nominal strength (kips)	Load on LP/web/DP at 0.05 radian (kips)
1B	1288	957	1235	-	768	898 / 898 / -
2B	2488	957	1235	657	768	1248 / 611 / 637
2B _f	2488	957	1235	657	768	1366 / 669 /697
3B	2488	957	1235	657	768	1476 / 723 / 753
4B	1288	957	1235	-	768	954 / 654 / -
5B	2488	957	1235	657	768	1691 / 828 / 863
6B	1119	175	874	-	528	667 / 667 / -
7B	2259	175	874	467	528	819 / 401 / 418
8B	2259	175	874	467	528	919 / 450 / 469
9B	1119	175	874	-	528	849 / 849 / -
10B	2259	175	874	467	528	1287 / 630 / 657

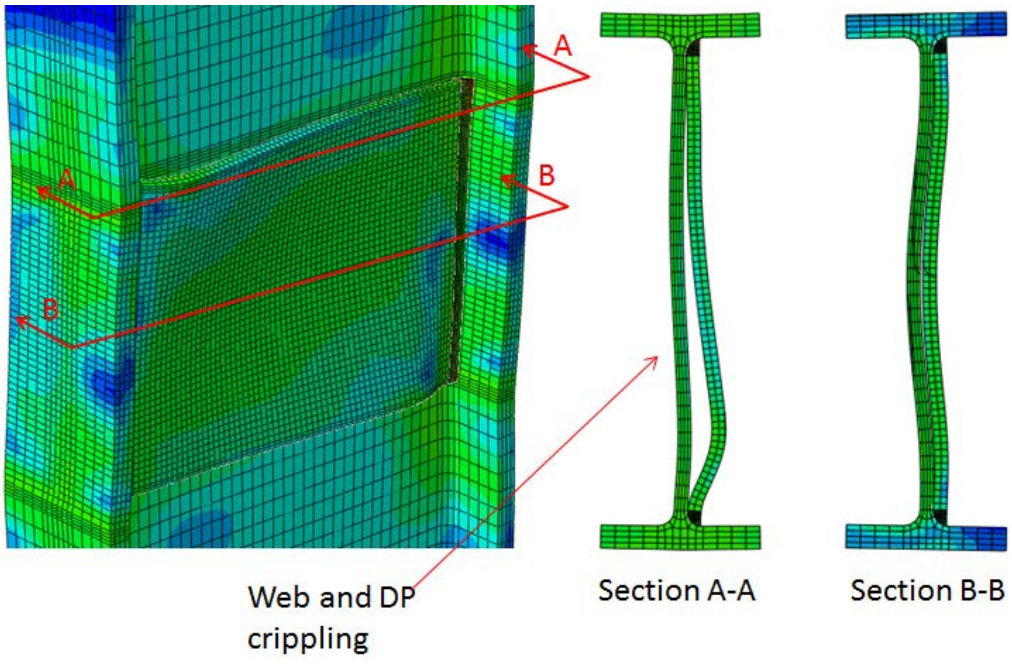

Figure 5.72: Web/DP crippling in case 2B (Deformation scale of 1).

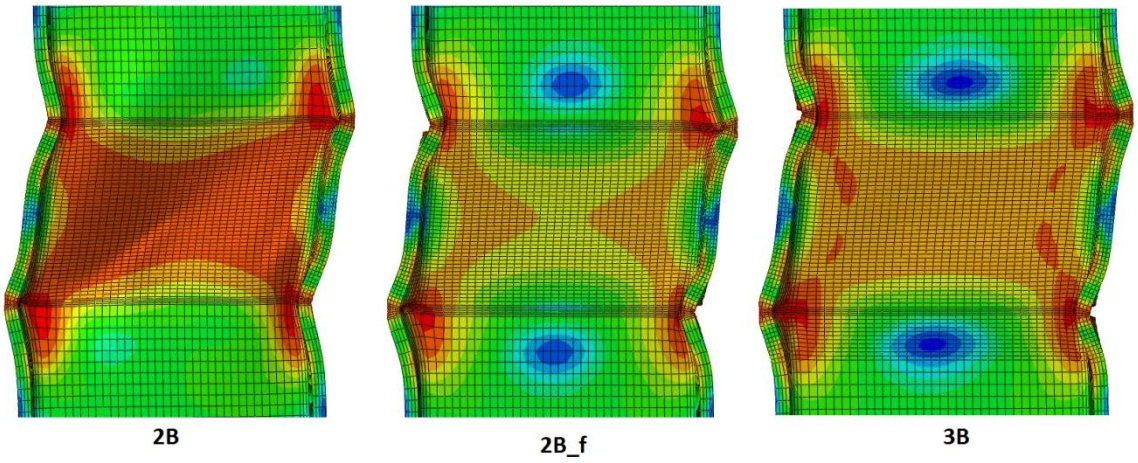

Figure 5.73: Localized flange bending in case 2B, 2B_f and 3B (Deformation scale of 5).

The strengths for different limit states and the load on one LP for each case are tabulated in Table 5.13. The quantity R_n for limit states other than shear strength of the panel zone represents the concentrated/tensile loading on one LP. It is assumed that load on one LP gets divided into the web and DP in proportion to their thickness. The load on one LP in case 2B, 2B_f and 3B is greater than the flange bending nominal strength. Therefore, there is localized flange bending in these cases (see Figure 5.73). The localized flange bending is removed by introduction of CP's in case 5B and the limit state for case 5B is shear strength (see Figure 5.70). Similar kind of localized flange bending occur in cases 6B, 7B and 8B as nominal flange bending strength of 175 kips is much lesser than the force on one LP in these cases. So, the nominal strength for flange bending as per Eq. J10-1 in AISC (2010a) matches reasonably well with the observations seen in simulations.

Another interesting observation was made in case 2B. The web shear was not the limiting strength for this case. Instead, its limit was restricted well below the shear limit due to three different localized limit states i.e. crippling of web, crippling of DP and flange bending (see Figure 5.72 and 5.73). The localized flange bending is already

explained in the above paragraph. The load on the DP (637 kips) is of the order of the DP crippling strength (657 kips) from Table 5.13 leading to crippling of the DP in case 2B. The DP crippling can also be seen from section A-A in Figure 5.72. But some observations opposite to that suggested by the limit states in Table 5.13 are seen in case 2B. The load on the web is 611 kips which is well below the web crippling strength of 1235 kips but the crippling of the web can be seen in Figure 5.72. Similarly, in cases 2B_f and 3B, the load on the DP is well above the DP crippling strength but the DP crippling in not evident in the simulations. Thus, some questions may arise over the overall accurateness of Eq. J10-4 and Eq. J10-5a in accurately predicting the web and DP crippling respectively. Moreover, the boundary conditions on the DP like horizontal welding and extension above the LP level may be responsible for the mismatch between the predictions of the AISC (2010a) equations and the simulation findings.

Some other issues and concerns pertaining to the doubler plate attachment details are the basis of some equations provided in the *Provisions for Steel Structural Buildings* (AISC 2010b). Equation E3-7 specifies the required thickness of the DP / web while Eq. E3-8 and Eq. E3-9 control if CP's are required in the column.

Eq. E3-7 in *Provisions for Steel Structural Buildings* (AISC 2010b) says:

The individual thickness, t, of column webs and doubler plates, if used, shall conform to the following requirement:

$$t \geq \frac{(d_z + w_z)}{90}$$

where

$d_z = d - 2\,t_f$ *of the deeper beam at the connection*

t = *thickness of the column web or doubler plate (in)*

w_z = *width of the panel zone between column flanges (in)*

So, the required thickness of the DP is:

$$t_{req} \geq (22 + 34) / 90$$
$$t_{req} \geq 0.622 \text{ inches}$$

The thickness, t, provided in all the cases in the deeper columns is 1 inch. But some amount of buckling of the DP / web is seen in case 2B (see section B-B, Figure 5.72) while there is no buckling of the web or DP evident in other cases. In cases other than case 2B, the extension of the DP or provision of horizontal welds or provision of the CP welded to the DP may be helpful in restricting the buckling of DP / web. So, Eq. E3-7 provides a good judgment on the buckling of DP / web in these simulations (except case 2B) but the boundary conditions for these equations should be more explicitly explained in Provisions.

Eq. E3-8 and E-9 respectively says that:

When the beam flange is welded to the flange of a wide-flange or built-up I –shaped column having a thickness that satisfies Equations E3-8 and E3-9, continuity plates need not be provided:

$$t_{cf} \geq 0.4 \sqrt{1.8\, b_{bf}\, t_{bf}}$$
$$t_{cf} \geq \frac{b_{bf}}{6}$$

where

b_{bf} = *beam flange width (in)*

t_{bf} = *beam flange thickness (in)*

t_{cf} = *column flange thickness (in)*

Accordingly, the required t_{cf} is:

$$t_{cf} \geq 0.4 \sqrt{1.8 \text{ x } (0.75 \text{ x } 11.9) \text{x } 1} \rightarrow t_{cf} \geq 1.60 \text{ inches}$$

$$t_{cf} \geq (0.75 \times 0.90)/6 \rightarrow t_{cf} \geq 1.49 \text{ inches}$$

The thickness of the column flange for cases 1B-5B is 1.75 inches while it is 0.75 for cases 6B-10B. So, as per Eq. E3-8 and E3-9 CP's are not required for cases 2B-3B but the flange bending is evident in case 2B, 2B_f, and 3B (Figure 5.73). Moreover, it is not clear if these equations are applicable for cases having a DP welded to the column web or it is only applicable for columns sections without any DP (case 1B).

5.4 MAXIMUM VON MISES STRESS, PEEQ AND PEMAG

The maximum Von Mises Stresses, PEEQ and PEMAG in the different parts of the panel zone assembly are listed in Table 5.14 – 5.19. These quantities are reported at +0.01 radian (last cycle) and +0.05 radian (last cycle).The quantities at +0.05 radian suggests the structural behavior at target rotation while the quantities at +0.01 radian suggests behavior near first yield of the panel zone shear versus gamma curve. The main observations from these tabulated values (Table 5.14 – 5.19) are as follows:

- The maximum VMS in the column at +0.05 radian are similar in all the cases irrespective of the presence of DP and CP's. This suggests that column ultimately shares the same load though different load paths. Note that these stresses are similar even though different limit states control panel zone strength in different cases. But the maximum PEEQ and PEMAG are much larger in cases where there is localized flange bending (case 2B, 2B_f, 3B, 7B and 8B). The same conclusions can be drawn at +0.01 radian. Maximum stresses are located in the middle depth of the column in cases where web panel zone shear is the limiting strength but maximum stresses are located near the k-area of the column in cases where the localized flange bending or web/DP crippling is the limiting strength (see Figures for VMS in columns in section 5.2).

- The maximum VMS in the DP are similar to those in the column web for each case at 0.05 and 0.01 radian. So, the DP acts as a web in the column but the increase in panel zone shear strength is not proportional to the combined thickness of DP and web of the column due to localized limit states in some cases. The maximum PEEQ and PEMAG in the DP is less than the column in each case. The maximum PEEQ and PEMAG in DP in cases having localized flange bending (case 2B, 2B_f and 3B) is greater than the cases having CP's (case 5B).
- The maximum VMS at 0.05 radian in vertical CJP1 weld reduces by 10-15% when the localized flange bending in some cases are removed by introduction of CP's (case 2B, 2B_f, 3B and 5B).
- The maximum VMS in CJP2 are much greater than in CJP3 at +0.05 radian but they are almost similar at 0.01 radian. The reason behind this may be the high amount of forces flowing through the CJP2 weld in order to resist the localized flange bending in deep columns at 0.05 radian.
- The thickness of the column web is similar to the thickness of the DP. The maximum VMS in the CJP2, CJP3 and CP are similar at front and back sides of the panel zone at 0.01 radian but maximum VMS in CJP2 and CJP3 are slightly different at 0.05 radian. The front side (F) is the side where the CP is welded to the DP while the back side (B) is the side where the CP is welded to the column web.

Table 5.14: Maximum Von Mises stress at 0.05 radian rotation

Case	Column	DB	CJP1	CJP2	CJP3	CP
1B	71.75					
2B	75.87	76.43	131.5			
2B_f	80.61	74.75	167.4	115.40 (horizontal fillet weld)		
3B	76.74	73	133.3			
4B	71.8			126.5	86.77	68.19
5B	73.77	71.7	110.5	299.5 (F)	87.22 (F)	76.88 (F)
				360 (B)	103.5 (B)	77.56 (B)
6B	79.02					
7B	89.38	79.1	202.6			
8B	89.69	77.02	193.8			
9B	70.8			214.2	87.1	72.88
10B	87.43	75.82	177.2	411.7 (F)	97.1 (F)	87.52 (F)
				505.7 (B)	139 (B)	86.5 (B)

Table 5.15: Maximum Von Mises stress at 0.01 radian rotation

Case	Column	DB	CJP1	CJP2	CJP3	CP
1B	60.78					
2B	66.63	65.68	89.54			
2B_f	66.21	62	88.54	79.71 (horizontal fillet weld)		
3B	65.23	60.91	85.17			
4B	57.36			87.28	71.54	56.28
5B	62.73	55.46	81.56	98.21 (F)	64.87 (F)	62.69 (F)
				101.9 (B)	70.39 (B)	63.3 (B)
6B	63.87					
7B	72.09	66.83	102.3			
8B	71.29	63.72	93.86			
9B	60.7			94.46	70.01	61.28
10B	69.64	61.75	89.28	137.5 (F)	67.72 (F)	68.64 (F)
				135.1 (B)	69.01 (B)	67.8 (B)

Table 5.16: Maximum PEEQ at 0.05 radian rotation

Case	Column	DB	CJP1	CJP2	CJP3	CP
1B	1.337					
2B	4.236	3.014	9.059			
2B_f	5.56	2.109	10.44	3.635 (horizontal fillet weld)		
3B	3.638	1.551	6.46			
4B	1.17			6.292	0.8852	0.7104
5B	2.45	1.108	3.792	20.4 (F)	0.5027 (F)	2.962 (F)
				23.67 (B)	2.623 (B)	3.463 (B)
6B	5.089					
7B	11.06	4.251	17.45			
8B	9.857	2.606	13.43			
9B	1.616			14.18	0.9476	1.857
10B	8.09	1.993	10.36	32.4 (F)	0.6124 (F)	6.95 (F)
				32.83 (B)	1.314 (B)	6.599 (B)

Table 5.17: Maximum PEEQ at 0.01 radian rotation

Case	Column	DB	CJP1	CJP2	CJP3	CP
1B	0.2894					
2B	0.7359	0.5726	2.067			
2B_f	0.8431	0.3299	1.917	0.4571 (horizontal fillet weld)		
3B	0.5755	0.2372	1.113			
4B	0.1584			1.81	0.1297	0.1652
5B	0.3873	0.1292	0.5711	3.484 (F)	0.06458 (F)	0.3886 (F)
				4.079 (B)	0.06495 (B)	0.4532 (B)
6B	0.9062					
7B	2.338	0.7636	4.568			
8B	1.715	0.3862	2.707			
9B	0.3366			3.196	0.09218	0.3331
10B	1.21	0.2491	1.665	7.935 (F)	0.1077 (F)	0.9664 (F)
				7.225 (B)	0.07262 (B)	0.8925 (B)

Table 5.18: Maximum PEMAG at 0.05 radian rotation

Case	Column	DB	CJP1	CJP2	CJP3	CP
1B	0.0548					
2B	0.1938	0.1626	0.2799			
2B_f	0.3011	0.1094	0.4744	0.2007 (horizontal fillet weld)		
3B	0.1539	0.07491	0.2885			
4B	0.05526			0.2543	0.00401	0.03153
5B	0.009119	0.0054	0.167	1.191 (F)	0.00515 (F)	0.1538 (F)
				1.536	0.1424	0.175
6B	0.269					
7B	0.6148	0.2017	0.6684			
8B	0.6403	0.1559	0.6128			
9B	0.0537			0.7374	0.04151	0.08298
10B	0.491	0.1312	0.523	1.805 (F)	0.09972 (F)	0.383 (F)
				2.298 (B)	0.3233 (B)	0.3639 (B)

Table 5.19: Maximum PEMAG at 0.01 radian rotation

Case	Column	DB	CJP1	CJP2	CJP3	CP
1B	0.00675					
2B	0.02173	0.01806	0.05436			
2B_f	0.02312	0.008505	0.04906	0.01336 (horizontal fillet weld)		
3B	0.01669	0.007078	0.03127			
4B	0.004436			0.04261	0.00412	0.004108
5B	0.001001	0.00379	0.01489	0.1037 (F)	0.0023 (F)	0.01065 (F)
				0.1247	0.00357	0.01216
6B	0.02571					
7B	0.06608	0.02185	0.1237			
8B	0.05779	0.01379	0.07742			
9B	0.007993			0.08272	0.00357	0.008765
10B	0.04234	0.009127	0.05306	0.3213 (F)	0.00438 (F)	0.03298 (F)
				0.3167 (B)	0.00663 (B)	0.0304 (B)

5.5 FORCE FLOW THROUGH THE CONTINUITY PLATE

The amount of force entering the CP's depends on the flange thickness of the column. In the cases considered, the column flange thickness was progressively decreased to ascertain the load path when CP's are critical elements in the system. The amount of force on one LP in each case has been tabulated in Table 5.2 - 5.12. The force entering each CP is derived using the section forces command as described in section 3.4. The force passing through the CP's is the summation of the forces passing through the front (attached to DP) and back (attached to column web) CP's at a LP location. The percentage of force flow though the CP for each case having CP's is listed in Table 5.20 – 5.23. The major observations from these data are as follows:

- As the column flange thickness decreases, the percentage of force flow through CP's increases which make CP'S an increasingly critical element in columns with thin flanges. The thinner flanges have a higher tendency to bend and thus transfer higher forces to the CP's. The percentage of force flow through the CP's is 35%, 46%, 26% and 32% in case 4B, 9B, 5B and 10B.
- The amount of force passing through front and back CP's is similar in cases where a CP is welded to a DP on one side of the column.
- The percentage of force transferred through the CP's in each case remains almost constant as the loading progresses from 0.01 radian to 0.05 radian.

Table 5.20: Force flow through continuity plate (Case 4B)

γ_p (radians)	Force on one LP (kips)	SOF3 through CP's (kips)	% of Force through CP's
0.01	712.92	251.60	35.29
-0.01	713.52	251.00	35.18
0.02	840.46	301.20	35.84
-0.02	842.33	300.20	35.64
0.03	890.16	321.20	36.08
-0.03	891.62	320.00	35.89
0.04	927.83	333.60	35.96
-0.04	931.07	333.20	35.79
0.05	949.70	338.80	35.67
-0.05	956.67	341.00	35.64

Table 5.21: Force flow through continuity plate (Case 9B)

γ_p (radians)	Force on one LP (kips)	SOF3 through CP (kips)	% of Force through CP's
0.01	628.93	290.40	46.17
-0.01	629.45	288.60	45.85
0.02	765.36	349.40	45.65
-0.02	765.27	342.40	44.74
0.03	804.84	368.20	45.75
-0.03	805.84	357.20	44.33
0.04	830.77	380.80	45.84
-0.04	831.10	365.80	44.01
0.05	849.68	390.40	45.95
-0.05	849.64	371.80	43.76

Table 5.22: Force flow through continuity plate (Case 5B)

γ_p (radians)	Force on one LP (kips)	SOF3 through CP's (kips)	% of Force through CP's
0.01	1170.25	306.20	26.17
-0.01	1171.85	303.90	25.93
0.02	1485.32	369.60	24.88
-0.02	1489.90	357.10	23.97
0.03	1588.01	393.40	24.77
-0.03	1594.62	371.50	23.30
0.04	1653.13	411.50	24.89
-0.04	1653.56	378.50	22.89
0.05	1691.67	422.40	24.97
-0.05	1692.16	381.60	22.55

Table 5.23: Force flow through continuity plate (Case 10B)

γ_p (radians)	Force on one LP (kips)	SOF3 through CP (kips)	% of Force through CP's
0.01	954.53	306.20	32.08
-0.01	956.54	303.90	31.77
0.02	1108.06	369.60	33.36
-0.02	1110.55	357.10	32.16
0.03	1185.26	393.40	33.19
-0.03	1187.77	371.50	31.28
0.04	1236.45	411.50	33.28
-0.04	1251.38	378.50	30.25
0.05	1287.56	422.40	32.81
-0.05	1303.11	381.60	29.28

5.6 FREE BODY DIAGRAM OF A DOUBLER PLATE CUT AND CONTINUITY PLATE

The force on the LP's in the panel zone assembly is transferred to the DP, CP, column and the welds. The load can be transferred to web/DP by two paths: (1) LP -> Column flange -> Vertical CJP1 weld -> Column web/DP (2) LP -> Column flange -> CP -> Column web/DP. The FBD of the DP and CP can be drawn to investigate the load path in different analysis cases. Figures 5.74 to 5.88 shows the FBD of case 3B, case 4B and case 5B while Figures 5.89 to 5.103 shows FBD of case 8B, case 9B and case 10B at approximately 0.01, 0.02 and 0.05 radian rotation of panel zone. The following observations can be made by comparing theses FBD's:

- The shear force in the DP at a cut 2 inches below the LP level increases marginally in case 5B as compared to case 3B at 0.01, 0.02 and 0.05 radian rotation. Comparing the individual forces in cases 3B and 5B, it is found that forces through the vertical CJP1 weld reduces when CP's are introduced in the assembly. This force reduces because much of the force in case 5B is carried by the CP's to resist the local flange bending. Similar conclusions can be drawn for case 8B and case 10B. Thus, it can be concluded that it is safe to weld the CP to the DP in deep columns and it has an added advantage of reducing the forces in the vertical CJP1 weld.
- The forces entering through the left end of the DP and the shear force transmitted by CP to DP increases progressively as the loading increases from 0.01 radian to 0.05 radian in all cases.
- In case 5A and case 20A, the CP's attached to the DP and the column web transmit comparable shear forces to the DP and the column web.

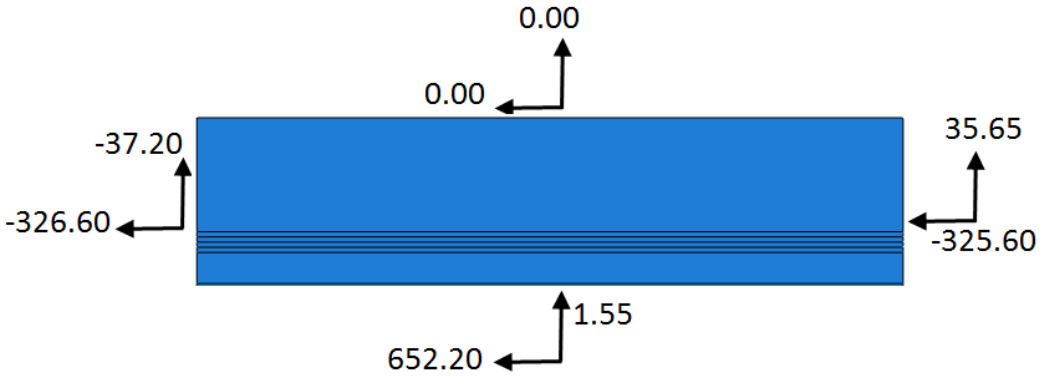

Figure 5.74: FBD of DP at 0.01 radian (case 3B)

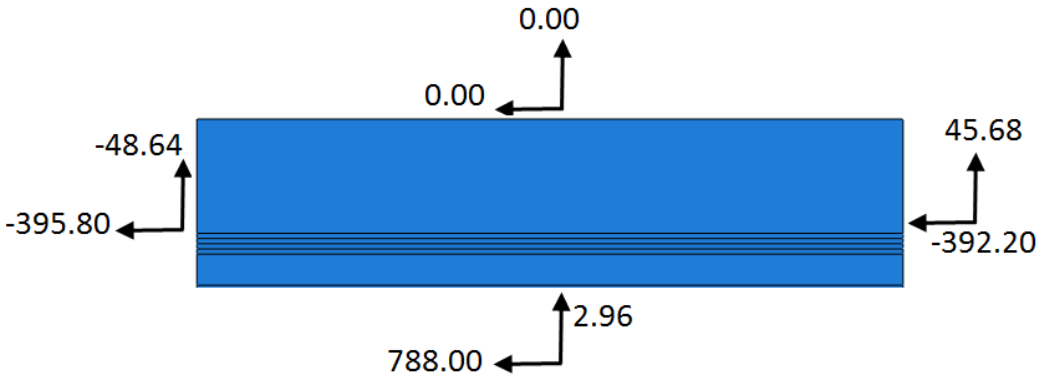

Figure 5.75: FBD of DP at 0.02 radian (case 3B)

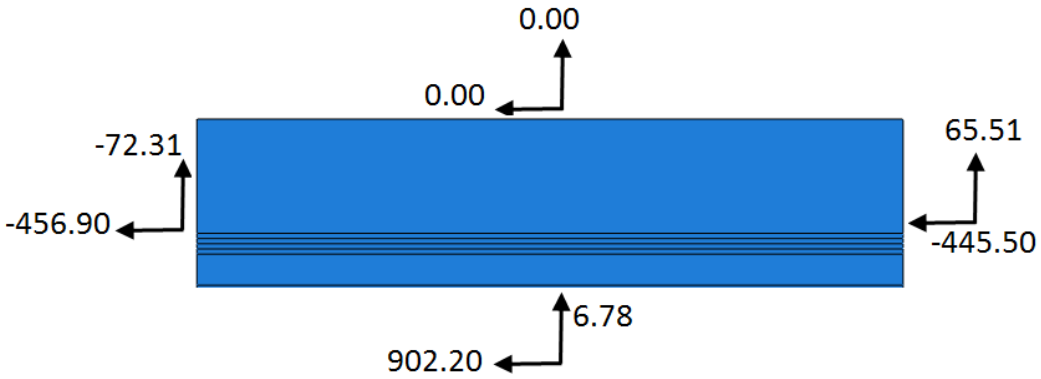

Figure 5.76: FBD of DP at 0.05 radian (case 3B)

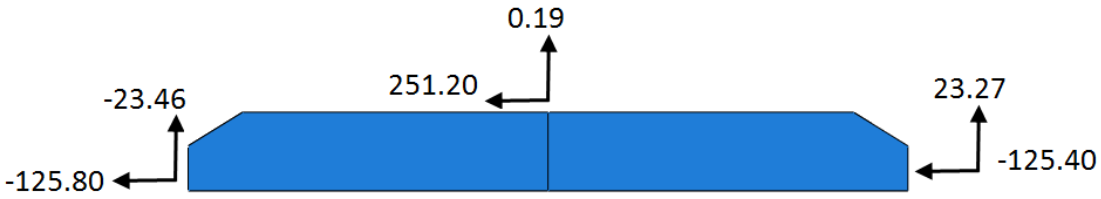

Figure 5.77: FBD of CP at 0.01 radian (case 4B)

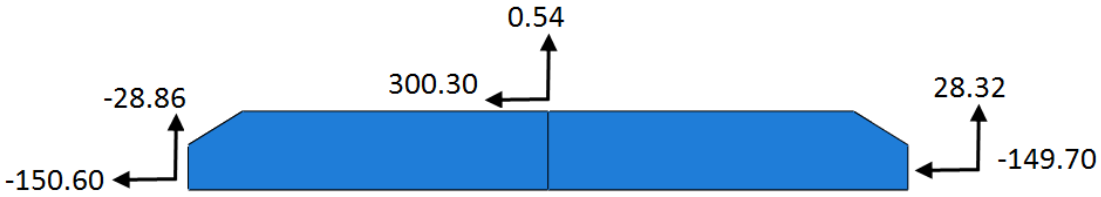

Figure 5.78: FBD of CP at 0.02 radian (case 4B)

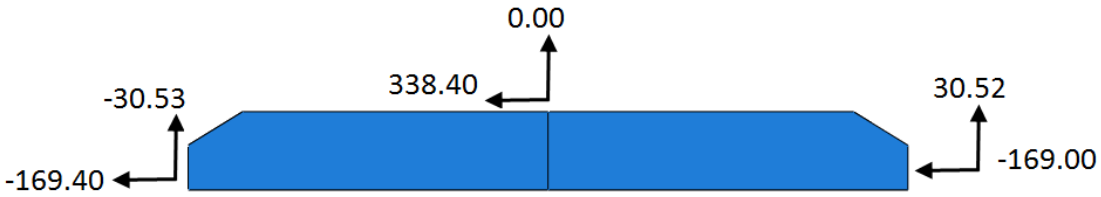

Figure 5.79: FBD of CP at 0.05 radian (case 4B)

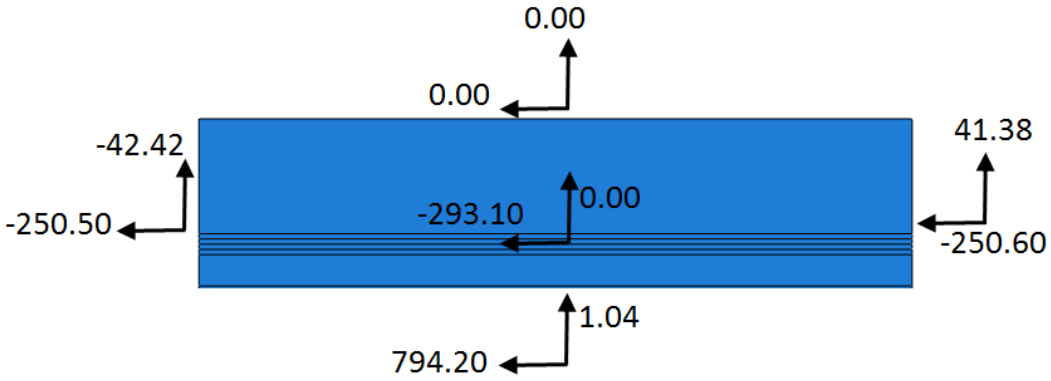

Figure 5.80: FBD of DP at 0.007 radian (case 5B)

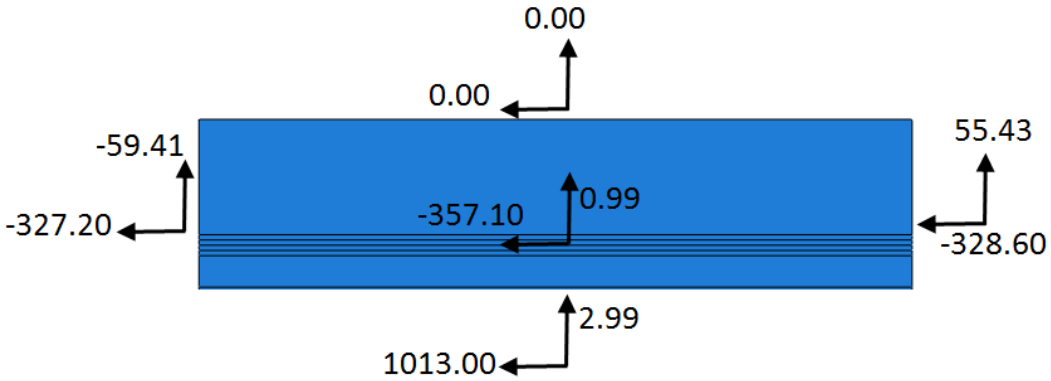

Figure 5.81: FBD of DP at 0.0159 radian (case 5B)

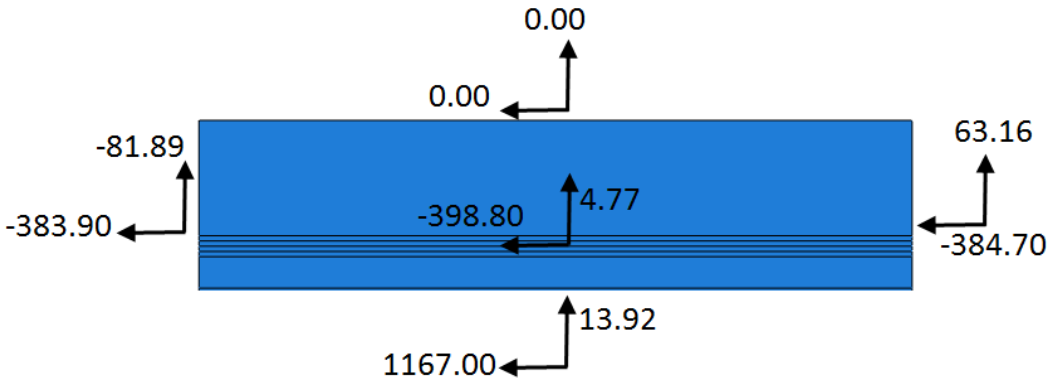

Figure 5.82: FBD of DP at 0.0407 radian (case 5B)

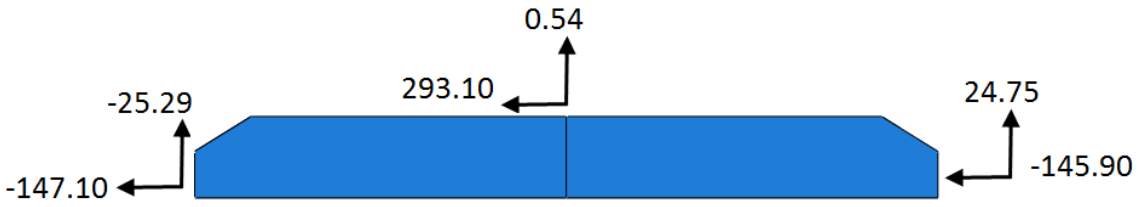

Figure 5.83: FBD of CP attached to DP at 0.007 radian (case 5B)

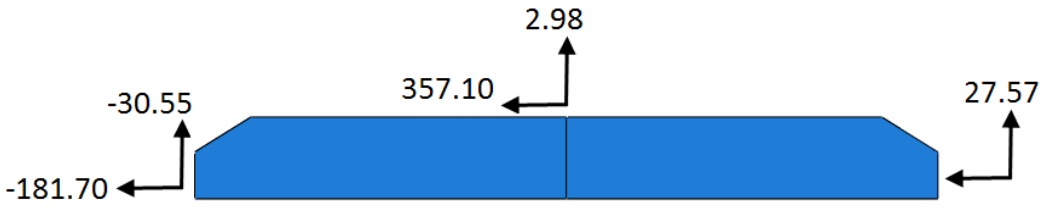

Figure 5.84: FBD of CP attached to DP at 0.0159 radian (case 5B)

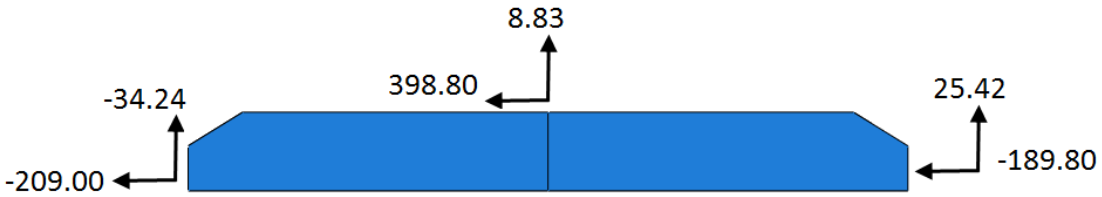

Figure 5.85: FBD of CP attached to DP at 0.0407 radian (case 5B)

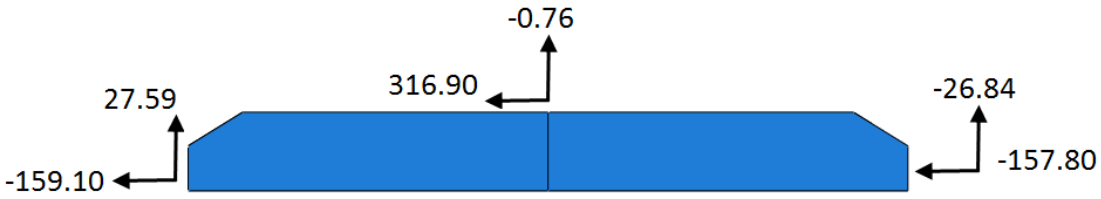

Figure 5.86: FBD of CP attached to column web at 0.007 radian (case 5B)

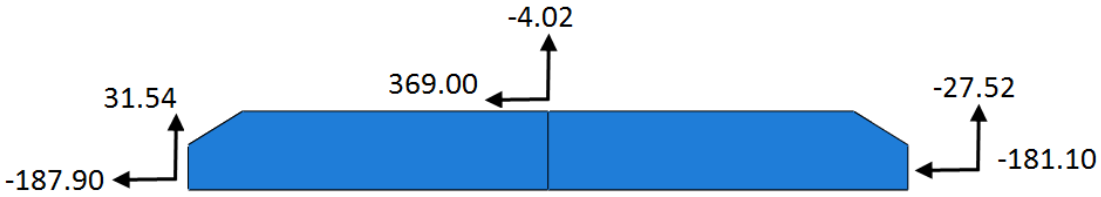

Figure 5.87: FBD of CP attached to column web at 0.0159 radian (case 5B)

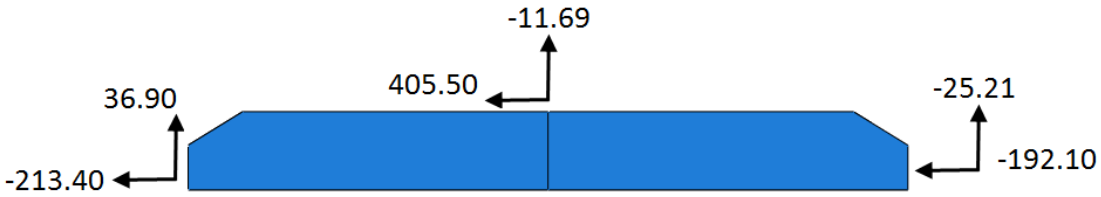

Figure 5.88: FBD of CP attached to column web at 0.0407 radian (case 5B)

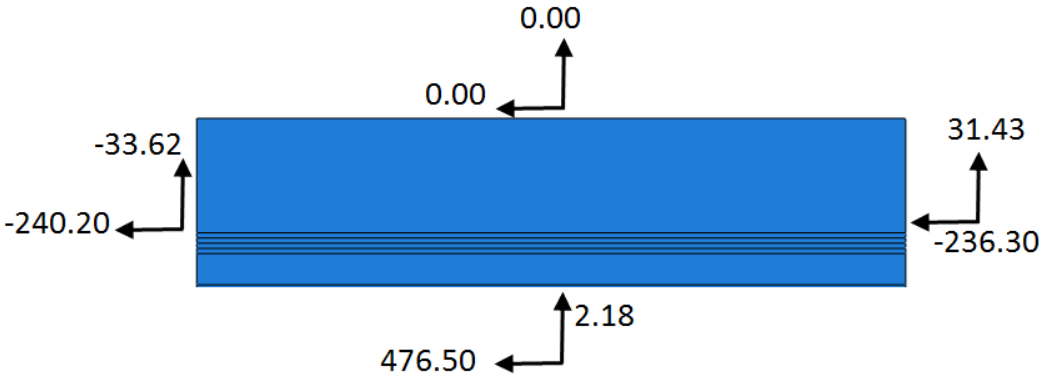

Figure 5.89: FBD of DP at 0.01 radian (case 8B)

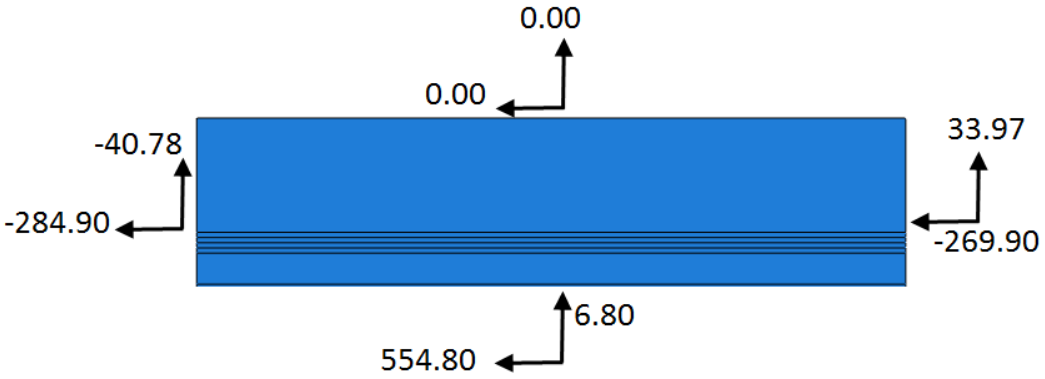

Figure 5.90: FBD of DP at 0.02 radian (case 8B)

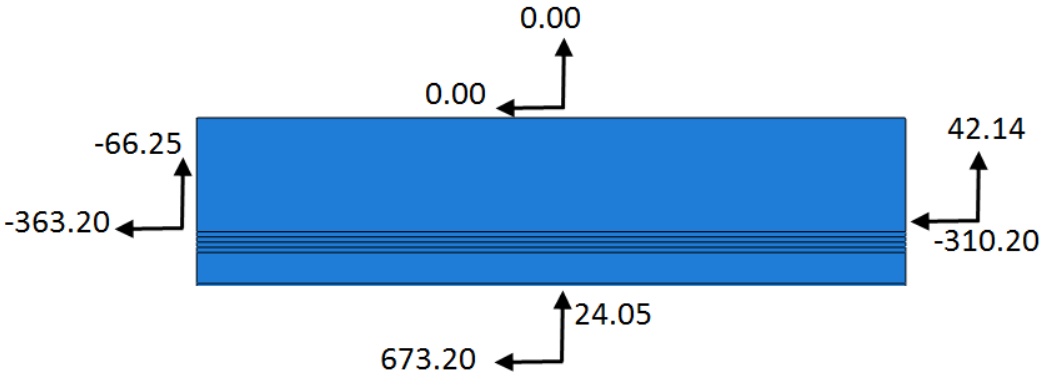

Figure 5.91: FBD of DP at 0.05 radian (case 8B)

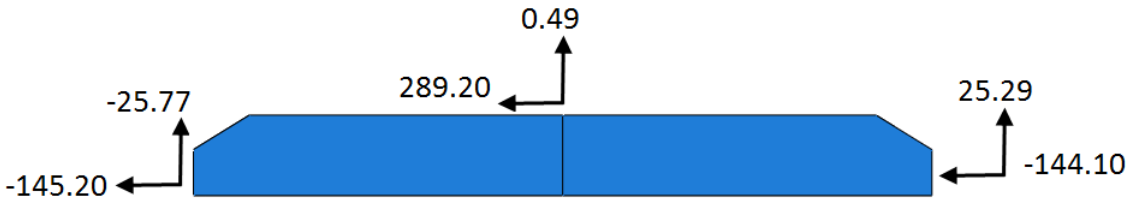

Figure 5.92: FBD of CP at 0.01 radian (case 9B)

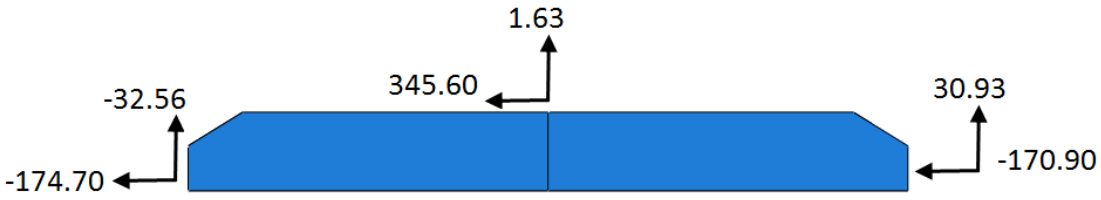

Figure 5.93: FBD of CP at 0.02 radian (case 9B)

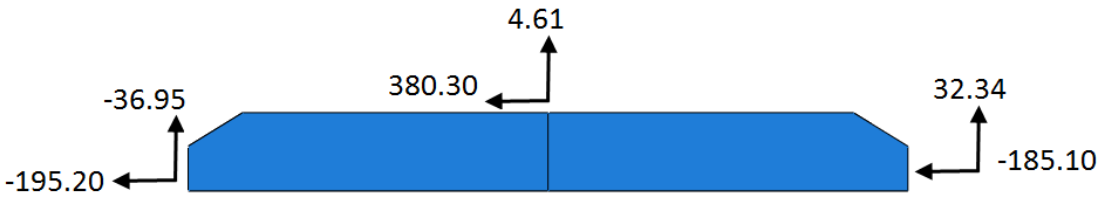

Figure 5.94: FBD of CP at 0.05 radian (case 9B)

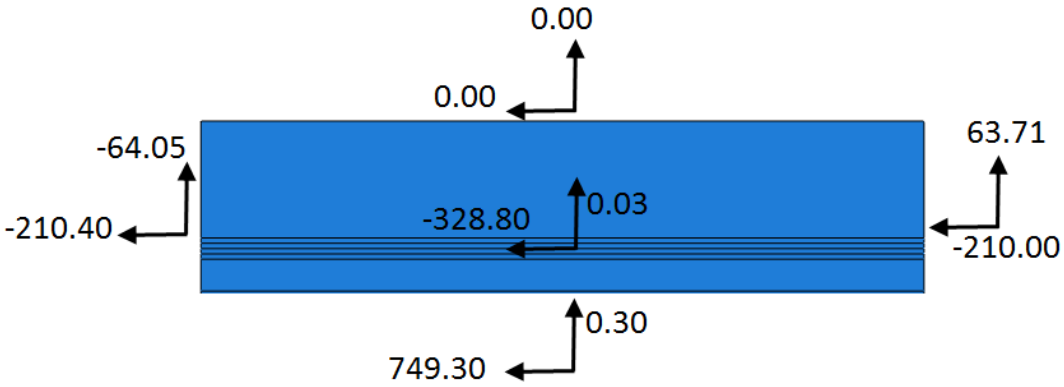

Figure 5.95: FBD of DP at 0.0062radian (case 10B)

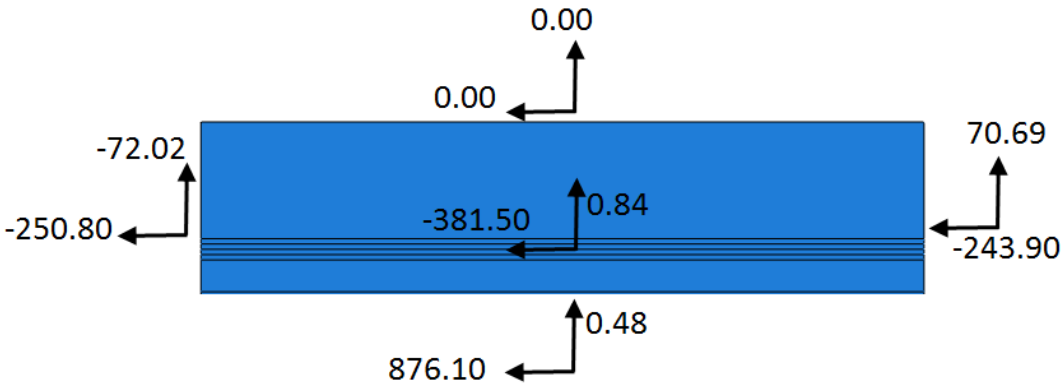

Figure 5.96: FBD of DP at 0.0118 radian (case 10B)

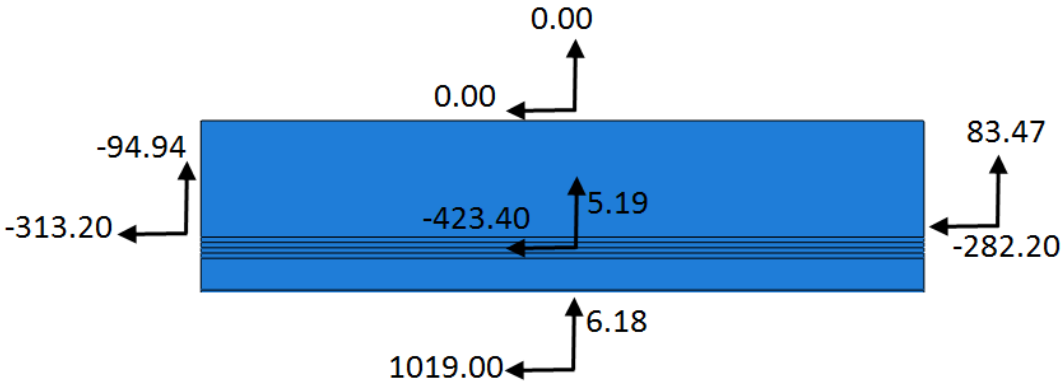

Figure 5.97: FBD of DP at 0.0322 radian (case 10B)

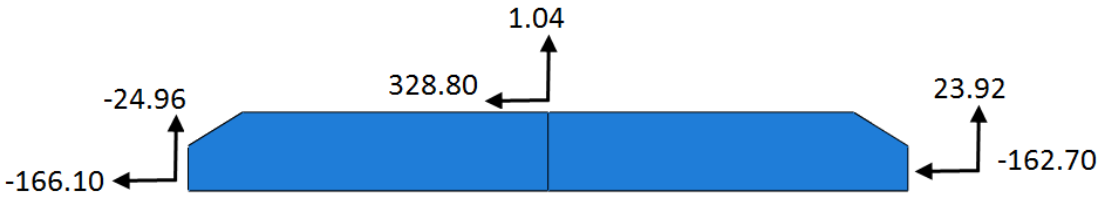

Figure 5.98: FBD of CP attached to DP at 0.0062 radian (case 10B)

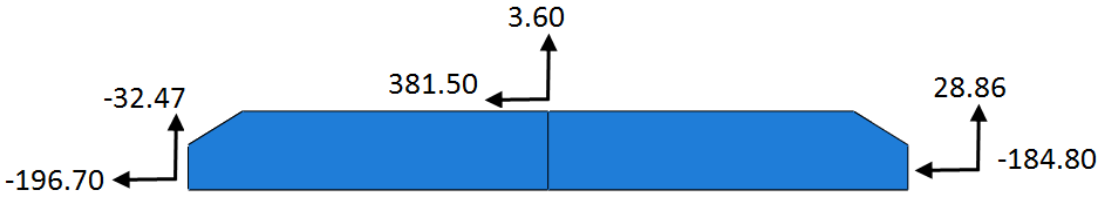

Figure 5.99: FBD of CP attached to DP at 0.0118 radian (case 10B)

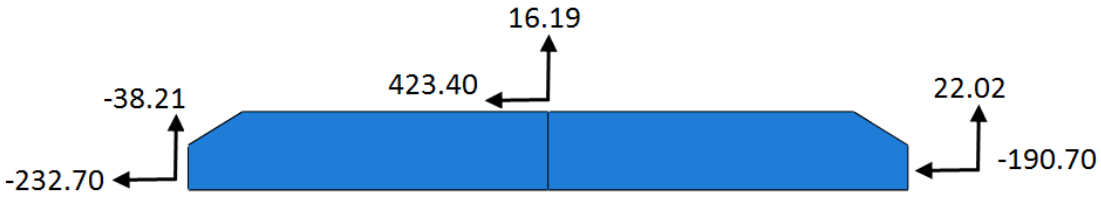

Figure 5.100: FBD of CP attached to DP at 0.0322 radian (case 10B)

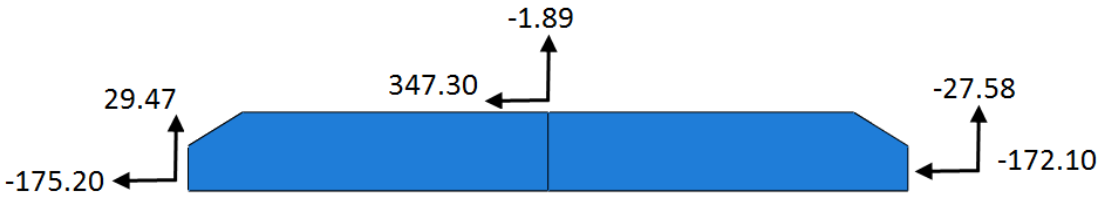

Figure 5.101: FBD of CP attached to column web at 0.0062 radian (case 10B)

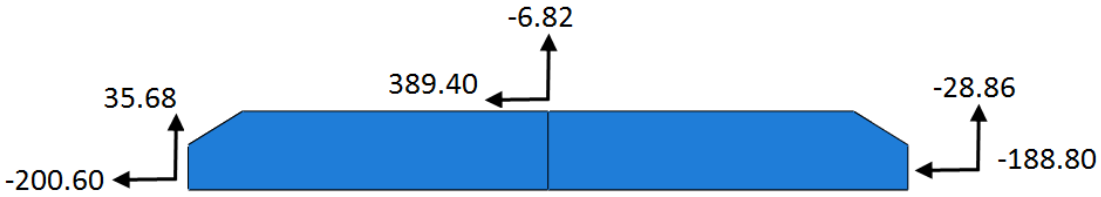

Figure 5.102: FBD of CP attached to column web at 0.0118 radian (case 10B)

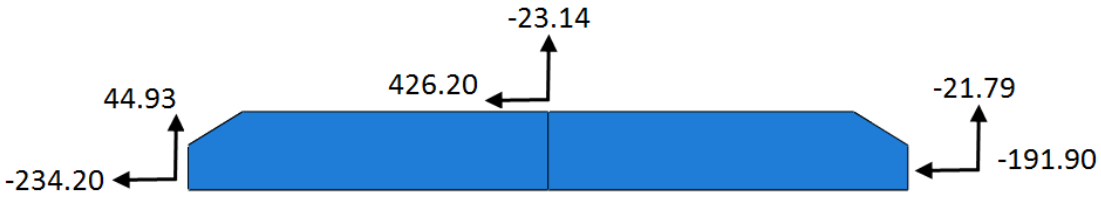

Figure 5.103: FBD of CP attached to column web at 0.0322 radian (case 10B)

5.7 SUMMARY

Not all of the simulations performed on the deep column (W40x264) were able to reach the nominal shear strength of the panel zone. The yielding in the column web/DP is concentrated near the k-area of the column due to localized flange bending in cases without CP's (except case 1B). The stresses at the middle depth of the DP are predominantly horizontal shear stress (S23) while stresses at the LP level are a combination of horizontal shear stress (S23) and horizontal normal stress (S33). The stresses in the vertical CJP1 weld at DP-CJP1 weld interface are predominantly vertical shear (S23) at the middle region of the weld and horizontal normal stress (S33) at the LP level. Thus the vertical weld should be designed to develop both the shear strength and tensile strength of the DP. The VMS in different parts of the panel zone may be similar at 0.05 radian rotation but the strain parameters like PEEQ and PEMAG are very different in cases having flange bending. The major conclusions from section 5.3, 5.4, 5.5 and 5.6 shows that there is some increase in the shear strength by extending the DP or by welding the DP on all four sides and it is safe to weld the CP over DP. The CP's are critical elements in the deeper column sections.

CHAPTER 6

Horizontal and Vertical Welds Cases of W14X398 and W40X264 Columns

6.1 INTRODUCTION

One of the major questions of this research is to see if there are any major benefits in providing horizontal fillet welds along the top and bottom edges of the DP. Some of the findings relevant to the above question are addressed in Chapter 4 and 5. This chapter provides further details and explanation. Section 6.2 lists the analysis cases for this study while the FBD of the DP cut and major observations are described in section 6.3 and 6.4 respectively.

6.2 ANALYSIS CASES

Table 6.1: Analysis cases for the study on effect of welding the DP both horizontally and vertically versus welding vertically only

Case	t_f (inches)	t_{dp} (inches)	l_{dp} (inches)	b_{dp} (inches)	CP	Horizontal Welds	Vertical Welds
2A	2.85 (W14X398)	0.50	24	10	No	No	Yes
2A_f		0.50	24	10	No	Yes	Yes
2B	1.75 (W40X264)	1.00	24	34	No	No	Yes
2B_f		1.00	24	34	No	Yes	Yes

Table 6.1 shows the analysis cases considered for this study. All the cases have vertical CJP1 groove welds to attach the DP to column. There are horizontal fillet welds at the DP – column web interface in cases 2A_f and 2B_f. The fillet weld dimensions are shown in Figure 3.3c. Figure 6.1 and 6.2 shows the comparison of panel zone strength versus rotation (gamma) for W14X398 and W40X264 column respectively. These figures only plots the last cycle of 0.05 radian in each case.

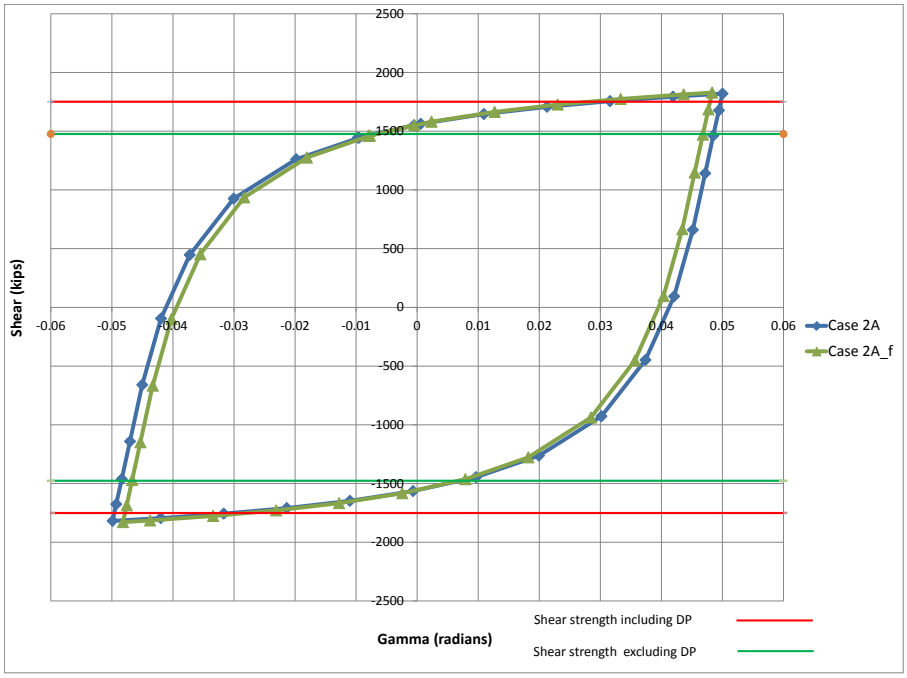

Figure 6.1: Panel zone shear versus gamma (W14X398 column)

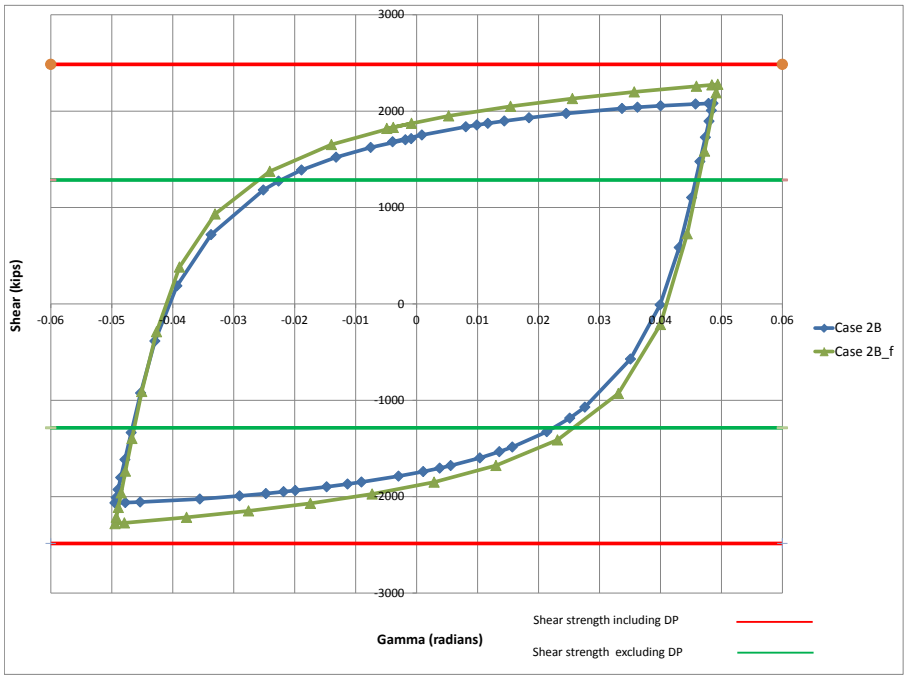

Figure 6.2: Panel zone shear versus gamma (W40X264 column)

6.3 FREE BODY DIAGRAM OF DOUBLER PLATE CUT

Figures 6.3 to 6.8 shows the FBD of a DP cut 2 inches below the LP level in case 2A and 2A_f while Figures 6.9 to 6.14 shows the FBD of case 2B and 2B_f at approximately 0.01, 0.02 and 0.05 radian rotation of panel zone.

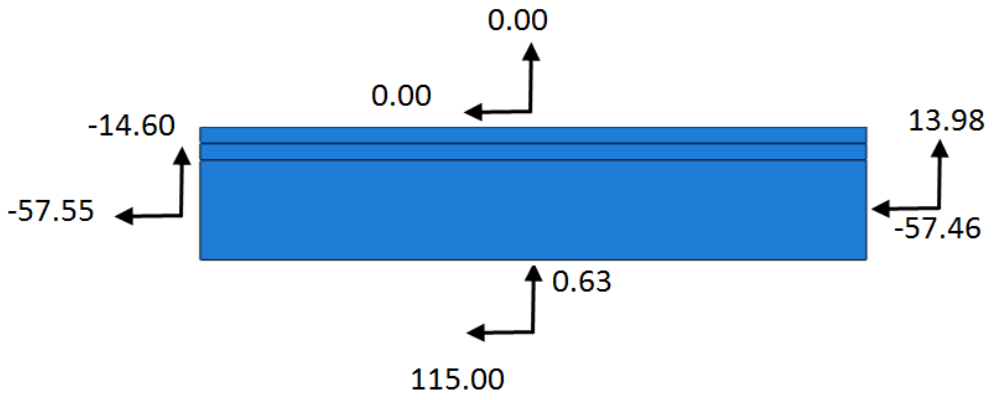

Figure 6.3: FBD of DP at 0.01 radian (case 2A)

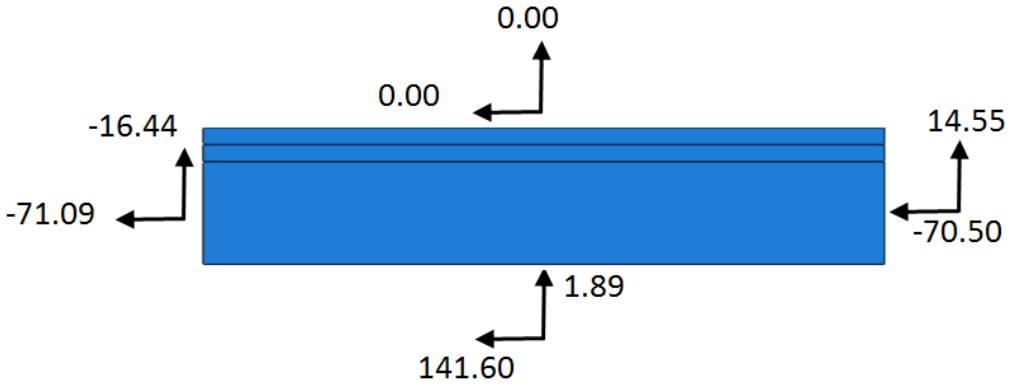

Figure 6.4: FBD of DP at 0.02 radian (case 2A)

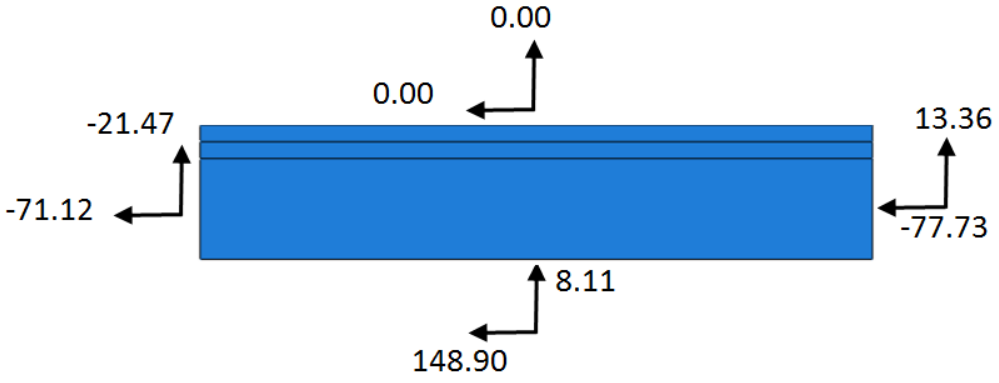

Figure 6.5: FBD of DP at 0.05 radian (case 2A)

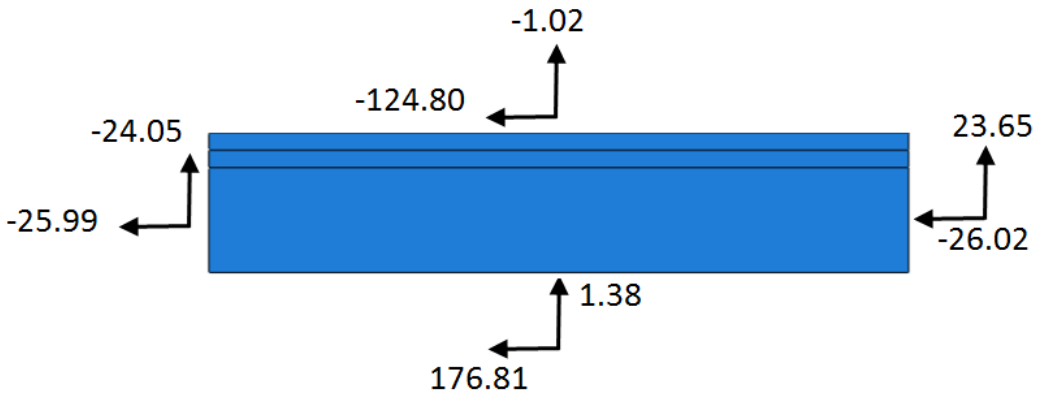

Figure 6.6: FBD of DP at 0.01 radian (case 2A_f)

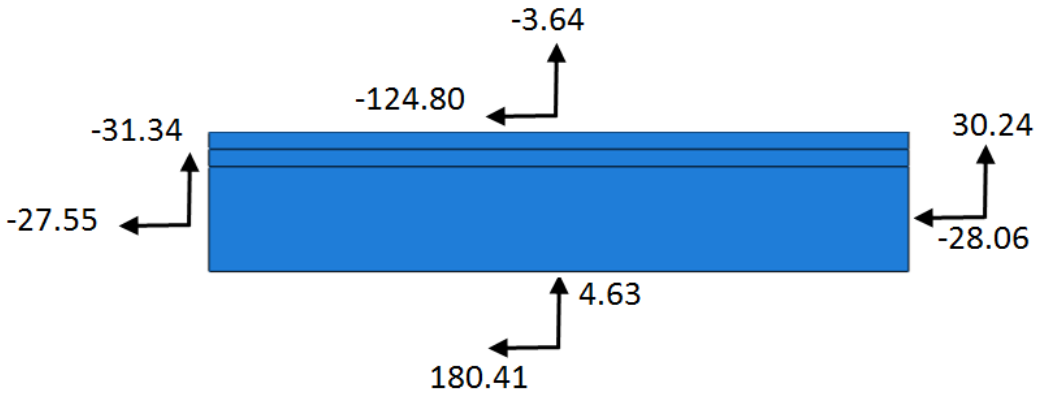

Figure 6.7: FBD of DP at 0.02 radian (case 2A_f)

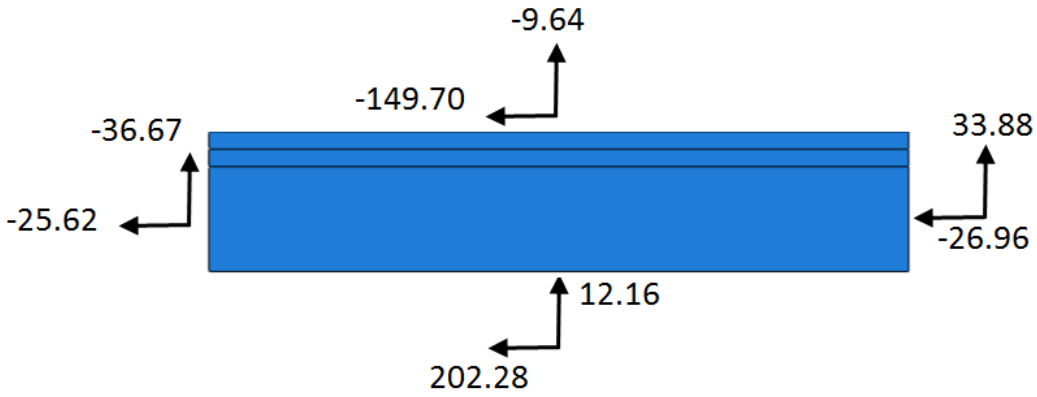

Figure 6.8: FBD of DP at 0.05 radian (case 2A_f)

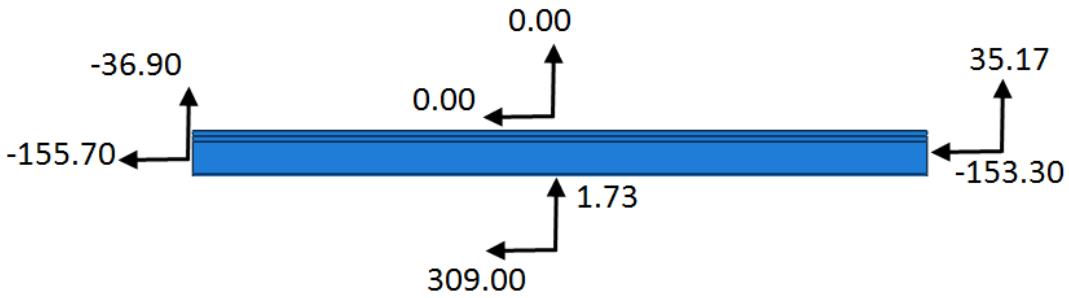

Figure 6.9: FBD of DP at 0.01 radian (case 2B)

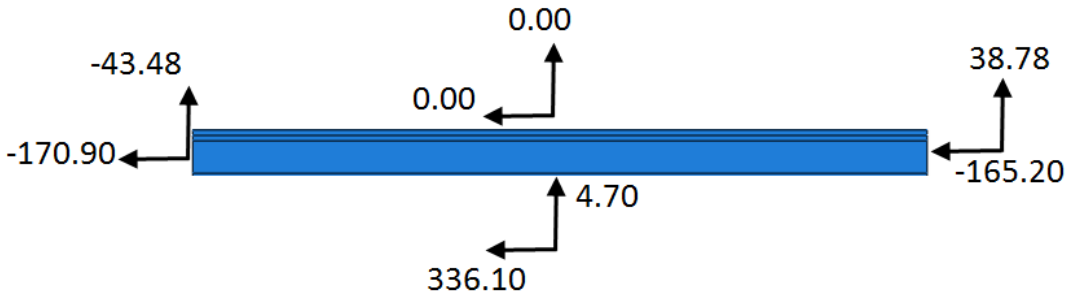

Figure 6.10: FBD of DP at 0.02 radian (case 2B)

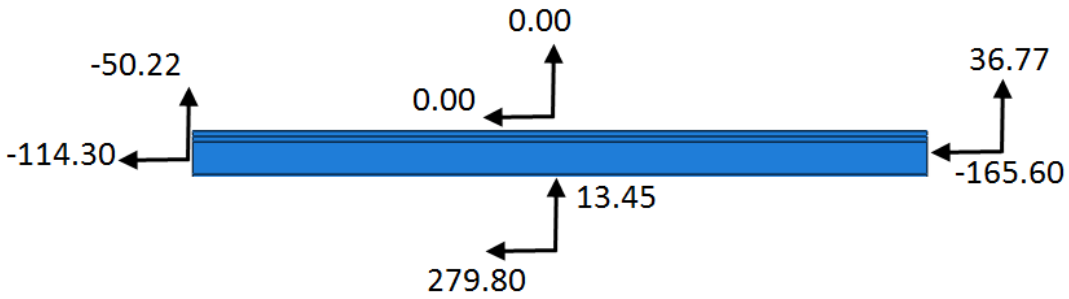

Figure 6.11: FBD of DP at 0.05 radian (case 2B)

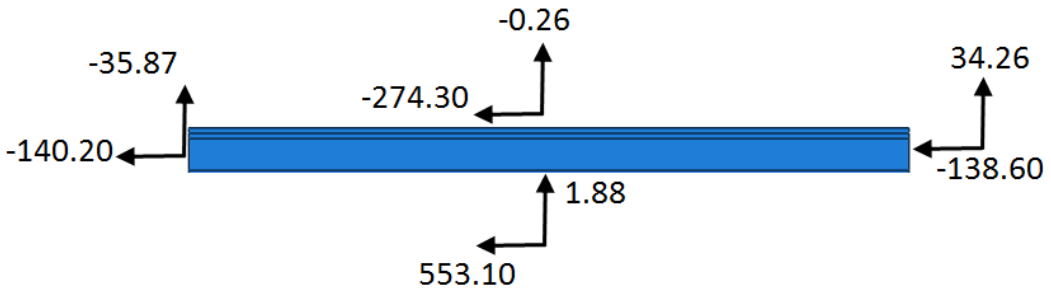

Figure 6.12: FBD of DP at 0.01 radian (case 2B_f)

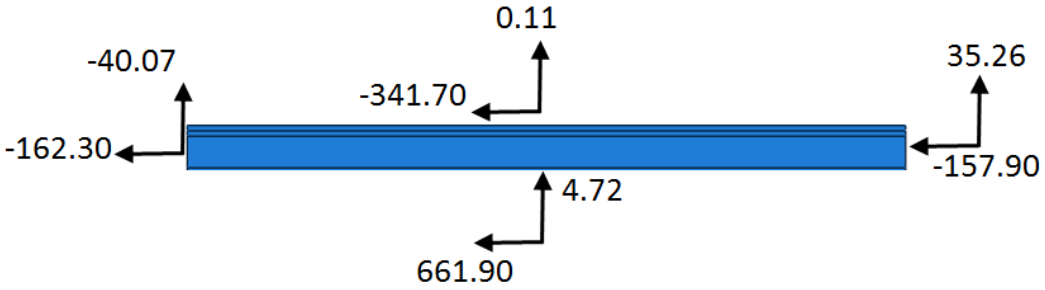

Figure 6.13: FBD of DP at 0.02 radian (case 2B_f)

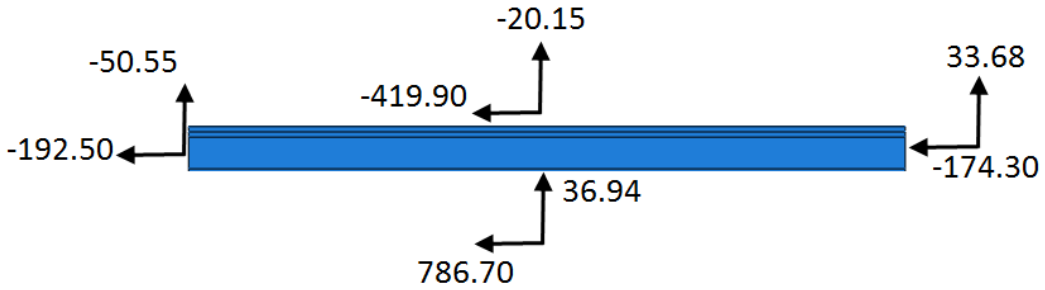

Figure 6.14: FBD of DP at 0.05 radian (case 2B_f)

6.4 OBSERVATIONS

The welding of the DP on all four sides (horizontally and vertically) did not increase the shear strength of the shallow column (W14X398) while there was a modest increase in the shear strength of the deep column (W40X264). The amount of this increase in the deep columns was about 10 percent. The possible reason for this different behavior in the shallow versus the deep column is that the web shear is the limiting strength in former case (case 2A) while local limit states like web /DP crippling and flange bending are the limiting strength in latter case (case 2B, see Figure 5.72, 5.73 for these local limit states). So, when the DP is welded on all four sides in deep columns, it stiffens the column against the localized limit states leading to an increase in the strength of the panel zone. Notice that in case 2B_f, still the panel zone is not able to reach its nominal panel zone shear strength (see Figure 6.2).

In shallow columns at 0.01 and 0.05 radian, there is no considerable change in the maximum VMS, PEEQ and PEMAG (see Table 4.33 - 4.38) values in DP and column when the DP is welded also horizontally. But there is considerable decrease in these quantities in the CJP1 vertical groove weld. The amount of percentage decrease of these quantities in CJP1 weld is tabulated in Table 6.2. The decrease in these quantities in CJP1 weld can also be explained by FBD's in Figure 6.3 – 6.8. The amount of force flowing through the vertical CJP1 weld reduces substantially when horizontal welds are provided and most of the force enters the DP though the DP - fillet weld horizontal interface. Another interesting observation is that the maximum VMS, PEEQ and PEMAG values are similar in the horizontal fillet weld and vertical CJP1 groove weld at 0.05 radian rotation of shallow column (case 2A_f).

In the deep columns at 0.01 and 0.05 radian, there is no significant change in the maximum VMS (see Table 5.14, 5.15) values in DP and column when the DP is welded

also horizontally. But there is considerable decrease in PEEQ and PEMAG values. At 0.01 and 0.05 radian in the DP as the DP is restrained against out-of-plane distortion when the DP is welded on all four sides. There is an increase in the maximum VMS, PEEQ and PEMAG values at 0.05 radian in the CJP1 weld when the DP is welded on all four sides. The increase of these quantities in CJP1 weld is tabulated in Table 6.2. This behavior in CJP1 weld can also be explained by FBD's in Figure 6.9 – 6.14. As the DP is welded on all 4 sides, the strength of the panel zone, force though the vertical CJP1 weld and force at the cut 2 inches below the LP level increases due to mitigating of local limit states. Notice that in case 2B_f, the force though the vertical CJP1 weld is higher than case 2B but still a large percentage of the force flow is through horizontal fillet weld (see Figure 6.14).

Table 6.2: VMS, PEEQ and PEMAG decrease in CJP1 weld as DP is welded on all sides

Case	VMS	PEEQ	PEMAG
0.01 radian			
2A -> 2A_f	-6.88 %	-46.76 %	-54.62 %
2B -> 2B_f	-1.11 %	-7.25 %	-9.75 %
0.05 radian			
2A -> 2A_f	-15.70 %	-62.70 %	-66.00 %
2B -> 2B_f	+27.30 %	+15.24 %	+69.50 %

The VMS along the width of the DP at the middle section is uniform around 70 ksi in both case 2A and 2A_f (see Figure 4.6 and Figure 4.11). The VMS along the width of the DP at the middle section is uniform around 60 ksi except at the left and right ends in both case 2B and 2B_f (see Figure 5.12 and Figure 5.19). The VMS at the left and right ends drops down to 40 ksi and 50 ksi in case 2B and 2B_f respectively.

In case 2A and 2A_f, the VMS along the depth of the vertical weld at the DP – CJP1 weld interface is constant around 80 ksi at the middle depths but rises locally to 90 ksi at the top and bottom ends (see Figure 4.7 and Figure 4.12). This localized high VMS

becomes less prominent in case 2A_f. The VMS values along CJP1weld in case 2B are around 90 ksi at the end region but dips down drastically to around 20 ksi at the middle depth. These stresses in case 2B_f are around 110 ksi at the ends but reduces slowly to around 50 ksi at the middle depth (see Figure 5.13 and Figure 5.20). The VMS along the depth is primarily a combination of horizontal normal stress (S33) and vertical shear stress (S23). The vertical shear stress is the main component of VMS at the middle depth while it is zero at the ends. The horizontal normal stress is maximum at the LP level while it is around zero at the middle depth except in case 2B (see Figure 5.13) where it varies almost linearly along the depth.

The VMS along the width of horizontal fillet weld in case 2A_f is uniform around 70 ksi with a slight dip at the middle width while in case 2B_f the VMS are around 70 kips at the left and right ends with a large dip to around 20 kips at the middle width (see Figure 4.13 and Figure 5.21).

The observations on welding of the DP on all four sides are summarized below. Note that these conclusions apply only to the case where the DP is not extended beyond the level of the LP's:

- The provision of horizontal welds in the shallow column (W14X398) does not increase the strength of the panel zone. However, the forces, stresses and strains in the vertical CJP1 weld are significantly reduced as a major portion of the forces in the DP flow through the DP – fillet weld interface.
- There is an increase of around 10 % in the strength of the panel zone if the DP is welded also horizontally as against having only vertical welds in the deep column (W40X264). Moreover, the DP has smaller strains due to restraint provided by the horizontal welds to the local DP crippling. Higher strength of panel zone at 0.05

radian increases the forces, stresses and strains in the vertical CJP1 weld but still a major portion of the forces in the DP flow through the DP – fillet weld interface.

CHAPTER 7

Thin and Thick Doubler Plates Cases for the W14X398 Column

7.1 INTRODUCTION

Most of the simulation cases in Chapter 4 were provided with a DP thickness of ½ inch which was slightly greater than the required DP thickness (0.37 inches) according to Eq. E3-7 in *Seismic Provisions for Steel Structural Buildings* (AISC 2010b). The equation states that required minimum DP thickness can be obtained as the summation of width of panel zone between column flanges and the web height of deeper beam at connection divided by 90. This provision served well as no considerable buckling or crippling of the DP that could lower the panel zone shear strength was observed in the analysis cases for the shallow column (W14X398). To investigate how a thinner (¼ inch) or thicker DP (1 inch) might affect the observations made in Chapter 4, some of the analysis cases were run with this new thickness of DP's. These new analysis cases are listed in section 7.2. All the major output figures and graphs for these cases are already given in Chapter 4. Section 7.3 provides the FBD of the DP cut and CP while section 7.4 discusses the results.

7.2 ANALYSIS CASES

Table 7.1 shows the analysis cases considered for this study. All the cases have vertical CJP1 groove welds to attach the DP to column. There are no horizontal fillet welds at the top and bottom edges of the DP. Figure 7.1 and 7.2 shows the comparison of panel zone strength versus rotation (gamma) for different cases. These figures only plot the last cycle of 0.05 radian in each case.

Table 7.1: Analysis cases for the thin and thick DP in W14X398 column

Case	t_f (inches)	t_{dp} (inches)	l_{dp} (inches)	b_{dp} (inches)	CP
3A	2.85	0.50	36	10	No
3A_quar		0.25	36	10	No
3A_one		1.00	36	10	No
5A		0.50	36	10	Yes
5A_quar		0.25	36	10	Yes
5A_one		1.00	36	10	Yes
13A	1.00	0.50	36	10	No
13A_quar		0.25	36	10	No
13A_one		1.00	36	10	No
15A		0.50	36	10	Yes
15A_quar		0.25	36	10	Yes
15A_one		1.00	36	10	Yes

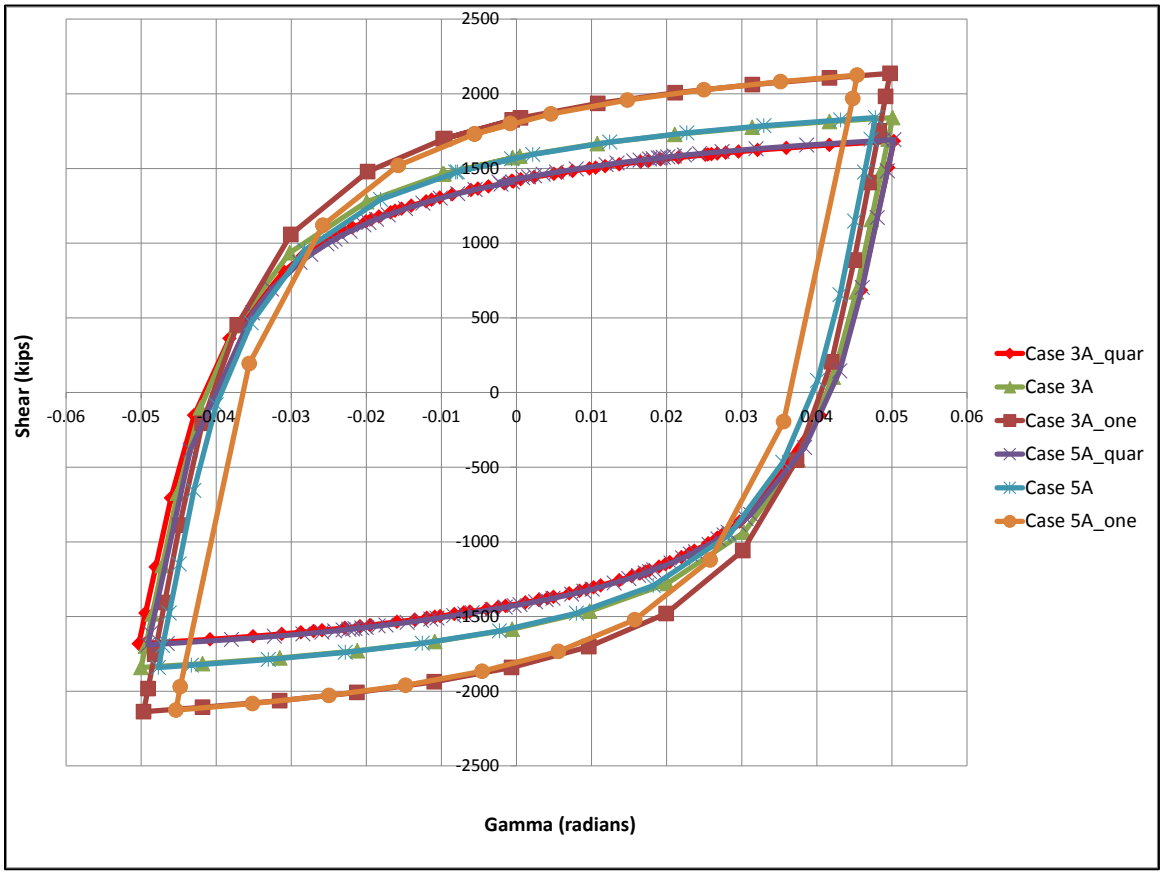

Figure 7.1: Panel zone shear versus gamma (W14X398 column, t_f = 2.85 inches)

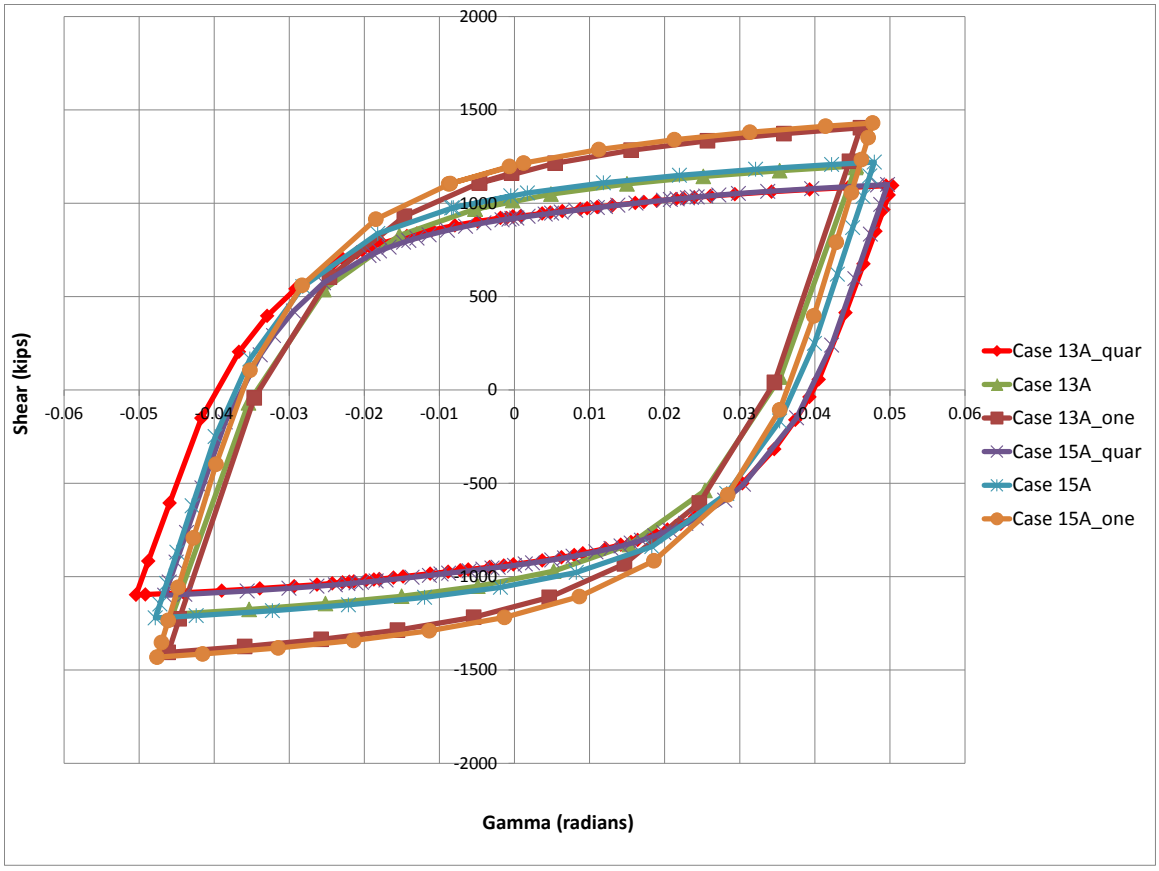

Figure 7.2: Panel zone shear versus gamma (W14X398 column, t_f = 1.00 inches)

7.3 FREE BODY DIAGRAM OF DOUBLER PLATE CUT

Figures 7.3 to 7.26 shows the FBD of the CP and the DP cut 2 inches below the LP level in case 3A_quar, 3A_one, 5A_quar and 5A_one. The FBD's for base case 3A and 5A are given in Figures 4.165 – 4.167 and Figures 4.171 – 4.179 respectively. Figures 7.27 to 7.50 shows the FBD of the CP and the DP cut 2 inches below the LP level in case 13A_quar, 13A_one, 15A_quar and 15A_one. All the FBD's are shown at approximately 0.01, 0.02 and 0.05 radian rotation of panel zone.

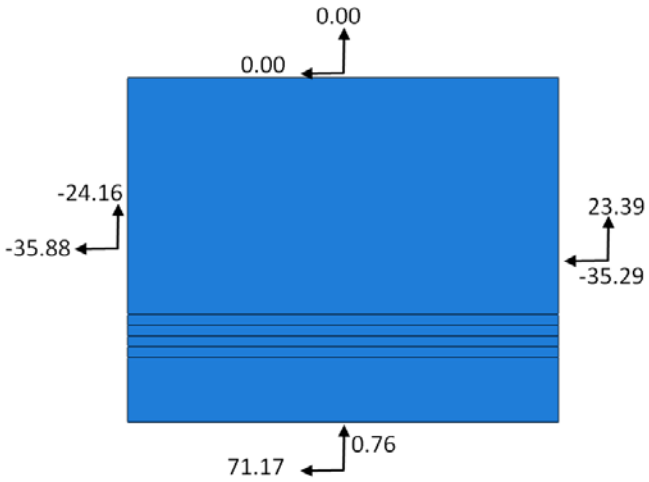

Figure 7.3: FBD of DP at 0.01 radian (case 3A_quar)

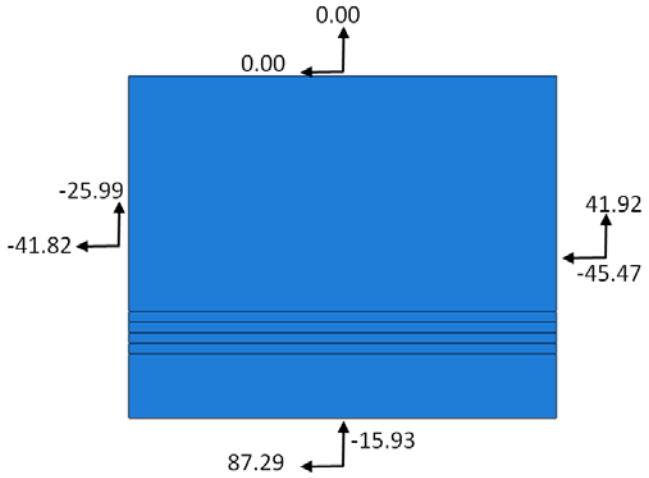

Figure 7.4: FBD of DP at 0.02 radian (case 3A_quar)

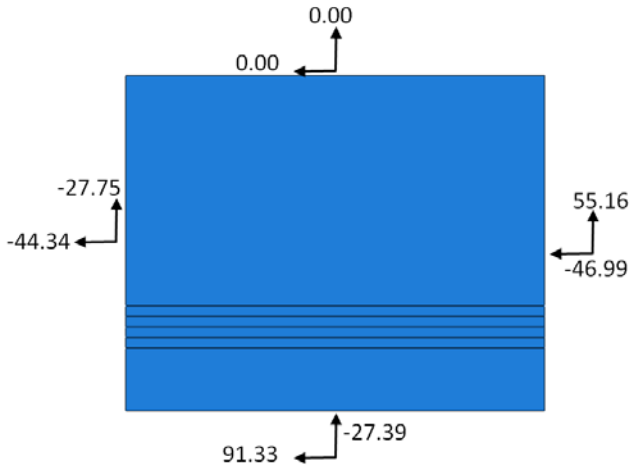

Figure 7.5: FBD of DP at 0.05 radian (case 3A_quar)

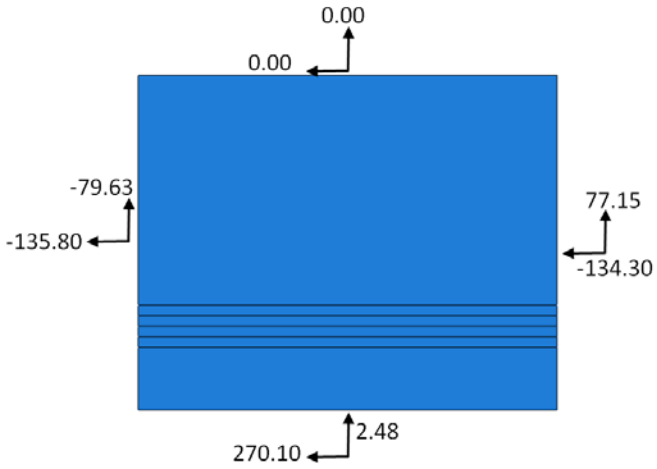

Figure 7.6: FBD of DP at 0.01 radian (case 3A_one)

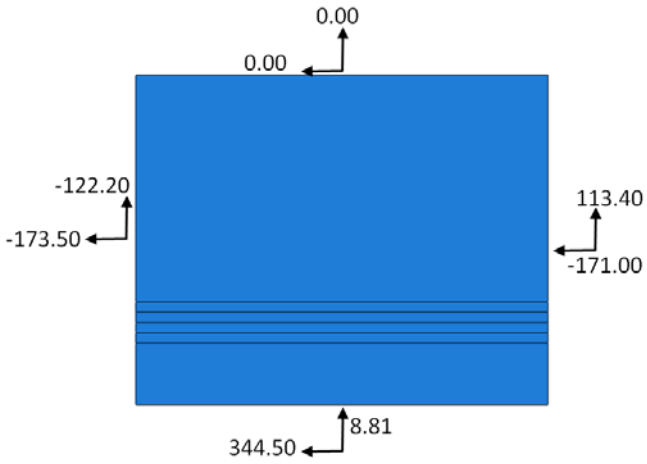

Figure 7.7: FBD of DP at 0.02 radian (case 3A_one)

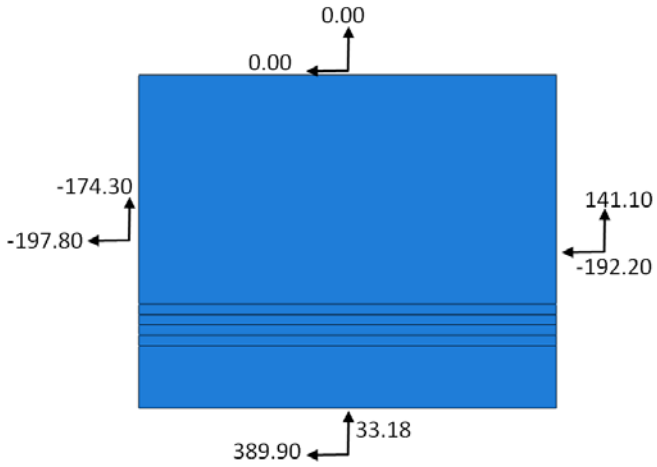

Figure 7.8: FBD of DP at 0.05 radian (case 3A_one)

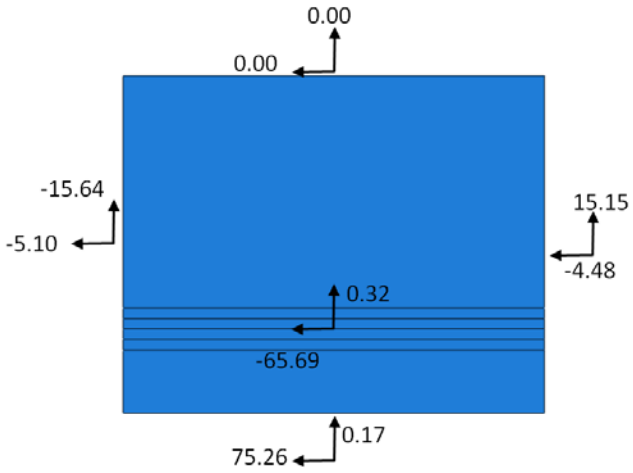

Figure 7.9: FBD of DP at 0.01 radian (case 5A_quar)

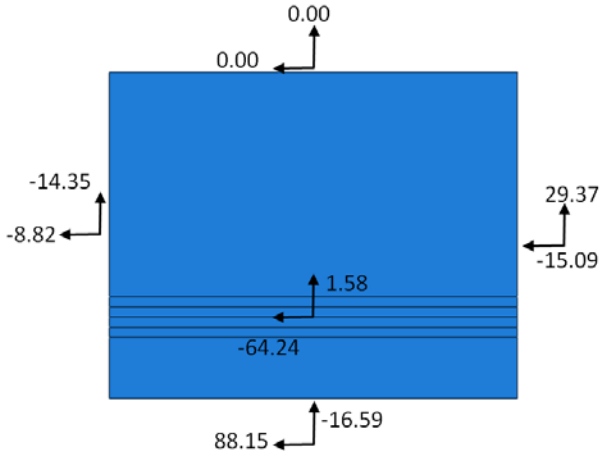

Figure 7.10: FBD of DP at 0.02 radian (case 5A_quar)

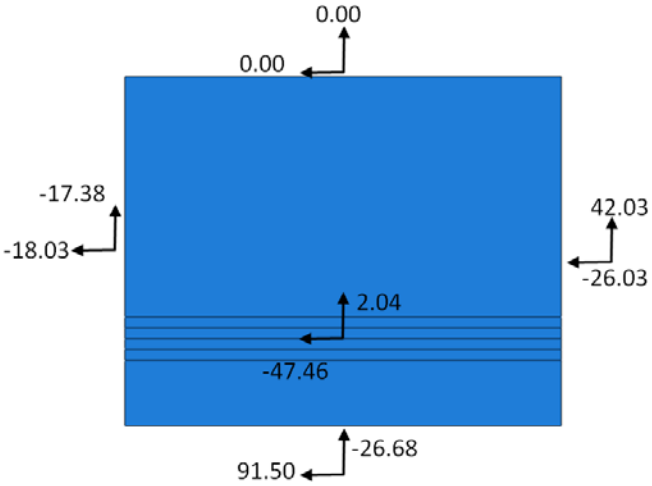

Figure 7.11: FBD of DP at 0.03 radian (case 5A_quar)

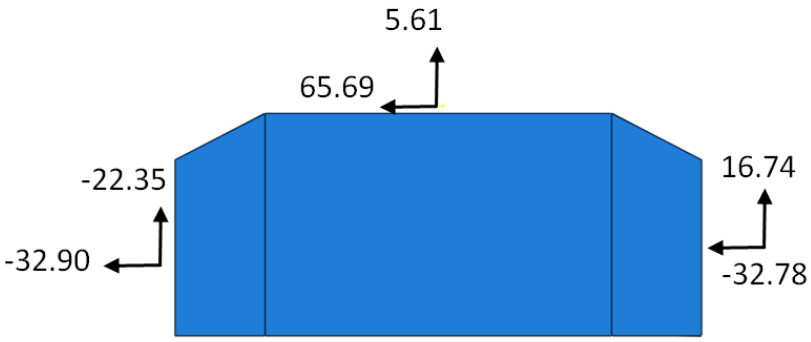

Figure 7.12: FBD of CP attached to DP at 0.01 radian (case 5A_quar)

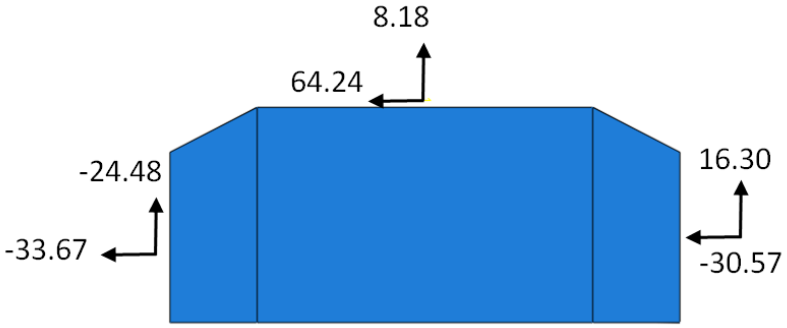

Figure 7.13: FBD of CP attached to DP at 0.02 radian (case 5A_quar)

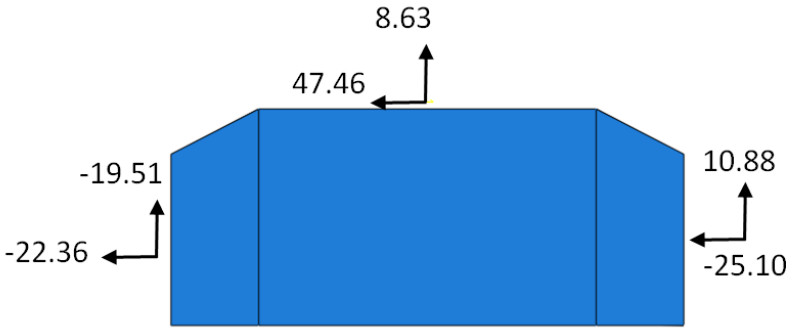

Figure 7.14: FBD of CP attached to DP at 0.05 radian (case 5A_quar)

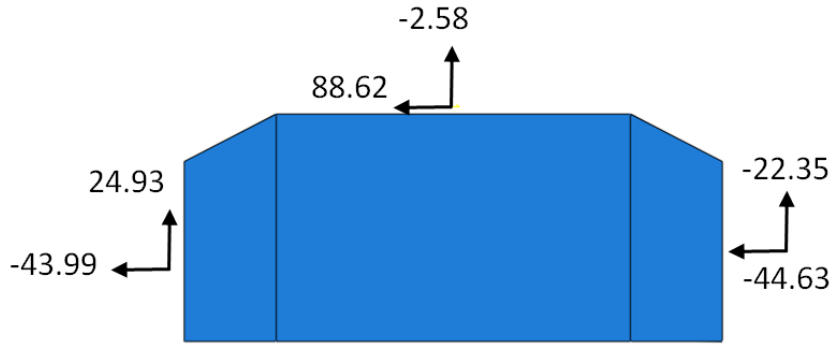

Figure 7.15: FBD of CP attached to column web at 0.01 radian (case 5A_quar)

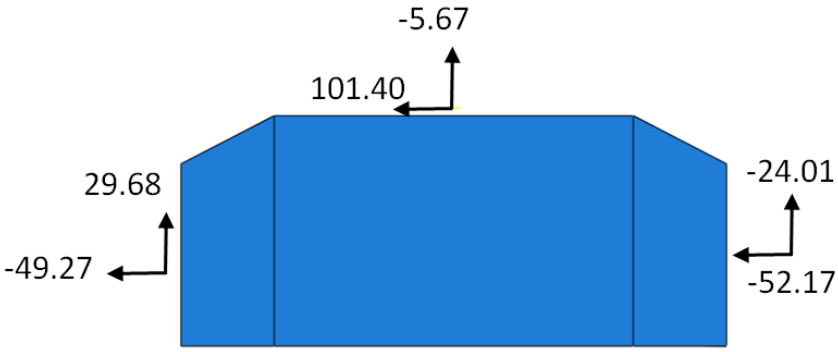

Figure 7.16: FBD of CP attached to column web at 0.02 radian (case 5A_quar)

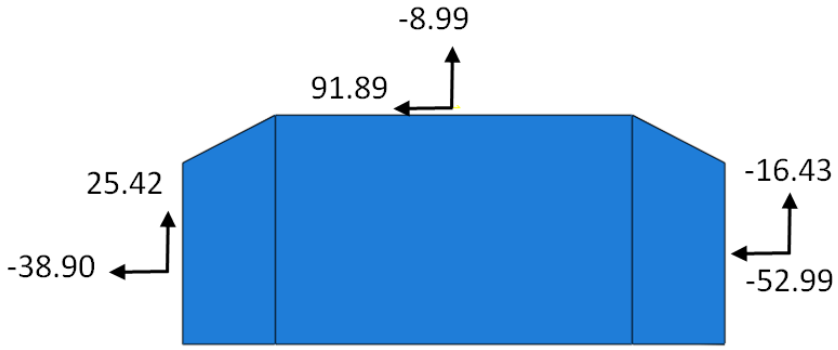

Figure 7.17: FBD of CP attached to column web at 0.05 radian (case 5A_quar)

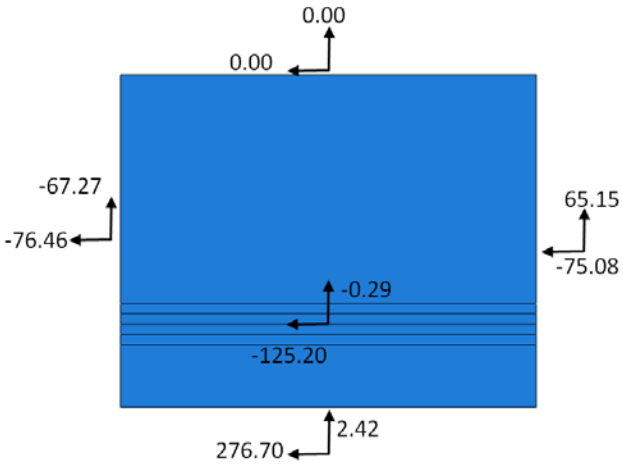

Figure 7.18: FBD of DP at 0.01 radian (case 5A_one)

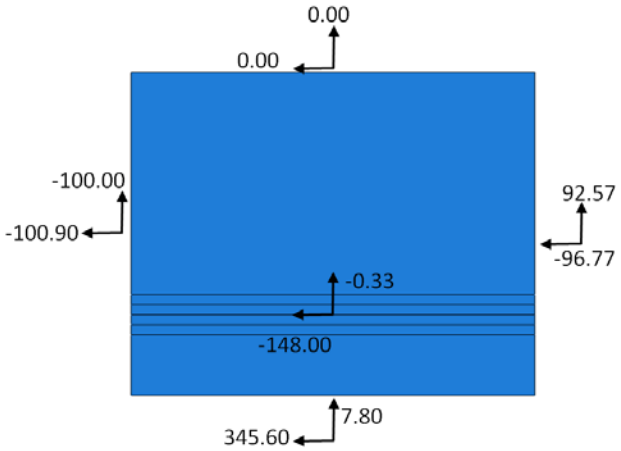

Figure 7.19: FBD of DP at 0.02 radian (case 5A_one)

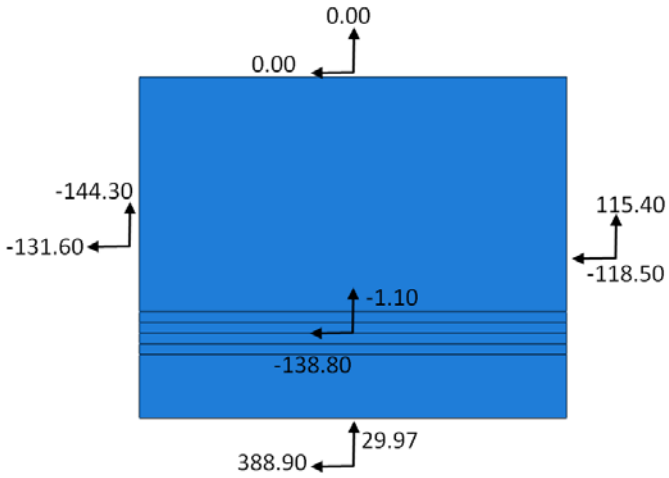

Figure 7.20: FBD of DP at 0.03 radian (case 5A_one)

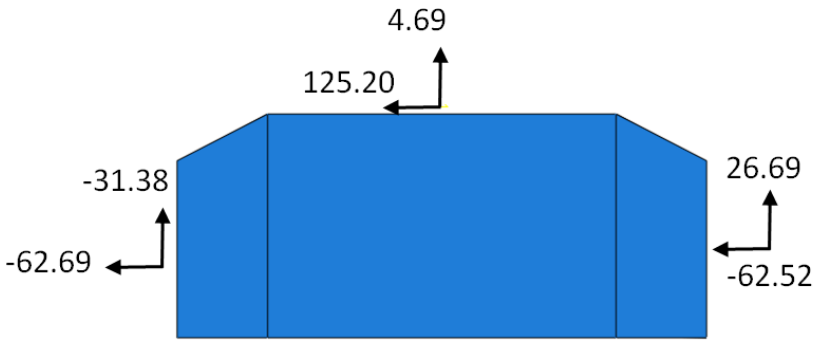

Figure 7.21: FBD of CP attached to DP at 0.01 radian (case 5A_one)

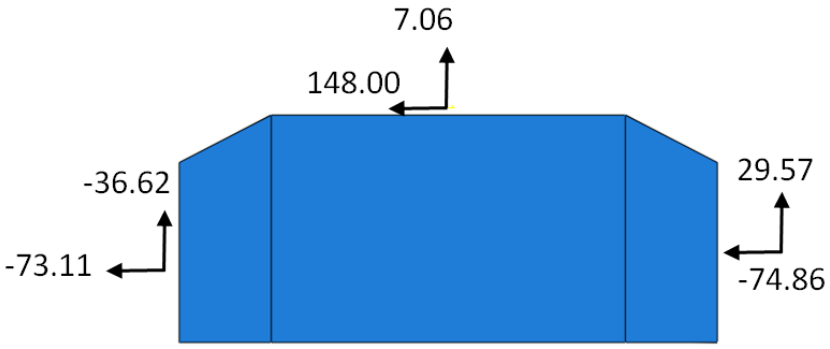

Figure 7.22: FBD of CP attached to DP at 0.02 radian (case 5A_one)

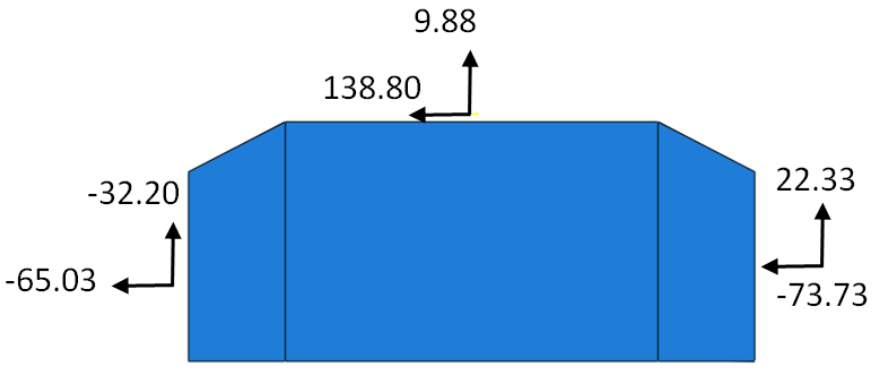

Figure 7.23: FBD of CP attached to DP at 0.05 radian (case 5A_one)

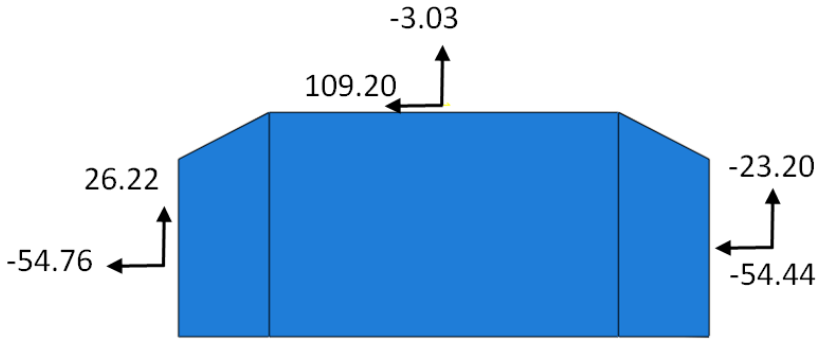

Figure 7.24: FBD of CP attached to column web at 0.01 radian (case 5A_one)

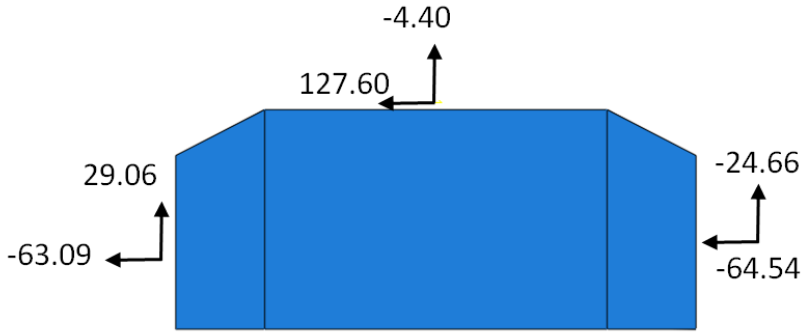

Figure 7.25: FBD of CP attached to column web at 0.02 radian (case 5A_one)

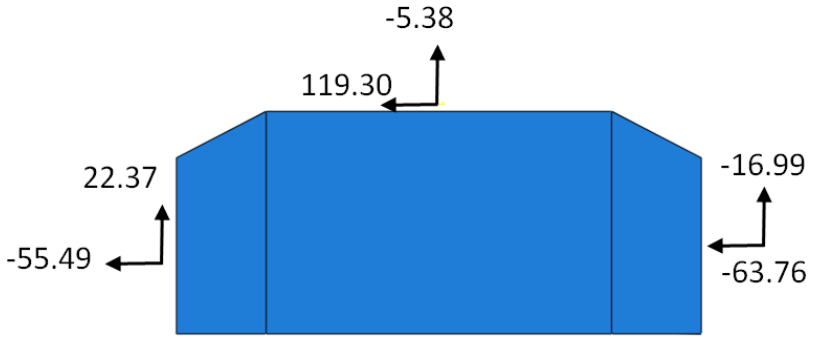

Figure 7.26: FBD of CP attached to column web at 0.05 radian (case 5A_one)

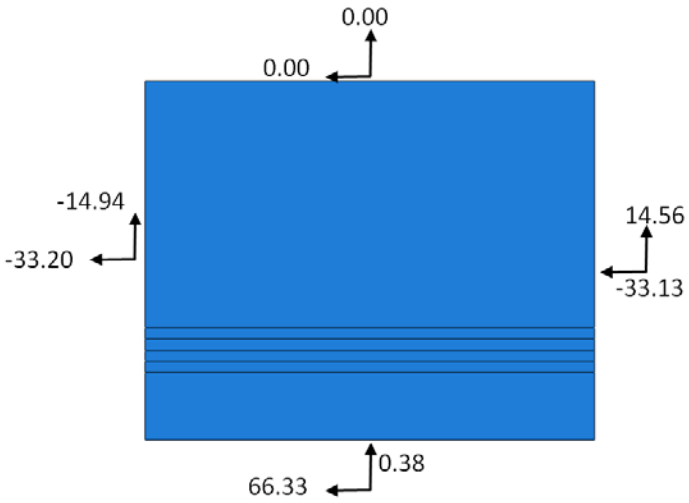

Figure 7.27: FBD of DP at 0.01 radian (case 13A_quar)

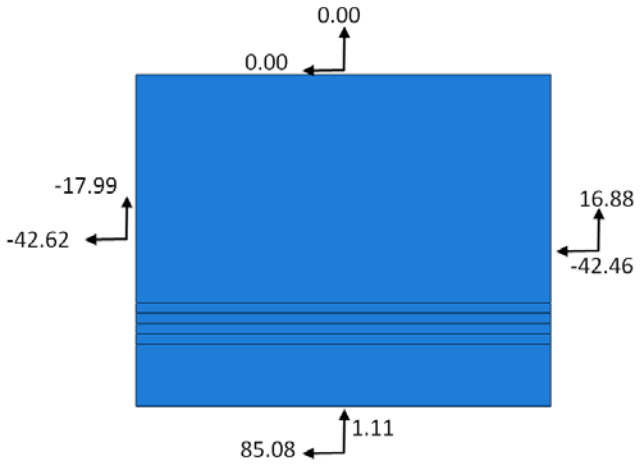

Figure 7.28: FBD of DP at 0.02 radian (case 13A_quar)

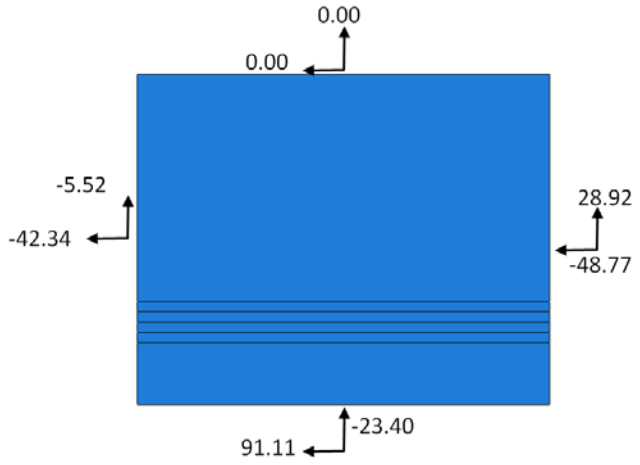

Figure 7.29: FBD of DP at 0.05 radian (case 13A_quar)

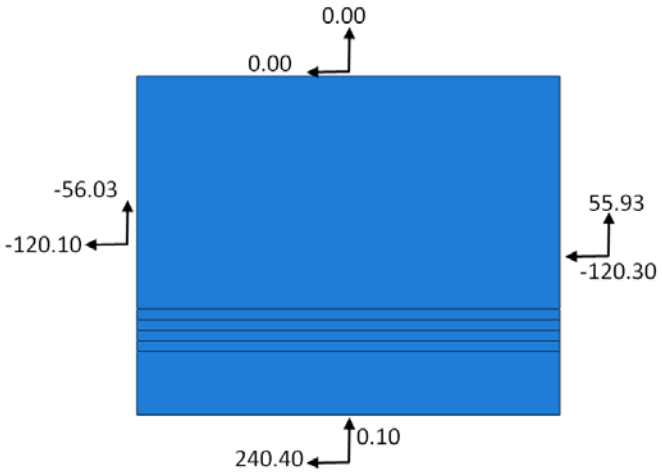

Figure 7.30: FBD of DP at 0.01 radian (case 13A_one)

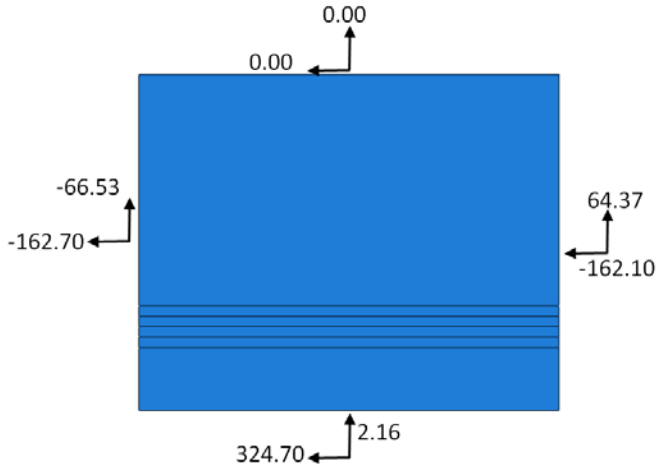

Figure 7.31: FBD of DP at 0.02 radian (case 13A_one)

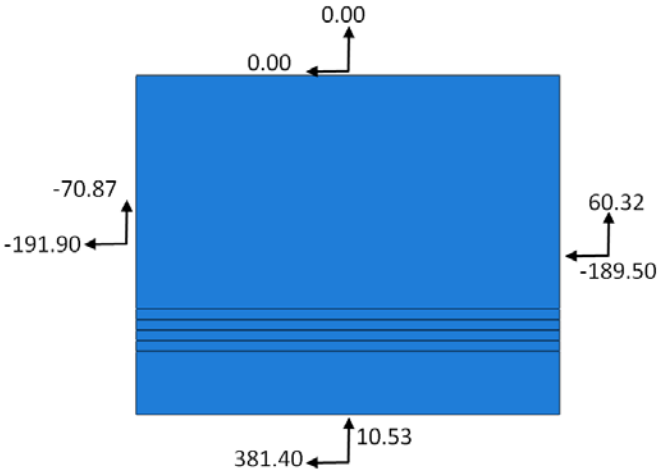

Figure 7.32: FBD of DP at 0.05 radian (case 13A_one)

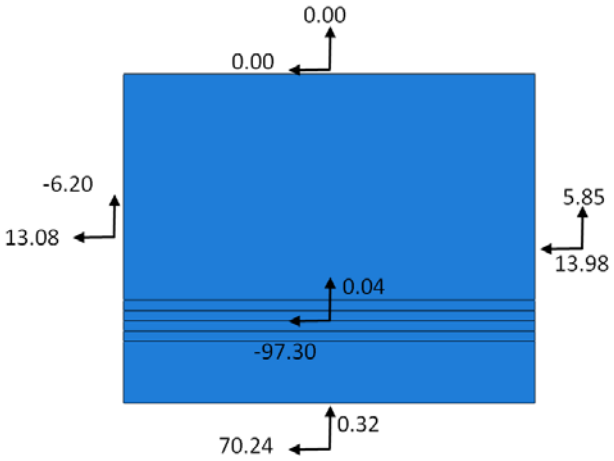

Figure 7.33: FBD of DP at 0.01 radian (case 15A_quar)

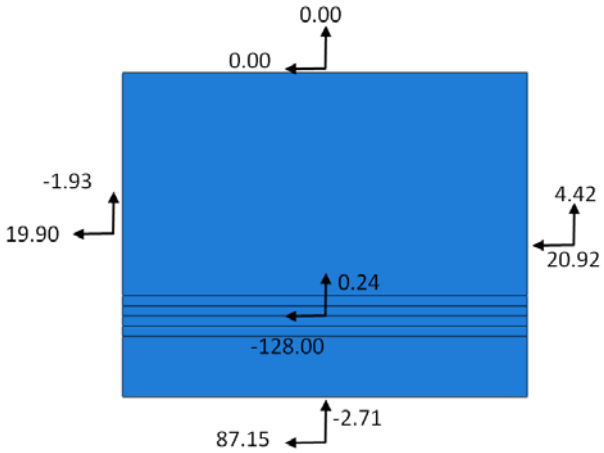

Figure 7.34: FBD of DP at 0.02 radian (case 15A_quar)

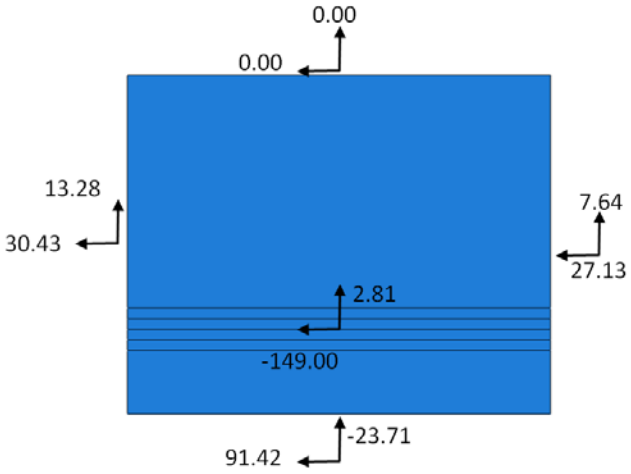

Figure 7.35: FBD of DP at 0.03 radian (case 15A_quar)

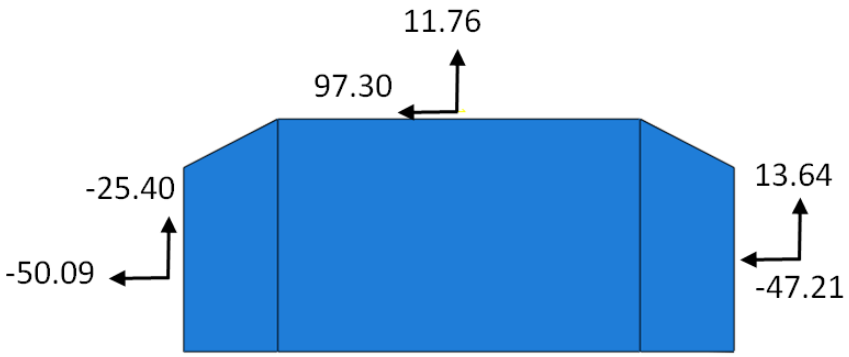

Figure 7.36: FBD of CP attached to DP at 0.01 radian (case 15A_quar)

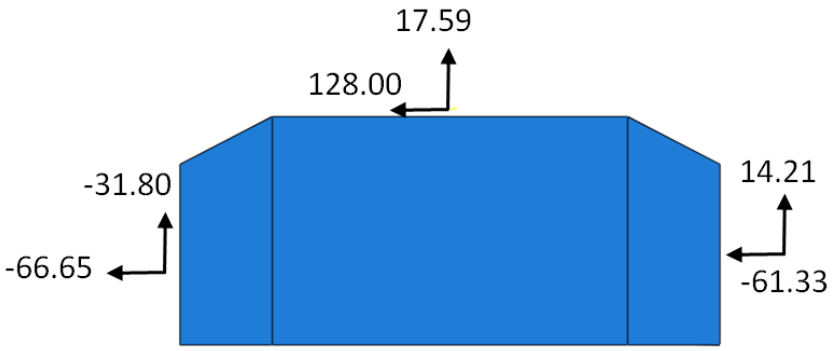

Figure 7.37: FBD of CP attached to DP at 0.02 radian (case 15A_quar)

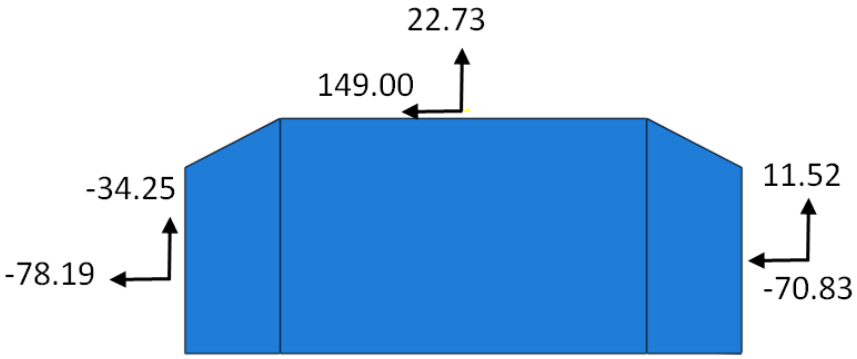

Figure 7.38: FBD of CP attached to DP at 0.05 radian (case 15A_quar)

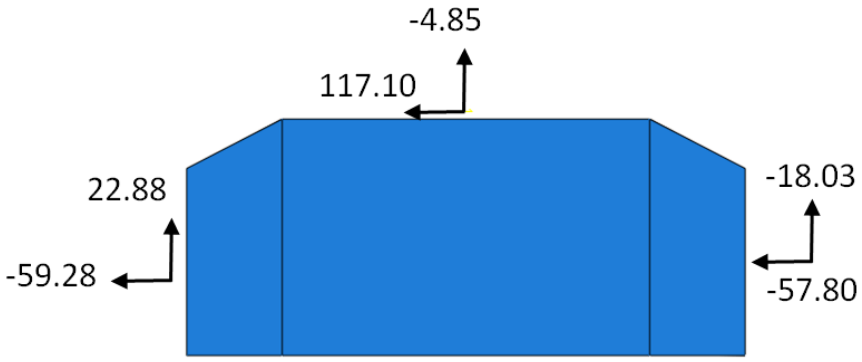

Figure 7.39: FBD of CP attached to column web at 0.01 radian (case 15A_quar)

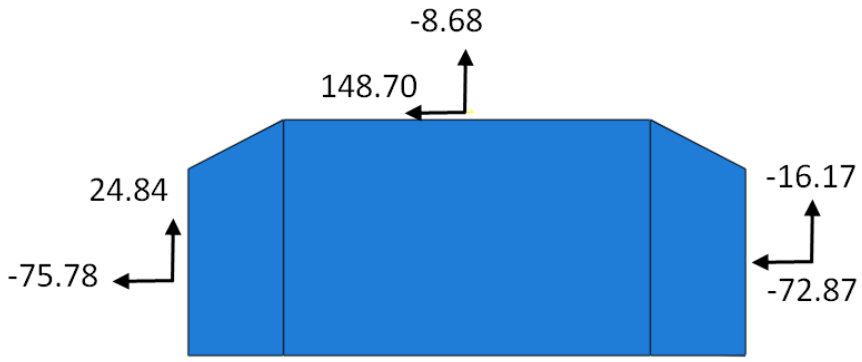

Figure 7.40: FBD of CP attached to column web at 0.02 radian (case 15A_quar)

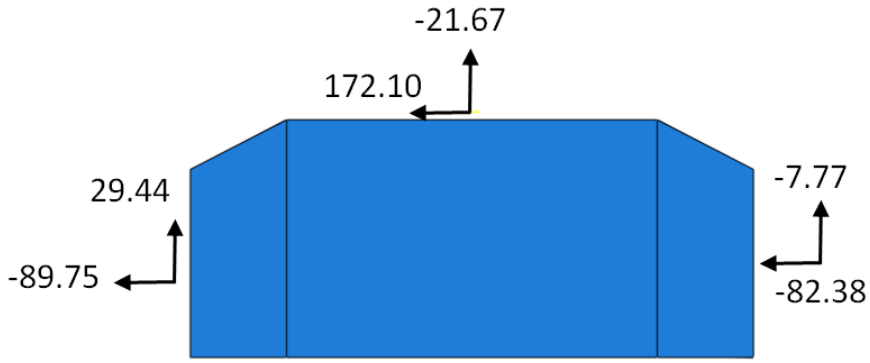

Figure 7.41: FBD of CP attached to column web at 0.05 radian (case 15A_quar)

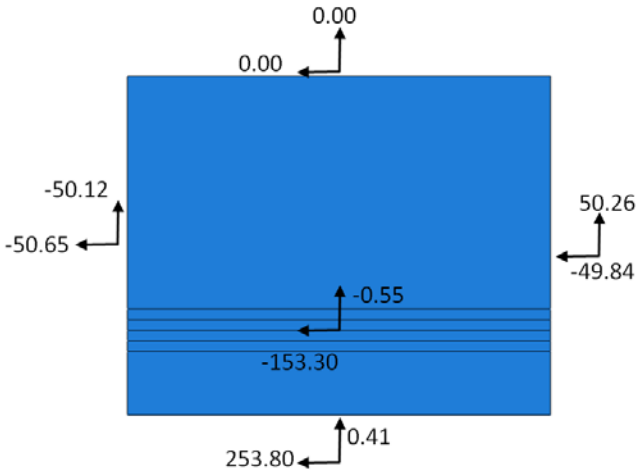

Figure 7.42: FBD of DP at 0.01 radian (case 15A_one)

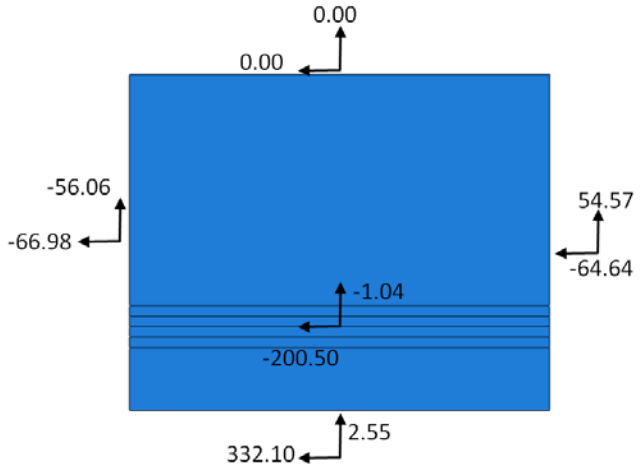

Figure 7.43: FBD of DP at 0.02 radian (case 15A_one)

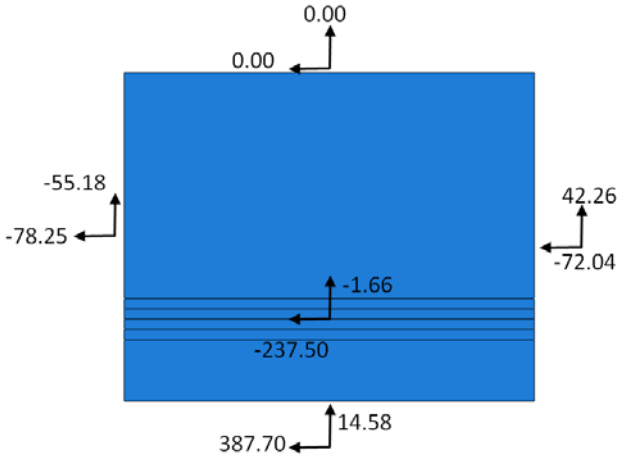

Figure 7.44: FBD of DP at 0.03 radian (case 15A_one)

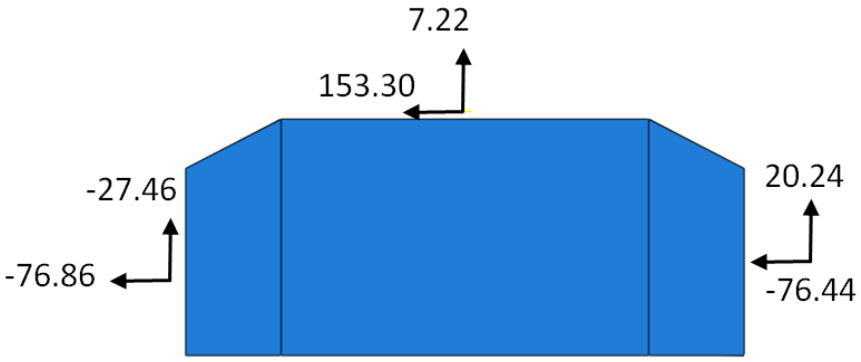

Figure 7.45: FBD of CP attached to DP at 0.01 radian (case 15A_one)

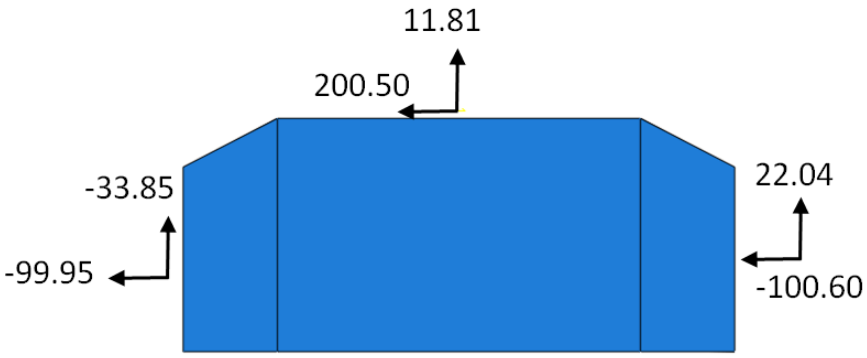

Figure 7.46: FBD of CP attached to DP at 0.02 radian (case 15A_one)

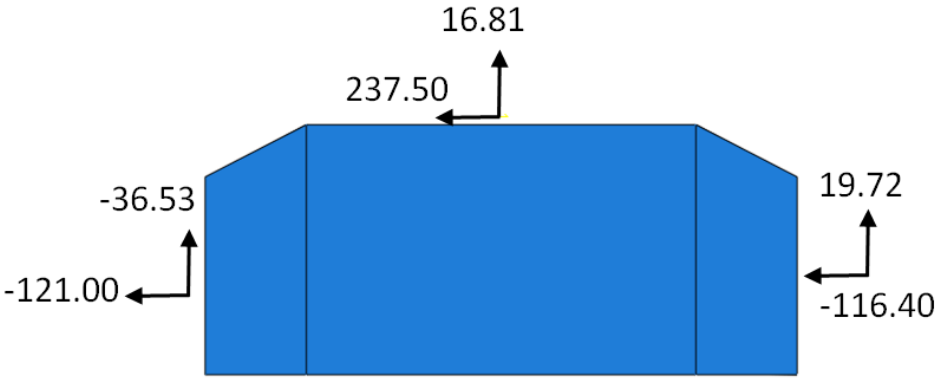

Figure 7.47: FBD of CP attached to DP at 0.05 radian (case 15A_one)

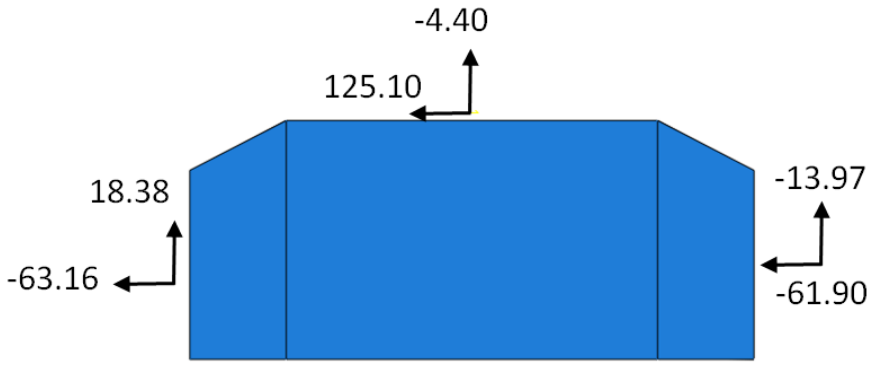

Figure 7.48: FBD of CP attached to column web at 0.01 radian (case 15A_one)

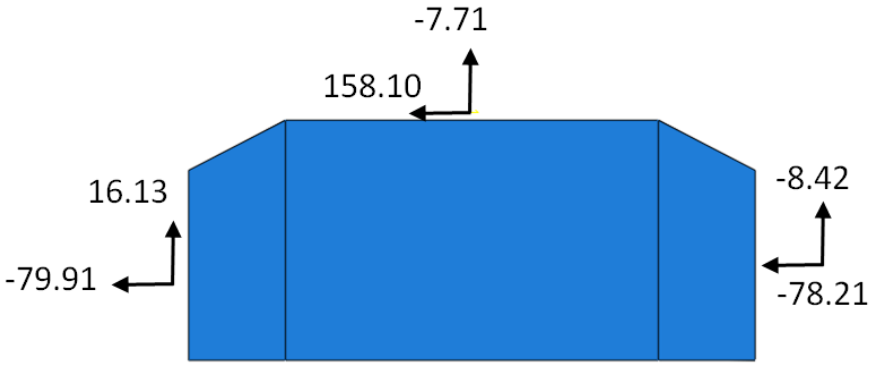

Figure 7.49: FBD of CP attached to column web at 0.02 radian (case 15A_one)

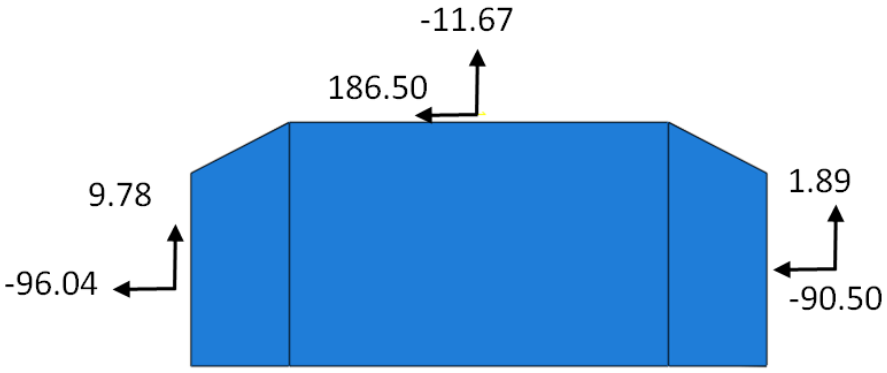

Figure 7.50: FBD of CP attached to column web at 0.05 radian (case 15A_one)

7.4 OBSERVATIONS

All the cases having undersized and oversized DP thickness were able to reach to the panel zone strength proportional to the combined thickness of the web and DP. This means that limiting strength in each case is web shear. However buckling of the DP (see Figure 4.21, Figure 4.42, Figure 4.92 and Figure 4.113) is noticed in cases having a ¼ inch thick DP, but these distortion are not high enough to cause any reduction in the panel zone strength.

In shallow columns at 0.01 and 0.05 radian, there is no considerable change in the maximum VMS, PEEQ and PEMAG (see Table 4.33 - 4.38) values in all the parts of the assembly in different cases (except case 13A_one). In case 13A_one at 0.05 radian, there is around 18 % increase in maximum VMS and around 260 % increases in maximum PEEQ and PEMAG in CJP1 weld as compared to base case 13A. The thicker welds may be the reason for this behavior.

In cases with a column flange thickness of 2.85 inches (see Figure 4.17, 4.22, 4.27, 4.38, 4.46 and 4.53), the VMS along the width of the DP at the middle section is uniform around 70 ksi while the VMS is uniform around 60 ksi at the top section (except case 5A, 5A_quarter). At the top section, the VMS near the central width is around 35 ksi in case 5A and around 20 ksi in case 5A_quarter rising sharply to 60 ksi at the ends (see Figure 4.38 and Figure 4.46). This reduction of VMS along the width of DP at the LP level (top section) in cases 5A and 5A_quar can also be explained by comparing the FBD of the DP at 0.05 radian in cases 5A (Figure 4.173), 5A_quar (Figure 7.11) and 5A_one (Figure 7.20). In case 5A_one, similar forces are transferred to the DP via vertical CJP1 weld and the horizontal CJP2 weld while in other cases 5A and 5A_quar, lesser amount of forces are transferred to DP via vertical CJP1 weld than via horizontal CJP2 weld. Thus the undersized DP may have high stress gradients near the LP level and the state of

stress is three-dimensional due to considerable buckling (see Figure 4.22 and Figure 4.46) rather than a two-dimensional state of stress observed in other cases.

In cases with a column flange thickness of 2.85 inches (see Figure 4.18, 4.23, 4.28, 4.39, 4.47 and 4.54), the VMS along the depth of the vertical weld at the DP – CJP1 weld interface is constant around 80 ksi at the middle depths but drop down drastically to 0 - 20 ksi at the top and bottom ends. The VMS along the depth is primarily a combination of horizontal normal stress (S33) and vertical shear stress (S23). The vertical shear stress is the main component of VMS at the middle depth while it is zero at the ends. The horizontal normal stress is maximum at the LP level while they are around zero at the middle depth (except in case 3A_quar and 5A_quar, see Figure 4.23 and Figure 4.47). The horizontal normal stress at the middle depth in cases with the thinner DP is non-zero.

Another interesting observation is seen in the FBD of the DP (see Figure 7.35) at 0.05 radian in case 5A_quarter where the direction of force at the left and right end of the DP is pull and push respectively while opposite directions are observed in all other cases as the loading on the LP's is push on left side and pull on right side. This is due to the fact that the DP and column flanges are so thin that the force transmitted via CP to DP is much higher than via vertical CJP1 welds.

Observations on thin / thick DP's are summarized below:

- With the thin doubler plate, the panel zone was still able to develop shear strength consistent with the full shear strength of the column web and DP combined. That is, the reduction in DP thickness did not reduce the contribution of the DP to panel zone shear strength. This was despite the noticeable amounts of out-of-plane displacement (buckling) observed in simulations with thin DP's. Three-

dimensional state of stress exists in the thin DP and stress gradients are higher at the LP level. More thorough research is required about the buckling of thin DP's in the panel zone.

- The panel zone strength is achieved when oversized DP is used in the panel zone but there are some concerns about the increase in stresses and strains in CJP1 groove weld when oversized DP is attached to the shallow column having thinner flanges.
- The DP is not overstressed in terms of increased stresses and forces when undersized or oversized DP's are used in the panel zone.

CHAPTER 8

Extension of the Doubler Plate beyond the Panel Zone for Cases of W14X398 and W40X264 Columns

8.1 INTRODUCTION

The possible advantages of extending the DP 6 inches beyond the LP level in shallow (W14X398) and deep (W40X264) columns are discussed in this chapter. Chapter 4 and Chapter 5 already summarized some of the findings of the extension of the DP, and these effects are explained in further detail here. Section 8.2 lists the analysis cases for this study and section 8.3 discuss major observations.

8.2 ANALYSIS CASES

Table 8.1: Analysis cases for the study on extension of DP

Case	t_f (inches)	t_{dp} (inches)	l_{dp} (inches)	b_{dp} (inches)	CP
2A	2.85 (W14X398)	0.50	24	10	No
3A		0.50	36	10	No
7A	2.00 (W14X398)	0.50	24	10	No
8A		0.50	36	10	No
12A	1.00 (W14X398)	0.50	24	10	No
13A		0.50	36	10	No
17A	0.50 (W14X398)	0.50	24	10	No
18A		0.50	36	10	No
2B	1.75 (W40X264)	1.00	24	34	No
3B		1.00	36	34	No
7B	0.75 (W40X264)	1.00	24	34	No
8B		1.00	36	34	No

Table 8.1 shows the analysis cases considered for this study. In all the cases, only vertical CJP1 groove welds were used to attach the DP to the column. There are no horizontal welds at the DP–column web interface. Figure 8.1 and 8.2 shows the

comparison of panel zone strength versus rotation (gamma) for W14X398 and W40X264 columns respectively. These figures only plots the last cycle of 0.05 radian in each case.

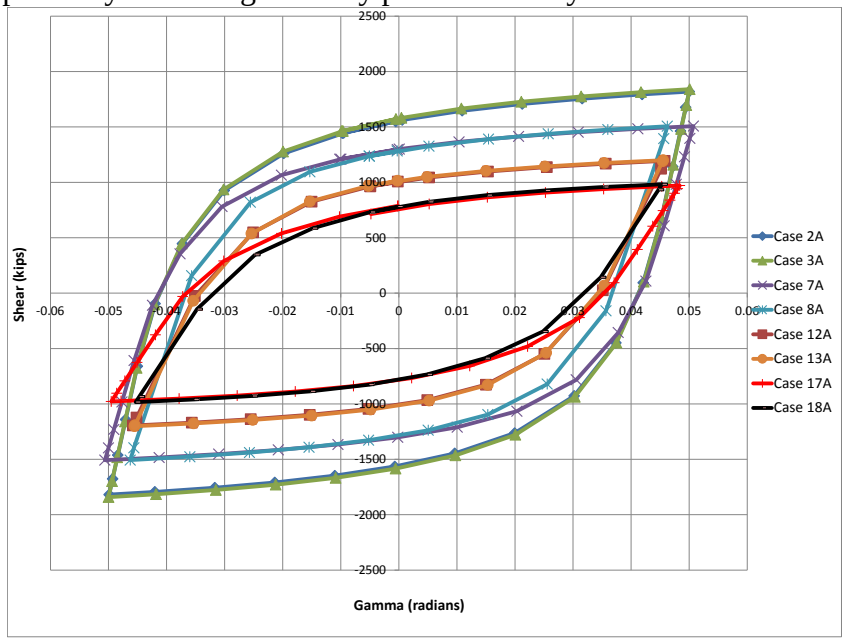

Figure 8.1: Panel zone shear versus gamma (W14X398 column)

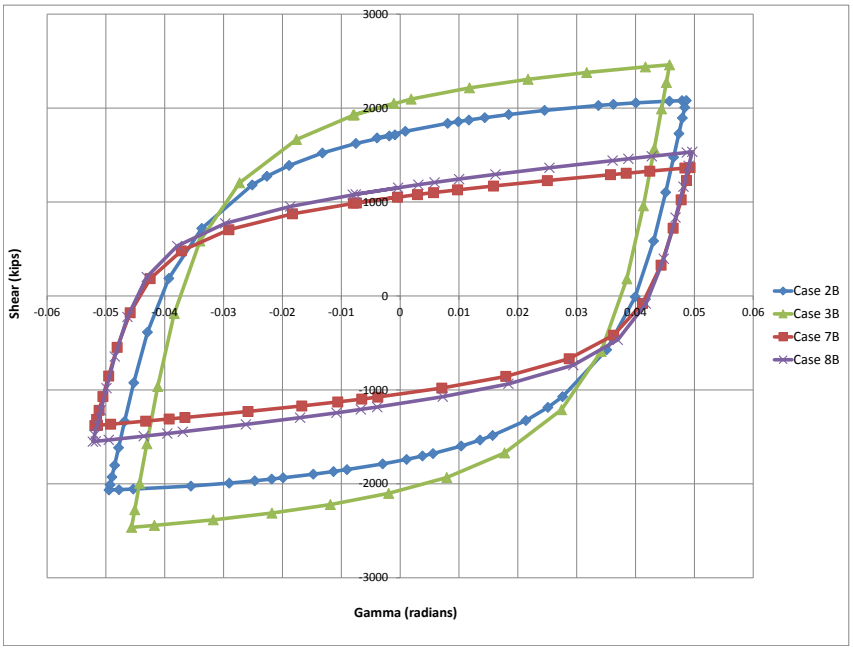

Figure 8.2: Panel zone shear versus gamma (W40X264 column)

8.3 OBSERVATIONS

The extension of the DP in the W14X398 column does not increase the panel zone shear strength (see Figure 8.1). However, there is appreciable increase in the shear strength in W40X264 column (see Figure 8.2). The increases in panel zone shear strength were: (a) 18 % (380 kips, case 2B and 3B) and (b) 12 % (167 kips, case 7B and 8B). The possible reason for this behavior is that the controlling limit state for shallow columns is web shear, while for deep columns (2B, 3B, 7B and 8B) the controlling limit states are local limit states like flange bending and web / DP crippling. The extension of the DB in deep columns stiffens the column web / DP against out of plane buckling/crippling and localized flange bending.

At 0.05 and 0.01 radian rotation of the W14X398 column, the maximum VMS, PEEQ and PEMAG (Table 4.33 to 4.38) in column and DP remains about the same whether the DP is extended or not. However, there is marked decrease of these quantities in the CJP1 weld in cases where the DP is extended. This decrease is tabulated in Table 8.2. These maximum values in the DP and column are located at middle depth (see Figure 4.4, 4.5, 4.15 and 4.16) while these maximum values are located near the LP level in CJP1 weld.

The maximum VMS (see Table 5.14 and 5.15) in different parts of W40X264 column at 0.05 and 0.01 radian remains similar as the DP is extended. The maximum PEEQ and PEMAG (see Table 5.16 and 5.19) at 0.05 and 0.01 radian decrease as the DP is extended (see Table 8.2). This may be attributed to the reduced localized flange bending or DP / web crippling as the extension of the DP stiffens the web. These maximum quantities are located near the k-area of the deep column due to the localized flange bending in that area (see Figure 5.5 – 5.8, 5.23 – 5.26).

The significant stresses along the width of the DP are plotted for each case in Chapter 4 and Chapter 5. As the DP is extended in the W40X264 column, the shear stress at the middle section (see Figure 5.27) becomes uniform along the width of the DP. In the case where the DP terminates at LP level, these shear stresses are low at the ends of the DP (see Figure 5.12 and 5.37). The shear stress at the middle section is uniform along the length in both cases (without extension and with extension) of W14X398 column (see Figure 4.6 and 4.17).

Table 8.2: VMS, PEEQ and PEMAG decrease in CJP1 weld as DP is extended

Case	VMS	PEEQ	PEMAG
0.01 radian			
2A -> 3A	-3.75 %	-30.70 %	-40.34 %
7A -> 8A	-10.00 %	-62.20 %	-62.10 %
12A -> 13A	-8.88 %	-66.40 %	-58.47 %
17A -> 18A	-3.22 %	-35.20 %	-35.52 %
0.05 radian			
2A -> 3A	-13.00 %	-52.35 %	-54.77 %
7A -> 8A	-15.17 %	-71.61 %	-70.00%
12A -> 13A	-18.26 %	-69.55 %	-76.00 %
17A -> 18A	-28.23 %	-50.22 %	-68.35 %
0.01 radian			
2B -> 3B	-4.88 %	-46.15 %	-42.47 %
7B -> 8B	-8.25 %	-40.73 %	-37.42 %
0.05 radian			
2B -> 3B	+1.37 %	-28.70 %	+3.07 %
7B -> 8B	-4.34 %	-23.04 %	-8.32 %

The stresses along the depth of CJP1 weld at the DP – CJP1 weld interface are plotted for each case in Chapter 4 and 5. The VMS along the depth is primarily a combination of horizontal normal stress (S33) and vertical shear stress (S23). The vertical shear stress is the main component of the VMS at the middle depth while it is zero at the ends. The horizontal normal stress is maximum at the LP level while they are around zero at the middle depth. In the deep columns, the VMS drops down to around 20 ksi at the

middle depth from around 90 ksi at the LP level in case 2B while the VMS drops down to around 60 ksi at the middle depth from around 90 ksi at LP level in case 3B (see Figure 5.13 and Figure 5.28). The VMS at the middle depth in case 7B was close to zero while the VMS at the middle depth in case 8B is around 30 ksi (see Figure 5.50 and Figure 5.57). In the shallow column, the VMS is uniformly around 80 ksi along the depth of CJP1 weld in between the LP's (see case 2A, Figure 4.7 and case 3A, Figure 4.18).

Observations regarding the extension of the DP can be summarized as follows:

- There is no increase in the shear strength of the W14X398 column as the DP is extended. However there is some reduction in stress in the vertical CJP1 weld at the LP level when the DP is extended.
- There is an increase of around 12 – 18 % in the shear strength of the W40X264 column as the DP is extended but there is no appreciable stress reduction in the CJP1 welds.

CHAPTER 9

Summary and Conclusions

9.1 SUMMARY

This thesis presented the results of an analytical study investigating attachment details for doubler plates in the panel zone of seismic-resistant steel moment frames. The panel zone is the portion of the column within the beam-column joint. When lateral load is applied to a moment frame, as occurs in earthquakes, very large shear forces are developed in the column panel zone. Doubler plates are sometimes used to increase the shear strength of the panel zone. Doubler plates essentially make the web thicker and thereby increase both the stiffness and strength of the panel zone.

While a significant amount of past research has investigated the behavior of the panel zone region in steel moment frames, very little research has been conducted on methods to attach doubler plates to the column. The doubler plate attachment details can have an important impact on the structural performance of the panel zone under seismic loading and also on the cost of construction. This research was aimed at developing an improved understanding of the advantages and disadvantages of various approaches for detailing and welding doubler plates to columns and how various details perform under cyclic inelastic loading. An additional goal of this research is to evaluate currently available doubler plate detailing requirements specified in the *Seismic Provisions for Steel Structural Buildings* (AISC 2010b) and to suggest improvements to these requirements where warranted. The research presented in this thesis builds on and extends recently completed work by Shirsat (2011) and Donkada (2012). The work by Shirsat and Donkada evaluated the performance of various doubler plate attachment details under monotonically applied loads. The research reported herein extends the work by Shirsat and Donkada by considering behavior of various doubler plate attachment details under cyclic loading.

This research, like that of Shirsat (2011) and Donkada (2012) focused on the case where the doubler plate is placed directly against the column web, and is then welded along its vertical edges to the column flange with groove welds. Some of the major questions addressed in the research include:

- For what level of stress or force should the groove welds along the vertical edges of the double plate be designed?
- Are there benefits to providing horizontal fillet welds at the top and bottom edges of the doubler plate, in addition the groove weld along the vertical edges?
- Are there benefits to extending the double plate 6-inches above and below the level of the beam flanges?
- When a continuity plate is welded directly to a doubler plate, what effect does this have on the doubler plate?
- Are the answers to the questions above different for double plates welded to shallow columns versus deep columns?

The research questions described above were addressed through an extensive series of finite element analyses conducted using ABAQUS. A simplified model was used wherein the beam was replaced by “loading plates” that were intended to represent the beam flanges. The model used three-dimensional solid elements and included both material and geometric nonlinearity. The finite element model used in this research was the same as that used by Shirsat (2011) and by Donkada (2012). The primary difference in this research, however, is that both the structural steel and welds were represented using a cyclic inelastic material model, compared to the monotonic material model used by Shirsat and Donkada.

This study was conducted using two different column shapes: a W14X398 (shallow column) and a W40X264 (deep column). These were chosen to evaluate differences in the performance of doubler plates in shallow heavy columns versus deep columns. All the columns were loaded cyclically to a displacement control loading of 0.05 radian rotation of the panel zone. The results for W14X398 column are presented in

Chapter 4 and Chapter 5 lists the results for W40X264 column. The results consisted of panel zone shear versus rotation (gamma) curves, stress and strain contours in the doubler plate and column, stress contours in the continuity plates, stress variation along the width of the doubler plate and stress variation in the vertical groove welds at the doubler plate-groove weld interface. Free body diagrams were developed for the continuity plates and a segment of the doubler plate to help understand the load path from the beam flange loading plates into the column, continuity plates, double plate and welds. The analyses were also used to study limit states other than panel zone shear yielding, including local column flange bending, and local crippling of the column web and/or doubler plate.

9.2 CONCLUSIONS

The major conclusions of this research are as follows:

- There is no increase in the panel zone strength in shallow columns when the doubler plate is welded on all four sides, i.e., horizontal fillet welds and vertical groove welds, as compared to the assembly where only vertical groove welds are used to attach the doubler plate to the column. However, in cases where the doubler plate does not extend above and below the level of the beam flange load plates, horizontal fillet welds help reduce stresses in the vertical groove welds.
- There is an increase of around 10% in the panel zone strength in deep columns when the doubler plate is not extended, but is also welded along the top and bottom horizontal edges. This increases the amount of force flow through the vertical groove welds to the doubler plate, so there is some increase in the stresses and strains in the top portion of the vertical welds. Here, the limiting strength is lower than the shear strength of deep columns due to the occurrence of localized limit states like column flange bending and doubler plate/column web crippling. So, this increase in strength by welding horizontally may be due to the restraint

provided by the horizontal welds to the doubler plate/column web crippling. Note that the doubler plate was terminated between the beam flange loading plates in these cases.

- Extending the doubler plate 6 inches beyond the loading plate level does not show any increase in the panel zone strength in shallow columns while there is around 12 – 18 % increase strength in the deeper columns. There is some reduction in stress in the vertical groove welds when the doubler plate is extended in shallow columns while there is a marginal stress increase in the vertical groove welds in the deeper columns.
- The use of doubler plates that are thinner than the minimum permitted thickness specified by Eq. E3-7 in the *Seismic Provisions for Steel Structural Buildings* (AISC 2010b) did not affect the panel zone strength in the shallow column, despite a considerable amount of buckling that developed in the doubler plate.
- In most of the simulation cases, the von mises stress in the vertical groove weld at edge of the doubler plate consists primarily of horizontal normal stress at the loading plate level and vertical shear stress at the middle depths of the doubler plate. Thus, the weld used to connect the doubler plate to column flanges should be designed to develop both the nominal shear strength and tensile strength of the doubler plate.
- The limit state that controlled panel zone strength for all cases of shallow columns was web panel zone shear. Thus providing continuity plates did not increase the panel zone strength. The amount of force flowing through the continuity plates into the column web increased as the column flange thickness decreased. The limit state that controlled strength for the deeper column was localized flange

bending for most cases without continuity plates. When continuity plates were added, the columns were able to develop the full shear strength of the panel zone.

- Welding a continuity plate directly to the doubler plate did not overstress the doubler plate in either the shallow or deep columns. Instead, the continuity plates reduced stresses in the groove welds at the vertical edges of the doubler plate in the shallow columns, and eliminated localized flange bending in deeper columns.
- In general, it was beneficial to extend the double plate 6-inches above and below the level of the beam flange loading plates. Extending doubler plates reduces stresses in the vertical groove welds, helps to reduce buckling of the doubler plate, and helps control local crippling of the doubler plate and/or column web large forces are applied at the beam flange load plate levels.
- Almost all analysis cases looked at columns were beams were attached to both flanges of the column, i.e. interior connections. Two cases were examined with the beam on only one side of the column, i.e., an exterior connection. Preliminary findings suggest that the doubler plate is not overstressed when a continuity plate is welded directly to it, similar to the findings for the interior connections.

9.3 FUTURE WORK

The research presented in this thesis considered a simplified model of the beam – column assembly and a cyclic material model accurate at higher levels of strains. Below are recommendations for future work.

- In this study, the beams connected to the column were replaced with loading plates. Additional analysis is needed using models that include the full beam and beam-to-column moment connection.

- The cyclic material modeled developed in this study is less accurate at lower cyclic strain levels. A more robust material model with more accurate hardening cycles at all strain levels can be developed to predict panel zone behavior accurately at both small and large rotations.
- It was assumed in this research that beam on both sides of column are of equal depth but in reality this may not be the case. Models having different beam depths on both sides should be investigated.
- Most of the cases investigated here represented an interior joint of a steel moment connection. More cases representing an exterior joint with the beam only on one side should be examined.
- Fillet welds instead of groove welds can be used for attaching the vertical edges of the doubler plate to the column flange. Additional research is needed to investigate this option.
- Additional work is needed to investigate the stability of doubler plates.

References

Abaqus Analysis User's Manual (2012). Dassault Systèmes Simulia Corp., Providence, RI.

Abaqus/CAE User's Manual (2012). Dassault Systèmes Simulia Corp., Providence, RI.

Getting Started with Abaqus: Interactive Edition (2012). Dassault Systèmes Simulia Corp., Providence, RI.

AISC (2010a), AISC/ANSI 360-10, *Specification for Structural Steel Buildings.* American Institute of Steel Construction, Inc., Chicago, IL.

AISC (2010b), AISC/ANSI 341-10, *Seismic Provisions for Structural Steel Buildings.* American Institute of Steel Construction, Inc., Chicago, IL.

AISC (2010c), *Steel Construction Manual, 14th Edition*, American Institute of Steel Construction, Inc., Chicago, IL.

Cofie, N.G., Krawinkler, H. (1985). "Uniaxial cyclic stress–strain behavior of structural steel". *Journal of Engineering Mechanics,* American Society of Civil Engineers.

Yongjiu, S., Meng, W., Yuanqing, W. (2011). "Experimental and constitutive model study of structural steel under cyclic loading". *Journal of Constructional Steel Research, 67*(8), 1185-1197. doi: http://dx.doi.org/10.1016/j.jcsr.2011.02.011

Mays, T.W. (2000). "Application of the Finite Element Method to the Seismic Design and Analysis of Large Moment End-plate Connections". *PhD Dissertation*, Virginia Polytechnic Institute and State University, Blacksburg, VA.

Shirsat, P.S. (2011). "Preliminary Analysis of Doubler Plate Attachment Details for Steel Moment Resisting Frames". *Master's Thesis*, The University of Texas at Austin, Austin, TX.

Donkada, S. (2012). "Finite Element Analysis of Doubler Plate Attachment Details and Load paths in Continuity Plates for Steel Moment Frames". *Master's Thesis*, The University of Texas at Austin, Austin, TX.

Okazaki, T. (2004). "Seismic Performance of Link-to-Column Connections in Steel Eccentrically Braced Frames". *PhD Dissertation*, The University of Texas at Austin, Austin, TX.

Richards, P. (2004). "Cyclic Stability and Capacity Design of Steel Eccentrically Braced Frames". *PhD Dissertation*, University of California, San Diego, CA.

Ryu, H.-C., (2005). “Effect of Loading History on the Behavior of Links in Seismic-Resistant Eccentrically Braced Frames”. *Master’s Thesis*, The University of Texas at Austin, Austin, TX.

Kaufmann, E.J., Metrovich, B.R., Pense, A.W. (2001). “Characterization of Cyclic Inelastic Strain behavior on Properties of A572 Gr. 50 and A913 Gr. 50 Rolled Sections”. *Final Report to American Institute of Steel Construction, ATLSS Report No. 01-13*, Lehigh University, Bethlehem, PA.

Engelhardt, M.D., Venti, M.J., Fry, G.T., Holliday, S.D. (2000). “Behavior and Design of Radius Cut Reduced Beam Section Connections”. *Report No. SAC/BD-00/17*, SAC Joint Venture

Ramberg, W., Osgood, W.R. (1943). “Description of Stress-Strain Curves by Three Parameters”. *TN902, 4943*, National Advisory Committee for Aeronautics.